Comments, suggestions, or corrections are welcome and should be sent to:

Y. F. Makogon
Petroleum Engineering Department
Texas A&M University
College Station, Texas 77843–3116
USA

PennWell Publishing Company
1421 South Sheridan Road/P.O. Box 1260
Tulsa, Oklahoma 74101

Library of Congress Cataloging-in-Publication Data

Makogon, IU. F. (IUrii Fedorovich)
Hydrates of hyrocarbons / Yuri F. Makogon.
p. cm.
Includes index.
ISBN 0-87814-718-7
1. Natural gas—Hydrates. I. Title.
TN884.M35 1997
665.7—dc21 96-51830
CIP

Printed in the United States of America

03 02 01 00 99 98 97

CONTENTS

LIST OF TABLES

LIST OF FIGURES

ACKNOWLEDGMENTS

This monograph contains a number of general solutions of the problems on natural and technogenic gas hydrates obtained by the author and by many researchers who work in research laboratories and industry around the world. Certainly, one monograph cannot embrace all aspects of the gigantic multifaceted problem of gas hydrates. A tremendous amount of specialized literature exists on gas hydrates—several thousands of scientific papers, several dozens of serious monographs, numerous reports, etc.

I am pleased to note that in my research I not only used the published works of the majority of hydrate researchers, but also discussed the results with many of them during visits to their laboratories, in meetings at numerous scientific conferences, and by correspondence.

I am pleased to present a letter which was sent by Professor Donald L. Katz a few months before his death. From his letter it is evident how highly he valued the achievements of his students and colleagues.

The most widely known works among the specialists are *Handbook of Natural Gas Engineering* by D. L. Katz et al. (1959); *Hydrates of Natural Gases* by Y. F. Makogon (1981); *Clathrate Hydrates of Natural Gases* by E. D. Sloan (1990); *Gas Hydrates, Studies in Organic Chemistry* by E. Berecz and Balla-Achs, (1983); and *Handbook of Gas Hydrate Properties and Occurrence* by Lewin (1983). However, the requirements of theory and industry exceed by far the boundaries of the earlier published results.

Mastering of the hydrocarbon resources in the polar regions and in deep sub-sea zones has sharply increased the importance of studying both the natural and technogenic gas hydrates. Many discussions with Professors E. D. Sloan, R. Kobayashi, P. R. Bishnoi, G. D. Holder, J. M. Brooks, G. Lisichkin, Drs. D. B. Robinson, A. Malyshev, Y. Batalin, V. Fomina, L. Krasnovskaya, Y. Steklianin, L. Smirnov, M. V. Tolkachev, Y. P. Handa, H. J. Ng, V. A. Kamath, R. D. Malone, P. Notz, A. Lund, T. Austvik, B. Kvamme, T. Svartas, A. Nerheim, T. Valand, J. Monfort, Adisasmito Sanggono and many others have resulted in a need to write the present monograph with the applied character. I express my deep gratitude to all of my colleagues who helped to create this monograph in one way or another.

This monograph resulted from collaboration between the Institute of Oil and Gas Problems of the Russian Academy of Science and Texas A&M University. This monograph was sponsored by the Russian Committee on Science, New Technologies, and Education; Russian Academy of Sciences; Texas A&M University; Amoco, Brown & Root Ltd.; Conoco; Marathon; Holditch Associates; and the Minerals Management Service of the U.S. Department of the Interior.

Special thanks are directed to Professor Wayne Dunlap of the Offshore Technology Research Center who edited the translated manuscript, and who arranged the funding from Texas A&M University and others.

As the experience of translating my previous monographs indicates, it is a complicated task requiring not only knowledge of Russian and English languages, but also a deep understanding of the presented material. With this I take a special pleasure in acknowledging my son, Taras, who performed this work on a highly professional level.

Yuri F. Makogon

Department of Chemical Engineering
H. H. Dow Building
Ann Arbor, Michigan 48109-2136
313/764-2383
College of Engineering
The University of Michigan

August 16, 1988

Prof. Yuri F. Makogon
147717 Moscow
Lenin Region
Rasvilka
VNIIGAZ, USSR

Dear Professor Makogon:

It is some time since Dr. Robert Lee brought me from Toronto your recent book with your greetings and the paper on Natural Gas Hydrates. I recall our meeting at the World Petroleum Congress in 1971 in Moscow. Also, I found your earlier book on Natural Gas Hydrates very informative.

The paper you gave at Toronto was excellent in bringing out the experiences of harvesting of natural gas which occurs in hydrate form in the earth. Your work with understanding gas hydrates and the communication with U. S. investigators is commendable.

Although my experimental work with hydrates has been a small part of my total activities, I have been interested in gas hydrates for 54 years. The repressured gas fields in Michigan used for gas storage starting in 1941 were at pressures and temperatures close to those at which hydrates form. When Normal Wells oil and gas field was drilled in Northwest Territories of Canada (1943), I inquired about the reservoir temperature and pressure there below permafrost but found no hydrate conditions. It was you and your associates who found the gas hydrates present in the earth.

My health and age keep me from doing technical work these days. It is good to see the technical developments made by the oncoming generations like yourself and my former students Kobayashi, Robinson, and Holder.

With thanks and best wishes, I am

Sincerely yours,

Donald L. Katz

Donald L. Katz
A. H. White Distinguished University Professor
of Chemical Engineering, Emeritus

DLK:bd

INTRODUCTION

The percentage of hydrocarbon fuel use in the world energy balance has increased during the 20th century from 3% to 63% worldwide, and is as high as 75% in some industrial countries. Table I-1 illustrates the dynamics of population growth and energy consumption in the world during the present millennium. This table shows that the world population has increased during this period by 20.5 times, specific energy consumption has increased by 37 times, and the total consumption of energy from mineral sources has increased by 814 times. Figure I-1 presents the dynamics of population and energy consumption growth in the world during this millennium. Figure I-2 shows the structure of specific energy consumption starting in 1800 and provides a perspective for the world energy balance during the next 50 years.

It is noteworthy that the percentage of coal usage in the 1800s did not exceed 5%. It reached 50% by 1880, reached a maximum of 74% by 1925, and at the present time it is under 27%. The percentage of oil and natural gas in the world energy balance did not exceed three percent at the beginning of the century. This percentage increased to 40% by 1950 and to 66% by 1975. Currently, oil and natural gas consumption is at 63%. The role of natural gas in the world energy balance will certainly increase in future decades based on the availability of resources and environmental factors.

Potential sources of energy minerals and energy consumers in the world are distributed unevenly. The social status of countries and populations and the development rate of individual countries are determined by the availability of energy resources and the rate of their consumption. However, even in countries with vast energy resources, the rate of energy consumption and social status also depend on political stresses.

The history of Russia, whose high energy potential is recognized all over the world, is a prime example. Major stresses in the present century have slowed down social development in this country. Early in the century Russia held the lead in oil production in the world and produced more oil than the United States. However, the First World War, the 1917 Revolution, and the following Civil War left Russia far behind. Despite the fact that Russia increased its oil production and exceeded the United States in oil and gas production in 1975, Russia never reached the specific

Table I-1 World consumption of energy.

Years	1000	1500	1900	1920	1940	1960	1970	1980	1989 July	1990	1992	1993	1994	1995
World population, 10^6 p.	275	450	1617	1811	2295	2982	3635	4500	5000	5090	5240	5350	5470	5650
Energy consumption, 10^9 T.O.E.	0.01	0.14	0.9	1.50	2.25	3.55	5.57*	6.50*	7.70*	7.81*	7.79*	7.80*	7.92*	8.14*
Energy consumption per capita, T.O.E./yr.	0.04	0.31	0.55	0.83	0.98	1.19	1.53	1.44	1.54	1.53	1.49	1.46	1.45	1.44

*BP Statistical Review of World Energy, 1996.

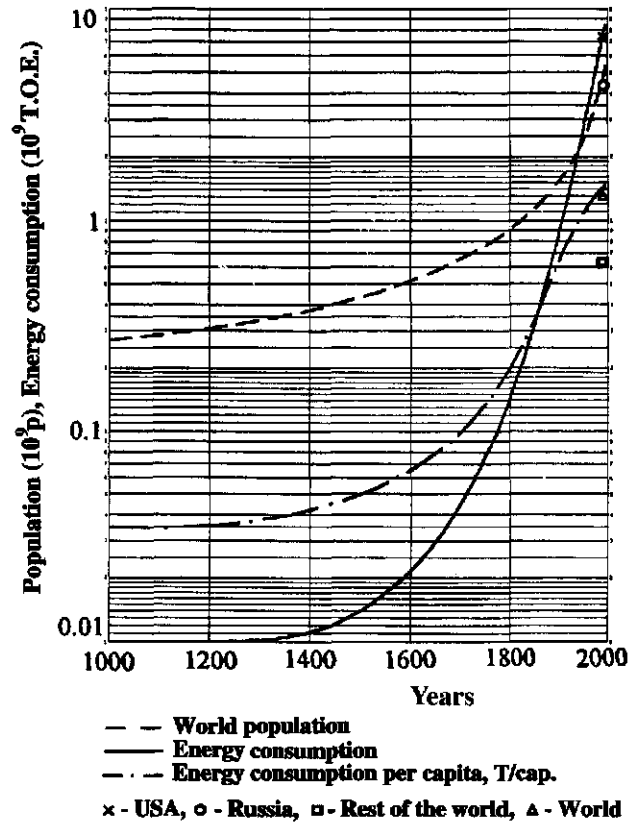

Figure I-1 World population and energy consumption.

rate of energy consumption per capita at the same rate as the United States (see Figure I-3).

Figure I-3 shows the growth dynamics of the three main energy industries in Russia: coal, oil, and gas production. There are three abrupt depressions on the production curves: the first is due to the Revolution and the Civil War; the second is due to the war with Germany, and the third is due to Perestroika in the political system.

This example illustrates dramatically that political aggression, either internal or external, is followed by destruction of economies and the degradation of a social system. In order to provide stable economic progress, mankind must find the power and wisdom to avoid political shocks and eliminate mutual claims.

Today increased rates in specific energy consumption are significantly higher than the population growth (see Figure I-1). Specific energy consumption is extremely uneven in different regions and fluctuates within a wide range from 0.1 to 7.5 tons of oil equivalent (TOE) per person

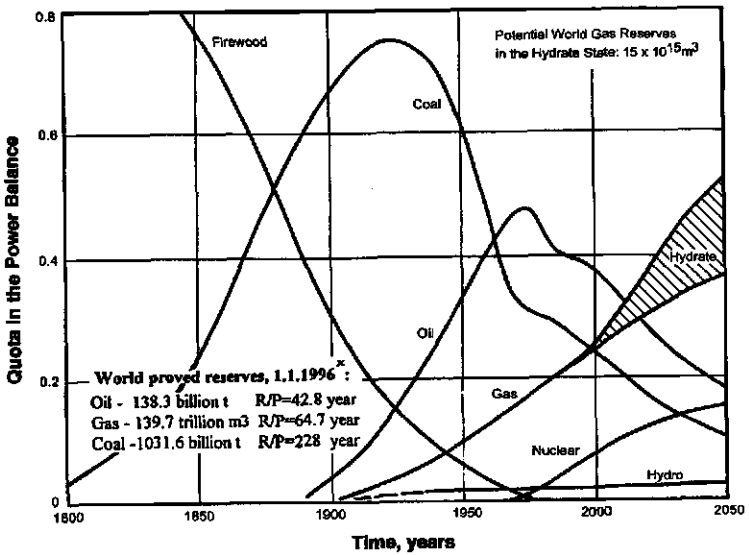

Figure I-2 World power balance dynamics.
x-BP Stat. Review of World Energy, 1996.

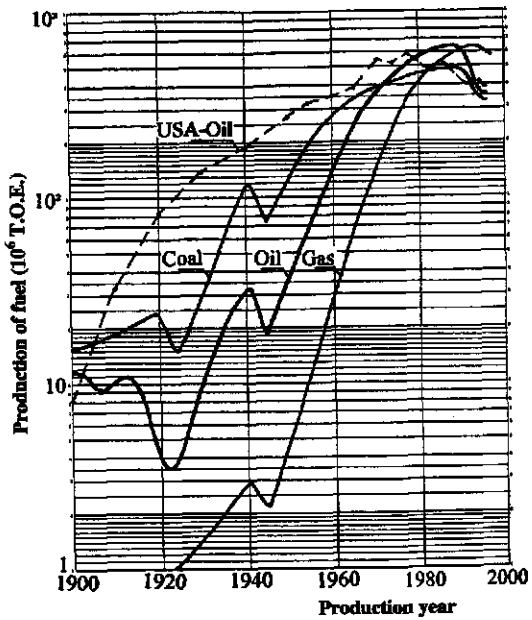

Figure I-3 Production of mineral resources in USSR.
(Oil Equivalent)—Oil = 10^7 kCal/T = 42.8 MJ/T; Gas = 0.9×10^7 kCal/1000 m^3 = 37.6 MJ/1000 m^3; Coal = 0.67×10^7 kCal/T = 28 MJ/T.

annually. Modern methods for survey and exploration of mineral energy sources allow us to determine the level of energy available for individual countries and regions in future decades. In the next 50–70 years, oil and natural gas will continue to be the main raw material for fuel and chemical industries, despite the investigation of new energy sources. So far, the share of oil in the world energy balance has reached its maximum and despite the annual increase in production oil's further role as a fuel will decrease. Active redistribution of hydrocarbon resources will take place in the world, as well as an active search for new unconventional hydrocarbon sources.

In modern conditions environmental requirements of energy sources, along with economic demands, have advanced to the forefront. Due to this the role of natural gas and unconventional hydrocarbons, sources will increase sharply. Some of the most prospective unconventional sources of natural gas are accumulations of natural gas hydrates which were proven to exist by Russian scientists in the 1960s. In 1969 a scientific discovery No. 75 was registered in the State Register of the USSR: "A Property of Natural Gases to Come into Combination with Water under Certain Thermodynamic Conditions in the Earth's Sedimentary Cover and to Form Gas Hydrate Deposits." This discovery by Russian scientists received international recognition and development.

The first gas hydrate deposits were revealed in the northern area of Siberia within the permafrost zone in the Messoyakhi and Ust-Vilyui fields. The first experience in producing gas from a gas hydrate deposit was obtained there.

Natural gas hydrates have become an exciting energy source for power engineers, space physicists, physical chemists, and other specialists over the last twenty years. Power engineers are interested in potential resources of hydrocarbon gases contained in the bowels of the earth in the hydrate state since those resources are by two orders of magnitude greater than the world's explored gas reserves.

The discovery of gas hydrate accumulations and the investigation of their properties have forced geologists to reconsider a number of principal statements on formation and conservation of oil and gas deposits both on land and offshore. Knowledge of the properties of hydrates allows us to evaluate in other contexts processes taking place in outer space. It gives us new insight into the formation of planets—particularly into the formation and dynamics of the earth's atmosphere and the ocean, as well as into the physics of comets and other space bodies.

Knowledge of the physical-and-chemical characteristics of hydrates and the processes of their formation, stable existence, and decomposition allow us to refine the impact of these phase transitions in the earth and on

the thermal characteristics of the sedimentary section, ocean, and atmosphere. The volumetric properties of hydrates appear to be unique: the specific volume of water at its transition into the hydrate state increases by 26–32%, whereas at freezing the increase is just 9%. The specific volume of gas at its transition into hydrate state changes sharply.

A large number of these problems remain to be investigated in order to get a quantitative result. However, it is noted that gas hydrates cannot be neglected when solving multiple fundamental problems connected with the dynamics of our planet and other space bodies.

Investigations on natural gas hydrates are underway in several scientific laboratories around the world—Russia, the United States, Norway, England, France, Japan, Indonesia, Brazil and other countries. The existence of natural gas hydrates is a global one, and these studies represent an example of international cooperation. Studies on gas hydrates are done under the United Coordination Program. The results of these studies are discussed annually at joint conferences.

Along with fundamental laboratory studies, intensive field work is being done to reveal gas hydrate fields on land and, especially, in the world's oceans. More than 60 large gas hydrate fields have been revealed to date in oceanic sediments and eight fields on land. Explored reserves of methane in the hydrate state are over 700 trillion m^3, exceeding seven fold the world's explored gas reserves. Potential gas resources concentrated on earth in the hydrate state exceed 1.5×10^{16} m^3. Figure I-4 provides a schematic map of the gas hydrate deposit occurrences (Kvenvolden, 1994). Figures I-5 through I-8 present the gas hydrate fields discovered on the North American Continent and in the seas of the USA.

An important concern is the economical feasibility of the development of gas hydrate deposits. There is an erroneous opinion among some specialists that in the regions abundant in natural gas resources, investing in the study of hydrates, surveys, and development of gas hydrate deposits is not appropriate. Unfortunately, the natural distribution of these energy resources is uneven. There are some regions low in mineral resources. The energy distribution of Russia's Far East, for example, is principally different from Western Siberia. Revealing hydrocarbons in the hydrate state and putting them into an energy balance of individual regions may radically change energy supply to industry and municipal consumers.

Despite some definite scientific achievements in hydrate studies, the basic properties of hydrates and hydrate-saturated porous media such as acoustic, electrical, thermophysical, thermomechanical, volumetric, and others remain practically unknown.

Preliminary results on the study of the acoustic properties of hydrates allowed us to design the means to reveal hydrate deposits in oceanic sediments and revealed the majority of hydrate occurrences known to

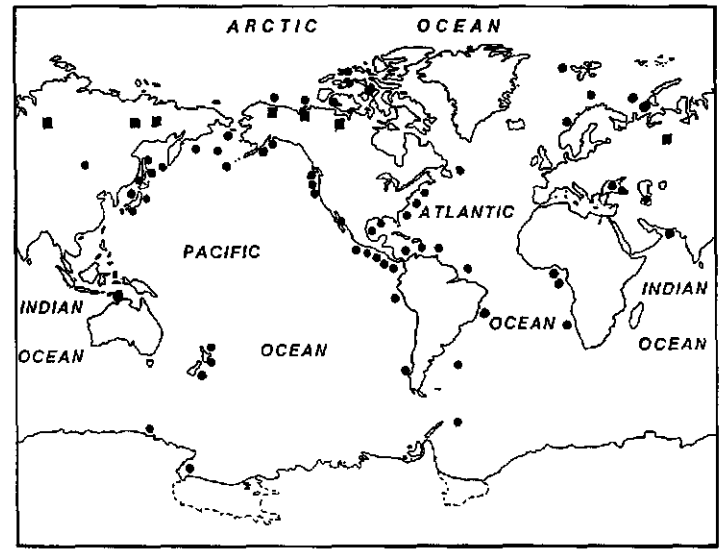

Figure I-4 Map of worldwide locations of gas hydrates occurrences in on-shore (■) and offshore (●) sediments.

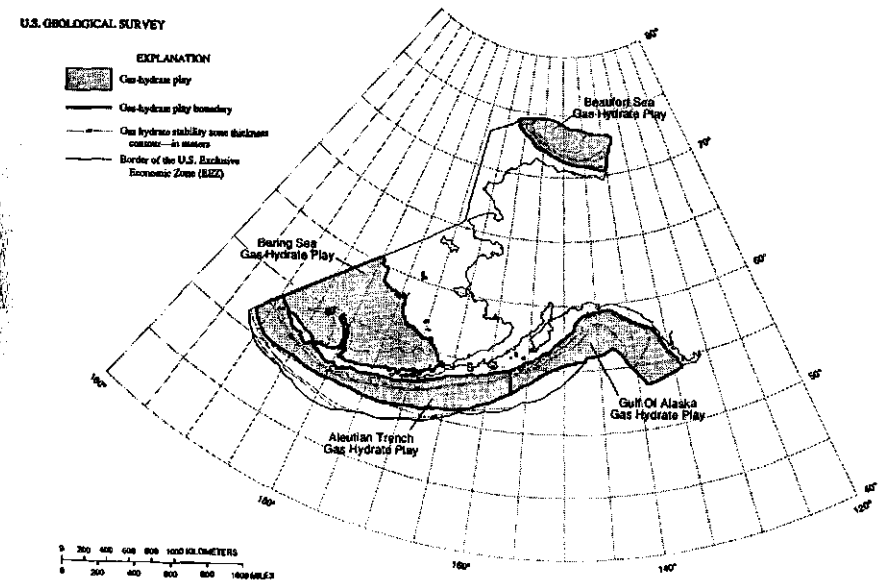

Figure I-5 Map of the Beaufort Sea, Bering Sea, Aleutian Trench, and Gulf of Alaska gas hydrate plays (Collett et al., 1994).

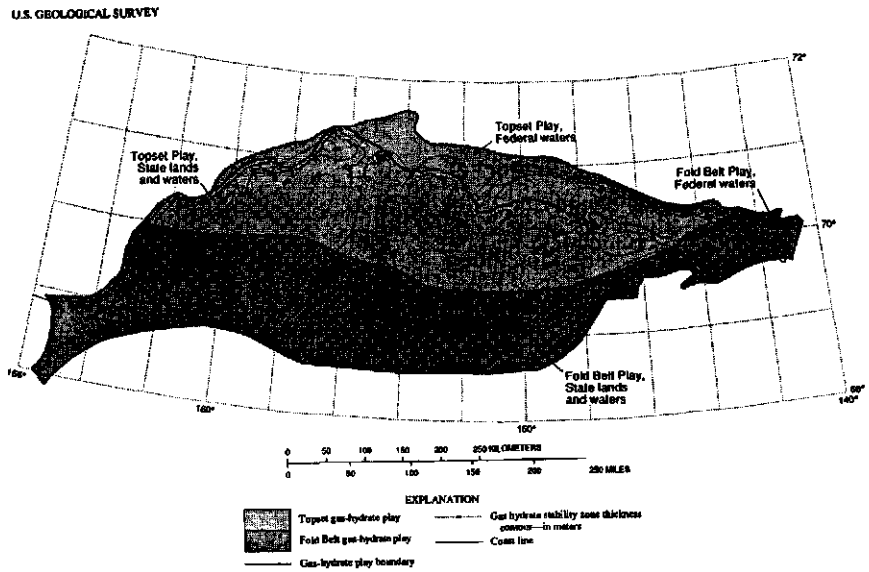

Figure I-6 Map of the Alaska topset and fold belt gas hydrate plays (Collett et al., 1994).

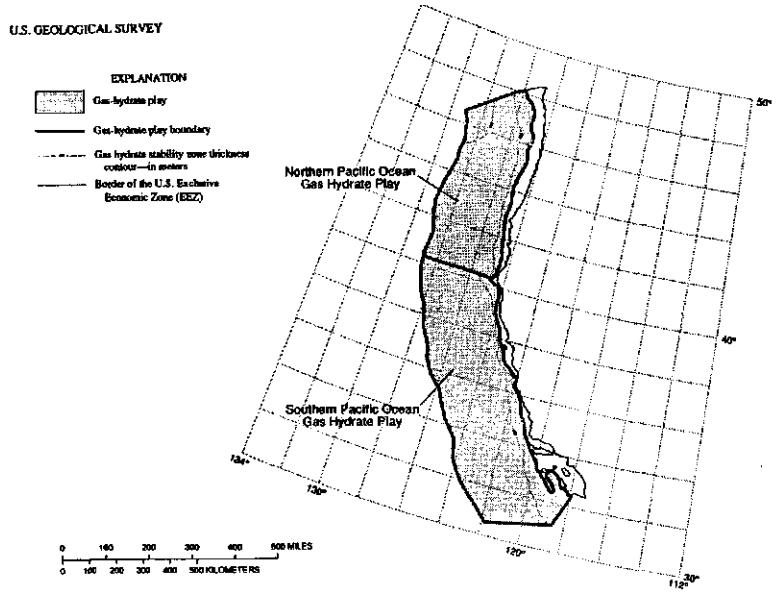

Figure I-7 Map of the Northern Pacific Ocean and Southern Pacific Ocean gas hydrate plays (Collett et al., 1994).

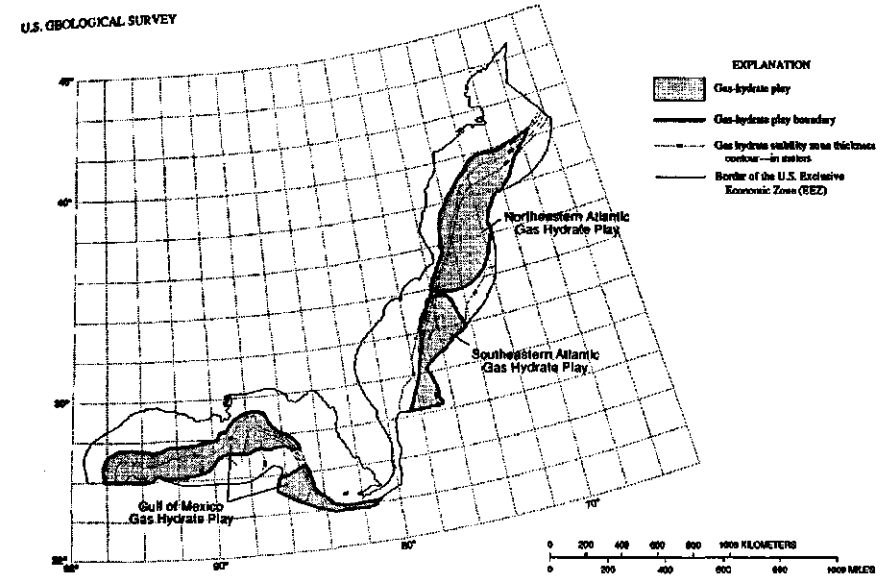

Figure I-8 Map of the Northeastern Atlantic Ocean, Southeastern Atlantic Ocean, and Gulf of Mexico gas hydrate plays (Collett et al., 1994).

date. However, the knowledge of seismoacoustic characteristics of gas hydrates does not allow us to determine the hydrate saturation of sedimentary layers in the zone of hydrate formation. For this, expensive wells must be drilled with core sampling and the full suite of logging.

Investigation of electrical properties of gas hydrates, and the processes of their formation and dissociation will allow us to develop highly efficient remote methods of outlining gas hydrate accumulations using aerial or satellite mapping.

Thermophysical properties of gas hydrates have been examined inadequately, within a very narrow temperature interval and for a limited number of hydrates.

The most difficult to examine are the thermomechanical and volumetric properties of hydrates. Absence of data on these properties has already resulted in a number of serious accidents in different parts of the world during construction and operation of wells in hydrate-saturated intervals of sedimentary rocks. It is important to know these properties of hydrates when designing, constructing, and operating offshore engineering installations.

Studies on properties of gas hydrates have made it possible to formulate the basic propositions of the influence of natural gas hydrates on the ecological situation on our planet. Natural gas hydrates stabilize the

thermal regime of the sedimentary section on one hand, and actively affect the dynamics of the ozone layer, greenhouse effect, and the earth's climate on the other.

Without revealing in detail the basic theses of the gas hydrates problem we would like to note that although hydrates were studied for over two centuries, the extent to which their properties have been determined is still in a primitive state, most notably at very high pressures and low temperatures. The basic technological features of hydrate formation and decomposition processes as well as kinetics and morphology of crystal hydrates have also been poorly studied. This considerably lowers the possibility for creating radically new technologies based on gas hydrate processes.

At the present time, fundamentally new instrumental methods and means of investigations have been developed for studies of gas hydrate properties and kinetic processes, which achieve new scientific and practical results.

Many problems of technogenic gas hydrates exist parallel with those of natural gas hydrates, complicating production, transportation, and processing of gases and volatile liquids. A regular trend can be seen in the example of gas hydrates—science solves only topical problems. Gas hydrates were first obtained in 1778, however, until the 1930s they were of no industrial interest. With the advance of hydrocarbon production and pipeline transportation, when formation of hydrate plugs resulted in emergency shutdowns of gas supply, hydrates came under study in the context of developing an effective means of their prevention and control. After the discovery of natural gas hydrates in the 1960s, they were studied in the context of gas production from hydrates and putting their resources into the energy balance. Unique properties of hydrates provide a basis for new efficient technologies.

Modern study of crystalline hydrates has two clear directions—technogenic and natural gas hydrates. Technogenic gas hydrates form in the technological system during production, transportation, processing, and storage of various gases and liquids having high vapor pressures. The goal of these studies is to create effective methods of prevention of hydrate formation and to develop new technologies utilizing gas hydrate properties.

Study of the natural gas hydrates pursues the goal of in-depth understanding of the genesis and properties of the natural hydrates. Based on this understanding, the following effective techniques are created:

- revealing and mastering the natural gas hydrate accumulations;
- assessment of hydrate influence on engineering constructions in hydrate formation intervals; and
- effect of hydrates on regional ecological situations and global changes.

1

CHAPTER

GAS HYDRATES: THEIR PHYSICOCHEMICAL ASPECTS

The History of Gas Hydrates

Revealing the truth in the history of development of any considerable scientific idea usually turns out to be very complicated. A scientist frequently would not pay proper attention to a natural phenomenon he had revealed, especially if the discoverer had no use for his contemporaries. The same phenomenon might be discovered by several scientists concurrently. Only after a period of time the idea progresses and is strengthened by factual evidence; society then should take an interest in the roots of the discovery and the researcher. When the idea is of considerable interest to the progress of civilization and has advanced to different parts of the world, the temptation is often to give priority to one of the national scientific schools when considering the history of discovery. But no matter what the national interests, only one truth exists and it must reflect the real contribution of each scientific school and each isolated scientist. The majority of scientific discoveries result from the absorbed work of some creative individuals searching and constantly filling in the blank spaces in science.

Gas hydrates are no exception. The boundary between 18th and 19th centuries was a time when developing industry acutely needed science, when every new discovery had a profound impact on the pace of civilized development and the hopes of the society were pinned to physics and chemistry. It was then that gas hydrates, solid molecular compounds of water with gas, were discovered.

The history of the discovery is not conventional. It is well known today there are vast natural gas hydrate accumulations on Earth, however the first hydrates were synthesized *in-vitro*. Their technological significance was found 150 years later. In several more decades hydrate deposits

were found in the earth, with their power potential many times exceeding conventional hydrocarbon resources.

Most specialists believed that gas hydrates were first obtained in 1810 in the laboratory of Sir Humphrey Davy, who cooled an aqueous solution saturated with chlorine gas below 9°C to yield a crystal/ ice-like material (Davy, 1811). However, analysis of the preceding works allowed us to obtain evidence of hydrate retrieval more than 30 years prior to H. Davy.

The great English philosopher and naturalist Joseph Priestley happened to obtain hydrate of sulphur dioxide (SO_2) both from its water solution and from the gaseous phase and ice. The results of the experiments were reported in his three-volume work *Versuche und Beobachtungen uber vershiedene Gattungen der Luft* (Priestley, 1778–1780).

Priestley had an opportunity to realize, in the frosty winter of 1778, in London, that "... water impregnated with vitriolic acid air (i.e., SO_2—auth. remark) may be converted into ice...."

> *I exposed in an open vial a quantity of water fully impregnated with vitriolic acid air, when the thermometer was at 17 degrees (i.e., –8.3°C—auth. remark), and observed that it was recently frozen quite through, the smell of it continuing to be very pungent. As it melted, the ice sunk to the bottom of the liquor, and when it was quite dissolved, the water appeared to be still very strongly impregnated.... Ice was not at all dissolved in vitriolic acid air. Letting it remain in this situation all night, the next morning I found all the air absorbed; but it appeared, by the form of the ice, that it had been melted, and frozen again; for it exactly fitted the glass vessel in which it was confined" (Priestley, 1790).*

Priestley also found the "ice" to decompose when put in an atmosphere of HCl, NH_3 and HF under the atmospheric pressure and low temperatures, and to remain stable under the same conditions in the air. Thus, the effect of hydrate inhibition was properly recognized. As fundamentally important as this discovery was, Priestley could not give it the correct appreciation.

Joseph Priestley was a highly curious and effective investigator. Nine new gases were discovered by him, with oxygen, hydrogen, carbon, and sulphur dioxide among them.

SO_2 is well known to form hydrate easily under atmospheric pressure and temperatures of +7°C. It is these conditions that allowed Priestley to obtain the SO_2-hydrate. However no serious importance was attached by him to the discovery, because there was no theoretical or practical value he could derive from it.

There is some evidence that the SO_2-hydrate has been obtained by at least three researchers following Priestley and prior to Davy: T. Bergman (1783), A. F. de Fourcroy and L. N.Vauquelin (1796, 1798), and A. F. de Fourcroy (1801) (Gmelins Handbuch, 1960).

It should be noted that the repeated discovery of gas hydrates by Sir Humphrey Davy during his experiments on chlorine and its aqueous solutions also caused no enthusiasm among scientists and industrialists. H. Davy, later the president of the United Kingdom Royal Society, never returned to his studies on hydrates. However, his disciple, later the great physicist, Michael Faraday in 1823 made a replica of his patron's experiment to obtain a composition formula of the chlorine hydrate: $Cl_2 \times 10H_20$ (Gregory, 1930). Several years later the SO_2-hydrate composition of $SO_2 \times 7H_20$ was gained by de la Rive (1829). The SO_2-hydrate primary obtained by Priestley had attracted the attention of scientists in the 19th Century. It was the SO_2-hydrate on which the quadruple points of the equilibrium curve were first obtained by Roozeboom (1884, 1885). The measurement techniques of that time did not allow precise results to be obtained. Thus, J. Pierre in 1848 showed the hydrate composition as $SO_2 \times 11H_20$ (Pierre, 1848) whereas Schoenfeld reported it in 1855 to be $SO_2 \times 14H_20$ (Schoenfeld, 1855). Only in 1927 was the correct formula given by W. Schroeder, who obtained the complete SO_2 hydrate phase diagram: $SO_2 \times 6H_2O$ (Schroeder, 1927).

Until 1934, more than 150 years following the discovery of gas hydrates, they were of a purely academic value. Hydrates did not cause any trouble in technologic systems of that time, and hydrate properties could not be studied to the extent that they could be used by industry. Hydrates of several significant gases were obtained during that period. Heterogeneous equilibrium diagrams were plotted and first attempts to theoretically summarize the experimental data were performed on synthesized CO hydrates (Wroblevsky, 1882), H_2S, CH_4, C_2H_6, C_2H_4, C_2H_2, N_20 hydrates (Villard, 1888), and C_3H_8 hydrate (Villard, 1890). Villard was the first to use the heats of phase transition of hydrate formation for calculating the water/gas ratio in the forming hydrate.

De Forcrand, in collaboration with Villard, studied conditions of H_2S and CH_3Cl hydrate formation. Hydrates of such gases as H_2S, H_2S mixed with C_2H_2, CO_2, and C_2H_6 were the major occupation of de Forcrand. He was the first to use the Clausius-Clapeyron Equation to specify the composition of 15 mixed hydrates (de Forcrand, 1897, 1902).

The production of hydrates of such inert gases as argon (Villard, 1896), krypton (de Forcrand, 1923), and xenon (de Forcrand, 1925) represented the apotheosis of the pre-technogenic period in hydrate research.

In the beginning of the 20th century oil and gas became important in the world energy balance. Figure I-1 illustrates changes in the world energy consumption. Deep borehole drilling and deep oil extraction were accompanied by substantial volumes of natural gas causing serious complications for the technology of oil extraction and transport. However, the industry soon learned how gas could be applied both in municipal services and industrial energetics. During the 1920s large gas pipelines were constructed and put into operation in the United States. Gas was supplied under pressure through these pipes from the gas fields to the consumption centers. Solid plugs complicated the transportation of gas during autumn and spring periods. Plugs were misinterpreted to form from water remaining in the pipelines after their construction and hydraulic pressurizing. This estimate led to a deadlock in solving the problem. However, an important conclusion was made by the American chemist E. G. Hammerschmidt in 1934. Not ice, but hydrate plugs were responsible for gas transport complications in the pipeline sections.

The 1930s and the 1940s characterized the second technological stage in the history of hydrates studies. Several fundamental works by Hammerschmidt (1934, 1939, 1940) formed the main principles to predict hydrate plug formation, and also created basic methods of hydrate control. Those methods gained further advancement and are being exploited today.

Studies by W. M. Deaton and E. M. Frost (1937, 1946) also date back to that time. These investigators, well skilled in physics and chemistry, were the first to show that individual gases and their mixtures were able to form hydrates not only in gaseous but also in a liquid phase (in technological systems of gas liquefaction, transport, and processing) as well.

However, the most significant results in hydrate studies from 1930 to 1950 are connected with D. Katz and R. Kobayashi, who devoted all their lives to the problem. In 1945 a very important universal diagram was reported by Professor Katz. It enabled the user to estimate a hydrate formation pressure, given a temperature and gas gravity, and covered the P-T range of the processes of gas extraction, transport, and processing.

The initial analytic method by Wilcox, Carson, and Katz (1941) enabled the user to determine the pressure and temperature of hydrate formation from mixtures. It was based on the gas-solid phase equilibrium constants similar to those for water-vapor phase. The method still continues to be used in the natural gas industry half a century later.

A long-time collaboration between D. Katz and R. Kobayashi gave rise to new research techniques and technology for hydrate study and strengthened its theoretical base. These investigators created the school of excellent young hydrate researchers in North America. These young

scientists are now leading in branches of the study. They are D. B. Robinson, E. D. Sloan, G. D. Holder, J. M. Brooks, M. S. Selim, P. R. Bishnoi, Y. P. Handa, H. J. Ng, V. A. Kamath, J. S. Tse, A. Vishniauskas, and many others.

Investigations into the molecular structure of hydrates occupies a special place in the history of their study. These investigations brought theory and experimental studies closer together and allowed more confident prediction of hydrate properties, etc. It should be noted that these investigations were initiated in Europe when Russian academician B. A. Nikitin turned his attention to the structure of inert gas hydrates and for the first time stated propositions on clathrate cage structure of crystal hydrates in the 1930s (Nikitin, 1936–1940).

Nikitin showed hydrates of individual gases and their mixtures to be non-stoichiometric compounds representing a crystal lattice built up from hydrogen-bonded water molecules, with cages filled by gas molecules bonded with water by the weak van der Waals forces. The theory was verified experimentally by German physicist von Stackelberg with his collaborators whose X-ray examinations established hydrates of two structures to exist (structures I and II) (von Stackelberg, 1949–1958). Experimental investigations were further developed by Dr. D. W. Davidson (Canada) and his disciples, S. A. Ripmeester, J. S. Tse, V. P. Handa, and others (Davidson et al., 1973–1978). This group engaged in research on the structure of hydrates and their thermal and electric properties.

Research in the technologic aspects of gas hydrates, started in 1934, is increasingly more intensive. Hydrate properties, hydrate formation and decomposition, effective means of hydrate control in systems of natural gas extraction, transport and processing, and new technologies based on the properties of hydrates are now the main subject of studies.

A number of methods of hydrate prevention in technological systems have been devised to date, and two of them have gained the most acceptance—drying of gas and injection of different inhibitors into the gas-liquid flow. A major contribution to the development of hydrate prevention methods was made by Prof. D. B. Robinson and his group (1976–1994).

A special place in the history of hydrates is the discussion that natural gas hydrates have been in existence long before the technogenic ones, and presumably have been of considerable importance in the formation of planets and other space bodies.

Initial proof of the existence of natural gas hydrates was the hydrate saturated cores extracted during the exploratory drilling in 1967. These cores were extracted at the Ust-Viliuisk and Sredne-Viliuisk fields in

Yakutiya, and at Messoyakhia field in Western Siberia (Makogon, 1972). Also ice cores containing air hydrate were extracted from the depth of 2164 m at the American Antarctic Station Byrd in 1968 (Miller, 1969).

However, the discovery of natural gas hydrates came from the Russian hydrate school, almost two hundred years after in-vitro hydrates were obtained. The first proposal that hydrates can exist in natural geological conditions was made by Prof. I. N. Strizhev (1946). He wrote: "There are vast areas in the North of the USSR where the strata temperatures are below zero at depths of 400–600 m, and gas deposits may be present. What is it about hydrates in such places? Won't these deposits contain significant amounts of hydrate even before the development? Won't all the hydrocarbon gas be in hydrate state? ..."

When analyzing thermodynamic properties of Yakutian geologic sections, Prof. N. V. Cherskiy repeated the hypothesis of hydrate existence in permafrost (Mokshantsev, Cherskiy, 1961). In 1963 a key well drilled in Markha, North-West Yakutia, showed permafrost rocks at depth of 1400 m. After analyzing thermodynamic data available and correlating it with the results of studies on hydrate formation at the free gas-water contact, the possibility of hydrate formation in porous layers was substantiated by Y. F. Makogon (1965, 1966).

The hypothesis needed to be verified instrumentally. For this, a series of direct experiments on hydrate formation and dissociation in natural and artificial core samples was set up by Makogon at Moscow Gubkin Oil and Gas Institute. The results of these experiments and first theoretical summaries were reported in 1965 and 1966. After close examination, those results and summaries were registered in the USSR State Register on December 25, 1969 as a scientific discovery No. 75, stated as follows: "Experimentally found is earlier unknown property of natural gases to form solid hydrate deposits in the earth's crust under certain thermodynamic conditions" (Vasil'ev et al., 1970).

Despite numerous publication in national newspapers and specialized journals, the discovery did not attract the attention of specialists in energetics. However, considerable public interest was generated by an address presented by Y. F. Makogon at the XI International Gas Congress (Moscow, 1970). Leading laboratories from several scientific centers in the USSR, the USA, Canada, and other large countries were drawn to the problem of natural gas hydrates. As a result of intensive investigations over several years, methods of survey and prospecting of both onshore and offshore hydrate deposits were devised, as well as methods of estimating hydrate gas resources.

World potential resources of hydrate methane were estimated by different authors and range widely from 7.6×10^{18} m^3 (Trofimuk et al., 1979) to 3.1×10^{15} m^3 (McIver, 1981). More detailed examinations showed the potential resources to be 1.5×10^{16} m^3 (Makogon, 1984) or 1.8×10^{16} m^3 (Kvenvolden, 1988).

More than 60 large hydrate accumulations have been revealed to date in the ocean and on the continents with total gas reserves exceeding 700×10^{12} m^3. Preliminary works for assessing hydrate deposits and bringing them into the energy balance are carried out intensively in a number of countries. It should be noted that the share of hydrate gas in the consumption of world energy may exceed 15% in the next century.

The history of studies on natural gas hydrates has been presented in numerous articles, scientific reports and addresses. A great number of patents have been taken out based on the investigations in hydrate properties.

The results of integrated studies on technogenic and natural gas hydrates are summarized in a number of monographs. More than 50% of these monographs were published recently (in the past 10 to 15 years). This shows the increasing topicality of these studies. A new powerful impetus to hydrate research is expected to be given very soon. It would be connected with assessment of hydrate deposits, with space developing and creation of new technologies based on hydrate properties, with the revealing of the gas hydrates' role in global geophysical, geochemical, climatic, and other processes.

Today two major directions have formed in the problem: technogenic and natural gas hydrates. Both these directions are based on the results of fundamental research of the genesis and properties of gas hydrates. Figure 1-1 presents a principal schematic of the major directions of studying gas hydrates.

General Description of Hydrates and Their Structure

Hydrates are solid metastable compounds whose properties and stability depend on the values of pressure and temperature. When hydrates are created in loosely consolidated sedimentary rocks, the hydrate will be a cementing material. If the hydrate dissociates, the rock formation becomes unconsolidated and loses its strength. Natural gas hydrates are dangerous during the construction and operation of wells, platforms, pipelines, and other offshore engineering structures.

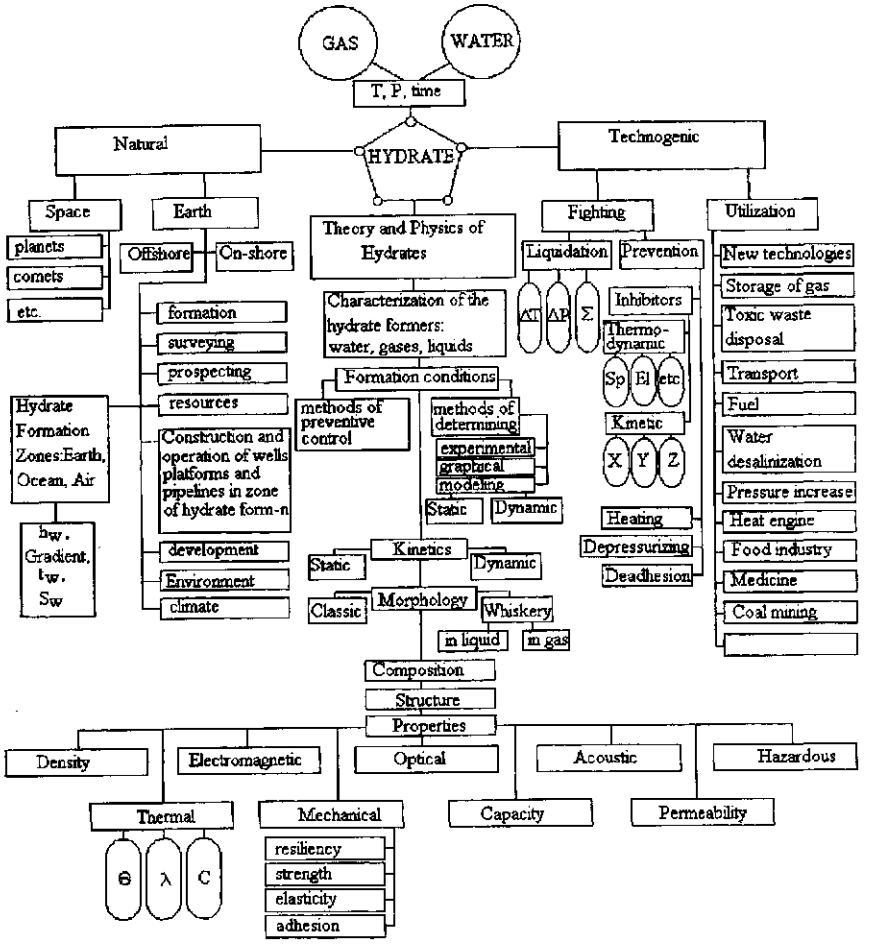

Figure 1-1 Schematic of gas hydrates knowledge.

Hydrates easily form in producing wells, or in gas and oil pipelines. The prevention of hydrate formation requires a substantial investment—as much as 10 to 15% of the production cost. Removal of continuous hydrate plugs from an onshore well costs up to $1 million, and from an offshore pipeline, $2–4 million and more.

Some hydrate properties are unique—one volume of water enclathrates 207 volumes of methane in gas hydrate. Crystallization pressure is up to 300–400 MPa. Pressure of free gas after dissociation of hydrate of methane in closed volume is up to 80–100 MPa. Electrical resistivity of hydrate is

very high. The specific volume of water during its transition into hydrate state increases by 26–32%, whereas during freezing the increase is just 9% which is considered abnormally high.

A large number of these problems are still to be investigated in order to get a quantitative result. The problem of natural gas hydrates is a global one. Potential gas resources concentrated on earth in a hydrate state exceed 1.5×10^{16} m^3. Explored reserves of methane in a hydrate state are more than 700 trillion m^3. It is very important to give an answer for both problems: how to prevent hydrate formation and to remove hydrate plugs from wells and pipelines, and how to produce gas from the natural hydrate deposits.

Inhibition, heating, different physical methods like a high frequency electromagnetic field and other methods can be used for preventing hydrate formation in a fluid flow. For preventing coagulation and sedimentation of microcrystals of hydrate in wells and pipelines different polymers, antiadhesives, and physical fields can be used.

Gas hydrates may formally be referred to as chemical compounds since they have fixed composition. However, hydrates are the compounds of a molecular type originating because of the van der Waals attraction forces between the molecules. Covalent bond is absent in gas hydrates because during their formation no pairing of valence electrons and no according spatial redistribution of electron cloud density occurs.

Hydrates of gases are widespread in nature and are formed easily in systems of production, transportation, and processing of gases and a number of volatile liquids. Hydrates have six different forms:

1. Molecular sieves, characterized by interconnected trough cavities-passages;
2. Channel complexes when hydrate forming molecules form a crystalline lattice with tubular cavities;
3. Layered complexes forming clathrates with interlaced molecular layers;
4. Complexes which form with large molecules having concavities or niches in which an inclusion molecule resides;
5. Linear polymeric complexes formed by clathrate molecules, having a tube-like shape;
6. Clathrates which form in cases when inclusion molecules fill in the closed cavities close in shape to a sphere. Hydrates of gases and volatile liquids are related to this type of clathrates.

Table 1-1 Schematic representation of hydrate types.

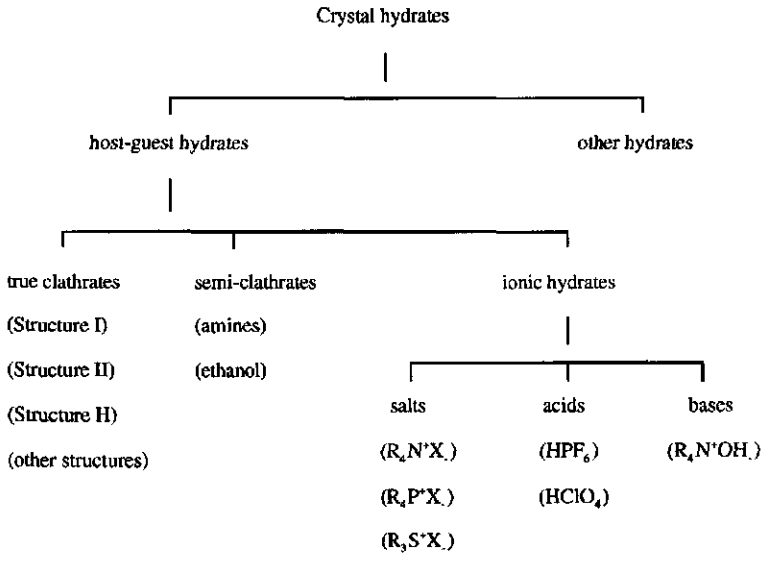

Gas hydrate is a mineral of the clathrate hydrate group widely spread in nature. Table 1-1 shows the major subdivisions of clathrate hydrates (Ripmeester et al., 1994).

Until now the unit cells of only three hydrate structures have been determined through the effort of Stackelberg with coworkers (1949–1954), and Davidson and Ripmeester with coworkers (1973–1994). These hydrates are formed with different size molecules. Each unit cell includes a fixed number of strongly bonded hydrogen water molecules. Size and shape of the unit cells are determined by the size and the energy of the enclathrated hydrate former guest molecule.

Figure 1-2 presents the shape of elementary polyhedral cavities and their characteristics (Ripmeester et al., 1994). Elementary cavities formed by the hydrogen bonded water molecules with encased hydrate former molecules agglomerate to form the hydrate crystals of different structure. Tremendous variety in shape and energy of the hydrate former molecules allows us to state that clathrate hydrates of gases can have numerous crystal structures. Only three structures characterized by the strict gas-water ratio and geometric parameters have been studied by now.

Figure 1-3 presents a schematic of a structure I hydrate formation from elementary cavities, and Figure 1-4 presents this schematic for a structure II hydrate.

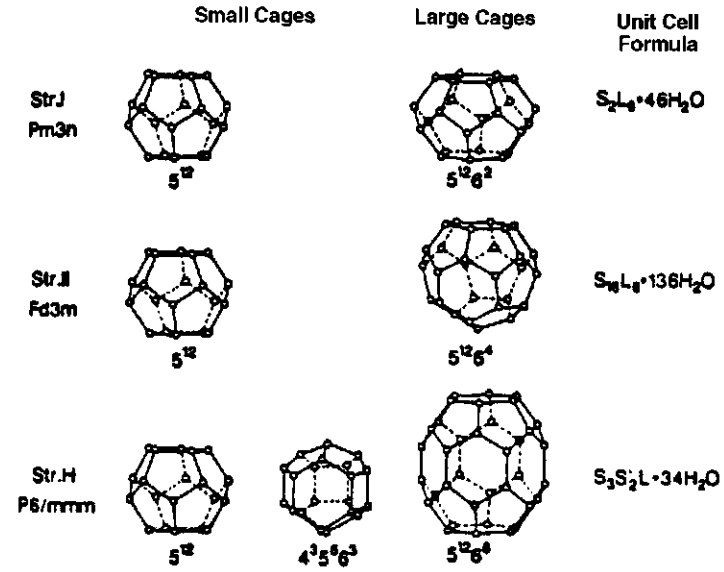

Figure 1-2 Clathrate hydrate polyhedra.

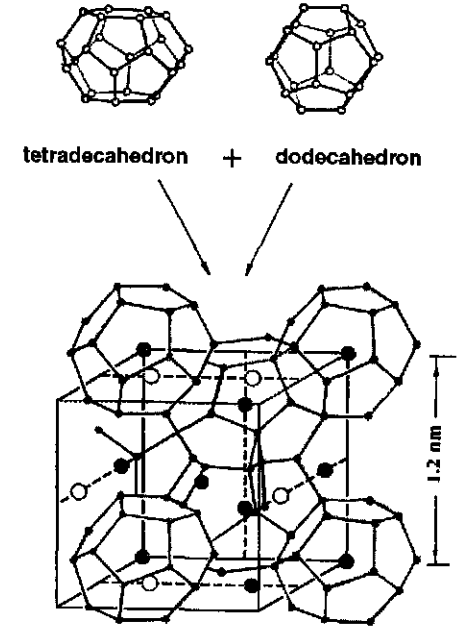

Figure 1-3 Crystalline lattice of gas hydrate, structure I.

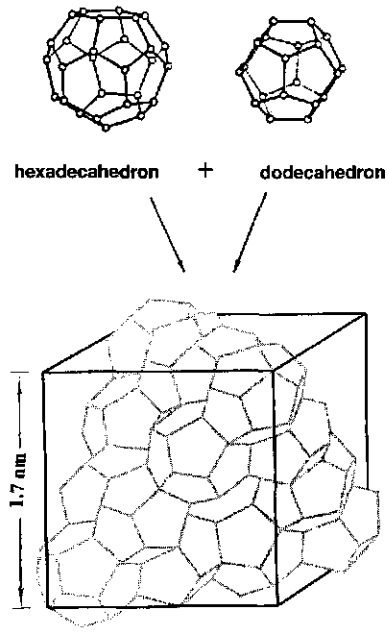

Figure 1-4 Crystalline lattice of gas hydrate, structure II.

Figure 1-5 shows the nomogram with data by Stackelberg and Ripmeester for explanation of the hydrate structure formed by gases and volatile liquids, depending on the molecule sizes.

Table 1-2 lists the most prevalent hydrate formers, participating in single and double hydrates of the different structures (Ripmeester et al., 1994).

Tables 1-3 and 1-4 present the most common characteristics of hydrates of the discovered structures.

The crystalline structure of forming gas hydrates is rather diverse and is not limited by the structures I, II, and H discovered through research of Stackelberg, Davidson, and Ripmeester. It should be noted that during the study of hydrate structures the used hydrates were obtained at relatively low pressures from gas and water at the free interface. Whiskery hydrates obtained at sub-zero temperatures and at pressures of 1–2 GPa will have a different structure.

Research conducted by the group of Dr. Yuri A. Dyadin together with Polish colleagues already has revealed a number of the new crystal hydrate structures. As it was indicated by our research (Makogon, 1974), formation of a hydrate crystal also is influenced by an electromagnetic field effect. In direct sunlight the growth rate of whiskery hydrate crystals

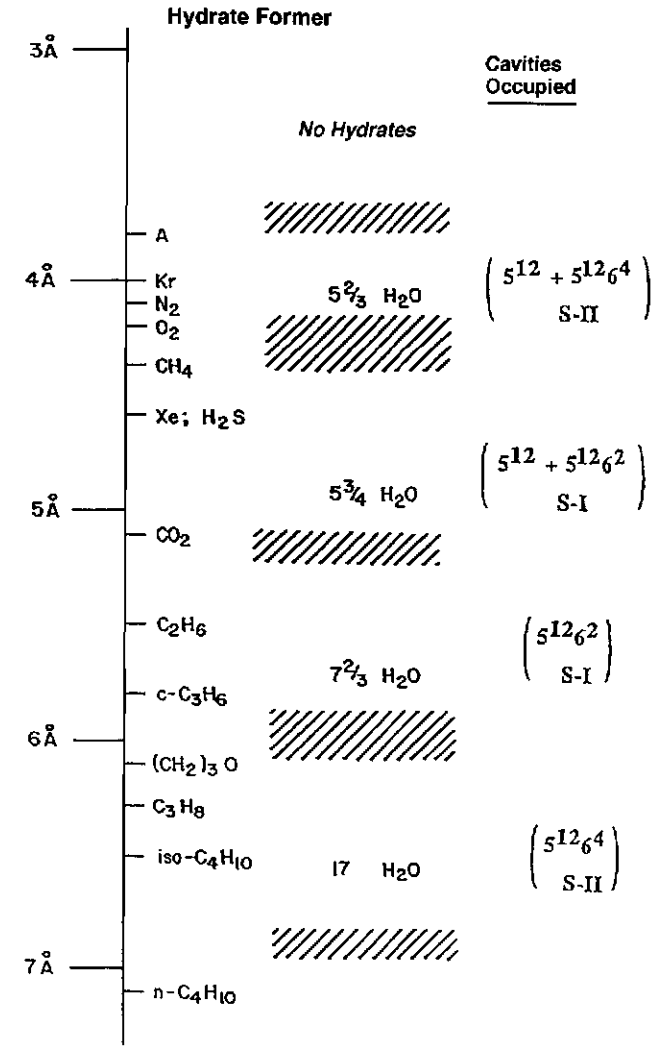

Figure 1-5 Guest size—hydrate structure relationships and hydration numbers.

is several times higher than in the dark. The density of a hydrate crystal obtained in a static electromagnetic field is much higher than the density of a hydrate grown in the same conditions without an electromagnetic field.

The study of hydrate structure is very complicated and depends highly on the accuracy of the instrumentation used. Nearly twenty years of research was dedicated by the highly qualified and well equipped group

Table 1-2 Some potential gas hydrate formers in natural and industrial environments.

Alkane	*Alkenes, Alkynes, Aromatics*
Methane (I)	Ethylene (I)
Ethane (I)	Propylene (II)
Propane (II)	Isobutylene (II)
Isobutane (II)	Allene (II)
Butane (II)*	cis-2-Butene (II)
Neopentane (II)*	2,3 Dimethyl-2-butene (H)*
2 Methylbutane (H)*	2,3 Dimetbyl-l-butene (H)*
2,2 Dimethylbutane (H)*	3,3 Dimethyl-2-butene (H)*
2,3 Dimethylhutane (H)*	Acetylene (I)
2,2,3 Trimethylbutane (H)*	Methylacetylene(II)
Hexamethylethane (H)*	3,3 Dimethyl-2-butyne (H)*
2,2 Dimethylpentane (H)*	Benzene (II)*
3,3 Dimethylpentane (H)*	

Cycloalkanes, Cycloalkenes	*Inorganics*
Cyclopropane (I, II)	0_2 (II)
Cyclobutane (II)	N_2 (II)
Cyclopentane (II)	H_2S (I)
Cyclohexane (II)	CO_2 (I)
Methylcyclopropane (II)	SO_2 (I)
Methylcyclopentane (H)*	Cl_2 (I)
Methylcyclohexane (H)*	CFCs
1, 2 Dimethylcyclohexane (H)*	
Cyclooctane (H)*	
Cyclopentene (II)	
cis Cyclooctene (H)*	

I, II, H refer to structure types. Entries with asterisks require a help gas for stability.

of Dr. D. Davidson. However, they managed only to confirm the results obtained by von Stackelberg and to discover the hexagonal structure H gas hydrates (Ripmeester, Tse, Ratcliffe, Powell, 1987, 1994).

Numerous studies of the structure of hydrates may be generalized in order to state that clathrate hydrates are compounds of fixed composition in a whole stability range.

Analysis of the experimental research indicated that the filling ratio of the large cages is equal or very close to one. At the same time the filling

Table 1-3 Characteristics of hydrate structures I, II, and H.

Designation	*Space Group Lattice Parameters*	*Cage Type*	*Ideal Stoichiometry*
Structure I	Pm3n 1.20 nm	D,T	$3M_D6M_T46H_2O$
Structure II	Fd3m 1.70 nm	D,H	$16M_D8M_H136H_2O$
Structure H	p6/mmm a = 1.22 nm, c = 1.02 nm	D′,D,E	$2M_D3M_D3M_E34H_2O$

Table 1-4 Structural characteristics of hydrates.

Parameter	*Structure I*	*Structure II*
Cage size, nm	1.203	1.731
Number of dodecahedra	2	16
Number of tetradecahedra	6	–
Number of hexadecahedra	–	8
Coordination number (number of water molecules in a single cage)		
in a small cage	20	20
in a large cage	24	28
Number of water molecules in the unit cell	46	136
Number of cages		
large	6	8
small	2	16
Cage diameter, nm:		
large	0.86	0.946
small	0.788	0.782
Ideal composition*	$6G\text{-}2M\cdot46H_2O$	$8G\text{-}16M\cdot136H_2O$

*Ideal composition of hydrate is obtained when all large cages are filled with the G molecules and small cages with the M molecules.

ratio of the small cages may vary from zero to nearly one. Thus the variable composition of hydrates in this case is caused mostly by the variable occupancy of the dodecahedral cages.

Unlike ice, where the hydrogen bonded water molecules form the six-membered rings, hydrate water molecules arrange into five- or six-membered rings, which, in turn, form the structural cavities enclathrating the gas molecules. Ice does not have cavities capable of including the gas molecules (except for helium and hydrogen). In hydrates the hydrogen bond length is about 0.275 nm, which is nearly the same as in plain ice (0.276 nm). Sizes of the dodecahedral cavities formed by water molecules in hydrates is sufficient to accommodate the molecules of argon (0.308 nm), krypton (0.338 nm), xenon (0.38 nm), methane (0.406 nm), and hydrogen sulfide (0.42 nm), etc. Space cannot be filled completely by dodecahedra with any positioning. Dodecahedra are positioned as atoms in diamond-like crystals or space centered cubic crystals. In each case a somewhat different distribution of space between dodecahedra will occur.

The elementary cage of gas hydrate consists of a fixed number of water and gas molecules. Molecular ratio of water and gas is a function of the size of the hydrate former gas molecules. One volume of water in hydrate state may enclathrate between 70 and 300 volumes of gas, depending on the properties of gas and hydrate composition.

Notably, in practice, the most often encountered hydrates have the cubic structures I and II. Their lattices are the least different energetically from the ice lattice, and the molar ratio of water and hydrate former varies between 5.75 and 17.

Instrumental research of hydrate structure performed by German and Canadian researchers revealed a wide variety of the hydrocarbons hydrate crystal structure. (Stackelberg, 1949; 1954 a, b; 1956; Stackelberg, Muller, 1951; Stackelberg, Meinhold, 1954 c; Stackelberg, Jahns, 1954; Stackelberg, Meuthen, 1958; Davidson, 1973; 1980; 1983; Davidson and Ripmeester, 1974; 1978; Davidson, Handa, 1984; Davidson, Garg, Gough, Handa, Ratcliffe, Ripmeester, Tse and Lawson, 1986 a; Davidson, Handa and Ripmeester, 1986 b; Davidson, Gough, Handa, Ratcliffe, Ripmeester, Tse, 1986 c; Ripmeester, Tse, Ratcliffe, 1987; 1994).

Morphology of the clathrate hydrates varies a lot and is determined by the shape of the hydrate former gas molecules, hydrate formation medium, phase state of water and hydrate formers, conditions of molecular transport to the crystal growth surface, crystallization type, pressure, temperature, degree of the process subcooling, physical fields in which the hydrate crystal formation is taking place, etc

Figures 1-6 through 1-13 present photographs of hydrate crystals of several gases. These photographs were taken with an ordinary camera

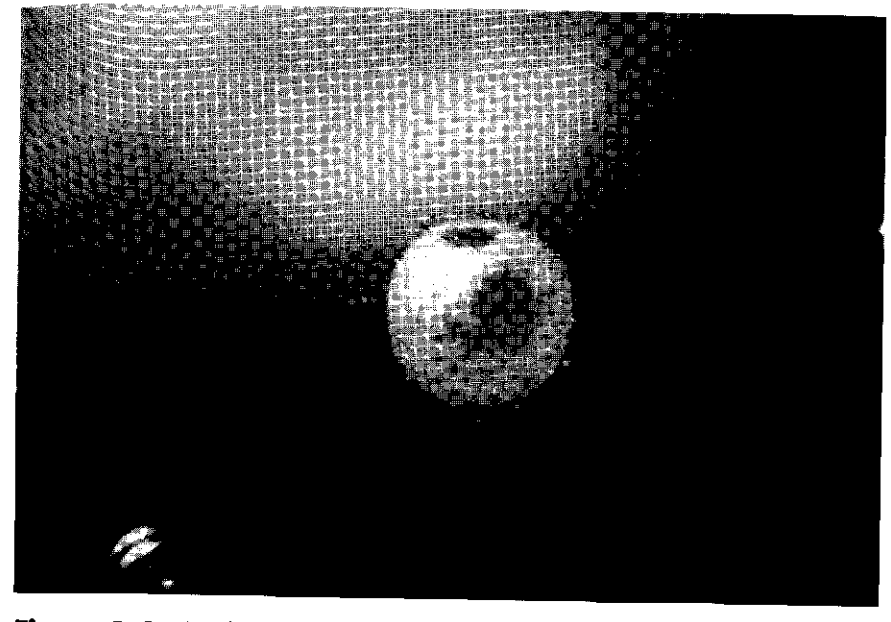

Figure 1-6 Methane hydrate formed on the water drop surface (P = 96 bar; T = 4°C).

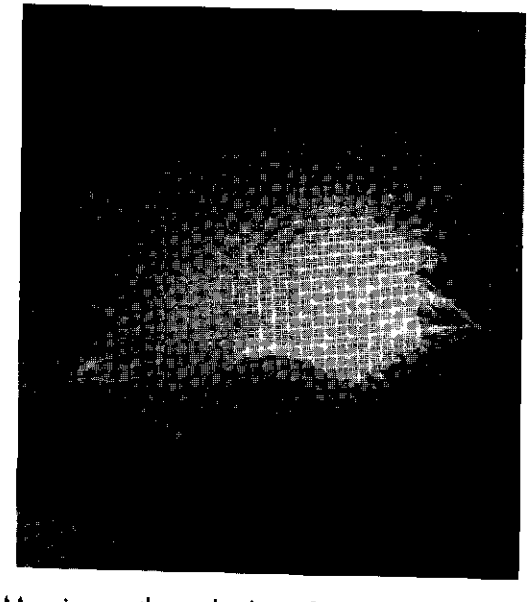

Figure 1-7 Massive methane hydrate formed in the gas sphere (P = 95 bar; T = 7°C).

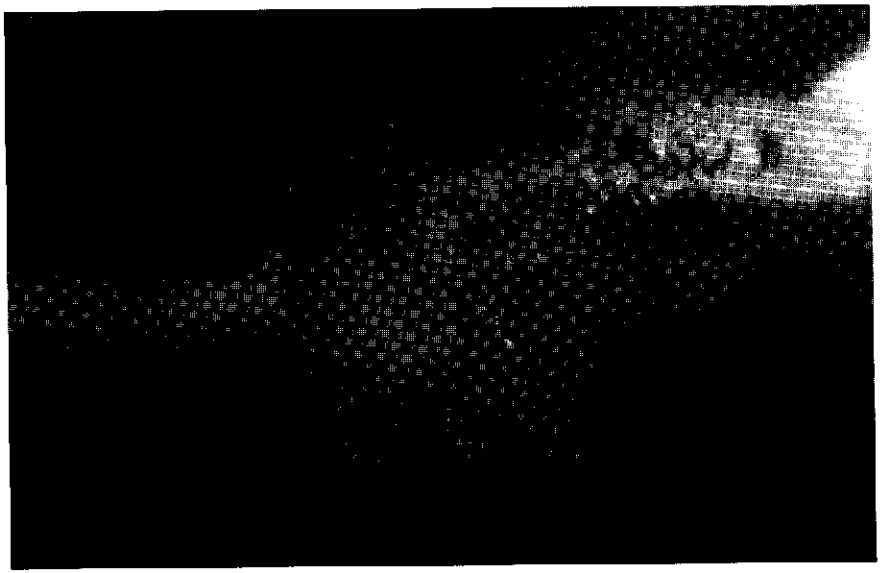

Figure 1-8 Soft massive methane hydrate, formed in the water volume in dynamic situation (P = 107 bar; T = 12°C).

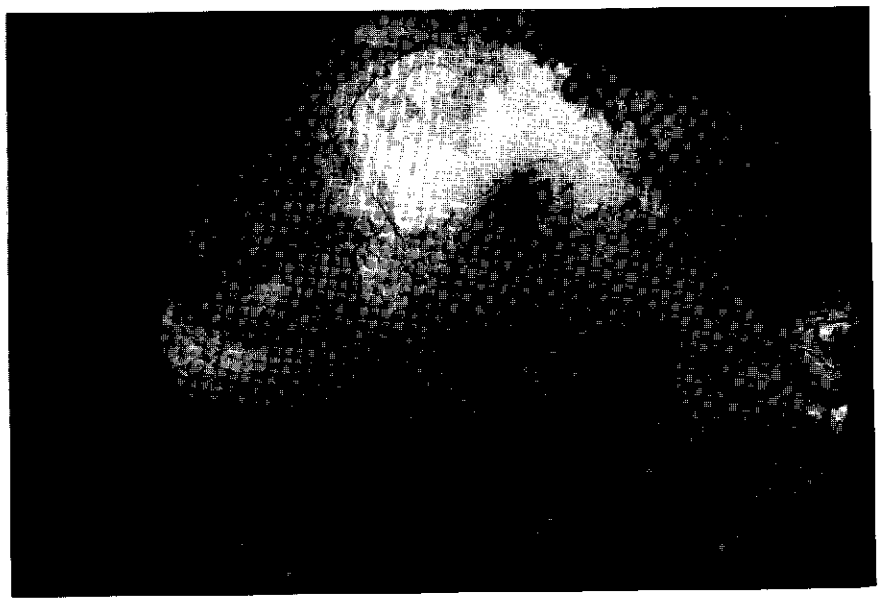

Figure 1-9 Massive and whiskery crystals of methane hydrate formed in gas sphere and water volume (P = 91.4 bar; T = 3°C).

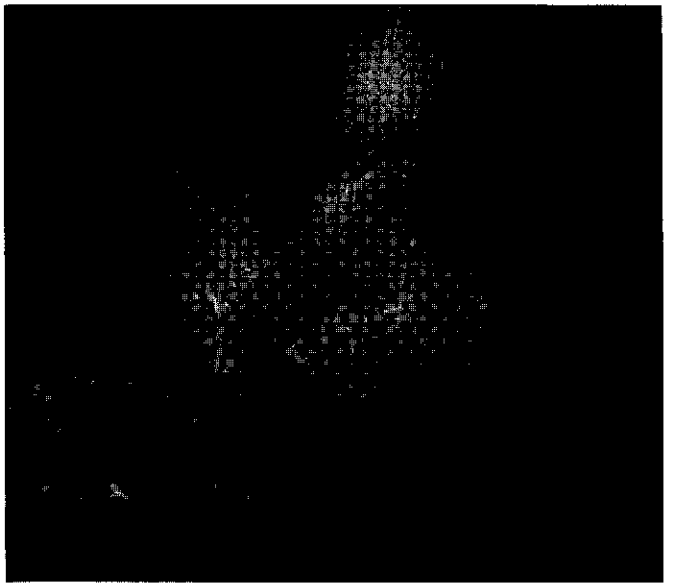

Figure 1-10 Massive ethane hydrate, formed in gas sphere (P = 11.5 bar; T = 1.6°C).

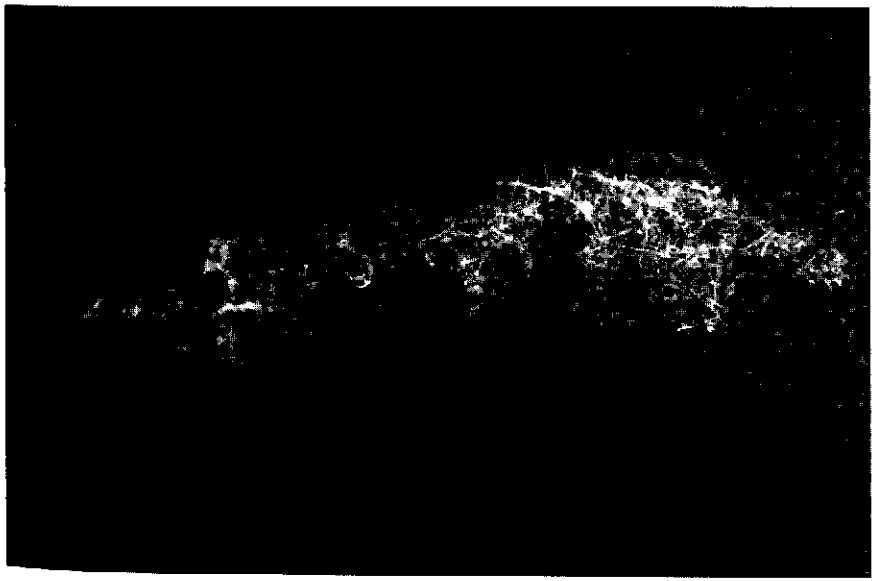

Figure 1-11 Massive hydrate of ethane, formed on the free gas-water surface, and on the surface of hydrate film (P = 14 bar; T = 5°C).

Figure 1-12 Propane hydrate formed in a gaseous medium (P = 12.9 bar; T = 274.6°C).

Figure 1-13 Propane hydrate formed in a bulk of water (P = 6 bar; T = 1°C).

(without the use of microscopes and other devices). These crystals were formed at different thermobaric conditions at the free contact interface, in the vapor phase, and in the volume of water. Shape and growth rate of crystals were defined by the formation conditions.

Determination of the Hydrate Formation Conditions

Hydrate formation conditions are usually determined during the design of the production technology, processing, and transportation of gas, during the development of measures for prevention of hydrate formation, and removal of the hydrate plugs. However, in the last several decades a critical need has appeared to determine the conditions of formation and stability of natural clathrate hydrates in earth and in outer space.

The most accurate parameters of hydrate formation from a real gas of complex composition usually can be obtained experimentally in a defined range of pressure and temperature. In practice different companies use the software programs written for gases of different compositions in a sufficiently broad range of pressures and temperatures. Such programs are based on the experimental results for hydrate dissociation equilibrium conditions: pressure-temperature-hydrate former composition. At the present time a multitude of such programs have been created, and each company prefers one of them according to criteria known only to the company. It can be noticed that there is no universal program that would embrace the whole industrial range of pressures, temperatures, and compositions of vapor and liquid phases. However, there are two programs, one written by Drs. Ng and Robinson (Canada) as well as the CSMHYD program by Professor E. D. Sloan, that satisfy these requirements the most. These two programs allow obtaining satisfactory data for the gases of various compositions at positive temperatures and at the pressures of up to 40 MPa with consideration of the presence of some hydrate inhibitors in water.

Dr. Batalin (1993) has developed a universal program for calculation of hydrate and wax formation in oil and gas flows, which produces good results at the pressures of up to 30 MPa. A computer program by Dr. Malyshev (Tiumen) can be applied for determination of hydrate formation conditions from the wide fraction of light hydrocarbons and in oil wells to obtain satisfactory results.

Currently, a number of analytical methods for estimation of the hydrate formation equilibrium parameters from gases of complex compositions is available. Let us briefly review several analytical techniques for determination of the conditions of natural gases hydrate formation.

The most generalized solution, based on the achievements in studies of molecular structure of crystal hydrates, was proposed by Barrer and coworkers (Barrer, Ruzichka, 1962), who made a number of assumptions:

1. Enclathrated hydrate former molecules do not form stable chemical bonds with the surrounding water molecules.
2. Interaction is taking place through the dispersion forces approximately described by the Lennard-Jones potential or its various modifications.
3. Energy of the dispersion interaction is much weaker than that of a hydrogen bond. This allows one to neglect the effect of enclathrated guest molecules on the state of water molecules in the hydrate lattice.

It follows from these assumptions that gas hydrates may be considered as "ideal" solid solutions in which solute (hydrate former) does not influence the solvent (water in the hydrate lattice).

Let us consider a closed system at equilibrium which contains M moles of vapor phase with composition X_i ($I = 1, 2, \ldots, n$), N moles of water in hydrate and S moles of water in liquid or in solid (ice) phases. Free energy of the hydrate phase F and equilibrium conditions are expressed as:

$$F = MF^{\beta} - RT\sum_{i=1}^{2}\nu_i\sum_{j=1}^{n}Q_{ij}\times\left[\ln\frac{Q_{ij}}{\left(1-\sum_{j=1}^{n}Q_{ij}\right)\times Z_{ij}}\sum_{j=1}^{n}Q_{ij}+\ln\left(1-\sum_{j=1}^{n}Q_{ij}\right)\right] \quad (1.1)$$

$$\mu_B = \mu^{\beta} - RT\sum_{i=1}^{2}\nu_i\ln\left(1-\sum_{j=1}^{n}Q_{ij}\right) \quad (1.2)$$

$$\mu_j = RT\ln\frac{Q_{ij}}{\left(1-\sum_{j=1}^{n}Q_{ij}\right)\times Z_{ij}} - RT\ln f_j + RT\ln\phi_j \quad (1.3)$$

where

F is the molar free energy of water in an empty hydrate lattice;

Q_{ij} is the filling ratio of hydrate cavity of type i ($i = 1, 2$) with gas molecules of type j ($j = 1, 2, \ldots, n$);

Z_{ij} is the statistical sum of type j molecules enclathrated in type j cavity;

ν_i is the ratio of number of type i cavities to the number of moles of water in hydrate;

μ_B is the chemical potential of water in liquid or solid (ice) and

μ^{β} is the hydrate phases;

f_j is the volatility of j-th gas component;

ϕ_j is the state function of gas with composition X_j under low pressure.

Gibbs potential ϕ of the considered system is an additive quantity of potentials of the liquid and solid (ice) $S\phi_B$, hydrate $N\phi_H$, and vapor $M\phi_V$ phases. Based on the general laws of thermodynamics and using the Gibbs-Duhem Equation (Equations 1.1–1.3), enthalpy H of the considered system is expressed as:

$$H = -T\frac{2d}{dT}\left[\frac{\phi}{T}\right] = -T\frac{2d}{dT}\left[\frac{N\left(F^{\beta}+PV_H\right)+S\phi_B}{T}\right] -$$

$$NRT2\sum_{i=1}^{2}\nu_i\sum_{j=1}^{n}Q_i\frac{d\ln Z_{ij}}{dT} + MH_g \quad (1.4)$$

where

V_H is the volume of hydrate containing one mole of water;

H_g is the molar enthalpy of the gas phase.

Suppose that some amount of heat was added to the system from outside, resulting in some of the hydrate decomposing into water (ice) and gas. Enthalpy of the new system H' containing M' moles of gas, S' moles of water in liquid or in solid (ice), and N' moles of water in hydrate phases, will be equal to:

$$H = -T\frac{2d}{dT}\left[\frac{\phi}{T}\right] = -T\frac{2d}{dT}\left[\frac{N'\left(F^{\beta}+PV_H\right)+S\phi'}{T}\right] -$$

$$NRT2\sum_{i=1}^{2}\nu_i\sum_{j=1}^{n}Q_{ij}\frac{d\ln Z_{ij}}{dT} + M'H'_g \quad (1.5)$$

Assuming that during hydrate decomposition the composition of the residual part does not change, the heat of hydrate decomposition is found per 1 mole of water:

$$\Delta H = \frac{H - H'}{N - N'} = -T\frac{2d}{dT}\left[\frac{F^{\beta} + PV_H - \phi_B}{T}\right] - RT2\sum_{i=1}^{2}\nu_i\sum_{j=1}^{n}Q_{ij}\frac{d\ln Z_{ij}}{dT} + \frac{MH_g - M'H'_g}{N - N'} \quad (1.6)$$

Assuming $M - M' << M$ and using the thermodynamic relation between gas enthalpy and volatility, reorganize the last part of the Equation 1.6 as:

$$\frac{MH_g}{N - N'} = RT2\sum_{i=1}^{2}\nu_i\sum_{j=1}^{n}Q_{ij}\frac{d\ln f_j}{dT} + H_j^0 \quad (1.7)$$

where

H_j is the enthalpy of component j in gas mixture under low pressure.

Let us introduce a new variable C_{ij} – Langmiur's constant (Davidson, 1973)

$$C_{ij} = \frac{Z_{ij}}{kT\phi_j} \quad (1.8)$$

Dependence of Langmiur's constants of separate components of natural gas on temperature is described by equation:

$$C = \exp(A - BT) \quad (1.9)$$

values of constants A and B are given in Table 1-5.

Water vapor pressure over the hypothetical empty hydrate lattice is determined by the equation:

$$\lg P_B^0 = a - b\lg T - \frac{c}{T} \quad (1.10)$$

Values of the constants a, b, c in Equation 1.10 for hydrate structures I and II are given in Table 1-6.

Using the correlations (1.2; 1.3; 1.8), rearrange Equation 1.10 to:

$$\Delta H = T\frac{2d}{dT}\left[\frac{F^{\beta} + PV_H - \phi_B}{T}\right] - RT2\sum_{i=1}^{2}\nu_i\sum_{j=1}^{n}Q_{ij}\frac{d\ln C_{ij}f_j}{dT} \quad (1.11)$$

The first term of the right hand side in Equation 1.11 expresses molar heat of transition of water from an empty hydrate lattice to liquid or ice, existing in equilibrium with hydrate ΔH_B. The second term is the heat of transition of enclathrated molecules from a hydrate cavity into gas phase (ΔH_{INCL}).

Table 1-5 Values of the coefficients A and B in Equation 1.9.

	Cavities			
	Small		*Large*	
Components	*A*	*B*	*A*	*B*
	Structure I			
CH_4	6.9153	0.0316	6.0966	0.0279
C_2H_6	9.4892	0.0406	11.9410	0.0418
C_2H_4	18.1735	0.0729	20.2959	0.0729
H_2S	6.0658	0.0117	4.4568	0.0117
CO_2	14.9976	0.0588	15.2076	0.0589
N_2	3.2485	0.0262	3.0116	0.0248
	Structure II			
CH_4	6.0499	0.0284	6.2957	0.0285
C_2H_6	9.4892	0.0406	11.9410	0.0418
C_2H_4	18.1735	0.0729	20.2959	0.0729
C_3H_8	–	–	18.2760	0.0462
C_3H_6	–	–	9.6250	0.0182
C_4H_{10}	–	–	13.6924	0.0277
H_2S	4.8258	0.0093	2.4030	0.0063
CO_2	23.0350	0.0904	25.2710	0.0978
N_2	3.2485	0.0262	3.0116	0.0248

Table 1-6 Values of the constants a, b, c in Equation 1.10.

Structure	*a*	*b*	*c*
I	–52.7149	–22.0937	84.0985
II	–47.3503	–20.2241	299.8385

Energy characteristics of water molecules' interaction in vertices of dodecahedral lattice composing the hydrate structure and in ice are close, but the presence of ice-like surrounding of water molecules is preferred. That is why in the first approximation it can be accepted that internal energy change in water during the transition from hydrate phase into ice is expressed by a linear function of temperature.

Then the heat of empty hydrate lattice decomposition into ice is described by equation:

$$\Delta H_B^0 = AT + B + PV(V_H - V_l) \quad \textbf{(1.12)}$$

where

A, B are the constants for a given type of hydrate lattice;

V_H, V_i are the molar volumes of water in hydrate and ice.

Water (ice) in equilibrium with hydrate contains dissolved gas. Gibbs potential of water is equal to (Davidson, 1973):

$$\phi_B = \phi_B^0 - RT \ln a \quad \textbf{(1.13)}$$

where

ϕ_B^0 is the Gibbs potential of pure water (ice);

a is the activity coefficient of water in liquid or solid (ice) phases, containing dissolved gas.

Assuming water and hydrate to be incompressible, and integrating the correlation:

$$\Delta H = T\frac{2d}{dT}\left[\frac{F^\beta + PV_H - \phi_B^0}{T}\right] = T\frac{2d}{dT}\left[\frac{\phi_B - \phi_B^0}{T}\right] = AT + B - P\Delta V \quad \textbf{(1.14)}$$

the difference between Gibbs potentials of water in an empty hydrate lattice ϕ_B^0 and in pure liquid (ice), equal to the difference of their chemical potentials μ_B and μ_B^0:

$$\phi_B - \phi_B^0 = \mu_B - \mu_B^0 = AT \ln T - B + CT - P\Delta VP \quad \textbf{(1.15)}$$

where

C is the integration constant.

Reorganizing Equations 1.2, 1.3 and using 1.8, 1.13, and 1.15, the correlation is given which describes the hydrate-ice-gas system equilibrium condition:

$$RT^2\sum_{i=1}^{2}\nu_i \ln\left(1 + \sum_{j=1}^{n} C_{ij}f_j\right) - P\Delta V + RT \ln a = AT \ln T + CT - B \quad \textbf{(1.16)}$$

and the equilibrium condition for hydrate-water-gas system:

$$RT^2\sum_{i=1}^{2}\nu_i \ln\left(1 + \sum_{j=1}^{n} C_{ij}f_j\right) - P\Delta V(V_H - V_{Liq}) + RT \ln a = A'T \ln T + C'T - B \quad \textbf{(1.17)}$$

where

C' is the constant for each type of hydrate structure.

Calculation of Hydrate Formation Parameters in Different Thermodynamic Systems

Conditions of hydrate formation are the basic initial information during the design of field development construction, choice of hydrate removal means, or creation of hydrate formation and utilization installations.

The equilibrium conditions of the water-hydrate-gas and hydrate-ice-gas systems are found by analogy with the derivation of Equations 1.16 and 1.17:

$$RT^2\sum_{i=1}^{2}\nu_i \ln\left(1 + \sum_{j=1}^{n} C_{ij}f_j\right) - P\Delta V + RT \ln a_w = AT \ln T + BT - C \quad \textbf{(1.18)}$$

$$RT^2\sum_{i=1}^{2}\nu_i \ln\left(1 + \sum_{j=1}^{n} C_{ij}f_j\right) - P\Delta V + RT \ln a_w = A'T \ln T + B'T - C' \quad \textbf{(1.19)}$$

In the quadruple point T_0 (hydrate-water-ice-gas) compositions of the hydrate phase formed from water + gas and ice + gas are the same, as follows from Equations 1.3, then from Equations 1.16 and 1.17 we determine:

$$T_0(A - A')\ln T_0 + (B - B')T_0 + (C - C') = RT_0 \ln(a_w/a_i) + P(V_W - V_i) \quad \textbf{(1.20)}$$

The existing relation between the coefficients A and A', B and B', C and C' may be determined from analysis of equilibrium conditions, heat of formation, and heat capacity of hydrates under quadruple point conditions at $t \approx 0$°C.

Because of continuity of the phase diagram in this quadruple point where water, hydrate, ice and gas phases are in equilibrium, we find from Equation 1.20:

$$T_0(A - A')\ln T_0 + (B - B')T_0 + (C - C') \approx 0$$

Thus, in order to describe hydrate formation conditions and heat of hydrate decomposition at $T = 273$ K, it is sufficient to know the constants A, B, C, A', B', C' for hydrate structures of both types. Values of the coefficients A, B, C were determined through processing of experimentally found parameters of methane hydrate formation (structure I) and propane-methane mixture (structure II). Results for coefficients A, B, C, A', B', C' for hydrate structures I and II are presented in Table 1-7.

Table 1-7 Values of the coefficients for equations describing hydrate formation conditions in different systems.

Structure of Hydrate Lattice	*A J/mol,K*	*B J/mol,K*	*C J/mol,K*	*A′ J/mol,K*	*B′ J/mol,K*	*C′ J/mol,K*
I	31.4	185.1	3702.5	6.3	42	–272.2
II	35.6	–212.9	4511.2	–2.1	14.1	235

Comparison of the calculated and experimental data for pure components and natural gas mixtures shows good convergence. Results of calculations indicate that an error in computation of the hydrate formation temperature under pressure change up to 30 MPa (nitrogen hydrates) and 16 MPa (natural gas hydrates) does not exceed 1°C.

In engineering practice simplified heterogeneous diagrams are used for estimation of the hydrate formation conditions for individual gases and for natural gas mixtures. Such diagrams are usually drawn on the basis of experimentally obtained points of dependence of hydrate of the studied gas formation (decomposition) conditions in the given range of pressures and temperatures.

Diagram of the heterogeneous state of hydrate-water-gas system is characterized by the presence of several quadruple points. For gases which the critical temperature is above the hydrate formation temperature at $t > 0$°C there exist four quadruple points. The first quadruple point represents the equilibrium of hydrate, ice, solid or liquefied gas, and gas phases. Usually this point occurs under high vacuum and low temperatures. At the second quadruple point hydrate, ice, water, and gas phases are in equilibrium. In the third point—hydrate, liquefied gas, water, and gas phases. In the fourth point corresponding to the maximum temperature of hydrate stability in the liquid water region the coexisting phases are hydrate, "hot" ice, water-gas. For the gases whose critical temperatures are below the water freezing point, three quadruple points are characteristic.

Figure 1-14 shows the plot of pressure—temperature dependence of methane and CO_2 stability—for low temperature and for high pressure, respectively.

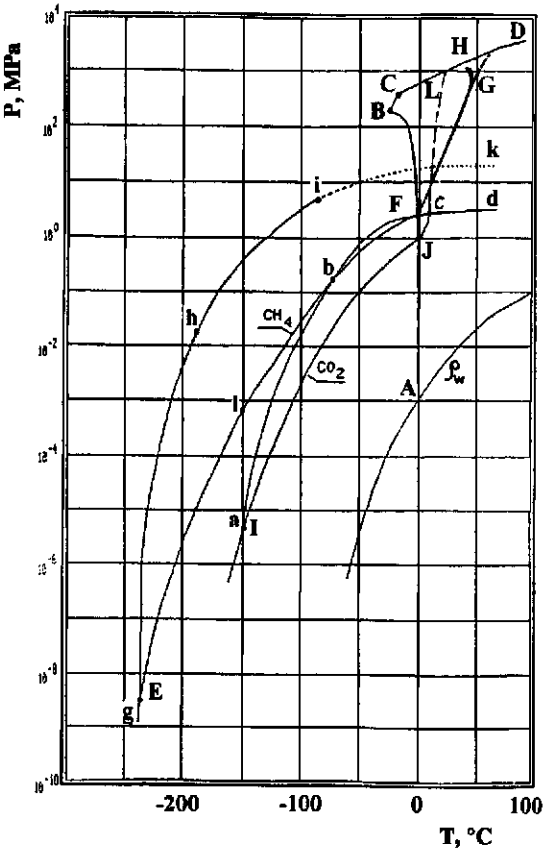

Figure 1-14 Conditions of methane and CO_2 hydrates formation.

ABCD	is the water-ice phase transition curve;
ghik	is the methane vapor pressure curve (CH_4);
abcd	is the carbon dioxide vapor pressure curve (CO_2);
glbFGH	is the methane hydrate P-T equilibrium curve;
aJcL	is the carbon dioxide hydrate P-T equilibrium curve;
ρw	is the water vapor pressure curve.

Figure 1-15 gives a more detailed picture of the P-T dependence of methane hydrate formation in the high pressure region. (Data for methane hydrate formation are shown in Table 1-8 by Makogon and Sloan, 1994; Marshal, Saito, and Kobayashi, 1964; Diyadin, Aladko and Larionova, 1966.)

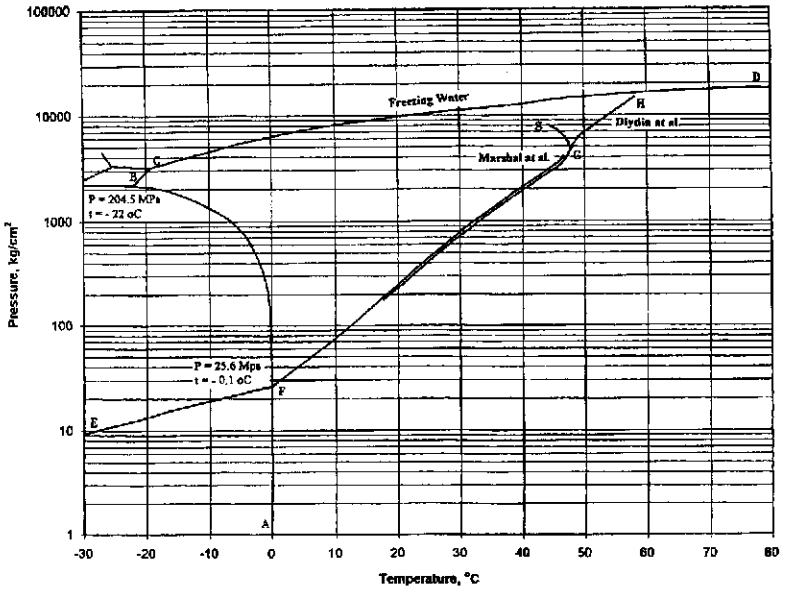

Figure 1-15 Equilibrium pressure—temperature of methane hydrate. (By: T. Y. Makogon, E. D. Slone, 1994; D. R. Marshal, S. Saito, R. Kobayashi, 1964; Y. A. Dyadin, E. Y. Aladko, E. G. Larionova, 1996.)

Table 1-8 Equilibrium pressure—temperature of methane hydrate.

P,MPa	*T,K*	*P,MPa*	*T,K*	*P,MPa*	*T, K*
2 × 10	37	67.41	301.2†	600.0	320.3‡
1 × 10	85	114.18	306.3†	658.0	319.1‡
1 × 10	128	157.33	309.9†	707.0	322.8‡
1 × 10	157	192.95	312.3†	784.0	319.0‡
8.25 × 10	190.15*	212.56	313.2†	786.0	325.0‡
1 × 10	193	244.62	314.6†	814.0	325.3‡
1.31 × 10	198.15*	279.85	316.3†	816.0	316.8‡
2.22 × 10	208.15*	329.32	317.8†	840.0	325.1‡
3.57 × 10	218.15*	378.86	319.3†	874.0	325.6‡
9.55 × 10	243.15*	409.42	319.7†	902.0	326.0‡
1.798	262.4	37.0	296.5†	956.0	326.2‡
2.6	273.1	59.9	300.7†	1000.0	327.7‡
7.5	283.1	162.0	310.4	1106.0	327.2‡
10	285.6	317.0	318.3‡	1200.0	328.0‡
16.40	290.3†	358.0	319.0‡	1219.0	328.4‡
30.89	295.1†	405.0	320.0‡	1335.0	329.6‡
33.8	295.8†	450.0	320.1‡	1426.0	330.1‡
45.65	297.7†	506.0	320.5‡	1500.0	330.4‡
58.63	299.8†	548.0	320.6‡	1525.0	330.4‡

†Makogon T. Y., Sloan E. D., 1994.
‡Marshal D. R., Saito S., Kobayashi R., 1964.
*Diyadin Y. A., Aladko E. Y., Larionoval E. G., 1996.

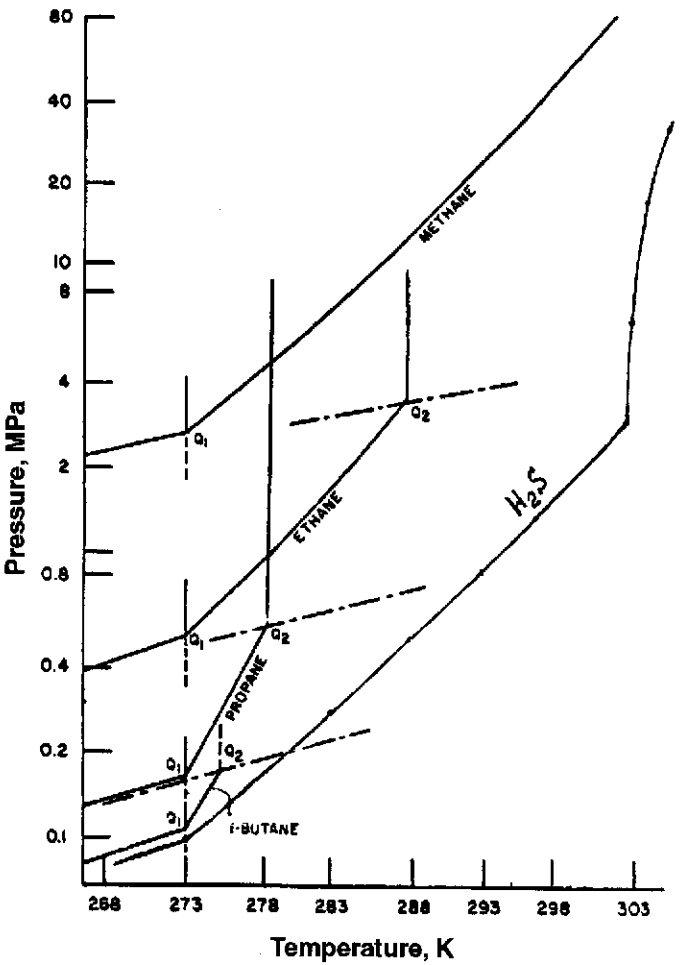

Figure 1-16 Phase diagrams for some simple natural gases that form hydrates (Katz et al., 1959).

AFBCD is the water-ice phase transition curve;

EFGgH is the methane hydrate P-T equilibrium curve.

Figure 1-16 shows the dependence of pressure and temperature for several pure gases.

In addition, the hydrate formation parameters for several gases are given in Table 1-9. Table 1-10 shows the formation conditions of hydrates stable at atmospheric pressure and T > 0°C.

Table 1-9 Parameters of quadruple points for hydrates of some gases.

Gas	Molecular Diameter, nm	Critical P,MPa	Critical T,K	T, K at MPa	Quadruple Points I P,MPa	I T,K	II P,MPa	II T,K	III P,MPa	III T,K	IV P,MPa	IV T,K
Ar	0.38	4.604	150.85	149.15			8.7	272.35				
Kr	0.4	5.43	209.35	245.35			1.46	273.05				
Xe	0.458	5.764	289.74	269.75			0.16	273.15	1.835	297.85		
N_2	0.41	3.469	126.05				14.338	271.9				
O_2	0.42	5.133	154.38				10.1	272.5				
CH_4	0.436	4.60	190.75	191	2×10^{-9}	36	2.563	272.9			1650	331
C_2H_6	0.55	4.98	305.42	241			0.53	273.1	3.39	287.8		
C_3H_8	0.628	4.341	369.95	262.1			0.172	273.1	0.556	278.8		
iC_4H_{10}	0.65	3.534	408.12	270.0			0.113	273.1	0.167	275.0		
H_2S	0.458	9.005	373.51	273.55			0.093	272.8	2.239	302.7		
CO_2	0.512	7.382	304.19	217.0	5×10^{-6}	121	1.256	273.1	4.499	283.0	900	287
Cl_2				282.85			0.0316	272.93	0.84	283.1		
SO_2				279.95			0.039	270.55	0.233	285.25		
SF_6				274.15			0.08	273.15	1.99	277.15		

Table 1-10 Conditions of stable existence for hydrates of some compounds at atmospheric pressure and at T > 273.15 K.

Agent	Nomenclature	Chemical Formula	Parameters of U.I.P. T, K	Parameters of U.I.P. P, kPa	Temperature Decomposition at 101.3 kPa, K	Pressure of Decomposition at 273.15 K, kPa
Ethyl bromide	F-160B1	C_2H_5Br	274.56	22.1	274.55	20.26
Dichloromethane	F-30	CH_2Cl_2	274.86	21.3	274.85	15.46
Ethyl chloride	F-160	C_2H_5Cl	277.96	78.6	273.93	26.79
Methyl mercaptan		CH_3SH	285.16		283.15	31.86
Sulfur dioxide		SO_2	285.16	233	280.25	39.51
Methyl bromide	F-40B1	CH_3Br	287.89	153.5	284.25	24.93
Methyl chloride	F-40	CH_3Cl	293.56	485	280.65	41.46
Ethyl fluoride	F-161	C_2H_5F	295.96		276.85	33.46
Hydrogen selenide		H_2Se	303.15		281.15	45.59
Hydrogen arsenide		AsH_3	301.45		274.75	81.71
Hydrogen antimonide		SeH_3			284.05	
Chlorine dioxide		ClO_2	291.35		288.15	21.33
Bromine chloride		BrCl			287.15	16.66

Figure 1-17 shows the generalized graph (Katz, 1945) for determination of the hydrates formation conditions from natural gases with different densities relative to air. Using these graphs produces satisfactory results for gases not containing acid components at pressures of up to 60–70 bar.

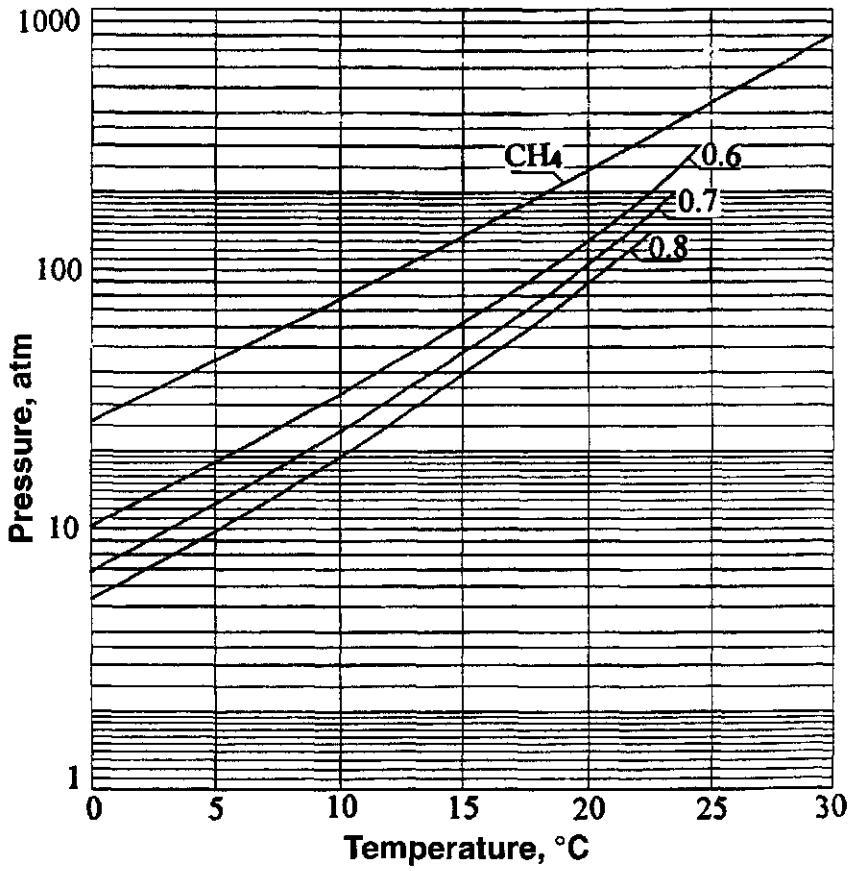

Figure 1-17 P-T of hydrate formation with CH_4 and natural gases.

Determination of the Hydrate-Gas Solution in Mineralized Water System Equilibrium

Hydrate formation in real conditions often occurs from gases dissolved in mineralized water through the equilibrium diffusive influx of gas molecules from the solution to the surface of hydrate. Equilibrium conditions of multiphase systems are described by the equality of chemical potentials of components in different phases. Chemical potentials of water μ_w^H and gas μ_i^H ($i = 1, 2, \ldots, n$) in the hydrate are expressed by the following equations:

$$\mu_W^H = \mu_W^\beta - RT\sum_{j=1}^{2} \nu_j \ln\left(1 - \sum_{i=1}^{n} Q_{ij}\right) \tag{1.21}$$

$$\mu_i^H = RT \ln \frac{Q_{ij}}{\left(1 - \sum_{j=1}^{n} Q_{ij}\right) \times Z_{ij}} RT \ln F_j + RT \ln \phi_j \tag{1.22}$$

where

- μ_W^β is the chemical potential of water in the empty lattice;
- n_j is the ratio of number of j-type cavities ($j = 1, 2$) to number of water molecules in an elementary cage of a hydrate structure;
- Q_{ij} is the ratio of j-type cavities filled with i-type gas molecules ($i = 1, 2, \ldots, n$);
- Z_{ij} is the energy function of condition of a molecule in a hydrate cavity;
- R is the universal gas constant.

Chemical potential of a water solution of salts and gases μ_W^L is expressed through the chemical potential of pure water μ_W^0 at the corresponding pressure P and temperature T and its activity a:

$$\mu_W^L = \mu_W^0 + RT \ln a \tag{1.23}$$

From the condition of equality of the correlations 1.21 and 1.23 it follows:

$$-RT \ln a + RT\sum_{j=1}^{2} \nu_j \ln\left(1 - \sum_{i=1}^{n} Q_{ij}\right) + \int_{P_0}^{P} \Delta V dP = \mu_W^0(P_0, T) - \mu_W^\beta(P_0, T) \tag{1.24}$$

where

ΔV is the difference of the molar volumes of water in the hydrate and liquid phases;

P_0 is the a fixed pressure assumed to be equal to 0.098 MPa.

The right part of the Equation 1.24 depends only on the temperature and the type of hydrate lattice being formed, and may be approximated on the basis of experimental data. Equation 1.24 is universal for all types of equilibrium where hydrates coexist with liquid phase; thus the temperature dependence of the right part may be determined on the basis of experimental studies on the hydrate-water-gas system equilibrium. Under the assumption that water and hydrate are incompressible, the Equation 1.24 may be presented as follows:

$$RT \ln a - RT\sum_{j=1}^{2} \nu_j \ln\left(1 - \sum_{i=1}^{n} Q_{ij}\right) - P\Delta V = AT \ln T + BT + C \qquad \textbf{(1.25)}$$

Calculated values of the coefficients A, B and C are given in Table 1-11.

Chemical potential μ_i^S of a gas component in water solutions of various mineralization s is expressed through the Sechenoff coefficient K and Henry's constant H_i in a form of equation (Namiot, 1976):

$$\mu_i^S = RT \ln H_i(P_0, T) Y_i \times 10^{K_i \times S} \exp\left[\frac{V_i(P - P_0)}{RT} + \mu_i^0\right] \qquad \textbf{(1.26)}$$

where

μ_i^0 is the standard value of chemical potential;

Y_i is the concentration of an i-th component in the solution;

V_i is the partial molar volume of an i-th component in the solution.

Table 1-11 Values of coefficients A, B and C from Equation 1.25 and values of V for structure I and II hydrates.

Type of Hydrates	*A, J/K*	*–B, J/K*	*C, J*	*ΔV, cm³/mol*
I	31.405	185.132	3702.492	4.6
II	35.592	–212.945	4511.172	5.3

When examining the equilibrium of a gas-water-hydrate system, the chemical potential of an i-th component in the gas phase μ_i' is expressed by an equation of the following type:

$$\mu_i' = RT \ln \frac{f_i}{P_0} + \mu_i^{St} \qquad \textbf{(1.27)}$$

where

f_i is the volatility of an i-th component of gas phase;

μ_i^{St} is the standard value of the chemical potential of gas phase at a pressure assumed to be equal to atmospheric ($P_0 = 0.098$ MPa).

For convenience of calculations of equilibrium conditions for this system a new variable is introduced—the Langmiur's constant C_{ij} which is the temperature function for the given component and hydrate cavity and may be determined from the equality of the Equations 1.22 and 1.27:

$$\frac{Q_{ij}}{\left(1 - \sum_{j=1}^{n} Q_{ij}\right)} RT = f \frac{Z_{ij}}{P_0} \exp\left[\frac{\mu_i^{St}}{RT}\right] = C_{ij}(T) f \qquad \textbf{(1.28)}$$

Langmiur's constant is determined by the peculiarities of molecular behavior in a hydrate cavity and by the choice of the standard value of the gas phase chemical potential. It is obvious that having chosen equal values of standard chemical potentials of a component in gas phase μ_i^{St} and in solution μ_i^0, values of the Langmiur's constants obtained after processing experimental data for gas-water-hydrate system equilibrium will be applicable to describing the equilibrium of a solution of hydrate-forming components in water with different degrees of mineralization system. Hence from the equality of Equations 1.22 and 1.26 and considering the determined from (1.28) Langmiur's constant, we obtain:

$$\frac{Q_{ij}}{\left(1 - \sum_{j=1}^{n} Q_{ij}\right)} = H_i(P_0, T) Y_i \times 10^{K_i \times S} \exp\left[\frac{V_i(P - P_0)}{RT}\right] C_{ij}(T) \qquad \textbf{(1.29)}$$

Introducing a new variable Φ converts Equation 1.25 to:

$$\Phi_{ij} = H(P_0, T) \times 10^{K_i \times S} \exp\left[\frac{V(P - P_0)}{RT}\right] Y_i \qquad \textbf{(1.30)}$$

$$RT\sum_{j=1}^{2} \nu_j \ln\left(1 + \sum_{i=1}^{n} C_{ij}\Phi_i\right) + RT \ln a - P\Delta V = AT \ln T + BT + C \qquad \textbf{(1.31)}$$

The obtained equation in a generalized form describes the equilibrium condition of a hydrate-gas solution in water with different degrees of mineralization system.

Results of calculations of methane solubility in water show that the CH_4 concentration in the solution increases as the pressure grows, reaching its maximum at the equilibrium conditions of a gas-water-hydrate system. Subsequent increase of pressure in the region of equilibrium of hydrate-methane-water solution system leads to a decrease of CH_4 concentration because of the transition of gas into hydrate.

It follows from Equation 1.25 that at isothermal compression of hydrate the equilibrium degree of filling cavities with gas molecules increases, which is due to the necessity of internal stabilization of cavities against the increasing external pressure such that reduction in partial molar volume of water is more energetically favorable.

The methane concentration φ both in pure and mineralized water decreases as the pressure grows. Depending on the hydrate and water volumes ratio in a closed system, pressure growth may lead to either the increase or decrease of the hydrate volume. At a high hydrate to water volume ratio the amount of gas released from the liquid phase will not be sufficient to stabilize the whole hydrate mass and the hydrate will partially decompose releasing gas necessary to fill the cavities of the remaining solid phase volume. It is worth noting that degassing of the water, which is in contact with hydrate or the water laterally migrating from the hydrate-formation zone, will occur at a lower pressure because of the depression in water saturation with gas.

Besides the equilibrium conditions for hydrate-water solutions systems, determination of the heat of hydrate formation ΔH_h in such systems is also of considerable interest. The heat of hydrate formation is a sum of the heat of crystal lattice formation ΔH_l, and the heat of inclusion of hydrate-forming gas molecules into a hydrate cavity ΔH_i with allowance made for according changes in the composition of equilibrium phases.

The heat of transition of water molecules from the solution into hydrate is equal to the heat of transition from the solution into pure water ΔH_s (the negative heat of diluting the solution) and to the heat of transition from pure water into hydrate ΔH_l^0:

$$\Delta H_l^0 = AT - C - P\Delta V \qquad (1.32)$$

where A, C, ΔV are the parameters provided by Table 1-12.

The heat of transition of gas molecules from water solutions into hydrate may be presented as a sum of heats of transition from the solution into gas ΔH_1 and from gas into the solution ΔH_2.

Table 1-12 Heats of diluting the water solutions of electrolyte inhibitors, ΔH, kJ/mole of an inhibitor.

Concentration of NaCl,						
% Mass	24.4	11.5	6.0	3.0	1.6	
$-\Delta H_s$, kJ/mole NaCl	0	1.35	2.6	3.75	2.9	
Concentration of $CaCl_2$,						
% Mass	38.0	23.8	11.0	5.6	0.1	
$-\Delta H_s$, kJ/mole $CaCl_2$	0	7.5	10.0	10.2	11	
Concentration of $MgCl_2$,						
% Mass	34.6	20.8	10.0	5.1	2.5	0.3
$-\Delta H_s$, kJ/mole $MgCl_2$	0	10.0	14.0	14.8	15.6	16.0

Table 1-13 Heats of dissolving of gases in water.

Gas	CH_4	CO_2	H_2S	SO_2	CO
ΔH_2, kJ/mol	13.14	19.75	21.71	40.71	10.96

The heat of transition of gas molecules from the solution into hydrate is equal to:

$$\Delta H = RT^2 \frac{d}{dT} \ln C_{ij} \qquad (1.33)$$

where

C_{ij} is Langmiur's constant.

Differential heats of dissolving of gas in water ΔH_2 are presented in Table 1-13.

The heat of hydrate formation in the system in question is expressed by equation:

$$\Delta H_H = AT - C - P\Delta V - \Delta H_P + RT^2 \sum_{j=1}^{2} \nu_j \sum_{i=1}^{n} Q_{ij} \left(\frac{d}{dT} \ln C_{ij} - \Delta H_{2i} \right) \qquad (1.34)$$

The results of the calculations show (see Table 1-14 and 1-15) that the heat of methane hydrate formation increases with temperature and decreases with pressure.

Table 1-14 Heats of formation of methane hydrates, ΔH kJ/mole H_2O.

	Pressure, MPa					
Temperature, °C	*3*	*5*	*10*	*20*	*35*	*50*
0	5.252	5.241	5.222	5.174	5.107	5.038
5	–	5.399	5.377	5.331	5.262	5.193
10	–	–	5.545	5.500	5.442	5.358

Table 1-15 Heats of formation of methane hydrates, ΔH kJ/mole H_2O at t = 10°C and various concentrations of NaCl in the solution.

Concentration,	*Pressure, MPa*					
% mass	*10*	*20*	*30*	*40*	*50*	*60*
14	5.543	5.523	5.501	5.489	5.468	5.347
23	–	5.550	5.497	5.492	5.486	5.480

The influence of inhibitors on the heat of hydrate formation is insignificant and one may neglect the heat of dilution in technical calculations. Heats of formation of hydrates from free gas and from gas dissolved in water differ by 30 to 35%.

Hydrates at Sub-Zero Temperatures

Both technogenic and natural gas hydrates form, stably exist, and decompose in a very broad range of temperatures. A temperature range below 0°C is very important during the development of hydrocarbon deposits in the Arctic regions, in several gas processing technologies, and in the solution of the problems in outer space.

Regrettably, there have been very few works devoted to studying the conditions of hydrate formation at temperatures below 0°C, and often the reported results are contradictory. So for a methane hydrate the range of decomposition temperatures at atmospheric pressure reported in the literature varies from –29 to –83°C, but actually it is –80.4°C (Makogon and Sloan, 1994).

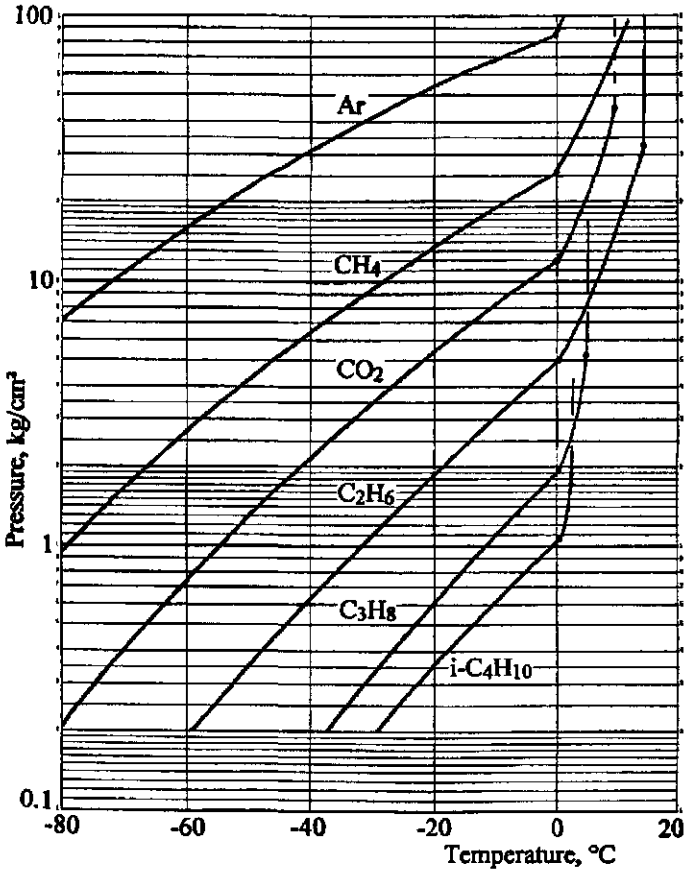

Figure 1-18 Hydrate formation with different gases at T < 0°C.

Knowledge of the hydrate's characteristics at sub-zero temperatures is extremely important in case of emergencies, when a sharp decrease of pressure in the pipeline is accompanied by a fast decomposition of hydrates and a temperature drop below the freezing temperature of the released water. A porous ice plug is formed in the pipeline, which is much more difficult to remove than a gas hydrate plug.

Figure 1-18 presents the equilibrium curves for hydrates of several gases at temperatures below 0°C. Equilibrium content of water vapor above hydrate is significantly lower than above liquid water or ice. Figure 1-19 shows the curves describing the vapor content in methane under saturation conditions at $T < 0$°C (Kobayashi et al., 1987) above ice and hydrate. It should be noted that hydrate is a good absorbing agent and may be used in several techniques for drying of gases.

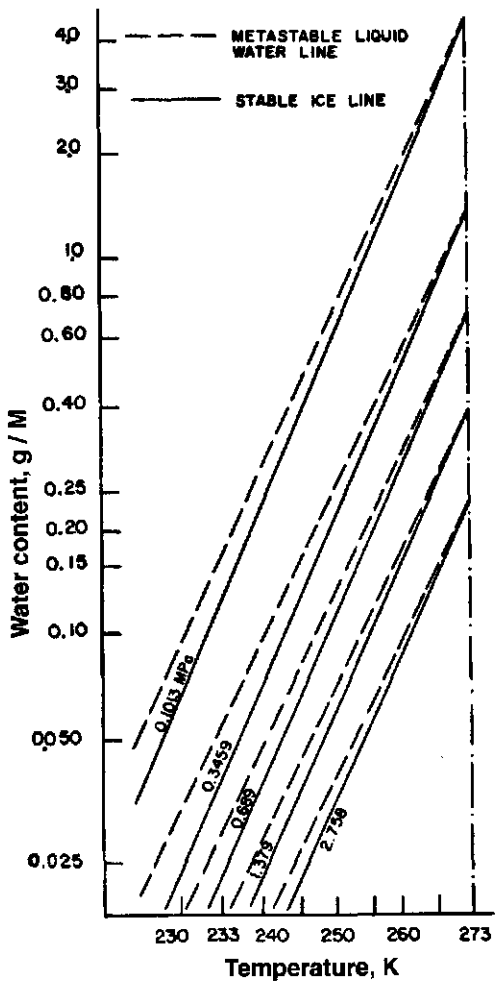

Figure 1-19 Equilibrium (solid) and metastable (dashes) water content chart for methane gas in equilibrium with ice. (Reproduced with permission from *Petroleum Engineering Handbook*, Kobayashi et al., 1987.)

In a hydrate formation zone a transition of water from ice to gas hydrates occurs. During the flow of bone dry gas over hydrate or ice, they decompose through sublimation. This is the basis for one of the applied methods of removal of hydrate and ice accumulations from the pipelines.

The capacitative and thermal properties of the phase transitions "hydrate-gas-water-ice" at $T < 0°C$ which determine thermomechanical properties of hydrates and their effect on the stability of engineering constructions, especially in the Arctic offshore conditions are very important.

The difference in thermal conductivity of ice and hydrate increases significantly with temperature decrease. This should be considered when solving the problems in dynamics of permafrost rock and gas hydrate deposits on our planet, and ice-hydrate ratio calculation on space bodies, in particular on Mars, Halley's Comet, etc. It is the difference in thermal conductivities of ice and hydrate in the bulk of Halley's Comet which explained the formation of "flares" on it during its approach to the sun. Temperature in its near-surface layers had risen above the hydrate decomposition temperature, but stayed below the surface ice melting temperature (Makogon, 1987).

Experimental determination of hydrate formation conditions below $T = 0°C$ is complicated because of the very slow kinetic characteristics of the transition process of ice to hydrate. However, the equilibrium parameters of the process are easy to determine through controlling the hydrates decomposition process by isothermal decreasing of pressure above hydrates accumulated at $T < 0°C$.

Decomposition of hydrate boulders in space may occur by several mechanisms: reforming in structure and composition, sublimation, thermomechanical destruction during collisions with other boulders, and thermal decomposition, etc.

Gas Hydrate Composition

Gas hydrate composition is determined by the initial parameters of a hydrate crystal formation, by the compositions of gas and water, and by pressure and temperature.

Composition of a single component hydrate remains practically fixed over a wide range of pressures and temperatures. Only a molar ratio of water and gas (n) is changed as a consequence of different filling of cavities with the hydrate former. With the complete filling of cavities and without structural changes, n remains constant. Composition of natural or technogenic gas hydrates formed from gas mixtures depends on the composition of the gas, pressure, and temperature.

Most accurately the composition of hydrates obtained under different conditions can be determined experimentally using physical or physicochemical methods of study. A high surficial absorbing ability of hydrates has to be taken into account during the composition study.

Achievements of statistical mechanics allow us to determine the hydrate composition analytically from the composition of gas above hydrate and partial pressures of separate components considering the filling ratios of the large and small cavities with hydrate forming components

based on Langmiur's constants. Having the partial pressure of components in the gas phase and Langmiur's constants, the filling ratio of hydrate cavities with separate components can be determined:

$$Q_{ij} = \frac{C_{ij} f_{ij}(P_H, T) \exp\left(-\frac{P - P_H}{RT} V_{ij}\right)}{1 + \sum C_{ij} f_{ij}\left(-\frac{P - P_H}{RT} V_{ij}\right)} \qquad (1.35)$$

Having determined the filling ratio of the large and small hydrate cavities with separate components, the relative composition of the components is calculated.

For hydrates of structures I and II we have:

$$N_{i,I} = \frac{Q_{i,Small} + 3Q_{i,Large}}{\sum Q_{i,Small} + 3\sum Q_{i,Large}} \qquad (1.36)$$

$$N_{i,I} = \frac{2Q_{i,Small} + Q_{i,Large}}{2\sum Q_{i,Small} + \sum Q_{i,Large}} \qquad (1.37)$$

In order to find new and more complex structures, new terms which account for the filling ratio of new cavities are added to the Equations 1.36 and 1.37.

Composition of hydrates of natural gases is determined mainly by the forming gas composition, pressure and temperature of formation. Table 1-16 and Figure 1-20 present the calculated compositions of sweet gas hydrates as a function of gas composition, temperature, and pressure. Composition of hydrate presented are given for the equilibrium decomposition temperature and pressure. Hydrate composition calculations utilized the computer model of Drs. Robinson and Ng of Edmonton.

Analysis of the hydrate composition study for 99% to 80 volume percent methane mixture compositions resulted in the following conclusions:

1. The amount of heavy components in hydrates increases with the molecular weight of the forming gas.
2. The relative content of CO_2 in hydrate structures I and II decreases with the molecular weight of the forming gas.
3. The amount of heavy components in hydrates decreases and methane content increases with temperature and pressure.
4. Hydrate formation pressure has the most significant effect on the propane and isobutane content in hydrate.
5. Content of CO_2 and *n*-butane varies little and usually decreases with pressure and temperature.

Table 1-16 Hydrate composition (volume %).

Component	Gas Composition, Volume %	P(MPa) T (K)	2.875 2	4.28 6	6 9.3	10 13	20 19.3	30 22.2
CH_4	99		99.364	96.711	97.025	97.534	98.165	98.410
C_2H_6	0.4		2.504	2.217	1.961	1.556	1.083	0.918
C_3H_8	0.1		0	0	0	0	0	0
CO_2	0.5		1.132	1.072	1.014	0.911	0.751	0.672
		P(MPa)	1.286	2.055	6	10	20	30
		T (K)	2	6	14.5	17.7	21.7	24.7
CH_4	95		62.430	65.215	71.527	75.425	92.072	93.138
C_2H_6	3		2.874	2.908	3.157	3.309	7.360	6.347
C_3H_8	1		23.132	21.428	17.697	15.348	0	0
i-C_4H_{10}	0.3		9.864	8.906	6.479	5.016	0	0
n-C_4H_{10}	0.3		1.537	1.375	0.962	0.719	0	0
CO_2	0.4		0.163	0.168	0.179	0.183	0.568	0.515
		P(MPa)	0.9	1.47	6	10	20	30
		T (K)	2	6	17	19.8	23	25.2
CH_4	90		55.189	58.480	66.285	69.636	75.078	77.349
C_2H_6	4		1.880	1.895	2.250	2.539	2.826	2.815
C_3H_8	2		23.054	21.435	18.131	16.808	14.127	12.791
i-C_4H_{10}	1		16.598	15.129	10.950	8.970	6.365	5.597
n-C_4H_{10}	1		2.594	2.344	1.619	1.276	0.842	0.713
CO_2	2		0.686	0.716	0.764	0.771	0.762	0.735
		P(MPa)	0.705	1.17	6	10	20	30
		T (K)	2	6	18.3	21	23.7	26
CH_4	80		49.664	53.782	63.393	66.377	70.665	72.257
C_2H_6	10		2.756	2.734	3.286	3.817	4.393	4.433
C_3H_8	5		34.002	31.174	25.007	23.122	19.984	18.723
i-C_4H_{10}	1		9.839	8.856	5.849	4.652	3.390	3.141
n-C_4H_{10}	2		3.079	2.751	1.715	1.302	0.876	0.784
CO_2	2		0.661	0.703	0.749	0.731	0.692	0.515

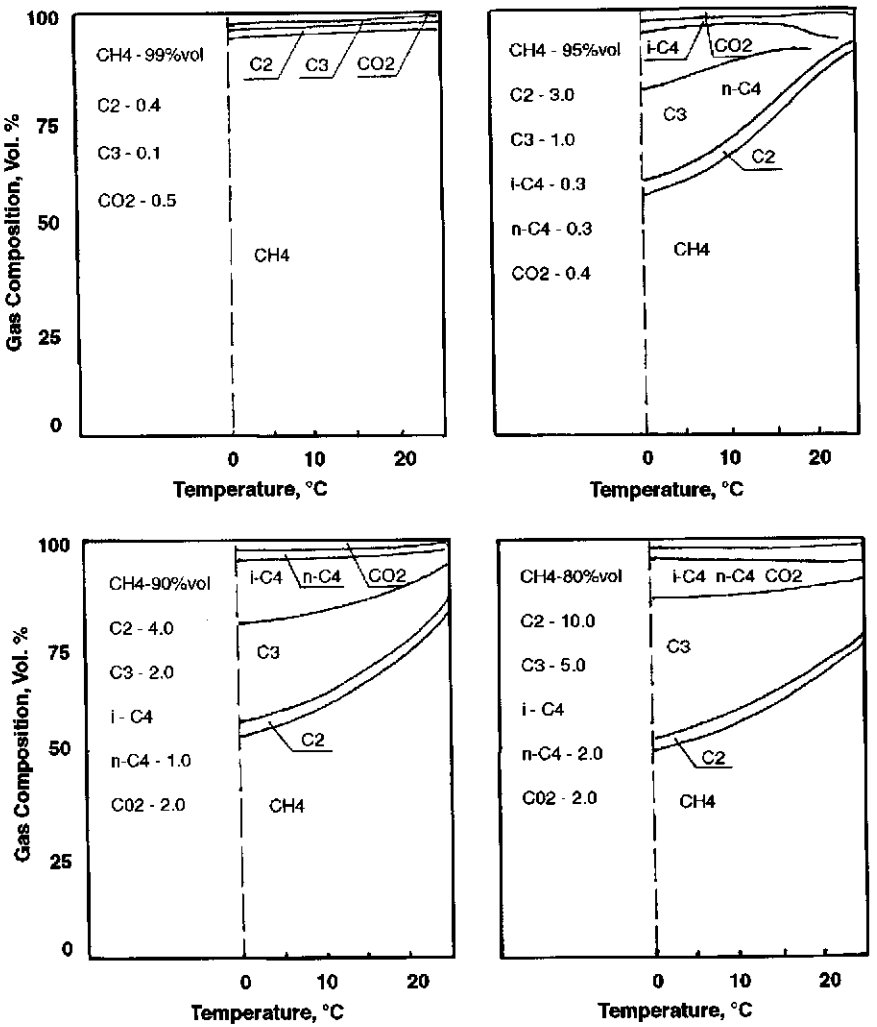

Figure 1-20 Hydrate composition dependence on free gas composition, pressure, and temperature.

6. Methane content increases in hydrate with pressure and temperature of hydrate formation, independent of the former gas composition. There possibly exists a range of high pressures where the content of methane in hydrate is higher than in the forming mixture.
7. It is suitable to maintain low temperature and pressure during the hydrate-based separation.

Table 1-17 Gas and hydrate compositions from the Orenburg gas field.

	Gas Composition (Volume %)		*Hydrate Composition (Volume %)*	
	Deposit Part			
Component	*Roof*	*Wing*	*Roof*	*Wing*
CH_4	84.1	84.86	29.3	12.9
C_2H_6	4.9	3.8	1.8	0.75
C_3H_8	1.58	1.3	23.08	18.57
i-C_4H_{10}	0.3	0.3	8.95	11.57
n-C_4H_{10}	0.51	0.5	–	–
C_5H_{12}	0.6	0.41	–	–
C_6H_{14}	1.21	0.23	–	–
H_2S	1.3	4.5	36.68	56.12
N_2	4.89	2.5	0.2	0.05
CO_2	0.53	1.5	0.05	0.04
He	0.065	0.055	–	–
Ar	0.01	0.009	–	–

Table 1-17 shows the effect of H_2S and nitrogen presence in the forming gas on the hydrate composition under the deposit conditions. The Orenburg gas field is used as an example data source. It can be seen from this table that the H_2S content in hydrate is 12–28 times higher than in the forming gas. This allows an effective pretreating of industrial gases. It should be noticed that the ratio of H_2S extraction from gas increases with the temperature and pressure of hydrate formation.

It can be seen from this table that the content of gases highly soluble in water increases in the roof part of the deposit and the presence of H_2S in gas sharply affects the hydrate composition through substituting the components filling the small cavities, such as CH_4, CO_2, and N_2.

Mechanism of Gas Hydrates Formation in the Lithosphere

Studies of the gas hydrates in the lithosphere discovered by Russian scientists have several directions. The leading specialists in a number of research laboratories in the world pursue academic and applied aspects of

the gas hydrates. Their persistent work has resulted in more than 60 discoveries of large gas hydrate deposits of hydrocarbon gases exceeding by several times the hydrocarbon reserves found to date in non-hydrate state.

In many cases gas hydrate accumulations are formed within the boundaries of natural hydrocarbon deposits. In such cases study of the gas hydrate accumulation effects on safety of construction and operation of engineering installations becomes imperative. This includes study of thermomechanical properties and carrying ability of the hydrate saturated rock, their location, conditions of their situation, and stability. Insufficient consideration of these factors may result in errors in prognosis of the offshore platforms stability, selection of the drilling method, and engineering of the offshore wells, pipelines and other offshore objects. Such errors may result in emergencies during construction operation of wells, destruction of engineering installations, capsizing of the offshore platforms, and ecological harm.

One of the most important and least studied problems is providing the basis of the mechanism of hydrate formation, accumulation, and dynamics of existence in porous rock under their natural situation conditions. Discovery of such a mechanism will allow us to determine the shape of gas hydrate accumulations, their spread in the sedimentary rock, sizes of inclusions, and stability, etc.

Often the hydrate saturated cores contain large inclusions of pure hydrate. The shape and size of hydrate inclusions depend on a number of factors. The most important factors are the capacity and strength of the carrier rock, fluid saturation with gas, pressure and temperature, and time of inclusions formation, etc. We have proposed a concept for the mechanism of the initial gas hydrate formation and their accumulation in sedimentary rock.

Development of the gas hydrates classification proposed by R. Malone (1989) lets us notice that hydrates in porous rock may be dispersed when the size of hydrate inclusion does not exceed the size of the pores of carrier rock; granular-dispersed when the inclusion size may exceed the pores size without destroying the pores; nodular inclusions when the size of hydrate inclusions varies from several millimeters to a few centimeters. Formation of hydrate nodules is accompanied by destruction of the carrier rock and hydrates act as a concrete. The further growth of the nodules may result in formation of lens-shaped hydrate accumulations extending up to several meters in width and tens of centimeters thick. Under favorable conditions, the lens-shaped accumulations may result in large gas hydrate deposits several meters thick extending for tens and hundreds of kilometers. From the thermomechanical characteristics viewpoint, the nodular-layered hydrate accumulations are the most dangerous ones.

The first studies of the hydrate formation process in the porous rock synthesized from natural specimens of granular rock were performed by Makogon (1966). The integral characteristics of the process were studied, while the gas hydrate formation mechanism was not detailed. This work pays primary attention to the analysis of the nucleation process and growth of mass and stability conditions for gas hydrate formations in porous rock. Specific details of the terrigenic sedimentary porous rock are reviewed which affect the process and make it differ substantially from that in a free volume.

The unit cell of a hydrocarbon gas hydrate consists of 54 to 146 molecules including 8 to 10 guest molecules, depending on the structure. In different structures of hydrate crystal 4 to 17 water molecules are present per each gas molecule.

The problem is reviewed on the example of methane hydrate, which is the most widespread hydrate former in the earth's sedimentary layer. The starting position in the analytical chain is that gas hydrate forms at the vapor-liquid interface, namely hydrate former in the vapor phase and water in the liquid phase. The proof of this statement is simple. It is required for the hydrate formation that 8 to 10 gas molecules and 46 to 135 water molecules come together in the same location. If both components are in vapor phase, then the probability of such event is negligible. If gas is soluble in water the probability of this event increases.

During the methane hydrate formation, the structure of water becomes loose and its volume increases by 26%. A water molecule occupies 3.3×10^{-29} m^3 in liquid, while in hydrate it occupies 4.158×10^{-29} m^3. Increase of the water specific volume requires an internal pressure of 1100 MPa (Telesnin, 1973).

Required energy for increasing the water specific volume in the hydrate state is found using the equation:

$$T = \frac{P(V - V_0)}{k} = \frac{(11 \times 10^8) \times (8.58 \times 10^{-30})}{1.38 \times 10^{-23}} = 684K \qquad \textbf{(1.38)}$$

where

T is the temperature required for the volume increase, K;

P is the internal pressure, Pa;

k is the Boltzmann's constant equal to 1.38×10^{-23} J/mol K;

$(V\text{-}V_0)$ is the increase of volume V_0 occupied by a water molecule in liquid state during its transition to solid hydrate state V, m^3.

At such a temperature, gas hydrate formation is thermodynamically impossible. Consequently, gas hydrate formation from a solution of gas in water is impossible.

Evolution of gas from the solution in mineral water to a free state separate phase always occurs in a supersaturated solution for either of these reasons: influx of additional gas from generation sites or change of thermodynamic conditions, etc. Usually the evolution of free gas from a solution occurs in portions as microbubbles that may then coalesce.

Radius of the gas bubble of the minimum size can be calculated based on the following statements:

1. Pressure of gas in such a bubble is defined by the action of the two components: surface tension force equal to $P_S \times S$, and the deposit hydrostatic pressure force $P_H \times S$, where S is the bubble surface in water medium.

$$P \times S = P_S \times S + P_H \times S$$

or

$$P = P_S + P_H \tag{1.39}$$

According to the Laplace's law $P_S = 2\sigma/r$, where σ is the surface tension coefficient and r is the bubble radius (Geguzin, 1975)

$$P = P_H + 2\,\sigma/r \tag{1.40}$$

Figure 1-21 presents the dependence of σ at the water-air and water-methane interface as a function of temperature and hydrostatic pressure (Gimatudinov, 1974; McKay, 1992).

2. Molecular ensemble of hydrocarbon molecules with its weight less than the buoyancy force acting on it in water in accordance with Archimede's law is considered a gas bubble.

$$N\,m\,g < \rho\,V\,g \tag{1.41}$$

where

- N is the number of non-condensed molecules of the substance in the studied thermodynamic situation;
- m is the mass of each bubble;
- V is the volume of the bubble;
- ρ is the density of the liquid (water);
- g is the gravity acceleration.

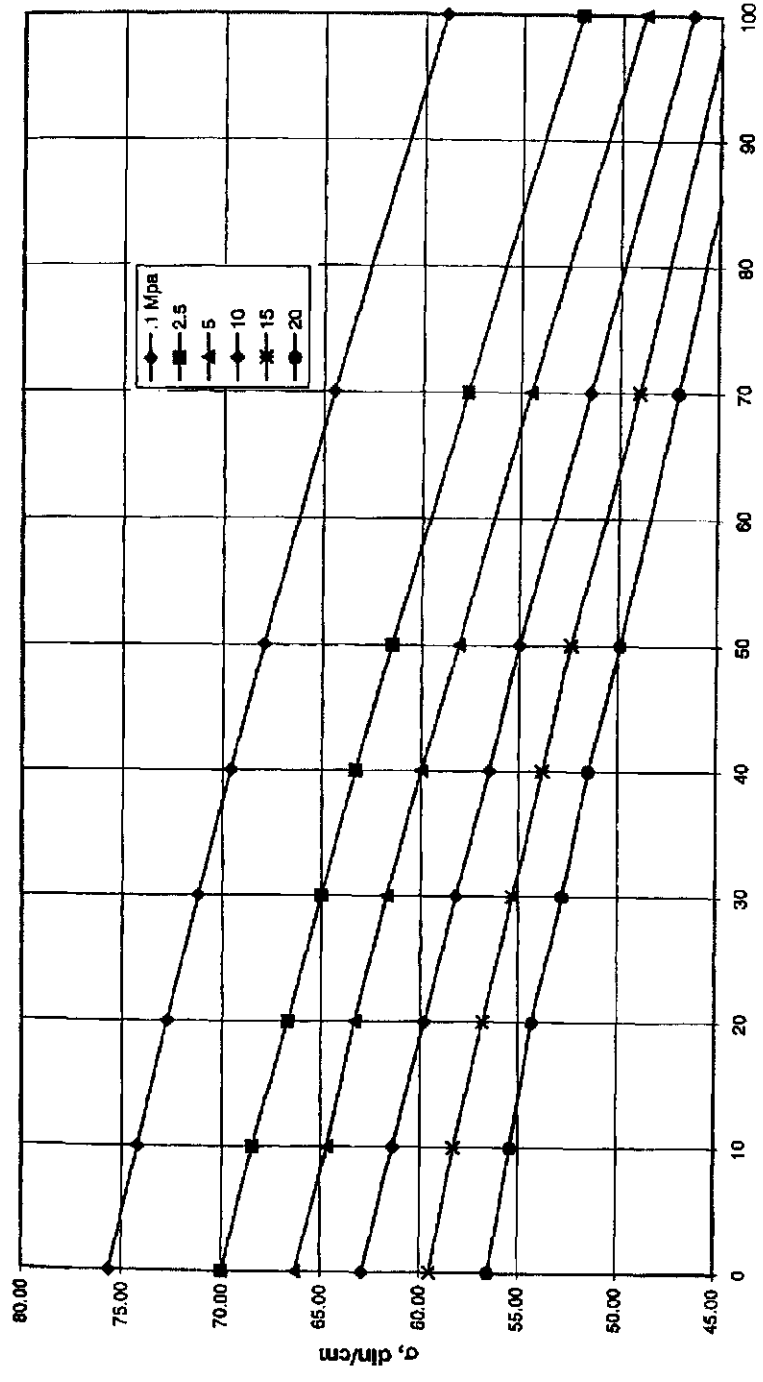

Figure 1-21 Surface tension (σ, dyne/cm) free water-methane dependence of pressure and temperature.

3. Pressure inside the bubble which prevents it from collapsing is determined from the van-der-Waals equation. Since the non-condensed media is considered, the intermolecular attraction can be neglected. Then

$$P = \frac{NkT}{V_0 - W_0} \tag{1.42}$$

where

W_0 is the total volume of gas molecules equal to $V_0 \times N$;

V_0 is the volume of one gas molecule at critical pressure (1.15×10^{-28} m^3 for CH_4).

From (1.42) it follows that

$$N = \frac{PV}{kT + PV_0} \tag{1.43}$$

where

P is the pressure in terms of (1.40).

Solving (1.40) and (1.41) simultaneously for P we obtain:

$$P = \frac{kT}{m/\rho - V_0} \tag{1.44}$$

4. Sum of all forces equals to zero at the bubble surface.

$$P = PH + 2\,\sigma/r = 0 \tag{1.45}$$

which results in

$$P = PH + 2\,\sigma/r \tag{1.46}$$

and

$$P_H + 2\,\sigma/r = \frac{kT}{m/\rho - V_0} \tag{1.47}$$

which after simple rearrangement produces the desired value of the gas bubble minimal radius:

$$r = \frac{2\sigma(V_0 - m/\rho)}{kT - P_H(V_0 - m/\rho)} \tag{1.48}$$

For example, the minimal radius of the bubble, particularly methane at a depth of 1500 m at $\rho = 10^{-3}$ kg/m^3, m = 27.2×10^{-27} kg, $V_0 = 1.15 \times 10^{-28}$ m^3, $k = 1.38 \times 10^{-23}$ J/K, $T = 277$ K, and $\sigma = 62 \times 10^{-3}$ N/m according to Equation 1.48, will be 4.3×10^{-9} m.

Gas bubbles emerging at a depth of 500 m require space with effective cross-section of 4.19×10^{-9} m or larger. Figure 1-22 presents the dependence of pressure inside a gas bubble formed in the bulk of water on bubble diameter and hydrostatic pressure. It can be seen from this figure that pressure inside the bubble is significantly higher than the hydrostatic pressure.

The determining factor of hydrate crystal nucleation in the bulk of water is not the pressure magnitude, but rather the rate of its lowering (pulsation) which determines the formation of microbubbles of gas.

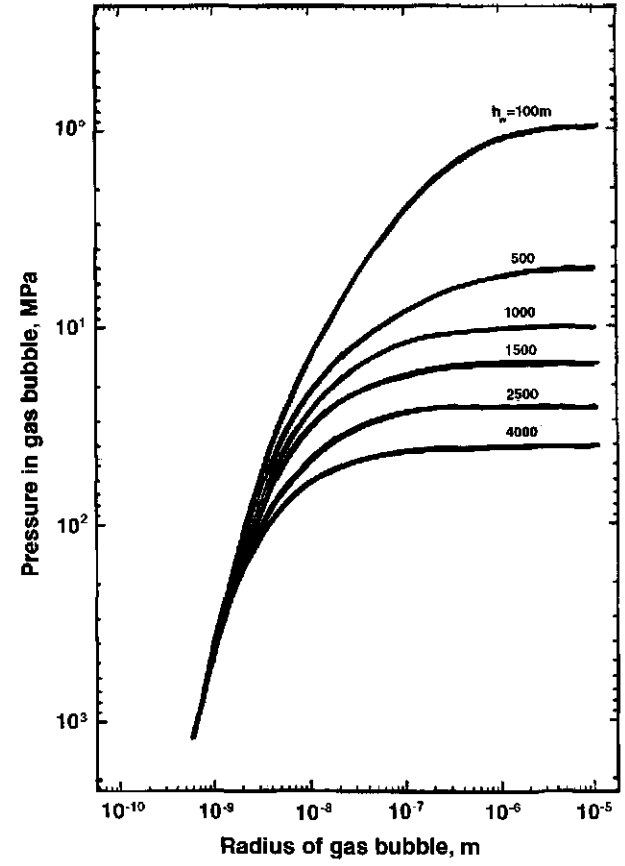

Figure 1-22 Gas bubble pressure dependence on the radius of gas bubble and hydrostatic pressure.

Pressure inside these microbubbles significantly exceeding the hydrostatic pressure is the driving force of the hydrate nuclei formation.

If the porous space is saturated with gas and water and sufficiently large bubbles (over 10^{-6} m diameter) of free gas are present at hydrate equilibrium conditions, still no hydrate formation happens because there is no driving force and there is no necessary subcooling for the hydrate nuclei to develop.

The change of thermobaric conditions is accompanied by evolution of microbubbles in the bulk of gas-saturated water. Microbubbles are characterized by a high concentration of gas molecules per unit volume and pressure much higher than the hydrostatic pressure. With such change of conditions, a process of hydrate crystals nucleation and growth develops.

Most experimenters are familiar with the fact that when the P-T conditions for hydrate formation are created in a gas-water system, hydrate formation does not start. Significant subcooling or overpressurization is required for the hydrate formation process to start. A relevant example was described by Ann Rigmor (1992) where the gas-water system was maintained at an equilibrium pressure of 8.6 MPa and a temperature of 287 K for 15 hours without hydrate formation. Afterwards pressure was increased to 15.5 MPa at a rate of approximately 0.15 MPa/minute. During the 20 minutes, water was saturated with gas and no hydrate nuclei started to form. Only after lowering the pressure in the system at a rate of 0.45 MPa/minute, the first nuclei were observed in the bulk of water at the pressure of about 10 MPa. Supersaturation of water and evolution of microbubbles has occured and the hydrate nuclei formed on their surface.

After the formation of hydrate nuclei only those which are stable grow, due to a sufficient diffusive influx of gas molecules from adjacent space. During this, a zone of decreased gas content is formed around microcrystals. If there is no source of active influx of gas molecules (a large bubble of gas, for example) then the hydrate microcrystal dissociates reforming the gas microbubbles which either coalesce or dissolve in water.

Decreased gas content zone around the microcrystal has significant dimensions and may reach the gas macrobubble. During this, a tunnel is formed in the water through which the gas molecules diffuse from the macrobubble towards the hydrate microcrystal promoting its growth (Burruss, 1995).

The tunnel is gradually filled with a hydrate needle crystal developing from the hydrate microcrystal towards the gas macrobubble. When the hydrate needle reaches the surface of the macrobubble, the touch point is the crystallization center and the free surface of the macrobubble is

quickly covered with a hydrate film isolating free gas from free water bulk where the macrobubble was formed. An interface process becomes a bulk diffusion one when water molecules diffuse through the hydrate film forming new hydrate layers (Makogon, 1974; Sloan, 1990). A simultaneous counterdiffusion of gas from macrobubble into the bulk of water forming new layers of hydrate on the outside of the macrobubble occurs.

High pressure inside the microbubbles provides a sufficient subcooling for active hydrate nucleation. Thus, local subcooling zones are formed in a bulk of water which provide the intense formation of hydrate nucleation centers.

Thermodynamic conditions of hydrate formation reaction are defined by the equation:

$$\mu_G + n\,\mu_W = \mu_H \tag{1.49}$$

where μ_G, μ_W, μ_H are chemical potentials of hydrate former gas, liquid water, and hydrate, accordingly. Reaction proceeds only if

$$\mu_G + n\,\mu_W > \mu_H \tag{1.50}$$

where μ_G and μ_W are the chemical potentials of hydrate former gas and liquid water prior to the reaction. The shape of crystals and kinetic parameters are defined by the hydrate formation mechanism and state of the system as a whole.

An important detail in formation of hydrate from microbubble is the significant increase in volume occupied by the gas bubble upon its transition into hydrate state. Figure 1-23 illustrates the schematic of gas redistribution in a volume of water during the gas transition from the dissolved to the hydrate state.

During the hydrate formation, a crystallization pressure is developed which is actively demonstrated during the crystal formation in a fixed volume, for example rock pores. The magnitude of the crystallization pressure may exceed the binding force of the carrier rock agglomerated particles.

As an example, one liter of hydrate contains 796 grams of water and 104 grams of gas. A bubble of 3.38×10^{-9} m radius formed at the hydrostatic pressure of 15 MPa and the temperature of 290 K contains 4,860 methane molecules. An elementary hydrate cavity composed of eight methane molecules and 46 water molecules has a volume of 1.77×10^{-28} m^3. Thus, the total volume of such clathrates of methane molecules contained in the bubble is 1.24×10^{-24} m^3. The volume of the considered bubble was initially 0.56×10^{-24} m^3, then the volume of a hydrate formed from the gas bubble exceeds the bubble size by 2.21 times, and the

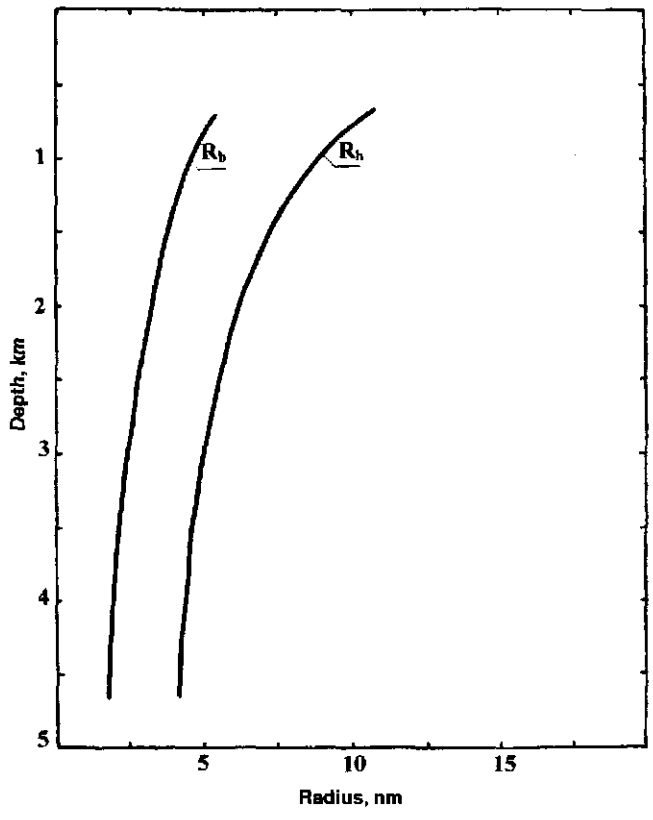

Figure 1-23 Dependence of the gas bubble radius (R_b) and of hydrate nuclei (R_h).

volume of hydrate exceeds the volume of gas bubble from which it was formed by 0.68×10^{-24} m^3. This amount of hydrate requires 4.7×10^{-16} Joules to form. Since all energy goes to the volume increase of the new formation, it follows from the energy conservation law that

$$U = P \times \Delta V, \tag{1.51}$$

where U is the energy required to form 726 hydrate unit cells (by the number of hydrate former molecules in the bubble);

- P is the crystallization pressure developed at a given hydrostatic pressure;
- ΔV is the difference in volumes of initial bubble and formed hydrate.

From which:

$$P = \frac{U}{\Delta V} = \frac{4.7 \times 10^{-16}}{0.68 \times 10^{-24}} = 6.91 \times 10^{8} Pa = 691 MPa \tag{1.52}$$

At these conditions the pressure developed during methane hydrate formation attains 691 MPa.

Based on the previous discussion, we can suggest that the natural gas hydrate nodules formation happens in the following way. A gas bubble with a radius of several nanometers which evolved or was trapped in a sufficiently large pore (10^{-4} – 10^{-6} m size) of rock, forms a primary associate of gas hydrate at appropriate temperature and pressure (both internal and external). The size of the hydrate is larger than size of the bubble, consequently the other bubbles, if present in the same pore, start to accumulate on the hydrate surface. A formed continuum is hindered by its size to leave the pore, and new portions of gas increase the volume of initial agglomeration and pressure against the pore walls increases. If the hydrostatic pressure, at a depth of 1500 m, is around 40 MPa, and a tear strength of the strongest rock does not exceed 10 MPa (on the order of magnitude) (Groysman, 1985), then the strength of pore walls is much lower than the pressure developed during the hydrate formation. The pore wall fractures, allowing inside additional gas and hydrate microcrystals. New portions of gas stimulate the volume increase of hydrate which fractures and densifies the rock around it, including pushing up the rock above it. Several cases are possible.

Mutual Solubility of Water and Hydrocarbons

Nucleation of crystals happens at the gas-water free interface. Growth of crystals and accumulation of hydrates may occur at the gas-water free interface, in the bulk of water from dissolved gas diffusing to the hydrate growth surface, or in the volume of free gas through diffusional sorption of water molecules in the saturated gas. The rate of hydrate crystals formation is determined by the intensity of diffusional and sorption processes and the effective removal of crystallization heat.

In order to determine the conditions of hydrate formation, to design a method for hydrate prevention and removal in the systems for production and transportation gases or volatile hydrocarbons, their moisture content has to be known. Several methods are available for determining the moisture content of natural gases. These are computational-analytical, direct experimental, and graphical.

A simple and reliable method suitable for engineering practice is the graphical method proposed by Mcketta (1947). This method resulted from the processing of numerous experimental data. Figure 1-24 shows the diagram for determining the moisture content of natural gas with 0.61 relative density at saturation conditions over a wide range of pressures and temperatures. Gas moisture content determination using this diagram produces an answer with less than 4% error which is quite acceptable for practical calculations.

Moisture content of gas depends on the environment with which it is in contact—liquid water in a free volume water, in a porous space of rock, or water in a solid state (ice or hydrate). Moisture content of the gas in contact with water in porous space or with ice or hydrate is always lower than in gas contacting water in a free liquid state. Moisture content of gases in contact with ice or hydrate was studied by R. Kobayashi (1955), E. D. Sloan (1976), G. D. Holder (1982), and others.

On the diagram (Figure 1-24), equilibrium moisture content curves were corrected in order to consider the gas-ice and gas-hydrate contact.

Table 1-16 gives the moisture content values for the natural gas in contact with water, ice, and hydrate.

It can be seen from Table 1-18 that the natural gas moisture content increases with temperature and decreases with pressure increase. Moisture content of gases also decreases with their increasing molecular weight and water salinity. Two graphs are present in the diagram for determining the correction factors to gas density C_γ and water salinity C_S. C_γ coefficient is applicable to all components of natural gas. Coefficients are determined using the correlations

$$C_\gamma = W_\gamma / W_{0.61} \text{ g/m}^3, \tag{1.53}$$

and

$$C_S = W_S / W_{0.61} \text{ g/m}^3 \tag{1.54}$$

where

$W_{0.61}$ is the moisture content of gas with specific gravity of 0.61 in contact with fresh water,

W_S is the moisture content of gas in contact with saline water.

Coefficient C_S is considered during calculation of natural gas moisture content in deposit conditions where gas is in contact with highly mineralized water. During moisture content calculations for a gas in pipelines where gas is in contact with nearly fresh water condensing from gas, the coefficient C_S is taken as 1.

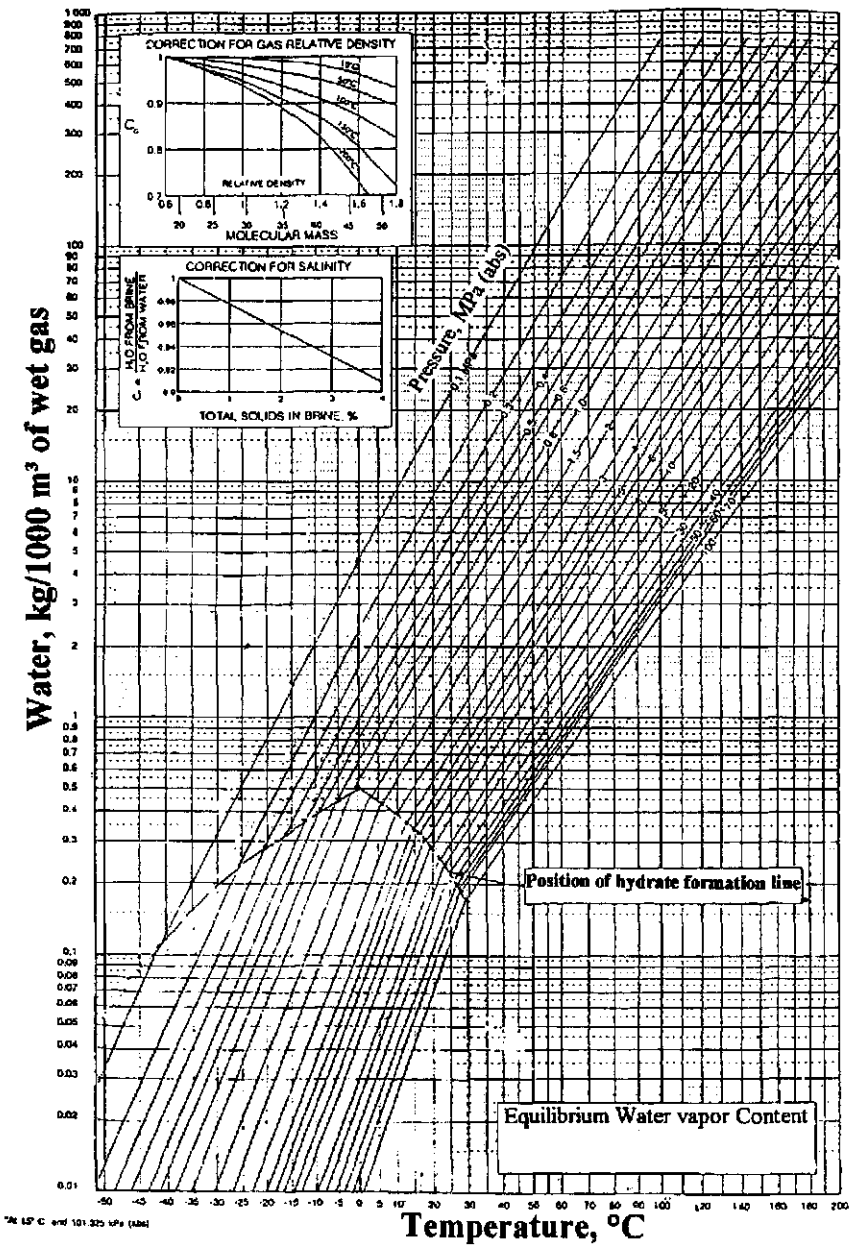

Figure 1-24 Nomogram for the determination of the water content of natural gases.

Table 1-18 Moisture content in g/m³ of the natural gas in equilibrium with water (W), ice (I), and hydrate (H) at different temperatures and pressures.

	P, MPa									
	10.0			*7.5*			*5.0*		
T,K	*W*	*I*	*H*	*W*	*I*	*H*	*W*	*I*	*H*
283	0.1651		0.127	0.1967		0.170	0.2599		0.220
273	0.0885	0.0885	0.0680	0.1041	0.1041	0.0843	0.1352	0.1352	0.1178
263	0.0457	0.0418	0.0317	0.0529	0.0485	0.0386	0.0675	0.0618	0.0529
253	0.0227	0.0185	0.0140	0.0260	0.0212	0.0168	0.0324	0.0264	0.0225
243	0.0110	0.0077	0.0059	0.0123	0.0087	0.0069	0.0150	0.0106	0.0090
233	0.0051	0.0031	0.0023	0.0056	0.0034	0.0027	0.0067	0.0040	0.0034

The presented nomogram is applicable to calculating the moisture content of sweet gases. Presence of CO_2 and H_2S increases the moisture content of gas significantly. Figure 1-25 shows the diagram for correcting the gas moisture content based on molar content of CO_2 and H_2S (Wichert, 1993). Use of the diagram in Figure 1-25 is explained in the following example.

What is the equilibrium water-vapor content of sour gas containing 30 mole % CH_4, 10 mole % H_2S, and 60 mole % CO_2 at 107°C and 8.36 MPa?

Figure 1-25 Water content for sour natural gas.

Solution:

1. Determine the equilibrium water-vapor content of sweet gas at the same condition using the chart in Figure 1-24 (approximately 14.2 kg/1000 m^3).
2. Calculate the equivalent H_2S content of the mixture by adding the mole % H_2S to 3/4 of the mole % CO2 (that is 10 mole % + 0.75 × 60 mole % = 55 mole % equivalent H_2S).
3. Enter the *SI* water-content-ratio chart (Figure 1-25) at 107°C and move to the right to the 55% equivalent H_2S line. From this point move vertically to the absolute pressure of 8.36 MPa. Move to the left side of the chart and obtain the corresponding water vapor content ratio (approximately 1.2).
4. To obtain the equilibrium water vapor content of the sour gas mixture, multiply the water vapor content ratio by the equilibrium water vapor content of sweet gas obtained in step 1 (14.2 kg/ 1000 m^3 × 1.2 = 17.04 kg/1000 m^3). Thus, the equilibrium moisture content of this particular gas is 20% higher than for the sweet gas.

Content of Dissolved Water in Liquid Hydrocarbons

Knowledge of the amount of water dissolved in liquid hydrocarbons (liquid gases, wide fraction of light hydrocarbons, petroleums) is of primary importance in view of the intensive development of oil and gas production in the polar and deep-water offshore regions characterized by harsh hydrate formation conditions. Designing of the methods for preventing hydrate formation in the product pipelines is impossible without having knowledge about water content and dynamics of phase state changing with the flow temperature and pressure. This problem is extremely complicated, insufficiently studied, and requires serious experimental and theoretical study. In large projects, usually, the necessary information on water content is obtained for the specified temperature and pressure conditions of the fluid.

Figure 1-26 presents the results of experimental determination of water content in several liquid hydrocarbons (Katz et al., 1959) These data may be used to evaluate approximately the fluids of close composition in the given pressure and temperature range.

One of the most complicated practical problems may be determination of moisture redistribution between vapor and liquid phases with a change of conditions. These conditions are pressure, temperature, composition,

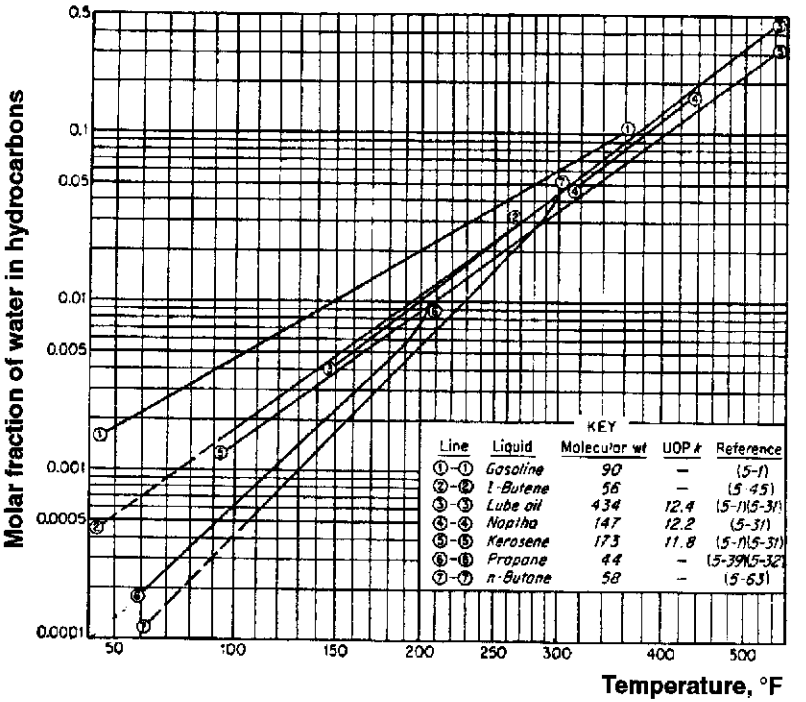

Figure 1-26 Solubility of water in liquid hydrocarbons.

and mass ratio of phases, especially in the presence of dissimilar substance injected into the flow; for example, a hydrate formation inhibitor, corrosion inhibitor or wax (paraffin) solvent. Under such conditions the W-S experimental data obtained from the analysis of in-field phases composition control are the most reliable ones.

If the thermodynamic conditions change, water dissolved in petroleum will condense and will be in a suspended dispersed state as microdroplets of 1 to 10 micrometers size. In static condition the microdroplets gradually coalesce and precipitate forming a plane mirror of liquid water saturated with gas. This liquid water, at necessary conditions may actively form hydrates both at the plane surface and at the surface of microdroplets. Formed hydrate microcrystals may have a film of condensed water or heavy liquid hydrocarbons and be carried by the flow to the separation point without coagulation. At flow stop even a small difference in a flow component's specific weight results in layering of components, coagulation, and sedimentation of hydrate microcrystals followed by plugging of the pipeline.

Figure 1-27 presents a typical pressure and temperature change diagram for a fluid flow in a layer-well-pipeline system. Figure 1-28 shows

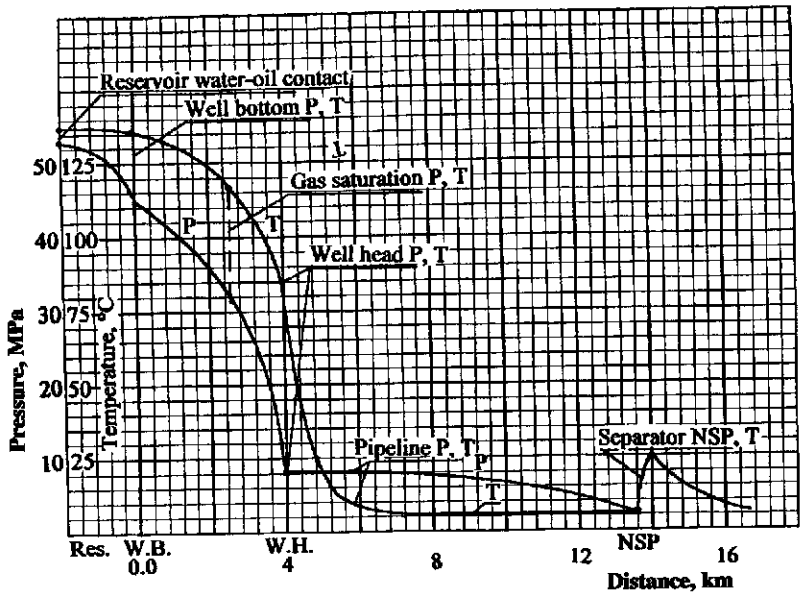

Figure 1-27 Change in fluid flow pressure and temperature in a well and in a pipeline.

a schematic of phase redistribution of water in the layer-well-pipeline system. It can be seen from Figure 1-28, that all fluid components are in a single-phase liquid state. At the bottom of the well, a condensed water appears as temperature and pressure change. The amount of this water increases with temperature decrease along the well (line A–B, Figure 1-28). With the decrease of pressure to a saturation pressure, dissolved gas evolves from oil to a free state. Part of the condensed water evaporates and saturates the free gas (line F–G, Figure 1-28). Point F corresponds to the gas saturation pressure temperature and point G to the well head pressure temperature.

In a horizontal pipeline a further decrease of temperature and pressure and a redistribution of components between the vapor and the liquid phases occurs. Part of the gas condenses, and water saturating the free gas also condenses (line G–H, Figure 1-28). As seen from Figure 1-28, close to 85% of the water dissolved in oil at layer conditions is condensed inside a well and pipeline and goes with the flow to the separator. As the temperature of the flow decreases below the hydrate formation temperature, action must be taken to prevent hydrate formation.

In a number of cases the only effective method is adding the inhibitors. Consumption of inhibitors is proportional to the mass of water in the flow. This question will be discussed in detail.

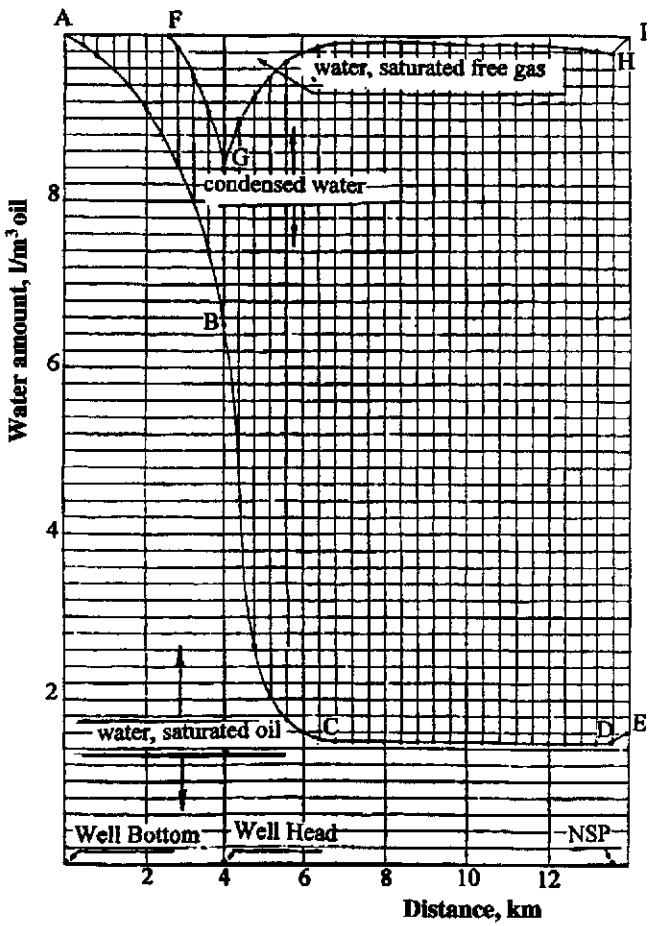

Figure 1-28 Changes of dissolved, condensed, and vapor water in fluid flow.

Solubility of Gas in Water

As shown previously, hydrate crystallization centers form and grow at necessary pressure and temperature from gas dissolved in water. Crystallization centers are formed in the bulk of water at the surface of gas microbubbles. Pressure in these microbubbles is significantly higher than in the system, as shown in Figure 1-22. The hydrate accumulation rate in the bulk of water is determined mainly by the intensity of a diffusive flow of gas dissolved in water to the crystal's surface. The driving force of the process is then the difference in the chemical potentials of gas molecules dissolved in water and those in a hydrate lattice. An area of decreased gas content is formed around the forming centers of crystallization in water.

Knowing the solubilities and chemical potentials for different gases dissolved in water and in a hydrate lattice, it is easy to calculate the rate of hydrate accumulation.

Natural gases rather actively dissolve in water even at low pressures. Solubility decreases with the increasing molecular weight of hydrocarbons. Acid gases CO_2 and H_2S increase the solubility of natural gases in water. Nitrogen, hydrogen, and helium decrease the gas solubility in water.

Content of gas dissolved in water can be determined analytically from the expression:

$$RT \ln(f_i/N_i) = RT \ln K_i + V_i (P - P_0) \qquad (1.55)$$

where

- f_i is the volatility of gas in the gas phase;
- N_i is the molar fraction of gas dissolved in water-ratio of number of moles of this component in solution to a total number of moles of water and all dissolved components;
- K_i is the Henry's coefficient;
- T is the temperature, K;
- P is the pressure;
- P_0 is the solvent (water) vapor pressure at temperature T;
- R is the gas constant;
- V_i is the partial molar volume of gaseous component dissolved in water.

Figures 1-29 and 1-30 show the dependence on temperature and pressure of methane and natural gas ($\Delta = 0.61$) solubility in water for temperature over equilibrium hydrate formation temperature (Katz et al., 1959).

In the literature there are no data for solubility of gases in water under hydrate formation conditions. At Texas A&M University the author studied solubility of gases in water under hydrate formation P-T conditions. Without reviewing the well-known principles of solubility of gases in water, we will only present some results of experimental research conducted at Texas A&M University on gas-water system in the region of hydrate formation.

During a complex study of kinetics and phase correlations of the gas-water system, it was determined that the content of gas dissolved in water decreases significantly as a result of the gas-water interface by the hydrate, and as a result of a sharp change in the surface tension forces at the gas-water and hydrate-water interface. Solubility of gas in water and supercooled water depends on the pressure and temperature (increases

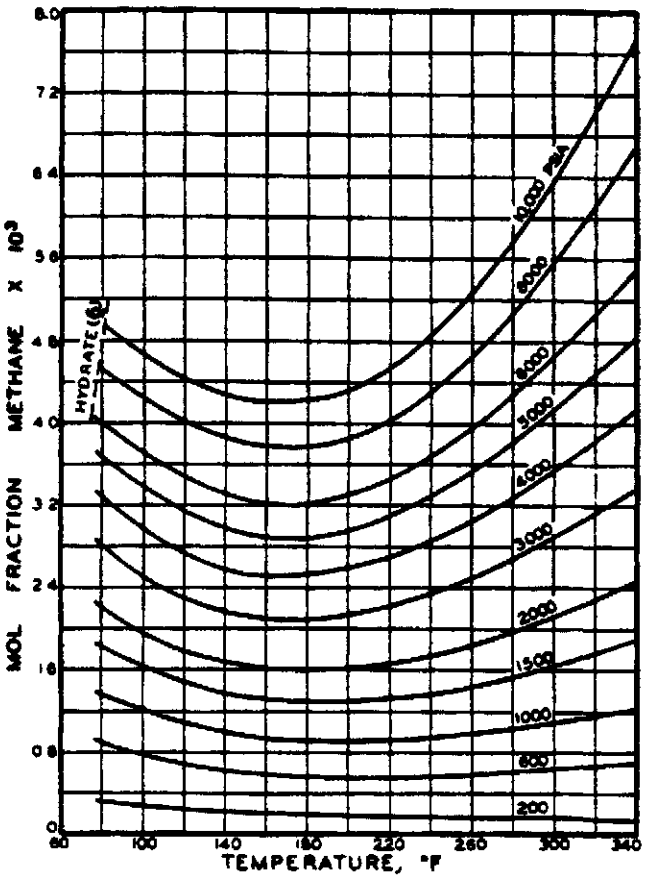

Figure 1-29 Solubility of methane in water (Katz et al., 1959).

with pressure and with lower temperature of hydrate formation and in the presence of hydrates on the gas-water surface increases with pressure and decreases with lower temperature (Figure 1-32). The content of gas dissolved in supercooled water increases with pressure and decreases with lower temperature. For constant pressure, lowering temperature increased the deficit of soluble gas in water (Figure 1-33). This data is very important for kinetic of hydrate formation in bulk volume of water or in the pore media. The process of hydrate formation always starts at the gas-water interface. After the gas-water interface becomes blocked by hydrate, the process of hydrate formation transforms from a surface-contact type to a bulk-diffusion process when hydrate crystals may grow both in bulk of liquid and in a volume of gas.

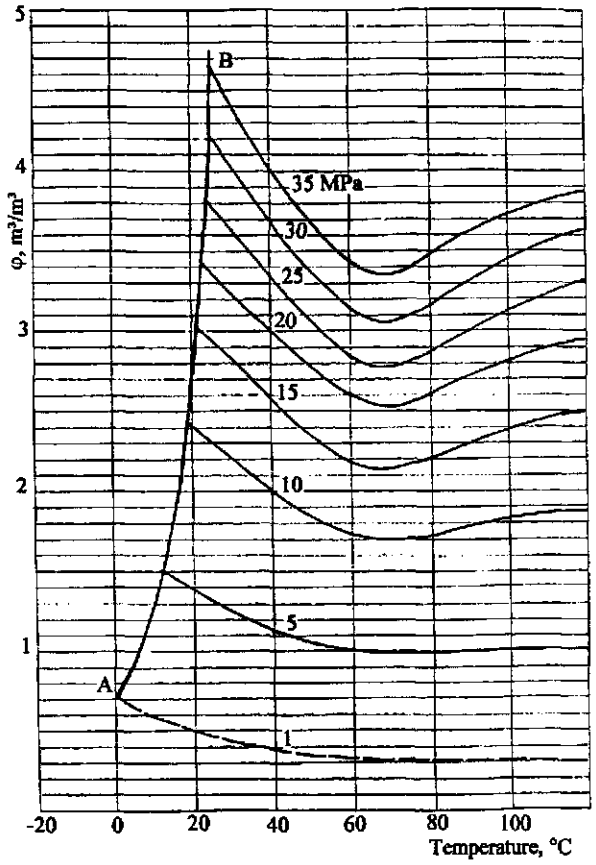

Figure 1-30 Solubilities of natural gas (Δ0.61) in water.

Figure 1-31 illustrates the same dependence for methane in water solubility for high temperature (up to 330°C) and for temperature lower than hydrate formation temperature for supercooling water. These plots show that in real conditions, gas solubility always increases with pressure. The effect of temperature is different. Up to 60–80°C solubility of gases decreases with the temperature; however, at higher temperatures, the solubility increases with the temperature.

Diagrams for solubility of gas in water (Figures 1-29 and 1-33) show a curve A-B delimiting the solubility growth with decreasing temperature. This curve corresponds to the hydrate formation conditions in the system when the structuring of water with its phase transition occurs and the gas-water molar ratio changes sharply (line CD in Figure 1-34).

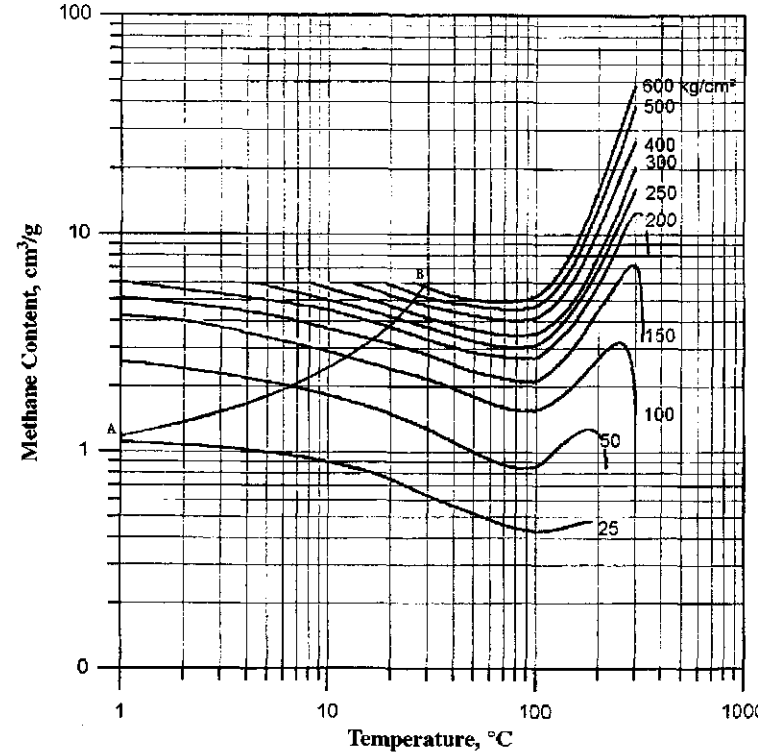

Figure 1-31 Solubility of methane in water as a function of T and P.

For example, a pressure of 2.6 MPa and a temperature of 0°C dissolves 1.2 volume of methane in a liquid water and 206.6 volume in a hydrate state. For a pressure of 10 Mpa and a temperature of 20°C, one volume of water dissolves four volumes of methane (point E in Figure 1-34). While at the same conditions in hydrate state, one volume of water binds 208 volumes of gas (point F in Figure 1-34). A specific volume of water increases by 26–32% during a transition to hydrate state and a high crystallization pressure is developed.

It is noteworthy that during the hydrate formation in water there is a flux of dissolved gas to the surface of a growing crystal. A kind of sorptional "vacuuming" of dissolved gas from water takes place. A difference in partial pressures of dissolved gas in water and at the surface of a growing hydrate crystal is the driving force that induces the diffusion of gas molecules and a crystal growth. This phenomena is very important in nature for formation of gas hydrate deposits from gases generated and

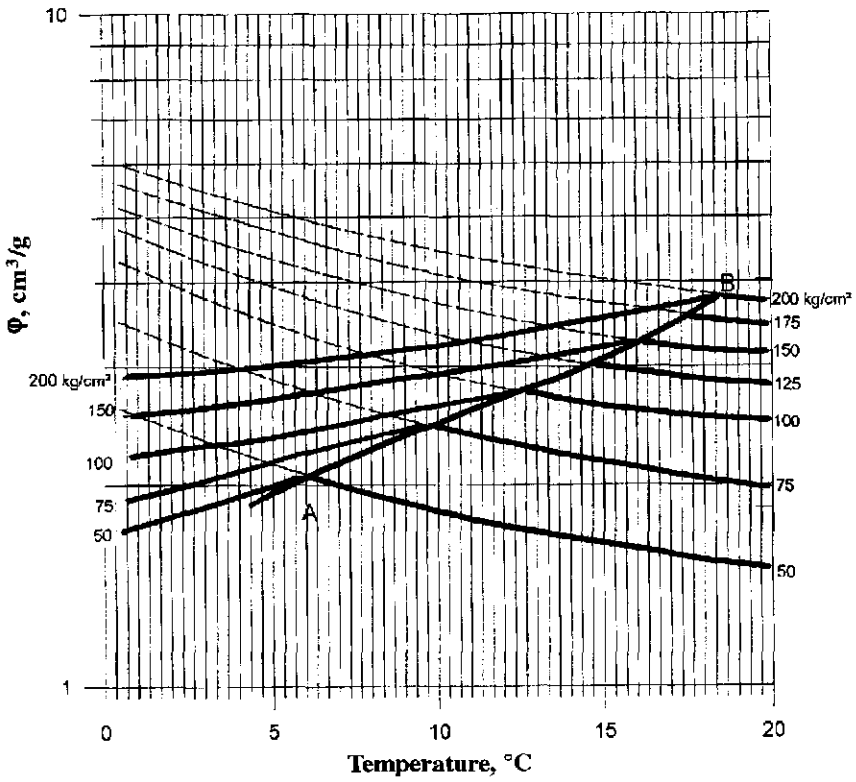

Figure 1-32 Dependence of the solubility of methane in water on pressure and temperature under hydrate film on the gas-water border.

diffusions in a pore water. Accordingly, gradient pressure-temperature and solution gases in the sedimentary rock hydrate deposits can form much quicker than natural gas fields (Figure 1-35).

Change of Moisture Content in Layer Hydrocarbons during the Field Development

A change in the moisture content of the deposit fluid during pressure changes is the key factor when choosing the system for hydrate prevention in operating wells and pipelines. Often, especially in offshore regions, the input of an inhibitor into the system is limited by the flow capacity of inhibitor pipelines. If such a pipeline was designed for the initial operation period, when the layer pressure is maximal, then after several years of operation a need may arise to decrease the production rate, to increase the inhibitor pipeline diameter, or to substitute the inhibitor for a more effective one. Most often the problem results in decreasing the oil production, which is usually unsuitable.

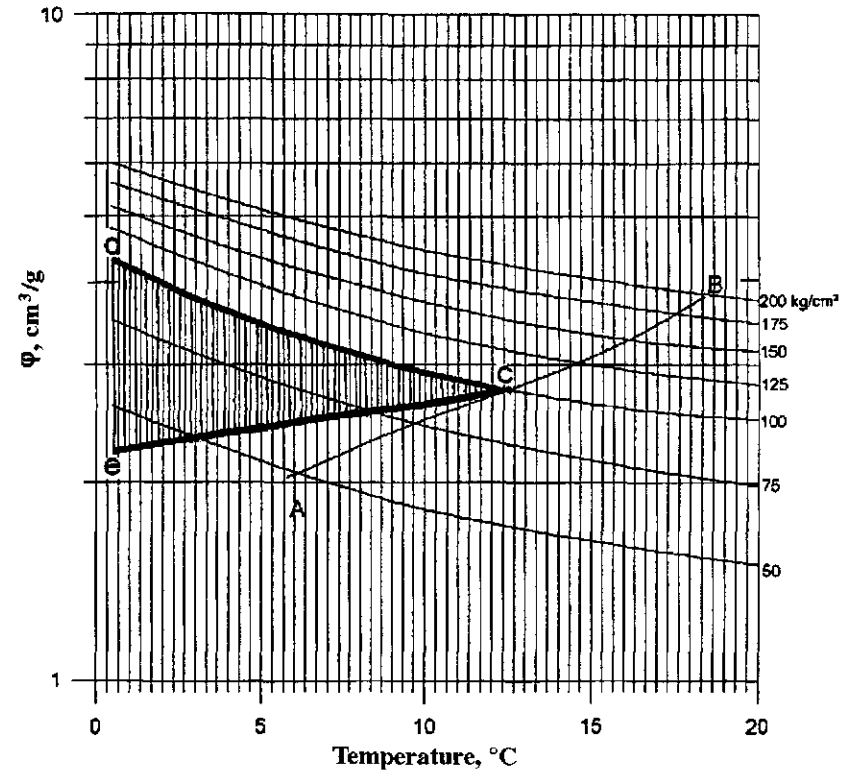

Figure 1-33 Dependence of the solubility of methane in water on pressure and temperature with a free interface *(c–d)*, and under hydrate film on the water border *(c–e)*.

Accurate knowledge about the hydrocarbons moisture content in layer conditions precludes the mistakes in selecting the hydrate prevention methods and provides more optimized regimes of system operation.

During the recovery of gas or oil saturated with gas, the layer temperature remains practically constant in most cases for at least the first few years. Pressure in the layer changes in time. Rates of pressure decrease are determined by the regime of layer operation—gas, water flooding, or combined. The highest rates of pressure drop are with the gas regime, when the gas recovery is not compensated by the energy of surrounding

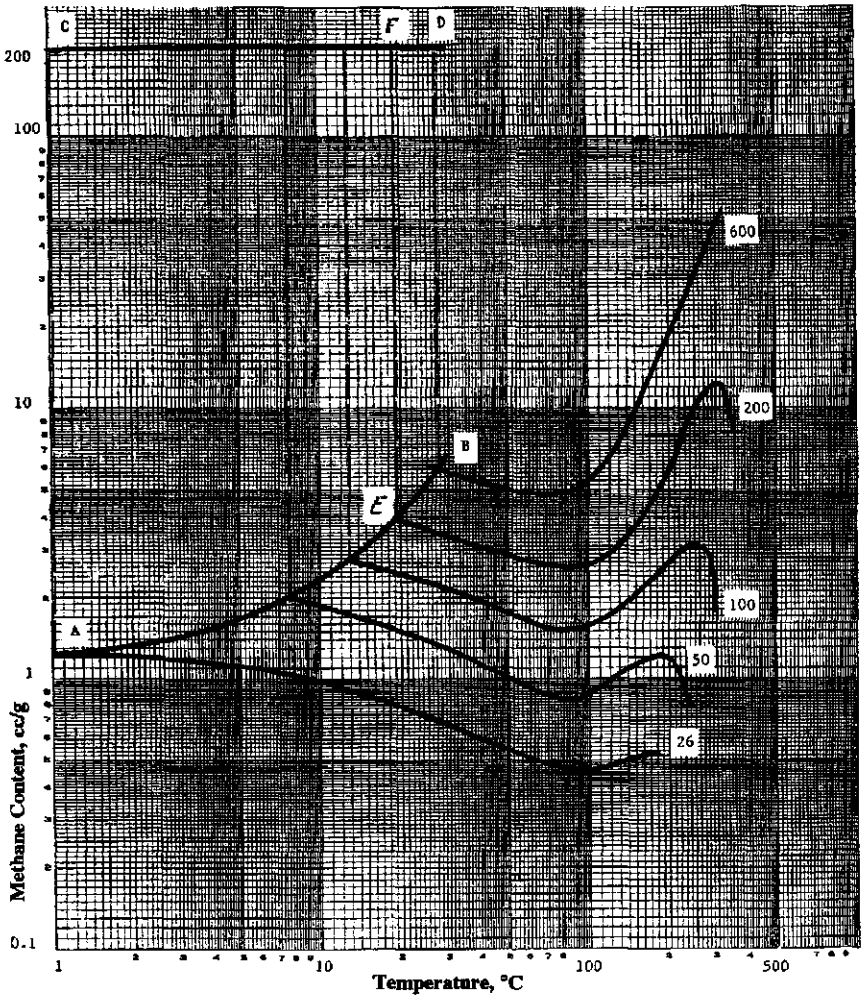

Figure 1-34 Gas-water ratio (cc/g) in liquid water and hydrate state *(C–D)* dependence on pressure and temperature *(A–B* - equilibrium hydrate formation curve).

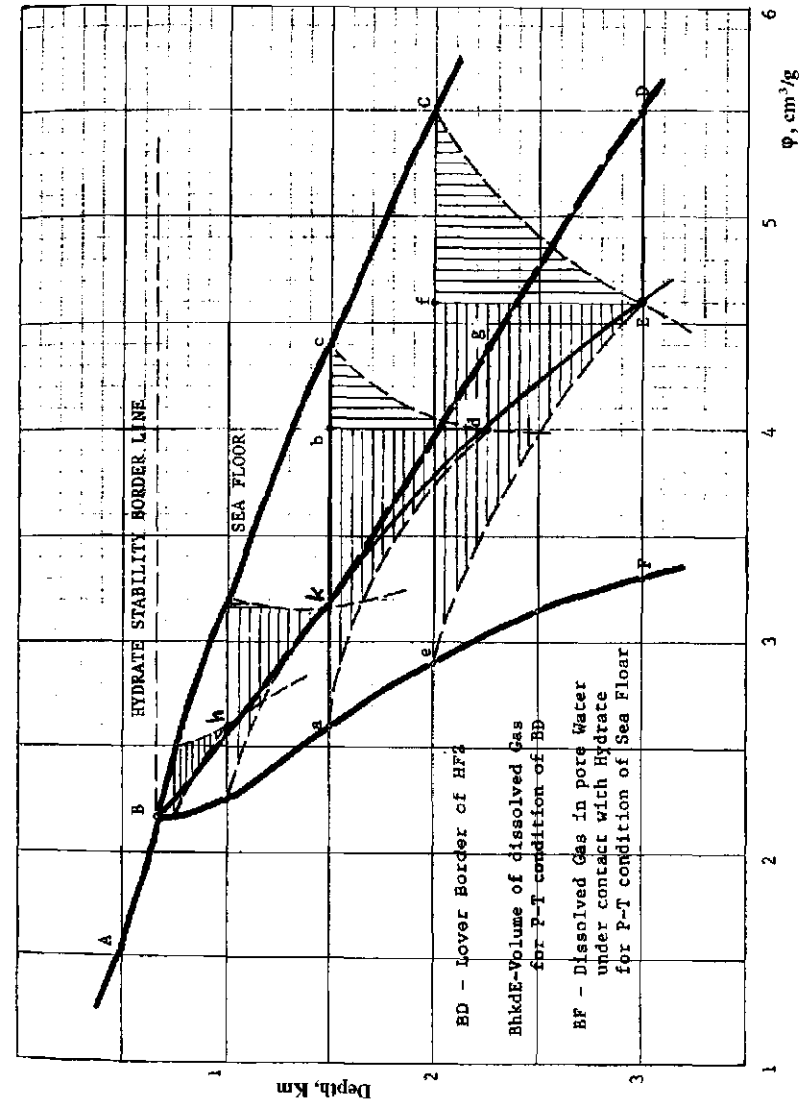

Figure 1-35 Variation of methane content in an offshore hydrate formation zone at geothermal gradient of 2°C/100m.

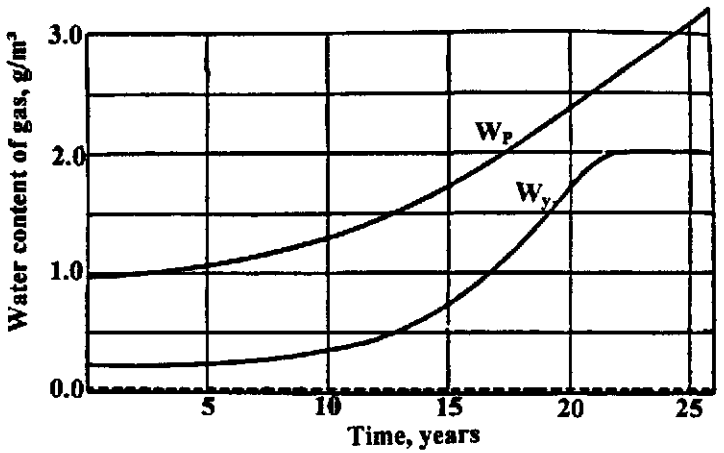

Figure 1-36 Changes in the water content of the gas during development of the gas field (W_p is water content of gas in the formation; W_y is water content of gas in the wellhead P-T).

rock. As a rule, the rate of fluid saturation with moisture exceeds the rate of pressure drop. Figure 1-36 presents the characteristic lines of change in hydrocarbons' moisture content in a layer, at a well head, and in a pipeline during the period of field development.

Formation Conditions for the Hydrates of Liquefied and Dissolved Gases

The experience of operating pipelines which carry the wide fraction of light hydrocarbons (WFLH) testifies about the presence of danger of serious complications due to hydrate formation. The problem of hydrate plugs removal came up and has been solved at all product pipelines in Russia. Measures for hydrate prevention require significant material resources.

An analysis of the literature on prevention of gas hydrates indicates that the main attention of researchers is directed to solving the problems of hydrate removal in oil and gas wells, and prevention of plug formation in the field and transportation pipelines. Only a small number of works deal with the hydrate plugs removal and prevention in the light hydrocarbons pipelines, describing only part of the problem. The literature reviews published recently, focus mainly on the details of phase equilibria for methanol-water-hydrocarbon-hydrate systems based on experimental research. Methods of hydrate prevention in pipelines currently in use are based on techniques developed during gas well and pipeline operations. In particular, the most widely used are hydrate inhibitors (methanol) and drying of gas going into the pipeline.

However, the field experience and studies show that hydrate formation in the liquid hydrocarbon transportation systems have substantial distinctions. Without consideration of these details, the traditional approach to hydrate plugging does not only have little effect, but brings negative results.

Among the main distinctions are:

- a small dependence of the hydrate of liquid hydrocarbons formation temperature on pressure;
- a substantial difference of conditions of repeated hydrate formation from gas released after decomposition of the hydrate of liquid hydrocarbons;
- an ability of the system liquid hydrocarbons-gas-released-from-hydrate to exist for a long time in pipelines.

The use of inhibitors (methanol) also has special distinctions. Mutual solubility of inhibitors, liquid hydrocarbons, and water with changing temperature and pressure of the flow require a radically different approach in selecting the method for hydrate prevention in the product pipelines.

The existing methods of hydrate plug prevention and removal handle the equilibrium state parameters of the hydrate-decomposition products system. While for the practical applications a more important factor is the determination of nonequilibrium parameters expressed in the change in time of the hydrate accumulations formation and decomposition processes. Hydrate formation is a first order phase transition accompanied by significant heat release. That is why the heat exchange analysis of the ground-product pipeline system basically must describe in the models the hydrate accumulation growth and decomposition dynamics, which have not been practically reviewed in any technique.

This section contains a generalized review of the many properties of the hydrates of liquid hydrocarbons, effect of inhibitors on the hydrate formation conditions, and details of preventing the formation and removal of hydrates from the product pipelines.

Carson and Katz (1942) suggested a prediction method based on the equilibrium constants K by analogy with vapor-liquid equilibrium. Numerical values of equilibrium constants were determined experimentally. This method was based on the idea that, with a good degree of accuracy, the gas hydrates can be considered as ideal solid solutions. Naturally, the equilibrium constants obtained from the analysis of the vapor and

hydrate phases composition are suitable for use only with that hydrate structure for which they were obtained. When applied to natural gases of high density the Katz-Carson method results in an error up to 30%.

The most general approach to the description of hydrates had been formulated in the statistical theory of the clathrate inclusion compounds. It was shown in the works of van der Waals (1959), Barrer and Stuart (1957) that the following equations are obtained from the chemical potentials equivalence condition for gas and water in the hydrate and free phases:

$$\Delta\mu_w = kT\sum_{i=1}^{2} \nu_i \ln\left(1 - \sum_{j=1}^{n} Q_{ij}\right), \tag{1.56}$$

$$\Delta\mu_i = kT \ln \frac{Q_{ij}}{1 - \sum_{j=1}^{n} Q_{ij}}, \tag{1.57}$$

where

- $\Delta\mu_w$ is the difference between chemical potentials of water in an empty hydrate lattice and in the liquid phase.;
- ν_i is the ratio of the number of type i cavities (i = 1, 2) to the number of water molecules in the hydrate unit cell;
- Q_{ij} is the filling ratio of hydrate cavity of type i with the gas component j;
- μ_j is the chemical potential of j-th component of hydrate former in equilibrium with hydrate;
- k is the Boltzmann's constant;
- T is the absolute temperature.

It is impossible to determine instrumentally the magnitude of chemical potentials for water and hydrate formers and prevent the use of Equations 1.56 and 1.57 for practical purposes. For this reason, in the work by Malyshev and Tyushniakov (1973), this system was transformed to the equations describing the equilibrium equations for the gas-water-hydrate and the gas-ice-hydrate systems:

$$\sum_{i=1}^{2} \nu_i \ln\left(1 - \sum_{j=1}^{n} C_{ij} f_j\right) - \alpha - \frac{P}{T} + \ln a = A \ln T + B + \frac{C}{T} \tag{1.58}$$

$$\sum_{i=1}^{2} \nu_i \ln\left(1 - \sum_{j=1}^{n} C_{ij} f_j\right) - \alpha' - \frac{P}{T} + \ln a = A' \ln T + B' + \frac{C'}{T} \tag{1.59}$$

where

- C_{ij} is Langmiur's constant for component j in cavity i of hydrate;
- f_j is the volatility of the j-th component of gas mixture (j = 1, 2, ..., ν), 10 × MPa;
- P is the hydrate formation pressure, 10 × MPa;
- A, B, C are the constants for each type of the hydrate structure for gas-water-hydrate system;
- A', B', C' are the constants for each type of the hydrate structure for gas-ice-hydrate system;
- a is the activity of water in the liquid state;
- T is the temperature, K.

Finding the conditions of hydrate formation with these equations is possible when constants A, B, C are determined for both hydrate structures. Experimentally obtained values of the coefficients A, B, C, A', B', C' (Tables 1-19, 1-20) provide the maximal coincidence of the calculated

Table 1-19 Values of parameters in equation 1.58 for the hydrates of structure I and II formed from gas and water (T > 273.15 K).

Type of Hydrate	*Parameter*					
	A	*B*	*C*	α	ν_1	ν_2
I	3.907	22.245	445.055	0.561	0.0435	0.1304
II	4.315	25.297	542.262	0.683	0.1176	0.0588

Table 1-20 Values of parameters in equation 1.59 for the hydrates of structure I and II formed from gas and ice (T < 273.15 K).

Type of Hydrate	*Parameter*			
	A'	*B'*	*C'*	α
I	0.755	5.050	68.785	0.317
II	0.255	1.659	28.246	0.415

and empirical dependencies of hydrate formation for pure gases and their mixtures, heats of hydrate formation, and heat capacity of hydrates.

An error in finding the temperature of hydrate formation in the pressure range up to 30 MPa (nitrogen hydrate) and 16 MPa (natural gas hydrate) does not exceed 1°C.

Equations 1.58 and 1.59 are used in the computer estimation of the parameters of hydrate formation from gas with low (under 2%) content of acid gases (CO_2 and H_2S) at pressures below 15 MPa. For the gas-condensate mixtures this computation may be used only for estimates with condensate factors below 150 ml/m³.

Equilibrium of the hydrate-liquid hydrocarbon-water system is expressed in the equality of chemical potentials of the hydrate forming components and water in different phase states. Equality of chemical potentials of water in a liquid phase is expressed through a generalized equation similar to 1.56

$$-kT\sum_{i=1}^{2}\nu_i \ln\left(1-\sum_{j=1}^{n}Q_{ij}\right) - P\Delta V + kT\ln a = AT\ln T + BT + C \qquad \textbf{(1.60)}$$

Chemical potential of the hydrate former in a hydrate cavity is described by the Equation 1.57, its magnitude in a liquid phase $\mu_j(P, T)$ is expressed by correlation (Roomer and Ryvkin, 1969):

$$\mu_{ij}(P,T) = \int_{P_B}^{P} V_{ij}dP + \mu_j^L(P_B,T) \qquad \textbf{(1.61)}$$

where

V_{ij} is the partial volume of a component in liquid phase;

P_B is the bubble point of liquid hydrocarbon at temperature T.

On the bubble line $P_B(T)$ chemical potentials of a component in vapor and liquid phases are equal, thus

$$\mu_j^L(P_B,T) = kT\ln f_j(P_B,T) + \mu_{jST}(T), \qquad \textbf{(1.62)}$$

where

$f(P_H, T)$ is the volatility of a component in vapor phase at bubble pressure $P_B(T)$.

From the condition of equality of components, chemical potentials in liquid and hydrate phases 1.59 and correlation 1.61 we obtain:

$$f_j(P,T)\exp\left(\frac{1}{kT}\int_{P_B}^{P}V_j dP\right) = \frac{Q_{ij}}{\left(1-\sum_{j=1}^{n}Q_{ij}\right)} \qquad \textbf{(1.63)}$$

After combining the Equations 1.60 and 1.63 a general correlation is obtained that expresses the thermobaric conditions of equilibrium existence of the hydrate-liquid hydrocarbon-water system:

$$RT\sum_{i=1}^{2}\nu_i \ln\left[1+\sum_{j=1}^{n}C_{ij}f_j(P_B,T)\exp\left(\frac{1}{kT}\int_{P_B}^{P}V_j dP\right)\right]$$

$$P\Delta V + kT\ln a = AT\ln T + BT + C \qquad \textbf{(1.64)}$$

To perform calculations, the values of partial molar volumes of components V_j in a liquid phase have to be known. In the first approximation the values of V_j for hydrocarbon components with critical temperatures greater than 280 K are equal to the specific volume of a pure component at a specified temperature. They correspond in the temperature range of 263 K < T < 283 K to the values for T = 273 K (Katz, Cornell, and Kobayashi, 1965) presented in Table 1-21 with a 5% uncertainty.

Partial volume of methane in liquid hydrocarbon V_H(cm³/mole) is calculated from the solvent density ρ(g/cm³) using the formula:

$$V_H = \frac{16}{0.45\rho - 0.01143} \qquad \textbf{(1.65)}$$

Hydrate formation pressure at the liquid hydrocarbon-water-hydrate equilibrium changes sharply with temperature, practically linearly. An estimate on a correctness of the calculation can be made using the Clausius-Clapeyron Equation:

$$\frac{dP}{dT} = \frac{\Delta H}{T(V_H - V_{Sdn})}$$

Table 1-21 Specific volume of liquid hydrocarbons.

Component	C_2	C_3	iso-C_4	n-C_4	*iso*-C_5	n-C_5	C_6
V, cm³/mole	71.4	83.3	100.0	97.1	112.5	111.1	128.6

The heat of hydrate formation from pure liquid hydrocarbons and water may be taken as the difference between the heat of hydrate formation from gas and water H_H and heat of gas condensation H_K. The difference of volumes in the denominator is calculated with the formula:

$$V_H - V_S = V^{\beta} - V_L - \sum_{j=1}^{n} V_j \sum_{i=1}^{2} \nu_i Q_{ij} = \Delta V - \sum_{j=1}^{n} V_j \sum_{i=1}^{2} \nu_j Q_{ij} \qquad \textbf{(1.66)}$$

The calculations indicate that the Clausius-Clapeyron Equation (*C-C*) and the Equation 1.62 produce close results for *dP/dT* for the hydrates of pure liquefied hydrocarbons (see Table 1-22). The characteristic detail is the *dP/dT* sign variation: for the hydrates of ethane, carbon dioxide, and isobutylene it is positive, whereas for the propane hydrate it is negative.

Quantity *dP/dT* for the structure II hydrates formed with the liquid hydrocarbon mixtures may vary in sign, depending on the liquid phase content of the molecules able to enter the small cavities of hydrate lattice inaccessible to propane and isobutane. At certain compositions of liquid hydrocarbons, the $dP/dT = 0$ condition can be satisfied. The $dP/dT = 0$ condition is impossible for the structure I hydrates because, in such a case, the fraction of the filled large cavities must not exceed the certain value, when the energy of interaction between the guest and the host molecules is insufficient to stabilize the hydrate lattice.

Experimental study of the pure propane and distilled water hydrate formation conditions indicated that during the first series of experiments with fresh water, the hydrate formation process happens near 273 K, and decomposition near 278.7 K. Consequent tests decreased the metastable subcooling by 2–3 K, and the temperature of the propane hydrate decomposition approached the tabulated values. The temperature differential between the formation and decomposition temperatures of the hydrate formed from a freshly double-distilled water is explained by the breaking of the hydrogen bonds characteristic for liquid water at elevated temperatures. During repeated tests there was no indication of such a significant (up to 5 K) difference.

Experiments with the liquid hydrocarbon (WFLH) (the composition is presented in Table 1-23) hydrate formation conditions indicated (see Figure 1-37) that the value of $dP/dT > 0$.

Through a similar method the conditions of hydrates formation from water and reservoir oil whose composition is shown in Table 1-24.

The bulk of hydrates formed from the reservoir oil can be easily observed (through sight windows) at the oil-water interface and is a flake-shaped gray mass. Results of the experimental study are presented in Table 1-25.

Table 1-22 Calculated values of *dP/dT* for the hydrates of pure liquids.

Component	ΔV, cm³/mol	Q_1	Q_2	V_j, cm³/mol	$V_H - V_S$, cm³/mol	$\Delta H_H'$, kJ/kg	$\Delta H_K'$, kJ/kg	*dP/dT Calculated by Equation* 1.4.7	*dP/dT Calculated by Equation* (C'–C)
C_3H_8	5.32	0	0.0582	84.0	0.379	134.4	370	–36.7	–64.2
iC_4H_{10}	5.32	0	–0.582	100.0	–0.562	138.2	353	19.8	16.2
C_2H_6	4.62	–	–	81.0	–	68.46	313.4	–	–
C_2H_4	4.62	–	–	62.9	–	63.0	314.4	–	–
CO_2	4.62	–	–	51.04	–	59.6	200.0	–	–

Table 1-23 Composition of the liquid hydrocarbon.

Sample Number	*Component Volume Fraction, %*								
	CH_4	C_2H_6	C_3H_8	iC_4H_{10}	nC_4H_{10}	C_5H_{12}	C_6H_{14}	CO_2	N_2
1	0.013	3.509	42.697	12.51	25.156	2.09	2.006	0.019	–
2	0.007	3.460	44.260	12.86	25.130	11.17	2.893	0.220	–
3	0.560	4.690	40.780	14.15	25.860	11.07	2.850	0.040	–
oil	24.6	5.87	8.82	2.65	6.14	–	–	0.32	0.80

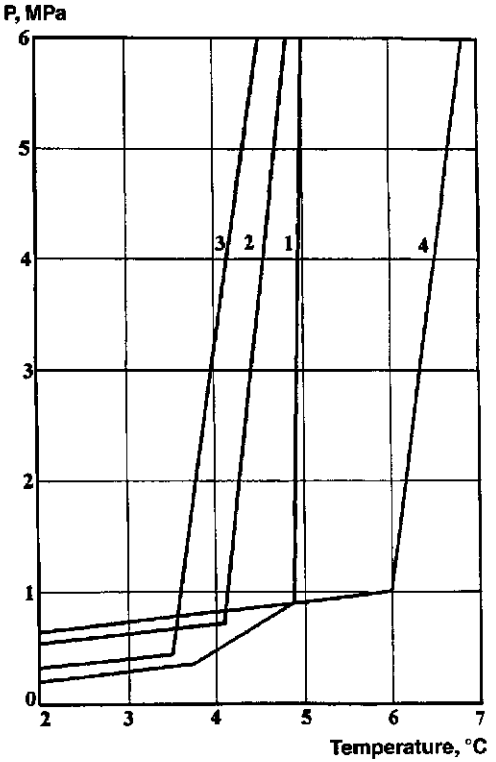

Figure 1-37 Hydrate formation conditions for wide fraction of light hydrocarbons (WFLH).

Table 1-24 Content of the hydrate forming components in the reservoir oil.

Oil Field	*Layer*	*Composition, Mole %*						
		N_2	CO_2	*Methane*	*Ethane*	*Propane*	*i-Butane*	*n-Butane*
Samotlor	AV1-2	0.64	0.06	37.9	1.21	2.93	1.25	3.24
	AV2-3	0.43	0.04	29.26	2.08	3.72	1.76	5.22
	AV4-5	0.21	0.39	33.52	1.02	2.51	1.62	2.67
	BV8	0.12	0.08	22.84	2.68	6.53	2.04	5.73
Vatinsk	AV1	0.57	0.12	21.34	0.94	2.77	2.02	4.36
	AV8	0.52	0.09	21.88	1.89	5.96	1.84	4.97
	BV5	0.30	0.06	16.4	2.10	3.41	1.86	5.14
	BV8	0.45	0.08	23.26	3.11	7.03	1.67	5.08
	U	0.63	0.77	24.14	5.13	8.30	1.47	5.41
Pravdinsk	BU6	0.80	0.32	24.6	5.87	8.82	2.65	6.14

Table 1-25 Conditions of formation and decomposition of hydrates obtained with the sample of reservoir oil.

Test Number	*Formation Conditions*			*Decomposition Conditions*	
	P, MPa	*T, °C*	*Observation Time, Hours*	*P, MPa*	*T, °C*
1	15.3	10	36	1.1	10
2	15.3	12	34	15.3	22
3	18.8	13	39	18.8	23
4	18.8	12	33	12.2	22
5	12.2	12	44	12.2	22
6	12.2	12	38	1.1	12
7	21.1	13	28	21.1	22

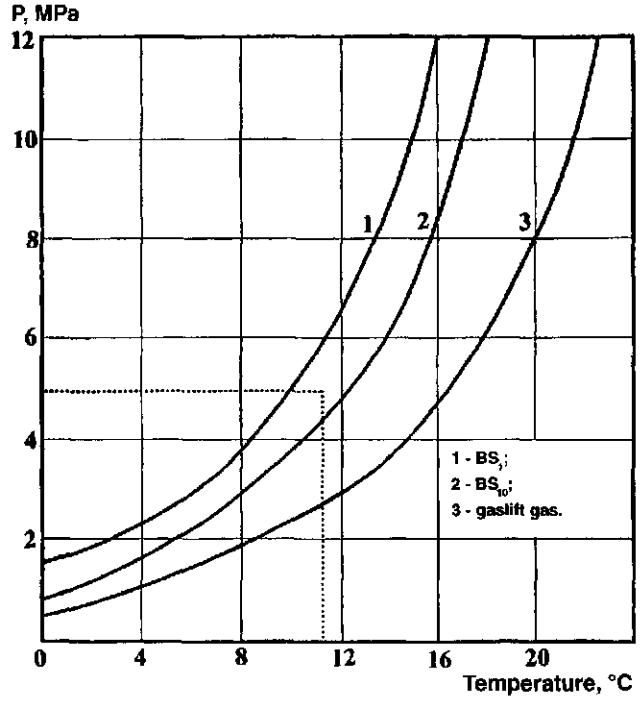

Figure 1-38 Hydrate formation conditions from water and oils of BS_1 and BS_{10} strata at the Feodorovskoe field.

Calculation of the formation conditions of hydrates with the reservoir oils from a number of the West Siberia fields whose compositions are given in Table 1-22 using the Equation 1.64 indicated that the hydrate formation pressure varies practically linearly with temperature with a positive gradient *dP/dT* (Figure 1-38). Hydrate formation conditions are presented in Table 1-26.

In order to make calculations it is necessary to determine the hydrate formation temperature at the oil saturation pressure. The calculation is made using the Equation 1.64 with $P = P_{sat}(T)$. Saturation pressure for each temperature is determined based on the constants of vapor-liquid equilibrium $K_i(P, T)$ using the formula:

$$\sum_{i=1}^{n} X_i \sum_{i=1}^{n} K_i Y_i = 1 \qquad (1.67)$$

where X_i, Y_i are the mole fractions of i-th component ($i = 1, 2, \ldots, n$) in the liquid and vapor phases, respectively.

Table 1-26 Conditions of hydrate formation at the saturation curve for oils from a number of the West Siberia fields.

Field	*Layer*	*Well No.*	T_{layer}, °C	P_{sat}, MPa at		*Hydrate Formation Conditions at Saturation Curve*			*T, at P = 30*
		No.		$T = 20$°C	T_{layer}	*P, MPa*	*T, °C*	*dP/dT*	*MPa*
Samotlor	AV1-2	2026	59	12.8	15.2	12.9	19.6	8.9	21.5
	AV2-3	2902	60	8.5	9.9	8.4	17.0	10.1	19.4
	AV4-5	1638	72	10.8	10.9	10.9	17.7	9.4	20.0
	BV8	4644	71	9.2	10.8	9.3	19.3	9.2	21.4
Vatinsk	AV1	125	68	7.0	7.6	7.0	14.4	10.4	16.7
	AV8	82	80	6.7	8.9	6.8	15.8	10.6	18.0
	BV5	80	81	5.1	5.9	7.9	13.5	11.1	15.9
	BV8	1004	91	7.5	10.1	7.4	17.5	10.2	19.8
	U	1003	90	8.9	11.9	9.0	20.4	10.1	22.5
Pravdinsk	BU6	717	82	8.8	11.6	8.8	20.5	10.1	22.6

P_{sat}—Saturation pressure, MPa

Dependence of the equilibrium constants on pressure and temperature during calculation of the oil saturation pressure are determined using the formula:

$$P_{sat}(T) = P_{sat}(20°C) + \frac{T-20}{T_{lay}-20}\left[P_{sat}(T_{lay}) - P_{sat}(20°C)\right] \quad (1.68)$$

where $P_{sat}(T_{lay})$, $P_{sat}(20°C)$ are the saturation pressures at layer temperature and at 20°C, accordingly.

Calculation of the hydrate formation conditions using the Equation 1.64 is possible only with a computer which limits its application in engineering practice. It is much simpler to determine the characteristics using the method based on the constants of gas-hydrate and gas-water phase equilibria.

It was shown earlier that in the hydrate-liquid hydrocarbon-water equilibrium region the hydrate formation pressure varies nearly linearly with the pressure-temperature gradient of 9 MPa/K or higher. In the practice of pipeline transportation of WFLH pressure in the pipelines does not exceed 5 MPa, and in the pressure range below 5 MPa, the hydrate formation temperature may be assumed to be constant, independent of pressure. Thus, it is sufficient to determine its value at one fixed pressure, for example at the WFLH boiling point $P_{sat}(T)$, which is the upper quadruple point.

In the upper quadruple point (P_0, T_0), gas, water, hydrate, and liquid hydrocarbon are in equilibrium. It is obvious that the hydrate-WFLH equilibrium constant $K_i(P, T)$ of the i-th component ($i = 1, 2, \ldots, n$) on the saturation pressure curve is expressed through the constants of gas-hydrate $K_{iH}(P_0, T_0)$ and gas-liquid $K_i(P_0, T_0)$ equilibria in an equation (Malyshev, 1985):

$$K_{iH}(P_0, T_0) = \frac{X_i}{Z_i} = \frac{X_i/Y_i}{X_i/Z_i} = \frac{K_{iL}^G(P_0, T_0)}{K_{iH}^G(P_0, T_0)} \quad (1.69)$$

where X_i, Y_i, and Z_i are the mole fractions of i-th component ($i = 1, 2, \ldots, n$) in the liquid, vapor, and hydrate phases, correspondingly.

In order to determine the upper quadruple point, it is necessary to solve simultaneously a system of equations describing the dependence of degassing start pressure on temperature and the temperature of hydrate formation from condensate on the condensate degassing start curve, which are

$$\sum_{i=1}^{n} Y_i = \sum_{i=1}^{n} \frac{X_i}{K_L^G(P, T)} = 1 \quad (1.70)$$

$$\sum_{i=1}^{n} Z_i = \sum_{i=1}^{n} X_i \frac{K_H^G(P, T)}{K_L^G(P, T)} = 1$$

In a number of works it is erroneously stated that "the process of hydrate formation in liquid hydrocarbons, including oils, occurs at high (up to 10 K) degrees of the system subcooling because of the water blockage by the waxy-paraffinic components." Note that the kinetics of origination and growth of the crystallization centers in a liquid hydrocarbons-water system are the least studied problem.

There are no principal distinctions between the crystal nucleation in gaseous and liquid phases. There are differences in the growth of hydrate crystals determined by the diffusive mass transfer characteristics of the processes, in coagulation and sedimentation of microcrystals which depend on the kinematic properties of the environment. These details are yet to be studied from several perspectives.

Hydrate composition (see Tables 1-27 and 1-28) differs significantly from the composition of the initial mixture, which stabilizes as a result of hydration. Experimental studies of the temperatures of hydrate formation

Table 1-27 Composition of liquid hydrocarbons.

Composition	CH_4	C_2H_6	C_3H_8	iC_4H_{10}	nC_4H_{10}	iC_5H_{12}	nC_5H_{12}	C_6H_{14}+
1	1.67	2.49	34.62	12.89	31.4	5.74	4.83	4.36
2	0.63	1.91	33.60	14.89	31.93	6.46	5.90	4.71

Table 1-28 Gas compositions in a hydrate formed with WFLH (volume fractions, %).

Sample Number	*Formation Conditions*		*Component*			
	P, MPa	*T, °C*	*Methane*	*Ethane*	*Propane*	*Isobutane*
1	0.40	3.5	0.12	11.40	76.68	11.80
2	0.42	5.0	0.08	10.72	76.50	12.70
3	0.55	6.5	5.30	9.96	73.62	11.02

from WFLH of these compositions indicated that the hydrate decomposition temperatures were 8.5 and 4.5°C.

An insignificant change in the methane concentration in a liquid hydrocarbons phase affects substantially its content in the hydrate phase. The increase of the methane concentration in hydrate stabilizes the hydrate structure, resulting in an elevated temperature of the hydrate formation, which was confirmed by experimental study with WFLH.

During the pretreating of the WFLH for transportation, the maximum extraction of methane from the transported product must be achieved. Special attention should be paid to the CH_4 content in the product during winter, when the product temperature is minimal and plug formation often occurs.

The characteristic property of hydrate formation from liquid hydrocarbons is the sharp difference between the gas contents in hydrate and in liquid. During the hydrate decomposition in pipelines, the gas released in large quantities cannot dissolve quickly in liquid hydrocarbon. That is why after the pipeline startup, the gas phase will eminently accumulate in the elevated parts of the pipeline that may substantially affect the flow characteristic of the pipeline.

Another detail is that the conditions of repeated hydrate formation from released gas changes significantly, and the equilibrium temperature grows with pressure. Figure 1-39 shows the dependence of the conditions of hydrate formation from gas released after decomposition of the hydrate plug formed with liquid WFLH whose composition is presented in Table 1-21. The data indicate that during plug removal, it is necessary to prevent the possibility of repeated formation of hydrate from the released gas, for example through gas venting.

For a primary estimation of the conditions of hydrate formation from a mixture of liquid hydrocarbons and water, it is essential to find the upper quadruple point temperature TK, which characterizes the intersection of dependencies of hydrocarbons saturated vapor pressures $P_{sat}(T)$ and the equilibrium pressure of hydrate formation from water and gas $P_H(T)$ on temperature T. In the first approximation the dependence $P_H(T)$ is described by the Ponomarev Equation (Degtiarev et al., 1969):

$$T = 18.47 \log P - B \qquad (1.71)$$

in which the coefficient B is calculated through the gas composition X_i on the saturation curve $P_{sat}(T)$, which is:

$$T_K = 18.47 \ln P_{sat}(T) - B(X_i) \qquad (1.72)$$

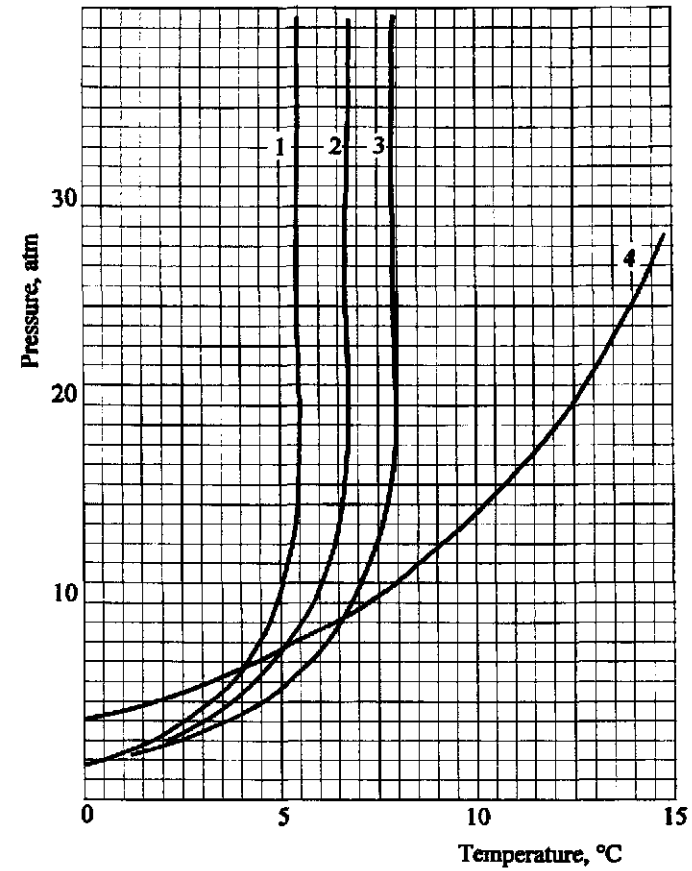

Figure 1-39 Conditions of hydrate formation with a wide fraction of light hydrocarbons at propane content (%:1-20; 2-30; 3-40; 4-equilibrium of formation of a secondary hydrate).

An analysis of the calculation results indicates that at pressures up to 7 MPa the difference during T_K temperature calculation using the Equations 1.61 and 1.69 does not exceed 1°C, however, this correlation is much simpler, and its solution does not require special computing facilities.

Gas is slightly soluble in water, thus the hydrate formation in a gas-water-liquid hydrocarbon system can be represented as the gas-water-hydrate equilibrium, when the gas composition corresponds to the gas-liquid hydrocarbon equilibrium. The hydrate formation conditions are

described by the Equation 1.58, and the gas-oil equilibrium—by the correlations using the gas-liquid equilibrium constants (Barrer, Stuart, 1957; Namiot, 1976). (The author has a universal PC program for the calculation of phase correlations in the multicomponent gas-oil-water systems. It is available to all willing to use it.) Thus the conditions of hydrate formation from water and gas-liquid mixture are described by the following system of equations:

$$RT\sum_{i=1}^{2}\nu_i \ln\left(1+\sum_{j=1}^{n}C_{ij}f_j\right)-P\Delta V+RT\ln a=AT\ln T+BT+C \qquad \textbf{(1.73)}$$

$$\sum_{i=1}^{n}\frac{Z_iK_i}{1+V(K_i-1)}=\sum_{i=1}^{n}X_i=1$$

where

V is the mole fraction of components in the liquid hydrocarbon phase;

K_i is the equilibrium constant for i-th component;

Z_i is the concentration of i-th component in the mixture;

X_i is the concentration of i-th component in the gas phase.

2
CHAPTER

PROPERTIES OF HYDRATES

Despite more than 200 years of gas hydrate history, their properties were studied very little because the research is extremely complicated. The properties of gas hydrates are determined by their composition and crystal structure. Currently more than 100 types of molecules are known to form hydrates of various structures. All these molecules, as well as some large molecules whose size does not allow them to form a stable single component hydrate, may form multicomponent hydrates.

An in-depth study of the properties of hydrates and characteristics of their formation and decomposition allows the development of new technologies based on these properties. The study of the hydrates' properties was initiated with the advent of modern measurement techniques. At the present time, hydrates are studied on a molecular level using the most advanced instruments, such as X-ray diffraction, NMR, proton NMR, infrared (IR) spectroscopy, and quantum microcalorimetry, etc.

In the 1950s X-ray structural analysis revealed the structure of gas hydrates (structure I and II). A further application of this method allowed the expansion of the class of the gas hydrate structures and showed that some clathrate hydrates have a theoretically improbable symmetry group.

Infrared spectroscopy allowed us to determine the level of molecular interactions (host-guest, host-host, and guest-guest) in the gas hydrates. This interaction, related to the vibrational, rotational, and translational motion of molecules in the gas hydrate, broadens the spectrum lines. In particular, it has been shown that for a wide range of gas hydrates the spectral characteristics of the guest molecules are practically not modified.

The paramagnetic resonance method (NMR and EPR) plays an immense role in the cycle of gas hydrate properties investigation. This method is based on the study of the hydrate sample resonance properties.

The quantum transitions occur in the sample's system of energy levels under the influence of an alternating magnetic field.

The NMR and EPR methods allow us to determine, with a high degree of accuracy, the magnitude of spin-spin and spin-lattice interactions, the character of relaxation processes in a gas hydrate, and their dependence on temperature and pressure. These methods also allow us to judge the various defects, thermal fluctuations, translation and rotation of molecules in hydrate; and to identify the enclathrated guest molecules and their concentration.

The dielectric relaxation method permitted us to increase the knowledge about internal dynamics of gas hydrates related to electrical properties (multipolarity) of gas and water molecules. In particular, the temporal relaxation constants of water and gas molecules were revealed. It was shown that these constants cover a broad range of values which depend on electrical multipolarity, its polarity, mutual geometry of the cavity, and guest molecules' fields, etc. The fact is interesting that the water and gas absorption bands are clearly separated, when they are usually distinctly spread apart.

The neutron diffraction method is used very little. It allows us to study the dynamics of the molecules participating in hydrate, and to obtain the characteristics of vibrational, rotational, and translational motion in gas hydrate. A number of works show a good match of the results from neutron diffraction and from IR spectroscopy.

The electron spectroscopy method is based on the diffraction of electrons by hydrate samples. In this spectroscopy, electrons with a well-defined energy are scattered from a target. The energy distribution and frequently the angular distribution of the electrons are measured.

Using these methods revealed a number of basic properties of hydrates of several gases which are presented briefly in this chapter.

Density of Gas Hydrates

One of the main characteristics of hydrates is density. A need for direct measurements of volume and weight at high pressures sharply complicates the ability to obtain reliable data on hydrate density. It required nearly two centuries of research on hydrates for an accurate measurement of hydrate density. Only after the study of gas hydrates structure using the NMR and EPR were the methods for calculating the hydrate density developed.

Knowing the parameters of a hydrate lattice *(a)*, the filling ratio of cavities in the structure I and II hydrates crystal lattices (α_1 and α_2) respectively, and the density of hydrate of a former gas with molecular mass *M*, we can find the density of a hydrate:

density of structure I hydrate:

$$\delta^{I} = \frac{(46H_2O + 6M\alpha_1)(1/N)}{a^3} \tag{2.1}$$

density of structure II hydrate:

$$\delta^{II} = \frac{(136H_2O + 8M\alpha_2)(1/N)}{a^3} \tag{2.2}$$

where

- M is the molecular weight of a hydrate former;
- α_1, α_2 are the filling ratios of cavities in hydrates of structures I and II, respectively;
- N is Avogadro's number;
- a is the hydrate unit cell lattice constant.

This method produces good results for equilibrium pressure at $T = 273$ K.

At higher pressures and temperatures the density of a hydrate can be determined with sufficient accuracy using Equation 2.3 which is expressed in a general form as:

$$\delta = \frac{\sum M_{hi}}{\sum V_i 18 n_i} = \frac{\sum K_i (M_{gi} + 18 n_i)}{\sum K_i V_i 18} \cdot \left[g/cm^3\right] \tag{2.3}$$

where

- M_{hi} is the molecular weight of the hydrate of *i*-th component;
- V_i is the specific volume of water in a hydrate state, g/cm^3;
- K_i is the mole fraction of *i*-th hydrate former gas component with molecular weight M_{gi} in hydrate;
- n is the ratio of the number of water molecules to the number of *i*-th component hydrate former gas molecules found from Equations 2.4 and 2.5. The magnitude depends on pressure and temperature.

For structure I hydrate:

$$n^{I} = \frac{23}{\sum_{A,B,C,K} \Theta_1 + 3 \sum_{A,B,C,K} \Theta_2} \tag{2.4}$$

For structure II hydrate:

$$n^{II} = \frac{17}{2 \sum_{A,B,C,K} \Theta_1 + \sum_{A,B,C,K} \Theta_2} \tag{2.5}$$

where

Θ_1 is the filling ratio of small cavities in hydrate lattice;

Θ_2 is the filling ratio of large cavities in hydrate lattice.

One can calculate n for all gas mixtures using the Equations 2.4 and 2.5.

Magnitude of V_i at various temperatures and pressures is found from the formula:

$$V_i = V_0(1 + 1.125 \times 10^{-4} \times \Delta t) \tag{2.6}$$

where

V_0 is the specific volume of water in a hydrate state for different gases at $T = 273.15$ K and specified pressure;

Δt is the temperature differential between equilibrium and $T = 273.15$ K.

Knowing the hydrate composition and specific volume of water in a hydrate state for different components (see Table 2-1), we can find the hydrate density at specified conditions using the Equation 2.3.

The density of hydrate increases with pressure. The densities of CH_4 and H_2S hydrates are presented in Table 2-2 at different equilibrium pressures.

Elasticity of Hydrates

Elasticity of hydrates depends on the formation conditions, composition and structure of the hydrate, degree of subcooling, and time of stabilization. Despite the importance of knowing the compressibility and strength properties of hydrates, these have not been studied much. Knowledge of the compressibility and strength characteristics of hydrates is required during the designing of methods for removing complete hydrate plugs from wells and pipelines, during the drilling of sedimentary rock in the hydrate formation zones, and during the construction and operation of engineering installations in the natural gas hydrate formation zones, to name a few.

The number of works related to the direct study of mechanical, thermal deformation parameters of hydrates and hydrate-saturated media is limited. These works were done by Parameswaran and Paradis (1985,

Table 2-1 Properties of the single gas hydrates.

Gas	*Molecular Weight g/mole*	*Dissociation Pressure at T = 237 K, MPa*	*Lattice Constant a, nm*	*Specific Volume of Water in Hydrate State at T = 273 K, cm³/g*	*Hydrate Density at T = 273 K, g/cm³*
CH_4	16.04	2.56	1.202	1.26	0.910
C_2H_6	30.07	0.53	1.203	1.285	0.959
C_3H_8	44.09	0.172	1.740	1.307	0.866
i-C_4H_{10}	58.12	0.113	1.744	1.314	0.901
CO_2	44.01	1.248	1.207	1.28	1.117
H_2S	34.08	0.096	1.202	1.26	1.044
N_2	28.01	14.3	1.202		0.995
Ar	39.95	8.7	1.202	1.26	
Kr	83.8	1.46	1.202	1.26	
Xe	131.3	0.156	1.200	1.252	

Table 2-2 Densities of hydrates in g/cm³ at equilibrium pressures.

Hydrate of Gas	*Pressure, MPa*				
	0.1	*1*	*10*	*100*	*1000*
CH_4		0.895	0.917	0.95	1.053
H_2S	1.004	1.044	1.053	1.087	

1989); Cameron, Baker and Handa (1989); and Jeanjean and Briaud (1990). Numerous works are related to the study of acoustic properties of hydrates determined by their elasticity and density.

Obtaining reliable results from the study of hydrate resiliency properties is complicated by the difficulties in producing a monolith hydrate crystal sample in laboratory conditions and in extracting the undeformed core samples during well drilling.

Hydrate properties of elasticity and strength have been studied in laboratories using the samples stable at relatively low pressures and temperatures above 263 K. Commonly, the elastic properties of hydrates are studied using the samples of pure hydrate, or using the hydrate saturated sand or sandstone cores with a hydrate saturation ratio varying between 0 and 1. A typical diameter of the cores is 25–100 mm, and length is 100–200 mm.

During the preparation of the samples for tests, its grain composition, porosity, moisture saturation, hydrate saturation, ice content, and volume and weight compositions of phases are determined. The samples are stored at the certain P-T conditions for 48–72 hours prior to the tests.

In order to correlate results of the tests, identical hydrate saturated samples containing ice were tested. Deformation and stresses in the samples depend on the magnitude, rate, and time length of applied force. Linear deformation e in time t is determined as

$$e(t) = \Delta L(t)/L_i \tag{2.7}$$

where

L_i is the initial sample length;

ΔL is the change of the sample length under pressure with time.

Mechanical stress in the sample (s) under pressure is defined as

$$\sigma(\tau) = \frac{M_a(\tau)g}{A_i}\left[1 - \varepsilon(\tau)\right] = \sigma_i\left[1 - \varepsilon(\tau)\right] \tag{2.8}$$

where

$M_a(\tau)$ is the mass applied to a sample;

g is the gravity;

A_i is the sample cross-section under pressure;

$\varepsilon(\tau)$ is the sample length change in time under pressure;

σ_i is the initial stress in a sample under pressure.

Table 2-3 Strength parameters of the samples (d = 50.8 mm, l = 108 mm).

Sample No.	$\dot{\varepsilon}, s^{-1}$	ε,%	*Strength for Sand (MPa) Filled with*	
			Hydrate	*Ice*
3	9.54×10^{-4}	1.51	16.81	17.5
4	9.84×10^{-4}	0.83	18.82	17.5
6	1.69×10^{-4}	1.79	18.00	15.2
11	1.68×10^{-4}	1.61	15.34	15.2
5	9.84×10^{-5}	1.94	16.65	14.7
10	9.84×10^{-5}	2.41	16.34	14.7
8	9.84×10^{-6}	3.06	17.22	12.3
9	9.84×10^{-6}	3.32	17.13	12.3
12	1.00×10^{-6}	4.01	16.07	10.5
13	1.00×10^{-6}	3.31	15.95	10.5

Samples were tested for axial compression at deformation rates of 10^{-6}–$10^{-3}s^{-1}$. It was found that at low deformation rates the strength of the hydrate saturated samples was less than that of samples filled with ice. At high deformation rates the strengths were practically the same. Table 2-3 presents several results of the ice- and hydrate-bearing rock testing.

Figure 2-1 shows the general dependence of the stress increase in the hydrate sample under load in time. Inflection on the stress-time curve corresponds to the stress magnitudes at which the microscopic fractures start to form in a sample. Further stress increase results in the destruction of a sample. During this, the magnitude of elastic deformation reaches 1–4% or more (see Figure 2-2). The maximum of the elastic deformation depends on the intensity of applied stress—on their magnitude and extent of application. Figure 2-3 presents the diagram of stress development in the sample during the gradual load increase.

The time of peak stress during the sample deformation increase under load can be defined as (Cameron, 1989)

$$\tau_1 = 221 \times 10^{-3}(\varepsilon)^{-0.95}, [s] \tag{2.9}$$

and

$$\tau_2 = 6.42 \times 10^{-3}(\varepsilon)^{-1.11}, [s] \tag{2.10}$$

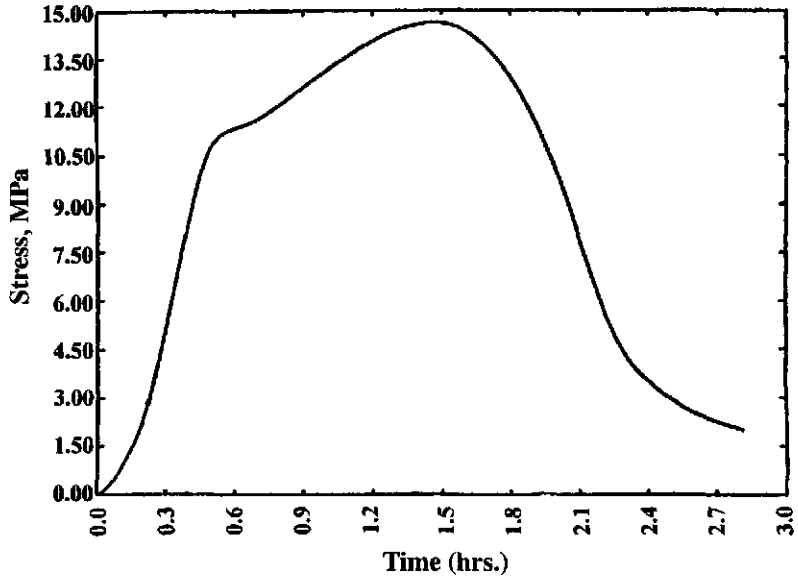

Figure 2-1 Stress for Instron Run on sample.

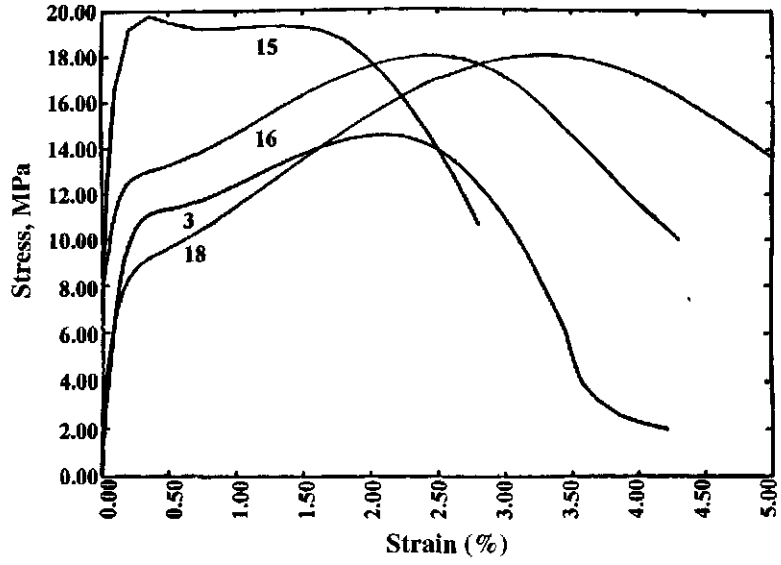

Figure 2-2 Stress-strain curves for Instron Runs.

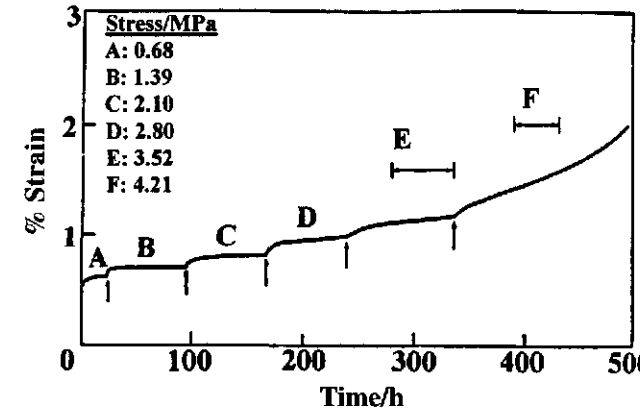

Figure 2-3 A typical creep curve for frozen sand containing THF hydrate tested at 270K. Arrows indicate an increase in stress on the sample (Parameswaran et. al., 1987).

It should be noticed that the deformation of samples depends on the load magnitude. Rate of deformation increases with load. The first peak in deformation (see Figure 2-1) is within the limits of 0.12–0.34% strain; the second peak is in the limits 0.72–3.2% strain, which corresponds to

$$\varepsilon(\tau_1) = 7.11 \times 10^{-2}(\varepsilon)^{0.0847} \tag{2.11}$$

and

$$\varepsilon(\tau_2) = 8.49 \times 10^{-2}(\varepsilon)^{0.151} \tag{2.12}$$

where $\varepsilon(\tau_1)$ and $\varepsilon(\tau_2)$ are in percent, and ε - in σ^{-1}.

The correlation between stress (σ) and deformation (ε) for the peak cases is defined as

$$\sigma_1 = 8.453(\varepsilon)^{0.151} \tag{2.13}$$

and

$$\sigma_2 = 20.42(\varepsilon)^{0.00886} \tag{2.14}$$

where σ is in MPa, and ε - in σ^{-1}.

P. Handa (Cameron, 1989) compared the strength characteristics of ice- and hydrate-saturated sandstone and obtained interesting results. At temperatures of –10°C the ice-saturated sandstone failed under a stress of P = 7 MPa, while the hydrate-saturated sandstone failed at P = 12.2 MPa.

Thus, hydrate-cemented samples are significantly stronger than ice-cemented ones.

Table 2-4 presents several parameters of the resiliency characteristics of hydrates compared with ice.

Research by Kiefte and coworkers (1985) verified the values calculated by Pearson et al., (1983) sound velocity in the hydrates of methane, propane, and hydrogen sulfide as equal to 3.3 km/s, 3.7 km/s, and 3.35 km/s, respectively.

It is noteworthy that the thermomechanical properties of the hydrate saturated rock depend on the structure and composition of the rock. It is

Table 2-4 Comparison of the properties of ice and hydrate.

		Hydrate	
Property	*Ice*	*Structure I*	*Structure II*
Isothermal Young modulus at $T = 268$ K (10^9 Pa)	9.5	8.4	8.4
Modulus of volumetric compression, units ($T = 272$ K)	8.8	5.6	–
Shear modulus at $T = 272$ K, units	3.9	2.4	–
Poisson's ratio	0.33	0.33	0.33
Time of water molecules reorientation at $T = 273$ K (ms)	21.0	10.0	10.0
Thermal conductivity at $T = 263$ K (W/m K)	2.23	0.49	0.51
Coefficient of linear thermal expansion at $T = 223$ K (10^{-5} K)	5.6	10.4	6.4
Dielectric constant at $T = 273$ K	94.0	58.0	58.0
Coefficient of adiabatic volumetric compression at 273 K 10^{-11} Pa)	12.0	14.0	14.0
Parallel sound velocity at $T = 273$ K (km/s)	3.8	3.3	3.6
Ratio of velocities (longitudinal/ transverse) at $T = 273$ K	1.88	1.95	–

difficult to consider the change in the load-carrying ability of the rock containing dispersed nodules of gas hydrates that may decompose as the temperature changes. In such cases the strength characteristics and the load-carrying ability decrease sharply.

The data are preliminary and cannot be applied completely to the natural conditions during the calculations of construction and operation of engineering objects in the hydrate-bearing rock intervals. The strength and deformation characteristics of methane hydrate, which is encountered the most in nature, have not been studied. Studies were performed only with samples containing structure II hydrate, which is relatively soft.

Electrical Properties of Hydrates

Electrical properties of hydrates are important to know during the interpretation of electrical testing results in wells which penetrate hydrate saturated rock; during the development and application of methods and means for hydrate field development; and during the hydrate formation and decomposition processes control through applying electric fields of various strength and frequency.

For the first time during experiments on the conditions of the natural gas hydrate formation and accumulation in real cores, we noted (Makogon, 1974) that the hydrate formation process is accompanied by a sharp increase in the sample's electrical resistance. During the hydrate formation cycle, electrical resistance of the core increased from 6 to 42 Ohm × m, i.e., seven fold. Thus, along with visual and thermobaric approaches, a new method of indication of hydrate formation and accumulation in a porous rock had been found.

Further investigations of the electrical resistivity of hydrates and hydrate saturated cores were performed by Pearson et al. (1983), who studied THF hydrates (structure II); Collett (1983), who measured the electrical resistance in real cores saturated with hydrates; Mathews (1985), who studied cores extracted in the Gulf of Mexico; Tzirita, who studied the THF hydrate and hydrate-saturated cores at frequencies 100 to 1000 ns^{-1}, and others.

Figure 2-4 presents the general nomogram for electrical resistance of hydrate and hydrate saturated cores. It can be seen from this figure that the scatter of resistance values is several orders of magnitude (Tzirita, 1991).

It is premature to make a generalized conclusion about electrical resistance of hydrates and to give practical recommendations on determining the

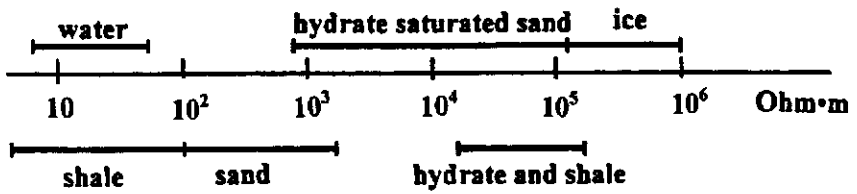

Figure 2-4 Range of electrical resistance of hydrate, sand, and shale.

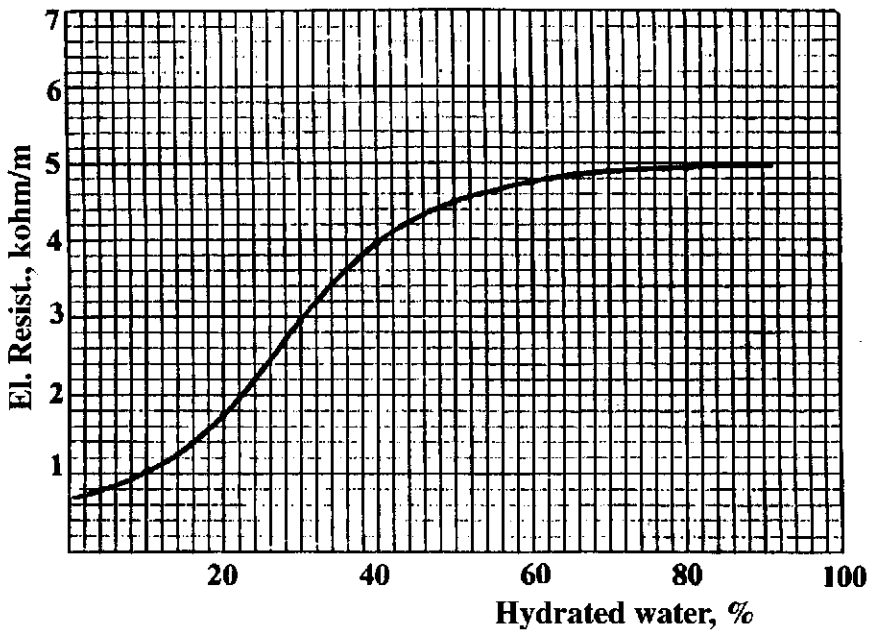

Figure 2-5 Electrical resistivity of hydrated sample.

hydrate content in layers during electrical testing of wells. A clear process of preparing the samples and finding their electrical resistance has not been developed. Electrical properties of the hydrates are yet to be studied.

Figure 2-5 shows the dependence of growth of electrical resistivity of a porous core sample saturated with gas and water as a function of its hydrate content.

Effect of Electromagnetic Field on the Process of Hydrate Formation

Electrical and magnetic stationary fields affect significantly the equilibrium formation conditions and growth kinetics of ice from water (Kachurin, 1978). Currently, there are no reliable experimental and theoretical data about the effect of these fields on a hydrate formation. Makogon (1975) indicated the effect of a stationary magnetic field on density and structure of hydrates. Denser hydrates with a more regular structure formed under the influence of a field. However, there was no complex research done on the effect of electrostatic fields on hydrate formation.

Theoretical consideration of this question is directed primarily at investigating the effect of stationary fields on equilibria. An external electrostatic field, acting on a system gas solution hydrate, changes the Gibbs potential of the system and chemical potentials of the components:

$$F = F_{E=0} + F_{E^*} \tag{2.15}$$

$$m_h = m_{h,E=0} + m_{h,E} \tag{2.16}$$

$$m_W = m_{W,E=0} + m_{W,E} \tag{2.17}$$

where

$E = 0$ means that this part of potential is equal to potential without field;

m_h and m_W are the chemical potentials of water in hydrate (h) and in a solution of gas in water (w).

Dependence of the potentials on an electrostatic field is revealed in the appearance of parts in the thermodynamic equilibrium conditions depending on the applied field and the parameters of material. Consider the hydrate-solution equilibrium in an electrostatic field. The chemical potential of water in a hydrate lattice $m_{h,E=0}$ is known from the van der Waals and Platteeuw theory (1959). In a field (E) it looks like

$$\mu_h^E = \mu_e + RT\sum_i \nu_i \ln(1-\theta_i) + \mu_{h,E} \tag{2.18}$$

where

$m_{h,E} = m_{h,E}(e_k, E, V_k)$,

where

k is the index of a component;

e is the dielectric permeability;

V_k is the volume of the type i cavity;

θ_i is the filling ratio of the type i cavity;

ν_k is the ratio of the number of type i cavities to the number of moles of water in hydrate;

m_e is the chemical potential of an empty hydrate lattice.

The chemical potential of water in a solution of gas in water in an electrostatic field is

$$\mu_W^E = \mu_W^0 + RT \ln X_1 + RT \ln \gamma_1 + \mu_{W,E} \tag{2.19}$$

where

μ_W^0 is a standard chemical potential of water without a field;

X_1 is the mole fraction of water in a solution;

γ_1 is an activity coefficient of water.

In equilibrium

$$\mu_h^E = \mu_W^E \tag{2.20}$$

from which

$$RT\sum_i \nu_i \ln(1-\theta_i) = \mu_W^0 - \mu_e + RT\ln(1-X_2) + RT\ln\gamma_1 + \Delta\mu_E \tag{2.21}$$

where

X_2 is the mole fraction of gas in solution,

$$\Delta m_E = m_{WE} - m_{hE} \tag{2.22}$$

Further, since the Langmiur's law is valid for the cavities filling ratio:

$$\theta_i = \frac{c_i f_2}{1 + c_i f_2} \tag{2.23}$$

where

c_i is the Langmiur's constant;

f_2 is the gas fugacity,

and the Henry's law is valid for the fugacity of gas above water, which looks like the following with consideration of the field:

$$f_2 = X_2 H \exp\left\{\frac{\bar{\nu}_2(P-1)}{RT} + \frac{\Delta\mu_{E,\Gamma}}{RT}\right\} \tag{2.24}$$

where

H is Henry's constant at $E = 0$;

$\bar{\nu}_2$ is the partial volume of gas in solution,

then one may write:

$$\sum \nu_i \ln\left(\frac{\theta_i}{c_i}\right) - \sum \nu_i \left\{\ln H + \ln X_2 + \frac{\bar{\nu}_2(P-1)}{RT} + \frac{\Delta\mu_{E,\Gamma}}{RT}\right\}$$

$$= \frac{\Delta\mu^0}{RT} + \ln(1-X_2) + \gamma_1 + \frac{\Delta\mu_E}{RT_1} \tag{2.25}$$

$\Delta\mu^0 = \Delta\mu_W^0 - \mu_e$

Let us denote $\alpha = \sum \nu_i \ln\left(\frac{\theta_i}{c_i}\right)$, and $\beta = \sum \nu_i$, (α»const in the P, T region of interest, b»0). Then

$$\ln X_2^\beta (1-X_1) = \alpha - \beta\left(\ln H + \frac{\bar{\nu}_2(P-1)}{RT}\right) \frac{\Delta\mu^0}{RT} \gamma_1 \frac{\Delta\mu_E + \Delta\mu_{E,\Gamma}}{RT} \tag{2.26}$$

Let us denote $X_2^\beta(1-X_1) = F_1(X_2, E=0)$, $X_2^\beta(1-X_2)\big|_{E=0} = F_1(X_2, E=0)$. Then

$$F_1(X_2, E) = F_1(X_2, 0) \exp \frac{\Delta\mu_E + \Delta\mu_{E,\Gamma}}{RT} \tag{2.27}$$

Further, since

$$\ln \frac{\theta_i}{1-\theta_i} = \ln c_i + \ln X_2 + \ln H + \frac{\bar{\nu}_2(P-1)}{RT} + \frac{\Delta\mu_{E,\Gamma}}{RT} \tag{2.28}$$

then after denoting $F_1(\theta_1, X_2, E) = \frac{\theta_i}{1-\theta_i}\frac{1}{X_2}$,

and $F_2(\theta_i, X_2, E = 0) = \ln c_i + \ln H + \dfrac{\bar{v}_2(P-1)}{RT}$

we obtain

$$F_2(\theta_i, X_2, E) = A_2(\theta_i, X_2, 0)\exp\frac{\Delta\mu_{E,\Gamma}}{RT} \qquad (2.29)$$

The effect of a field on the equilibrium of a gas-solution of a gas-hydrate system is described by Equations 2.27 and 2.28, allowing us to calculate the hydrate lattice filling as well. The numerical estimates of the field magnitude, which substantially affects the system equilibrium, produce the strength value of $E \sim 10^5$ V/cm. Notice that the presented scheme of describing the electrical field also works for describing the effect of a stationary magnetic field on hydrate formation ($E > H$, $\varepsilon > \mu$, etc.).

Heat of Formation, Heat Capacity, and Thermal Conductivity of Hydrates

The thermophysical properties of hydrate formation and decomposition processes are extremely important in all problems of the natural and technogenic gas hydrates. Regrettably, these characteristics are poorly studied and bear the pointwise rather than the generalized character. The most reliable results have been obtained through instrumental methods. Accurate experimental determinations of the thermophysical characteristics allowed us to be more precise and justify the analytical methods of calculating the heat of hydrate formation process, their heat capacity, and thermal conductivity.

The process of hydrate formation is simultaneous fixation of freely moving molecules of a hydrate former gas and water. During this process, the specific volume of water increases by 26–32% and the energy is consumed to loosen the water lattice. A specific volume of gas sharply decreases, and gas is simultaneously compressed from the ambient hydrate former pressure P_0 to the pressure of gas in a hydrate state P, accompanied by a significant change of the internal energy of a gas.

Usually, the hydrate formula is written as $M \times n\mathrm{H_2O}$, where n is the molar ratio of water and gas in a hydrate. The enthalpy of hydrate formation-decomposition is determined by the reaction

$$M \times n\mathrm{H_2O}\ (\text{solid}) = n\mathrm{H_2O}\ (\text{solid}) + M\ (\text{gas}) \qquad (2.30)$$

and

$$M \times n\mathrm{H_2O}\ (\text{solid}) = n\mathrm{H_2O}\ (\text{liquid}) + M\ (\text{gas}) \qquad (2.31)$$

Heat released during hydrate formation is one of the most important parameters characterizing both the hydrate formation process as a whole, and its elementary parts, such as consumption of molecules into cavities of a hydrate lattice and their behavior in these cavities. The thermal effect of hydrate formation is the basic parameter during the development of hydrate formation and removal techniques.

Within the boundaries of the statistical theory of hydrates, an equation expressing the heat of hydrate formation from water and gas looks like

$$\Delta H = AT - C - P\Delta V + RT^2\left(\frac{\partial \ln a}{\partial T}\right)_P - RT^2\sum_{i=1}^{2}\nu_i\sum_{j=1}^{n}Q_{ij}\left(\frac{\partial \ln C_{ij}}{\partial T}\right)_P \qquad (2.32)$$

$$\Delta H' = A'T - C' - P\Delta V' + RT^2\left(\frac{\partial \ln a}{\partial T}\right)_{P'} - RT^2\sum_{i=1}^{2}\nu_i\sum_{j=1}^{n}Q_{ij}\left(\frac{\partial \ln C_{ij}f_j}{\partial T}\right)_{P'} \qquad (2.33)$$

Magnitudes of the coefficients A, B, C, and V were defined earlier and presented in Chapter 1.

An analysis of the Equations 2.32–2.33 indicates that the heat of hydrate formation equals the sum of heats of an empty hydrate lattice decomposition with an account for an increase of the water molar volume $A'T + B' - P(V_H - V_L)$, a solvation of gas in water released after the hydrate decomposition $RT^2(\partial \ln a/\partial T)_P$, an incorporation of a molecule of the j-th component in the i-th type cavity from an expanded state of the phase $RT^2(\partial \ln C/\partial T)_P$, and the transition of gas from an expanded state to the equilibrium pressure $RT^2(\partial \ln f_i/\partial T)_P$.

As a rule, the heat of hydrate formation is determined from the Clausius-Clapeyron Equation (Davidson, 1973)

$$\frac{dP}{dT} = \frac{\Delta H_{KH}}{T(V_H - V_D)} \qquad (2.34)$$

where V_H and V_D are the volumes of hydrate, and of the products of its decomposition, respectively.

The absence of precise experimental studies on the heat of hydrate formation from gases of variable compositions does not allow us to estimate directly the accuracy of the ΔH calculation using Equation 2.32. Most often the Clausius-Clapeyron Equation 2.34 is used in order to find the heat of a hydrate formation.

The characteristic difficulty of using the Equation 2.34 for practical calculations is the indefinite volume difference $\Delta V = V_H - V_D$, which is described with sufficient accuracy within the statistical theory of hydrates through the filling ratio of cavities Q_{ij}:

$$\Delta V = V_H - V_D = V^{\beta} - V_L - \sum_{i=1}^{2} \nu_i \sum_{j=1}^{n} Q_{ij} \frac{ZRT}{P} \qquad (2.35)$$

where

Z is gas compressibility.

The Clausius-Clapeyron Equation is applicable to the calculations of hydrate formation heats of pure gases and mixtures of gases and liquids. Compositions of hydrate formation differ in the solid and in free fractions. That is why the difference of volumes $V_H - V_D$ is only approximately described by the Equation 2.32. The main drawback of the Clausius-Clapeyron Equation, with respect to the calculation of heat of hydrate formation from mixtures, is the impossible task of considering the heat of mixing of hydrate former during a hydrate decomposition. This heat mixing is taken into account in Equation 2.32 in the term $RT^2(\partial \ln f_i/\partial T)_P$.

From a technological viewpoint, the heat of hydrate formation related to a mole of water in a hydrate ΔH is more informative than the quantity $\Delta H'$ because of a small variation in hydrate lattice volume with pressure and temperature (below 5%), and a possibility of a direct use during the thermophysical calculations for a removal of the hydrate plugs of known volume. At the same time $\Delta H'$ is more representative during the development of measures on mastering gas hydrate deposits, since it describes the energy consumption per mole of produced gas. That is why the engineering practice needs operative methods for estimating both parameters.

Accuracy of magnitudes of the heat of hydrate formation obtained from the Equation 2.32 is quite acceptable for engineering calculations. The mean deviation from the values obtained with precise experimental methods is about 3%.

Experimental values for the heats of hydrate formation (decomposition) of hydrocarbon gases at T-273 K are (Handa, 1986)

CH_4	18.1 ± 0.3 kJ/mole
C_2H_6	25.7 ± 0.3 kJ/mole
C_3H_8	27.7 ± 0.3 kJ/mole
i-C_4H_{10}	31.0 ± 0.2 kJ/mole

and at $T > 273$ K

CH_4	54.2 ± 0.3 kJ/mole
C_2H_6	71.8 ± 0.4 kJ/mole
C_3H_8	129.2 ± 0.4 kJ/mole
i-C_4H_{10}	133.2 ± 0.3 kJ/mole.

The heat of hydrate formation from liquid hydrocarbons and water may be represented as the sum of a heat of lattice crystallization ΔH_l, the heat of gas molecules transition from an expanded state into the liquid phase ΔH_L, the heat of gas molecules transition from an expanded state into a hydrate lattice ΔH_T, i.e.,

$$\Delta H_H = AT - C - P\Delta V - RT^2 \sum_{i=1}^{2} \nu_i \sum_{j=1}^{n} Q_{ij} \left(\frac{d \ln C_{ij}}{dT} - H_{Li} \right) \qquad (2.36)$$

Definition of the filling ratio Q_{ij} was discussed previously.

For pure liquids the quantity H_{ij} depends on the temperature and practically does not vary with pressure. For example, for liquid propane at $T = 280$ K with pressure increase from 3.5 to 20 MPa, H_{ij} increases by 2% (Reed and Sherwood, 1971).

Figure 2-6 shows the dependence of the heat of hydrocarbon hydrates phase transition, from which it is seen that it weakly depends on temperature.

When the hydrates form from a mixture of liquid hydrocarbons, and the compositions of liquid and hydrate phases are different, then during the calculation of heat of hydrate formation a heat effect of the solvation in the liquid hydrocarbon phase of the components evolution during a hydrate decomposition has to be considered. Methods of calculation were presented in the works of Katz (1959), Katz, Cornell and Kobayashi (1965), and Reed and Sherwood (1971).

Heat of solvation can be determined using the additivity rule:

$$H = \sum_{i=1}^{n} X_i \times \Delta H_i(T) \qquad (2.37)$$

where

X_i is the concentration of the i-th component in hydrate, mole fraction;

$\Delta H_i(T)$ is the heat of condensation of a pure i-th component at temperature T.

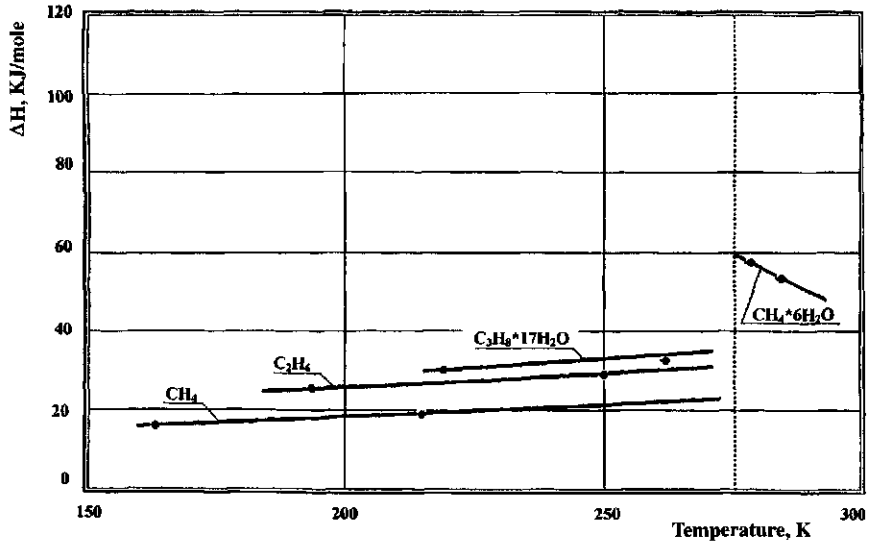

Figure 2-6 Heat of formation/decomposition of hydrates.

For the approximate calculations of the heat of hydrate formation (kJ/mole of gas) from natural gases at $T > 0°C$ the following expression can be used:

$$\Delta H = 33.44n[(1 + 2475g)T + 282.5 - 42.12g] \quad \textbf{(2.38)}$$

where

- g is the relative density of gas with respect to air;
- T is the temperature of a hydrate formation process, °C;
- n is the molar ratio of water and gas in hydrate.

Heat Capacity of Hydrates

Heat capacity of hydrates is one of the major thermodynamic parameters determining the technology of their accumulation, decomposition, and structural characteristics, etc. The heat capacity of hydrates depends on the composition and type of hydrate and on the pressure and temperature.

Heat capacity of any substance can be determined by the double differentiation of its free energy by temperature at a constant volume

$$C = -T\left(\frac{d^2F}{dT^2}\right)_{V,Q_{ij}} \quad \textbf{(2.39)}$$

For stable existence of a gas hydrate, the constant volume can be interpreted as the invariability filling ratio of the hydrate lattice with gas molecules quantities Q_{ij}. It was shown previously that the free energy of a hydrate containing one mole of water and enclathrated gas is expressed by the Equations 1.2 and 1.3.

Differentiating twice this expression on temperature at constant Q_{ij} and considering the condition 2.32, we obtain:

$$C = C^{\beta} + RT\sum_{i=1}^{2}\nu_i\sum_{j=1}^{n}Q_{ij}\left[\frac{5}{2T} + \frac{d^2T\ln C_{ij}}{dT^2} + \frac{n}{2T} + \frac{d^2T\ln Z_{ij}}{dT^2}\right] \quad \textbf{(2.40)}$$

where $C^b = -T(d^2F/dT^2)$.

Heat capacity of an ideal gas is equal to

$$C_P^0 = \frac{5+nj}{2}R + RT\frac{d^2T\ln\Phi_j}{dT^2} \quad \textbf{(2.41)}$$

Solving Equations 2.32 and 2.33 with 2.34, we obtain the equation for determining the heat capacity of a hydrate:

$$C_H = C^{\beta} + \sum_{i=1}^{2}\nu_i\sum_{j=1}^{n}Q_{ij}(C_{Pj}^0 + Rq_{ij}) \quad \textbf{(2.42)}$$

The molar heat capacity for the hydrates of hydrocarbon gases can be found from the expression 2.42 (Handa, 1986)

$$s_{p,m} = a + bT + cT^2 + dT^3, \text{ [J/mole} \times \text{K]} \quad \textbf{(2.43)}$$

where a, b, c, and d are the coefficients presented in Table 2-5 for different gases and temperatures.

Table 2-5 Value of coefficients a, b, c, d.

Gas	*T, K*	*a*	*b*	*c* × *10²*	*d* × *10⁵*	*s, J/mole* × *K*
CH_4	85–270	6.6	1.454	–0.364	0.631	0.8
C_2H_6	85–265	22.7	1.872	–0.536	1.076	1.0
C_3H_8	85–265	–37.6	4.86	–1.625	3.291	1.9

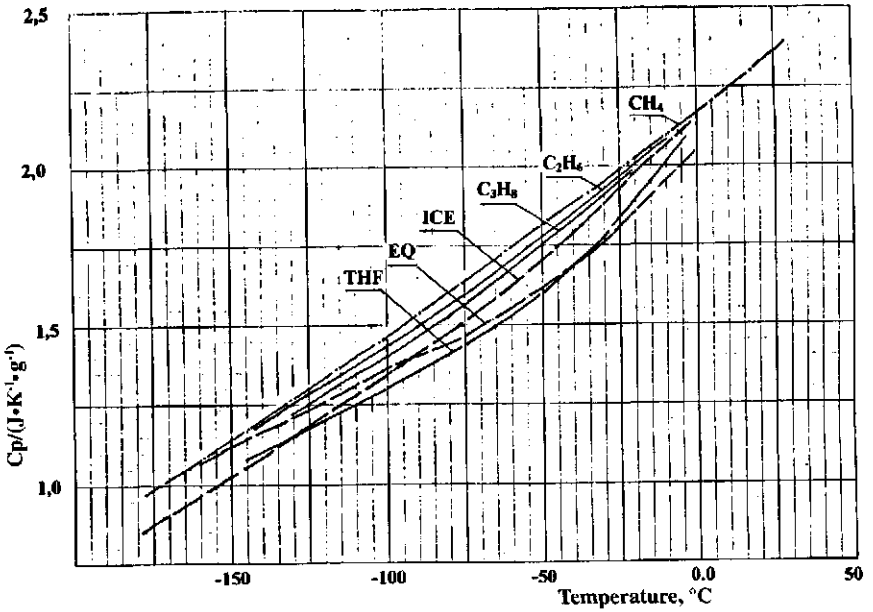

Figure 2-7 Specific heat capacity C_p of bulk ice and hydrates.

Figure 2-7 presents the curves of the hydrate heat capacity change with temperature.

Thermal Conductivity of Hydrates

Studying the thermal conductivity of hydrates is extremely important during the development of thermal methods of treatment of hydrate-saturated deposits for gas production; during the removal of hydrates in the technological systems of gas production, transportation, and processing; and during the climate calculations.

The theory of thermal conductivity in solids presumes that heat is transferred mainly by the transverse acoustic phonons. That is the reason why a number of works have appeared stating that the thermal conductivity of hydrates is close in magnitude to that of ice. However, the experimental studies of Davidson, Handa, Stoll, and others showed a difference.

Figure 2-8 presents the results of an experimental study on the thermal conductivity for hydrates of methane and several other gases, as well as for ice and water at various temperatures and equilibrium pressures. From

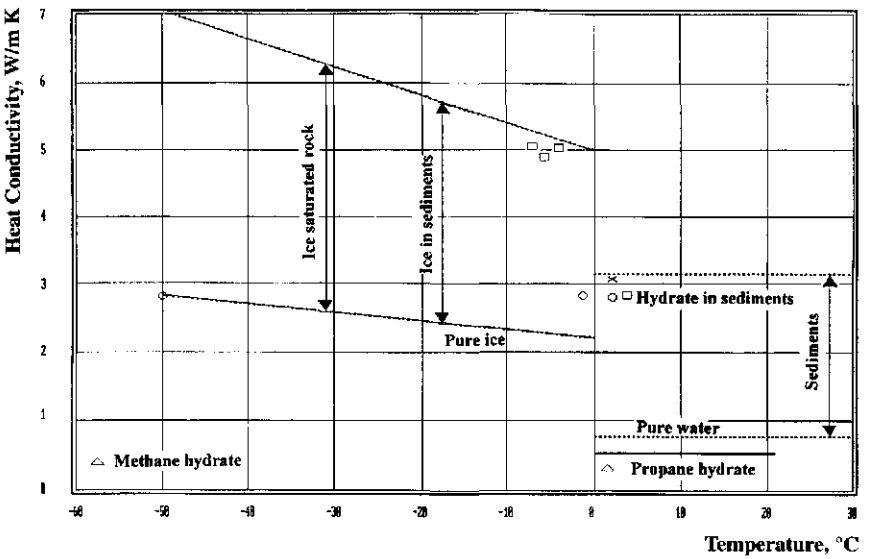

Figure 2-8 Heat conductivity of hydrate, water, and ice.

this figure, it is shown that the thermal conductivity of hydrates is close to that of water and slightly increases with temperature. Thermal conductivity of ice at $T = 0°C$ is four times higher than that of hydrate and decreases significantly with temperature. Already at $T = -80°C$ the thermal conductivity of ice is 7.5 times higher than that of a methane hydrate.

These results indicate that further research of the thermal conductivity of hydrates of pure gases and natural gas mixtures, and of the hydrate-saturated rock at various pressures and temperatures is extremely important.

3
CHAPTER

THE MECHANISM OF HYDRATE FORMATION

Experimental Methods of Studying Crystal Hydrates

Everything that is known about the process of gas hydrate formation and its properties has resulted from experimental studies. Several of the relationships were given an analytical description which is based on commonly known statements and empirical coefficients. The current level of knowledge about the structure and energies of intermolecular bonds in complex multicomponent systems is not sufficient to allow the development of an accurate theory of hydrate crystal formation and to predict hydrate properties.

Today researchers use dedicated experimental apparatuses and appropriate techniques to study various gas hydrate parameters. A majority of apparatuses constructed before the 1990s are based on a cell of a known volume. The pressure, temperature, and composition of a studied fluid are known and its consumption can be controlled. The hydrate formation and decomposition processes may be observed visually. Operating pressure in such cells varies between several MPa and 1200 MPa. In the near future the Institute of Inorganic Chemistry of the Siberian Branch of the Russian Academy of Sciences will put into operation the visual cell rated to 2,200 MPa. The operating temperatures can range from that of liquid helium to about 350 K. Volumes of cells range from several cm^3 to several liters. The most common volumes are 200 to 700 cm^3 and the pressures of 20–70 MPa.

A majority of researchers study the hydrate formation conditions in dynamics, simulating the real gas-liquid flows by bubbling the hydrate former through a layer of water, or by mechanical shaking, mixing, etc. This creates a gas-water or a gas-aqueous solution of inhibitor interface.

However, the processes of hydrate crystal nucleation and growth, coagulation, and sedimentation of the growing hydrate crystals are determined by many variable factors which are more difficult to consider in the dynamics of a flow. Thus, the interpretation of results is often controversial and unconvincing.

Location of Hydrates Formation

Gas hydrates may form in any location where a free gas, water, the appropriate temperature and pressure exist—in space, in the atmospheres of planets, inside the planets, and in the technical systems of production, transportation, and processing of gases. In real conditions, the technological hydrates form in the layer prior to putting the development of a deposit in the well-bottom zone of a layer, if the deposit is located in the hydrate formation zone. Hydrates also form when the fluid temperature falls below the equilibrium temperature as a result of large depressions, or during the pumping of water having a temperature below hydrate equilibrium into the well bottom zone of a gas or a gas-oil well.

Hydrates may form in the well bottom in a column of production pipes, especially if the throttle devices are present in these pipes, in the annular space, and in the christmas-tree equipment. The startup period is the most hydrate prone when the wellbore is cold.

During the long shutdown of wells in Northern or offshore fields, the forming hydrates may completely plug the wellbore, even destroy the well construction under certain conditions and result in an emergency fountain. Hydrates may form in any section of the technological line of gas collection and pretreatment, in the long distance transportation systems, and in the underground storage and distribution of gases and a wide fraction of liquid hydrocarbons.

In order to determine the location of hydrate formation, one has to know the gas composition, salt content of water, and the vapor composition in the gas phases before and after the hydrate formation, equilibrium pressure and temperature conditions of hydrate formation, and the effective change of pressure and temperature. During the lowering of the temperature below equilibrium, hydrates will form and start to accumulate. In a gas pipeline several hydrate plugs may form in a series. Intensity of the hydrate accumulation is determined by many factors, the most important being the state of water, the degree of subcooling and turbulence of the flow, rate of a gas-water free interface formation, intensity of hydrate formers diffusion, and other factors.

Mechanism of Formation and Types of Gas Hydrates Crystallization

The process of gas hydrate formation, as with any crystallization process, comes in stages—from birth of the crystallization nuclei through the growth of crystals to critical size. Crystals can be massive and whiskery. Massive crystals grow by surface sorption of gas and water molecules. Whiskery crystals grow by tunnel sorption of gas and water molecules. Formation of the hydrate crystallization nuclei usually happens at the gas-water free interface. Growth of the hydrate crystals in the presence of crystallization nuclei can occur at the gas-water interface (surface film hydrate), and in the volume of gas or in the volume of water (volumetric—diffusional or whiskery hydrate growth process). The surface contact growth of the hydrate is characterized by a relatively high rate whose magnitude is determined by the kinetic parameters and the intensity of removal of the heat released during the crystallization.

The diffusive flux of the gas and water molecules through the layer of a forming hydrate is also a determining factor, depending on the phase state of the medium where the hydrate crystal growth occurs—at the gas-water free interface, in the volume of gas, or in the volume of water. The formation rate of a hydrate at the gas-water free interface, where the water and gas molecules are available in excess directly at the surface of the sorptional formation, is the highest.

The mechanism of the hydrate formation process is rather diverse and has been studied the least in the multifaceted problem of gas hydrates. The process of formation of crystallization nuclei may happen only at saturation (possibly local) of gas with the water vapor, or saturation of water with gas. Two cases are then possible: water is in the single phase vapor state, and water is in the two-phase state—liquid-vapor and ice-vapor. The process of the hydrate growth on the formed nuclei may occur both at water vapor saturation, and at incomplete saturation when the water vapor partial pressure is higher in the vapor phase than the partial pressure above the hydrate.

Formation of the hydrate crystal nuclei is discussed in Chapter 1. The gas-water interface during the precrystallization period is a structural surface of single boiling clusters. Depending on the thermodynamic characteristic of the gas-water interface, the clusters of water molecules are in a metastable state (Figure 3-1). The adsorbed molecules of gas are located between the separate clusters of water. The maximum gas-water molar ratio is located at the gas-water interface and the surface layer is saturated with the gas molecules. In turn, the gas medium in immediate contact with water is supersaturated with the water molecules leaving the bulk of

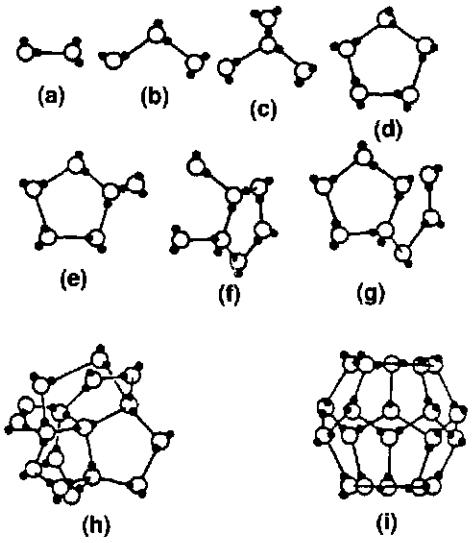

Figure 3-1 Form of water molecule aggregates.

liquid because of its kinetic energy and returning back because its energy is not high enough.

Thus, at the gas-water interface a "boiling" transitional layer is located where both water and gas exist in a supersaturated state. During the creation of the appropriate thermodynamic conditions, this layer is where the crystal nuclei form, and the water and gas molecule orientation is fixed in their crystalline state. As the difference between the chemical potentials of water and gas further increases, the hydrate formation process occurs through simultaneously-consequential adsorption of the gas and water molecules. (Layers of the crystal unit cells continue to grow.) The process of a hydrate film formation at the gas-water interface continues until the complete coverage of the water surface.

Formation of the crystal nuclei occurs at the following interfaces:

- liquid water to gas, liquid water to liquid gas, or ice to gas
- at the surface of water film and droplets condensed in the volume of gas
- at the surface of gas bubbles emerging in the volume of water
- at the surface of dispersed liquid gas droplets saturated with water vapor and evaporating in the volume of gas
- at the water to metal interface where the gas molecules dissolved in water adsorb

An intensive formation of the crystal nuclei at the metal-water interface (without the visual presence of free gas bubbles) takes place during the formation of hydrate from water which comes from melted ice frozen in the presence of liquid gas. The adsorbed gas molecules gradually become denser and form a structural surface together with the water molecules on which the nucleation and growth of hydrate crystals occurs.

When a hydrate forms from a liquid gas at saturation pressures, usually the temperature in the cell has to be lowered below freezing in static conditions in order to initiate the nucleation. Freezing of water saturated with gas is accompanied by the emanation of dissolved gas and its adsorption on the walls of the cell. (Solubility of gas in ice is much lower than in liquid water). During the following melting of ice at the pressure above hydrate equilibrium (through external heating of the cell) a film of hydrate forms on the cell walls from the adsorbed gas and water molecules. Molecular tunnels, through which the gas molecules flow to the whiskery hydrate crystals growing in the volume of water, are formed at the hydrate-cell walls interface. During this process a relatively high crystallization pressure is developed, the magnitude of which is yet to be studied. Although we do have facts about when the crystallization pressure of hydrate forming in an annular space at the temperature of 8°C crushed the 3-inch fountain pipes with the wall thickness of one-fourth inch.

Another explanation of the mechanism of hydrate nuclei formation on the walls of the cell underwater is possible. During the initial period of water freezing, when an ice-like structure similar to the structure of a hydrate is formed at the cell walls, a thin film of hydrate is formed from the gas dissolved in water. However, during this period, the process of hydrate formation is limited by the diffusive influx of hydrate forming gas from water to the centers of crystallization. The kinetic rate of water transition into ice is significantly higher than into the hydrate state. The rate of accumulation of ice is determined by the intensity of phase transition heat removal during the bulk freezing of water, and also important is the diffusion of water and gas molecules to the surface of a forming hydrate during the hydrate accumulation.

The rate of hydrate nuclei formation is determined significantly by the magnitude of external pressure and the degree of subcooling. With pressure the rate of hydrate nucleation increases. With the increasing degree of subcooling the nucleation sharply increases, and after reaching a certain value at a specified pressure, smoothly decreases.

The dependence of the methane hydrate nuclei formation rate at the gas-water free interface on pressure P and subcooling ΔT can be described by the equation

$$J = a \times e^{-b\Delta T/20\times\sqrt{P}} \times \sqrt{\Delta T} \tag{3.1}$$

where a and b are the coefficients whose values depend on the pressure (see Table 3-1).

After the emergence of hydrate nuclei, hydrate spreads and covers the whole gas-water free contact surface. The rate of the complete hydrate film formation at the gas-water interface depends on many factors, of which the most important are the composition and the phase state of gas, degree of subcooling, structural state of water and pressure, and temperature of the process.

The critical size of the nucleus around which the hydrate crystal forms, is determined as (Sloan, 1990):

$$r_{cr} = \frac{2\sigma V_H}{RT\left[\sum_{j=1}^{2} Q_j \ln(f_j / f_{\infty,j}) + \frac{n_W V_W (P - P_\infty)}{RT}\right]} \tag{3.2}$$

where

- σ is the surface tension of water at the hydrate-water interface;
- V_H and V_W are the molecular volumes of hydrate and water, respectively;
- Q_1 and Q_2 are the molar fraction of the guest molecules (gas) in the free cells of the hydrate lattice;
- f_j and $f_{\infty,j}$ are the experimental and equilibrium volatilities of the component j at temperature T and excess pressure $(P - P_\infty)$;
- n is the number of water molecules per each molecule of gas in hydrate.

According to the laser study of the hydrate nuclei formation (Nerheim, 1992), the critical nuclei sizes are between 5 and 30 nm. However, the crystals of this size are metastable and easily agglomerate into larger ones with the sizes from 100 to 2000 nm which are stable and surely developing.

Table 3-1 The a and b coefficients depend on pressure.

P, MPa	*5*	*6*	*7*	*8*	*9*	*10*
a	0.705	0.838	3.09	12.99	27.28	37.75
b	1.65	3.55	5.68	8.18	12.65	51.39

Under the supersaturation conditions the crystal nucleation process proceeds most actively in the layer of water near the surface which is supersaturated with gas during the pressure decrease, when a large number of microbubbles emerge whose internal pressure is significantly larger than the ambient pressure. Even with a small amount of subcooling the microcrystals actively form and grow in the near-surface region.

It is worth noting that a direct experiment (Bishnoi, 1983) and the laser probing (Nerheim, 1992) of nucleation and growth of the hydrate crystals have proved the presence of the water structural memory retaining the cluster form for a long time after the decomposition of hydrate (Makogon, 1970). Stability of the structural memory of water depends on the pressure, temperature, initial hydrate composition, and other parameters.

Hydrate grows around the crystal nuclei as spherical films covering the gas-water free interface. Figures 3-2 and 3-3 show two photographs of methane hydrate crystals obtained at the gas-water free interface at various pressures and degrees of subcooling.

The radial rate of a hydrate film formation on a free interface is rather high reaching hundreds of microns per second. It stays constant for the given thermodynamic conditions. With the pressure rise, with the decrease of the specific volume of gas, with the increased subcooling, and with the increased structuring of water, the rate of surface-film increases. Dependence of the surface-film methane hydrate radial growth rate on pressure can be determined from:

$$V_r = a \times e^{b\Delta T/10P} \tag{3.3}$$

Thickness of the hydrate film formed at the gas-water free interface for methane, depending on pressure and degree of subcooling, ranges between 0.5 and 200 μm.

The mass rate of the hydrate formation M_H is determined by the expression

$$M_H = \pi h \rho V_r^2 J \tau \tag{3.4}$$

where

- ρ is the density of the hydrate;
- h is the thickness of the forming film;
- J is the rate of crystal nuclei formation;
- τ is the growth time.

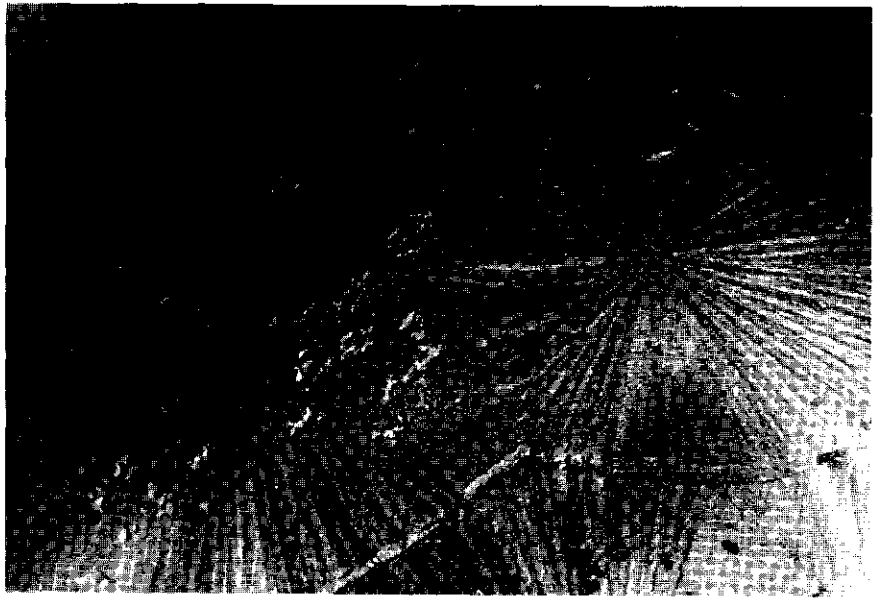

Figure 3-2 Hydrate of methane formed on the free gas-water surface.

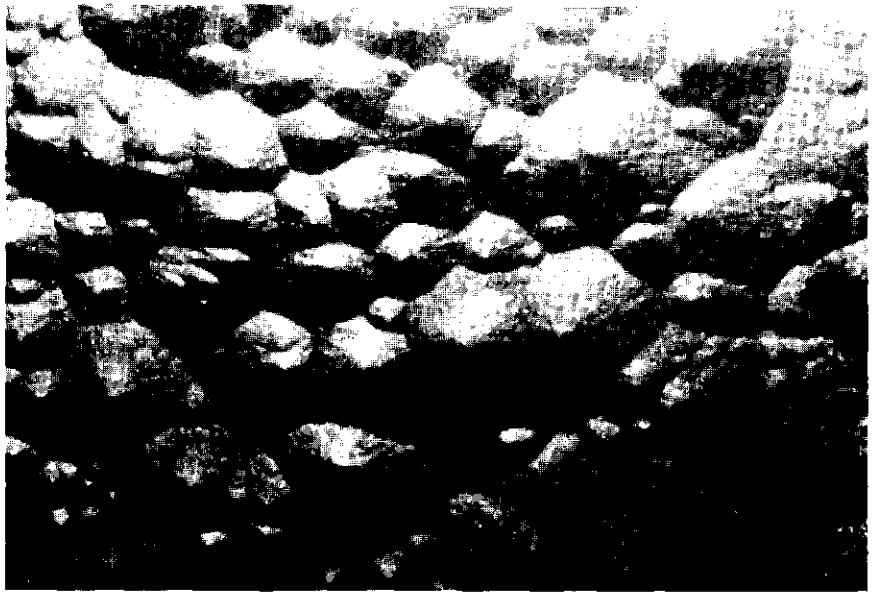

Figure 3-3 Hydrate of methane formed on the free gas-water surface.

After the formation of a hydrate film on the whole gas-water free interface, the process of hydrate formation goes from a surface-film type to a volume-diffusive type when the hydrate former diffuses through the film of formed hydrate. During the first time period, the rate of the volume-diffusive growth is rather high because the film of hydrate separating the hydrate formers is relatively thin. Besides that, the influx of a hydrate former from the supersaturated transition layer takes place during the initial period. As the thickness of hydrate film grows on the interface, the growth rate of hydrate in a closed volume bears the exponential decay character.

When liquid water is absent but saturated water vapor is present, the mechanism of hydrate formation has a somewhat different character. Water molecules in vapor during the precondensing stage form clusters (see Figure 3-1) composed of chains and cages of ice-like structure. With the appropriate thermodynamic conditions, these water clusters enter the fixed bonding with the gas molecules and with each other, thus forming the basis of crystal nuclei, around which the crystal nuclei form and hydrate crystal grows.

Liquid gas-former dispersed in the environment, undersaturated with water vapor, causes the nucleation and growth of hydrate crystals in the local zones of subcooling. These zones of subcooling are formed during the intensive evaporation of the dispersed hydrate former (Krasnovskaya, 1976).

At certain thermodynamic conditions, the hydrate growth centers form in the bulk of water at the solid metal-water interface. Initial hydrate formation can happen in both a large volume of water and at the surface of the condensed film or droplet.

Whiskery crystals usually grow when the hydrate nuclei are present in a bulk of water. Whiskery crystals are pushed from the base when the source materials (in our case the molecules of water and gas) arrive at the same geometric location, to the base of a crystal. The growing crystal is pushed from its base. Shape of the whiskery crystals, independent of the gas composition, can be a straight, smoothly bent, or spiral needles, or more often whole colonies of thread-like crystals.

The axial growth rate of hydrate whiskers, both in the gas and in the liquid phases for gases of different compositions, ranged between 0.05 and 1 μm/second during the crystal incubation period. In the gas medium the rate of whiskery crystals formation is sometimes larger by several orders of magnitude than the crystals formation rate in a volume of water.

After the hydrate decomposition, most of the hydrate-like structure of water is retained. With the heating of water above 30°C the structured

state of water almost completely disappears. Formation of hydrate from the freshly condensed water requires large subcooling, and the process of hydrate formation then is characterized by larger energies.

The temperature of initial hydrate formation is strongly influenced by the elevated water temperature. The higher temperature of water heating and the longer time of water held at the given temperature correspond to the larger subcooling required to start hydrate formation at a specified pressure. The effect of water preheating on the process of hydrate crystals nucleation increases as the pressure decreases. The maximum values of heating temperature at which the effect on the initial hydrate formation conditions is pronounced, range from 30 to 35°C. Heating of water above these temperatures does not produce a noticeable difference.

The conditions of gas hydrate formation can be determined from the equation:

$$\mu_W^L - \mu_W^0 = \frac{kT_m}{(m+1)n}\ln(1-Q_1) + \frac{kT_m}{(m+1)n}\ln(1-Q_2) \qquad \textbf{(3.5)}$$

where

μ_W^L is the chemical potential of liquid water in equilibrium with hydrate;

μ_W^0 is the chemical potential of a hypothetical "empty" hydrate lattice (all $Q = 0$);

m, n are for structure I hydrate $m = 3$, $n = 5.67$;

Q_1 is the filling ratio of the small cavities with hydrate former gas;

Q_2 is the filling ratio of the large cavities with hydrate former gas;

$$Q_1 = \frac{C_1P}{1+C_1P},\ Q_2 = \frac{C_2P}{1+C_2P} \qquad \textbf{(3.6)}$$

where

C_1, C_2 are Langmiur's constants for the small and the large cavities, accordingly;

P is the pressure of hydrate formation.

It can be seen from Equation 3.5, the difference of starting hydrate formation temperatures at a constant pressure from the condensed water and the heated water after hydrate decomposition is determined by the different magnitudes of its chemical potentials. The water obtained from hydrate decomposition and the retention of the hydrate-like structure has a larger chemical potential than the freshly condensed water or water heated to a high temperature.

Lowering the temperature of hydrate formation from a preheated water can be explained by the destruction of the structure of a liquid crystalline state of water. Hydrate decomposition leads to a destruction of a solid crystal state (molecules of water and gas are strictly fixed). Upon the hydrate decomposition through lowering the pressure or raising the temperature, the molecules of gas emerge from the fixed cavities formed by water molecules, and the cavities themselves generally remain intact. These cavities exist in water as large aggregates.

An increase of the water temperature after decomposition of hydrate increases the kinetic energy of water molecules and the rate of translation and destruction of fixed water molecules orientation. The increasing number of the aggregates and separate cavities decompose. The water structure fades. In order to form the new crystal nuclei and new cavities, a certain subcooling is required with a magnitude that is proportional to how much the initial (native) water structure faded.

The heat of hydrate formation from a freshly condensed water is significantly larger than the heat of hydrate formation from a structured water obtained after hydrate decomposition.

Pressure-Temperature Conditions of Well Operations

In order to develop maintenance measures and prevention of the hydrate formation it is necessary to know the equilibrium conditions of hydrate formation from a gas of known composition and the change of gas flow parameters in the well, in the field systems of collection and pretreatment, and in the pipelines.

Dependence on the equilibrium temperature and pressure is determined by one of the previously described methods. Conditions of hydrate formation and accumulation in the reviewed part of the technological system exist at $P_S > P_E$ or $T_S < T_E$, where P_S, T_S equals operating pressure and temperature of the system; P_E, T_E equals equilibrium pressure and temperature of forming hydrate of the specified composition.

Since hydrate can form in the well-bore during the well shutdown period and during its operation, let us consider the definition of parameters for both cases in the easiest statement. Well bottom pressure in the stopped gas well is determined by the formula

$$P_B = P_H \exp(0.03415\rho L / z_C T_{Ave}) \qquad \textbf{(3.7)}$$

or

$$P_B = P_H e^S \tag{3.8}$$

where

$$S = 0.03415\rho L / z_C T_{Ave} \tag{3.9}$$

Here

- P_H, P_B are the pressures at well head and at the specified depth, accordingly, MPa;
- L is the well depth at which the pressure is estimated, m;
- ρ is the relative gas density;
- z_C is the gas compressibility at average pressure and temperature.

The average temperature in the well equals

$$T_{Ave} = (T_B - T_H) / \ln(T_B / T_H) \tag{3.10}$$

where

- T_H, T_B are the temperatures at well head and at well bottom, accordingly, K.

The well bottom pressure is determined either by a direct measurement with the well pressure gauge (which is preferred), or calculated from the measured well head pressure:

$$P_B = \sqrt{P_H^2 e^{2S} + 1.377 \times \lambda \frac{z_C^2 T_{Ave}^2}{d_{Int}^5} (e^{2S} - 1) Q^2} \tag{3.11}$$

where

- λ is the coefficient of hydraulic resistance;
- d_{Int} is the internal diameter of the fountain pipes, 10^{-2} m;
- Q is the gas debit at the standard conditions, 1.157×10^{-3} m^3/s.

The hydraulic resistance coefficient λ depends on the gas flow regime and the surface structure of the pipe walls (Figure 3-4). For a precise calculation the real coefficient is determined in practice by measurements during the well operation

$$\lambda = \frac{(P_B^2 - P_H^2 e^{2S}) d_{Int}^5}{1.377 Q^2 z_C^2 T_{Ave}^2 (e^{2S} - 1)} \tag{3.12}$$

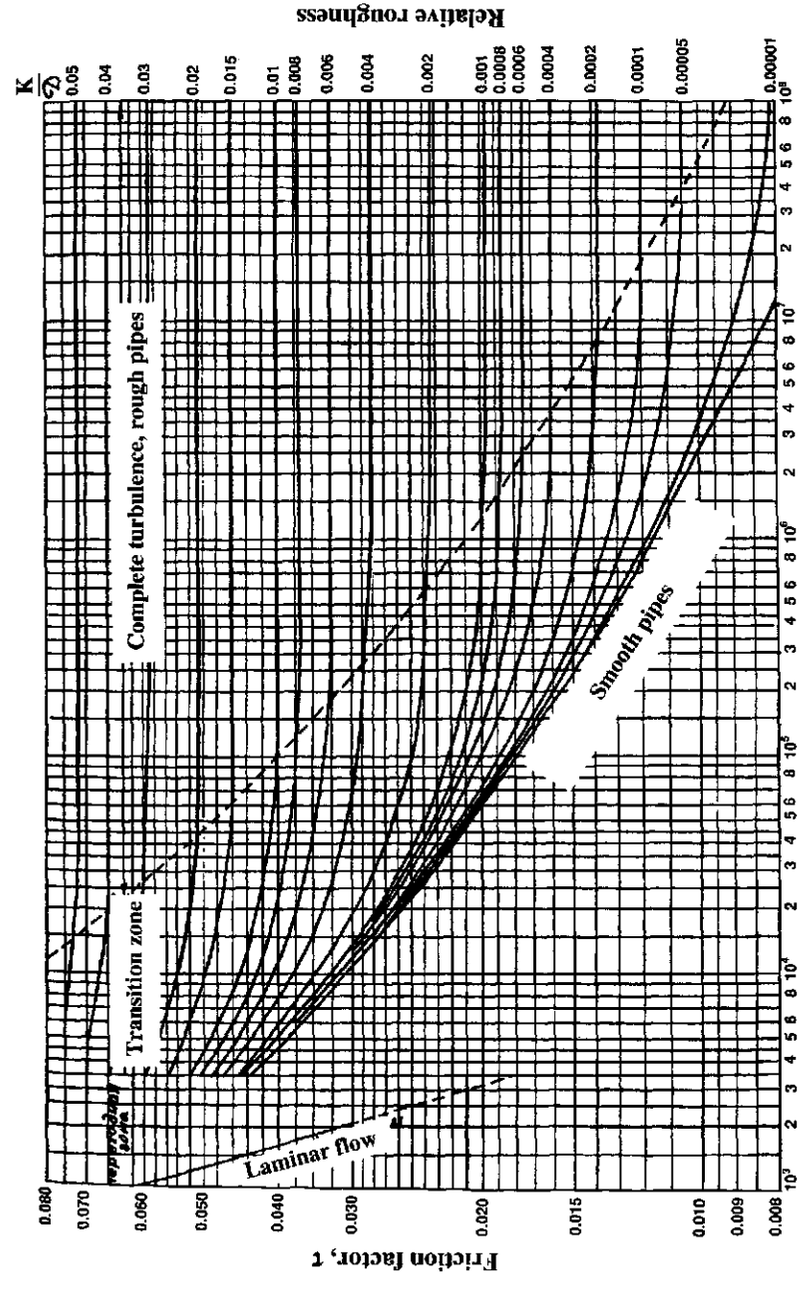

Figure 3-4 Friction factor for flow of fluids in pipe (Katz et al., 1959).

At the large temperature gradients along the well bore and when the high accuracy of calculations is required, the following formula is recommended for the well bottom pressure determination

$$P_B = P_H^2(T_B / T_H)^{2S} + 1.377\lambda \frac{z_C^2 T_H^2 Q^2}{d_{int}^2}\left[(T_B / T_H)^2 - (T_B / T_H)^{2S}\right] \quad (3.13)$$

where

$$S = 0.03415\rho L / z_C(T_B - T_H) \quad (3.14)$$

During the pressure determination, the presence of liquid in the well should be accounted for.

A change of the gas temperature along the well bore is determined by the initial layer temperature T_L; the production characteristic of the layer (rate of flow), and the magnitude of the well operating debit Q, kg/s; the well structure, and the thermal conductivity of its walls; the geothermal gradient of the rock Γ, K/m; the heat capacity of gas, and the Joule-Thompson coefficient D_i.

During the calculation of gas temperature change along the well bore, the following should be taken into consideration:

- the presence of phase transitions of water and gas in the well and in the rock around the well,
- the hydrate formation in the gas stream, the ice melting in permafrost zone,
- the hydrate decomposition in hydrate saturated layers, and
- the hydrocarbons condensation or evaporation.

The temperature in a stopped well is gradually changing, and, after a certain amount of time, it stabilizes approaching the natural temperature of the rock. For practical calculations, the change of the temperature with depth in a well after stabilization can be determined using the formula

$$T_L = T_S - \Gamma(L - l) \quad (3.15)$$

where

T_L is the temperature at depth L, °C;

T_S is the stratum (layer) temperature, °C;

Γ is the average geothermal gradient, °C/m.

$$\Gamma = (T_S - T_0) / (L - l_0) \quad (3.16)$$

where

T_0 is the temperature of the neutral layer at depth l_0, °C.

During the presence of a permafrost the geothermal gradient in the rock below permafrost is calculated by the equation

$$\Gamma = (T_S - T_P) / (L - l_P) \quad (3.17)$$

where

T_P is the frozen ground temperature, °C, at the lower permafrost boundary h_M.

Within the regions of permafrost the geothermal gradient is determined by

$$\Gamma_P = (T_P - T_0) / (h_P - h_0) \quad (3.18)$$

The temperature of gas in the stem of the operating well at depth l is determined with

$$T_l = T_S - \Gamma l - \Delta T e^{-al} + \frac{1 - e^{-al}}{a}\left[\Gamma - \frac{D_i(P_B - P_l)}{l} - \frac{A}{c_P}\right] \quad (3.19)$$

where

T_l is the temperature of gas at depth l measuring from the middle of the perforation interval, °C;

ΔT is the change of temperature in the layer, and can be calculated from the Equation 3.22, °C;

D_i is the differential Joule-Thompson coefficient in the well stem, °C/MPa;

P_l is the pressure at depth l measuring from the middle of the perforation interval, MPa;

A is the thermal work equivalent, 9.8 kJ/kg × m;

c_P is the average heat capacity of gas in the well stem, kJ/kg × °C;

a is the coefficient determined by the formula:

$$a = 2\pi\lambda_R / Gc_P f(\tau) \quad (3.20)$$

where

λ_R is the thermal conductivity of the rock, kJ/m × s × °C;

$f(\tau)$ is the dimensionless function of time:

$$f(\tau) = \ln\left(1 + \sqrt{\pi\lambda_R \tau / c_R R_C^2}\right) \quad (3.21)$$

$$T_B = T_S - D_i \Delta P \frac{\log[1 + Gc_P\tau / \pi H c_R R_W^2]}{\log[R_P / R_W]} \quad (3.22)$$

where

T_S, T_B is the temperatures of stratum and of well bottom, accordingly, °C;

D_i is the Joule-Thompson coefficient;

ΔP is the pressure difference between the stratum and the well bottom, MPa;

R_P, R_W are the radii of the pay-zone and the well, accordingly, m;

H is the perforated thickness of the production layer (pay zone), m;

c_P is the heat capacity of gas, kJ/kg × °C;

c_R is the heat capacity of rock, kJ/kg × °C;

G is the mass flow of gas, kg/s, is determined from the known debit by:

$$G = \rho Q \quad (3.23)$$

where

ρ is the density of gas, kg/m^3;

Q is the well debit at normal conditions, m^3/s;

The temperature in the stem of an operating well with the presence of permafrost is determined from the Equation 3.19 in the interval from the well bottom to the lower boundary of the permafrost. The temperature of gas at the entrance into the permafrost zone $T_{0,P}$ is found from the formula

$$T = T_{0,P} - \Gamma l_{0,P} - \Delta T e^{-a l_{0,P}} + \frac{1 - e^{-a l_{0,P}}}{a}\left[\Gamma - \frac{D_i(P_B - P_{l_{0,P}})}{l_{0,P}} - \frac{A}{c_P}\right] \quad (3.24)$$

where

$l_{0,P}$ is the distance from the middle of the perforation interval to the permafrost zone, m;

Γ is the geothermal gradient of the rock below the permafrost °C/m, found from the Equation 3.17.

Within the permafrost region the temperature distribution is described by equation:

$$T_l = T_{0,P} - \Gamma_P l + \frac{1 - e^{-apl}}{a_P}\left[\Gamma_P - \frac{D_i(P_{l_{0,P}} - P_l)}{l} - \frac{A}{c_P}\right]\beta \quad (3.25)$$

where

T_l is the temperature of gas at a distance l from the lower boundary of the permafrost, °C;

Γ_P is the geothermal gradient found from the Equation 3.18;

l is the distance from the lower boundary of the permafrost zone to the point of interest, m;

$P_{l0,P}$ is the pressure at the entrance into the permafrost zone, MPa;

P_l is the pressure in the point of interest, MPa.

The coefficient a_M is calculated from expression

$$a_M = 2\,\pi\,\lambda_P / G\,c_P f(\tau) \quad (3.26)$$

and the function $f(\tau)$ from the formula

$$f(\tau) = \ln\left(1 + \sqrt{\pi\lambda_P\tau / c_P R_W^2}\right) \quad (3.27)$$

where

λ_R is the thermal conductivity of the permafrost rock, kJ/m × s × °C;

c_P is the heat capacity of the permafrost rock, kJ/m^3 (see Figure 3-5);

β is the dimensionless coefficient accounting for the change in the rate of heat exchange at sub-zero temperatures. It can be estimated approximately depending on the temperature of frozen ground by the formula

$$\beta = (T_P - T_0)^2 / T_0^2 \quad (3.28)$$

where

T_0 is the temperature of the neutral layer, usually taken equal to the annual average temperature of the region, °C;

T_P is the average temperature of rock in the permafrost zone, °C.

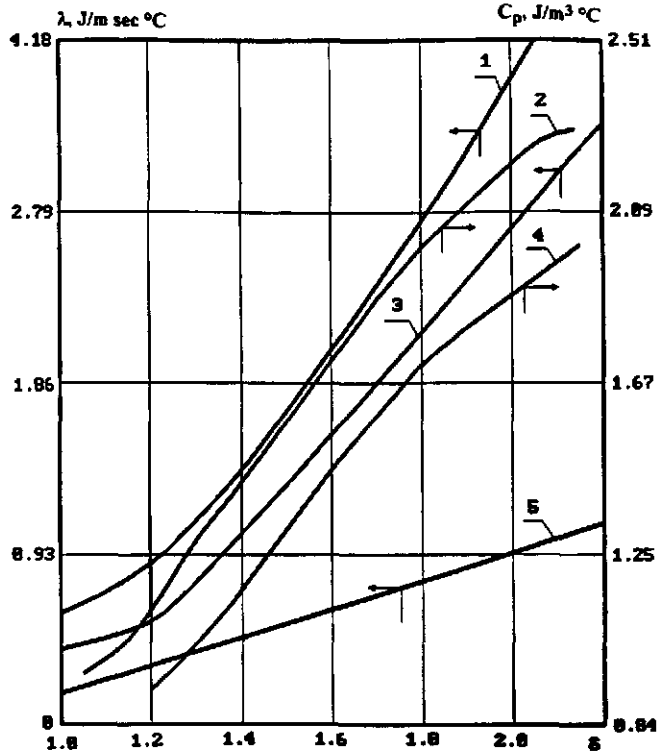

Figure 3-5 Change of heat conductivity and heat capacity of frozen rock.

1 - Heat conductivity of sandstone
2 - Heat capacity of sandstone
3 - Heat conductivity of shale
4 - Heat capacity of shale
5 - Heat capacity of dry rock frame

Hydrate Formation in the Near Well Bottom Part of the Layer

Hydrates can form in the well bottom part of the layer during:

1. Lowering of the gas temperature in the well bottom zone below the hydrate equilibrium temperature due to high depressurization during gas production;
2. Cold water injection into the layer during the drilling or repairing of a well;

3. Injection of the cold gas into the underground reservoir;
4. Cooling of the well bottom zone due to an intensive evaporation of the highly volatile hydrate inhibitors or surfactants, etc.

In order to determine the radius of hydrate formation in the well bottom zone, two temperature curves are necessary—one for the hydrate formation equilibrium and one for the actual temperature depending on the magnitude of the layer temperature, debit of the produced gas, and the temperature depression in the well-bottom zone. The point of intersection of these curves will define the radius of hydrate formation. One has to know the pressure and temperature in the well-bottom zone of the layer at different well production rates in order to construct such a diagram.

Pressure change in the well bottom zone of the layer is calculated using the formula

$$P = \sqrt{P_{Layer}^2 - AQ\frac{\ln(R_P / R)}{\ln(R_P / R_W)} - BQ^2 R_W / R} \qquad (3.29)$$

where

Q is the gas debit, m³/s;

A, B are the coefficients of filtration resistance depending on the well bottom zone parameters and on the well bottom design;

R_p, R_W are the radii of the pay-zone and of the well, respectively.

The temperature of gas at the well bottom with gas filtration through the layer due to the pressure difference $\Delta P = P_{Pay} - P_{Bot}$ is determined by using the Equation 3.22.

A change in the gas temperature and in the equilibrium temperature in the well bottom zone of a cooled deposit with the layer temperature of 10.5°C and pressure of 7.7 MPa is shown in Figure 3-6. The filtration resistance coefficients A = 129.6 c/m³ and B = 0.864 c/m³ are determined from the results of the well testing.

The production rate of the well ranged from 1 to 7 m³/s. The equilibrium curve of hydrate formation corresponds to the deposit gas composition—about 99% methane. Hydrates start to form at a debit of up to 2.14 m³/s—on the well walls, and at a debit of up to 7 m³/s the radius of the hydrate formation zone increased to 1.25 m.

The technological regime of wells in deposits with cooled layers must preclude the formation of hydrate in the layer, because the cyclic formation and decomposition of hydrate will result in destruction of the well bottom zone, formation of large caverns, and a sequential destruction of the well.

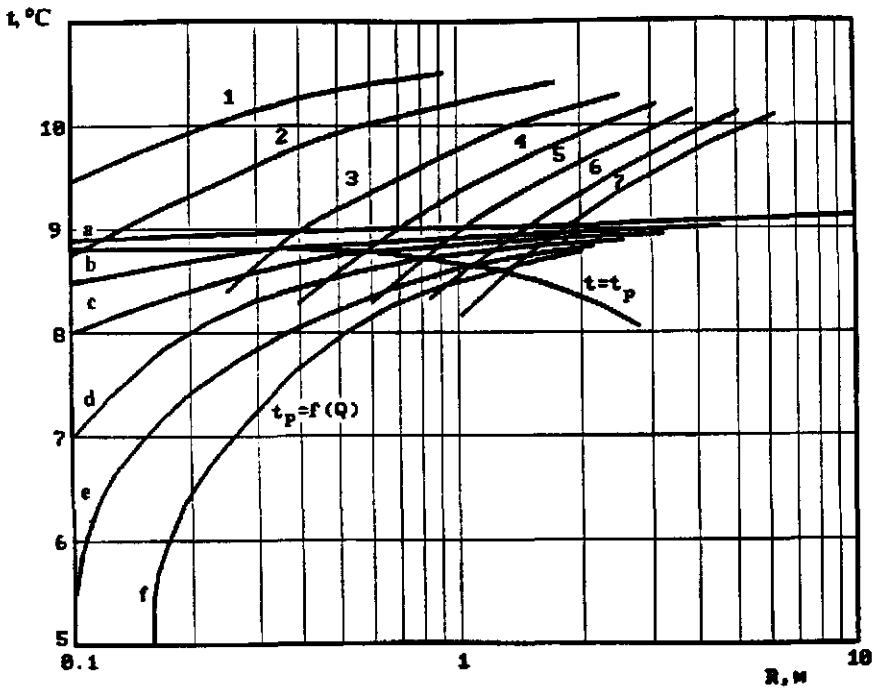

Figure 3-6 Change in hydrate formation conditions in the bottom part zone of a gas well (1–7 are gas temperature at different production rates; a–f are equilibrium temperature of hydrate formation change at different gas flow rates).

Formation of Hydrates in Wells

Hydrate formation in wells is one of the most important problems that must be solved during oil and gas production. Prevention of the hydrate plugs formation in wells is related to the complication of the well design and large consumption of energy and inhibitors, since the flow coming from the wells does not undergo preliminary separation into water and gas. The number of such complications increases significantly as wells are relocated to the north, or to deep offshore zones, with the development of the deposits having anomalously high pressures, and with locating the oil and gas wells having pressure below saturation pressure into operation.

Hydrates can form in any place where water and gas are present at the appropriate temperature and pressure—in a layer (in sediments); in the well bottom zone; in the fountain pipes and in the annular space; in the well head equipment before, inside, and after the orifices; and in separators and pipelines. Hydrates may form in the drilled well if drilling utilizes the fresh water solutions in the low temperature and high pressure intervals, during the drilling while entering the pay-zone, during mastering and testing of a well, and during the well shut-in period. Hydrates actively form at the appropriate temperature and pressure not only in the gas and gas condensate wells, but also in the oil wells when the well operating pressure is lower than the gas saturation pressure, and temperature is below hydrate equilibrium. Presence of the low-temperature wax promotes the formation of hydrate plugs and sharply complicates the formation of solid phase in the flow.

Hydrates in the well is a well's disease. Hydrate formation, as with any disease, is easier and less costly to prevent than to liquidate. Later in this chapter the conditions of hydrate formation and liquidation on an example of the Czechoslovakian well Karlin-1 are considered.

Location and intensity of hydrate accumulations in a well vary and depend on the operation regime, design and geothermal gradient in a well, fluid composition, and other factors. In order to determine the interval of hydrate formation in a well, it is necessary to draw a diagram of the hydrate equilibrium curve dependent on the well operating parameters and the actual temperature in a well. The lower boundary of hydrate formation is determined by the intersection of both temperature curves. The equilibrium curve is constructed from the hydrate equilibrium pressure values for a known gas composition, the actual temperature curve—from the results of the well thermometer measurements, or from the values calculated using Equation 3.19.

Under certain conditions, when the well is operated only in the annular space, the hydrate formation may bear the localized character—in the gas throttling locations during its flow through loose junctions. Cases more often encountered are of hydrate formation in the stems of wells which were inoperative for a long time or formed during well conservation.

Usually, temperature stabilization in a shut well filled with gas results in the cold zones of the rock to the temperature lowering below the hydrate equilibrium. Nuclei form from the films of water on the tube walls. The following crystallization, as usual, results in a total plugging of the well bore. Length of the hydrate plugs reaches tens or hundreds of meters. Under certain conditions of hydrate formation and accumulation of plugs in sections of the pipe, great stresses can develop in the pipe which result in crushing and breaking the well columns (Figure 3-7).

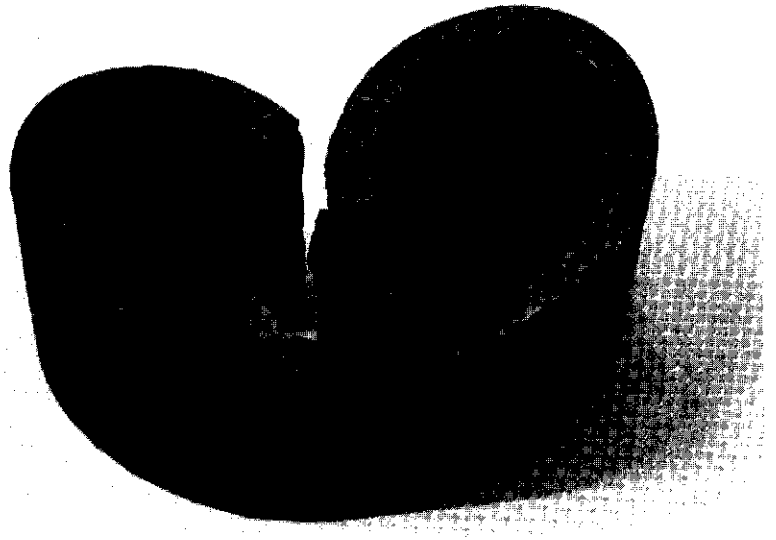

Figure 3-7 Cut of a 64 mm diameter pipe with 6 mm thick wall crushed in a well by hydrate at depth of 1245 m, temperature = 7°C.

Prevention of Hydrate Formation during Construction and Testing of Wells

Hydrate formation is observed during the construction and testing of most oil and gas wells in the north or deep-water offshore fields. The cause of hydrate formation is an intensive cooling of the well product. In such conditions, special importance should be directed at proper planning measures to fight hydrate formation.

Length of the survey drilling with the low temperature of the injected drilling mud results in a sufficient change of the thermal field of the rock surrounding the well and significantly influences the intensity and depth of the hydrate formation during the following well testing.

During the well drilling, the drilling mud in contact with the deep high-temperature rock warms up, and, depending on the heat losses in the surface system of mud preparation, the temperature distribution in the downcoming and upcoming flows can vary within a wide range. However, in all cases the temperature of the well bottom zone is lower, and of the well head, higher than the static geothermal temperature.

In a thermally insulated surface system the well head temperature of the drilling mud T_H of the well of depth h with a constant geothermal

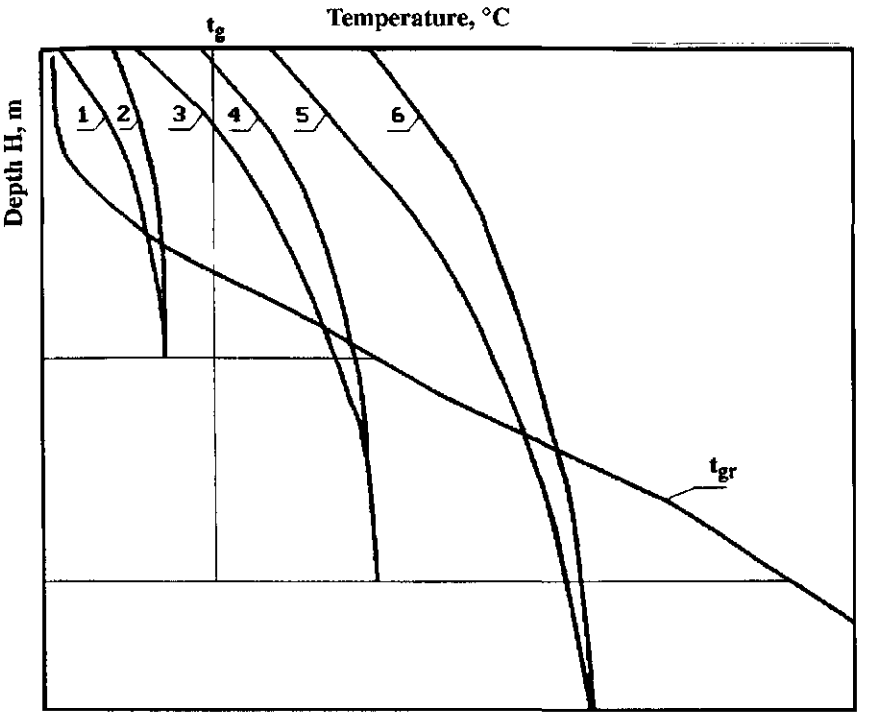

Figure 3-8 Temperature of downgoing (1, 3, 5) and upcoming flows (2, 4, 6) during drilling mud circulation in wells with different depths (t_g is temperature of hydrate formation as a function of depth; t_{gr} is geothermal temperature distribution).

gradient Γ and the temperature of the neutral layer being 0°C can be estimated using the correlation:

$$T_H = 0.5\,\Gamma\,h \tag{3.30}$$

Apparently, the hydrate formation is impossible when the temperature T_H is higher than temperature of hydrate formation at the layer pressure $T(P_L)$, at depths larger than

$$H > 2\,T(P_L)\,/\,\Gamma \tag{3.31}$$

Depending on the geothermal distribution of temperature and the well depth, temperature of the downgoing and upgoing drilling mud (Figure 3-8) can be lower than (lines 1, 2) in Figure 3-8 close to (lines 3, 4), and higher than (lines 5, 6) the temperature of hydrate formation at the layer pressure. In the first case, when gas enters the drilling mud, the probability

of hydrate formation in the well bore during the drilling is high. In the second case, hydrate formation is possible near the well head, and in the third case, impossible.

Temperature distribution in the well bore depends on the initial temperature of the injected mud. If the temperature in the well bore must be maintained below the temperature of hydrate formation due to technological reasons (for example, in order to prevent hydrate decomposition in the intervals of hydrate-saturated layers), it is necessary to cool the drilling mud coming from the well.

Prevention of the hydrate formation in a well during mastering and testing is accomplished through several methods: preheating of the well-bore by circulation of the hot drilling mud immediately before the mastering, treatment of the well bottom zone with inhibitors of hydrate formation, using the inhibitor based shut-down muds, and using the heating cables lowered to the total depth of the potential hydrate formation interval.

The application of each of the methods listed above depends on the expected regime of operation and on composition of the product. The most versatile and easily applicable method is electrical heating with the cable lowered in the well production tubing, or mounted on the outer side of the fountain tubing throughout the zone of potential hydrate formation.

The temperature distribution in the well in which a linear heat source is located at depth l with a specific power w is determined using the correlation:

$$Q\, c_p\, dT/dx = k\,(T - T_0 - \Gamma x) + w \qquad (3.32)$$

where

- k is the heat transfer coefficient between the product and the surrounding rock, W/m °C;
- w is the specific linear power of heating, W/m;
- Q is the well production rate, kg/s;
- c_P is the heat capacity of oil, J/kg °C;
- T_0 is the temperature of the neutral layer, °C;
- Γ is the geothermal gradient, °C/m.

Solution of the equation for the interval of potential hydrate formation is

$$T(x) = T_0 + \Gamma x + \frac{\Gamma Q c_P}{k}\left[1 - e^{k(x-L)/Qc_P}\right] + \frac{w}{k}\left[1 - e^{k(x-L)/Qc_P}\right], \qquad (3.33)$$

where

- L is the depth of the middle of the perforation interval, m.

The maximum difference between the temperatures of the flow and of hydrate formation is found near the well head. The magnitude of a minimum specific power of heating providing a sufficient prevention of hydrate formation for the wells with large depths is expressed by the formula

$$w_0 = \frac{k(T_\Gamma - T_0 - \Gamma Q c_P / k)}{1 - \exp(-k / Qc_P)} \approx k(T_\Gamma - T_0) - \Gamma Q c_P \qquad (3.34)$$

It follows from this correlation that at a fixed length of the cable the required power decreases proportionally to the well production rate.

Calculations for the deposits of West Siberia ($k = 2$ W/m °C, $\Gamma = 0.033$°C/m, $T = 0$°C) with the different values of T, indicate that at the cable length of 500 m the maximum specific electrical heating power is 50 W/m, and the total maximum power is 25 kW (Figure 3-9).

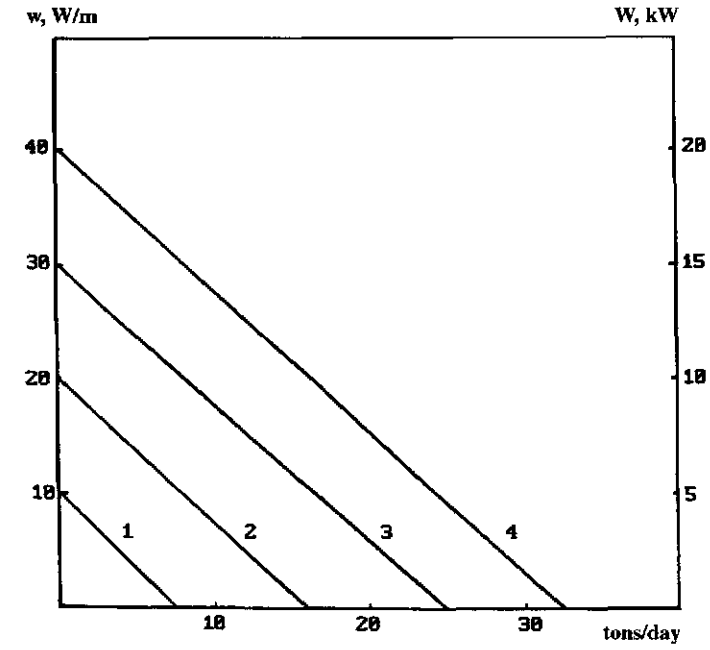

Figure 3-9 Specific (w) and total (W) electric heating power for hydrate prevention at different T_g (1 is T_g = 5°C; 2 is T_g = 10°C; 3 is Tg = 15°C; 4 is T_g = 20°C).

The heating cables may be substituted with geophysical cables having a low resistance of wires. The cables lowered into the production tubing must be weight-bearing, must have low specific electrical resistivity, and must withstand high temperatures. It is most suitable to use the three- or seven-wire cables, because attaching them to the three-phase electrical source does not cause the phase load shift. A choice of cable, according to its electrical characteristics, is done by using the correlation:

$$W = \alpha U_m 2/R_0\ 12 \geq w_0 \qquad (3.35)$$

where

- U_m is the maximum source voltage corresponding to the technical characteristics of the cable, *V;*
- R_0 is the specific resistivity of the cable wire, Ohm/m;
- l is the required depths of lowering the cable, m;
- α is the coefficient equal to 1 for the three wire, and to 2 for the pair-parallel seven wire cables.

Tests of the efficiency of the heating cables were performed in the wells of the Feodorovskoe, Varieganskoe, and Talinskoe fields in West Siberia. The field works indicated that using the seven-wire cables of the type KG-7-70-180 and the three-wire cables of the type KG-3-40-90 was effective for preventing the hydrate formation. The necessary characteristics of electrical heating in the other regions, for example, in the Krasnoyarsk region, are presented in the Table 3-2.

In order to prevent hydrate formation during the field testing at the sites whose fluid compositions are not expected to have large amounts of water present (absence of the gas-water or oil-water contact near the perforation interval), it is efficient to treat the well bottom zone with the inhibitors of hydrate formation. The mechanism of the anti-hydrate action is a matter of creating a buffer between the layer fluid and the depression liquid from the mobile zone of an agent injected into the well bottom zone, and of the consequent treatment of the fluid coming from the layer in the well bottom zone by contacting the layer fluid with the residual agent bound and the layer. This buffer provides the separation of the layer fluid and the depression liquid during the entering of fluid into the well and its flow through the fountain tubing cooled after a prolonged shut-in period. Thus, an effective prevention of plug formation is ensured from the very first moment.

The inhibitor, tied up in the porous volume, desiccates the layer fluid and partially is carried out into the well with the flow. During this process

Table 3-2 Characteristics of the electrical well heating for preventing hydrate formation at all regimes of operation.

Name of the Oil and Gas Field Sites	*Depth of the Hydrate Formation Zone from the Well, m*	*Heating Characteristic*			
		Maximum Required Power		*Source Voltage*	
		Specific, W/m	*Total, kW*	*KG 7-70-180*	*KG 7-95-180*	*KGGN 10*
Anabaro-Khataganskaya	1470	32	47	–	914	570
Yenisey-Khataganskaya	1330	22	29	660	683	430
Pur-Tazovskaya	1330	22	29	660	683	430
Southern-Tungusskaya	2040	22	45	–	100	630
Baktiyskaya	1800	14	25	–	737	460
Khataganskaya	2000	18	36	–	933	580

its concentration and effectiveness decrease. Thus, during the planning stage it is necessary to quantify the decrease in the concentration of the tied inhibitor ensuring an effective prevention of hydrate formation through the whole testing period.

Laboratory research indicated that after the inhibitors are passed through the rock collector core sample and displaced by oil and gas, the residual inhibitor content does not practically differ from the residual water content. The volume of the created buffer V_B can be estimated using the formula:

$$V_B = V_0 (1 - \gamma) \tag{3.36}$$

where

V_0 is the volume of inhibitor injected into the layer, m^3;

g is the residual water content of the collector, volume fraction.

On the other hand, the buffer volume must prevent gas contact with the depression liquid, during the time the buffer goes from the bottom of the production tubing to the well head the gas must not penetrate the buffer layer. The following condition must be maintained:

$$\frac{L_B}{V_G} \le \frac{L - L_B}{V_F} = \frac{(L - L_B)S_F}{Q} \tag{3.37}$$

where

L_B is the height of the buffer in the production tubing before the fluid entering the well bottom, m;

L is the depth of the production tubing in the well, m;

V_F is the flow velocity in the well, m/s;

Q is the production rate m^3/day;

S_F is the cross section area of the fountain tubing, m^2;

V_G is the slip velocity of the gas through the buffer layer, relative to the agent, m/s;

When oil ($V_F = 0.1$ *m/s*) and gas ($V_F = 0.5$m/s) enter the fountain tubing with the diameter 62 mm, the ratio L_B/V_G is correspondingly 0.5 and 0.8 for the well with the production rate $Q = 30$ tons/day. The minimum effective buffer volume is estimated using the formula:

$$V_B = L_B S_F = \frac{LS_F}{1 + Q / S_F V_G} \tag{3.38}$$

The estimates indicate that for an oil well the depth of $L = 2000$ m, the minimum buffer volume is approximately 3 m^3, and the optimum volume of inhibitor at $\gamma = 0.3$ equals 4.5 m^3.

The testing performed at the Tagrinskoe field indicates that this technology is highly effective for wells in which the hydrate formation conditions exist during the well start-up period with a consequent transition into a hydrate-free regime after the well bore heating.

Using the hydrate inhibitor based shut-down mud is suitable for prevention of hydrate formation during the testing of a well with a large area of permafrost rock and with an expected high production rate, during which, in a short period of time, the well will enter a hydrate-free P-T regime. The inhibitor concentration in the shut-down solution must provide an effective prevention of hydrate formation in the most dangerous initial period of time. The main feature of this method is the guaranteed prevention of plug formation in the production tubing during the time of ejection of the solution film on the production tubing walls, which occurs only at the high flow rates of gas. In the opposite case, the solution accumulates moisture, and, under the hydrate formation conditions, it can promote the plug formation in production tubing.

The exploratory wells in West Siberia utilize well bore preheating by circulating hot fluid for a long time through the fountain tubing lowered to the hydrate-potential depth before testing to prevent hydrate formation. The heat accumulated by the rock prevents hydrate formation during the consequent testing at all regimes of well operation. Technologically, the heating can be performed through the production tubing, as well as through the annular space.

In order to obtain the optimum parameters of preheating, a system of transient heat transfer equations must be solved

$$\begin{aligned} c_P \frac{dT_1}{dt} + Qc_P \frac{dT_1}{dx} &= k_1(T_1 - T_2) \\ c_P \frac{dT_2}{dt} + Qc_P \frac{dT_2}{dx} &= k_1(T_2 - T_1) - g_0 \end{aligned} \tag{3.39}$$

where

T_1, T_2 are the distribution of temperature in the production tubing and in the annular space of the well, °C;

Q is the liquid flow rate, m^3/day;

c_P is the heat capacity of liquid, J/m^3 °C;

k is the heat transfer coefficient, W/m °C;

g_0 is the transient function of heat exchange with rock.

A numerical solution of equations for the case of hot oil injection through the production tubing and annular space at the rate of 300 tons/day indicate (Figure 3-10) that after 12 hours the temperature practically stabilizes and does not depend on time. The calculations show that it is best to supply hot oil through the annular space. Water is less effective because of the high coefficient of heat transfer and low heat capacity which results in a fast cooling of the injected agent by the upgoing flow.

The rapid temperature stabilization at different well depths (Figure 3-11) allows us to assume it constant over the whole period of heating. The dependence of temperature change in the near-well rock with the heating time t is approximately described by the formula

$$\Theta = \frac{T(x,t) - T_R(x)}{T(x,0) - T_R(x)} = \frac{\ln(1+\sqrt{4/\pi})}{\ln(1+\sqrt{4\tau/\pi+\pi\tau})},$$

$$\tau = at/R^2 \qquad (3.40)$$

where

- $T(x,t)$ is the temperature dependence at depth x on time from the end of heating, °C;
- $T(x,0)$ is the temperature at depth x during the preheating, °C;
- $T_R(x)$ is the undisturbed temperature of rock, °C;
- t is the time of preheating, s;
- a is the thermal conductivity of rock, m^2/s;
- R is the well radius, m.

In order to evaluate the time of preheating with hot oil (T_{head} = 100°C), depending on the time of expected testing, the data in Figure 3-11 obtained for $\Theta = 0.2$ which corresponds to the minimum possible numerator of 20°C and a maximum possible denominator of 100°C in Equation 3.40, may be used.

Preheating consumes a lot of energy and has a lower efficiency rate, because after the heating during mastering the hot liquid is removed from the well. For example, the unproductive heat loss with removal of hot oil (T_{head} = 100°C) from the depth of 4000 m of the 160 mm diameter well is 17 GJ.

For a comparison, the total energy consumption for the cable heating of a well during the well testing for four days and the required power of 25 kW is 8.64 GJ. The dependence on the power of heating required to maintain the oil temperature at well head of 100°C during the preheating time with the rate of injection of 300 tons/day and well depth of 2000 m is presented in Figure 3-12.

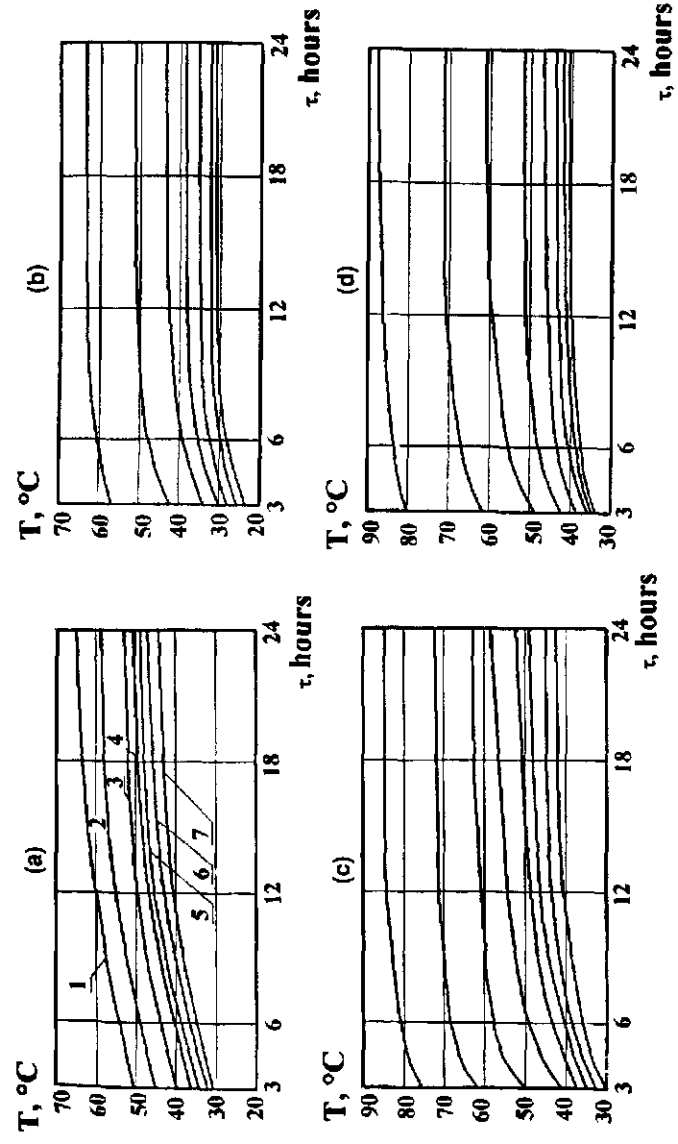

Figure 3-10 Dependence of temperature on time τ at various locations in production pipes (a, c) and annual space (b, d) during injection of hot oil at T = 100°C through the annular space (a, b) and production pipes (c, d) at a rate Q = 300 tons/day with production pipes lowered to 800 m depth.

1 is L=100 m 2 is L=200 m 3 is L=300 m 4 is L=400 m
5 is L=500 m 6 is L=600 m 7 is L=700 m 8 is L=800 m

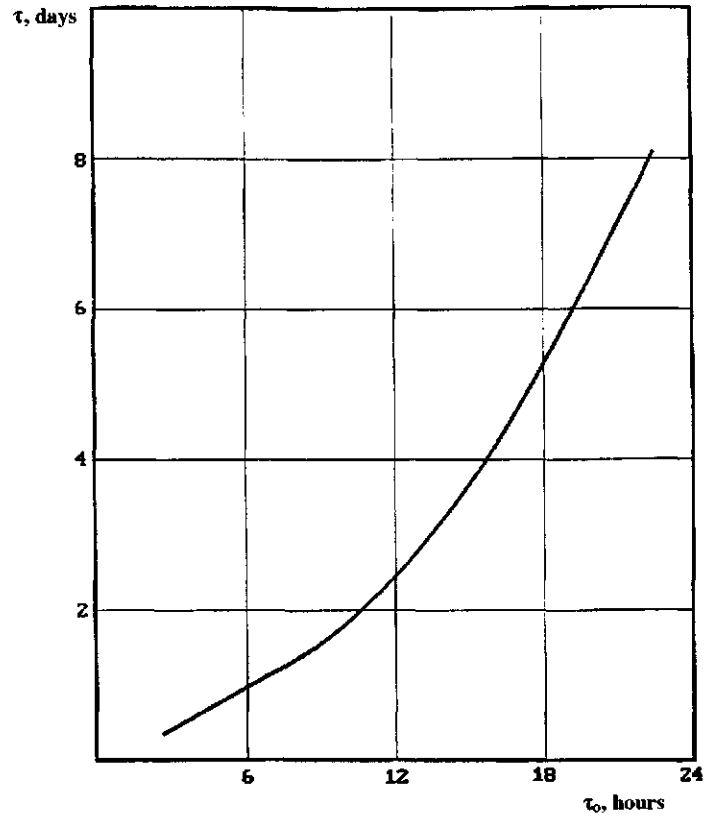

Figure 3-11 Dependence of well bore cooling time τ to T = 50°C on the time τ_0 of initial oil preheating (T = 100°C) with initial rock temperature = 0°C.

Preheating is suitable for use at the sites which do not have large electric power sources. The simplicity of the furnace construction with moderate safety requirements when water is used as the heat carrier, allows us to implement this technology in the majority of cases.

The methods listed were tested at the West Siberia fields. It was concluded that the use of a heating cable is most rational. This method can be easily controlled and is reliable, safe, environmentally clean, and energy efficient. When an appropriate cable (e.g., KG7-70-180) and the connection schematic are selected, the operations of measuring the well bottom pressure and temperature with probes lowered on the heating cable, used to transmit the obtained information, are carried out simultaneously with heating.

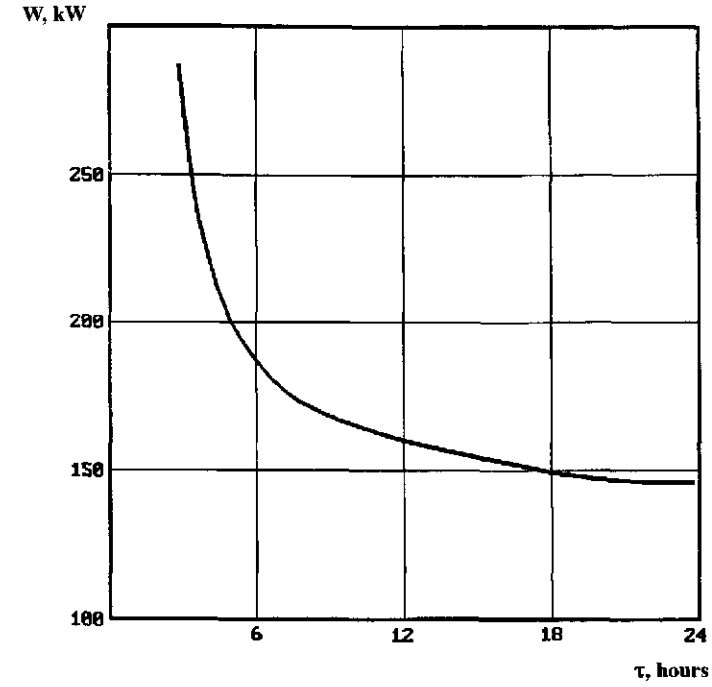

Figure 3-12 Dependence of required heating power to maintain inlet temperature = 100°C at oil flow rate = 300 tons/day in the 2000 m deep well with geothermal gradient Γ = 0.033°C/m.

Complications during the Drilling of Wells

The hydrate saturated layers are characterized by an extremely low permeability, which prevents the filtration of drilling mud into the layer and the formation of a protective layer of dry mud on the well walls. The absence of a protective layer on the walls of a well, which opens the gas hydrate deposit during the drilling at temperature above hydrate equilibrium and with chemically active solutions, results in hydrate decomposition. Decomposition of hydrate in a well bottom zone of the layer is accompanied in a number of cases with a sharp weakening of the bonds between the grains, fluidizing of a part of the rock, and ejection into a well. This process is accompanied by an intensive formation of caverns, and shearing rock may cause seizing of tools. A gas evolving from hydrates at a high pressure results in an intensive saturation and ejection of drilling mud from a well.

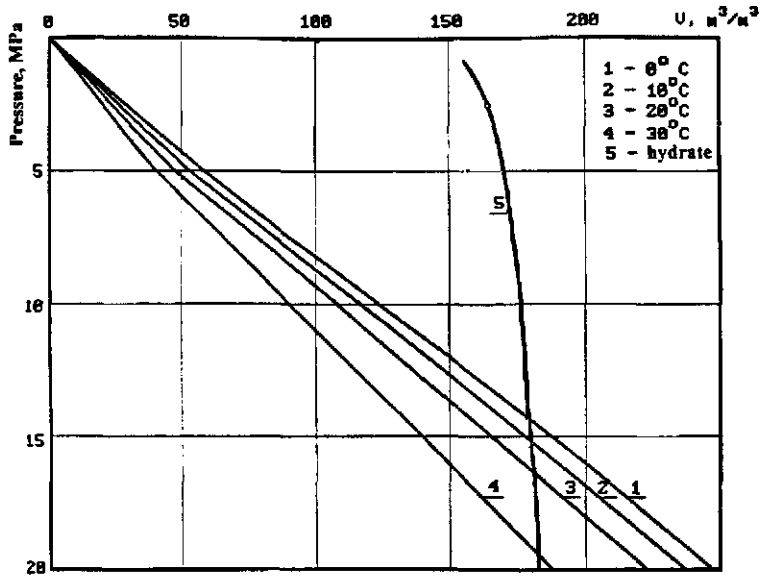

Figure 3-13 Amount of gas contained in the unit volume as a function of pressure and temperature in free (1–4) and hydrate state (5) for methane.

Figure 3-13 shows the curves relating the volume of gas contained at equilibrium in a unit volume of hydrate for different gases. Curves of a specific gas content in a free state at similar P-T conditions also are given for comparison in this figure. It can be seen from the comparison of the presented curves that, in the gas hydrate deposit at hydrostatic pressure of up to 14 MPa (at 1400 m depth), volumes of methane and carbon dioxide released at hydrate decomposition exceed significantly the volumes of gas in a free state at similar conditions. For example, at the 750 m depth of a drilled layer at $T \geq 10°C$, 157 m^3 of methane is released from one cubic meter of rock pore space filled with methane hydrate, and 85 m^3 from a cubic meter of rock filled with methane in a free state.

The depth at which the volumes of gas contained in a unit volume in a free and in a hydrate state are equal and can be determined from the expression:

$$H = \frac{22.4 \times 10^5 \rho_H P_0 T z}{T_0 \gamma (M_G + 18n)}, m \qquad (3.41)$$

where

ρ_H is the density of hydrate, g/cm³;

P_0 is the atmospheric pressure, MPa;

T is the temperature at depth H, K;

z is the compressibility at layer conditions;

T_0 = 273.15 K;

γ is the average density of solution in the rock, g/cm³;

M_G is the molecular weight of the hydrate former gas;

n is the molar ratio of water and gas in the gas hydrate deposit.

Intensity of hydrate decomposition and gassing of a drilling mud are determined mainly by the excess temperature of drilling mud above the equilibrium temperature of hydrate in a layer. Released gas then flows in a well, dissolves in the drilling mud, decreases its density, and results in an emergency ejection of the mud from a well. The pressure of the released gas is determined, not by a hydrostatic pressure, but by the temperature of hydrate decomposition. However, the ejection of drilling mud is accompanied by a sharp intensifying of hydrate decomposition, which, in turn, results in a significant cooling of the rock in the zone of hydrate decomposition and decay of a process of hydrate decomposition.

To prevent an intensive formation of cavities, seizing of the drilling tools, and gassing and ejection of a drilling mud due to hydrate decomposition, it is necessary to increase the density of a drilling mud, decrease the mud temperature below hydrate equilibrium, or a combination of these two methods. The necessary density of a drilling mud ρ_γ at which hydrate can not decompose in a drilled layer can be determined from the equation

$$\rho_\gamma = \frac{100 P_{EQ}^{T_\gamma}}{H} \qquad (3.42)$$

where

$P_{EQ}^{T_\gamma}$ is the equilibrium pressure corresponding to the drilling mud temperature T_γ;

H is the depth of the drilled gas hydrate deposit, m.

The quantity P_{EQ} can be found from expressions $\log P_{EQ} = 1.415 + 0.0417(T_\gamma + 0.01\ T_\gamma^2)$ for methane, and $\log P_{EQ} = 1 + 0.0497\ (T_\gamma + 0.005\ T_\gamma^2)$ for a natural gas with the relative density 0.6.

Figures 3-14 and 3-15 present the curves of the drilling mud density needed to prevent decomposition of hydrates of methane and of a natural gas with the relative density 0.6 as a function of depth and the temperature of mud.

In reviewing Figures 3-14 and 3-15 for methane hydrate for drilling at the following conditions we see: depth of a gas hydrate deposit H = 500 m

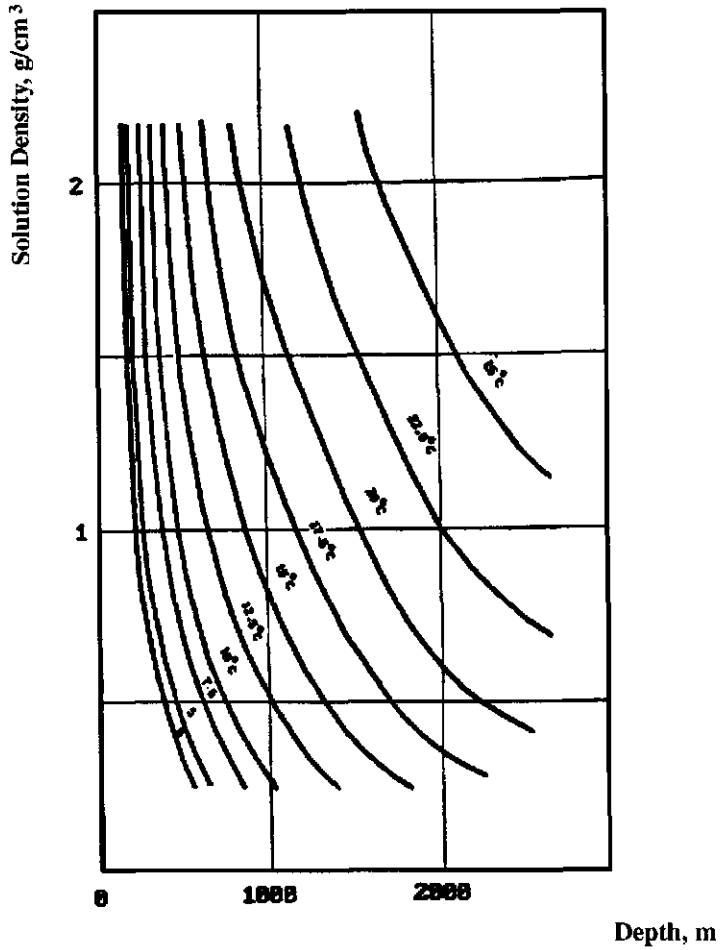

Figure 3-14 Density of the drilling mud necessary to prevent methane hydrate decomposition as a function of mud temperature and depth of gas hydrate deposit.

and 1200 m; layer temperatures in a gas hydrate deposit are 2°C and 10°C, accordingly; hydrostatic layer pressure in a gas hydrate deposit $P = 5$ MPa and 12 MPa, accordingly; equilibrium temperatures of hydrate decomposition equal 6.5°C and 14°C, accordingly; drilling mud temperatures T_γ are 0°, 5°, 10°, 15°, and 20°C. Let us find the density of a drilling mud to prevent hydrate decomposition.

The equilibrium pressure for the upper gas hydrate deposit boundary at $T_\gamma = 0°$, 5°, 10°, 15°, and 20°C will be 2.6, 4.5, 7.5, 14.0, and 25 MPa,

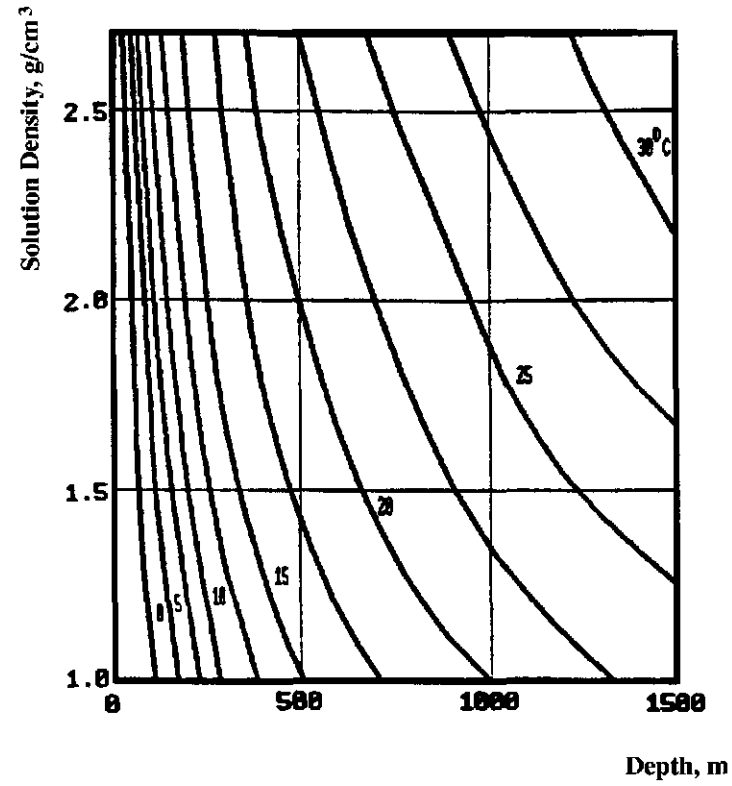

Figure 3-15 Density of the drilling mud necessary to prevent natural gas hydrate decomposition as a function of mud temperature and depth of gas hydrate deposit.

accordingly. The needed density of a drilling mud is then 0.52, 0.9, 1.5, 2.6, and 4.6 g/cm3, respectively. From the presented values we see that maintaining the mud temperature at 0° and 5°C prevents hydrate decomposition in a layer and ensures a completely safe regime of drilling. Increase of the drilling mud temperature to 10° and to 15°C requires us to increase the mud density to 1.5 and 2.6 g/cm^3, and it is almost impossible to prevent hydrate decomposition at the mud temperature of 20°C by increasing the mud density. (It would require an increase to 4.6 g/cm^3.) By using a combined method for the last case: decrease the mud temperature to 12.5°C and increase the density of mud to 2 g/cm^3 we ensure a safe drilling operation. Additionally, a closed drilling system with the maintaining of an excess well head pressure can be recommended. For example, at $\rho_\gamma = 2$ g/cm^3 and

$T = 20°C$ an excess head pressure of 36 MPa must be maintained, which sharply complicates the technique and equipment for drilling.

The equilibrium pressure for a gas hydrate deposit at a 1200 m depth at drilling mud temperature $T_y = 0°$, 5°, 10°, 15°, and 20°C will be similar to that at the upper layer because the gas composition is the same: 2.6, 4.5, 7.5, 14.0, and 25 MPa, accordingly. The density of a drilling mud needed to prevent hydrate decomposition is then 0.22, 0.38, 0.63, 1.1, and 1.92 g/cm^3, respectively.

During the calculation of an allowed temperature and required density of a drilling mud during a hydrate bearing layer, drilling it is necessary to know the composition of a hydrate former gas, equilibrium temperature, and pressure of hydrate decomposition. In each case, certain values of a drilling mud density and temperature are recommended, judging by the technological possibility and by economical expediency.

Formation, Prevention, and Removal of Hydrates in Product Pipelines

Hydrate formation in product pipelines is possible under certain thermobaric conditions and when water is in contact with a liquid hydrocarbon. Formation of a hydrate phase is thermodynamically possible from moisture dissolved in a hydrocarbon. However, accumulation of the amount of water sufficient to form hydrate cavities in some areas is very improbable because of a low concentration of water molecules in hydrocarbon liquid. Thus, this method of hydrate formation in an operating pipeline can be discarded.

Formation of hydrates from a hydrocarbon supersaturated with water proceeds by the mechanism of water adsorption on solid inclusions or on the metal of pipes with the consequent transformation of microscopic volumes of water into hydrate. Further growth may proceed by a direct transition of water molecules from a hydrocarbon solution to hydrate without the intermediate microscopic volumes of water when a hydrate phase is present.

The most important questions in the practice of product pipeline operation are the determination of sections where hydrate formation is thermodynamically possible, and choosing a method for preventing formation and removal of hydrate plugs. Locating of hydrate prone sections of product pipelines is done by finding the temperature and pressure distributions along the line. Comparison of the found values with the equilibrium conditions of hydrate formation allows us to locate confidently a boundary of a hydrate prone zone.

Comparison of data about the equilibrium conditions of hydrate formation and the actual temperature distribution along a pipeline allows us to estimate a boundary of a hydrate prone area, to determine the effect of the seasonal temperature fluctuation on the length of the zone where hydrate formation is likely, and to estimate thermophysical properties of the rock. This information is important to establish the emergence of the fact of hydrate plug formation danger.

Distribution of Pressure in a Product Pipeline

Pressure distribution P along the pipeline during the transportation of a single phase liquid through a pipeline is expressed as (Silash, 1980):

$$Q = 0.0656\ \mathrm{K}\ (\Delta P / L)^{0.552}\ d^{2.656}\ \mathrm{m}^{-0.104}\ \rho_L^{-0.448} \qquad (3.43)$$

where

- Q is the liquid flow rate, m^3/hour;
- K is the friction factor of pipe ($K = 10$ for new pipes);
- $\Delta P/L$ is the pressure drop because of friction, atm/km;
- d is the internal pipe diameter, cm;
- μ is the viscosity, cP;
- ρ is the specific weight of a product, g/cm^3.

The given equation does not provide high accuracy of computation. However, the inaccuracy in the calculation does not affect the estimation of a hydrate prone location because of a little effect of pressure change on the conditions of hydrate formation from liquid hydrocarbons.

Calculations indicate that an 0.5 MPa inaccuracy in calculating a pressure when the pressure in a pipeline is greater than 1.5 MPa results in a 3% or a lesser error in estimating the temperature of repeated hydrate formation. Consequently, Equation 3.43 is fairly applicable also to the analysis of a repeated hydrate formation. Analysis of Equation 3.43 indicates that the pressure differential between the starting and the ending points of a pipeline at a fixed flow rate is influenced most significantly by changes in a pipe diameter. A 1% decrease in a pipe diameter results in a 5% increase of the pressure gradient. Thus, monitoring the pressure along the product pipeline can be an effective method of revealing the segments of pipeline whose diameter has decreased because of hydrate formation and accumulation.

As an example, a plot of $\Delta P/Q$ as a function of time is presented in Figure 3-16 for the Nizhnevartovsk-Yuzhnyi Balyk product pipeline for

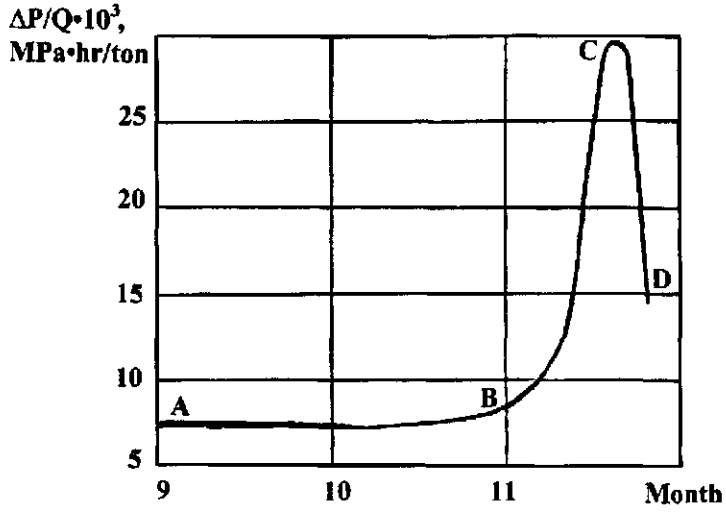

Figure 3-16 Dependence of specific pressure losses in the Nizhnevartovsk–Yuzhnyi Balyk product pipeline during the formation of a hydrate plug.

1982, when at the 50 km and at the 150 km segments large hydrate plugs formed. It can be seen from Figure 3-16 that the process of hydrate formation in the pipeline had started in November (A-B). A gradual accumulation of hydrates on the pipe walls was happening during the first decade of December, and during the second 10 days (C) the volume of hydrate had reached a critical value, pressure drops had increased sharply and an emergency shutdown of the pipeline and removal of the hydrate was required (D).

A change of the physical properties of the pumped products (viscosity, density) with temperature also affects the distribution of pressure in a pipeline. Estimates indicate that a temperature change of 20°C (from 0 to 20°C) results in a 10% decrease of the pressure gradient dP/dx because of a decrease in viscosity. A 20°C temperature increase causes a 5% decrease of the pressure gradient because of a decrease in density. As a whole, the changes of physical characteristics result in a 1% change of pressure gradient per 1°C which should be considered during design calculations.

The presented analysis indicates that the control over a pressure distribution is an effective method of diagnosing the processes of a pipeline cross section change because of hydrate accumulation in the critical sections of a pipeline.

Temperature Regimes of Pipeline Operation

The temperature regime of a pipeline operation is a determining factor for hydrate formation. As a rule, the temperature in a starting part of a pipeline is above the hydrate equilibrium temperature. Thus, the starting location of a hydrate prone interval and its length are determined by the intensity of a heat exchange between the moving product and the medium surrounding a pipeline.

In northern conditions, product pipelines are laid in freezing grounds where thermophysical characteristics depend both on a heat exchange with a pipe and on ambient conditions (air temperature at the surface, depth of a snow layer, etc.). A complex profile of the land, an inhomogeniety of ground and the seasonal changes of their thermophysical characteristics, a presence of sections going on the bottom of rivers, and sections on land prevent the possibility of an accurate description of the thermal regime of a product pipeline.

When the phase state of a pumped product is constant, then the heat losses depend on the type of heat exchange between a pipe and ground and between ground and surface. Transport of heat in the ground can be conductive or convective, depending on the moisture and on the presence of liquid flow in the ground. The temperature conditions on the surface of the ground significantly affect the character of heat loss from a pipeline. Types of cover (grass, snow, etc.), moisture evaporation or freezing, and many other factors have to be considered.

Various approximations are used because of the difficulties of describing in detail the temperature distribution. The simplest one is a calculation based on the assumptions that the effect of surface is negligible, and that the heat transfer coefficient is constant with time and with length. Then, from a heat balance on an element of length dx at a position x of a product pipeline we have:

$$0.28\, Q\, C_p\, dT/dx = k\, \pi\, D\, [T(x) - T_{GR}], \qquad \textbf{(3.44)}$$

where

- Q is the average liquid flow rate, tons/hr;
- C_p is the liquid heat capacity, J/kg °C;
- k is the heat transfer coefficient between a liquid and a ground, W/m2 × °C;
- D is the diameter of a pipeline, m;
- $T(x)$ is the average product temperature at a position x, °C;
- T_{GR} is the average ground temperature at the depth of a pipeline, °C.

Solution of the equation is:

$$T(x) = T_{GR} + (T_0 - T_{GR}) \exp(-k \pi D x / 0.28 Q C_p), \quad (3.45)$$

where

T_0 is the temperature at the beginning of a pipeline ($x = 0$), °C.

Analysis of the calculations on the temperature distribution along a product pipeline with a length of 250 km, a diameter of 0.5 m, an average heat transfer coefficient of 1.54 W/m² °C, indicates (Figure 3-17) that at certain temperatures (initial $T_0 = 20$°C, and ground $T_{GR} = 0$°C) the hydrate formation is impossible. This is with a temperature of hydrate formation from a pumped product being 5°C along the whole length of the line only at 1000 tons/hr or higher flow rates.

Average values of k are typically used during product pipeline design in calculating the temperature distribution. A study of the temperature regime of the Urengoi-Surgut-Cheliabinsk gas pipeline operation has shown that the average values of k vary significantly with seasons (due to phase changes of water in the carrier rock) between 0.53 W/m² × °C in

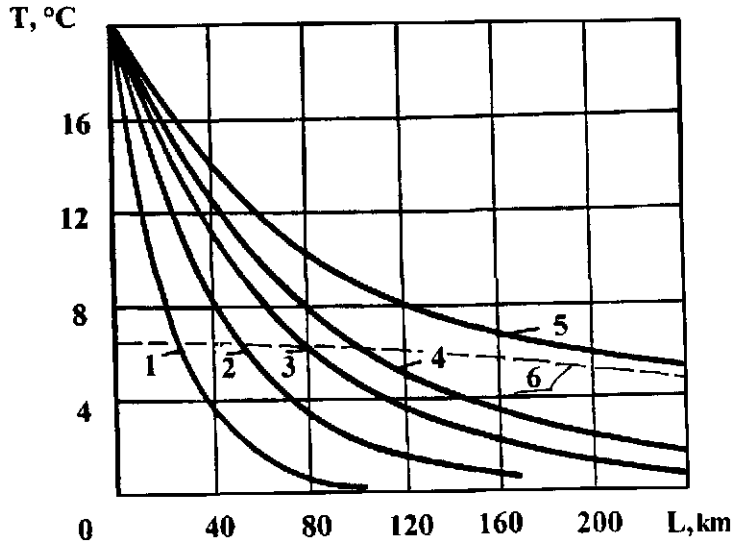

Figure 3-17 Dependence of the temperature distribution in a product pipeline on the volume of flowing liquid (1 is 90 tons/hr; 2 is 140 tons/hr; 3 is 270 tons/hr; 4 is 500 tons/hr; 5 is 1000 tons/hr To = 20°C; 6 is equilibrium temperature).

June and 3.53 W/m² × °C in January. It follows that the average values of the heat transfer coefficient k must be corrected during estimation of hydrate prone zone locations of product pipelines. In practice, the values of temperature measurements in the beginning T_0, and at some point along a pipeline where the temperature is being measured, are used to calculate the current value of k. Then the mark x of the start of a hydrate prone area with a temperature T_H of the pipeline of length L is calculated with the correlation:

$$x_H = L \frac{\ln[(T_H - T_{GR})/(T_0 - T_{GR})]}{\ln[(T(L) - T_{GR})/(T_0 - T_{GR})]} \quad (3.46)$$

The temperature regime of pipelines is stabilized during the first day after startup. Thus, the heat transfer coefficient k between the flow and ground can be assumed constant in time because of an insignificant temperature variation of the pipeline bearing ground with the surface temperature variation. Then the temperature distribution $T(x,t)$ along the pipeline distance x is described by an equation similar to Equation 3.45, but with the values of initial temperature $T_0(t)$ and a temperature at pipeline depth $T_{GR}(t)$ variable with time:

$$T(x,t) = T_{GR}(t) + [T_0(t) - T_{GR}(t)] \exp(-k \pi D x/0.28 Q C_p) \quad (3.47)$$

Calculations of temperature change in product pipelines are important for designing and evaluation forecasts. It is a safe practice to use the results of actual temperature and pressure measurements along a product pipeline for determining the boundaries of hydrate prone sections and for revealing the more probable locations of hydrate accumulation.

The curves of light hydrocarbon fraction temperature changes with time are shown in Figure 3-18 at inlet 1, at outlet 2 (max) and 3 (min), and hydrate equilibrium 4.

Details of the Flow of Immiscible Liquids and Gas-Liquid Mixtures in Pipelines

Some amount of stagnant water accumulates in the low areas of product pipelines from poor cleaning of pipes after construction and pressurizing. Liquid water accumulates in the rising sections of a pipeline during its operation, and the liquid level is in a quasistatic state. Presence of water decreases the active cross section of a pipeline and increases the hydraulic resistance to the flow, while its presence in a hydrate prone section promotes the formation of plugs.

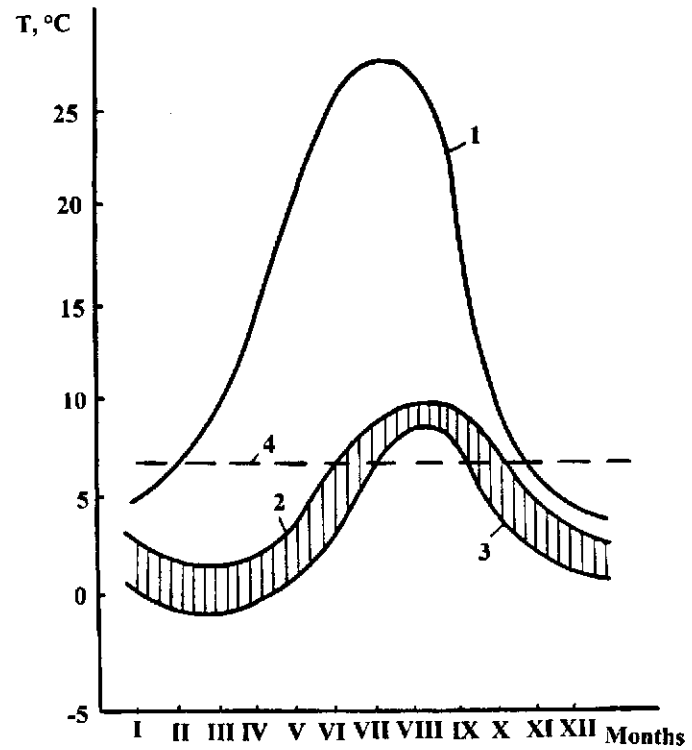

Figure 3-18 Dependence of the operating temperature variation in the Nizhnevartovsk–Yuzhnyi Balyk product pipeline (1 is on entrance; 2 is on exit [max.]; 3 is on exit [min.]; 4 is equilibrium temperature).

A differential equation was obtained for a hydrocarbon liquid flow in the rising section of a pipeline with a stationary water phase, which describes the position of a phase separation boundary along the section rising at an elevation angle a (Figure 3-19) as follows:

$$\frac{dy}{dx} = \frac{\left(\frac{\Delta\rho}{\rho}\right)\sin\alpha - \frac{\lambda Q^2 p(y)}{8gS^3(y)}}{\left(\frac{\Delta\rho}{\rho}\right)\cos\alpha - \frac{\beta_0 Q^2}{S^3(y)}\frac{dS}{dy}} \qquad (3.48)$$

where

y is the depth of the moving liquid flow (Figure 3-19), *m;*

x is the coordinate of the pipeline section, m;

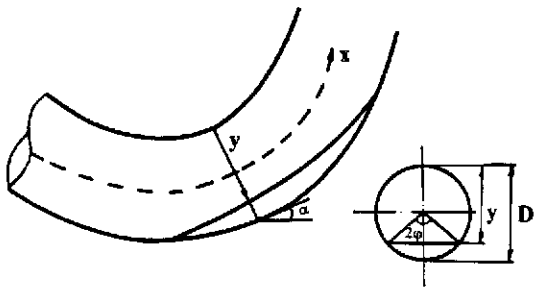

Figure 3-19 Schematic of a liquid flow in a shallow section of a pipeline in presence of water.

$\Delta\rho$ is the density difference between water and hydrocarbon, kg/m^3;

α is the elevation angle of a pipeline, rad;

λ is the hydraulic friction factor;

Q is the liquid flow rate, m^3/s;

g is the gravity acceleration, 9.8 m^2/s;

p is the hydrocarbon flow cross section perimeter at a distance x, m;

S is the hydrocarbon flow cross section area at distance x, m^2;

β is the empirical coefficient equal to 1.1 for a turbulent flow and 2 for a laminar flow.

The volume of water contained in a pipeline is described by an equation:

$$V(L) = d^2 \Big/ 4\int_0^L \left[\varphi(x) - \sin\{2\varphi(x)\}\right]dx \qquad (3.49)$$

or

$$V = \frac{\pi d^2}{4}L - 2^{1/3}\int_0^L \frac{y^{3/2}(1-y)^{1/6}}{(0.01464)^{1/3}} \qquad (3.50)$$

For approximate calculations of the amount of water in a pipeline, the value $y(x)$ can be assumed constant with length and equal to the normal value y_N, then

$$V = L\left[\frac{\pi d^2}{4} - \frac{y_N^{3/2}(1-y_N)^{1/6}2^{1/3}}{(0.01464)^{1/3}}\right] \qquad (3.51)$$

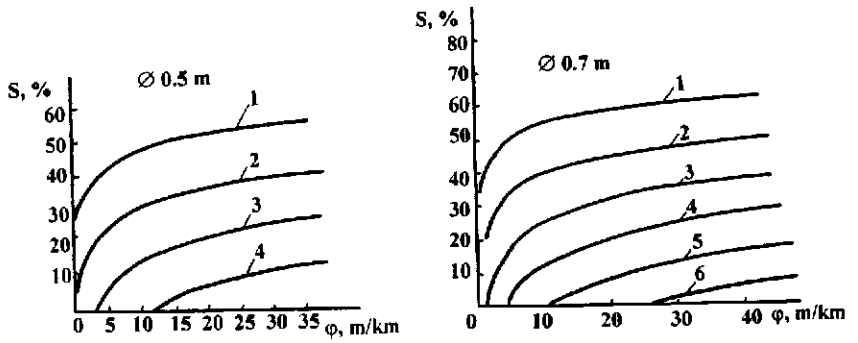

Figure 3-20 Correlation of the specific volumes of stationary water and methanol in a product pipeline as a function of liquid hydrocarbons flow rate: 200, 300, 400, 500, 600, and 700 tons/hour.

Ratio of volumes of free stationary water and methanol as the functions of characteristics of pipeline operation with diameters of 0.5 m and 0.7 m are presented in Figure 3-20.

The normal depth of a flow, and consequently, the volume of a liquid phase decrease with a decreasing density of a non-hydrocarbon liquid. A relative decrease of the normal flow depth as a function of ρ is described by a correlation

$$y_N(\rho)/y_{N,W} = [(\rho - \rho_L)/(\rho_W - \rho_L)]^{1/4}, \qquad (3.52)$$

where

$y(\rho)$ is the normal level of a liquid with a density ρ, *m*;

$y_{N,W}$ is the normal level of water, *m*.

Results of calculations show that the maximum volume of stagnant water decreases with the increasing flow rate. A brief increase in the flow rate of a pumped product to a maximum value with a following transition into a nominal regime is the most realistic method of decreasing the water content in the stagnation zones filled with water to the limit.

The following correlation can be used to estimate the specific volume of removed water per unit length of a pipeline ΔV with a flow rate increase ΔQ:

$$\Delta V = -\left(\frac{\partial V}{\partial Q}\right)\Delta Q = -\left(\frac{\partial V}{\partial \varphi}\right)\left(\frac{\partial \varphi}{\partial y}\right)\left(\frac{\partial y}{\partial Q}\right)\Delta Q = 2R^2 \sin\varphi\left(\frac{\partial y}{\partial R}\right)\Delta Q \qquad (3.53)$$

In a field practice extremely filled stagnation zones are seldom encountered. To evaluate the volume of water in a pipeline and the condition of its motion, the length of an aqueous phase, that is, the length of water-containing sections of a pipeline has to be known. The simplest method used to determine the length of a water-containing section consists of measuring the pressure differential across a stagnation zone, or across a section which includes the stagnation zone. The pressure drop in the zone where stagnant water is present ΔP is from Pascal's law:

$$\Delta P = P_U - P_L = \rho_w g\, h \sin\alpha \qquad (3.54)$$

where

P_U is the pressure in the upper part of a water-containing zone, Pa;

P_L is the pressure in the lower part of a water-containing zone, Pa;

ρ_w is the density of water, kg/m^3;

g is the gravity, m/s^2;

h is the elevation difference, m;

L is the length of the water-containing zone, m;

α is the angle of a pipeline elevation, rad.

Evaluation of the Conditions of Aqueous Accumulations Ejection from the Lowered Sections of Product Pipelines

The main cause of hydrate plug accumulation in product pipelines is the existence of water accumulations in the lowered sections of a line. Removal of these accumulations is determined by the regimes of the pipeline operation. In the most generalized form these conditions are characterized by the minimum flow velocity V_E which provides the water ejection. The minimum velocity of accumulations ejection from lowered sections is described by an equation which directly follows from the correlation (3.48) and looks as:

$$V_E = \sqrt{\frac{2}{\lambda} gD \sin\alpha \frac{(\rho_W - \rho_L)}{\rho_L}}, \qquad (3.55)$$

where

V_E is the minimum velocity of accumulations ejection, m/s;

λ is the hydraulic friction factor.

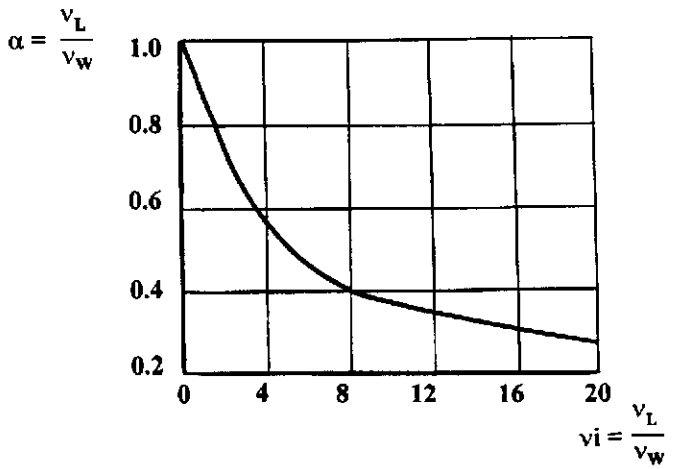

Figure 3-21 Dependence of the carry-out velocities of liquid (ν_l) and water (ν_W) from a product pipeline on their viscosities ratio.

Experimental study has shown that the ejection velocity is affected insignificantly by the changes in the surface tension at the boundary between phases and in the density of pumped products. The quantity V_E depends mainly on the ratio of kinematic viscosities of the transported hydrocarbon and of the accumulated liquid ν_L/ν_W, and also on the angle of the rising section of a product pipeline (Figure 3-21). The dependencies of the minimum flow rate by weight, providing the removal of the accumulations at laminar and at turbulent (in the part of smooth pipes) flow regimes, are described by correlations:

for a laminar flow

$$G = 8.7\, D^4\, (\rho_W - \rho_L)\, (\sin\alpha)^{1/3} / \nu_W^{0.726} \times \nu_L^{0.274}, \qquad (3.56)$$

for a turbulent flow

$$G = \rho_L^{0.4}\, (\rho_W - \rho_L)^{0.6}\, D^{2.7}\, (sin\ \alpha)^{0.19}\, \nu_L^{0.272} / \nu_W^{0.415} \qquad (3.57)$$

At the present time, methanol is used to fight hydrate formation in product pipelines. Calculations of the ratio of aqueous methanol solution ejection velocity to the ejection velocity of water V_M/V_W dependence on methanol concentration C indicate (Figure 3-22) that by increasing C the ratio υ_L/υ_W first decreases, and then increases. The minimum value occurs at $C = 40\%$ weight.

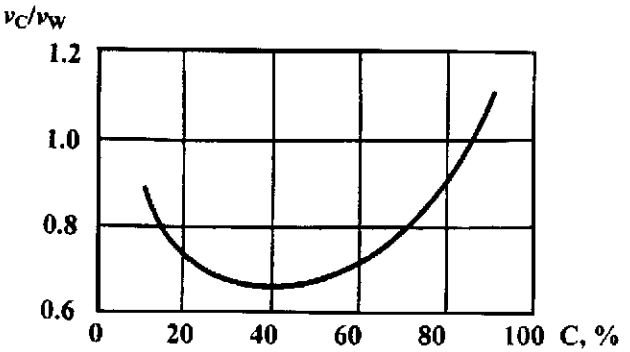

Figure 3-22 Dependence of the ratio of the velocity of aqueous methanol solution carry-out to the velocity of water carry-out on methanol concentration (C, wt%).

The limiting case of using the effect of ejection velocity increases with the increase in viscosity of the transported liquid is the use of viscoelastic compounds (gels) ensuring a nearly complete removal of water at all velocities of product flow. The experience of using these systems witnesses to their high effectiveness.

Effect of Product Pipelines Stops on the Formation of Hydrate Plugs

Unlike gas wells and pipelines, the formed hydrate phase can move along the water-liquid hydrocarbon interface and get into the upper part of a rising section in the product pipelines of light hydrocarbons fraction. The specific volume of water increases by 32% during hydrate formation of light hydrocarbon fraction hydrate. Thus the depth of flow h decreases, and at a fixed liquid flow rate hydrate phase must be removed from a stagnant zone because of its overfilling with a flow of hydrocarbon.

Experimental study indicates that hydrate formed from liquid hydrocarbons and water do not coagulate at an intensive mixing, but adhere on the walls of equipment and are easily moved by the flow of a liquid. However, during long stops the stagnant hydrate phase gains the ability to aggregate and to form a stable adhesive bond with the metal of a pipe without being carried away with the liquid flow.

To evaluate the degree of danger from a product pipeline shutdown as a stimulus of plug formation, let us consider a section which consists of lowering an elevation with equal lengths L and heights h (Figure 3-23)

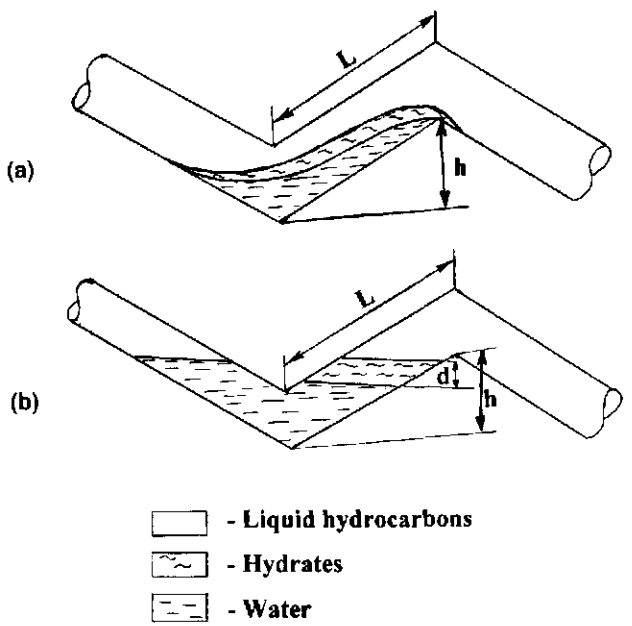

Figure 3-23 Schematic of distribution of hydrates and water in a stagnation zone in an (a) operating and a (b) shut-down product pipeline.

with a volume of stagnant water V_w in the elevation section. Hydrate continuously accumulate in the elevation section because of hydrate formation. After the product pipeline shutdown, water and hydrate flow into the lower part of a pipe under the force of gravity and block the pipe diameter at certain conditions. Then the hydrate thickness d is:

$$d = g\frac{t}{S_0}\sin\alpha = g\frac{ht}{LS_0} = h\frac{gt}{V_{Pipe}}, \qquad (3.58)$$

where

g is the specific rate of a hydrate film growth, m²/s;

t is the time of hydrate formation at this interval;

S_0 is the pipe cross section area, m²;

V_{Pipe} is the volume of the rising pipe section, m³.

Let us assume that the product pipeline downtime was sufficient for a hydrate to densify into an impenetrable monolith formation which will be considered to be a solid plug if it withstands the maximum pressure differential ΔP_M allowed for this pipeline with the pumping compressors turned on, i.e.

$$\frac{\pi D_0^2}{4}\Delta P_M = \frac{\pi D}{h}\sigma_H L d, \qquad (3.59)$$

or

$$t \geq \frac{\Delta P_M D^2 \Delta H_H}{4LK\Delta T_H \sigma_H}, \qquad (3.60)$$

where

σ_H is the shear stress of hydrate removal from pipe walls.

It can be seen from the obtained correlation that the minimum time of hydrate accumulation in the stationary zone, in amounts sufficient to form a plug, does not depend on the angle of pipeline elevation. The value of a minimum volume of aqueous phase V_M, at which the total filling does not occur at the lowering-elevation border during a pipeline shutdown, is determined as:

$$V_M = 2S_0\frac{D}{\sin 2\alpha} = \frac{\pi D^3 L^2}{4h\sqrt{L^2 - h^2}} \qquad (3.61)$$

At inclinations h/L ~ 0.01 the value of V_M for pipes with a diameter of 0.5 m is about 20 m³.

To the Question of Preventing Hydrate Plugs in Product Pipelines

The main reasons for hydrate plug formation in product pipelines are in a violation of the technology of preparing a line for operation after construction, and in a low quality of drying hydrocarbons. The presence of water accumulations in lowered sections of product pipelines is the consequence of insufficient cleaning of pipes after their pressurizing, or of using an inferior technology to remove water. The most effective method of preparing a pipeline for operation is to pass pigs through a pipe until water stops coming out of it.

When the requirements for the conditions of a hydrocarbon entering a pipeline are met, the possibility of water condensing out is excluded, and consequently, hydrates cannot form in a whole pipeline. However, the shutdowns and violations of technology in product pretreatment at facilities result in the condensation of moisture dissolved in hydrocarbons on

the pipe walls as the flow cools down and water accumulation in the lowered sections promote hydrate formation.

At this time, a periodic or a continuous injection of inhibitors is used in industrial product pipelines to prevent plug formation. The consumption of inhibitors is determined experimentally. Simultaneously, a study of works on the prevention and removal of hydrate plugs from the Nizhnevartovsk-Yuzhnyi Balyk-Tobolsk indicates that an effective use of inhibitors is possible only when a pipeline operation is thoroughly prepared and controlled. Otherwise, the injection of inhibitors will not only be useless, but could also promote plug formation.

A highly effective method of removing liquid water is passing pig pistons through a pipeline. However, this method is applicable in pipelines during the summer season where a hydrate free regime is established, and water does not lose its mobility. The periodic passing of gaseous plugs that pass easily through narrow sections and bends, brings good results.

Prevention of Hydrate Formation through a Continuous Injection of a Hydrate Inhibitor

This method is used similarly to the hydrate formation prophylactics in gas wells and gas pipelines. The essence of this method is to saturate a hydrocarbon with methanol, during which the motion along the line and the temperature decrease interacts with the residual water in lowered sections. By doing this, it is assumed that the concentration of alcohol in water prevents hydrate formation. Usually, a continuous injection of methanol is made into a product pipeline where free water accumulates in lower sections, or during a poor preparation of a hydrocarbon for transportation.

A distinguishing feature of an aqueous methanol solution equilibrium with liquid hydrocarbons is a sharp growth of solubility of water and methanol in a hydrocarbon at an 80% weight or greater concentrations of alcohol (Figure 3-24). The use of a technical grade methanol with a greater than 80% concentration of alcohol results in an oversaturation of hydrocarbon with water relatively to the conditions of equilibrium between a liquid product and water.

An equilibrium is established between phases in the nearest part of a stagnant zone during the product flow in a pipeline at the designed rates of 0.5–1.0 m/s because of a hydrocarbon-water interaction. The saturation of hydrocarbon with water and methanol at the end of this section is determined by the concentration of methanol in water. Initially, the water contained in a pipeline does not contain methanol. The concentration of alcohol in a transported fluid at the outlet from the stagnation section will sharply decrease, compared to the inlet concentration. Consequently, water in the stagnation zone nearest the pipeline begins to absorb the methanol dissolved in a transported fluid and blocks it from coming to the remote hydrate prone sections. The volume of liquid in the stagnation zone increases during this process due to the evolution of alcohol from a transported hydrocarbon.

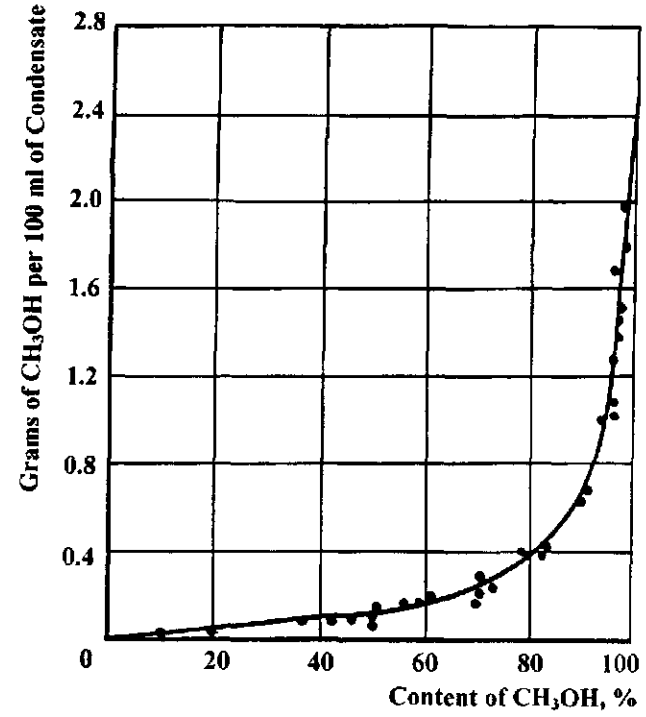

Figure 3-24 Dependence of methanol solubility in liquid hydrocarbons on its concentration in aqueous solution.

A generalized material balance equation for a stationary aqueous phase and a moving hydrocarbon phase is:

$$C(t) = \frac{M_0 C_0 + Q X_M^0 t - \int_0^t Q X_M(C)dt}{M_0 + Q(X_M^0 + X_W^0)t - \int_0^t Q X_M(C)dt - \int_0^t Q X_W(C)dt} \qquad (3.62)$$

where

$C(t)$ is the concentration of methanol in aqueous solution at time t, mass frac.;

M_0 is the initial mass of water+methanol solution of concentration C_0 in stagnant zone, kg;

C_0 is the initial concentration of methanol in the liquid in stagnant zone, mass frac.;

Q is the hydrocarbon liquid flow rate, kg/h;

X_M^0 is the concentration of methanol in the incoming hydrocarbon, mass frac.;

$X_M(C)$ is the equilibrium concentration of methanol in hydrocarbon in contact with the solution with a concentration C, mass frac.;

X_W^0 is the concentration of water in the incoming hydrocarbon, mass frac.;

The solubility of methanol in hydrocarbons is much higher than the solubility of water ($X_W << X_M$), then the correlation 3.62 is transformed into:

$$\frac{dC}{dt} = -(10C)Q\frac{[X_M(C) - X_M](1-C) + CX_W}{M_0(1-C_0) + X_W Qt} \qquad \textbf{(3.63)}$$

At approximation $X_W << X_M$ we can find the solution of the Equation 3.63 in the interval of a linear variation of X(C) to be:

$$X_M(\mathrm{C}) = \mathrm{A\,C}\,;$$

$$\ln\frac{(AC - X_M)(C_0 - 1)}{(AC_0 - X_M)(C-1)} + \frac{(A - X_M)(C_0 - C)}{(1-C)(1-C_0)} = \frac{A}{X_W}\left(\frac{X_M}{A-1}\right)^2 \ln\left[1 + \frac{QtX_W}{M(1-C_0)}\right] \qquad \textbf{(3.64)}$$

Calculations show that at methanol concentrations less than 40%, the aqueous solution consumes over 70% of the incoming dissolved methanol. The increase of mass of a liquid during this process in a stagnant zone with time is described by the correlation:

$$M(t) = M_0 + Q\,X_M\,t \qquad \textbf{(3.65)}$$

If the volume of water in the first stagnant zone were 50 m^3, then the concentration of methanol in the hydrocarbon flow coming out of the zone after contacting water is below 25% of the initial value. The unproductive loss of methanol due to dissolution into water is then 20 m^3.

If several water-containing zones are present on a section of a pipeline operated in a hydrate-free regime, then according to the Equation 3.64, the methanol concentration in hydrocarbon in the beginning of a hydrate prone interval does not exceed 5% of the initial concentration until the methanol concentration reaches 25% in water in the last zone. For example, in a system of six stagnant zones, each having a volume of 50 m^3 at a product flow rate of 200 tons/hr this is reached after 140 days.

The correlations 3.62–3.65 hold true for a period of time during which the volume of stagnant zone is not overfilled. In an opposite case, the magnitude of volume is fixed, depending on the pipeline operation regime. In the first approximation, at methanol concentrations less than 40% a change in the quantity $C(t)$ for a completely filled stagnant zone is described by an equation:

$$C(t) = \frac{Z_{in}}{A}[1 - \exp(-AQt / M_0)] + C_0 \exp(-AQt / M_0) \qquad \textbf{(3.66)}$$

where

C_0 is the initial methanol concentration in aqueous solution during an overfilling of a stagnant zone ($M = M_0$);

Z_{in} is the methanol content of a hydrocarbon at entrance into a stagnant zone.

Equation 3.66 expresses the concentration of methanol in a flowing aqueous solution. The main influx of an inhibitor to the following sections occurs in an aqueous methanol solution because of a sharp difference in methanol concentration in liquid hydrocarbon at the inlet and outlet of a stagnant zone.

It follows from the presented data that a constant injection of methanol is suitable only before a hydrate prone section with small amounts of water present in stagnant zones. Injection of an inhibitor can be done in the nearest location because of the change in position of the beginning of a hydrate prone section. Such injection can be started well before the time of a hydrate season to ensure the saturation of all stagnant zones with methanol and supplying of methanol to all the hydrate prone sections. It should be noted that the supply of an inhibitor can be stopped during the hydrate season, because then a reverse process of methanol dissolving from water into light hydrocarbon fractions takes place, and methanol gets carried to more remote sections. Necessary calculations can be made using the Equations 3.62–3.64.

A number of product pipelines contain sections with stagnant water, some of them being in hydrate prone locations. Since methanol dissolved in a hydrocarbon is consumed at closer sections which contain water, it is necessary to know the time required for an inhibitor to reach a hydrate prone section for a successful application of the technology.

A review of a product pipeline which consists of N stagnant sections in a row filled with water to the limit follows. The last K of N sections are operated in a hydrate regime. In such case the influx of additional liquid (for example, due to absorption of alcohol dissolved in light hydrocarbons) will first of all cause its overfilling and its consequent flow from one zone into another. Let us assume that the incoming additional amounts of inhibitor dissolve immediately and evenly in each of the separate volumes of aqueous methanol solution. Then the change of the inhibitor concentration in the i-th ($i = 1, 2, \ldots, N$) stagnant zone is described by an equation:

$$\frac{dC_i}{dt} = \frac{q}{M_i}(C_0 - C_i) \qquad (3.67)$$

where

C_i is the inhibitor concentration in the i-th stagnant zone;

q is the specific flow rate of an inhibitor;

M_i is the mass of liquid in the i-th stagnant zone;

A boundary condition for a system of Equation 3.67 is the rate of inhibitor flow into the first zone which is described by Equations 3.62–3.64. For low inhibitor concentrations in solution (C < 40%) the following correlation can be used as the boundary condition.

$$q = Q \times t \times Xm \qquad (3.68)$$

Under the assumption of the volume equality of all stagnant zones, $M_i = M_0$ and if the solubility of water in hydrocarbon is neglected, compared to the solubility of methanol in hydrocarbon at initial saturation with methanol (Xm), the solution for Equation 3.67 is:

$$C_i(t) = \left[1 - \sum_{j=0}^{i-1} \frac{1}{ji}(Q \times Xm \times t / M_0)^j \exp(-Q \times Xm \times t / M_i)\right] \qquad (3.69)$$

From this equation, the time t_H after which an inhibitor at the concentration C_H sufficient to effectively prevent hydrate formation will arrive to the section $i = k$ can be determined:

$$C_H = \left[1 - \sum_{j=0}^{i-1} \frac{1}{j!}(Q \times Xm \times t_H / M_0)^j \exp(-Q \times Xm \times t_H / M_0)\right] \qquad (3.70)$$

Injection of an inhibitor must be started during the hydrate-free regime of operation to saturate stagnant water zones with the inhibitor and to ensure an effective prevention of hydrate formation by constant injection. Injection of an inhibitor in the beginning of a product pipeline, during the period when the temperature at remote sections drops below the hydrate equilibrium temperature, may result in an opposite effect. Water can flow from the overfilled stagnant zones into a subcooled section and form a hydrate plug.

Injection of an inhibitor at a constant rate is appropriate in the beginning of a hydrate prone section which prevents the saturation of hydrate-free stagnant zones with methanol and decreases methanol consumption. Thus, the use of this method of inhibition requires us to predict the dynamics of changes of a hydrate prone section in time, the optimum concentration of an inhibitor at different locations, and the times of start and end of inhibitor injection.

It should be noted that the considered cases are applicable only in situations when there is no possibility to remove liquid water from a pipeline by passing pig pistons, drying, or other methods.

Prevention of Hydrate Formation by a Periodic Injection of Portions of Inhibitors

One of the prophylactic means of fighting hydrate plugs is to periodically pass through a pipeline large volumes of hydrate inhibitor liquids poorly soluble in hydrocarbons, for example, alcohols or glycols. This method most often is used to clean pipelines constructed of pipes with different diameters and where pig pistons cannot be used effectively to clean water from a pipeline.

This method is based on a piston displacement of water from stagnant zones with inhibitors which then provide effective protection of the line for a long time. However, some complications occur during the implementation of this method which decreases its effectiveness, and in a number of cases produced the opposite results. Thus, it is necessary to thoroughly justify this technology and to evaluate the degree of risk from negative results prior to solving questions concerning this method.

The average flow rate of hydrocarbons is assumed to be, at most, 1 m/s during the design of pipelines. Interaction of a stationary water phase in a

stagnant zone with a hydrocarbon during the movement of such flows can be considered as equilibrium. Influx of a portion of a water soluble agent results in it dissolving in water and in a decrease in the concentration.

Look at a pipeline as a system of connected filled vessels with volumes V_i to describe the process of inhibitor concentration change in coexisting stagnant zones. Any amount V of reagent entering the first zone results in an immediate dissolving and flow of the same volume with the new concentration into the next zone, etc. Change of concentrations in the given zones is then described by a system of Equations 3.67. A boundary condition is the volume entering the first zone of a pipeline, i.e. $q \times t = V$.

After the transportation of a complete portion of inhibitor with volume V the concentration of inhibitor in each stagnant zone with equal volumes of water V_0 is described by the correlation:

$$C_i = C_0\left[1 - \sum_{j=0}^{i-1} \frac{1}{j!}(V / V_0)^j \exp(-V / V_0)\right] = C_0 F(i, M) \qquad (3.71)$$

where

C_0 is the concentration of agent in the liquid entering the first zone.

Calculations indicate that at least 150 m^3 of methanol with the initial concentration of 96% must be injected into a product pipeline with seven stagnant zones, each having a volume $V_0 = 50$ m and a minimum agent concentration C = 10% to prevent hydrate formation. The obtained correlations allow us to quickly determine the required volume of an agent to prevent hydrate formation in the whole pipeline.

It is worth mentioning that the obtained correlations are universal and are applicable to calculate an injection of any agent. Differences in agents will be accounted for in the value of the maximum concentration preventing hydrate formation and in the initial injected concentration of an agent.

A detail for using inhibitor jackets as a means of preventing hydrate plugs formation in a product pipeline is the advanced movement of water into a hydrate prone zone, compared to an average flow velocity. In some cases this may cause plugging because it promotes the movement of the hydrate phase from stagnant zones into separate sections where hydrate can accumulate. The scenario of hydrate plug formations in the Nizhnevartovsk-Yuzhnyi Balyk product pipeline in December 1982 can be considered as an example. With winter coming and temperatures decreasing to 5–6°C, a single 50 m^3 portion of methanol was injected into the pipeline from the Nizhnevartovsk gas processing plant on December 11 to prevent hydrate formation. The average product velocity was decreased to V_{Ave}~0.66 m/s. A sharp decrease of the pipeline flow capacity was noticed on December 12, and work on removing plugs from pipeline sections started at a distance of 150 km were started on December 13.

Based on earlier statements, injection of an inhibitor had promoted the movement of water into hydrate prone areas (150 km and beyond) one to one and a half days after the injection of methanol, although it was expected to take three days. This time interval was interpreted as a lateness in treatment, although it was the injection of methanol which caused the plug formation.

Kinetics and Morphology of Gas Hydrates

Introduction

Many articles have been published concerning the process of gas hydrate formation (Makogon, 1970, 1974, 1981, 1996; Visniauskas and Bishnoi,1983, 1985, 1994; Englezos,1987, 1993; Selim and Sloan, 1989; Sloan 1990; Makogon and Sloan, 1994; Elperin and Fominykh, 1996; Mori, 1996; Mori and Mochizuki, 1996; Narita and Uchida,1996; Sugaya and Mori,1996; Svartas et al., 1996); however, very few studies have been carried out on the formation of crystallization centers of hydrates and on their growth. A majority of researchers have obtained hydrates under dynamic conditions. They created the surface of gas-water contact either by mixing, including bubbling of gas through the water, or by mechanical agitation of the chamber by means of various crank gears or electromagnetic mixers. These conditions, in turn, exert great influence on the structure of the crystals being formed. Through experiments, the researchers became well aware that at the beginning of hydrate formation the temperature can vary widely, at one and the same pressure.

As a result of experimental studies it was determined (Makogon, 1974; 1981) that the process of hydrate formation starts at the free gas-water surface:

a. on a free contact surface of liquid water-gas or liquid water-liquid gas

b. on the surface of the water drop-water film that condensed in a gas volume

c. on the surface of gas bubbles that separate out within a water volume

d. on the interface of the condensed gas drops-dispersed condensed gas, as the condensed gas evaporates within a volume of free gas saturated with water vapors

e. on the water-metal interface where the adsorption of the molecules of gas dissolved in the water takes place

After the formation of critical size nuclei, a hydrate film forms around them and blocks the free interface. Radial growth rate and thickness of the hydrate film depends on the gas and water compositions and pressure and supercooling of the process.

After the hydrate film formation over the whole gas-water interface, the surface-contact process becomes a diffusive one, when the molecules which form hydrate to the sorptional surface of the growing crystal through defects in the formed hydrate film.

Sorptional surface can be on the free surface of growing crystal (massive hydrate crystals) and at the base of the growing crystals (whiskery crystals).

Molecules of water and gas diffuse to the sorptional surface both from a volume of gas and from a volume of water through the hydrate film at the gas-water interface. During the formation of whiskery crystals, hydrate forming molecules go to the sorption surface on the surface of growing whiskery crystals by means of a tunnel diffusion. Tunnels are formed at the vessel-growing hydrate interface. During tunnel diffusion the size of the diffusion channels are much smaller than during the sorption by an open surface of a growing crystal. The whiskery hydrate crystal growth prevails in a closed volume.

Massive crystals grow more often in a volume of gas. Whiskery crystals grow both in a volume of gas and a bulk of water. Gel-like crystals are formed at certain conditions in a bulk of water, whose nature will be studied further. In redistribution of mass and volume of crystals a change occurs in P-T conditions—possibly changes in crystals also occur. Crystals may sublimate in a volume of gas, dissolve in a volume of water, form new forms of crystals. Further discussion and examples of these crystals can be seen in figures later in this chapter.

Unfortunately, the absolute majority of research done was not aimed at discovering the physics of hydrate formation and dissociation. The mechanism of nucleation and growth of hydrate crystals in static conditions and in fluid flow is unknown at this time. Previous models for hydrate kinetics that are quantified have normally been limited to the regime of steady crystal growth. There are not satisfactory descriptions of

possible mechanisms and corresponding induction times for the stage of primary and secondary nucleation.

Kinetics of hydrate formation was viewed only from the aspect of hydrate accumulation, depending on the degree of flow supercooling and turbulence. These are only the external factors of hydrate formation. The kinetics of hydrate dissociation was studied very little.

Morphology of hydrate crystals has hardly been studied at all, although it allows us to discover the crystals nucleation and growth. Our research in 1995-96 showed the existence of different types of crystallization and a large variety of crystal morphology types, depending on conditions. The modern theory of hydrate formation processes cannot answer many fundamental questions.

Several results of our experimental research performed at the Texas A&M University are presented here.

Experimental Technique

The experiments were carried out in a bathyscaph chamber with a volume of 890–1060 cm^3 (Figure 3-25). The chamber design made visual monitoring of the process possible from five sides, through flat 40 mm round thick glass windows, with a diameter of 84 mm. This chamber allowed us to conduct a complex investigation of both formation and decomposition of hydrates in static and in dynamic conditions. The operation pressure was up to 20 MPa.

Determination of the rate of crystallization nuclei and of hydrate formation was done under isothermal conditions, with the temperature of the process maintained at $+/-0.1°C$. The temperature was controlled in gaseous and liquid phases with an accuracy 0.05°C, and a pressure control system with an accuracy 0.1%. The chamber was equipped with a special mechanism that allowed us to measure the solubility of gas in the water with free gas-water contact, and in water with hydrate film on the water-gas surface, and determine the dynamics of phase correlation of components during hydrate formation without disturbing the P-T and kinetic conditions.

The precision of measuring the volume of the sampled solution of gas and water is to 10 mm^3. The cell pressure could be constant or preset, varying with the supply of gas into the volume of gas or by bubbling gas through a layer of water. The pressure could also be controlled by an injection of fresh water or of water pre-saturated with gas through a micropump with a water flow rate of 0.01–0.1 cm^3/min. Water could be

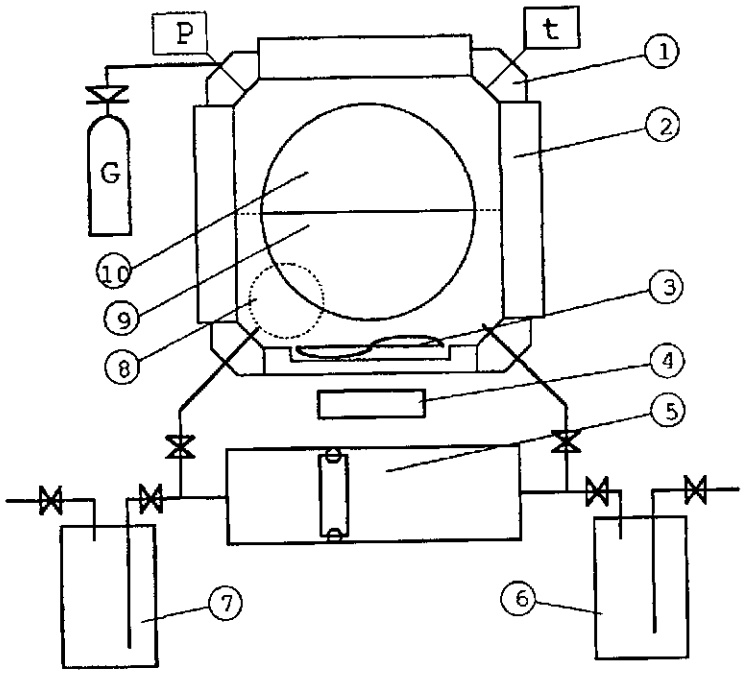

Figure 3-25 Schematic of the apparatus for studying the gas-water phase ratios and kinetics of hydrate formation.

1 - reactor cell
2 - windows for visual control
3 - magnetic stirrer
4 - magnetic stirrer drive
5 - compensation system of liquid withdrawal
6 - system of measuring phase ratios
7 - system of injected liquid pre-treatment
8 - two-layer elastic vessel
9 - liquid water
10 - gas
11. high pressure gas source
12 - pressure control system
13 - temperature controller

supplied into the cell as a bulk liquid or in a microdispersed state with a pressure drop at a throttle of up to 20 Mpa.

The cell allows us to study the formed hydrate film, and to determine various properties of hydrates. Results of experiments showed that three types of hydrate crystals may form simultaneously at the same ambient P-T conditions: massive; whiskery, and gel-like crystals. The results were obtained for methane Ultra High Purity, and a double-distilled water.

The cell pressure could be kept constant, or preset—varying by supplying gas into the gas volume, bubbling gas through a layer of water, or pre-saturating water with gas with a micropump. Water could be supplied into the cell in a bulk liquid or in a microdispersed state with a pressure drop at the throttle of up to 20 MPa.

The reactor cell was equipped with a remote magnetic stirrer, and a mechanical system provided for the creation of a free gas-water interface at a rate equal to the rate of a hydrate film formation.

The cell allows us to study the morphology of crystals, to conduct direct measurements of thickness of the formed hydrate film, and to determine various properties of hydrates.

Conditions and Places of Hydrate Formation

The study of morphology of hydrates allows us to understand the basics of the hydrate formation and decomposition.

A majority of experimentalists study the process of hydrate formation in dynamics, trying to approach the real conditions of well and pipeline operation. Such an approach prevents the study of crystal morphology.

In order to approach the understanding of the basics of hydrate crystal nucleation and growth kinetics, we constructed a number of experimental apparatuses during the 1960s which allowed us to study hydrate morphology in static conditions, both in a free volume and in porous media. Several generalizations of the obtained results were presented in the monograph (Makogon, 1966, 1974, 1981). It was shown that the process of crystal nuclei formation occurs at the free gas-water interface. This can be a boundary between a large volume of liquid water and gas. At that stage the gas can exist in a free or in a condensed state. This can be a spherical surface of a gas bubble in a volume of water or a water drop in a volume of gas. This can also be a very thin film of water condensed in the gas phase on the walls of a container (a well, a pipeline, a separator). Lastly, it can be a mono or a multimolecular layer of gas molecules released from an aqueous solution during a change in P-T conditions and adsorbed on the surface of the container.

Study of the locations of formation and growth of hydrate nuclei has shown that with large volumes of water in the presence of a free gas-water interface, nucleation proceeds at the surface of a gas-water interface and at the surface of gas microbubbles in a near-surface layer of water. Gas hydrate grows to the gas-water interface because of a diffusive influx of gas, and a film forms rapidly around the nucleation "center."

A dependence of the rate of hydrate nuclei formation at the free gas-water interface and of the rate of linear crystal growth on pressure, temperature and the degree of supercooling of the process was established (Fig. 3-26).

Kinetics and morphology of hydrate crystals depend on many factors—composition of hydrate formers, pressure, temperature, rate of cooling, rate of formation of a free gas-water interface, intensity of diffusive processes, etc.

In the first stage of the hydrate formation process, when a hydrate forms at a free gas-water interface, the thickness of the forming film ranges from 0.005 to 0.2 mm. For example, the thickness of the hydrate film for methane obtained at 8.3 Mpa and 6.6°C (a supercooling 4.4 K) and measured 60 seconds after its formation 0.005 mm, and at P = 8.12 Mpa and T = 1.8°C (a supercooling of 9 K) measured 90 seconds after its formation—0.01 mm. Thickness of the above film kept at constant pressure and temperature for 293 hours was 0.08 mm. However, the method of measurement with a precision micrometer doesn't tell us whether it is a solid monolithic hydrate film or an agglomeration of microcrystals formed on the initially formed hydrate film.

In order to start the formation of crystal nuclei and hydrate growth there must always be a certain supercooling whose magnitude depends on pressure, temperature, composition of gas, and state of water (Figs. 3-27, 3-28, and 3-29). The degree of supercooling of the hydrate formation depends on the pre-crystallization state of water and reaches 1–12°C for methane at pressures of up to 12 Mpa.

It was shown that water has a structural memory after hydrate decomposition. Stability of clusters of water molecules depends on the degree of superheating of water obtained after hydrate decomposition. The less the superheating of water above the hydrate melting point, the less supercooling is needed in order to start the process of hydrate formation.

At a low rate of cooling (under 0.1–0.6 K/hour), there is no large temperature gradient between the walls of the container and the cooled water in the container. Crystal nuclei form at the free gas-water interface, which is remote from the effect of capillary forces and from meniscus at the gas-water-metal interface.

At a high cooling rate (1–3 K/hour and higher), when the temperature of the cooling metal surface is much lower than the temperature of the cooled water (beyond the meniscus), the process of hydrate formation can start at the gas-water-metal boundary. The lower the rate of cooling, the lower the degree of supercooling and the more hydrate nuclei are formed. The lower the rate of hydrate formation around the nuclei, the thinner the formed hydrate film.

Growth of hydrates at the gas-water interface proceeds at a constant rate determined by P-T conditions. Figures 3-30 and 3-31 present the dependencies of the radial growth rate and thickness of the forming hydrate film on pressure and supercooling of the system.

A system supercooled by 6–10°C can exist in a metastable state for many hours without forming hydrates (see Figures 3-32 and 3-33). Hydrate formation proceeds at a high rate in such system.

After the nuclei forms on the free gas-water surface, a hydrate film grows around the nuclei and closes off the free surface (see Figures 3-27, 3-28, and 3-29). This hydrate surface allows the formation of massive hydrate crystals. Figure 3-34 shows a photograph of unique methane hydrate crystals which formed at the surface of a film hydrate at P = 7.7 Mpa and T = 5°C. The maximum length of crystal rays was 40 mm; diameter of spheres which composed the rays was up to 0.2 mm. Rays were characterized by a very high resilience and strength and easily withstood a vibration of a relative frequency. With time the ray crystals of a slim purity will get amorphous formations growing and lose their resilience. Each elementary sphere composing such a ray crystal contains 4.64×10^{15} hydrate cavities.

Figure 3-35 shows the bunches of methane hydrate rays formed simultaneously in the same conditions as the hydrate shown in Figure 3-34. It should be noted that the rate of such ray formation is rather high. Formation is completed within a fraction of a second. These are shooting crystals. Hydrate formation proceeds from the water vapor contained in gas. Figure 3-36 shows a spiral crystal of methane hydrate, grown in a volume of gas.

At certain conditions, when there is a large diffusive flow of water molecules through the non-curing defects in a hydrate film, the process of massive hydrate crystal formation may proceed until the complete conversion of water into hydrate. Figure 3-37 presents a photograph which shows the development of such a process.

Massive hydrates are characterized by a large variety of crystal shapes that depend on the composition of gas and water, pressure and temperature, etc. (see Figures 3-34 through 3-42). Massive hydrates can start to form on the steel of a cell from condensed water vapor film (see Figures 3-37 and 3-38). Figure 3-39 shows a photograph of methane hydrate formed on the surface of a water droplet. Figures 3-40a and 3-40b show two massive crystals of methane hydrate grown under different circumstances of supercooling in a volume of gas. Figure 3-41 shows the growth of a massive ethane hydrate, P = 1.4 Mpa; T = 5.5°C. Figure 3-42 shows

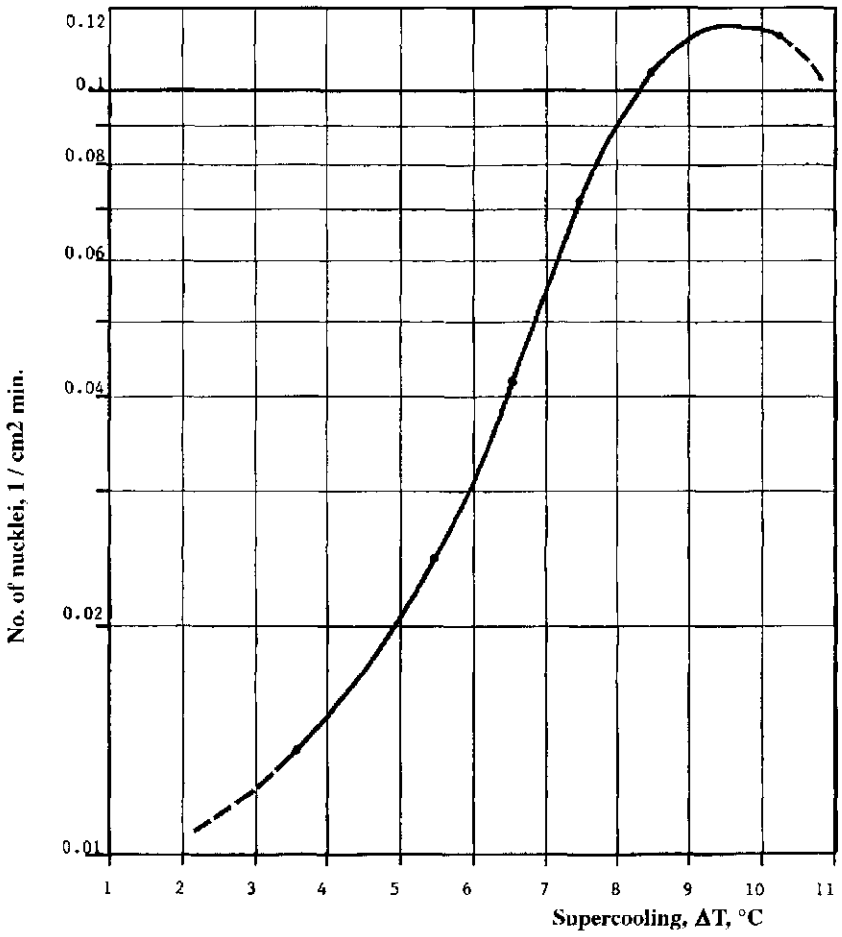

Figure 3-26 Dependence on supercooling of formation rate of methane hydrate nuclei on the free gas-water surface.

a series of photographs of a gradual growth of a massive propane hydrate at P = 1.4 Mpa; and T = 2.2°C.

Hydrate formation may start on the wall of a cell and spread over the whole gas-water interface in the presence of intensive cooling (1–3°C/hour or more) and in the presence of a large thermal gradient.

Only massive hydrate crystals whose growth is determined by adsorption of gas and water molecules on the growing crystal surface form at supercooling up to 3°C (Figures 3-29 and 3-31).

Massive crystals grow mostly in the gas phase because of different molecular sizes of gas and water and different diffusion coefficients

through a previously formed hydrate film at the gas-water interface. The growth rate of massive hydrates is determined by diffusive and sorption influx of gas and water molecules and intensity of heat removal from the forming crystal surface.

In the present solid hydrate film and increase in the degree of supercooling over 2.8–3.2 K, whiskery crystals start to grow in the area of strong capillary force action. In this area, water pressure is lower than the vapor pressure by the amount of the capillary pressure, and favorable conditions for whiskery hydrate formation are created. A change of capillary pressure P_c can be written as

$$\Delta P_S = \frac{dP_s}{dP_c} P_c \tag{3.71}$$

Whiskery colonies of thread-like crystals grow in volumes of both gas and water and have high stability and crystallization pressures. The linear growth rate of whiskery crystals is three to four orders of magnitude less than of massive hydrates on a free gas-water surface.

The sorptional activity of whiskery crystals is much higher than that of massive crystals because of smaller sorption channels (between the solid steel surface and cavities of forming hydrates). Table 3-3 and Figures 3-43 and 3-44 present the dependence of the formed whiskery hydrates' length on pressure and degree of supercooling in time. The rate of whiskery crystals growth is much higher than that of the massive crystals without free gas-water interface.

Their main distinction is that they grow, not from the crystal's surface, but from its base by the diffusion of gas and water molecules on the surface of the growing crystal to its base and by a tunnel sorption (between the solid surface of steel and base of growing crystal) that "pushes off" the growing crystal (similar to grass growth).

As displayed in these photos, three different types of crystals form at different pressure-temperature conditions: massive (Figures 3-27 through 29; 3-34 through 42), whiskery (Figures 3-45 through 58), and gel-like crystals (Figures 3-59 through 60) may form.

Figure 3-45 shows a colony of whiskery crystals of methane hydrate grown in water under a hydrate film on the gas-water surface. The growth time for this colony was 25 hours.

Figure 3-46 shows the colony of whiskery crystals grown in the same P-T conditions as in Figure 3-45, only in a gas sphere. Figures 3-47 and 3-48 show two colonies of whiskery crystals of hydrate methane formed simultaneously in the same conditions: P = 87 bar; T=275.1 K; only with different views. Figure 3-48 is the frontal view and Figure 3.47 is from

Table 3-3 Dependence of the length (mm) of the formed whiskery methane hydrate on pressure, and degree of supercooling (Teq-Th) in time.

		Teq -Th	*Growing Time, Hours Growing in the Bar*							
No.	*P,*	*°C*	*1*	*2*	*6*	*12*	*24*	*48*	*96*	*120*	
1.	48.6	4.5	1.0	2.0	4.3	7.4	10.0	14.0	18.3	–	Gas/Water
2.	102.0	6.1	0.6	1.0	2.7	4.8	8.0	13.2	22.0	25.6	Gas/Water
3.*	96.0	16	1.8	6.0	12.5	16.9	23.0	29.0	–	–	Nat. Gas
4.	84.0	6.6	2.0	3.2	7.2	14.0	24.0	34.5	42.0	43	Gas/Water
5.	63.8	7.5	3.6	8.0	20.0	26.0	32.0	39.4	46.0	47	Gas/Water
6.	57.8	6.9	5.0	10.0	24	32.2	38.2	42	–	–	Gas
7.	98.0	9.3	37.0	47.0	72	86	–	–	–	–	Gas/Water
8.	85.9	5.6	6	10	25	38	–	–	–	–	Water
9.	85.4	5.6	10	18	40	64	88	–	–	–	Water
10.	84.2	5.6	6	11	26.5	43	61	66 (32 hr)	–	–	Water

*Nat. Gas-Natural Gas, Spec. Density 0.6
Gas/Water-Started on the Gas-Water border

above. The formation of these crystals starts under the hydrate film on the gas-water surface.

Figure 3-49 shows how a pipeline can be closed by hydrate crystals.

Figure 3-50 shows developing whiskery crystals in the gas and water volume.

Figure 3-51 shows the three different hydrate methane crystal types: massive; whiskery and gel-like. Whiskery hydrate crystals of propane formed in water are shown in Figure 3-52.

The solubility of gas in a volume of water under hydrate film on the gas-water surface is much lower than in bulk water with a free gas-water surface (chapter 1).

The high sorptional activity of whiskery crystals growing in a volume of water results in a significant decrease of the content of gas dissolved in water and in dissolving of the crystals. Figures 3-53 through 58 show this change with time.

Figure 3-59 shows the methane hydrate crystal types grown in the gas and water volume (gel-like is in the water). Figure 3-60 also shows soft gel-like methane hydrate crystal formed in water.

Figure 3-61 shows a "massive-amorphous" crystal formed on the gas bubbles in a volume of water in a dynamic situation.

Our control methods were insufficient for detecting sublimation of crystals in a gas volume after decreasing the amount of water molecules above the growing crystals.

The obtained experimental data correlates well with the new theory of hydrate formation proposed by Kvamme (1994–1996). Comparison of the obtained experimental data with the main positions of the new theory of hydrate formation makes a solid base for the theory. The use of a number of empirical coefficients will be required for engineering calculations, but this problem can be solved.

Let us briefly review the essence of Kvamme`s theory for the hydrate formation processes. The theory presented here is based on the assumption that the primary nucleation takes place on the hydrate former side of the interface. The theory is formulated in four steps:

1. Adsorption of hydrate former on water surface
2. Restructuring to form partial hydrate cavities
3. Closing of cavities and growth/decay of metastable particles
4. Steady growth of stable nuclei

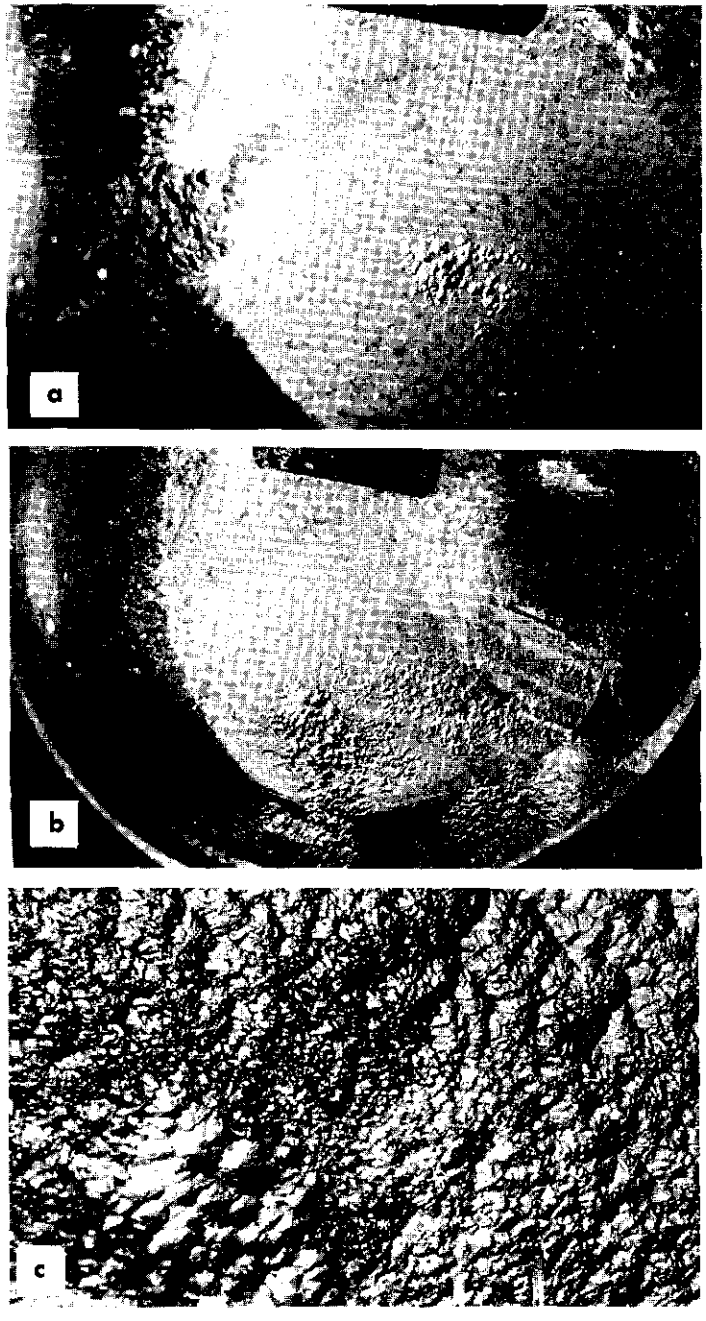

Figure 3-27 The dynamic of formation of methane hydrate crystallization nuclei on the surface of gas-water contact (P = 98kg/cm^2; Δt = 0.5°C).

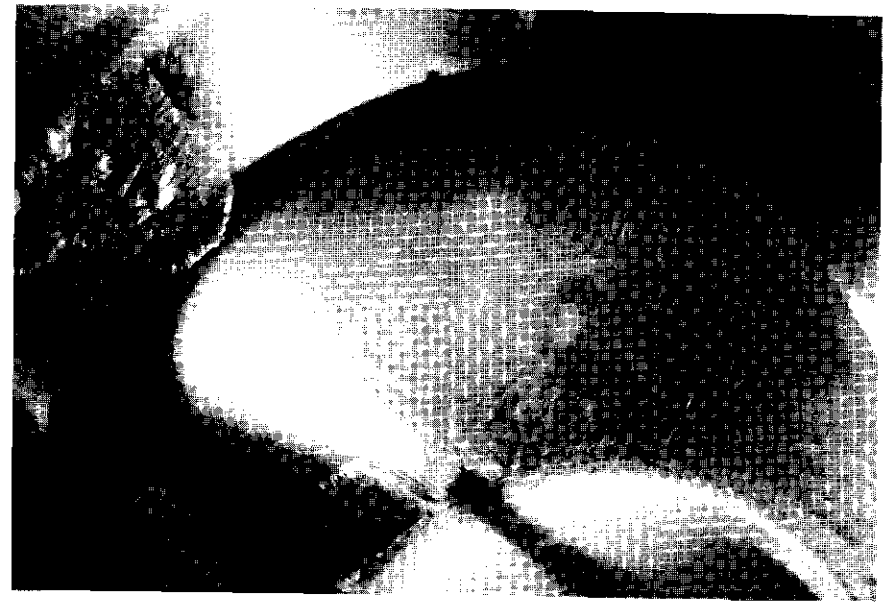

Figure 3-28 Photograph of a growing methane hydrate film on the water surface (P = 41.4 atm.; T = 277 K).

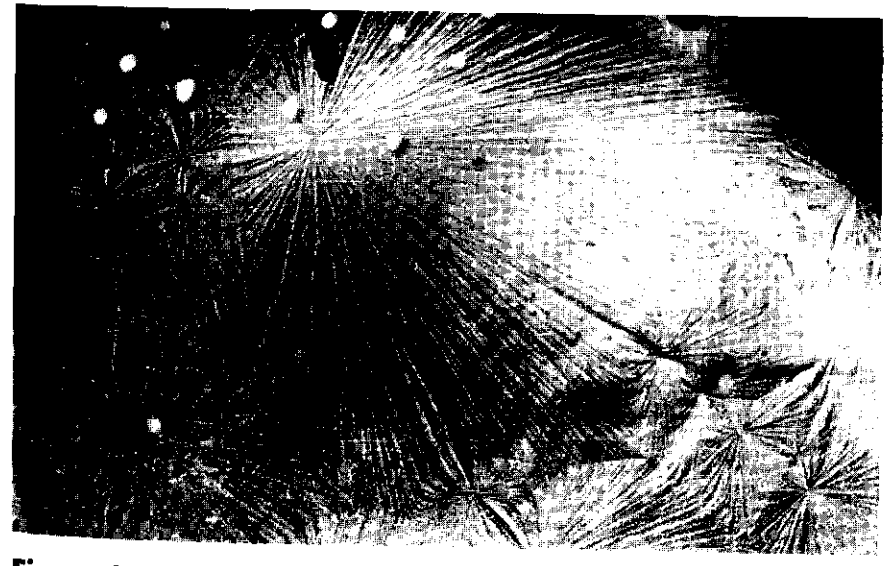

Figure 3-29 Methane hydrate film (P = 57 kg/cm^2; T = 5.5°C).

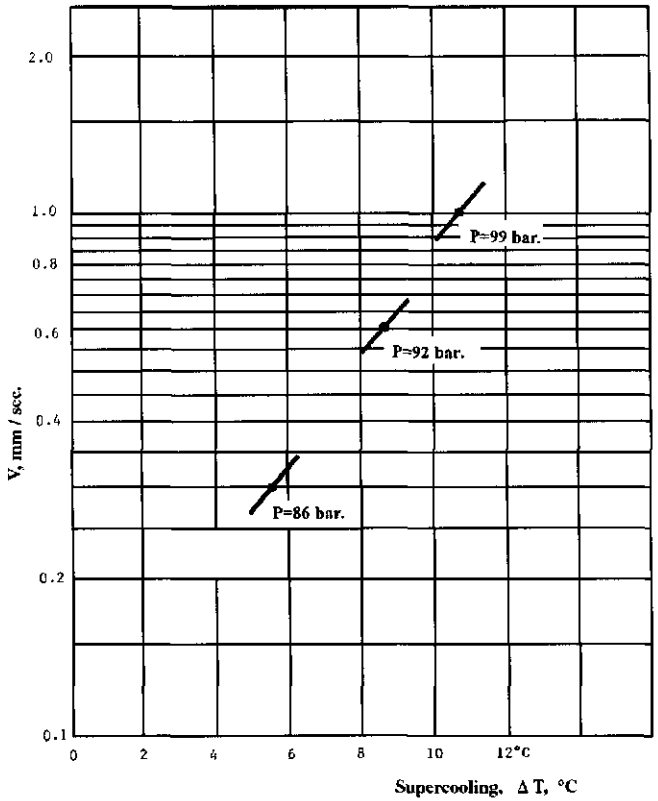

Figure 3-30 Dependence of the rate of radial growth of surface-contact hydrate of methane on supercooling.

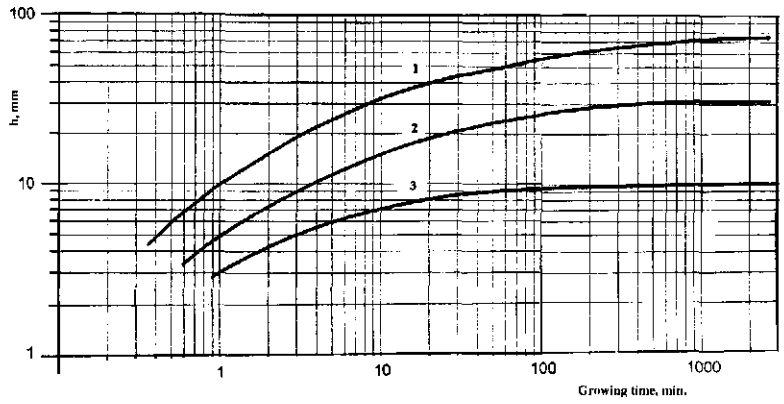

Figure 3-31 Dependence of thickness of methane hydrate film, formed on the free gas-water surface on pressure and supercooling (1 is P = 8.1 Mpa, $\Delta t = 9°C$; 2 is P = 8.3 Mpa, $\Delta t = 4.4°C$; 3 is P = 8.4 Mpa, $\Delta t = 2.7°C$).

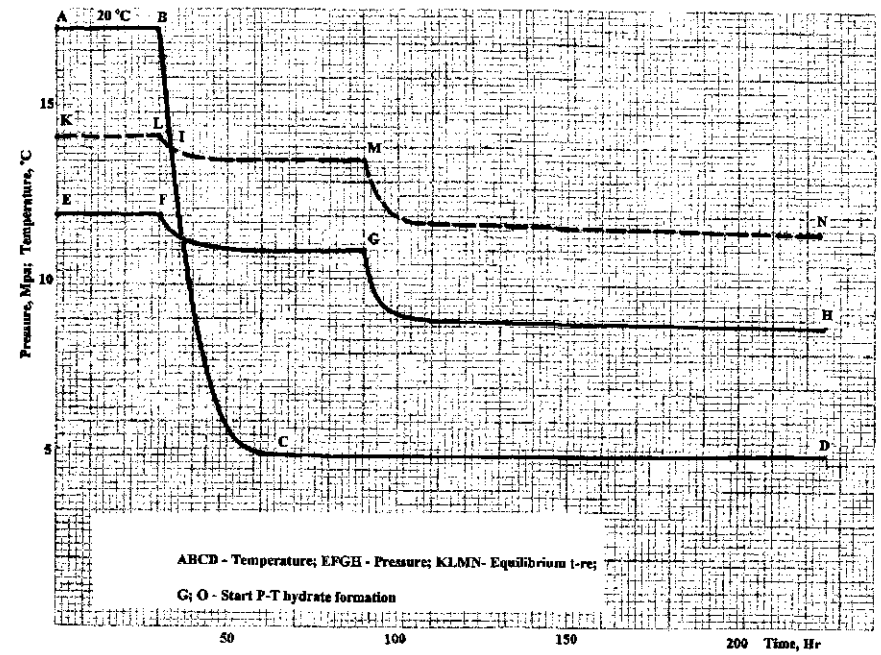

Figure 3-32 Dependence of start time methane hydrate formation.

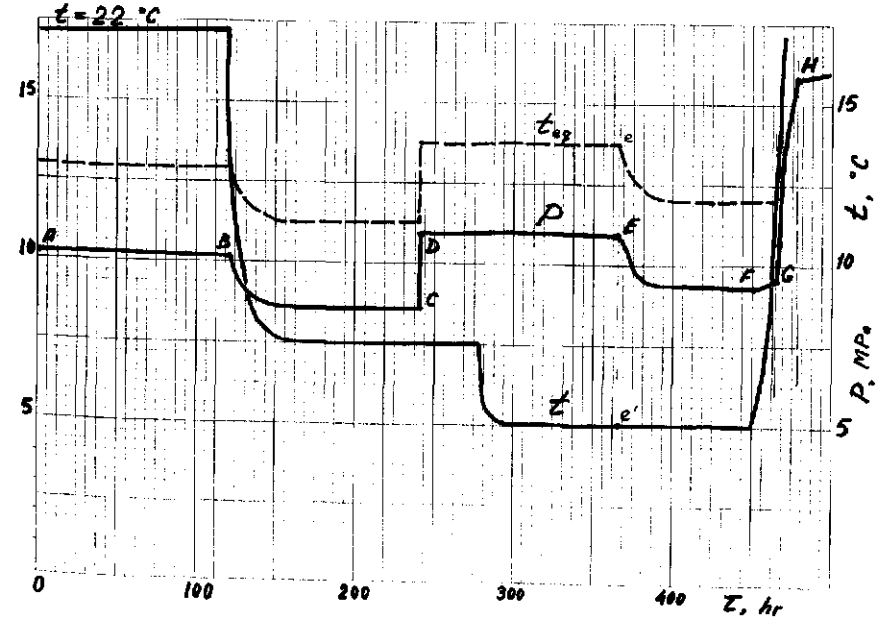

Figure 3-33 Dependence of P-T methane hydrate formation in the time.

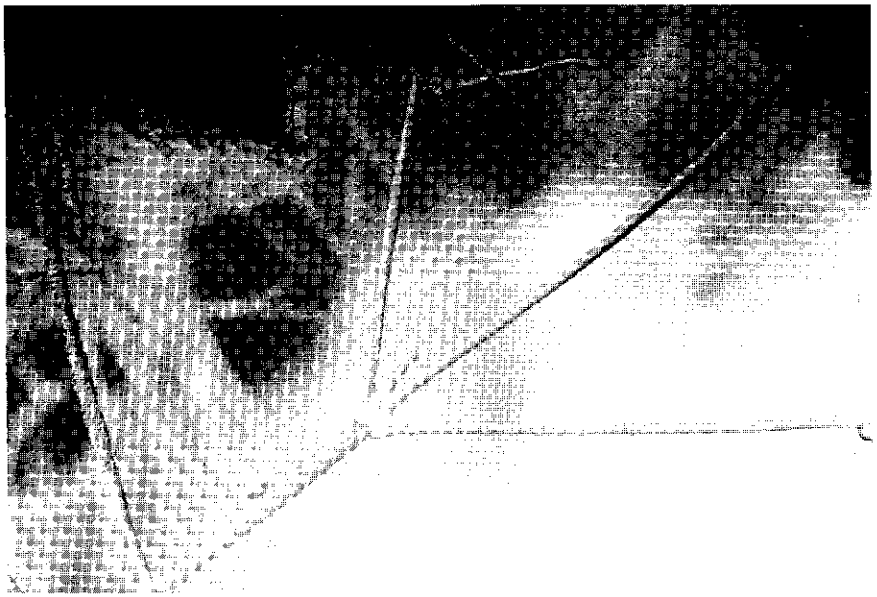

Figure 3-34 Massive methane hydrate crystals (P = 77 kg/cm^2; T = 283.3 K).

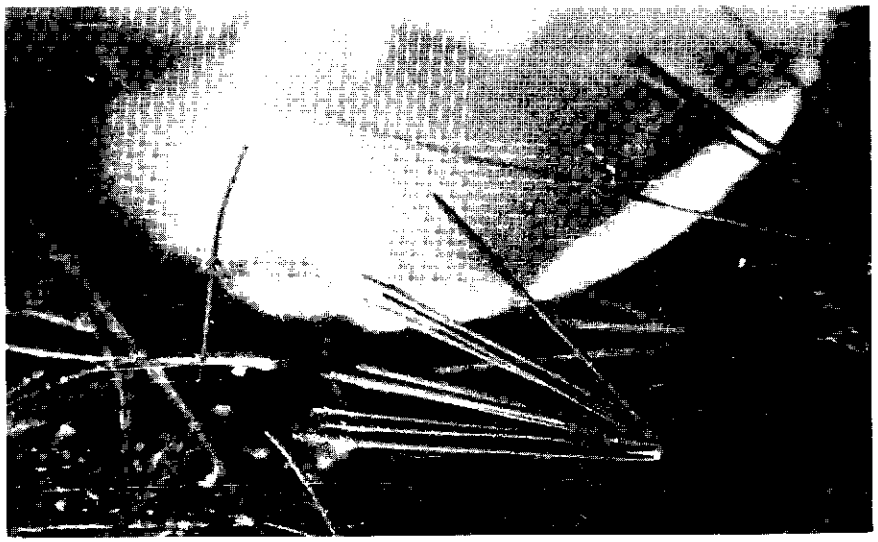

Figure 3-35 Massive methane hydrate crystals (P = 77 kg/cm^2; T = 283.3 K).

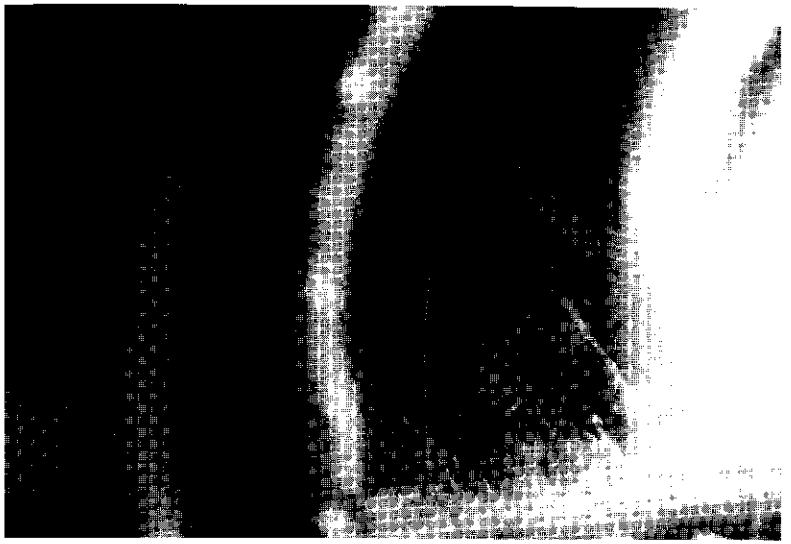

Figure 3-36 Spiral crystal of methane hydrate (growth P = 86 kg/cm^2; T = 27 K). A spiral with a total of 82 turns with outside diameter of spiral 0.2 mm and constant filament diameter of 0.05 mm. Total length of spiral was 42 mm with only one point of support.

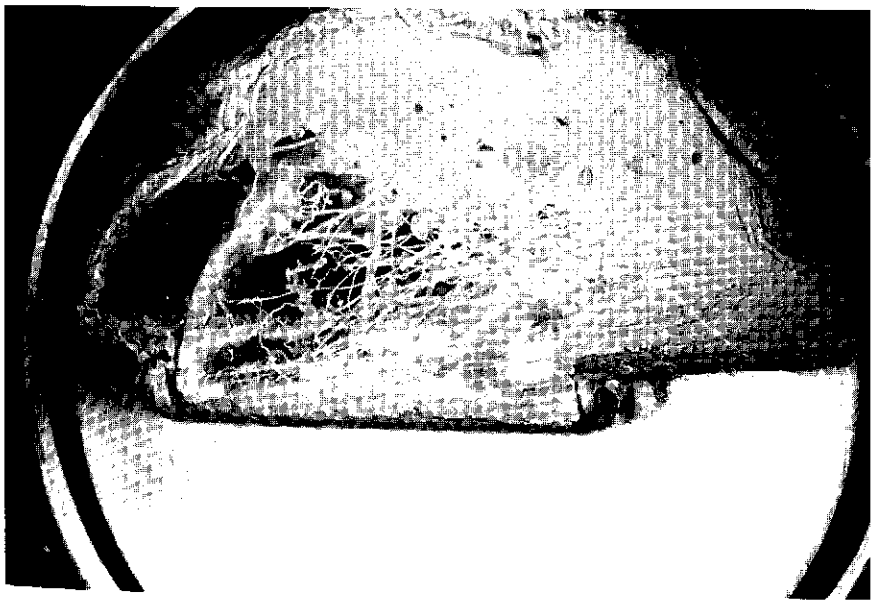

Figure 3-37 Massive crystal of methane hydrate grown over hydrate film in a gas volume (P = 56.4 kg/cm^2; T = 275 K).

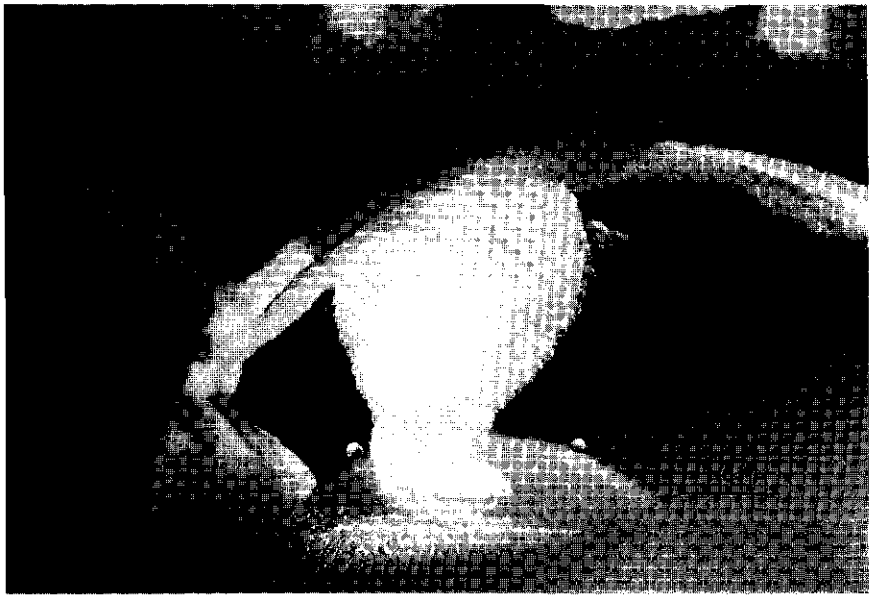

Figure 3-38 Massive methane hydrate in a gas volume (P = 60 bar; T = 275.5 K).

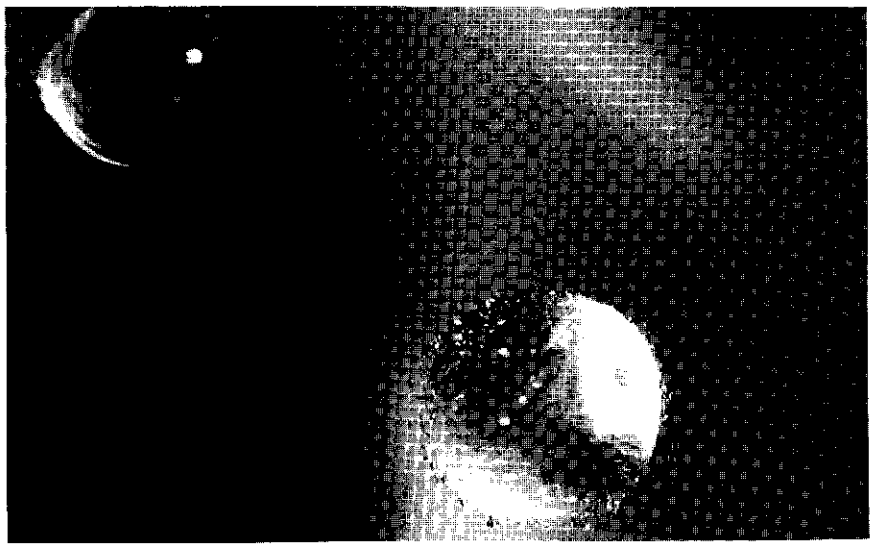

Figure 3-39 Massive methane hydrate grown on the water drop surface (P = 95.2 bar; T = 278.7 K).

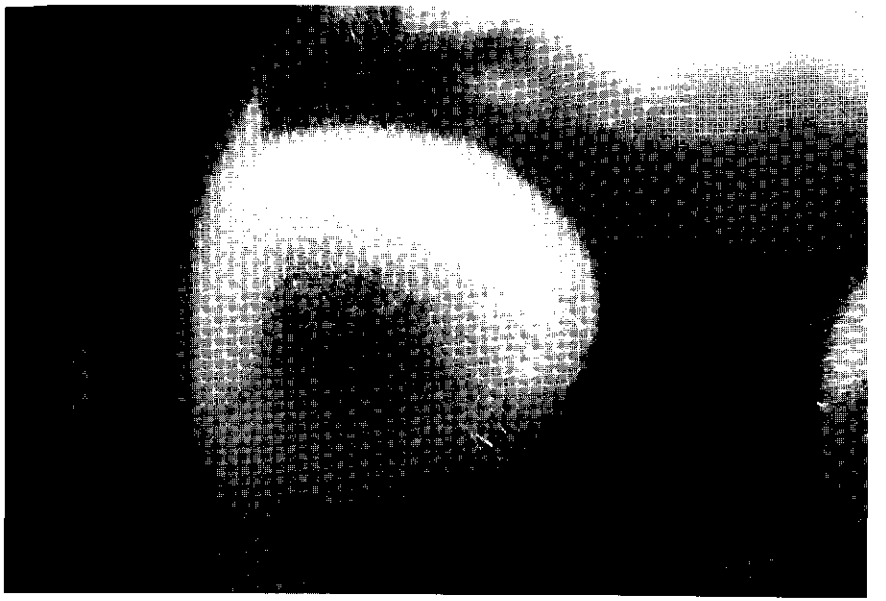

Figure 3-40a Massive crystals of methane hydrate grown in a gas volume (P = 74.9 kg/cm^2; T = 281.2 K. supercooling 1.7 K).

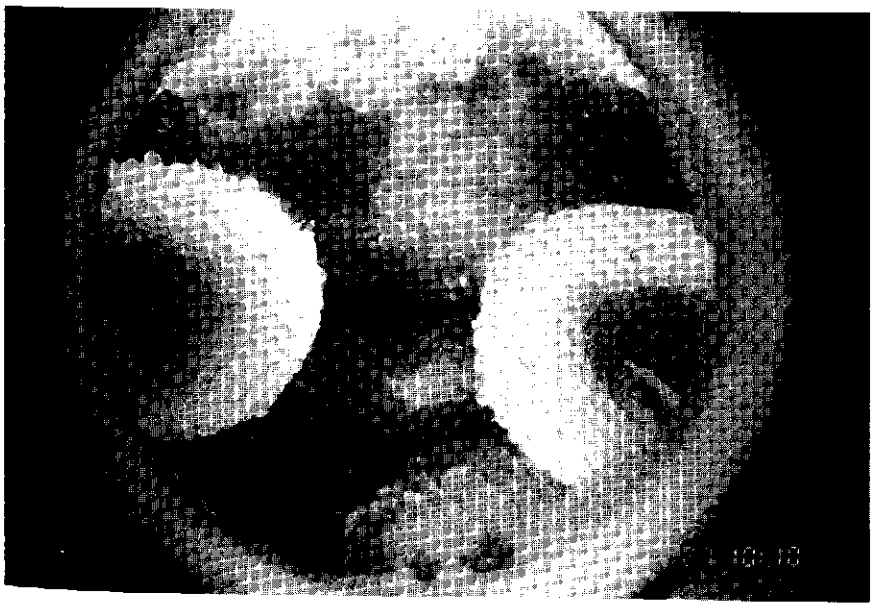

Figure 3-40b Massive crystals of methane hydrate grown in a gas volume (P = 61.25 kg/cm^2; T = 281.0 K. supercooling 0.2 K).

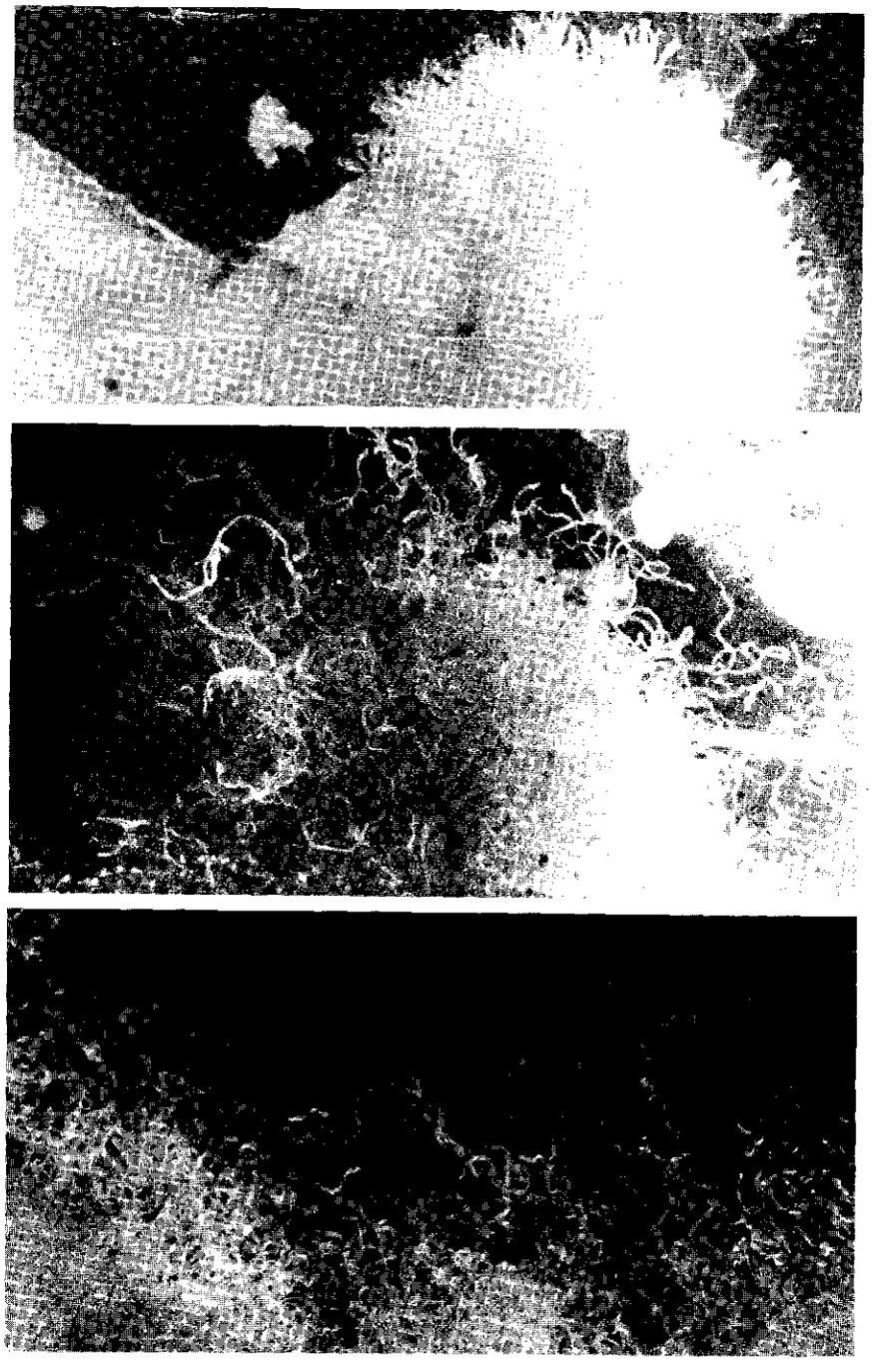

Figure 3-41 Growth stages of a massive ethane hydrate (P = 1.4 Mpa; T = 5.5°C).

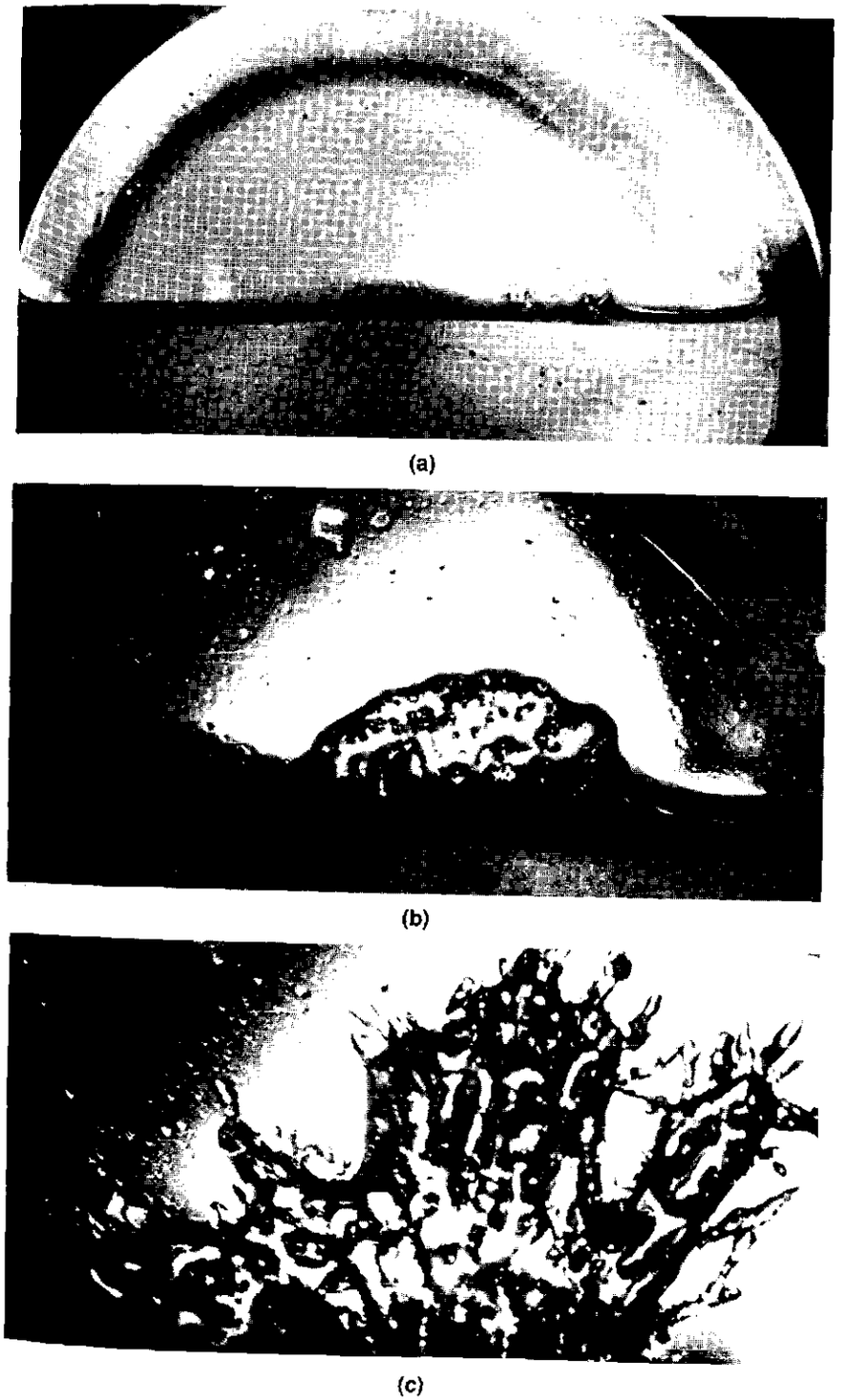

(d)

(e)

Figure 3-42a–e Dynamic growth of propane hydrate formation (a–e); P = 12.8 kg/cm^2; T = 274.5 K.

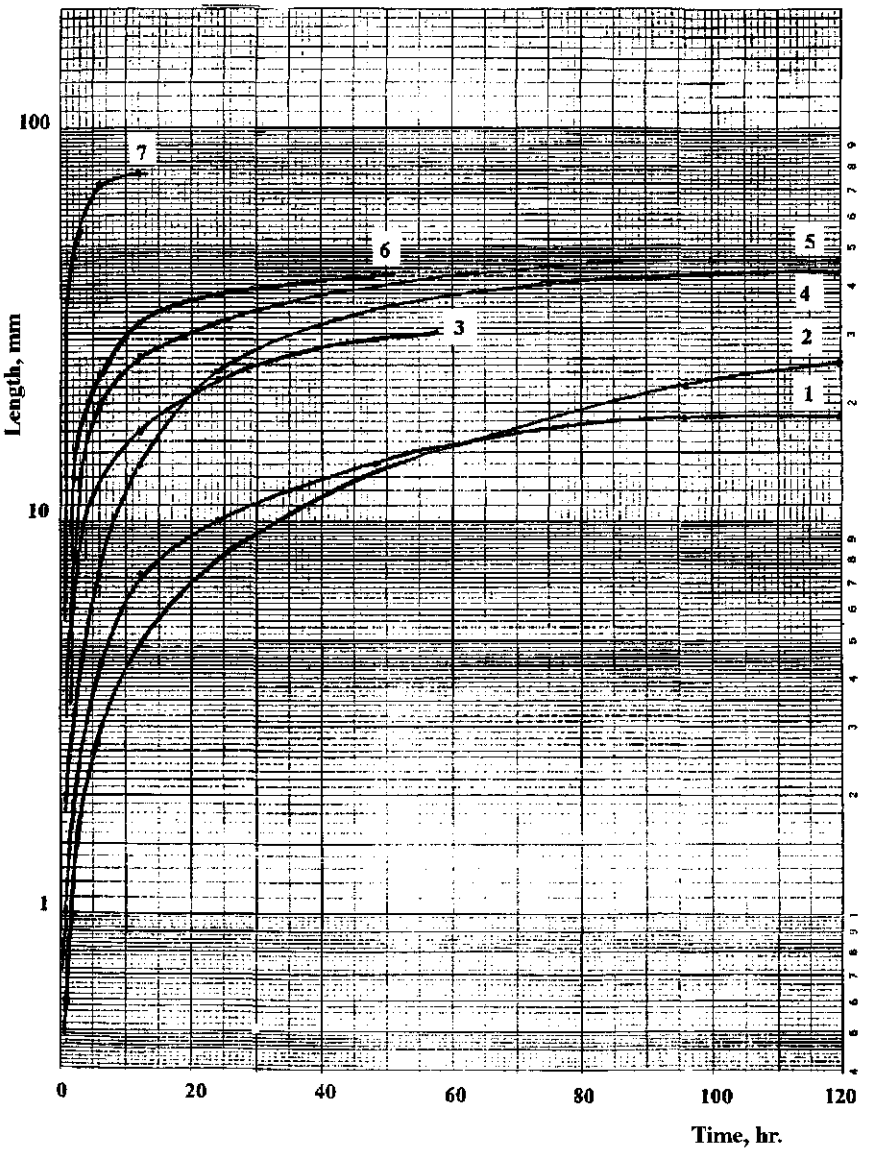

Figure 3-43 Dependence of the length (mm) of the formed whiskery colonies of methane hydrate on pressure, temperature and degree of supercooling. (Experiment 1–7, Table 3–3.)

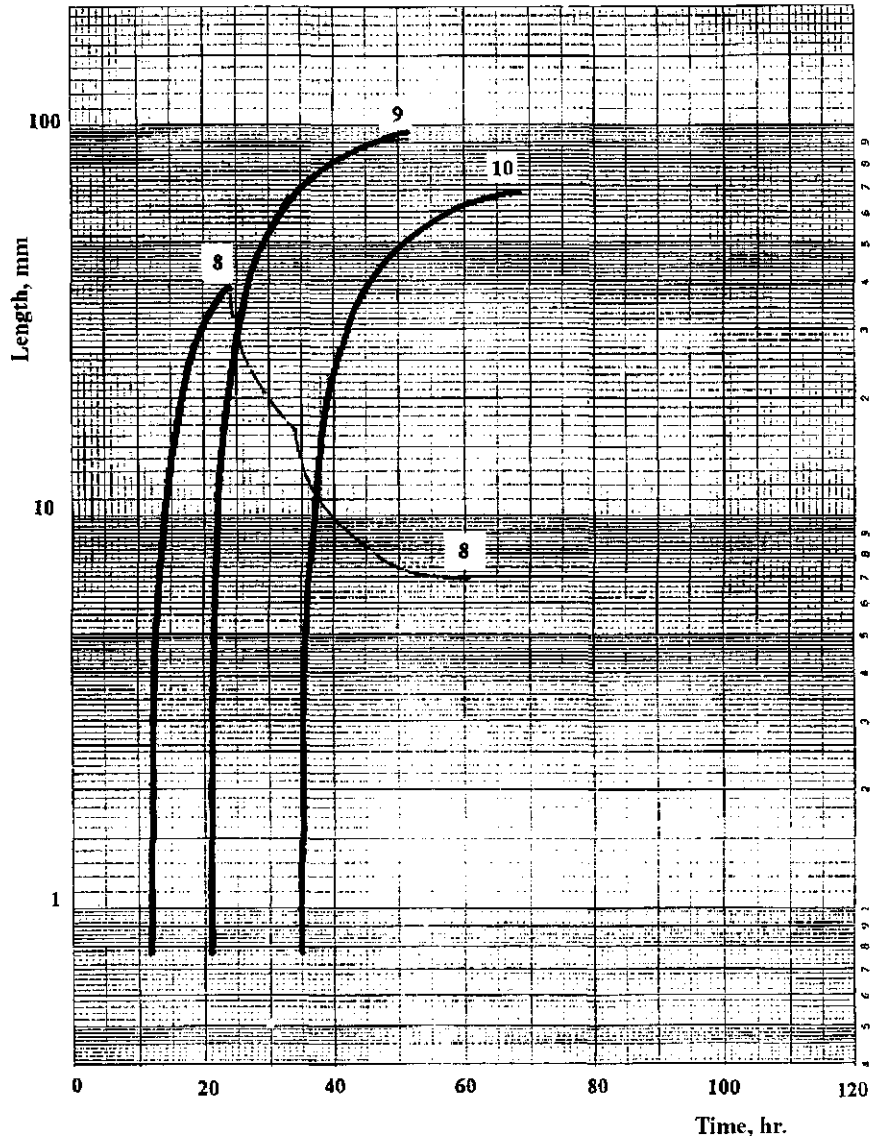

Figure 3-44 Dependence of the length of the formed and dissolved whiskery colonies of methane hydrate on pressure, temperature and supercooling. (Experiment 8–10, Table 3–3).

Figure 3-45 Whiskery crystals of methane hydrate, growing in a water volume (P = 86.5 bar; T = 276.9 K).

Although individual equations that are part of the theory may have a theoretical significance, additional assumptions induce empirical elements to the theory presented. In addition, some of the data—for instance the critical core size and thickness of the "effective" interfacial layer—that are applied in the illustration of the theory are rough estimates based on approximate calculations or consideration of dynamic aspects.

Surface Adsorption

This study is a system of liquid water in contact with a gas phase containing the hydrate forming molecules. As an approach for the adsorption process we may use the grand canonical ensemble as a starting point in the

Figure 3-46 Whiskery crystals of methane hydrate, growing in a gas volume (P = 86.5 bar; T = 276.9 K).

development of a dynamic model. A grand canonical ensemble is defined as that part of the gas water interface that contains the first layer of adsorbed gas molecules and the first layer of water molecules in contact with these guest molecules. We also assume that the water layer has a constant number of water molecules, since water molecules that may be connected to growing structures will be replaced by new water molecules from the bulk phase. Gas molecules may penetrate the boundaries of this ensemble and enter the remaining part of the gas side of the interface and subsequently the bulk gas phase. The water molecules are free to enter the

Figure 3-47 Whiskery crystals of methane hydrate (P = 87 bar; T = 275.1 K).

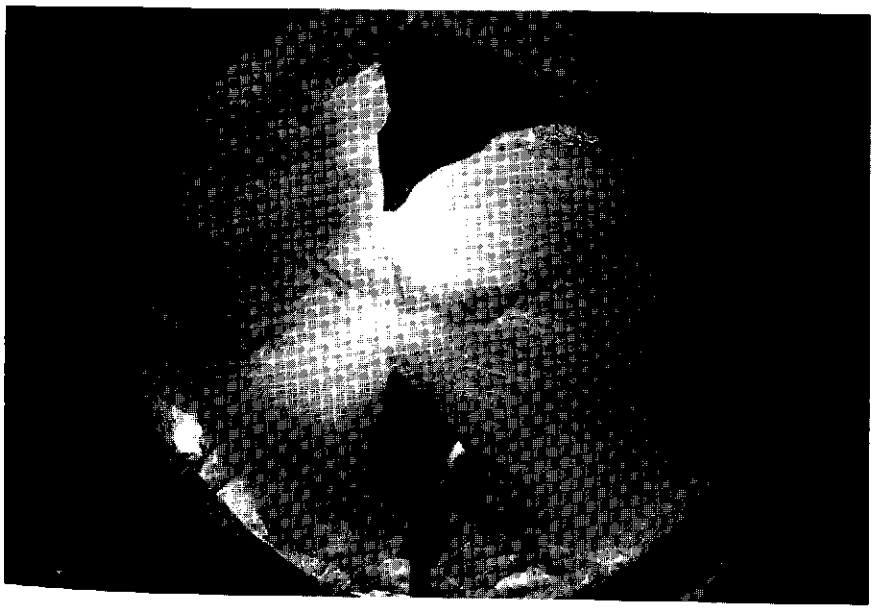

Figure 3-48 Whiskery crystals of methane hydrate, growing in a gas volume (P = 87 bar; T = 275.1 K).

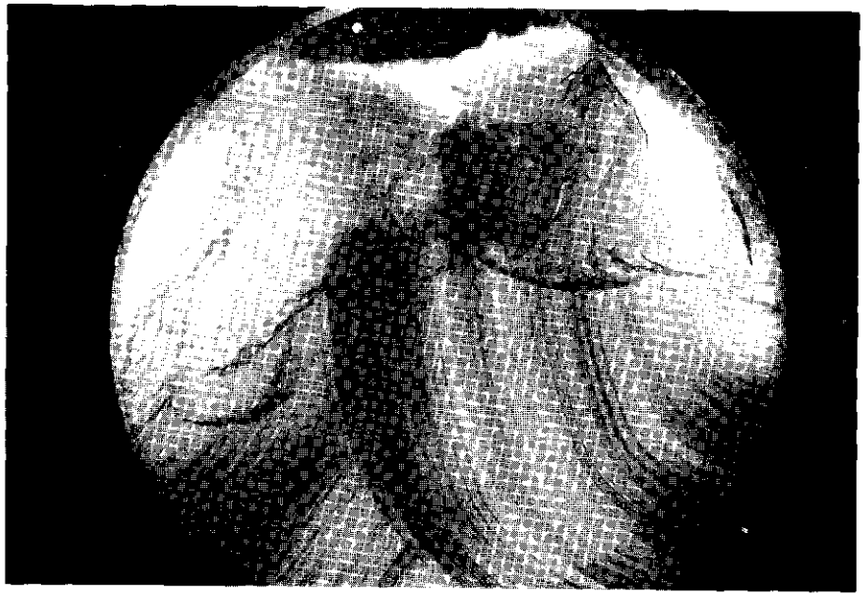

Figure 3-49 Two whiskery colonies of methane hydrate, grown in water over whiskery colony massive hydrate film, formed on the free gas-water surface (P = 80.22 kg/cm²; T = 278.4 K).

Figure 3-50 Whiskery methane hydrate growing in gas and water volume (P = 97.9 atm; T = 2.7 K).

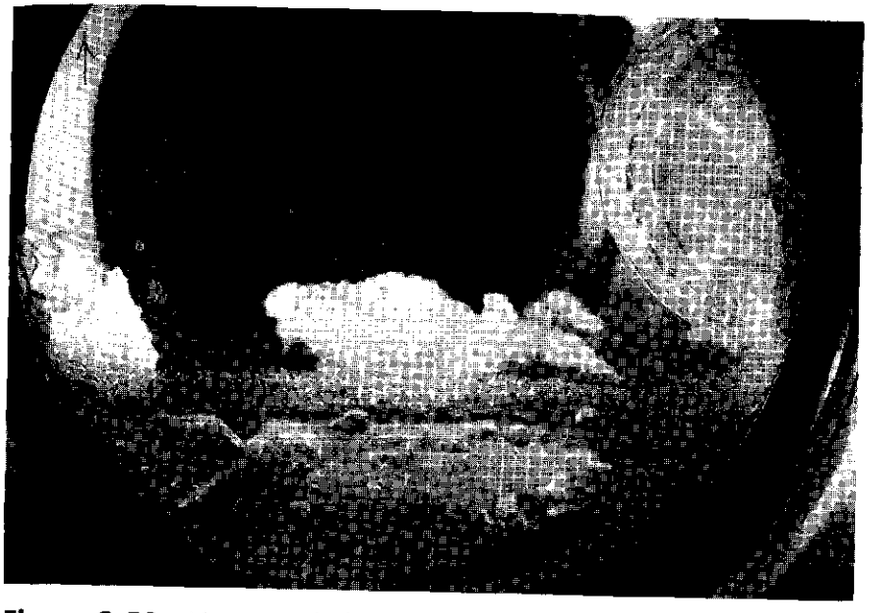

Figure 3-51 Massive, whiskery, and gel hydrates of methane (P = 84.6 bar.; T = 3.4 K).

Figure 3-52 Whiskery propane hydrate crystals growing in water volume (P = 12.8 bar.; T = 1.5°C).

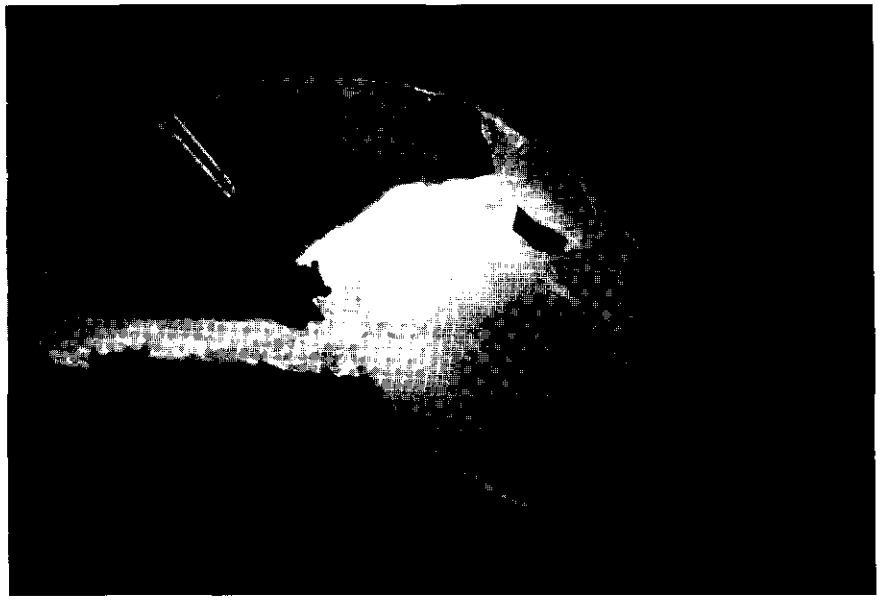

Figure 3-53 Methane whiskery crystals dissolving in water (P = 96.6 bar.; T = 277.6 K; $\Delta\tau$ = 6 hr.).

Figure 3-54 Methane whiskery crystals dissolving in water (P = 96.6 bar.; T = 277.6 K; $\Delta\tau$ = 12.5 hr.).

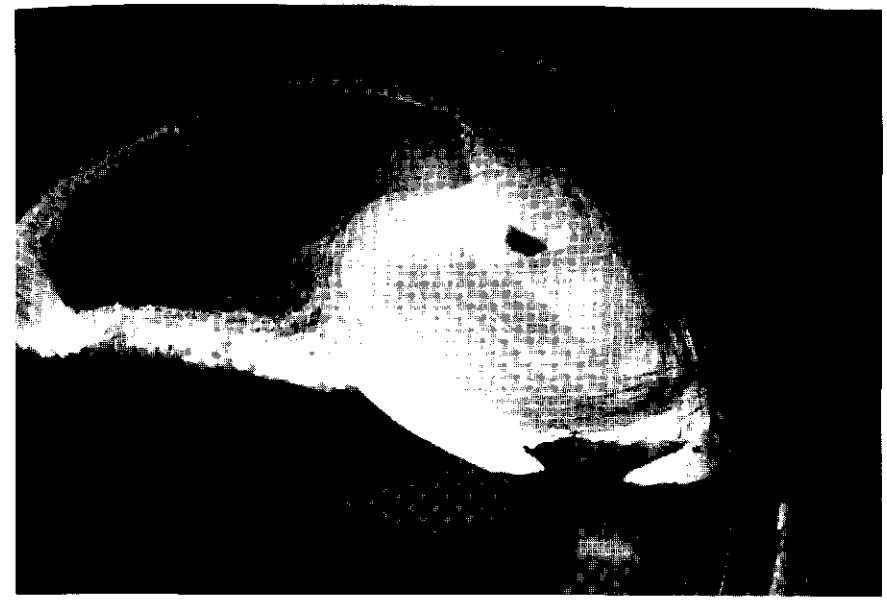

Figure 3-55 Methane whiskery crystals dissolving in water (P = 96.6 bar.; T = 277.6 K; $\Delta\tau$ = 30.5 hr.).

Figure 3-56 Methane whiskery crystals dissolving in water (P = 96.6 bar.; T = 277.6 K; $\Delta\tau$ = 38 hr.).

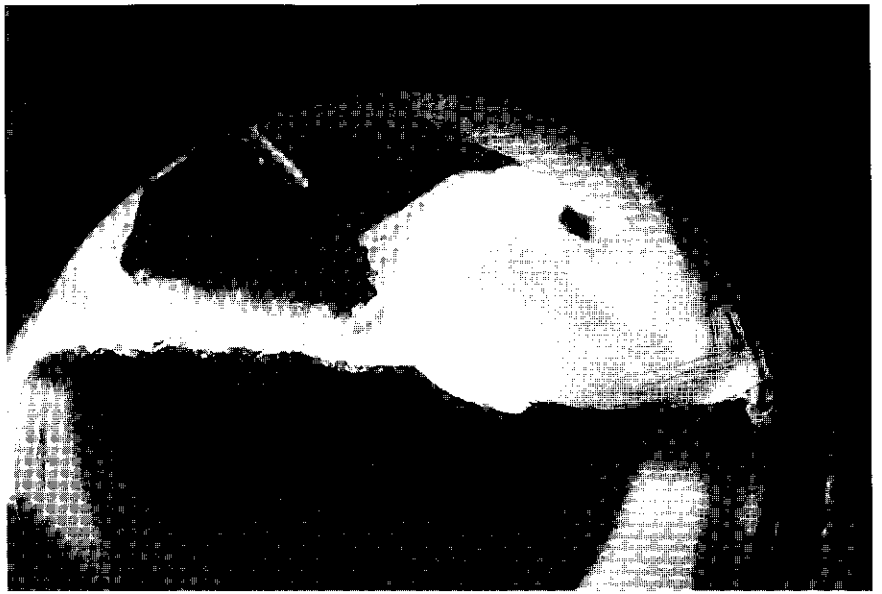

Figure 3-57 Methane whiskery crystals dissolving in water (P = 96.6 bar.; T = 277.6 K; $\Delta\tau$ = 52 hr.).

Figure 3-58 Methane whiskery crystals dissolving in water (P = 96.6 bar.; T = 277.6 K; $\Delta\tau$ = 66 hr.).

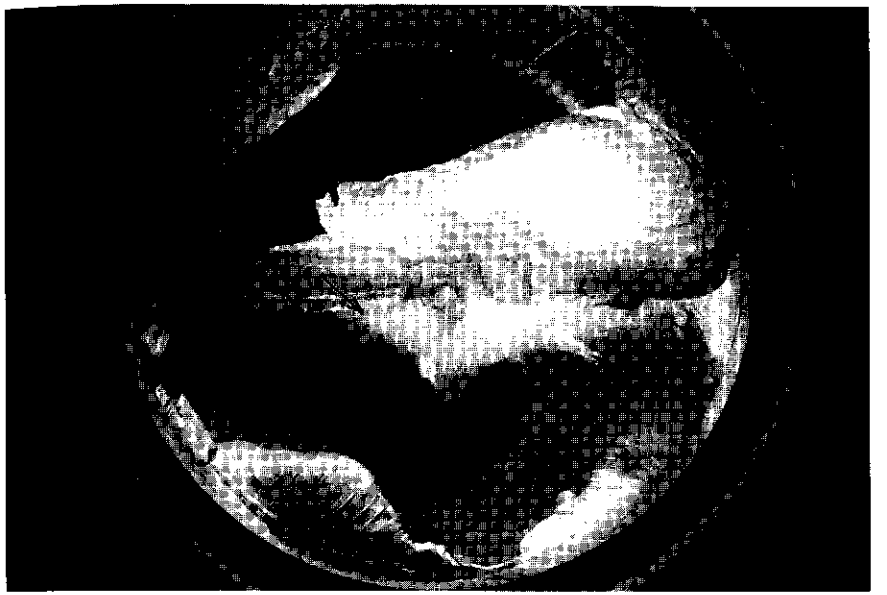

Figure 3-59 Whiskery methane hydrate growing in volume of gas and water and soft-gel crystals (marked by an arrow) growing in volume of water (P = 83 atm.; T = 275.9 K).

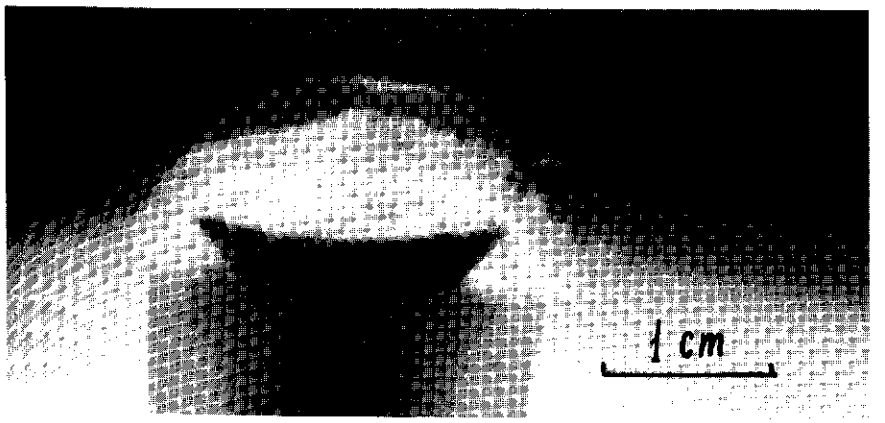

Figure 3-60 Gel-like methane hydrate crystal formed in volume of water (P = 9.3 Mpa; T = 7.5°C).

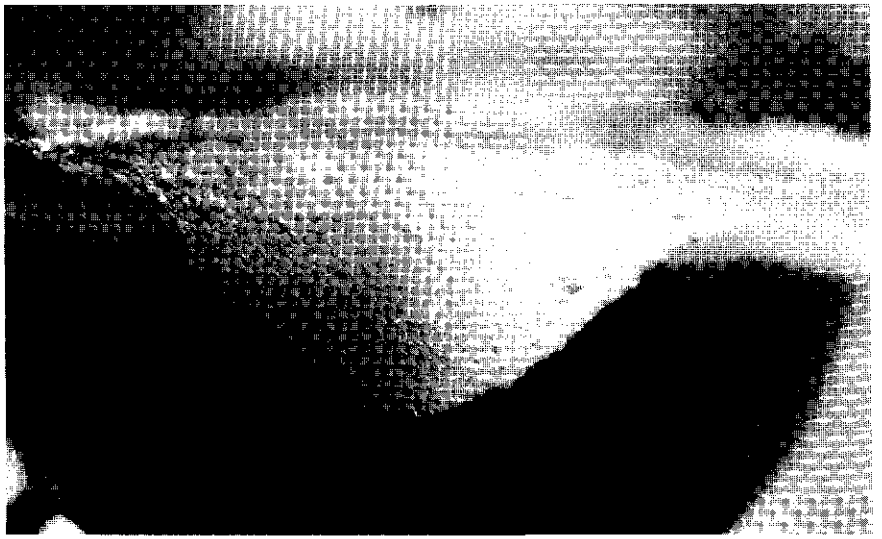

Figure 3-61 Cone-like accumulation of gas hydrate bubbles in water (P = 95.2 atm; T = 282.1 K).

remaining part of the liquid water interface and subsequently the water bulk phase, or they may enter the gas phase in a similar manner depending on local driving forces for molecular transport.

We will assume that the initial nucleation takes place on the surface of water (on the gas side of the interface) and will neglect effects of dissolved gas on the adsorption rate of gas on the surface and subsequent reorganization of water molecules around adsorbed molecules. It is assumed that the surface adsorption establishes a quasi equilibrium state. The sum of the two bulk phases (gas and water) and this grand canonical ensemble is closed at constant temperature and will as a total represent a canonical ensemble for the entire system.

The grand canonical partition function for this absorbed layer may be written as:

$$\Xi = \prod_{i=1}^{i=p} (1 + e^{\frac{\mu^{w,surf.}}{\nu_i}} a_i)^{\nu_i N_w} \qquad (3.72)$$

where μ with superscript w, surf. is the chemical potential of water at the surface and N with subscript w and N_w is the average number of water-molecules in the first layer around the adsorbed gas molecule of type i. The average number of adsorbed molecules per number of water molecules surrounding these adsorbed molecules is ν_i. N_p is the total number of gas molecules of type p that are absorbed on the surface.

In our first approach it will approximate the chemical potential for water at the surface with the corresponding value in the bulk phase but corrected for the enthalpy corresponding to approximately only a half configurational integral for water-water interactions. This applies to the initial configuration where the surface water molecules are only in contact with gas. After the onset of hydrate growth this picture gets more complicated and water chemical potential of the surface molecules will change toward a more uniform value compared to water in its environment, i.e., growing crystals on the gas side and liquid water. For residual chemical potential we have used the values of Table 3-4 of Kvamme and Tanaka (1995). The corresponding enthalpies are obtained by numerical differentiation. Calculation of ideal gas chemical potential for the TIP4P model from the ideal gas partition function is trivial using the ideal gas partition function and the moments of inertia for TIP4P.

$$a = \exp[\beta(\mu + kT \ln b)] \qquad (3.73)$$

where β is the inverse of Boltzmann's constant times temperature and μ is the chemical potential of the specific gas molecule that is absorbed. b is given by:

$$b = (mkT/2\pi\hbar^2)^{(3/2)} \int_{x=-\infty}^{x=\infty} \int_{y=-\infty}^{y=\infty} \int_{z=-\infty}^{z=\infty} \exp[-\beta w(x, y, z)] dx dy dz \qquad (3.74)$$

Equation 3.75 applies to spherical gas molecules. The surface is oriented in the x-y-plane. Negative z is in the direction of bulk water and positive z is in the direction of bulk gas phase. If we assume that an adsorbed gas molecule enters the surface of the liquid water so that the center of the adsorbed molecule is located at $z = 0$, the contribution to w from negative

Table 3-4 Water parameters. H-O-H angle is 112.52°, O-H bond length is 0.93109 Å and Z denotes the partial charges on the atoms.

	O	*H*
σ(Å)	2.77025	1.21863
ε/k_B(K)	86.3212	1.93816
Z	-0.78478	0.39239

z is that due to interaction between the gas molecules and water, and that for positive z is for interactions between the gas and surrounding gas molecules. If we assume that water molecules in this first stage are still approximately uniform liquid, we may estimate the interaction as:

$$dw(x, y, z) = \frac{1}{2}\rho_w \phi_{w,i}(x, y, z)\, g_{w,i}(x, y, z)dxdydz \qquad (3.75)$$

for negative z and:

$$dw(x, y, z) = \frac{1}{4}\sum_{j=1}^{j=p}\rho_j \phi_{j,i}(x, y, z)\, g_{j,i}(x, y, z)dxdydz \qquad (3.76)$$

for positive z. The additional factor of 0.5 in Equation 3.76 accounts for the double-counting of gas-gas interactions that would otherwise be present in Equation 3.72. $F(x,y,z)$ is the interaction energy, modelled as Lennard-Jones 12-6 for gas gas interaction and gas water interactions. Subscript i is the index of the particular gas molecule in consideration and subscripts w and j denote surrounding water and gas molecules, respectively. The pair correlation-function for pairs is indicated by the subscripts is g. The average filling fraction is obtainable from Equation 3.72 by differentiation of the logarithm with respect to adsorbed molecule chemical potential. See also Equation 3.95.

The pair correlation functions involved in Equations 3.75 and 3.76 may be estimated from an integral type of theory if we assume that within the effective extension of the gas gas and gas water interactions there is a uniform density and molecular distribution in the two phases (water interface and gas interface). Furthermore, if we approximate the integral of Equation 3.74 by the corresponding expression for fixed molecules we obtain the simple result:

$$b = \left(mkT/2\pi h^2\right)^{(3/2)} \exp[-\beta < w >] \qquad (3.77)$$

where <w> is the sum of the three-dimensional integrals of Equations 3.75 and 3.76 for negative and positive z-directions, respectively.

The extension of Equation 3.75 to an interaction-site model for water is straightforward. It may seem somewhat arbitrary to calculate these energies based on a half liquid structure. However, it is expected that the situation is rather chaotic at the interface, with gas molecules entering and leaving the liquid side of the interface continuously. A theoretical description of the "true" behavior at this interface is probably beyond scientific status in these areas today. As such Equations 3.74 and 3.75 represents a feasible and simple approximation for an assumed average adsorption energy. At least we expect it to be more representative than approximating the water surface to be a flat homogenous surface, which would be another simple alternative. Strictly speaking, the evaluation of Equation 3.76 using correlation functions from a uniform theory is in contrast to the concentration gradient that is expected in this region. (See the discussion at the end of this section.) The gas-gas interactions are small compared to the interactions with liquid water as represented by Equation 3.75 and as such Equation 3.76 may serve as a first approximation.

In this part of the work consider only spherical Lennard-Jones 12-6 models of the guest molecules. The model for water is presented in Table 3-4. Lorentz-Berthelot mixing rules are applied for cross interactions. A plot of estimated structure for this model at 298.15 K and a density of 998.0 kg/m^3 is presented in Figures 3-62 through 3-64 together with experimental neutron data of Soper (1993). The structure is estimated from dielectrically corrected RISM with HNC closure. For computational details see Kvamme (1994–95).

The Molecular Dynamics (MD) simulations are performed in an NVT ensemble consisting of 256 molecules. The simulation box is cubic and periodic boundary conditions are applied in all three dimensions. Temperature is controlled according to the thermostat procedure of

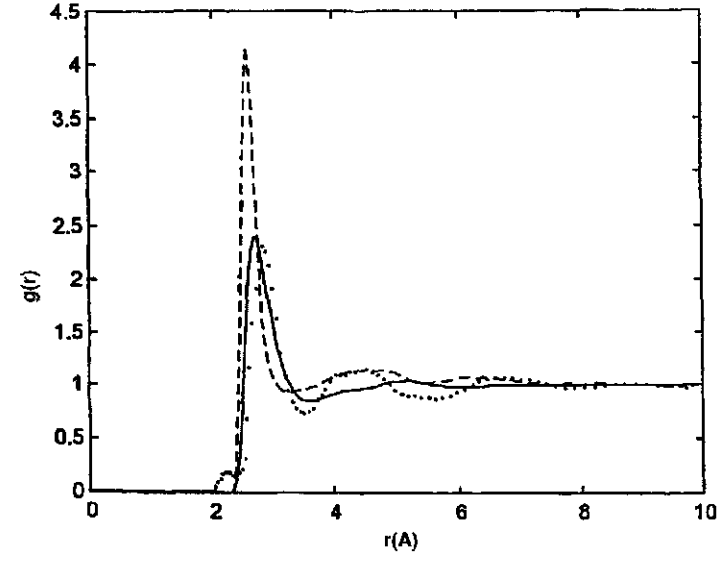

Figure 3-62 Correlation functions for oxygen-oxygen at 293.15 and a density of 991 kg/m^3. Solid line is the result from integral equation theory and dashed line is the corresponding result from NVT molecular dynamics simulations, both for water model described in the text. Dotted line is neuron data for real water by Soper (1993).

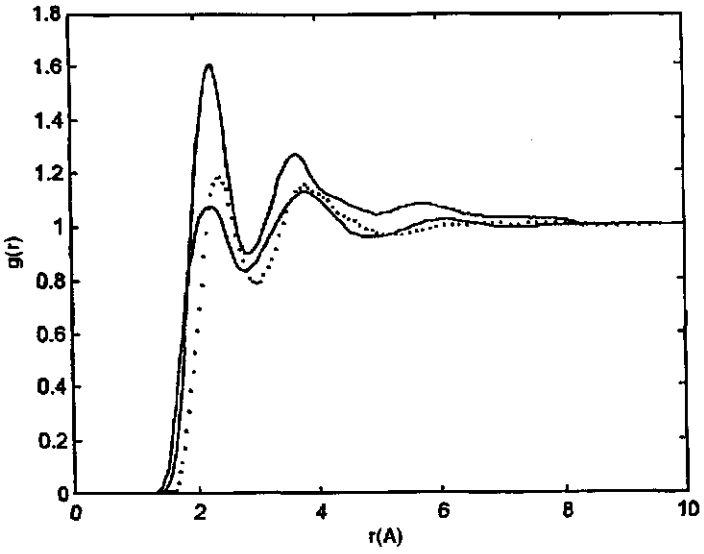

Figure 3-63 Correlation functions for hydrogen-hydrogen at 293.15 and a density of 991 kg/m^3.

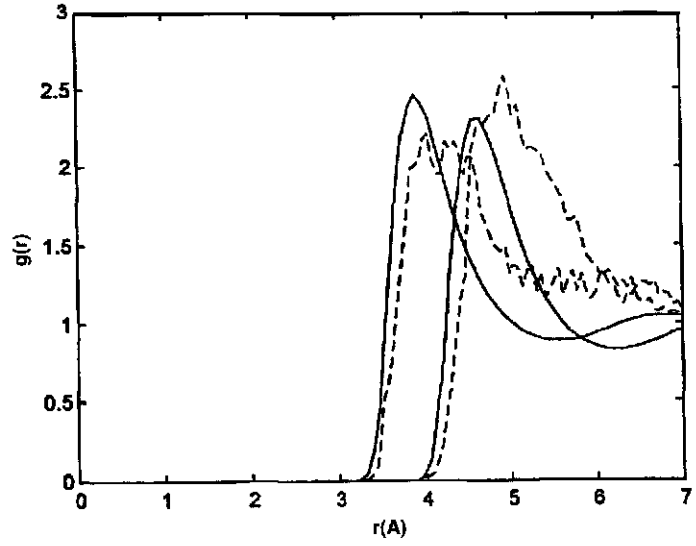

Figure 3-64 Correlation functions between solute molecules at a 5 mole % solution in liquid water at 273.15 K and a density of 998.7 kg/m^3. Dashed lines are calculated form MD and reflects the average of phase separated system. Solid lines are the RISM calculated results for methane and ethane in a uniform mixture with water. The distinction between the two solutes is obvious from the different sizes according to Table 3-4.

Hoover (1985) using separate thermostats for the rotational and transitional degrees of freedom. The control parameters for the two thermostats are fixed according to an analysis of the frequencies for pure liquid model water at 273 K according to the procedures originally suggested by Nose (1984) and discussed in more detail by Di Tolla and Ronchetti (1993).

In Figure 3-65, plotted correlation functions between the water oxygen and solute molecules, are at a concentration of 5 mole %. The corresponding MD simulations are performed in an NVT ensemble (as described above) consisting of 13 solute molecules and 243 water molecules (potentials of Table 3-4). The concentration is somewhat arbitrary since the degree of supersaturation in the liquid part of the interface layer is unknown. In the MD simulations the system is likely to split into two phases and, as such, the correlation functions from MD are likely to reflect an average of the methane rich and water rich parts of the ensemble. The corresponding solute-solute correlation functions are presented in Figure 3-66. Gas phase correlation function for spherical molecules is fairly trivial and can even be predicted by analytical approximation. We calculate these by RISM, more for convenience since our RISM program package is already included in the FORTRAN coding for the complete model described in this paper.

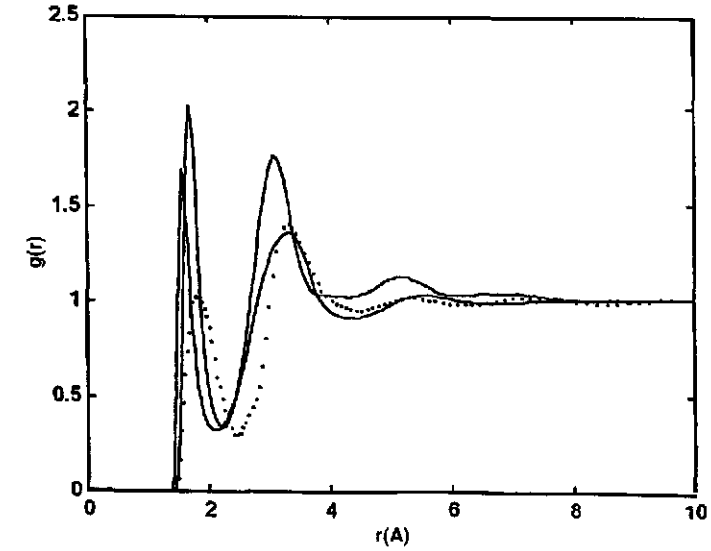

Figure 3-65 Correlation functions for hydrogen-oxygen at 293.15 and a density of 991 kg/m^3.

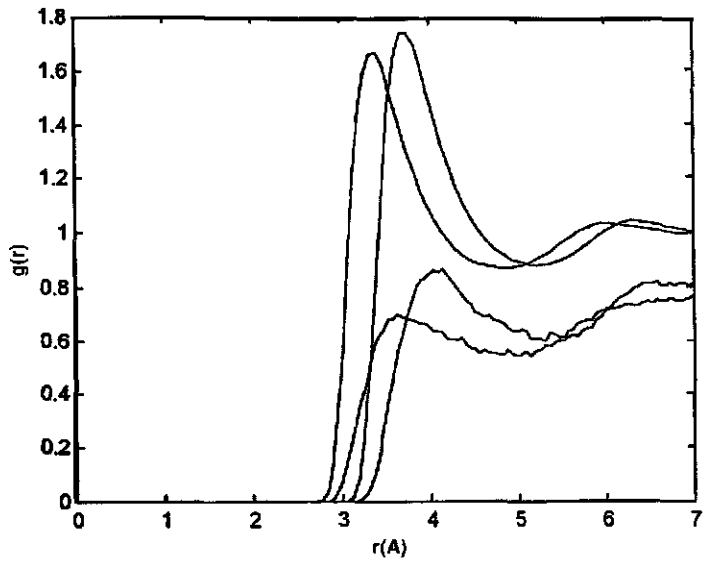

Figure 3-66 Correlation functions between water oxygen (model of Table 2) and the models for methane and ethane at a 5 mole % solution in liquid water at 273.15 K and a density of 998.7 kg/m^3. Dashed lines are calculated from MD and reflect the average of phase separated system. Solid lines are the RISM calculated results for methane and ethane in a uniform mixture with water. The distinction between the two solutes is obvious from the different sizes according to Table 3-4.

At present there are no rigorous theories with simple analytic solutions for the self diffusion of Lennard-Jones molecules in gas phase. The self diffusion of square well molecules at low to moderate densities has been investigated by Dufty, Mo, and Gubbins (1991). An approximate translation of the Lennard-Jones potential into a corresponding square well potential is made by requiring that the second virial coefficient of the two models should be the same and that the integral over the net attractive part of the Lennard-Jones potential should equal a similar integral over the negative well of the square well potential. At this stage we have not made any attempts to verify the effect of these approximations on the different terms of the diffusion model. The repeated ring approximation is expressed in terms of the diffusion coefficient relative to the Boltzmann diffusion coeffisient (superscript * indicate diffusion coefficient divided by the corresponding Boltzmann value at the same condition) as:

$$d^* = [\omega_{R\sigma^+} g(R\sigma^+) - (\omega_{R_{\sigma^-}} + \omega^{bs}_{R_{\sigma^-}}) g(R\sigma^-) + (\omega_{\sigma^+} + \omega^{bs}_{\sigma^+}) g(\sigma^+)]^{-1} \qquad (3.78)$$

In this equation all the ring integrals ω for different regions of particle separations (indicated by subscripts) were evaluated and presented in convenient form by Marcheti and Dufty (1981). The hard core diameter is σ, and $R\sigma$ is the location of the end of the well depth. Superscript *bs* indicates bound state conditions. The pair correlation functions *g* for different separations as indicated in parentheses are listed as Equation 3.78 in the paper by Dufty, Mo, and Gubbins (1991).

In summary it is assumed that Equation 3.78 determines the rate of gas transport at all locations in the gas phase. Equations 3.72–3.77 determine the instant fraction of these molecules that are adsorbed on the surface initially (Equation 3.95, for time > 0). A thickness of the gas side of the interface layer of 100 Å is applied as a constant value in this study. Calculation of the density gradient in the interfacial layer is made using a first order Fick's law with a linear assumption for starting values in an iterative loop. It is assumed that the density changes linearly from the density corresponding to an adsorbed layer at an estimated fraction (from Equation 3.72) to bulk density at 100 Å from the water surface. This density profile is used to calculate diffusivities at different distances from the surface, and average g(r) for the gas phase (for use in Equation 3.76) is calculated. Solving Fick's law for this profile of diffusivities gives a new density profile. This cycle is essentially convergent in two steps, at least within the approximate nature of the calculations presented in this work.

Initial adsorption fractions calculated from Equation 3.72 is in the order of .6 to .8 for the systems and temperatures in this study. The effective range of the intermolecular potentials between gas and liquid water is in the order of 15–20 Å for the models of Table 3-4. Although a value of 100 Å for the thickness of the interfacial layer on the gas side may seem arbitrary, it is obvious that the interaction between the gas and the surface is zero at these separations. Essential parts of the "memory" of dynamical effects at the surface also will be wiped out at this distance. For illustration purposes it is expected that this value should be reasonable and that a solution to Fick's law can provide the neccesary solution to the transport in this part of the interfacial region. Note that Equation 3.78 takes no account of the particular interactions at the water surface.

Restructuring and Cavity Closure

The partial cavities surrounding the guest molecules (represented by the g(r)'s in Equation 3.75 will not energetically have the most favorable strucure of water molecules with respect to hydrogen bonding. At some stage the system will decompose or rearrange into cavities similar to those

observed in stable hydrate. Due to the neccesary expansion involved in this prosess it is likely that such rearrangements take place on the the water surface or at least close to this surface. As the next step in the hyphothesis we assume that the structure of the partial cavities approaches that of the final structure. For Structure I this means a ratio of 3 to 1 for complete cavities with coordination number 24 and 20, respectively, and half this number for the half-cavities at the surface. We also assume at this stage that the water molecules have approached a rigid structure similar to that of the final cavities of hydrate and that this structure is unaffected by the gas water interactions. The grand canonical partition-function for this stage will then be:

$$\Xi = \exp\left(-\beta N_w A_W^0\right)\left(1+\sum_{p=1}^{p=N_s} a_{p_s}\right)^{N_s}\left(1+\sum_{r=1}^{r=N_l} a_{rl}\right)^{N_l} \tag{3.79}$$

This is the equation of van der Waals & Platteuw (1959) but at this stage only for partial cavities on the water surface. The cell partition-functions a are given by Equation 3.73 or alternatively, a corresponding expression estimated from the harmonic oscillator approach (Tanaka, 1992–1994).

Some of these partial structures will close and start growing as hydrate cores. Dynamically there are a number of different processes that can participate in the support of the extra water molecules needed for completion of cavities. Water molecules may condense from the supersaturated interface and eventually support the closure of cavities. The structuring of water will imply an expansion of the water network around the adsorbed solute, from liquid-like situation to something more in the direction of hydrate density for the partial cavity. It is possible that these expansions induce extra forces of movement due to gravitational forces. Partial cavities may, as a result of this, turn and bring the unclosed parts in contact with the liquid water surface. Other possible mechanisms also may be able to support the extra water molecules needed for closing of the cavities. But the fact remains that very little is known about the behavior at the interface. Molecular simulations of the water/solute inteface is one of the subjects for our future efforts. In the meantime we consider the theory as a an unverified hyphothesis.

We will as a first approach assume that the rate of this restructuring prosess may be modeled as a set of first order kinetic equation as:

$$\frac{1}{N_{W,0}^{ads.}}\frac{\partial N_W^{str.}(t)}{\partial t} = \frac{K_1}{RT}\left(\mu_W^{str.}-\mu_w^{ads.}\right)N_W^{ads.}(t)$$

$$\frac{K_2}{RT}\left(\mu_W^{surf.}-\mu_W^{str.}\right)N_W^{str.}(t)-\frac{K_3}{RT}\left(\mu_W^{core}-\mu_W^{str.}\right)N_W^{str.}(t)\times$$

$$\frac{1}{N_{W,0}^{ads.}}\frac{\partial N_W^{core}(t)}{\partial t} = \frac{K_3}{RT}\left(\mu_W^{core}-\mu_W^{str.}\right)N_W^{str.}(t)-\frac{K_4}{RT}\left(\mu_W^{core}-\mu_W^{surf}\right)N_W^{core}(t) \tag{3.80}$$

N with subscript w is number of water molecules at different stages of the formation prosess (as indicated by superscript). Equation 3.80 is total number of molecules and are related to a specific surface and the corresponding number of molecules initially adsorbed on that surface. Superscript ads. means adsorbed. The rate of absorbed gas molecules is calculated according to the gas diffusion rate and a time dependent filling fraction that depends on adsorption characteristics of all different particles at the interface. Superscript str. means structured and corresponds to the structured state of partial cavities described in Equation 3.79. The K-values are rate constants, assumed independent of temperature, pressure, and type of component. Superscript core means closed structure corresponding to small cores (below the critical size).

The chemical potential for water in such a core is approximated in the following manner. A crystal corresponding to 130 unit cells or larger are assumed to have a constant chemical potential. For hydrate structures smaller than this, the chemical potential is corrected for the change in enthalpy due to reduced number of long range interactions. We correct the interaction energy for all water-water interactions at separations larger than the closest neighbor, relative to the number of water molecules. The final result of this analysis may be expressed as:

$$\mu_w^{core} = \mu_w^{hydrate} - h_w^{hydrate}\left(1-\lambda(n_w^{core})\right) \tag{3.81}$$

where:

$$\ln\left[\lambda(n_w^{core})\right] = \sum_{i=0}^{i=4} a_i\left[\ln\left(\frac{n_w^{core}}{n_{w,c}}\right)\right]^i \tag{3.82}$$

with fitted parameters given in Table 3-5: n with superscript core and subscript w denote the number of water molecules in the core and n with subscript w, c denote the number of water molecules in a core of critical diameter. The chemical potential of water in a spherical core containing 16478 (appr. 55 Å in radius) water molecules (Structure I) according to Equation 3.81 is very close to the chemical potential of water in complete hydrate crystals. For the purpose of illustration we will designate this size as the critical size, although we make no arguments that this is the "true" critical particle. Laser experiments (Nerheim, 1993) indicate that the critical diamater may be in the range of 50–150 Å.

Table 3-5 Parameters in Equations 3.82 and 3.94 for structure I.

Parameter	*Equation 3.82*	*Equation 3.94*
a_0	$1.154019241278448 \cdot 10^{-11}$	7.25417657179056
a_1	-0.185272729622668	-2.54388439347909
a_2	-0.252863019630854	0.510590288962651
a_3	$-4.434861643222207 \cdot 10^{-2}$	$-4.95155249186003 \cdot 10^{-2}$
a_4	$-3.011039798979578 \cdot 10^{-3}$	$1.732267668148799 \cdot 10^{-3}$

This is applied using the following distribution of core sizes. Although not theoretically rigorous, it is similar to the distribution that will arise from a steady state situation between the different sizes of particles that are growing.

$$f(n_w) = \frac{e^{-\beta\mu_w^{core}(n_w)}}{\int_{n_0}^{n_{w,c}\cdot 6} e^{-\beta\mu_w^{core}(n_w)}} \tag{3.83}$$

The corresponding average number of water molecules that are transformed into metastable cores of different sizes may be reformulated to:

$$N_w^{core}(t) = M_W^{core}(t) \int_{n_{w,0}}^{n_{w,c}} n_w f(n_w) d\, n_w \tag{3.84}$$

where M now is defined as the average number of cores at a specific time t.

Equation 3.84 does not account for the fact that the true chemical potential of the core also will be a result of the medium surrounding the particle. Since the particle is assumed to move and rotate in its neighborhood to other particles it may be exposed to gas phases at some instances and to liquid water surroundings at other instances. There will therefore be a field of forces from the nonpolar and polar parts of the interactions from surrounding particles. The chemical potential of the core is thus the chemical potential of an isolated core of a specific size. Simultaneous solution of Equations 3.80–3.82 with number of adsorbed molecules gives the necessary equations for the growth rate untill critical size of particles.

Equation 3.80 is formulated for one average unstable core size. The alternative would be to use a coupled set of equations where we consider a gradual change in discrete steps toward critical size particles. The total change in number of water molecules from a unit cells toward critical size

is divided into a number of a gradual change in chemical potential of water in Equation 3.81 and considers a set of discrete extensions in the size of the core. Since Equation 3.82 was fitted to data for extensions of spherical sizes of the core we may define:

$$\frac{\partial M_{w,i,j}^{core}}{\partial t} = K_{w,i,j} M_{i,j} - K_{wp,i,j+1} M_{i,j+1} \tag{3.85}$$

$$\frac{\partial M_{g,i,j}^{core}}{\partial t} = K_{g,i,j} M_{i,j} - K_{gp,i+1,j} M_{i+1,j} \tag{3.86}$$

K are rate constants. Subscript w means water and subscript g means gas. M is the number of cores of a particular size as indicated by subscripts. The first constants are the constants for net increase in M at a size j while the second term is the decease in j due to creation of larger sizes $j + 1$. In the following we shall treat the system as a system with one type of hydrate former only. The extension can, at least in an approximate manner, be made by interpreting Equations 3.85 and 3.86 as the rates of flow of a stoichiometric mixture of guest components according to the equilibrium ratio. The rate constants for net forward and progress to larger cores are denoted by subscripts w and wp for water and similarly for the guest component g in Equation 3.86. Subscript j is the running number for discrete sizes with respect to number of water molecules. The corresponding running number for discrete sizes with respect to guest molecules is i. Equations 3.85 and 3.86 are connected if we require that the filling of the clathrate with guest molecules should be in accordance with the equilibrium ratio, i.e. a homogeneous hydrate during all stages of growth:

$$\dot{N}_g^{core} = \left(\frac{\theta_g^{small}}{23} + \frac{3\theta_g^{large}}{23} \right) \dot{N}_w^{core} \tag{3.87}$$

where θ is the filling fraction of a particular type of cavity as indicated by superscript. If we assume that the rate constants for a particular size may be modeled by a set of universal constants k_ξ and the differences in chemical potential for a particular size we may write:

$$K_{w,i,j} = \frac{k_w}{RT} (\mu_{w,i,j}^{core} - \mu^{surf}) \tag{3.88}$$

$$K_{g,i,j} = \frac{k_g}{RT} (\mu_{g,i,j}^{core} - \mu_g^{gas}) \tag{3.89}$$

for water and gas. Note that Equation 3.89 will be redundant in the case of stoichiometric fillings according to Equation 3.87. The destruction

rates may not neccesarily involve stoichiometric destruction but the further growth rates will depend on the actual situation of the previous core size, denoted by j-1 and i-1, respectively. In order to get a consistent and simple set of equations for the growth phase, it is now assumed that both growth and decay of particles are stoichiometric. This means that:

$$K_{g,i,j} = \left(\frac{\theta_g^{small}}{23} + \frac{3\theta_g^{large}}{23} \right) K_{w,i,j} \tag{3.90}$$

$$K_{gr,i+1,j} = \left(\frac{\theta_g^{small}}{23} + \frac{3\theta_g^{large}}{23} \right) K_{wr,i+1,j} \tag{3.91}$$

Thus within these approximations, Equation 3.86 is redundant.

Within this discretization we will interpret Equation 3.80 as the step needed to create the smallest core size. In order to ensure stoichiometry and symmetry within the core, we use a unit cell as the smallest core size to be calculated by Equation 3.80. Rewriting Equation 3.80 for this purpose gives the following equation in terms of number of such cores:

$$\frac{\partial M_W^{str.}(t)}{\partial t} = \frac{n^{ads}}{n^{str.}} \frac{K_1}{RT} \left(\mu_W^{str.} - \mu_W^{ads.} \right) M_W^{ads.}(t) - \frac{K_2}{RT} \left(\mu_W^{surf.} - \mu_W^{str.} \right) M_W^{str.}(t) - \frac{K_3}{RT} \left(\mu_W^{core} - \mu_W^{str.} \right) M_W^{str.}(t) \tag{3.92}$$

$$\frac{\partial M_W^{core}(t)}{\partial t} = \frac{n^{str.}}{n^{core}} \frac{K_3}{RT} \left(\mu_W^{core} - \mu_W^{str.} \right) M_W^{str.}(t) - \frac{K_4}{RT} \left(\mu_W^{core} - \mu_W^{surf} \right) M_W^{core}(t)$$

where now $n^{ads.}$, $n^{str.}$ and n^{core} are the number of water molecules in an adsorbed situation, a structured state or a minimum core size. The number of water molecules in an adsorbed state is taken to be the first coordination shell as calculated from the pair correlation functions, but divided by 2 in accordance with the approximations for surface strucure. $n^{str.}$ is approximated to be half the number of a closed cavity for the particular type of guest molecule and n^{core} is 46 or 136 depending on structure (I or II, respectively). These numbers are for independent cores not sharing any water molecules. The first two numbers are reduced according to the double counting due to the number of shared water molecules at the surface.

The major contribution to the free energy change with increasing size is due to the change in chemical potential of water. When the system is in equilibrium, Equation 3.85 equals zero. The assumption of a Boltzmann

distribution of sizes gives the following relation between the back and forward rate constants:

$$K_{wr,i,j} = K_{w,i,j-1} e^{-\beta(\mu_{w,i,j-1}^{core} - \mu_{w,i,j}^{core})} \tag{3.93}$$

where β is the inverse of temperature times the gas constant. In linear algebraic notation Equation 3.91 may be written as:

$$\underset{\rightarrow}{K}_{wr} = A k_w \tag{3.94}$$

where $K_w^T = \left[K_{w,1}, K_{w,2}, \ldots\ldots, K_{w,l} \right]$ and $K_{wr}^T = \left[K_{wr,1}, K_{wr,2}, \ldots\ldots, K_{wr,l} \right]$ The elements of A are:

$$A_{i,j-1} = \frac{1}{RT} (\mu_{w,j-1}^{core} - \mu^{surf.}) e^{-\beta(\mu_{w,j-1}^{core} - \mu_{w,j}^{core})} \tag{3.95}$$

for all elements $i = j$ and $j = 2, \ldots, 1$ when 1 is the number of discrete core sizes. Also note that Equation 3.94 presumes that additional water molecules, which result in further growth of the core, come from the surface water molecules even though there is also the possibility that water molecules from the gas phase may condense on the surface of a growing particle.

The coupled set of equations may now be written as:

$$\frac{\partial \underset{\rightarrow}{M}}{\partial t} = \underset{\leftrightarrow}{B} \underset{\rightarrow}{M} \tag{3.96}$$

where $M^T = [M^{ads.}(t), M^{str.}(t), M_{w,i,1}(t), M_{w,i,2}(t), \ldots M_{w,i,l}]$. Elements of B are zero except for the elements described below. $B_{11} = 1$ and:

$$B_{2,1} = n^{ads} \frac{K_1}{RT} (\mu_w^{str.} - \mu_w^{ads.}) \tag{3.97}$$

$$B_{2,2} = -n^{str.} \frac{K_2}{RT} (\mu_w^{surf} - \mu_w^{str.}) - n^{str.} \frac{K_3}{RT} (\mu_w^{core} - \mu_w^{str.}) \tag{3.98}$$

$$Bj, j = \frac{k_w}{RT} (\mu_{w,i,j}^{core} - \mu^{surf}) \tag{3.99}$$

$$B_{j,j+1} = -K_{wr,j}, j \le l + 1 \tag{3.100}$$

Since the attraction between cores at different stages and liquid water molecules at the surface is stronger than the attraction between water and single guest molecules, it is reasonable to anticipate that the distribution at the surface will be dominated by growing stable cores and unstable hydrate precursor particles. As such we will estimate the free area that may be subject to adsorption of new gas molecules as the free area given by the packing of these particles at the surface.

Growth of Nuclei

Shneidman & Weinberg (1992) have presented analytical results for the nucleation theory due to Zeldovich (1943).

The final results for two limits of this theory may be expressed by:

$$\frac{1}{\tau}t_{0,b} = \alpha + \ln\alpha + \ln\eta + \gamma - 1 \tag{3.101}$$

for the "ballistic" type of situation or:

$$\frac{1}{\tau}t_{0,p} = \frac{1}{2}\alpha^2 + 2\alpha + \ln\alpha + \ln\eta + \gamma - \frac{3}{2} \tag{3.102}$$

for situations which are typically controlled by diffusion of monomers. γ is euler's constant, 0.5772. t with subscript 0 indicate nucleation time and:

$$\alpha = \left(\frac{n_w(t)}{n_{w,c}}\right)^{\frac{1}{3}} - 1 \tag{3.103}$$

where n_w is the actual size of the nuclei (in terms of number of water molecules) and subscript w,c denote critical size. Equation 3.103 estimates the average number of water molecules $n_w(t)$ that are in a state of stable growth. ψ is the minimal work needed to form a nucleus a specific size (again subscript c denote critical size) and η is given by:

$$\eta = \beta 6\,\psi_c \tag{3.104}$$

τ can be expressed as:

$$\tau = \frac{\chi^2}{2D_c} \tag{3.105}$$

$$\frac{1}{\chi^2} = -\frac{1}{2}\beta\frac{\partial^2\psi}{\partial n_w^2}\Big|_{n_{w,c}} \tag{3.106}$$

The vapor pressure of water at hydrate forming conditions is generally small and, even though the gas layer above the liquid water will be supersaturated, we will assume that most of the growth will take place at surfaces that are facing the liquid water. In the calculations presented in this paper we now assume that transport of hydrate forming molecules from the immediate vicinity of the cores to the core surface, and subsequent reorganization onto established nuclei may be one of the limiting factors.

We hypothesize two possible ways of accomplishing this process: 1) gas molecules on the surface, neighboring the growing core can be encapsulated in incomplete cavities and by rotation of the crystal they may enter the liquid phase of the interface, and 2) dissolved gas-molecules leaving the liquid phase may be trapped by a crystal and encapsulated in a cavity. There is no scientific evidence for these possible mechanisms. And at this stage it is not clear whether Equation 3.85 or 3.86, if either of the two, are the most appropriate according to the limiting kinetic term in this process. It is our intention to investigate these types of systems by molecular simulations. For the present calculations we assume that transport of gas monomers toward the core is the limiting factor and Equation 3.86 is applied in all calculations presented in this paper.

On a macroscopic scale it is experimentally observed by several research groups that hydrate formation starts at the wall of the experimental cell. Sloan (1994) discusses some recent experiments where these aspects appear very clear in the experiments. The roughness of the wall will create areas of disrupted water that have a lower barrier for creating closed cavities. Gas may also enter into microscopic "pockets" at the wall.

Using the definition of the surface tension together with the available data for chemical potential of water in hydrate and liquid phase we may write ψ as:

$$\psi = -\left(\mu^{w,hydrate} - \mu^{w,liq.}\right)\left(n_w + \frac{s(T)\,n_w^{2/3}}{\beta\dfrac{\partial A}{\partial n_w}}\right)_{n_{w,c}} \tag{3.107}$$

where the partial derivative of area with respect to the number of water molecules at critical size is obtainable from Equation 3.94 below and $s(T)$ is proportional to the surface tension, empirically modeled as:

$$s(T) = s_0 + s_1\beta \tag{3.108}$$

s_0 and s_1 are deterministic constants related to the surface tension. The specific form of s in Equation 3.87 is empirical. The rate constant D will in many cases be a power-law of the form:

$$D = D_0 n_w^{\kappa} \tag{3.109}$$

where k will be 2/3 for the "ballistic" situation and 1/3 for the diffusion-controlled situation. D_0 is a deterministic constant. Since monomer diffusion control is assumed in this work we use 1/3 for κ.

Cores that reach a critical size according to the solution of Equations 3.85–3.100 will enter Equation 3.102 for further steady growth. This generates a distribution of growing cores of different sizes depending on the time the particular core entered the region of stable growth.

In summary, the consumption of water molecules that are in hydrate form in unstable form are found from the sum of the elements 3 - 1 in the solution of Equation 3.96 for every time-step. The consumption of water molecules from the sum of cores in stable growth are given by Equation 3.103 for the solution of Equation 3.102 for the particular time after the particular core entered the region of stable growth.

The diffusion prosess is expected to be rather non-ideal and dependent on the actual situation in the system. Experimentally a number of different situations may appear. In static equilibrium, cell growth frequently starts along the walls of the cell, giving rise to one particular situation of diffusion of monomers toward the growing sites. Several hydrate particles at the gas/water interface may seem to grow independently and eventually connect. Initial hydrate formation may also appear as a thin hydrate film that grows more or less homogeneously out from the interface. In general there is no reason to believe that the diffusion factor D_0 should be a constant value during the growth period. This type of changes in the limiting growth factor is not accounted for in the theory, as is also obvious from Equations 3.85 and 3.86 above.

The specific surface area (area in square Ångstrøms per molecule) of a spherical particle with n_w water molecules.This specific surface may be calculated directly from the crystallographic data of Stackelberg et al. (1949–1954) and correlated to a polyonomial of the form:

$$\ln\left[\frac{A(n_w)}{n_w}\right] = \sum_{i=0}^{i=4} a_i \left[\ln\left(\frac{n_w}{16478}\right)\right]^i \qquad \textbf{(3.110)}$$

where the coefficients are fitted to number of water-molecules for a given unit cell size. Although this cell constant will be a function of temperature, we will use a constant value of 12.03 Å for structure I and 17.31 Å for structure II in this work.

Summary and Numerical Evaluation

It is assumed that the initial ($t = 0$) adsorption rate may be calculated according to the appropriate derivatives of Equation 3.72. After this initial adsorption, new guest molecules may adsorb on the surface in competition with existing particles that are at different stages in the nucleation process. For times larger than zero the extension of Equation 3.72 is straight forward and leads to the following expression for adsorption fraction at times larger than zero:

$$\theta(t) = \frac{Y(t)^{ads.}}{Y(t)^{ads.} + Y(t)^{str.} + Y(t)^{core} + Y(t)^{hyd.}} \qquad \textbf{(3.111)}$$

where Y is given by:

$$Y^j = \delta_j a_j (n_w^j) \exp(-\beta \mu_w^j) \qquad \textbf{(3.112)}$$

$$a_j(n_w^j) = \exp(-\beta \langle u^j \rangle) \qquad \textbf{(3.113)}$$

δ_j is zero whenever particles of type j are absent. At time zero it will be zero for all particles exept the adsorbed gas molecules. The average interaction energy, $\langle u^j \rangle$, for the adsorbed species of type j are described by Equations 3.73–3.77 for adsorbed gas molecules. For structured partial cavities it is assumed that the gas molecule is in the center of the half-cavity and the structure (i.e., distances) is known. For metastable cores that are growing and for stable cores, we apply a very simple approximation where the static force balance between the force of the particle (assumed spherical) due to gravitational forces determines the contact area between the particle and the liquid water as the area of the spherical cap at the interface. The water-water interaction energy at this interface area is approximated to be the average of liquid water average interaction energy (from MD) and average interaction energy of water in hydrate.

The number of water molecules at this specific contact area is calculated by assuming that the hydrate surface consists entirely of water molecules that are arranged in pentagons equal to the pentagonal sides of hydrate.

A simple euler integration scheme is sufficiently accurate for the integration of the complete set of equations with respect to time, at least within the simplifying assumptions implied in the application of the theoretical scheme.

In experimental situations stirring of the fluids and other processes that disrupt the surface will increase the gas/water interface since the stirring will create different sizes of micro bubbles as well as small pockets containing gas. These pockets and bubbles will vary in size and amount of gas. Some of these may even be in the visible size range depending on the rate of stirring relative to the size and shape of the vessel. The potential driving force towards a nucleation process in each of these situations of entrapped gas surrounded by water will vary since the amount of entrapped gas and the exposed water surface is different. It is beyond our present scientific level to describe this complicated and complex non equilibrium process in detail. It will probably not be possible to distinguish between the different possible initiation sites related to the different bubbles and pockets. An empirical correction to the non-stirred, ideally flat surface may be written as:

$$A^{ads.} = A_0^{ads.}(1 + \vartheta) \qquad \textbf{(3.114)}$$

Where υ is a function of the sizes and shapes of the vessel and the stirrer, and the stirring rate. A^{ads} means average effective adsorption area and the corresponding term with subscript 0 means the cross section area between gas and water as defined by the vessel.

Rate constants for Equation 3.80 for pure methane as gas phase are given in Table 3-8 together with coefficients D_0, s_0 and s_1.These constants are fitted using the experimental data of Englezos et al. (1988) at a pressure of 48.6 bar.

Provided there is an adequate description of the terms in Equations 3.96 and 3.97 there is no limit in the theory with respect to types of components. In particular, we find in a separate study (Maliniak, 1990) that, for the model systems applied in that study, a monomer of poly (N-vinylpyrrolidone) (PVP) will form hydrogen bonds with liquid water through the double bounded oxygen on the PVP ring. It is likely that the ring will be soluble in the water phase due to the nitrogen and oxygen groups in the ring while the hydrocarbon backbone will not be significantly soluble. As such, the corresponding adsorption energies can be calculated from the correlation functions between the PVP ring and liquid water.

A set of model parameters is given in Table 3-6. There are a total of 78 distinct site correlation functions for the system of water and PVP sequence. These results are for a 3.9% solution of PVP monomer in water. A solid line is calculated from dielectrically adjusted RISM equations (Kvamme, 1994). Details on the molecular dynamics results are given by Kvamme et al. (1995). If we assume that the ring will completely dissolve in water and that the backbone is completely insoluble, it is possible from the geometry of the ring to calculate an appropriate concentration of rings in the top water layers. A corresponding solution to the RISM integral equation will provide the necessary average energies between water and

Table 3-6 Parameters in Equations 3.83 and 3.95 for structure II.

Parameter	*Equation 3.83*	*Equation 3.95*
a_0	$3.49030862684 \cdot 10^{-8}$	2.82516756703427
a_1	1.00002699511846	0.723943574812951
a_2	$2.70593822371 \cdot 10^{-6}$	-0.259358799059289
a_3	$-4.25442763330 \cdot 10^{-6}$	$2.495924801238 \cdot 10^{-2}$
a_4	$2.22934566984 \cdot 10^{-6}$	$-8.38898661455 \cdot 10^{-4}$

different groups in the PVP rings. In addition to the energy between the functional group (for the PVP rings) and liquid water there will be adsorption energy associated with the methyl groups of the backbone which we may assume approximately float at the top of the liquid water. Correspondingly it should be possible to make an approximate estimate for the adsorption effects of the backbone for each sequence of the polymer.

In summary, it appears possible to obtain a simple estimate for the adsorption energies of each polymer sequence using integral equation theory and some simplified approximations for the backbone adsorption energies. Together with a length distribution of the actual polymer that is added, it is straightforward to estimate an average adsorption energy for use in Equation 3.95. We have not made a complete calculation of these energies, but at least for the dissolved ring at a concentration corresponding to 1/256 mole fraction of PVP monomer (Kvamme, 1995) in water, the total energy for a complete polymer will be large (Table 3-7). Even smaller concentrations in the ppm range relative to the amount of water is

Table 3-7 Interaction parameters and intramolecular structure for the PVP model (Kvamme, 1995).

	SITE	*τ (Å)*	*ϕ/k_B(K)*	*q (C)*	*X (Å)*	*Y (Å)*	*Z (Å)*
1	C[a] (ring)	3.63	51.000	0.38	–2.5390	–0.2815	–0.2411
2	CH2[a] (ring)	3.63	51.000	0.00	–3.9460	0.0016	0.2353
3	CH2[a] (ring)	3.63	51.000	0.00	–3.9460	1.5170	0.4812
4	CH2[a] (ring)	3.63	51.000	0.22	–2.4720	1.8600	0.7259
5	O[c]	2.95	63.600	–0.38	–2.2080	–1.3260	–0.8010
6	N[a]	3.32	46.900	–0.44	–1.7600	0.7690	0.0464
7	CH3[b] (chain)	3.87	88.061	0.00	0.5312	–0.2325	0.4549
8	CH[a] (chain)	3.63	51.000	0.22	–0.3026	0.8302	–0.2995
9	CH2[b] (chain)	3.87	59.381	0.00	–0.0146	0.8080	–1.8270
10	CH3[b] (chain)	3.87	88.061	0.00	–0.5320	2.0280	–2.6060

Table 3-8 Lennard-Jones-Parameters for different guest-molecules.

	CH_4	*C_2H_6*
s(Å)	3.758	4.418
e/k_B(K)	148.6	230.0

likely to cover large portions of the liquid surface. It may seem that PVP is an efficient kinetic inhibitor, since it will affect the liquid surface prior to nucleation as well as grow hydrate particles.

When hydrate particles have reached a significant size (above critical), the PVP polymer prefers to stick to the hydrate surface rather than to liquid water due to an energetically favorable hydrogen bonding which involves more than one hydrogen from the hydrate surface for each of the oxygens in the ring. In summary it appears possible to obtain reasonable approximate values for the adsorption of PVP on liquid water and growing hydrates.

Conclusions

A new theory was presented for the kinetics of hydrate formation. This theory is based on the assumption that the initial formation of hydrate takes place on the gas-water interface toward the gas phase. The theory is complete, but some intermediate results are obtained using approximations that have to be verified and eventually improved. The theory is demonstrated with comparison to previously published experimental data for methane hydrate. Effects of kinetic inhibitors can be included in the theory. The proper extension of the theory to a situation where the hydrate formers are in a liquid phase was also discussed.

Inhibition of Hydrate Formation Process

A tremendous amount of experience has been accumulated in preventing the process of hydrate formation—drying of gas, lowering the pressure, increasing the temperature, injection of inhibitors into the flow, etc. The physical significance of drying the gas consists of removing the liquid water medium itself, one of the hydrate formers. Chemical potential of water molecules contained in gas decreases them so much that they can not enclathrate gas molecules and form a hydrate.

Inhibiting the process of hydrate formation is a widely used practice. There are two kinds of inhibition: thermodynamic and kinetic. The essence of thermodynamic inhibition is that the third active component is added to a two-component system (water+gas) which changes the energy of intermolecular interaction and changes thermodynamic equilibrium between molecules of water and gas. There exists a certain dependence between the concentration of an inhibitor in water and the temperature of hydrate formation.

Alcohols and electrolytes are used as hydrate inhibitors. The chemical potential of water molecules decreases because hydrogen bonds form reactions

$$H_2O + CH_3OH \underset{\leftarrow}{\rightarrow} H - O \bullet\bullet\bullet H - O - CH_3 \quad (3.116)$$
$$\qquad\qquad\qquad\qquad\quad H$$

and

$$H_2O + CH_3OH \underset{\leftarrow}{\rightarrow} O - H \bullet\bullet\bullet O - CH_3 \quad (3.117)$$
$$\qquad\qquad\qquad\quad H \qquad\quad H$$

and equilibrium in the reaction of hydrate formation moves to the left.

$$CH_4 + n \times H_2O \underset{\leftarrow}{\rightarrow} [CH_4 \times nH_2O]_{Hydrate} \quad (3.118)$$

$$\mu_{CH_4} + n\mu_{H_2O} \underset{\leftarrow}{\rightarrow} \mu_{Hydrate} \quad (3.119)$$

For its development either pressure should be increased or temperature decreased. Electrolytes solutions are used as thermodynamic inhibitors beside alcohols.

A more effective inhibitor decreases the activity of water molecules to a larger extent, i.e., changes more the chemical potential of water. Kinetic inhibitors do not lower the temperature of hydrate formation, instead, they adsorb on the surface of hydrate microcrystals and microdispersed droplets of water in the flow of a fluid; sharply change the diffusive-sorptional exchange at the gas-inhibitor-water interface; decrease the rate of microcrystals growth, their coagulation, sedimentation and adhesive parameters, thus preventing the formation of large gas hydrate plugs in wells and in pipelines.

Thus, kinetic inhibitors do not preclude the process of hydrate formation, but only shift in time and in space the formation of large hydrate plugs. Kinetic inhibition is a temporary inhibition. It is effective in dynamics and dangerous in statics and forces the shutdown of systems of production and transportation of hydrocarbons. Nevertheless, kinetic inhibition is appropriate in conditions when the condensed water cannot be removed from the flow before the moment of hydrate formation.

Kinetic inhibitors must be very soluble in water, not hydrolyze to insoluble compounds, and adsorb well on a polar surface of hydrate microcrystals forming an external surface preventing the association of hydrate crystals. They also must have a low toxicity, be of moderate cost, and be available and environmentally friendly.

The fatty acids can be used as kinetic inhibitors like

$$C_3H_7COOH---C_7H_{15}COOH, \tag{3.120}$$

and mixtures of fatty alcohols and amines

$$C_3H_7OH---C_7H_{15}OH \tag{3.121}$$

$$C_3H_7NH_2---C_7H_{15}NH_2, \tag{3.122}$$

poly-N-vinylamides, poly-N-vinyl-N-methylapetamide, and other.

A kinetic inhibitor poly-N-vinylpyrrolidone $(-C_6H_9NO-)_x$ (PVP) has undergone sufficient and successful testing in industry. Figure 3-67 shows the curves comparing the relative effectiveness of the traditional (thermodynamic) inhibitors and PVP (Notz, 1994). PVP is injected as an alcohol or aqueous alcohol based solution into an oil and gas flow to create a 0.5% concentration. PVP is supplied as granules or as a liquid concentrate.

In some cases, organic silicon-based coatings, which sharply decrease adhesion of hydrate to metal are used to relocate the place of hydrate formation. Epoxy- or chlorine-group of antiadhesives which react with the hydroxyl oxidized layer of metal is used in coatings. An apolar part of an antiadhesive molecule, which is hydrophobic, and thus prevents the adhesion of polar molecules, appears on an external layer of the coating. For example, hydrophobization by means of a trimethylchlorosilane

$$Fe|FeO|-OH + Cl - Si(CH_3)_3 \rightarrow Fe|FeO|-O-\underset{\displaystyle CH_3}{\overset{\displaystyle CH_3}{Si}}-CH_3 \tag{3.123}$$

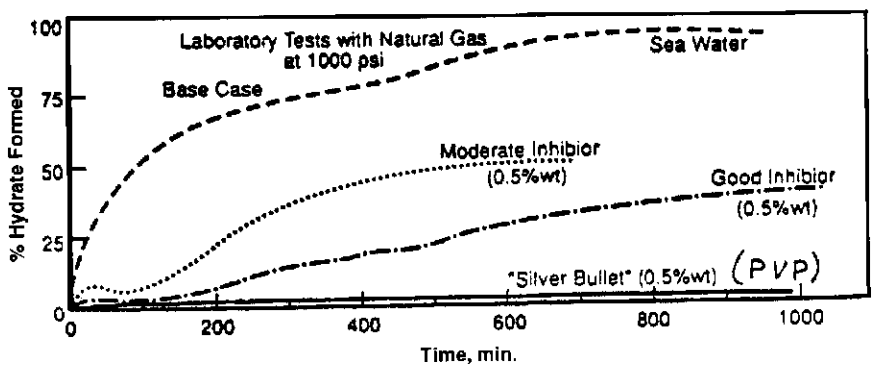

Figure 3-67 Laboratory tests of kinetic inhibitors.

or by siloxane oligomers containing Cl– or ethoxy group, fluorine-based antiadhesives, and others:

$$(C_2H_5O)-\underset{\displaystyle R}{\overset{\displaystyle Cl}{Si}}-O-\left(-\underset{\displaystyle R}{\overset{\displaystyle R}{Si}}-O-\right)_n-\underset{\displaystyle R}{\overset{\displaystyle Cl}{Si}}-(OC_2H_5) \tag{3.124}$$

Such compounds decrease adhesion, not only of water (hydrate), but also of oil, thus increasing the flow capacity of product pipelines.

Solution of a hydrocarbon gas in water is a typical example of a solution of apolar compound in a very polar solvent. Interaction between the molecules of gas and water is not large. It is based on weak van der Waals forces. Molecules of gas are located in voids formed by a structure of liquid water.

Injection of an inhibitor into water saturated with gas sharply decreases the solubility of gas in water. To explain this phenomenon, let us look at the structure of an inhibitor molecule. All inhibitors used can be separated into two groups: inorganic salts and organic compounds. It is very important that all inorganic compounds used are electrolytes, i.e., their aqueous solution contained not single molecules, but ions. A degree of ionization which determines the strength of an electrolyte is rather high with the used salts approaching 100%.

When a solid salt, or its concentrated solution enters the aqueous solution of gas, it ionizes under the effect of water dipoles. Both ions have a positive and a negative charge which attracts water dipoles which surround the ions like a "coat." As the concentration of ions increases in water, the structural parameters of water change. At high ionic concentrations, the molecular structure of a solution gradually approaches that of a crystal hydrate of a salt. Interaction between the water dipoles and ions of an inhibitor is of an electrostatic nature. It is significantly stronger than the interaction between the molecules of gas and water, and, as a whole, the process is energetically favorable. Simultaneously, the liquid crystal structure of water with voids is destroyed, and the solubility of gas decreases. A more significant energy or larger supercooling of the solution is required to form structural cavities of water molecules to form a hydrate. This phenomenon is known in physical chemistry as salting out. It is observed in a system when the polarities of solution components and a solvent differ. Aqueous solutions of methane, ethane, propane, butane, chlorine, noble gases, nitrogen, carbon dioxide, and other apolar molecules are extremely sensitive to the addition of inhibitors.

The dependence of gas solubility in an aqueous salt solution on the salt concentration is expressed by Sechenov's formula:

$$\ln(X/X_0) = -k\,C \qquad (3.125)$$

where

X, X_0 is the molar fraction of gas in salt solution with the salt concentration C and molar fraction of gas in pure water solution (at the same pressure of gas and temperature);

k is the constant of salting out characteristic for the given salt.

The salting out effect of separate ions increases with their charge and depends on the ionic radii. The larger is the ionic radius, the thicker is the "coat" of water dipoles covering it. The effect of an ionic radius on its salting out effect is explained, on one hand, by the fact that the decrease of ion size at the same charge results in an increase of ion-dipole interaction, i.e., in the strengthening of bonds between water molecules and ions; on the other hand, when the ionic radius decreases, the coordination number of ion also decreases which results in a decrease in the size of the water layer covering an ion. However, the first tendency is expressed stronger, and then the salting out effect of an ion decreases with its radius.

It is necessary to choose inorganic inhibitors which are highly soluble in water, strongly dissociate into ions, and, in turn, have a maximum charge and a minimum radius. Using the law of changes in charges and in radii of ions based on a periodic law, it is easy to choose the cations which have the maximum salting out effect. In the main subgroup of the three groups of the periodic table the salting out effect of ions has to increase, as a rule, from bottom to the top and from left to right.

Supposing that the salting out effect of ions is linearly dependent on their charge and radius, we can evaluate the salting out effect using the equation:

$$A_M = K\,q / r \qquad (3.126)$$

where

A_M is the salting out activity per 1 gram-ion;

K is the proportionality coefficient, m/Coulomb;

q is the ionic charge, Coulomb;

r is the ionic radius, m.

In the first approximation it can be assumed that K is constant from ion to ion. Then the salting out activity of considered ions can be evaluated quantitatively (see Figure 3-68 and Table 3-9)

It can be seen from an analysis of Table 3-9 and Figure 3-68 that the compounds of boron, beryllium, and aluminum are more active. However, because of the high cost of beryllium compounds and the absence of salts having the B^{+3} cation we limit our review to the cations of Na, Mg, Al, K, and Ca. It is clear that the aluminum ion has to have the highest salting out effect. The salting out activity of other ions (per 1 gram ion) decreases as Al > Mg > Ca > Na > K which is well supported by practice.

This row of activity is true for solutions containing the same number of gram-ions of metals. Since a weight percent concentration is more often used in practice, it makes sense to make evaluations of the salting out activity of an ion per 1 gram of metal besides the activity per 1 gram

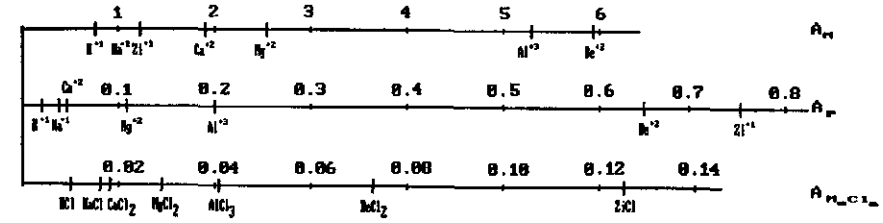

Figure 3-68 Relative activity of electrolytes based on A_M-gram-ion, A_p-gram-metal and A_{MgCl_2}-gram-salt.

Table 3-9 Activity characteristic of different electrolite.

Element	*Charge*	*Ionic Radius*	A_M	*Atomic Weight*	A_P	A_{MeCln}
Li	+1	0.78	1.28	7	0.75	0.124
Be	+2	0.34	5.88	9	0.65	0.073
Na	+1	0.98	1.02	23	0.04	0.0157
Mg	+2	0.78	2.56	24	0.11	0.028
Al	+3	0.57	5.26	27	0.20	0.041
K	+1	1.33	0.75	39	0.02	0.010
Ca	+2	1.06	1.89	40	0.05	0.018

ion. To do that the value of the salting out activity must be divided by the gram-atomic weight:

$$A_P = A_M / \alpha \qquad (3.127)$$

where

A_P is the salting out effect of 1 gram of cation;

A_M is the salting out effect of 1 gram of ion;

α is the gram-atomic weight of metal.

Salts of the same acidity have to be compared while comparing the inhibiting activity of salts, also paying attention to the content of crystalline or hygroscopic water in solid salt during the experiment.

This suggested scheme of calculation produces the following results for chlorides the salting out effect of one gram of the salts LiCl, $BeCl_2$, NaCl, $MgCl_2$, $AlCl_3$, KCl, $CaCl_2$ (assuming that the salts do not contain crystalline water and are dry). In one gram of LiCl there is $7/(7 + 35.5) = 0.165$ grams of lithium. The activity of Li^{+1} per one gram is 0.75. Then one gram of LiCl produces $0.75 \times 0.165 = 0.124$ from Li^{+1}. Similarly, one gram of $BeCl_2$ gives $9 \times 0.65/(9 + 71) = 0.073$;

NaCl	$23 \times 0.04/(23 + 35.5) = 0.0157$;
$MgCl_2$	$24 \times 0.11/(24 + 71) = 0.028$;
$AlCl_3$	$27 \times 0.20/(27 + 106.5) = 0.041$;
KCl	$39 \times 0.02/(39 + 35.5) = 0.010$;
$CaCl_2$	$40 \times 0.05/(40 + 71) = 0.018$.

i.e., to evaluate the salting out activity of a salt the activity of one gram A_P has to be multiplied by the fraction of metal in a salt molecule.

$$M_{MeCl_n} = A_P \frac{\text{Atomic weight}}{\text{Molecular weight}} \qquad (3.128)$$

Notice that the order of activity of one gram of metal ions and one gram of salts is the same, the only difference being in the quantitative ratios.

Comparison of salts of the same metal and different acids is complicated using the given scheme. However, assuming that the salting out activities of anions Cl^- and NO_3^- are close, the activities of one gram of $CaCl_2$ and one gram of $Ca(NO_3)_2$ can be compared:

$$A_{CaCl2} = A \frac{40}{40 + 71} = 0.05 \times 0.36 = 0.018 \qquad (3.129)$$

$$A_{Ca(NO_3)_2} = A \frac{40}{40 + 124} = 0.05 \times 0.24 = 0.012 \qquad (3.130)$$

i.e., calcium nitrate has to be one and a half times less active per unit mass than calcium chloride (this corresponds quantitatively to an experiment).

It is clear that the salting out activity per unit mass of an inhibitor sharply decreases when crystal hydrates of salts are used. Water-free calcium chloride is more active than its six-water hydrate $CaCl_2 \times 6H_2O$ by a factor of $(40 + 71 + 6 \times 18)/(40 + 71) = 2$ times. Use of cations of other metals is hardly suitable for inhibition because there is no multi-charge metal cation of a small radius which would combine a low cost, a high solubility in water, and a high degree of dissociation.

The choice of an anion of inhibiting salt follows the same rules, provided that salt as a whole has to be highly soluble in water. We will consider the acidic residues of only the most general acids while selecting anions. Although a principal possibility exists of enhancing the inhibiting effect through anions selection, we will not use it because the cost and shortage of the appropriate acids does not allow us to even consider a possibility of their use.

a. Carbonates: Na_2CO_3, K_2CO_3, $MgCO_3$, $Al_2(CO_3)_3$, $(NH_4)_2CO_3$.

None of the salts listed above, probably, can be recommended as an inhibitor. Carbonates of sodium, potassium, and ammonium hydrolyze in a solution produce acidic medium which can result in a high increase of a corrosion activity; carbonates of magnesium and calcium are practically insoluble in water; aluminum carbonate does not exist.

b. Nitrates: $NaNO_3$, KNO_3, NH_4NO_3, $Mg(NO_3)_2$, $Ca(NO_3)_2$, $Al(NO_3)_3$.

All of the above salts are soluble in water and strongly dissociate. They can be recommended as inhibitors, and their inhibiting activity per one gram mole of salt has to decrease in the following order:

$$Al(NO_3)_3 > Mg(NO_3)_2 > Ca(NO_3)_2 > NaNO_3 > KNO_3 > NH_4NO_3.$$

The drawback of nitrates is their relatively high cost which is mainly determined by the cost of a nitric acid, and their acidic effect. Sodium nitrate is, besides that, very hygroscopic.

c. Sulfates: Na_2SO_4, K_2SO_4, $(NH_4)_2SO_4$, $MgSO_4$, $CaSO_4$, $Al_2(SO_4)_3$.

All of these salts, except the low soluble calcium sulfate and corrosive ammonium sulfate, can be active inhibitors. Aluminum sulfate has the highest activity.

d. Chlorides: NaCl, KCl, NH_4Cl, $MgCl_2$, $CaCl_2$, $AlCl_3$.

Chlorides of sodium, potassium, magnesium, calcium, and aluminum are widely known salting out agents. Limitations in a row of chlorides consist of hydrolyzing, and thus, corrosion activity of aluminum chloride; potassium chloride is more expensive than sodium chloride, calcium chloride, and magnesium chloride, whose salting out activities are higher. Availability, low cost, and high activity of concentrated solutions of calcium chloride allow us to implement them widely as inhibitors of gas hydrate formation process.

Water is the most ionizing solvent since it has the highest dielectric constant. Solid salt of ionic structure dissociates in water into particles with opposite charges—ions. Tension of the electric field of these particles reaches 10^6 V/cm. Interaction of oppositely charged ions with water molecules and with ions results in significant changes in structure characteristic for pure water which is manifested the most at high concentrations of electrolytes.

Structural changes in a state of water caused by the addition of inhibitors alter the equilibrium of the reaction Gas + Water = Hydrate toward the decreased temperature. These changes can be characterized by the decrease in the value of chemical potential in a solution compared to pure water. Change of the chemical potential of solvent m in a solution with concentration C from the chemical potential of a pure solvent μ_0 is described by the equation:

$$\mu\,(P, T, C) = R\,T \ln a(C) + \mu_0\,(P, T) \qquad \textbf{(3.131)}$$

where

a is the activity of solvent in a solution.

Practically all substances used as anti-hydrate inhibitors are not consumed by hydrate cavities because the molecular diameter of inhibitor molecules is larger than the cavities' diameters. The chemical potential of water in a hydrate lattice is described by the Raoult-Langmiur's equations. The equation which describes the condition of a phase equilibrium in a system gas-water-inhibitor-hydrate can be written as:

$$RT\sum_{i=1}^{2} \nu_i \ln\left(1 + \sum_{j=1}^{n} C_{ij} f_j\right) - P\Delta V + RT \ln a = AT \ln T + BT + C \qquad \textbf{(3.132)}$$

where

ν_i, a, A, B, C are the constants for a hydrate of a specified structure (see Table 3-10);

T is the absolute temperature, K;

P is the hydrate formation pressure, MPa;

f_{ij} is the volatility of j-th component of a gas mixture ($j = 1, 2, \ldots, n$);

C_{ij} is the Langmiur's constant for a j-th hydrate forming component of a gas mixture in a cavity of type i ($i = 1, 2$).

Temperature dependence of the Langmiur's constants C_{ij} is described by an equation:

$$C_{ij} = T^{q_{ij}} \exp(\alpha_{ij} + \beta_{ij} / T) \qquad \textbf{(3.133)}$$

where

q_{ij}, α_{ij}, β_{ij} are the constants for each component ($j = 1, 2, \ldots, n$) and type of a hydrate lattice.

Values of the constants q_{ij}, α_{ij}, β_{ij} are given in Chapter 1. Volatility of the components in a vapor phase f_j is calculated using the Benedict-Webb-Rubin (BWR) equation of state.

Equations 3.132 and 3.133 with the BWR equation only can be solved using the method of successive approximations regarding P at the fixed composition of gas X and temperature T for each type of hydrate structure. The smallest among the obtained values of P characterizes the conditions of hydrate formation and the type of hydrate structure. From a comparison with experimental data, the error in evaluation of an equilibrium temperature of hydrate formation at a fixed pressure does not exceed 1°C. The

Table 3-10 Values of the parameters in Equation 3.132 for hydrates of structures I and II formed from gas and water (T > 273 K).

Hydrate	*Parameters*					
Type	*A*	*B*	*C*	*a*	o_1	o_2
I	3.807	22.254	445.055	0.0561	0.0435	0.1304
II	4.315	25.297	542.262	0.0683	0.1176	0.0588

Table 3-11 Values of activity coefficients for water in aqueous salt solutions (T = 25°C).

	Concentration, wt.%					
Electrolyte	*5*	*10*	*15*	*20*	*25*	*30*
ZnCl	0.96	0.90	0.83	0.72	0.57	–
MgC_2	0.98	0.94	0.88	0.79	0.68	–
$CaCl_2$	0.98	0.95	0.90	0.83	0.75	0.64
NaCl	0.97	0.94	0.90	0.84	0.78	–
NH_4Cl	0.97	0.94	0.90	0.85	0.82	
KCl	0.99	0.95	0.93	0.89	–	–

correlation (3.135) allows us to perform the calculation of hydrate formation conditions from solutions with inhibitors.

Dependence on the activity of water in a solution on the concentration of an inhibitor was determined from a change in vapor pressure of water. Table 3-11 presents the results of the parameter calculation for a number of inhibitors.

During the solution of agents in water, the chemical potential of water molecules decreases, and the temperature of hydrate formation decreases accordingly. The degree of change in the chemical potential of water in a solution is expressed by an activity coefficient a which depends on the concentration C of a water-soluble agent. The equation which expresses the dependence of water activity in an agent solution at which a system of a liquid hydrocarbon, hydrate, and an inhibitor solution exists in equilibrium at the specified pressure P and temperature T, is:

$$a = \exp[\frac{1}{RT}(AT\ln T + BT + C) - \sum_{i=1}^{2} \nu_i \ln(1 + \sum_{j=1}^{n} C_{ij} f_j A_{0j})] \qquad \textbf{(3.134)}$$

$$A_{0j} = \exp[-\frac{V_j}{RT}(P - P_H)]$$

In order to determine the concentration of an inhibitor which results in the prevention of hydrate formation in technological lines, Equation 3.133 must be solved with respect to a, and to determine the concentrations of an inhibitor from the dependence of water activity in a solution (Table 3-11). The dependence of water activity a on the concentration of

Table 3-12 Values of the constants A and B in equation 3.135 for a number of hydrate inhibitors.

	Inhibitors					
Coefficient	*ZnCl*	*$CaCl_2$*	*$MgCl_2$*	*NaCl*	*NH_4Cl*	*KCl*
A	2.84	1.95	2.55	1.34	1.35	0.21
B	3.18	2.57	3.13	1.86	1.89	0.33

electrolytes at C > 30% weight can be determined for engineering calculations from the correlation:

$$C = \frac{1 - a}{1 + A_a + Ba^2} \qquad \textbf{(3.135)}$$

The values of the constants A and B are shown in Table 3-12 for a number of inhibitors.

An activity of water a in an inhibitor solution is determined by the composition, pressure and temperature. Study of a liquid hydrocarbon—methanol solution equilibrium (Bukhgalter, 1987) indicates that at methanol content less that 70% weight in water, the solubility of hydrocarbon can be neglected Equation 3.133, and an activity of water a depends on the agent concentration C as follows:

$$C = \frac{0.4762a^2 + 0.5238a}{0.208a^2 + 0.229a + 0.5625}. \qquad \textbf{(3.136)}$$

Determining the Necessary Amount of an Inhibitor to Prevent Gas Hydrate Formation

Methanol, calcium chloride, glycols, mixtures of alcohols and electrolytes, and other chemicals have found a broad application in the practice of fighting hydrates. The main parameters that characterize different inhibitors are a decrease in the equilibrium temperature of hydrate formation and the temperature of inhibitor solution freezing (Figure 3-69).

The amount of inhibitor needed to prevent hydrate formation at the specified flow parameters consists of two parts: consumption to create an aqueous solution of required concentration and consumption to saturate the vapor flow of gas or light hydrocarbon with inhibitor. The necessary

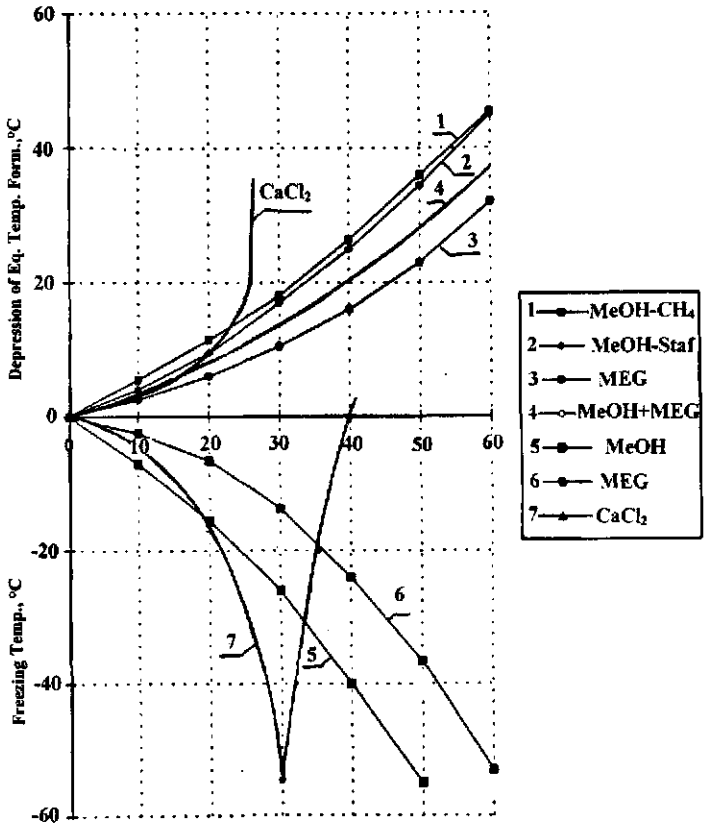

Figure 3-69 Effect of mass concentration of inhibitor on the temperature of hydrate formation, and on the temperature of water solution freezing.

amount of a non-volatile inhibitor (electrolytes) is determined from the condition of the chemical potentials equality between the hydrate, gas, and liquid inhibitor solution phases:

$$\mu_W^H = \mu_W^{sl} \tag{3.137}$$

The water vapor content in the vapor phase above electrolyte solution can be neglected (Englezos and Bishnoi, 1988). The amount of salt dissolved in water and in hydrate also can be neglected.

According to the van der Waals and Platteeuw (1959) theory, the chemical potential of water in a hydrate is then expressed as:

$$\mu_W^H = \mu_W^{MT} - RT\sum_{i=1}^{2} \nu_i \ln(1 + \sum_{j=1}^{n} C_{ij} f_j) \tag{3.138}$$

where

C_{ij} is Langmiur's constant;

ν_i is the number of cavities of type *i;*

f_j is the vapor pressures of hydrate forming gases;

n is the number of components present in system;

μ_W^{MT} is the chemical potential of water in an empty hydrate lattice.

Chemical potential of water in a solution is

$$\mu_W^{sl} = \mu_W + RT \ln a_W \tag{3.139}$$

where

a_w is the activity of water.

From the conditions (3.107)–(3.109) we find the criterion of equilibrium:

$$\frac{\Delta V_W}{RT} P + \Phi(T) - \ln a_W - \sum_{i=1}^{2} \nu_i \ln(1 + \sum_{j=1}^{n} C_{ij} f_j) = 0 \tag{3.140}$$

where

ΔW is the difference in volume of a cavity formed by water molecules in a hydrate and in a free state.

The following information is required in order to find the needed amount of a non-volatile inhibitor of hydrate formation:

1. the amount of water contained in a liquid state and condensing in a pipeline in a section where the conditions of hydrate formation are present,
2. equilibrium temperature of hydrate formation (T_{EQ}), and
3. actual temperature of gas in a pipeline (T_G).

Hydrate formation is possible when $T_G \le T_{EQ}$. A necessary decrease of hydrate formation temperature is determined from a condition $\Delta T = T_{EQ} - T_G$.

Dependence of hydrate formation on temperature decrease, ΔT, for pure and natural gases with inhibitor solutions of different concentrations was studied by many researchers: Hammerschmidt (1939, 1940), Katz (1959), Jakoby (1950, 1953), Makogon (1960, 1966), Bishnoi (1980), Vasilchenko (1965), Malenko (1979), Kobayashi (1951, 1987), and Bond

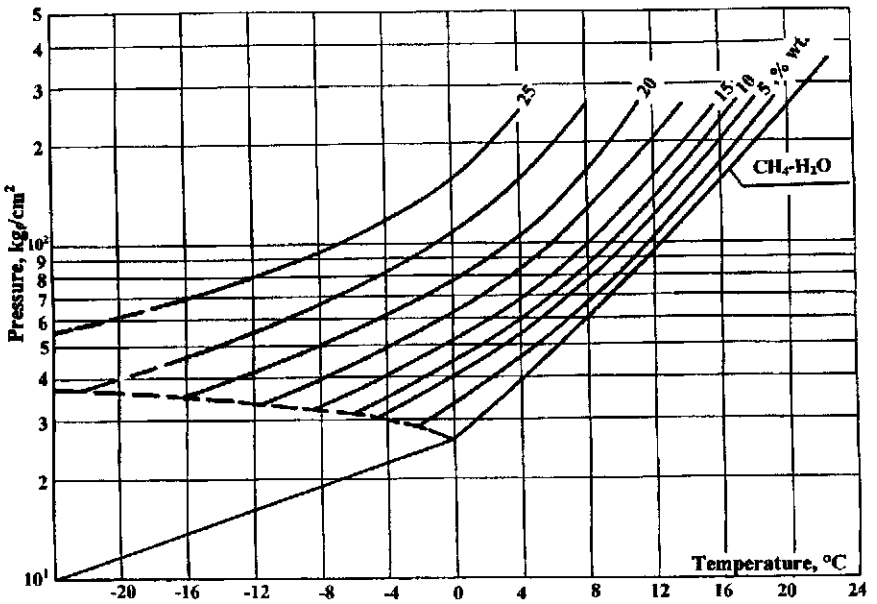

Figure 3-70 Conditions of methane hydrate formation during their inhibition with calcium chloride solutions.

and Russell (1949). However, the most comprehensive study was done by Professor Robinson's group (1965–1993).

Figures 3-70 and 3-71 present such dependencies for the solutions of $CaCl_2$ for methane and for natural gas with a relative density of 0.6, accordingly.

Having determined the minimum necessary concentration of an inhibitor C_2 and knowing the initial concentration of an injected inhibitor C_1, we find the specific consumption of a non-volatile inhibitor (e.g., electrolyte, glycol):

$$q_H = \frac{(W_1 - W_2)C_2}{C_1 - C_2} + q_K\beta, \ (g/m^3) \qquad (3.141)$$

where

W_1 is the moisture content of a gas entering a pipeline, g/m³;

W_2 is the moisture content of a gas leaving a pipeline in a point of hydrate formation, g/m³;

q_K is the liquid hydrocarbons content in a flow, g/m³;

β is the solubility of an inhibitor in a liquid hydrocarbons phase, g/kg.

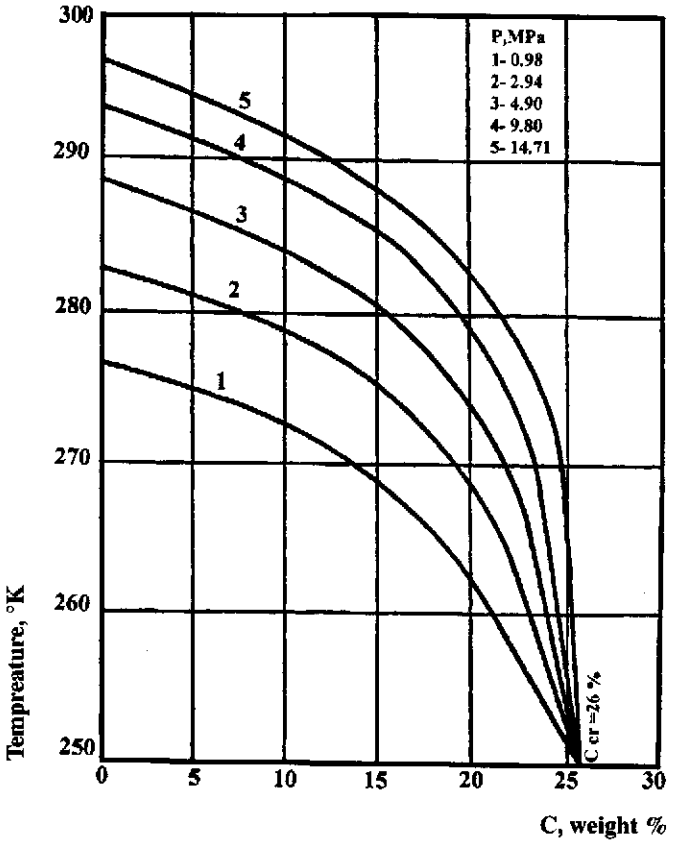

Figure 3-71 Dependence of hydrate formation temperature on $CaCl_2$ solutions concentration under different pressures.

A correction must be made when liquid water is present in a pipeline.

At operating temperatures below 0°C it is necessary to check the possibility of solution freezing during prolonged contact with gas. This check is done using the found value of C_2 with the graphs in Figure 3-69. If the temperature of inhibitor solution freezing is higher than the temperature of gas, then the necessary amount of inhibitor is determined from the condition of avoiding its freezing.

Values of W_1 and W_2 can be determined at specified P-T conditions from a graph in Figure 1-24 (see Chapter 1). It should be noted that a correction for the content of water vapor in gas above hydrate is made in this graph. Figure 1-25 shows the graph for finding the correction coefficient for the moisture content in gases containing H_2S.

Example 3.1. Determine the consumption of a 25% solution of calcium chloride required to prevent hydrate formation in a gas well at the following conditions:

relative density of gas Δ0.6; P_{layer} = 25.4 MPa; $P_{well\ top}$ = 14.9 MPa; T_{layer} = 53°C; $T_{well\ head}$ = 15°C; production rate Q = 10.4 m³/s (900000 m³/day).

Solution: First, we determine the moisture content of the gas in layer conditions W_1, and at well top W_2. Using the nomogram (Figure 1-24), W_1 = 0.88 kg/1000 m³, W_2 = 0.174 kg/1000 m³ of gas. Difference W_1-W_2 gives the amount of water (kg) condensing from every 1000 m³ of gas:

$$\Delta W = W_1 - W_2 = 0.706 \text{ kg} / 1000 \text{ m}^3.$$

Having found the equilibrium temperature of hydrate formation for P-T conditions in a well as 22°C, find the magnitude of equilibrium temperature decrease, ΔT, required to prevent hydrate formation:

$$\Delta T = 22° - 15° = 7°C.$$

From the graph in Figure 3-69 we determine that the temperature difference ΔT = 7°C corresponds to the 16.7% weight concentration of a used solution of calcium chloride. From a material balance equation we find a specific consumption of a 25% solution of $CaCl_2$:

$$q_H = \frac{0.706 \times 16.7}{25 - 16.7} = 1.42 \text{ (kg/1000 m}^3\text{)}. \quad \textbf{(3.142)}$$

Daily consumption will be $q_{daily} = Q \times q = 1.42 \times 900 = 1278$ (kg/day), where Q is the production rate of a well, (1000 m³/day). Density of a 25% solution of $CaCl_2$ is 1.23 kg/l, which results in a daily consumption of the solution being

$$q_H = \frac{1278}{1.23} = 1040 \text{ (l/day)}. \quad \textbf{(3.143)}$$

Regular consumption of the inhibitor will be 1040 × 1.1 = 1143 (l/day).

Determining the Required Amount of a Volatile Inhibitor

Volatile inhibitors are the compounds which decrease the temperature of hydrate formation and whose vapor pressure is higher than the water vapor pressure at a specified temperature (e.g., methanol, ethanol, and other light alcohols). It is necessary to consider the amount of an inhibitor dissolved in a compressed gas in contact with an aqueous inhibitor solution of a specified concentration when the amount of a volatile inhibitor required to prevent hydrate formation is determined along with finding the minimum concentration of a released aqueous inhibitor solution.

P-T dependencies of conditions of hydrate formation from different gases during inhibition with methanol or glycols are presented in Figures 3-72 through 3-76. In order to find the amount of methanol saturating a vapor phase, it is necessary to know its solubility in gas of a specified composition at the given temperature and pressure.

Let us consider gas and methanol phases coexisting at pressure P and temperature T. This state is characterized by an equality of chemical potentials of methanol in a liquid phase μ^L and in a gas phase μ^G.

$$\mu^L(P,T,X_i) = \mu^G(P,T,Y_i) = RT \ln f^G(P,T,X_i) + C(T) \quad \textbf{(3.144)}$$

where

X_i, Y_i are the compositions of liquid and gas phases for all components (i = 1, 2, …, n), accordingly;

n is the number of components in a gas phase, including methanol;

f^G is the volatility of methanol in a vapor phase;

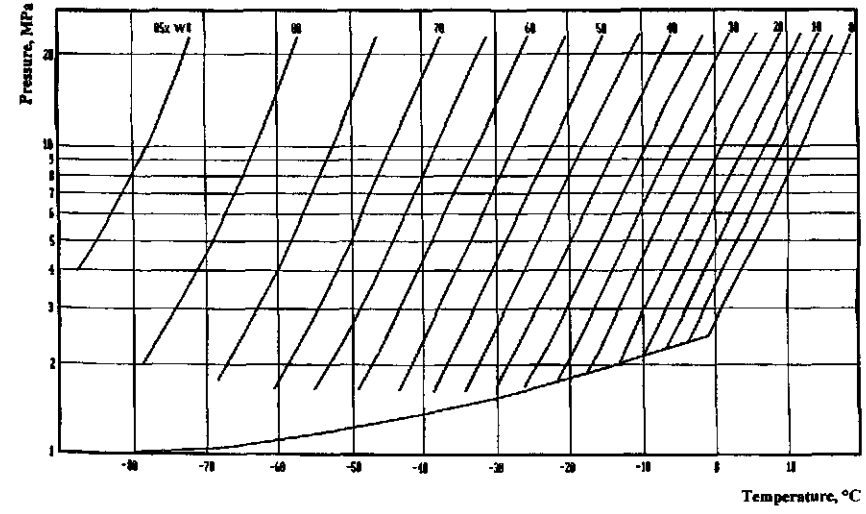

Figure 3-72 Lowering of methane hydrate formation temperature with methanol solutions.

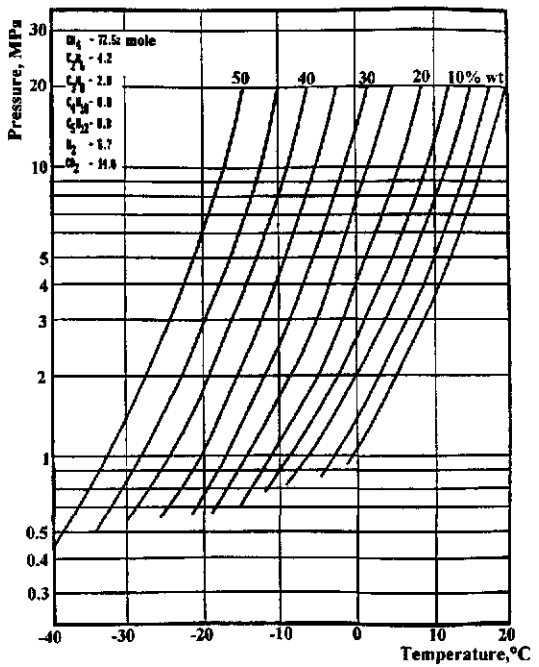

Figure 3-73 Effect of methanol on natural gas hydrate formation.

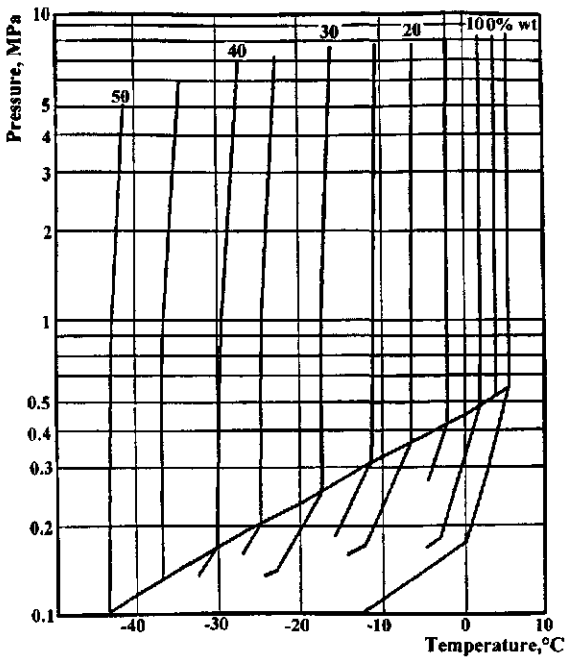

Figure 3-74 C_3H_8 hydrate formation with methanol solutions.

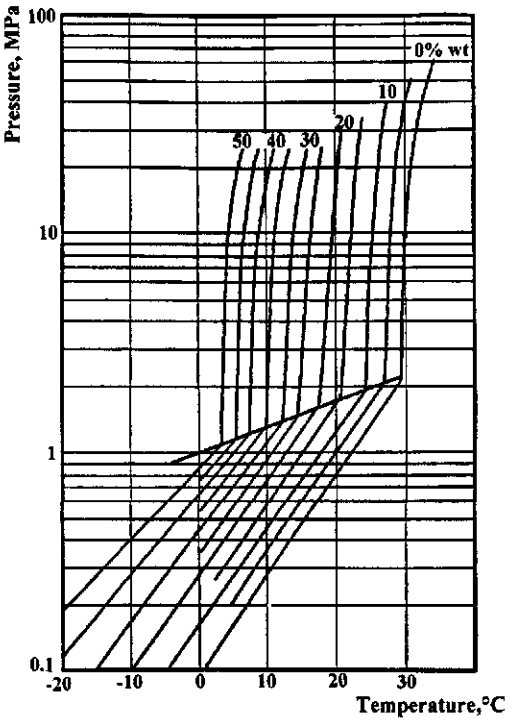

Figure 3-75 H_2S hydrate formation with methanol solutions.

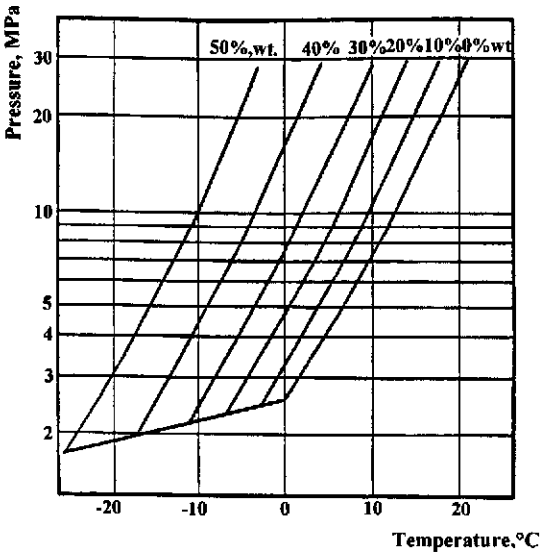

Figure 3-76 Lowering of hydrate formation temperature with ethylene glycol solutions.

$C(T)$ is the function of a temperature;

R is the gas constant.

Assuming the liquid to be incompressible, and neglecting the solubility of gas in the liquid, we obtain an expression:

$$\mu^L(P,T,X_i) \approx \mu_0^L(P_0,T) + V\,[P - P_0(T)], \tag{3.145}$$

where

V is the molar volume of methanol;

μ_0^L is the chemical potential of a pure methanol;

$P_0(T)$ is the vapor pressure of methanol at temperature T.

The following equation is true in the case of equilibrium between a pure liquid and its vapor:

$$\mu^L(P,T) = \mu_0^G(P_0,T) = RT \ln [f_0^G(P_0,T)] + C(T) \tag{3.146}$$

Combining the Equations 3.144 and 3.146 and expressing the chemical potential of methanol in a gas phase through volatility f^G, we obtain:

$$f^G(P,T,Y) = f_0^G(P_0,T) \exp [V^L(P - P_0)/RT] \tag{3.147}$$

Volatility of methanol vapor in a gas phase f^G(P,T,Y) is a function of pressure, temperature, and gas composition. The explicit form of this dependence can be obtained from a real gas equation of state. The Bitty-Bridgeman equation of state for which all constants required to calculate methanol content are known, is the most appropriate among the real gas equations of state:

$$PV^2 = RT\,[V + B_0(1 - b/V)](1 - c/VT^3) - A_0(1 - a/V) \tag{3.148}$$

where

B_0, b, c, A_0, a are constants depending on gas phase composition Y_i;

V is the volume of gas at the specified P and T.

For multicomponent gas mixtures the constants A_0, B_0, a, b, c are determined from equations:

$$A_0 = \left(\sum_{i=1}^{n} Y_i \sqrt{A_{0i}}\right)^2 \quad B_0 = \sum_{i=1}^{n} Y_i B_{0i} \tag{3.149}$$

$$a = \sum_{i=1}^{n} Y_i a_i \quad b = \sum_{i=1}^{n} Y_i b_i \quad c = \sum_{i=1}^{n} Y_i c_i$$

where

Y_i is the molar fraction of i-th component, including methanol vapor in a gas phase;

a_i, A_{0i}, B_{0i}, b_i, c_i are the values of the coefficients for pure components.

Volatility of methanol vapor in a gas phase expressed through a Bitty-Bridgeman equation of state is described by the expression:

$$f^G = \frac{RTY_M}{V} \exp\left\{\frac{1}{RTV}\left[RT(B_0 + B_{0M}) - 2\sqrt{A_{0M} - A_0}\right.\right.$$
$$-\frac{R}{T^2}(c + c_M) - \frac{RT}{2V}(B_0 b_M + B_{0M} b + B_0 b) + \frac{2a\sqrt{A_0 A_{0M}} + A_0 A_{0M}}{2V}$$
$$\left.\left. + \frac{B_0 c_M + B_{0M} c + B_0 c}{2V} + \frac{R}{3V^2T^2}(B_0 b c_M + b_M B_0 c + Bcb + bcB_0)\right]\right\} \tag{3.150}$$

where

B_{0M}, A_{0M}, a_M, b_M, c_M are constants for the Bitty-Bridgeman equation for methanol.

Dependence of the vapor pressure of methanol (MPa) on temperature (K) in the interval $253 < T < 353$ K is described by the correlation:

$$P = 4.941 - 2006.04\,T \tag{3.151}$$

We determine the value of gas saturation with methanol by solving Equation 3.147 together with 3.148–3.150 with respect to Y_M. It is necessary to account for the gas compositional change Y_i during its saturation with methanol vapor.

$$Y_i' = (1 - Y_M)\,Y_i \tag{3.152}$$

where

Y_i is the mole fraction of the i-th component in the specified composition of gas not containing methanol vapor;

Y_M', Y_i' are the content of methanol vapor and i-th component vapor at a vapor-liquid equilibrium.

The content of methanol in gas and in liquid hydrocarbons was determined using this method in the pressure range 0.5–30.0 MPa and in the temperature range –85° to +30°C (Figures 3-77 and 3-78).

To determine the required amount of a volatile inhibitor injected into a gas condensate flow with practical accuracy, the following expression is used:

$$q_C = \frac{(W_1 - W_2)C_2}{C_1 - C_2} + \alpha \times C2 * 10^{-3} + \beta q_K \qquad (3.153)$$

where

q_C is the specific consumption of an inhibitor, g/m^3;

W_1 is the moisture content of a gas at injection conditions, g/m^3;

W_2 is the moisture content of a gas of oil at conditions of an inhibitor leaving a flow, g/m^3;

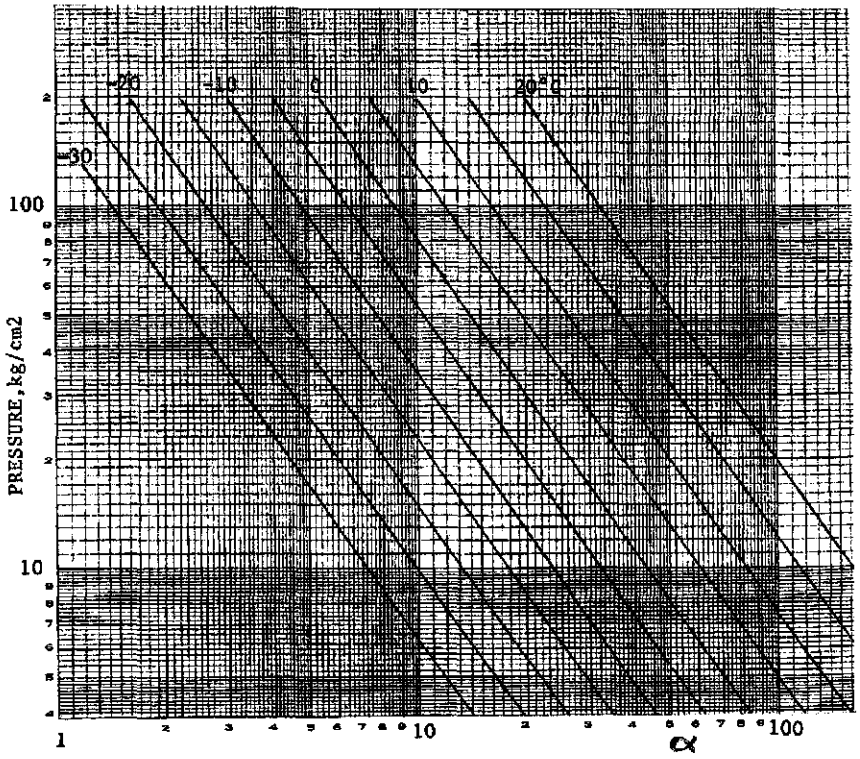

Figure 3-77 Dependence of coefficient α on pressure and temperature.

C_1 is the mass concentration of an inhibitor in an injected solution, fraction, (determined by technical capabilities);

C_2 is the mass concentration of an inhibitor in a solution leaving a flow; fraction, (determined from Figures 3-72–3-76);

α is the amount of methanol going into the vapor phase, saturating a gas flow, g/st.m^3, (determined from Figure 3-77);

q_K is the content of liquid hydrocarbons in a flow, g/m^3;

β is the solubility of an inhibitor in liquid hydrocarbons, g/kg, value of β can be found approximately from Figure 3-78.

The quantities W_i, C_i, q, and β are determined from current conditions during evaluation of a specific inhibitor consumption to prevent hydrate formation in a constructed well filled with a drilling mud of a complex composition, considering the water content of a drilling mud, and the

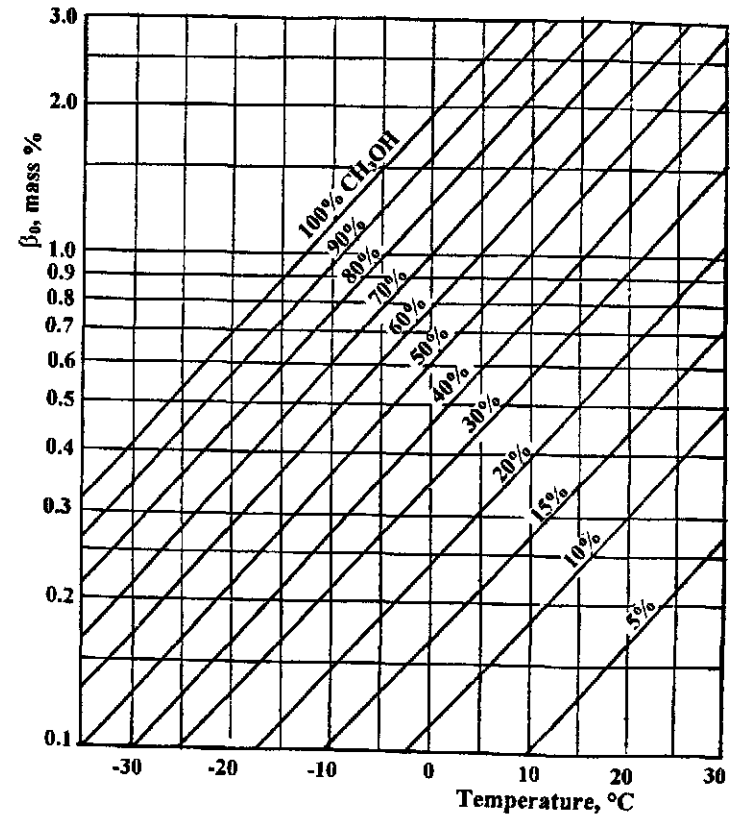

Figure 3-78 Solubility of CH_3OH in liquid hydrocarbons.

content of inhibiting salts and alcohols contained in a drilling mud as additives. The amount of an injected inhibitor must be calculated for a whole mass of free water contained in a drilling mud. It is also necessary to consider the solubility of an injected inhibitor in all components contained in a drilling mud.

Determining the Inhibitor Consumption for Preventing Hydrate Formation in Gas and Oil Wells

A specific inhibitor consumption for prevention of hydrate formation in compressor tubing or in the annular space during production of a gas-saturated oil is found from the expression:

$$q_O = S\left(\frac{C_2}{C_1 - C_2} + \Gamma C_2 \alpha - q_L \beta\right) \qquad \textbf{(3.154)}$$

where

- q_0 is the specific consumption of an inhibitor per ton of produced oil, ton/ton;
- S is the water content of oil, weight %;
- C_1 is the concentration of an injected inhibitor, mass fraction;
- C_2 is the minimum allowed concentration of an inhibitor at which hydrate does not form in a flow, mass fraction (determined from Figures 3-72–3-76);
- Γ is the gas factor, m^3/m^3;
- α is the amount of an inhibitor which saturated a gas flow (determined from Figure 3-77); for non-volatile inhibitors (glycols, electrolytes) $\alpha = 0$;
- q_L is the oil content of a flow, m^3/m^3;
- β is the coefficient of the solubility of an inhibitor in oil (determined approximately from Figures 3-78);

Example 3.2. Hydrocarbon gas is transported through a pipeline.

A relative density of gas by air is 0.8.

Gas parameters in the beginning of a pipeline are $P_1 = 6.4$ MPa, $T_1 = 20°C$;

in the end $P_2 = 3.0$ MPa, $T_2 = 0°C$.

Determine a specific consumption of methanol required to prevent hydrate formation in this section.

Solution: From moisture content curves (Figure 1-24; see Chapter 1) considering the gas density,

$$W_1 = 0.97 \times 0.40 = 0.388 \text{ g/m}^3,$$

$$W_2 = 0.97 \times 0.15 = 0.145 \text{ g/m}^3.$$

Equilibrium temperature of hydrate formation from a gas of a specified composition at the operating pressure is $T_{OP} = 17°C$. The necessary temperature of hydrate formation decrease $\Delta T = 17°C$. The final methanol concentration providing such a decrease is $C_2 = 27\%$ (Figure 3-73). The value of α at P = 3.0 MPa and T = 0°C is 15 (Figure 3-77). Specific methanol consumption calculated with Equation 3.144 is

$$q_M = \frac{(0.388 - 0.145) \times 27}{100 - 27} + 27 \times 10^{-3} \times 2.5 = 0.16 \text{ kg/1000m}^3.$$

At least 160 kg/hour of methanol must be injected at a gas flow rate of 1×10^6 m^3/hour.

Example 3.3. Determine the amount of methanol required to prevent the process of hydrate formation under following conditions:

Initial data:

layer pressure, $P_L = 22$ MPa;

layer temperature, $T_L = 4°C$;

moisture content of a gas at P_L and T_L: $W_L = 0.75 g/m^3$;

hydrocarbon condensate factor, $q_C^L = 180$ g/m^3;

molecular weight of a condensate = 70;

well production rate, $Q = 350000$ m^3/day;

pressure at the first stage of separation, $P_S^1 = 13$ MPa;

temperature at the first stage of separation, $T_S^1 = 25°C$;

moisture content of gas after the first stage of separation, $W_S^1 = 0.35$ g/m^3;

hydrocarbon condensate separation in the first stage of separation, $q_C^1 = 110$ g/m^3;

pressure at the second stage of separation, $P_S^2 = 6.5$ MPa;

temperature at the second stage of separation, $T_S^2 = -14°C$;

moisture content of gas after the second stage of separation, $W_S^2 = 0.04$ g/m^3;

hydrocarbon condensate separation in the second stage of separation, $q_C^2 = 70$ g/m³;

pressure of condensate stabilization, $P_C^{ST} = 1$ MPa;

temperature of condensate stabilization, $T_C^{ST} = 1$ MPa;

amount of stable condensate, $q_C^{ST} = 50$ tons/day.

Calculation data:

equilibrium temperature of hydrate formation at P_L, $T_{EQ}^L = 23.5$°C;

equilibrium temperature of hydrate formation at P_S^1, $T_{EQS} = 21$°C;

equilibrium temperature of hydrate formation at P_S^2, $T_{EQS} = 17.5$°C;

necessary decrease of a hydrate formation temperature:

– for layer conditions, $\Delta T_L = T_{EQ}^L - T_L = 23.5 - 43 = -19.5$°C;

– for the first separation stage conditions, $\Delta T_S^1 = T_{EQ,S}^1 - T_S^1 = 21 - 25 = -4$°C;

– for the second separation stage conditions, $\Delta T_S^2 = T_{EQ,S}^2 - T_S^2 = 17.5 - (-14) = 29.5$°C;

Since the equilibrium temperature of hydrate formation in the conditions of layer and of the first stage of separation is lower than the actual temperature, methanol should be injected into the gas flow after the first separation stage. The amount of condensate released in the first stage of separation is

$$\Delta q_K^1 = 180 - 70 = 110 \text{ g/m}^3. \quad \textbf{(3.155)}$$

The amount of condensate released in the second stage of separation is

$$\Delta q_K^2 = 180 - 110 = 70 \text{ g/m}^3. \quad \textbf{(3.156)}$$

The amount of water in a gas flow:

at layer conditions, $\Delta W_L = 0.75$ g/m³;

at the first separation stage conditions,

$$\Delta W_S^1 = W_L - W_S^1 = 0.75 - 0.35 = 0.4 \text{ g/m}^3 =$$
$$0.4 \text{ kg/1000 m}^3 = 0.4 \times 350000 \text{ m}^3\text{/day} = 140 \text{ kg/day};$$

at the second separation stage conditions,

$$\Delta W_S^2 = W_L - W_S^2 = 0.36 \text{ g/m}^3 =$$
$$0.36 \text{ kg/1000 m}^3 = 0.36 \times 350000 \text{ m}^3\text{/day} = 126 \text{ kg/day};$$

A calculation of the amount of methanol needed to prevent a hydrate formation process in the second separation stage is done using the Equation 3.156:

For the given conditions:

- coefficient of methanol content in a gas phase $\alpha = 1.2$;
- coefficient of methanol content in a condensate phase $\beta = 0.5\%$ mass $= 0.25 \times 1.4 = 0.35$;
- initial concentration of an injected methanol $C_1 = 98\%$ weight;
- minimum allowed methanol concentration which prevents a hydrate formation process at the specified parameters (see Figure 3-75) $C_2 = 44\%$ weight;

Then

$$q_{MS}^2 = \frac{0.4 \times 44}{98 - 44} + 10^{-3} \times 1.2 \times 42 + 0.35 \times 70 \times 10^{-2}$$
$$= 0.612 \text{ kg/1000m}^3 \quad \textbf{(3.157)}$$

Thus, a specific methanol consumption for preventing the process of hydrate formation in gas treatment installations at a hydrocarbons condensate content of 180 cm³/m³, considering the solubility of methanol in hydrocarbons, is 0.612 kg/103 m³. 612 kg/10^6 m³ of produced gas or 214.2 kg/day of 98% methanol must be injected into a gas flow.

Methanol must be injected after the first stage of liquid water separation before a heat exchanger placed between the first and the second stages of separation in an operating technological scheme at the specified regime.

Complex Inhibition of Hydrate Formation and Corrosion Processes

Two types of corrosion exist during well operation: corrosion of metal equipment and corrosion of cement and rock in the well bottom part of a layer. Corrosion of metals increases sharply in the presence of acid gases and of mineralized oxygenated gases.

It is known from the operation of northern field wells that during an injection of methanol into the well bottom zone of a layer to prevent hydrate formation, the cementing stone is destroyed and the process of carrying sand from a layer intensifies. Shale-based cement of a collector-layer dehydrates when methanol is injected into the near-well-bottom part of a layer, and consequently, the cement compresses, thus forming cracks between shale aggregates and spaces between the cement and rock grains. These cracks and spaces between the cement and rock grains are filled with water films during the following influx of moisture into a layer which

exerts a wedging effect. As a result, the aggregation forces weaken, and the surface water films grow. This promotes a disjunction of structural aggregates and a significant loss of mechanical strength of a collector. The strength (coherence) of the rock may decrease by several times.

Vaporized moisture in a filtering gas transforms into a liquid during well operation in the well-bottom zone in presence of methanol because methyl alcohol decreases the temperature and pressure of water vaporization. Thus, the salt content of a condensed moisture is much lower than the mineralization of a rock water. Contact with this pure water results in a decreased number of consumed cations in a shale-based cement. This, in turn, decreases the strength of a collector.

The processes of cement solidification are related to watering of CaO, SiO_2, Al_2O_3, etc. and the formation of oxide hydrates: $Ca(OH)_2$, $2CaO \times SiO_2 \times H_2O$, $2CaO \times Al_2O_3 \times 7H_2O$, etc. These hydrates are the binding compounds. Three periods in the process of cement solidification stand out: solution, colloidization and seizing, and crystallization and solidification. Water content in a solidified Portland-cement is 8.4% after 3 days, 9.1% after 28 days, and 13.3% after six months.

Contact of cement with concentrated methanol results in a dehydration of the stone, which slows down the crystallization process. The largest destructive action toward a cement stone is done by a concentrated methyl alcohol. A sample held in it for one month at the pressure of 0.1 MPa becomes soft, loses its strength, although no external signs of destruction are observed. At pressures of 5.0 MPa a sample held in methanol loses its strength completely and liquefies. A mixture of methyl alcohol, calcium chloride, and water does not exert a destructive action on a cement stone; on the contrary, the strength of a cement sample held in this mixture became higher than after treatment with other aqueous solutions of hydrate inhibitors.

The loss of mechanical strength of a cement stone is possibly related to the process of acidic corrosion because concentrated methanol is acidic (pH ≈ 5). Destruction of concrete or cement stones becomes noticeable at pH ≤ 6.5. The destructive action of methanol increases under pressure since methanol molecules intensively dissolve in water deposited as films with a thickness of several molecules on the surface of gel particles. Then a mechanical spreading of microscopic particles occurs, which results in a complete loss of mechanical strength of a stone saturated with methanol.

Destruction of rock and cement stone decreases the insulating properties of a cement ring, which, in turn, causes the influx of water. Filtration of the layer water slows down the process of rock and cement destruction. However, the irreversible consequences which occurred because of a hydrate inhibitor action will remain, i.e., there will be observed a constant influx of a layer water due to the loss of sealing.

The experience of the Messoyakh field operation indicates that during the development stage the amount of sand and water carried out progressively increased at a constant rate of methanol supply to the operating wells bottom. The carrying out of sand had stopped after the appearance of water in wells product (several cubic meters per day), which supports completely the suggestion above.

An aqueous solution containing 10% CH_3OH and 20% $CaCl_2$ can be recommended as an effective hydrate inhibitor decreasing the temperature of hydrate formation by about 35°C instead of a concentrated methanol. Volatility of methanol in this solution is nearly 15 times less than in a concentrated methanol. Therefore, this mixture of electrolytes and nonelectrolytes does not have a cooling effect on a well-bottom zone. Besides that, another effect of this solution is an insignificant decreasing of mechanical strength of a collector and strengthening of a cement stone.

Use of methanol or its solutions as hydrate inhibitors during testing and operation of wells at low layer temperatures even at a very low mineralization of layer water (up to 10 g/l) may promote the precipitation of carbonates and sulfates because of a change in pH. Concentration of hydrogen ions pH in a solution is determined by a pressure of dissolved CO_2, and solubilities of $CaCO_3$ and $CaSO_4$ depend on the pH of a solution.

Solubility of CO_2 in a concentrated methanol is about 11–12 times higher than in water. The content of CO_2 in aqueous solutions of methanol can be calculated using the formula:

$$\log \frac{X^0_{CO_2}}{X_{CO_2}} = 1.07 X_W \qquad \textbf{(3.158)}$$

where

X_{CO_2} is the mole fraction of CO_2 in an aqueous solution of methanol;

$X^\circ_{CO_2}$ is the mole fraction of CO_2 in pure methanol at the same conditions;

X_W is the mole fraction of water in a solution.

Addition of methanol to a layer water results in a decreased pressure of CO_2 because of its higher solubility in the presence of methanol, and consequently, in a precipitation of $CaCO_3$ and $CaSO_4$ from a solution. In order to prevent the precipitation of salts, it is necessary to add small amounts of acid, e.g., HCl to methanol. If $CaCl_2$ is a component of a hydrate inhibitor, then this mixture cannot be injected into a well without adding an acid because with the increase of pH of a layer water the amount of precipitated $CaCO_3$ may reach several grams per liter due to an additional influx of Ca^{++} ions (as $CaCl_2$) and because of a high content of CO_3^{--} (up to 3000 mg/l) in a layer water.

A precipitation of methanol salts (alcoholate) during the injection of methanol into a well bottom is a result of a reaction with layer water. This process proceeds especially intensely with highly saline water. This can be easily averted by adding an acid to methanol. It is necessary to account for the presence of highly saline water during the selection of a method for inhibiting hydrates during field development at the final stage, when the recovery of gas is accompanied by an active emergence of layer water. The presence of saline layer water must be considered not only from the point of their inhibiting action during an injection of methanol into a gas flow, but also from the point of possible salt precipitation in a well.

Figure 3-79a presents the curves indicating the amounts of salt precipitated from a solution of methanol in layer water (g/kg of solution). Figure 3-79b shows a solid salt plug in he well after injection of methanol. The weight concentration of cations in layer water was 38% (K^+ – 0.4%; Na^+ – 30.2%; Ca^{+2} – 6.2%; Mg^{+2} – 1.24%; B^{+2} – 0.02%) and anions – 62% (Cl^- – 61%; Br^- – 0.25%; I^- – 0.004%; SO_4^{-2} – 0.2%; HCO_3^- – 0.2%; NH_4^- – 0.1%). In Figure 3.79, maximum salts precipitation occurs at 30–60% of methanol concentration in layer water. Analysis of the precipitated salts indicates that their main mass (over 80%) is sodium chloride.

Safety during Work with Inhibitors

Among the known inhibitors of hydrate formation, methanol poses the greatest hazard to the operation personnel. Methanol is soluble in alcohols, infinitely soluble in water. Methanol vapor mixed with air has a very low flame concentration: 3.5%. Methanol vapor forms an explosive mixture with air. Temperature limits of forming explosive mixtures above aqueous solutions vary as follows (Table 3-13):

Methanol vapor density is 1.1 relative to air, flash point is 8°C, self-ignition temperature is 464°C. With the increasing dilution by water the specified temperatures increase (Table 3-14).

Table 3-13 Dependence of an explosive temperature on methanol vapor content.

		Methanol Content, %				
		100	*70*	*40*	*10*	*5*
Explosivity limits, °C	lower	7	15	30	60	–
	upper	39	49	55	76	–

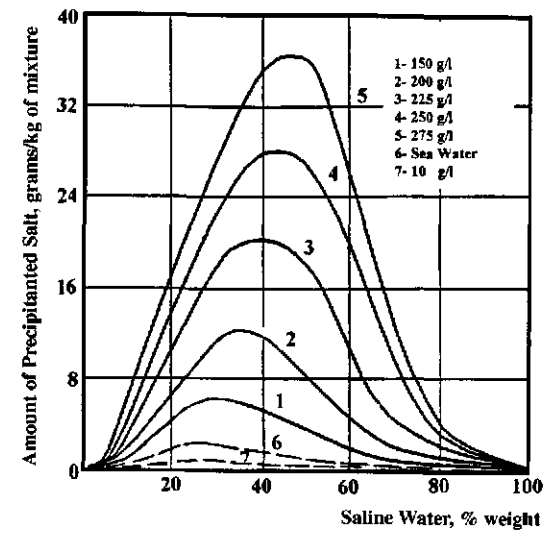

Figure 3-79a Dependence of the amount of salt precipitated from the methanol-saline water solution.

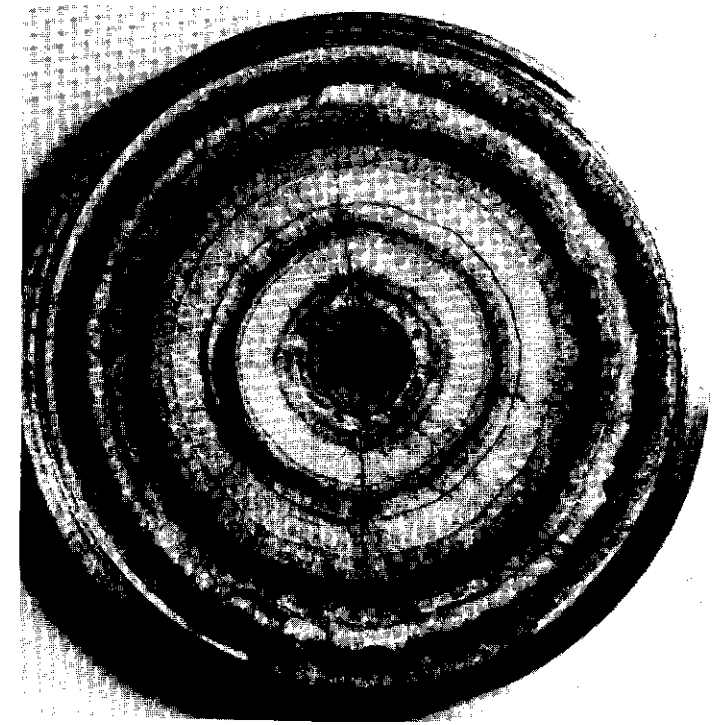

Figure 3-79b Solid salt plug in the gas-condensate well, 4" diameter (Orenburg field, well no. 197).

Table 3-14 Dependence of self-ignition temperature on water vapor content.

	Water Content, %							
	0	*15*	*45*	*60*	*75*	*85*	*90*	*95*
Self-ignition temperature, °C	464	500	545	565	580	600	610	–
Flash temperature, °C	8	11	22.75	30	44.25	58.75	65.25	–

Maximum velocity of flame propagation during the burning of methanol vapor mixed with air is 0.572 m/s, and 1.05 m/s in mixture with oxygen. The maximum flame temperature during the burning of methanol vapor mixed with air is 1750°C, and pressure of explosion of such mixture is 8.4 kg/cm^2. Rate of methanol burning on a free surface is 1.2 mm/min (or 57.6 kg/m^2 × h).

Toxicity of methanol is much higher than that of ethyl, butyl, and other alcohols. Methanol is a strong poison which affects primarily the nervous and blood vessel systems with a very expressed cumulative action (i.e., an ability to accumulate in an organism). First of all, methanol paralyzes blood vessels in an organism, then causes changes in cells. Toxicity of methyl alcohol is explained by the formation of formaldehyde and formic acid in an organism. Vision nerve and eye retina are always damaged during methanol poisoning. Methanol vapor is highly soluble in blood and fluids of a body. Accumulation of a methanol vapor in an organism continues over the whole period of vapor inhalation, whereas its consequent secretion through the respiratory system and kidneys occurs slowly.

Methanol is especially dangerous if swallowed: 5–10 grams of methanol may cause a severe poisoning, and 30 grams is usually a fatal dose. However, sensitivity to methanol is very inconstant even for the same person. Sometimes, sickness and vomiting appear right after drinking methanol, but the first symptoms also may appear several hours later, the next day, or even later. There is no relation between the degree of expression of the first signs of poisoning and its outcome. The body turning blue, deep and uneasy breath, cramps, weak and fast pulse happen in severe cases. The pupil reaction is absent. Death results from the cessation of breathing. Conscious poisoned patients complain about strong pain in the whole body, stomach pain, headache, or an aura before the eyes. If the

poisoning is not fatal, the healing process is slow. A persisting widening of pupils is a sign of a possible relapse or a stable sight disorder. A functional disorder of the liver remains after a clinical recovery.

The poisoning happens not only from swallowing methanol but also from breathing its vapor. Methanol vapor strongly irritates mucous membranes of the respiratory system and eyes. The threshold of smelling methanol is 0.9943–0.011 mg/l. Cases of fainting with a consequent sharp headache, vomiting, intoxication, and weakening of sight were observed after inhaling methanol vapor. The poisoning at low concentrations develops gradually and is expressed in an irritation of mucous membranes, headache, ringing in ears, neural disorder, and sight disorder. Inhalation of high concentrations of methanol is prevented by the irritation of mucous membranes of the respiratory system and eyes. The threshold of a reflex action on the sight sensitivity is 0.0035 mg/l which is lower than the threshold of a smell sensitivity. Methanol enters the body as a liquid and as a vapor after skin contact.

The remedy is to remove methanol from an organism, inhibit its oxidation, and prevent acidic products. A stomach washing with 2–4 liters of a 5% baking soda solution, an intravenous injection of 1 liter of this solution, and an injection of 500 ml of a 5% glucose solution must be done during the first two hours during a heavy oral methanol poisoning. Consequently, five grams of baking soda, lots of drinking, and a 1–3% solution of baking soda intravenously must be administered every 30 minutes (up to 4 liters of liquids daily) to fight acidic products. Constant monitoring levels of bicarbonates in plasma and the pH of urine should be done. Treatment with alkali solutions should continue for four days.

The main chemical antidote for methanol poisoning is ethyl alcohol which prevents the oxidation of methanol due to competitive reactions, and thus decreases the amount of toxic oxidation products circulating in an organism. Immediately after methanol poisoning, one liter of a 5% solution of ethanol and one liter of a 5% solution of glucose in water or in a 3.5% NaCl solution should be administered intravenously. The following method of treatment is also recommended: inject 0.75 g of ethyl alcohol per each kilogram of body weight immediately and 0.5g/kg every four hours after that for 72 hours monitoring the concentration of ethyl alcohol in blood (maximum of 10 g/kg) and in a buffer volume of a plasma.

Upon evaluation, the following procedures can be done: inhalation of oxygen, artificial respiration, phlebotomy (200–300 ml), injection of stimulants and heart medicine and use of Barbamyl or chloralhydrate during excitation with raving. Keeping the body warm is a must—use hot-water bottles and mustard plasters. Place the head high and apply cold

compression if the face is red. A positive effect during the sight disorder is observed from repeated injections of calcium chloride every six hours during the first day and from the use of Vitamin B. Carboxylic ammonium is recommended in order to decrease acidic products, because formaldehyde transforms into a hexamethyltetraamine.

It is necessary to add an odorant (ethylmercaptane in a 1:1000 ratio), kerosene (1:100) and chemical ink or other dark dye well soluble in methanol (2–3 liters per 1000 l of methanol) to prevent the possibility of drinking methanol by mistake as an alcoholic beverage. Only the personnel which have been instructed by a safety officer are allowed to work with methanol. All technical personnel must be equipped with appropriate clothing (rubberized aprons, rubber gloves), footwear, and filtering or isolating gas masks to prevent skin pollution and methanol vapor inhalation during work with methanol. All personnel working with methanol must undergo a physical examination (oculist, general practitioner, neuropathologist) at least once every 12 months. Methanol consumption must be controlled and recorded in a watch journal by gas collection operators.

It is necessary to use protective clothing and rubber gloves during the use of complex inhibitors of hydrate formation and corrosion (methanol + corrosion inhibitor I-1-A) to prevent its action on skin. Hands should be covered with a protective silicone cream when working without gloves, and at the end of this work, hands must be washed with soap and warm water. In the case of getting inhibitor I-1-A on unprotected areas of the skin it should be removed by washing with warm water, soap and a brush. I-1-A inhibitor entering an organism with food or water is inadmissible. All operations on preparing the complex inhibitors in field conditions should be done in open air, or under hood and using fully sealed vessels and installations, etc. in laboratory conditions.

One of the means of preventing methanol poisoning is its substitution, upon availability, of the non-toxic solutions of calcium chloride, less toxic glycols, and selecting other methods of fighting hydrate formation (oil treatment, heating gas at well top, etc.). The vessels containing methanol should be marked poison and flammable. Personnel must be instructed about the high toxicity of this substance in order to prevent drinking methanol. The field should have on file rules for handling methanol during its transportation, storage and use; general sanitary rules for storage and use of methanol; and instruction on the order of receiving methanol from suppliers, its transportation, storage, dispensing and use in gas fields, transportation pipelines and underground gas storage facilities.

A danger of heavy poisoning during work with glycols from inhaling the vapor is negligible, because all glycols have low volatility. However,

a chronic poisoning is possible. The toxic effect of ethylene glycol (EG) was studied the most. Air saturated with EG contains 0.5 mg of EG vapor per 1 liter at 25°C. After oral intake of EG, it acts as a protoplasmatic poison. Mainly, EG affects the central nervous system and kidneys. Both EG and the products of EG oxidation in a body, e.g., ethanedioic acid are toxic. Besides a weak irritation of eyes, flabbiness, and a loss of appetite, signs of kidney disorder are observed during EG vapor action. Highly concentrated EG solutions irritate the eyes and upper respiratory system and cause sleepiness and short narcosis. Nevertheless, the last symptoms are easily reversible. A brake fluid GTJ-22 which contains glycols is used in the northern regions in cars. An intake of 100 ml of this liquid may result in death.

It is thought that EG partly oxidizes in an organism to a ethanedioic acid. Toxicity of glycols decreases in a row: ethylene glycol > diethylene glycol > triethylene glycol. Toxicity of glycols decreases in aqueous solutions, compared to pure substances.

First aid in field conditions must be done during glycol poisoning. Induce vomiting and generously flush stomach with water or with a concentrated baking soda solution. Fighting the acidic products is done as in the case of methanol poisoning.

Preventive measures during work with glycols include detailed instructions to personnel about the danger of taking glycols inside, warning labels, and detailed instructions about work with each inhibitor, their storage, transportation, etc.

General poisoning of personnel with calcium chloride in field conditions is impossible. It should be kept in mind, however, that metal chlorides may contain the salts of hydrocyanic, arsenic, and other acids as impurities. A local action on an organism during work with a solid $CaCl_2$ is expressed in catarrhs of the mucous membranes of the nasal passages (during crushing salt). Concentrated solutions of $CaCl_2$, as all salts of the Group II metals, cause skin irritation after prolonged contact with unprotected skin. It is sufficient to use regular clothing, rubber gloves, and, sometimes, protective glasses to completely prevent the effect of calcium chloride and its solutions.

Prevention of Hydrate Formation in a Well by Controlling Its Regime of Operation

A method of preventing hydrate formation in a well by establishing an optimum hydrate-free regime of a well operation is widely used at gas and

gas condensate fields in the north. The location of hydrate formation can be relocated by controlling the P-T parameters of a well from a well bore into the well top equipment where it is much simpler and less expensive to prevent hydrate formation. Such controlling can be done for wells whose hydrate formation conditions are present between the well top and bottom. The closer the location with hydrate formation conditions to the well top, the easier it is to prevent accumulation of hydrate in a well by moving the gas throttling to the well bottom, by decreasing a loss of pressure and temperature of the flow in a well, and by artificial heating of the flow in a well, etc.

Figure 3-80 presents a diagram of well operation conditions—dependence of pressure and temperature at well bottom (abcdef) and at well top (ABCDEF) on flow rate. The curve GgBEhH is a P-T hydrate formation equilibrium curve for a produced gas. Intersection of the P-T equilibrium curve of hydrate formation and the technical temperature in a well determines the location of hydrate formation.

A curve of well top gas temperature dependence on a well production rate usually has a maximum in a certain point (on Figure 3-80—point C).

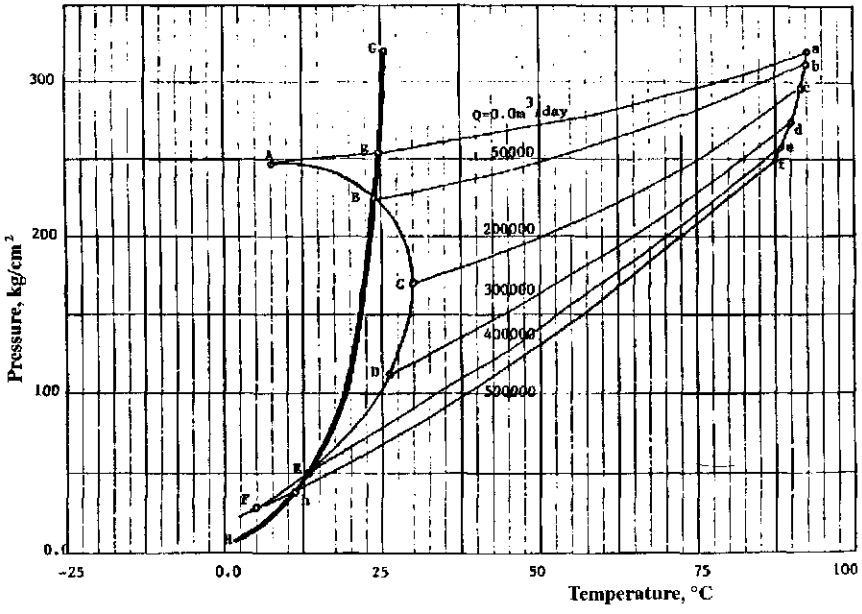

Figure 3-80 Temperature-pressure regime in the well. GH is equilibrium P-T hydrate formation; a,b,c,d,e,f are wellbottom P-T conditions; A, B, C, D, E, F are wellhead P-T conditions; Q is gas production rate, m^3/day.

At low production rates, the well top temperature of gas will be close to the rock temperature at a neutral level. The temperature of gas at a well top increases with an increased production rate because of a decrease residence time of a gas in a well and decreased heat transfer to the rock. However, the increased gas temperature with production rate continues only to a certain limit. The further increased production rate results in a temperature decrease because of a throttling effect. The presence of a maximum on a curve of a gas temperature dependence on production rate is determined by the existence of two factors—decrease of heat exchange between gas and well walls with increased production rate and the simultaneous increase of a throttling effect.

Such a diagram is constructed based on calculations or on results of hydrodynamic study. From the presented diagram we see that during the well shut-in (Q = 0) the well top temperature and pressure (A) do correspond to hydrate formation conditions—hydrates form in a near-well-top part of a well. During well operation with production rates of up to 50,000 m^3/day, hydrates form in a well bore. At production rates from 50,000 to 400,000 m^3/day, hydrates do not form in a well because the well top temperature (BCDE) is above hydrate equilibrium. The further increase of a production rate is accompanied by an increase of throttling of pressure in a well and temperature decrease at well top below hydrate equilibrium (F), and hydrates form in a well. Thus, by controlling the well operation regime, we can relocate the place of hydrate formation from a well into a well-top equipment where it is easier and cheaper to prevent and to remove hydrates. A hydrate free regime of well operation will be at gas production rates between 50,000 and 400,000 m^3/day.

The existence of a hydrate-free regime of well operation is established by a described method using the well testing data. This, of course, does not indicate that every well can be assigned a production rate which would ensure a hydrate-free regime of operation. There is a possibility that at high layer pressures or low temperatures, hydrate formation will happen in a well bore and sometimes in a well-bottom zone of a layer at all regimes of well operation.

Choice and assigning of a hydrate-free regime of well operation does not preclude the possibility of later hydrate formation in gas treatment and transportation facilities. Furthermore, hydrate formation is possible in wells operating in a hydrate-free regime during deviations from a hydrate-free regime or during long shutdowns. Thus, such wells must be provided with the necessary equipment for injection of inhibitors into a well bore to prevent hydrate formation during deviations from their normal regime of operation.

In a number of cases, controlling hydrate formation conditions can be done, not only through changing the production rate, but also by changing the location of gas throttling from a well-top equipment to a well bottom where the gas temperature increases by heat exchange with rock. We can also prevent hydrate formation in a well by a forced heating. The method of gas and liquid flow preheating in a well is most effective in those cases when the hydrate formation conditions are brief—during mastering and testing, and during well startup after a long conservation. The method of a gas and liquid flow forced heating is also effective in gaslift wells operation with a high water content in a flow, especially in arctic regions with low temperature profiles of the rock.

The most technological method of preventing hydrate plug formation in wells during mastering and operation is heating of the product by linear heat sources (such as heating cables) along the whole hydrate-prone interval. Usually, the cables with a diameter of 12–18 mm are lowered directly into production tubing. The presence of a cable does not significantly affect the hydraulic flow resistance.

Thermal regime of well operation $f(x)$ with a cable lowered to depth z_0 which releases heat q per unit of its length, is described by this equation:

$$Q\,C_p\,dT/dz = -k\,[\,T - T_R(z)] + q, \qquad \textbf{(3.159)}$$

where

Q is the well production rate, g/s;

C_p is the heat capacity of the product, J/g °C;

k is the linear heat transfer coefficient, W/m °C;

$T_R(z)$ is the temperature of rock surrounding a well at depth z, °C;

q is the specific power of a heater, W/m.

Solution of the Equation 3.159 is:

$$T(z) = T_R(z) + \frac{\Gamma}{a}\left(1 - e^{a(z-H)}\right) + \frac{q}{QC_p a}\left(1 - e^{a(z-H+z_0)}\right)\eta(z - H + z_0) \qquad \textbf{(3.160)}$$

where

$$a = \frac{k}{QC_p};\quad \eta = \begin{cases} 0 & \text{at} \quad z - H + z_0 < 0 \\ 1 & \text{at} \quad z - H + z_0 \geq 0 \end{cases}$$

z_0 is the depth of lowering a cable, m;

H is the depth of well, m;

Γ is the geothermal gradient.

The possibility of hydrate formation is usually evaluated by values of well-top pressure and temperature. A well is operated in a hydrate-prone regime if the well top temperature is below the equilibrium temperature of hydrate formation at a buffer pressure. Dependence of the well-top temperature T_{WT} on the operation regime looks like:

$$T_{WT} = T_{NL} + \frac{\Gamma}{a}\left(1 - e^{-aH}\right) + \frac{q}{QC_p a}\left(1 - e^{-az_0}\right) \qquad \textbf{(3.161)}$$

where

T_{NL} is the temperature of a neutral layer (usually at depth of 10–20 m from surface).

The last member of this equation expresses the thermal addition to the well-top temperature due to heating (by a cable). It follows from this that the evaluation of a required heating power q can be done using a value of well-top temperature without heating T_{WT_0} and an equilibrium temperature of hydrate formation at a buffer pressure $T_H(P_B)$ by the formula:

$$q = \frac{QC_p a[T_H(P_B) - T_{WT_0}]}{1 - \exp(-az_0)} \approx QC_p a[T_H(P_B) - T_{WT_0}] \approx k[T_H(P_B) - T_{WT_0}] \qquad \textbf{(3.163)}$$

Note that the obtained correlation is applicable at sufficiently high values of the buffer pressure ($P_B > 2$ MPa). A more accurate calculation of the required heating power is done by a simultaneous solution of the Equation 3.160 with a pressure distribution along the well bore $P(z)$ and P-T conditions of hydrate formation.

The use of three- and seven-conductor geophysical cables for heating whose characteristics are shown in Table 3-15 is acceptable.

Table 3-15 Characteristics of geophysical cables.

Cable Type	*Outer Diameter, mm*	*Conductor Resistance, Ohm/km*	*Cable Weight, kg/km*	*Thermal Resistance, m °C/W*	*Maximum Source Voltage, V*
KG7-70-180	10.3	25.5	602	0.2	660
KG7-95-180	16.5	25.5	530	0.2	1000
KG7-70-90	12.1	25.5	517	0.2	660
KGGN-10	18.0	5.0	1200	1.0	660

The maximum specific power of cables of different lengths is determined from the formula:

$$W = \alpha \frac{U^2}{R_0 l^2} n \qquad (3.164)$$

where

U is the maximum allowed source voltage, V;

R is the resistance of a cable wire, Ohm/km;

l is the cable length, km;

n is the number of conducting wires;

α is the coefficient depending on the cable connection method.

Seven-conductor cables (KG7) should be connected to a three-phase source as a "star" with a parallel connection of pairs of wires to a phase with one controlling wire. Dependence of the maximum specific power on the length of cables of different types with a star-type connection is presented in Table 3-16.

The equipment for electrical heating of wells using heating cables consists of a three-phase power transformer, linear electric heater-cable, lubricator, and an end cable holding socket. Transformers of the type TMPN-100/3 used during production of oil by electric centrifugal pumps can be used as a power transformer. A common geophysical lubricator with a reinforced gasket can be used. Different parts of geophysical depth equipment can be used as a cable tip, like the tip cover of the type NKBZ-36 with a GZBZ/36 head.

It is worthwhile to use mobile electric heater units in conditions of geology survey expeditions. These units include a logging raiser PKS-3.5,

Table 3-16 Dependence of a maximum specific power on a cable length with a star-type connection (W/m).

	Cable Length, m						
Cable Type	***400***	***500***	***600***	***700***	***800***	***900***	***1000***
KGGN-10	–	–	400	270	210	170	134
KG7-95-180	450	300	200	140	115	90	72
KG7-70-90	200	128	95	56	50	40	32

lubricator with sealing gaskets, transformer with a control station mounted on a separate platform or directly in a cabin.

Methods of Removing Hydrates

Despite the availability of technological recommendations and means providing an effective prevention of hydrate formation in systems of production, transportation and processing of gases and liquid hydrocarbons, the facts of formation of large hydrate plugs which have to be removed are fairly common. Choice of the method of hydrate liquidation is determined by the location of a hydrate accumulation, by the volume and character of a hydrate plug, by the hydrate composition, and by the available means of hydrate liquidation.

Hydrates may form and shut the gas flow partially or completely in the well-bottom zone of a layer; in a well bore—in fountain tubing column; in annular space; in well-top pipes or in near-well-top equipment; in a system of field pipelines and installations; in transport gas pipelines and product pipelines; and in underground systems of gas storage, including a layer, etc. Liquidation of accumulating hydrate simplifies in the case of partial plugging of an operating cross-section when a gas flow can be provided, because the gas flow can be used to carry an inhibitor or a heat carrier to the surface of a hydrate and to carry out hydrate decomposition products. A complete closing of a pipe cross-section sharply complicates removal of hydrates because a constant removal of liquid water and renewal of a free surface of hydrate decomposition are required, as well as a special care taken during the use of thermal methods of hydrate removal.

Hydrates in installations and in pipelines can be removed with or without stopping their operation. Usually, a shutdown of an installation or a pipeline is required in the case of a complete hydrate plug. Removal of hydrates should be done during operation in the case of an incomplete plugging of a pipeline or an installation.

General Requirements for Doing Works on Hydrate Removal

1. An emergency occurs in systems of production and transportation related to hydrate formation when a complete hydrate plug forms in a well, a technological installation or in a section of a pipeline, and it totally closes the cross-section and is the most difficult to remove. In order to prevent a complete plugging of a cross-section, it is necessary to do a continuous monitoring of equipment

operation, especially during the startup period at sections in which the gas parameters are close to the conditions of hydrate existence. The main parameter indicating a process of hydrate formation is an increase of pressure differential across a section. The reason for deviating from a normal regime should be determined when the differential increases more than by a factor of two. If the reason is related to hydrate formation, removal should be started immediately.

2. In case of a complete hydrate plug formation, it is necessary to determine the location of its accumulation and to attempt to break the continuity of hydrate. This can be attained by different means: heating of a pipeline, injection of an inhibitor, etc. Breaking the continuity of a solid hydrate plug should be started from its wings. An inhibitor cannot be injected into a continuous body of a plug, neither can the plug be heated from inside, because decomposition of hydrate in a closed volume can result in a sharp local increase of pressure and breakage of a pipeline.
3. Decreasing pressure in a section with hydrates during removal of hydrates at temperatures close to 0°C should be done only after injection of an appropriate amount of a heat carrier or an inhibitor in order to prevent lowering of the temperature below 0°C and to preclude the freezing of water released during the hydrate decomposition.
4. During any method of hydrate removal associated with accumulation of water in place of hydrate (except for a sublimation method), water should be removed from a pipeline. Water should be taken from the lower part of a pipeline in a section with the lowest position.

Removal of Hydrate Accumulations from a Near-Well-Bottom Part of a Layer

Hydrate formation is possible under certain thermodynamic conditions in the near-well-bottom part of a layer. The values of well-bottom pressure and temperature have to be compared with the equilibrium P-T conditions of hydrate formation in order to establish a possibility of hydrate formation in a near-well-bottom zone of a layer.

Calculation of a well-bottom pressure P_{WB} is done using the formula:

$$P_{WB} = \sqrt{P_L^2 - AQ - BQ^2} \qquad \textbf{(3.165)}$$

where

P_L is the layer pressure, MPa;

Q is the production rate of a well, 1000 m^3/day;

A, B are the filtration resistance coefficients.

The well-bottom temperature is determined from an equation:

$$T_{WB} = T_L - D\frac{P_L - P_{WB}}{\ln\frac{R_C}{R_W}}\ln\left(1 + \frac{GC_P\tau}{\pi h_{EF}C_R R_W^2}\right) \qquad \textbf{(3.166)}$$

where

T_L is the layer temperature, °C;

D is the Joule-Thompson coefficient, °C/MPa;

R_C, R_W are the radii of the production contour and of a well, accordingly, m;

G is the weight flow rate of gas, kg/hour;

C_P is the heat capacity of a natural gas at a constant pressure, kJ/kg × °C;

τ is the time from the start of well operation, hours;

h_{EF} is the effective thickness of a gas-saturated layer, m;

C_R is the volume heat capacity of rock, kJ/m^3 × °C.

The actual values of pressure and temperature in a near-well-bottom part of a layer and on a well wall are determined using these equations. The possibility of hydrate formation in a near-well-bottom part of a layer is established by their comparison with the equilibrium conditions of hydrate formation.

The formation of hydrates in a near-well-bottom zone can be evaluated more accurately from well testing results. The order of performing such testing has to be followed. Initially ensure that the fountain tubing and a space outside the pipes of a well selected for testing is free from hydrates. In order to do that, a static well-top pressure has to be measured before the start of work. If the pressure has a value typical for this moment of time, there is no solid hydrate plug in a well bore.

A lower value of static pressure at well top indicates a possible presence of liquid or a complete hydrate plug in a well. If the pressure at a buffer and in the space behind the pipes drops sharply after opening the

valves and does not recover after closing the valves, it confirms the presence of a hydrate plug in the compressor pipes and in annular space. Decomposition of hydrates in the compressor pipes is done by using the methods described in the following section.

Well testing is started after removing hydrates. Testing is done through compressor pipes with the injection of an inhibitor into annular space. The temperature of gas becomes lower than the equilibrium temperature of hydrate formation at a certain value of depression, which results in hydrate formation in a near-well-bottom zone of a layer. The start of this process is monitored by a manometer as a sharp pressure drop at well bottom. The start of hydrate formation is also marked on an indication curve. A sharp deviation of an indication curve toward the increased depression is registered in the case of hydrate formation in a near-well-bottom zone. The break point in an indication curve corresponds to the depression and production rate of a well at which the process of hydrate formation starts. Thus, the maximum allowed depression and production rate are determined by well testing.

Removal of hydrates is done by a cyclic injection of inhibitors in the case of hydrate formation in a well-bottom zone. The most appropriate inhibitors for hydrate decomposition in a well bottom zone are methanol and calcium chloride solutions. Keep in mind that the concentrated methanol solutions promote the dehydration of a well-bottom zone when injected into a layer, and they also decrease the strength of cement stone and rock. Dehydration of electrolytes during their cyclic injection may result in a crystallization of injected salts and in a decreased productive characteristic of a near-well-bottom part of a layer.

The volume of an inhibitor necessary to remove hydrates from a well-bottom zone of a layer is determined with the formula:

$$V = \pi\,(R2 - R_w2)m\,h_{EF}\,N, \qquad \textbf{(3.167)}$$

where

R is the radius of a hydrate formation zone, m;

m is the porosity of a layer;

N is the safety coefficient taken as 1.5–2.

The treatment of a near-well-bottom part of a layer with an inhibitor of hydrate formation is done in the following sequence:

- A well is blown until the end of liquid ejection.
- A necessary amount of inhibitor is injected at a temperature of 50–70°C through the compressor pipes;
- A well is shut-in after an inhibitor injection and left with a column of an inhibitor until a complete recovery of static pressure at well top. If the time of a complete pressure recovery exceeds one day, then the column of an inhibitor should be pressed into a layer with the help of neighboring wells or a compressor.
- A well is held with an inhibitor for one day after the well-top pressure recovery, after which it is actively blown into an atmosphere, and a hydrate-free regime of its operation is established.

Removal of Hydrates from a Well Bore Using a Thermochemical Method

Hydrates form in a well under certain thermochemical conditions where they accumulate during the period of gas production and during a well shutdown period, especially during a long conservation. Hydrates can be relatively easily removed by flushing a well bore with methanol, a heated solution of calcium chloride, or hot oil or water during a hydrate plug formation which partly closes a well cross-section. Hydrates can be removed in these conditions without stopping the well. The operational well is preferred in such conditions because an upgoing stream of gas is used to carry the injected inhibitor.

Hydrates are removed by heating via bringing heat through a section which is free from hydrates during a complete closing of a cross-section of only fountain pipes or only annular space behind pipes. The most convenient and available are liquid heat carriers which can be injected into a well bore until hydrate decomposition and ejection from a well.

Currently, there exist several thermal methods of removing a complete hydrate plug from a well bore. One effective method is heat released during a chemical reaction if a solid reactant lowered through a usual well-top lubricator into a well and reacting upon a direct contact with hydrate. The heat released during this reaction results in an intensive hydrate decomposition.

A solid phosphorus pentachloride PCl_5 or a phosphorous anhydride P_2O_5 enclosed in a solid metal capsule made of a magnesium metal foil are used as reagents. This capsule is completely dissolved in the products of the agent reaction with water released during hydrate decomposition.

The capsule has a window in its bottom which is made of a water-soluble compound, for example, metallic calcium. The thickness of this metal is determined by its dissolving rate in water and by the time of a capsule movement from the well top lubricator to the top of a hydrate plug. Upon dissolving an isolating window, the agent reacts with water

and an exothermic reaction which releases about 3 MJ/kg of agent develops. In practice the efficiency of such heater is near 0.7; the heat produced during the reaction of 1 kg of agent is sufficient to melt 5 kg of hydrate. One 5 kg capsule will decompose about 10 meters of a hydrate plug with a diameter of 62 mm.

A well is filled with water up to the top during hydrate decomposition (to ensure smooth lowering of a capsule to the hydrate surface) and a capsule is dropped through a lubricator. The cover dissolves during the capsule passage through a well bore, and when the capsule reaches the hydrate surface an exothermic reaction occurs:

$$PCl_5 + 4\,H_2O \rightarrow H_3PO_4 + 5\,HCl + 514\ kJ \qquad \textbf{(3.168)}$$

At the same time the magnesium body dissolving will occur in a formed phosphoric acid:

$$Mg + H_3PO_4 \rightarrow MgHPO_4 + H_2\uparrow \qquad \textbf{(3.169)}$$

Since magnesium forms a galvanic pair with a steel pipe in which it acts as a cathode, magnesium dissolves completely. Phosphoric acid is also consumed, which significantly reduces the risk of corrosion.

A capsule dissolves completely during the reaction without a precipitate which allows us to use these capsules until the total decomposition of a hydrate plug. A capsule window must be covered with grease in order to protect it from atmospheric moisture during its transportation. The window must be completely cleaned from grease before dropping a capsule in a well.

Formation and Removal of Hydrates in the Karlin-1 Well (Czechoslovakia)

Unique complications due to hydrates are encountered in practice despite significant experience and a large number of instructions available on the prevention of hydrate formation. The conditions of formation and removal of a large hydrate plug in the Karlin-1 well in whose removal we were able to participate in Czechoslovakia in April 1992 are reviewed in this work.

The Karlin-1 well had opened a gas condensate deposit at a depth of 3984 m with an anomalously high layer pressure of 806 atm at a low geothermal gradient of 2.3°C / 100 m. This was the reason for hydrate formation in the well. Hydrate formation conditions in the Karlin field are presented in Figure 3-81.

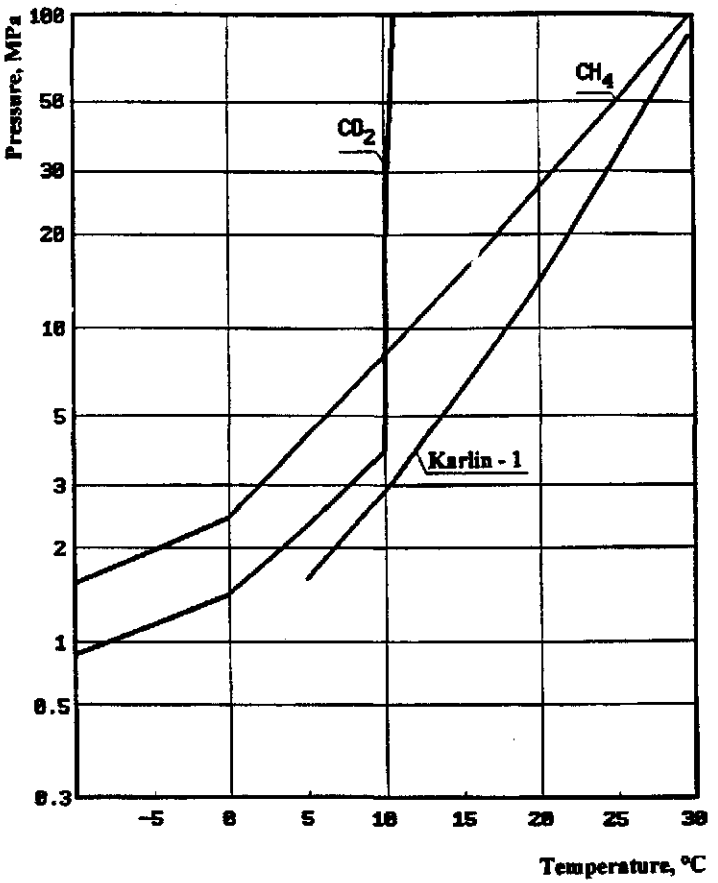

Figure 3-81 Methane, CO_2, and Karlin–1 well gas hydrate formation conditions.

Characteristics of the Karlin-1 Well

The well Karlin-1 was drilled in the southwestern part of Slovenia as a testing well and opened a productive layer at a depth of 3984 m with an anomalously high layer pressure of 806 kg/cm^2 and a layer temperature of 102°C. The static well-top pressure equaled 650 kg/cm^2. The temperature of the neutral layer was near 12°C. Rock profile was characterized by a low thermal gradient equal to 23°C/km. Composition of the layer gas is presented in Table 3-17.

Figure 3-82 presents the well construction. A production pipe with a diameter of 7 inches was lowered to a depth of 3934 m and fountain pipes

Table 3-17 Composition of a layer gas.

Component	CH_4	C_2H_6	C_3H_8	C_4H_{10}	C_5H_{12}	C_6H_{14}	N_2	CO_2	C_7+
Content, Mole %	90.6	5.5	1.55	0.36	0.42	0.23	0.4	0.95	0.61

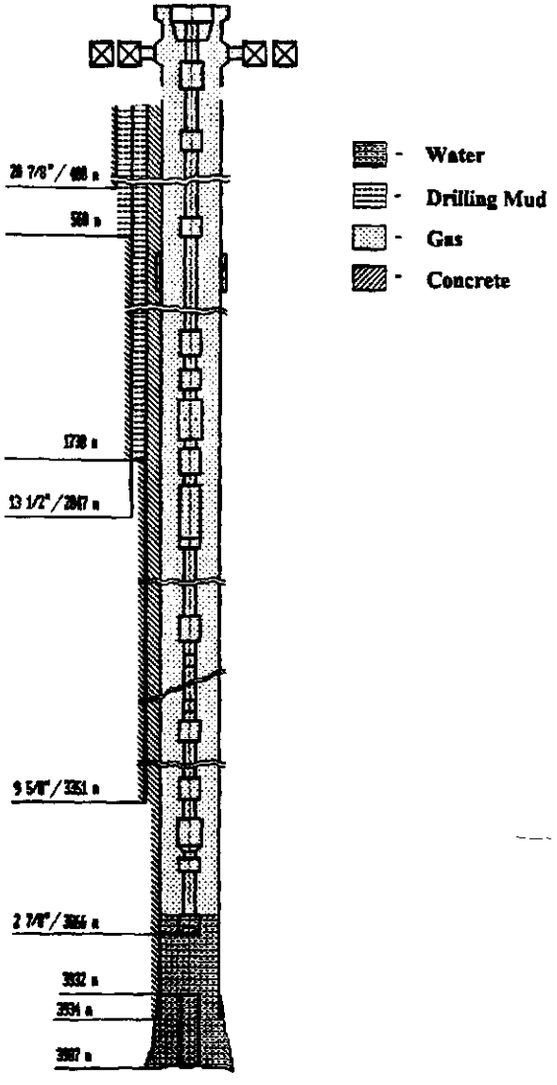

Figure 3-82 Karlin–1 well design.

with a 2 7/8 inch diameter to a depth of 3866 m into a well in presence of two technical columns of a 13 3/8 inch diameter and a length of 2017 m and a 9 5/8 inch diameter at a length of 3351 m. The well top was equipped with Romanian equipment rated to a pressure of 700 kg/cm with a passage cross-section of 2 7/8 inch diameter. The production column was cemented to the top. Technical columns—to depths 560 m and 1730 m decreased the strength of the well. There was no packer in the well.

Conditions of Hydrate Formation in the Well

The Karlin-1 well was drilled with a standard barite water-based mud with a density of 2.2 g/cm^3. Mastering of the well was done during early spring by gradual replacement of a drilling mud with a pure cold water. The well was operating through compressor tubing for two days with a production rate of 100–160 thousand m^3/day after causing an influx and blowing into atmosphere. Then the velocity of an upgoing flow did not exceed 1 m/s which did not provide a complete carrying out of a film water, and the water flowing down the tube walls promoted hydrate accumulation in the well. A total of near 300 thousand m^3 of gas was produced, after which the well was stopped for pressure stabilization.

Figure 3-83 presents the curves of the temperature change in rock profile, the equilibrium temperature of hydrate formation, and intervals of a possible hydrate formation in the Karlin-1 well. According to Figures 3-81 and 3-83, the interval of stable hydrate existence for the P-T conditions of the Karlin-1 well existed in the interval from well top to the depth of 880 m. However, a certain subcooling is required to start hydrate formation. The maximum subcooling of 17°C (a differential between the equilibrium temperature and well temperature) is observed in the near-well-top space. The minimum subcooling of 0°C was in the point of intersection of the hydrate equilibrium curve and the thermal gradient, at a depth of 880 m.

Shown by the results of a hydrate plug removal, the most dense plug formed in a near-well-top space. The rate of decomposition of this plug by a high-temperature washing did not exceed 1–4 cm per minute.

Nucleation of hydrate crystals occurred on a free surface of a water film which resided and condensed on pipe walls. Vapor pressure of water above the formed hydrate was much lower than above the free water surface, which provided an active diffusive influx of water vapor from gas to the surface of growing hydrate crystals.

The time of a hydrate plug formation in a well can be estimated by a heat exchange between a pipe element filled with a gas-water mixture

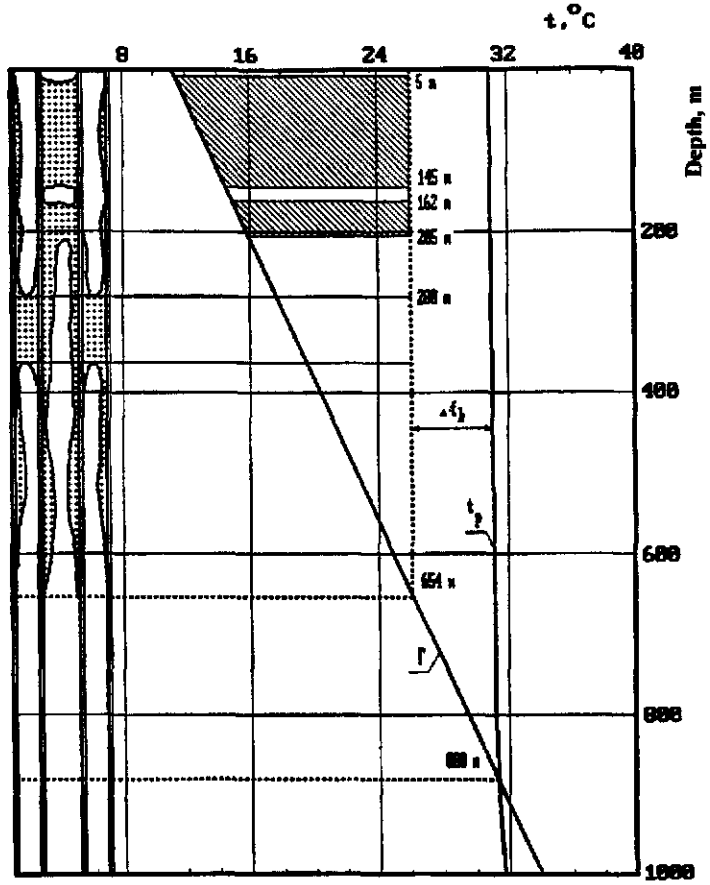

Figure 3-83 Hydrate plug formation in Karlin–1 well.

with surrounding rock, assuming that the forming hydrate does not flow down the walls, but accumulate at the site of formation:

$$\tau = \frac{D\Delta H}{4k(T_H - T_A)} \qquad (3.170)$$

where

- τ is the time of a complete hydrate plug closing the compressor pipes cross-section formation, s;
- D is the diameter of compressor pipes, m;
- ΔH is the heat of hydrate formation, J/m^3;
- k is the coefficient of heat transfer from compressor pipes to surroundings, W/m^2 × K;

- T_H is the temperature of hydrate formation, °C;
- T_A is the ambient temperature, °C.

The value of k after two days of well operation equals approximately 20 W/m^2 × K, then at T_H = 25°C, T_A = 12 °C, ΔH = 350 J/cm^3 the time of a complete hydrate plug formation covering the cross-section of a compressor pipe does not exceed seven hours. In real conditions, hydrates form on the surface of a film water and can flow down the tube walls localizing in separate places. The time of a complete plugging of a pipeline then decreases.

Location and Sizes of Formed Hydrate Plugs

A complete hydrate plug was discovered in a well at a depth of 5 m from well top during an attempt to lower a depth manometer two days after mastering a well and stopping it for pressure stabilization. Theoretically, the hydrate plug could protrude from the well top to a depth of 880 m. However, in wells shut down for a short period of time, several block plugs usually form which partially or completely close the pipe cross-section.

As shown by an analysis of hydrate removal, two complete plugs formed in a well in compressor tubing at depth intervals of 5–145 m and 162–202 m, and one complete plug in annular space between compressor tubing and a production column with the upper boundary at a depth of 280 m. Note that during the formation of several complete hydrate plugs, the pressure of free gas between plugs can drop significantly below the operating pressure in a well. In the considered example (Figure 3-83) the pressure in a column of fountain pipes between plugs could drop to an equilibrium value corresponding to the temperature at the specified depth, to 50 kg/cm^2. The operating pressure outside the column equal to 650 atm, in this example, can crush a column of fountain pipes in the interval 145–162 m between complete hydrate plugs.

Prevention of Hydrate Formation in a Well

In similar conditions it was simple and safe to inject methanol in a volume approximately equal to the volume of a film water in the interval of possible hydrate formation, but not less than 25% of the volume of pipes in the specified interval, to prevent hydrate formation after stopping the Karlin-1 well for stabilization. In the example, 0.5–0.7 m^3 of methanol injected into the well would have been sufficient, which would have promoted washing of a water film from pipe walls in the hydrate formation

interval and would have provided the concentration of methanol and water in vapor sufficient to prevent hydrate formation during the well shutdown period. Unfortunately, this was not done, and hydrates formed in the well.

Removal of Hydrates from a Well

Plug removal was complicated by an anomalously high pressure, low strength capacity of a well-top equipment to a possible hydraulic shock during plug opening, and an absence of experience on removing hydrates in analogous conditions. Czechoslovakian specialists had turned to their neighbors—Austrians and Germans, then to Italians and Hollanders to develop a program and technology of hydrate removal. Several possibilities were considered: drilling of a hydrate plug with an open well top; injection of methanol into fountain tubes and the space between columns; injection of hot water into the space between columns; and flushing a hydrate plug with diethylene glycol at a temperature of 30°C with a closed well top with admittance of pipes under pressure.

The first three cases were tried. It was decided to abandon the first method after drilling through the first tens of meters. This is an emergency method and should not be used.

Injection of two cubic meters of methanol with a 96% concentration under pressure into fountain tubes and the space between columns did not produce and could not produce results because a concentrated methanol on a hydrate surface decomposes it into gas and water whose density is higher than that of methanol. The further decomposition of hydrate stops. The fountain pipes were filled with methanol to the well top, and an 80 m column of methanol was found in the space between columns. Hydrate decomposition did not occur.

Then 4 m^3 of water with an initial temperature of 80°C was injected into the space between columns. The water was supplied for three and a half hours in insufficient portions and, having filled the space between columns, did not produce the desired effect. Thus, the upper boundary of the complete hydrate plug in annular space was determined to be at a depth of 280 m. The tools used did not answer the question as to the length of the hydrate plug in the space between columns. A significant error was the low rate of hot water injection whose volume did not exceed 4 m^3 into space outside tubes.

Keep in mind that decomposition of hydrates in a closed volume in the presence of a complete hydrate plug near the well top may result in a sharp increase of pressure, exceeding the strength of compressor tubes.

Heating of a well through the space outside tubes has to be over the whole interval of potential hydrate formation up to a temperature exceeding the temperature of hydrate decomposition in compressor tubes. This will prevent reforming of hydrate from water flowing down after hydrate decomposition.

It is necessary to make sure that there is no complete hydrate plug in annular space prior to injecting hot water into annular space outside tubes in order to decompose hydrates inside compressor tubes. This can be done by a partial venting of gas from annular space. We should determine the amount of heat required to decompose hydrates in compressor tubes and in annular space and to heat the whole column of pipes in the interval of possible hydrate formation because of water released during hydrate decomposition in near-well-top space flowing down.

The amount of water necessary (V) with a specified temperature (T_0) required to decompose hydrate in compressor tubes and to heat pipes in a hydrate formation interval to a temperature above the temperature of possible hydrate formation can be estimated using the following assumptions:

1. temperatures of water of volume V flowing down the tubes surface from well top to bottom and of the tubes surface are equal;
2. heat losses into surroundings are negligible.

The distribution of temperature, T, with depth, x, is described by a correlation:

$$M_W C_W \, dT + M_W C_W (T - T_0 - \Gamma x)\, dx = 0, \qquad \textbf{(3.171)}$$

where

M_W is the mass of supplied water, kg;
C_W is the heat capacity of water, J/kg × K;
M_{ST} is the mass of a unit length of well tubes, kg/m;
C_{ST} is the heat capacity of steel, J/kg × K;
Γ is the geothermal gradient, K/m;
T_0 is the temperature of the neutral layer, K.

Solution of the Equation 3.171 is:

$$T = \left(T_0^W - T_0 + \frac{\Gamma}{A}\right) \times \exp(-Ax) + \Gamma x + T_0 - \frac{\Gamma}{A}, \qquad \textbf{(3.172)}$$

where

$$A = M_{ST}C_{ST} / M_W C_W$$

An expression correlating the parameters $A(M_{ST}, M_W)$, T_0^W, T_0, Γ, L (L is the lower boundary of possible hydrate formation zone) can be found from the condition of compressor tube temperature elevations above the temperature of hydrate formation in the whole hydrate-prone interval:

$$AL < \ln\left(1 + \frac{T_0^W - T}{\Gamma / A}\right) \tag{3.173}$$

The results of calculations indicate that, in the case considered, at an injection temperature of 80°C, the minimum volume of injected water must be at least 6.5 m³. The heat of the pipes is then insufficient for a complete decomposition of a hydrate plug. Thus, an actual volume of water has to be much larger, so that a clearance sufficient for an unmelted plug to move down the pipe would form between a pipe wall and a hydrate plug.

The previous statements are true in the absence of a hydrate plug in annular space. In the last case not a whole volume of injected water participates in heating pipes in section x, but only a part $M_W(1-x/L)$, where L is a distance from surface to a hydrate plug in annular space. Temperature distribution along the pipe in this case is found from the solution of equation:

$$\frac{dt}{dx} = -\frac{C_{ST}M_{ST}}{C_W M_W}\left(\frac{T - T_0 - \Gamma x}{L - x}\right) \tag{3.174}$$

With the boundary condition $T(0) = T_0^W$ the solution of Equation 3.174 is

$$T = T_0 + \Gamma L + \left\{T_0^W - T_C - \Gamma L + \frac{A\Gamma L}{A-1}\right\} \times \left\{1 - \frac{x}{L}\right\}^A - \frac{A\Gamma L}{A-1} \times \left\{1 - \frac{x}{L}\right\} \tag{3.175}$$

A graph of temperature distribution along the along the pipe is shown in Figure 3-84 (curve 1) for the case when 4 m³ of water at a temperature of 80°C was injected into annular space (upper boundary of a hydrate plug was at a depth of 280 m). A temperature distribution for the case of a free water flow without a hydrate plug is also shown for comparison in the same figure (curve 2). The condition of a hydrate plug decomposition in compressor tubes is the temperature of water in annular space being higher than some value (curve 3) which equals:

$$T > T_{EQ} + \frac{k_1 + k_2}{k_1} \times \frac{M_H \Delta H + M_H C_H (T_{EQ} - T_C - \Gamma x)}{C_W M_W / L} \tag{3.176}$$

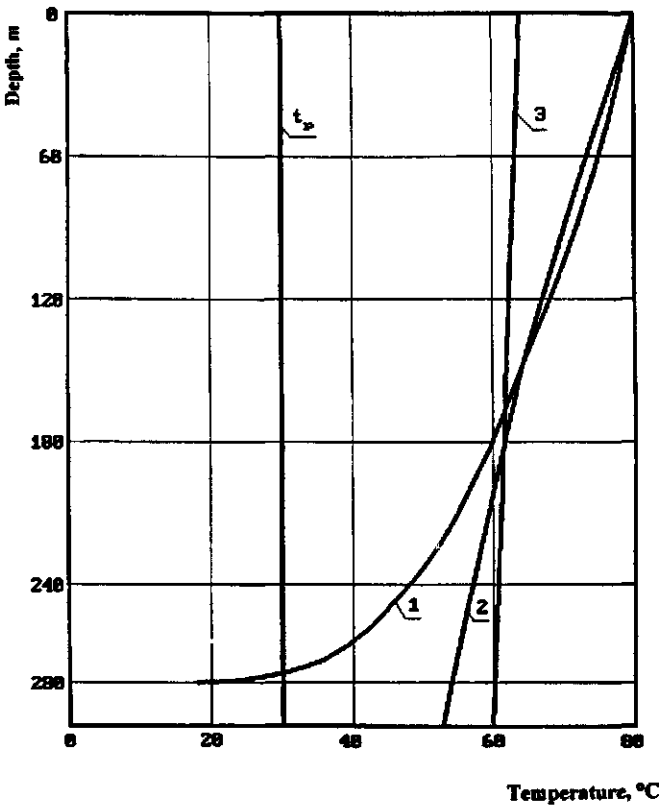

Figure 3-84 Temperature profile along the pipes (curve 3 was calculated with $k_1 = k_2$).

where

C_H is the heat capacity per unit length of a hydrate plug in compressor tubes;

M_H is the mass per unit length of a hydrate plug in compressor tubes;

ΔH is the heat of hydrate formation;

k_1 is the coefficient of heat transfer between annular space and compressor tubes;

k_2 is the coefficient of heat transfer between annular space and surroundings;

In real conditions liquid in a well moves not as a single pack, but as a film on compressor and production tubes walls. The process of water flowing down is lengthy. Thus, at certain conditions a part of supplied water will cool down and will transform into a hydrate phase. It is expedient to use hydrate inhibitors at concentrations which preclude hydrate formation at any P-T conditions in a well as heat carriers in order to prevent hydrate formation in space outside tubes and in annular space. The most acceptable is a mixture of inhibitors—90% of a twenty-weight-percent calcium chloride solution and 10% of pure methanol.

It was determined during sampling a liquid at well top of the Karlin-1 well from a space between columns that it is a 92% weight methanol solution. This means that the injected methanol did not dissolve in water but floated to the top. A hydraulic overthrow took place.

Thus, the three methods did not produce a positive result. A method of hydrate decomposition by a heat carrier injected into the well to a hydrate surface under pressure with a sealed well top remained an option. OTIS Company's equipment allowed the use of this method. The only items to select were a heat carrier and its temperature and the rate of circulation. Undoubtedly, a 20% solution of $CaCl_2$ with 10% of pure methanol supplied at a temperature of 80–90°C or a pure hot methanol could be best. Both of these options were declined by OTIS. The first because of the high corrosion activity of $CaCl_2$ solution, and the second because of the flammability of methanol and instability of couplings in well-top equipment.

Determining the parameters of a heat carrier injection providing decomposition of a hydrate plug in compressor tubes was done based on a solution of a heat problem on temperature distributions in a column through which a heat carrier is injected ($T_1[x]$) and in compressor tubes ($T_2[x]$) which are described by a system of equations:

$$\begin{cases} cq\dfrac{dT_1}{dx} = -k_1(T_1 - T_2) \\ -cq\dfrac{dT_2}{dx} = k_1(T_1 - T_2) - k_2(T_2 - T_D) \end{cases} \qquad \textbf{(3.177)}$$

where

- k_1 is the coefficients of heat transfer between a flow in a column and in compressor tubes;
- k_2 is the coefficients of heat transfer between a flow in compressor tubes and surroundings;

- q is the injection rate of a heat carrier;
- c is the heat capacity of a heat carrier;
- T_D is the temperature distribution with depth along well in rock around well; $T_D = T_C + \Gamma x$;
- T_0 is the temperature of a neutral layer;
- Γ is the geothermal gradient.

Solution of the system of Equation 3.177 with boundary conditions

$$T_1(0) = T_0^T,\ T_1(L) = T_2(L) + \Delta T, \qquad \textbf{(3.178)}$$

where

- L is the upper boundary of a hydrate plug (depth of column lowering);
- ΔT is the change in heat carrier temperature because of heat loss for hydrate decomposition

is:

$$T_1 = C_1 \times \exp(\lambda_1 x) + C_2 \times \exp(\lambda_2 x) + \Gamma x + T_C - c\,q\,\Gamma/k_1, \qquad \textbf{(3.179)}$$

$$T_2 = C_1(1 + \lambda_1\, c\, q/k_1)\exp(\lambda_1 x) + C_2(1 + \lambda_2\, c\, q/k_2)\exp(\lambda_2 x) + \Gamma x + T_C,$$

where

$$\lambda_{1,2} = \frac{k_2}{2cq}\left(1 \pm \sqrt{1 + 4k_1/k_2}\right)$$

$$C_1 = \frac{-\lambda_2\left(T_o^T - T_0 + \dfrac{cq\Gamma}{k_1}\right) \times \exp(\lambda_2 x) - \Gamma + \dfrac{\Delta T k_1}{cq}}{\lambda_1 \exp(\lambda_1 x) - \lambda_2 \exp(\lambda_2 x)}$$

$$C_2 = \frac{-\lambda_1\left(T_o^T - T_0 + \dfrac{cq\Gamma}{k_1}\right) \times \exp(\lambda_1 x) + \Gamma - \dfrac{\Delta T k_1}{cq}}{\lambda_1 \exp(\lambda_1 x) - \lambda_2 \exp(\lambda_2 x)}$$

Estimates indicate that heat losses from a heat carrier are insignificant during hydrate decomposition and the change in a heat carrier's temperature can be neglected ($\Delta T = 0$) (at $q = 5$ l/min the diameters of a column and compressor pipes are 42 mm and 75 mm, accordingly; $\Delta T \approx 0.1$°C).

It is necessary to know the temperature of a heat carrier at the depth of lowering a column in order to determine the parameters of a heat carrier

injection (temperature, rate) needed to establish the conditions of a hydrate plug decomposition:

$$T_1(L) = T_0^T - \left(T_0^T - T_0 + \frac{cq\Gamma}{k_1}\right)\left(1 - \frac{(\lambda_1 - \lambda_2)\exp(\lambda_1 + \lambda_2)L}{\lambda_1 \exp(\lambda_1 L) - \lambda_2 \exp(\lambda_2 L)}\right)$$
$$+ \Gamma L\left(1 - \frac{\exp(\lambda_1 L) - \exp(\lambda_2 L)}{L[\lambda_1 \exp(\lambda_1 L) - \lambda_2 \exp(\lambda_2 L)]}\right) \quad (3.180)$$

The temperature of a heat carrier at outlet is determined by an equation

$$T_2(0) = T_0^T + \frac{cq\Gamma}{k_1}\left\{1 - \frac{(\lambda_1 - \lambda_2)}{\lambda_1 \exp(\lambda_1 L) - \lambda_2 \exp(\lambda_2 L)} + \right.$$
$$\left.\left(T_0^T - T_0 + \frac{cq\Gamma}{k_1}\right)\frac{\lambda_1\lambda_2}{\Gamma}\frac{\exp(\lambda_1 L) - \exp(\lambda_2 L)}{\lambda_1 \exp(\lambda_1 L) - \lambda_2 \exp(\lambda_2 L)}\right\} \quad (3.181)$$

Figure 3-85 presents the graphs of $T_1(L)$ and $T_2(0)$ dependence on the depth of an upper hydrate plug boundary with the following parameters: $T = 80°C$; $q = 45$ l/min; outer diameter of a lowered column is 1 2/3″, and internal diameter is 1/2″; $k_1 = 75$ W/m × K; $k_2 = 65$, 5, and 1 W/m × K; $T_{amb} = 12°C$; $\Gamma = 0.023$ K/m. The rate of a hydrate plug decomposition can be then determined from a correlation:

$$v = \frac{\{T_1(L) - T_{EQ}\}k}{\Delta H} \quad (3.182)$$

where

k is the heat dissipation coefficient of a heat carrier during washing of a hydrate plug (in our case about 1.5–6 kW/m² × K);

When the temperature of a heat carrier is higher than the hydrate equilibrium temperature in the place of contact with a hydrate plug by 40°C, the rate of a complete hydrate plug decomposition is 1–4 cm/min.

Our proposal to flush the hydrate plug with diethylene glycol under pressure at a temperature of 80–90°C and at a rate of 40–50 l/min, which precludes a hydraulic shock during the opening of the lower end of the plug, was finally accepted after industrial discussions. The equipment allowed us to set a required rate of washing at an operating pressure of about 700 kg/cm². The lowered columns had an outer diameter of 1 2/3″, and internal diameter of 1/2″. Specific stress on the column was

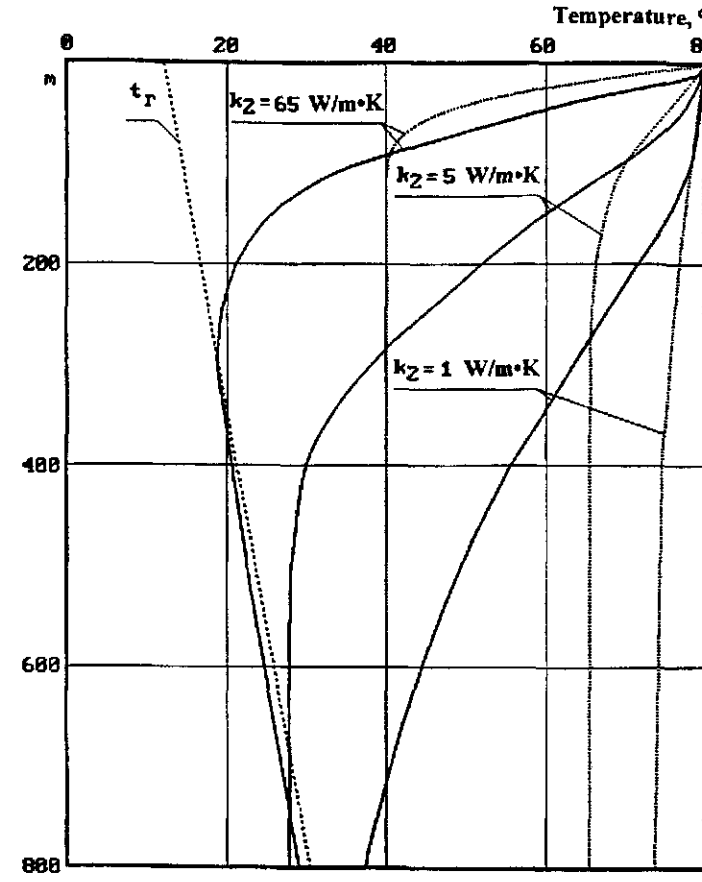

Figure 3-85 Dependence of heat carrier temperature on depth of upper boundary of the hydrate plug (—— is temperature at depth L; ····· is outlet temperature).

1000–1500 kg. The rate of complete hydrate plug removal was 2–4 cm/min in its upper part and about 20 cm/min in its lower part at the specified parameters.

Heating of the well bore was performed until the removal of hydrates from annular space with the following blowing of decomposition products through separators into atmosphere after the removal of hydrate plugs from compressor pipes. The well cleaned from hydrates was conserved with setting a cement bridge.

Conclusion

Our level of knowledge today allows us to forecast and to prevent hydrate formation in any point of a technological chain during production, transportation, and treatment of gases. Formation of hydrate plugs in wells is a result of a violation of a technological regime or an inaccurate prediction of hydrate formation conditions.

A hydrate plug in a well or in a gas pipeline is a benign tumor in a technological organism which has to be removed. The sooner it is spotted, the easier, cheaper and simpler it is to remove. Untimely prediction and prophylactics result in formation of a complete hydrate plug closing a well or a gas pipeline which can cause complete work stops, and, in some cases, explosions and deaths.

A timely, proper use of the known recommendations allow us to remove any hydrate plug formed in any location. The effect is determined by the qualifications of specialists and the quality of the equipment and technology used. Removal of hydrate plugs is always more expensive than their prevention, especially in deep seas. The author has experience of removing hydrate plugs from wells and pipelines operating in different climate conditions on land and under sea.

4

CHAPTER

TECHNOLOGICAL USE OF GAS HYDRATES

The properties of hydrates, parameters of a hydrate formation process, and a change of a hydrate former's characteristics during their transition from a free into a bound hydrate state and back allow us to create a number of principally new technologies.

One of the unique properties of hydrates is a change of the specific volume of hydrate formers during their transition from a free state into a hydrate state or from a hydrate into a free state. A specific volume of water increases by 26–32% during the transition into a hydrate state (by 9% during transition into ice state). A specific volume of gases changes by several orders of magnitudes during hydrate formation. This property allows us to create methods of storage and transportation for large volumes of gas in a hydrate state at low pressures, and to create effective methods of compressorless pressure increase for gases. Gas hydrates can be used to create clathrate accumulators of heat, cold, and mass. Gas hydrates also can be used for a machineless thermal compression of gases, generation of cold, and energy production during the use of a low-potential heat. The process of hydrate formation found unexpected uses for elimination of complicated gas-oil fountains (Makogon, 1980).

Recently a technology of using gas hydrates for desalinization of water was tested. Several gas-hydrate based desalinizators are operational. For example, desalinizators of the Coppers Freon Company have been used which produce 37.5 m^3 of fresh water per day (using Freon-12 agent) since 1968 (Smirnov, 1993). Desalinizators of the Lammus Development Company have been used to generate 76 m^3/day of fresh

water (using propane) since 1968. Operation of this installation for seven years was reported (Diamant, 1974).

Only water molecules go into a hydrate phase during hydrate formation from a saline water, while minerals dissolve in water concentrate. Thus, by using a hydrate formation process one can simultaneously obtain fresh water from saline water and concentrate mineral solutions with the consequent production of pure food concentrates, powders, salts, etc.

Water vapor pressure is lower above hydrates than above water in a free state at the same temperature. This property allows us to create methods of gas drying and also methods of dispersion of high-temperature fogs.

Various gaseous and liquid hydrate formers create hydrate at different thermodynamic parameters. This allows us to create methods of separation and enrichment of mixtures by a subsequent transition through a hydrate state at specified regimes.

Heavier isotopes of the same hydrate former enter hydrate easier. This property allows us to create effective methods of material enrichment, i.e., to enrich water with deuterium.

Different ways of using gas hydrates are at the proposal stage; experimental studies and technological solutions are being worked on.

A device in which the transition of water and an agent through a hydrate state and the use of specific properties of gas hydrates changes the quality of a gas stream can be named a gas hydrate transformer (GHT). A feed stream can be a stream of heat, and mainly, a stream of material.

All GHT classes consist of the same unified elements $Z \leq 5$: crystallizer, melter, hydrate converter (used to purify and to dry hydrate and to relocate it from a crystallizer into a melter), agent transformer, and an input-output system for feed materials and products. Many processes, regularities, and even construction solutions are the same in the functional elements of GHTs. In many classes of GHTs each element is represented by a few modifications. The indicated uniformity eases the representation of every GHT as a composition of technological solutions of GHT elements and an originality of thermodynamic cycle of a particular transformer.

Let us review the technological details and thermodynamic capabilities of the most prospective GHTs.

Desalinization, Concentrating, and Separation of Aqueous Solutions

Nearly 1.5 billion cubic kilometers of water exist on our planet. However, 97% of this water is saline and exists in seas and oceans.

Fresh water on earth is only 30.5 million km^3, 97% of which is located in polar and mountain glaciers. Less than 3% of fresh water or 0.88 million km^3 is located in rivers, lakes, and soil and is available to humans. This is just 0.06% of all water resources on earth. However, even this volume of water has an uneven global distribution. The majority of fresh water is concentrated in large rivers and lakes (Baikal, Ontario, Michigan, etc.). Improvements in the distribution of fresh water on land are accomplished by creating large artificial water reservoirs and irrigation systems on rivers, by recovering artesian water from underground sources, and by creating large desalinization systems.

The technology of water desalinization is based on properties of hydrate:

1. To form its structure from molecules of pure water and an agent, leaving impurities (organic and inorganic) in the solution;
2. To separately crystallize salt along with formation of gas hydrates in a saturated solution; then the crystals of two solid phases (gas hydrate and salt) have significantly different densities and are separated by weight in a saturated solution.

A gas hydrate method of water desalinization is similar to the method of freezing on contact. Similar to a freezing method, in a gas hydrate technology the initial solution is deaerated, cooled, and transformed into a solid. Gas hydrate is formed upon contact with a hydrate former (temperature of hydrate formation in solution is lower than in pure water by the amount of temperature depression due to the presence of salts). Hydrate crystals are separated and washed from brine and melted. Fresh water and brine coming out of the process are degassed.

However, the possibility of a hydrate former choice with a different position of a hydrate formation curve on a P-T diagram (compared to an almost vertical and fixed line of ice formation) is flexibly adaptable to different characteristics of desalinization, to the salt content of an initial solution S_j, to the required coefficient of fresh water extraction

$$\eta_{EN} = \frac{W_{\min} + e_X}{\sum_i l + e_T}$$

to the type and amount of energy, to the ambient temperature T_0, and to the temperature of hydrate formation in a crystallizer T_A.

The following schematics of hydrate crystal desalinizators (HD) were proposed:

1. Heat-pump—the heat of hydrate formation is removed by a boiling hydrate forming agent, agent vapor condenses on hydrates washed from brine, and the excess of the heat of agent condensation is released into surroundings at T_0 (see Figure 4-1).
2. Regenerative—the heat of gas hydrate formation at T_A and dissociation at T_B are regenerated, i.e., $T_A < T_B$ (Figure 4-2).
3. Cold-producing—uses an agent with a high T_{Upper} Invariant (quadruple) Point, so that $T_A > T_0$ and $T_B < T_0$; melting of hydrate at T_B = 276-280 K generates cold.
4. Heat use (Figure 4-3) $T_{UIP} > T_A > T_0$. The heat of hydrate formation is removed into surroundings by a direct heat transfer. Hydrate is melted by a low temperature heat, and the need for compressor equipment disappears. Independence of the desalinizator from electric power can be ensured by melting hydrate to a vapor state and its expansion in a turbine.
5. Temperature differential use—using temperature differential between a depth of cold water and warm surface water in sea

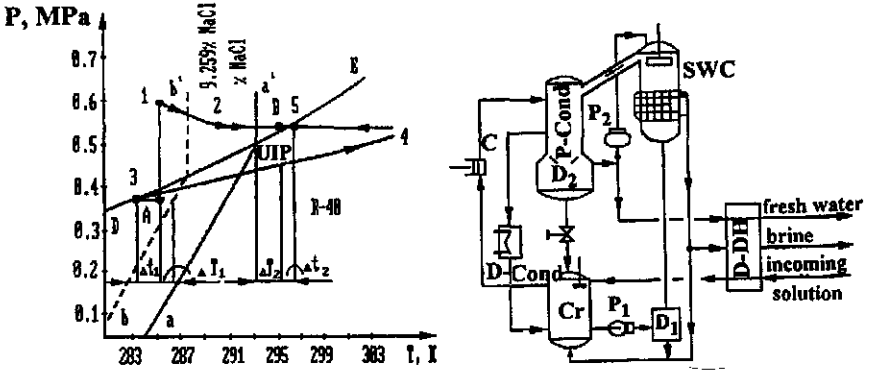

Figure 4-1 Cycle and schematic of a single stage heat pump clathrate hydrate desalinator (HD).

A-1: compression of hydrate suspension and moving it with pump (P_1) from crystallizer (Cr) to decanter (D_1), and then to separation and washing column (SWC); 1-2: separation and washing of hydrates from brine in SWC; 2-3: heating and melting of hydrates in P-Cond; 3-4: compression of agent vapor in compressor (C); 4-5: cooling and condensation of agent vapor in P-Cond (on hydrates) and in D-Cond; 5-3: valve expansion of liquid agent; 3-A: boiling and heating of liquid and vapor agent in Cr. UIP-upper invariant point.

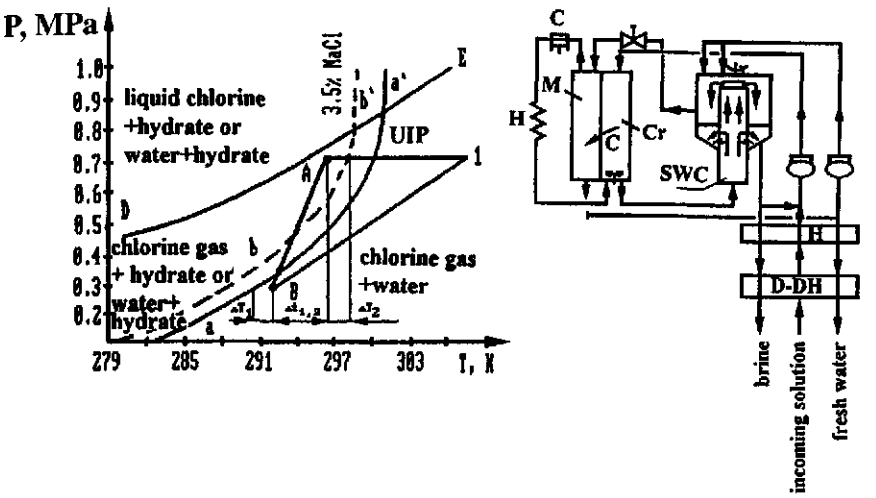

Figure 4-2 Cycle and schematic of a regenerative HD.

A-B: pressure drop during washing of hydrates in SWC and valve expansion of fresh water suspension during its moving from SWC to melter (M); B-1: agent vapor compression in C; 1-A: vapor cooling in heat exchanger (H).

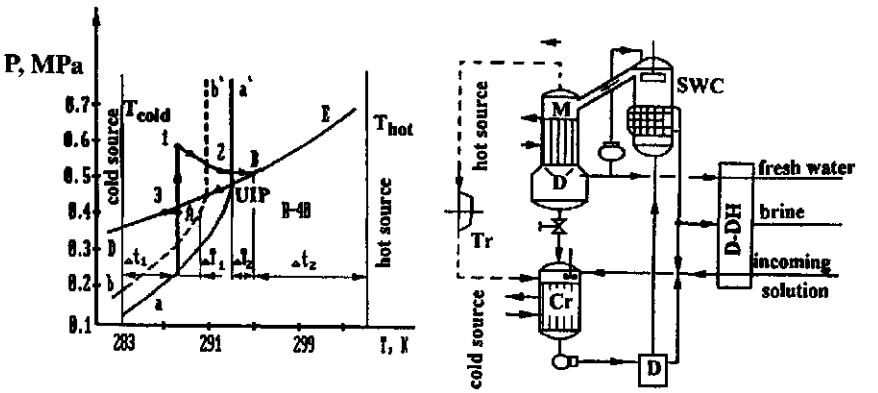

Figure 4-3 Cycle and schematic of a heat utilizing HD.

A-1: compression of gas hydrate suspension and its moving with P_1 from Cr to D_1 and then to SWC; 1-2: separation and washing of hydrates from brine in SWC; 2-B: heating, melting of hydrate in M and separation of water from liquid agent in decanter (D_2); B-3: moving and valve expansion of liquid agent from D_2 to Cr; 3, 3-A: boiling and heating in Cr.

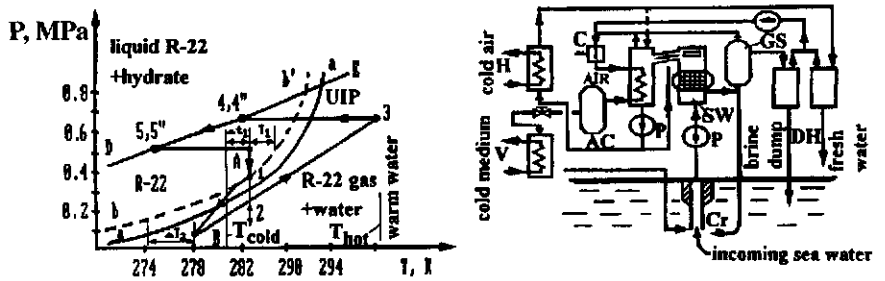

Figure 4-4 Cycle and schematic of a cold producing HD utilizing the temperature difference of sea water.

A-1: hydrate formation in Cr; 1-2: rising of gas hydrate suspension to the sea level; 2-1: compression of suspension and its moving with P_1 from Cr to SWC; 1-B: separation and washing of hydrate from brine in SWC; B: melting of hydrate in M; B-3: agent vapor compression in C; 3-4", 4-4": cooling and condensation of vapor in tube space of M; 4-5: valve expansion of liquid agent; 5-5": boiling of liquid agent in vaporizer (V); 5"-A: agent vapor heating; AC: air cooler; GS: gas separator.

(Martynovski, et al., 1974; Smirnov, et al., 1974, 1975). Hydrates form at T_A = 279–288 K and P = 0.4–2 MPa in a crystallizer (Cr) lowered into cold water to a depth of 30–200 m. After raising hydrate suspension to the surface and washing hydrates from brine, hydrates are melted by warm surface water. It is expedient to make such HDs as cold-producing type. Cold is generated both from melting of a hydrate and from boiling a hydrate forming agent (Figure 4-4).

6. Combination—this method is used for desalinization and purification of mine water, cooling the air in mines, and its cleaning from CO_2, CO, and H_2S. A cold-producing HD shown in Figure 4-5 was proposed for such purposes. Freon hydrates are transformed into ice at T_B = 273 K by decreasing pressure, and ice-water suspension reacts with warm polluted gases in an air cooler. Cold generation of ice during the production of 1 kg of fresh water is sufficient to cool 11 kg of moist hot air from 303 K down to 288 K. A combined condition of mine air (cooling and cleaning from gases) and desalinization of saline mine water increases the thermodynamic effectiveness by two to three times in comparison with a separate desalinizator of mine water and a mine air conditioner. Effectiveness is 15.2% for the schematic in Figure 4-5. This schematic is especially useful for deep mines in which air temperatures reach 313–323 K at depths of 1–1.5 km.

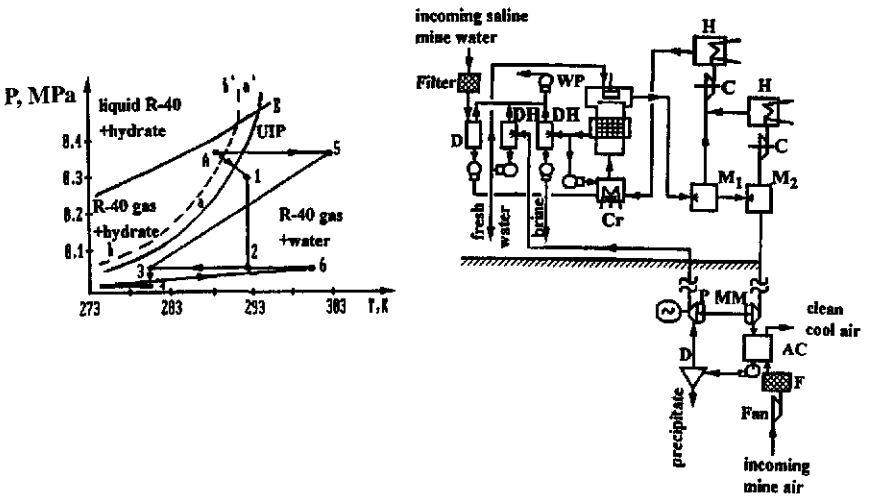

Figure 4-5 Cycle and schematic of a cold producing HD used for mine water desalination and mine air conditioning.

A-1: washing of hydrate from brine in SWC; 1-2,3-4: adiabatic pressure drop in melters M_1 and M_2; 2-3, 4-B: cooling of hydrate suspension in M_1 and M_2; B: melting of hydrate and formation of ice in M_2; B-6, 3-5: compression of agent vapor in compressors C_1 and C_2; 6-3, 5-A: cooling of compressed gas in heat exchangers H_1 and H_2; AC: air cooler.

The desalinization stages mentioned can be arranged into blocks creating combined installations with a new effect in order to increase the depth of conversion of salt solution. For example, a hydrate crystal desalinizator-separator (HDS) shown in Figure 4-6, is used for an extreme separation of a solution. An HDS consists of two similar heat-pump stages: desalinizing (initial solution as a feed and fresh water and brine having 7–9% of salts in product) and concentrating, eutectic contoured in Figure 4-6 (brine from stage 1 as a feed and a brine of high concentration, up to eutectic concentration, or dry salt in product).

An HDS is suitable for use in the following regimes: desalinization with a moderate concentration of brine (up to 7–9%); desalinization with a high concentration of brine, up to the concentration of a gas hydrate eutectic (24.8% for NaCl); desalinization with high concentration of brine and production of dry salt; and desalinization with production of dry salt (a particular case of an extreme separation of initial solution into water and salt). An HDS can be used for separation of an initial salt solution until production of a first crystallizing salt, a mixture of dry salts, or a component separation of salts (in cases when it is allowed by phase equilibria in multicomponent salt systems).

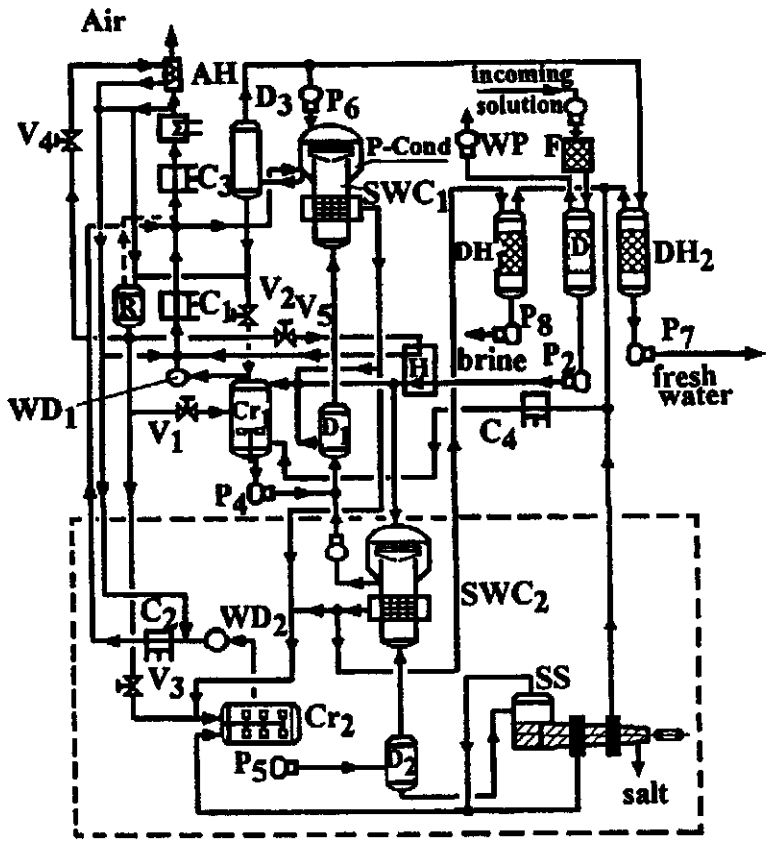

Figure 4-6 Schematic of clathrate hydrate desalinator-separator (HDS).

A saline solution contacts a hydrate forming agent. In a desalinization regime at a temperature of 278–283 K and a pressure of two to four bars, gas hydrates form in a crystallizer (Cr_1) from water coming from a polluted solution. Hydrate crystals are separated from a liquid agent in a decanter (D_1), washed from a surfacial brine film in a separation-washing column (SWC_1) and melted in a melter-condenser (P-Cond) at 283–293 K and four to six bars during their contact with a hot gaseous agent with releasing of a liquid agent and fresh water. The liquid agent is then recycled into C_{r1} and fresh water is released as a product after its degassing from a dissolved agent.

Brine enters the crystallizer Cr_2 after the desalinization stage SWC_1 in the regime of separation and forms hydrates at 263–253 K and one to two

bars. Two types of crystals appear—gas hydrates and salts in a concentrated brine. These crystals are separated in a decanter (D_2). Dry salts are removed through a salt separator (SS), and gas hydrates are pre-washed from a concentrated brine in SWC_2 and directed into a desalinizing stage where they are subjected to all operations mentioned above with the production of fresh water.

Environmental effects consist of preventing the pollution of nature with brines and recycling of fresh water into production. Salts can be produced as a mixture (in case of a single eutectic stage) or as pure components (with several eutectic stages). The purity of the salts produced depends on the purity of a phase crystallized from a multicomponent brine. Propane and ozone-friendly freons such as R22 and others, including 134a are recommended as hydrate formers.

This economically decreases specific expenses by two to three times, compared with multi-stage distillation (see Table 4-1) and with membrane methods (electrodialysis and reverse osmosis) by 1.5–2 times. Energy conserving gas hydrate technology is suitable for cleaning waste brines with different compositions of pollutants and on a large scale (with productivity of 500 to 100,000 m^3/day or more).

The crystal hydrate method has several advantages in comparison with distillation and membrane methods of desalinization.

It has the lowest energy consumption for brine separation. During separation of a 2% solution of NaCl 29 MJ/ton of fresh water is consumed and 54–65 MJ/ton of fresh water is consumed during an extreme separation of this solution into water and salt. The degree of thermodynamic perfection (exergetic efficiency) of crystal hydrate desalinizators is determined by the formula:

$$\eta_{EN} = \frac{W_{min} + e_X}{\sum l + e_T} \qquad (4.1)$$

where

W_{min} is the minimum work of desalinization or separation of a salt solution; $W_{min} = f(S_1, t, T_0)$;

e_X, e_T are the exergies of obtained cold and used heat;

Sl is the total consumed work (including all irreversible losses); Sl = 10-24% for heat pump HD and HDS.

The lower values relate to HD and a solution with low salt concentrations, the higher—to HDS, concentrated solutions and combined installations.

Table 4-1 Calculated technical and economical characteristics of hydrate crystal and distillation desalinators-separators (HDS and DDS).

	HDS			*DDS*
Characteristics	*2% NaCl*	*3.68% salts:*	*18% salts:*	*1.35% salts:*
Concentration of initial solution, %		NaF –1.53 NaCl –1.66 Na_2CO_3 –0.49 Na_2SO_4 –0.0003 K_2CO_3 –0.00016	NaCl –6 $CaCl_2$ –12	NaCl –0.9 $CaSO_4$ –0.2 salts Mg+K –0.25
Productivity, tons/day:				
by initial solution:	2400	1058.6	2400	2400
by fresh water:	2352	1000	1687.8	2280
by dry salt:	48	58.6	712.34	33.86
Electric energy consumption:				
specific, MJ/ton of fresh water	65.9	89.6	242.3	59.2
daily, kW × h/day	43133	24861	113614	37536
Coal consumption				
specific, ton/ton of fresh water	–	–	–	0.0276
daily, tons/day	–	–	–	63
Thermodynamic efficiency (4.1.1)	11.25	16	24.68	1

Effectiveness of heat-using HD utilizing heat of low potential, on the order of 313–323 K and difference in temperatures of sea water is 4 to 10%.

The efficiency shown is much higher than that of modern distillation multi-stage desalinization units for which $\eta_{Ex}^{Actual} = 1$ to 2%. The reason for energy inefficiency of distillation compared to gas hydrate methods of desalinization is loss of work due to high specific energy flows in a zone of salt solution separation because of irreversibility of temperatures difference above temperature depression (Martynovski, 1966).

Another advantage is contact heat exchange and the absence of heat transmitting surfaces.

Additionally, there is minimum corrosion and it is possible to use cheap construction materials because of low temperatures and pressures, for example concrete (which is especially important during purification of corrosive wastes). All units are contained in a single module. Productivity of an installation is controlled by the length of a module.

A significant decrease or a total absence of requirements for water pretreatment, insensitivity to pollution, and significant changes of initial water composition (up to a saturation concentration) are all advantages. At the same time the possibility to obtain fresh melted hydrate water which has an increased biological activity; the possibility of a low potential heat utilization with temperature of 323 K, or of a natural difference in temperatures of warm surface and cold depth sea water (e.g., in Black and Caspian seas); and the possibility of combining, when extraction and componental separation of salts, and production of concentrated heavy water (this is especially energetically favorable during desalinization of sea water) can be done along with production of fresh water.

Production of Food Powders from Fresh Fruit, Berries, and Vegetables

Water-soluble powders are prepared from vegetable or fruit juices and insoluble powders from their residue. Soluble powders can be used for the production of juices and to make beverages after long storage. Insoluble powders are used in the confectioner industry. Apples, grapes, pears, strawberries, tomatoes and other fruits, berries, and vegetables can be used as raw material. A technology is also being examined that processes vegetative raw materials used in cattle feeding (green corn biomass, etc.) for production of soluble and insoluble powders from silo usable for long storage and for use as vitaminized additives for cattle feeding during the winter.

Juice and residue contact with a hydrate forming agent (Freon 12, carbon dioxide, etc.) in various lines of treatment and form gas hydrates. Gas hydrates in juice (line of juice treatment is similar to the HDS schematic shown in Figure 4-6) crystallize at parameters of a gas hydrate eutectic. The obtained crystals of dry substances of juice are separated from crystals of gas hydrate and agent, blown with an inert gas (nitrogen), and removed as a soluble powder.

Moisture from fruit residue is crystallized into hydrate, residue is ground with gas hydrates which are then melted, and juice is pressed from the residue for the second time. The residue is dried by a warmed gas agent with a subsequent transformation of water vapor into a gas hydrate, blown with inert gas, and removed as insoluble powder.

The use of a new technology allows us to obtain two products from a raw material—soluble and insoluble powder, to decrease energy consumption (for example, to 65 MJ/ton of removed water for apple juice; compare to 3600 MJ/ton of water during sublimation freezing), to have a continuous process with a larger productivity, and to significantly decrease the length of drying.

Concentration of Heavy Water

This technology is based on the property of water and a hydrate former to change their isotopic composition during a transition through a hydrate state. A hydrate equilibrium curve for heavy water is located on a P-T diagram about 3–4 K to the right of a hydrate equilibrium curve for normal water. Our experience in transforming water (both natural and enriched to 10% of D_2O) through a hydrate state showed (water was analyzed by NMR before and after hydrate formation) that:

- Water from a hydrate melt is enriched with deuterium and tritium. The kinetic factor a of separating an elementary act of crystallization—melting was 1.05–1.075 for deuterium, and 1.045–1.06 for tritium.

$$\alpha = \frac{X/(1-X)}{Y/(1-Y)} \qquad (4.2)$$

  where X, Y are mass concentrations of heavy isotope in poor and enriched water, accordingly.

- The degree of enrichment depends of a P-T diagram zone in which hydrate formation is done, and on kinetic specialties of the process;

- The largest enrichment occurs at maximum approaching of temperature, T_A, to the temperature T_{EQ} of a point on a hydrate equilibrium curve for normal water at the same pressure (i.e., during hydrate formation with a small driving force $D_T = T_{EQ} - TA = 0.25–0.5$ K and with low rate), and removal of the last portions of a hydrate melt. In order to obtain the maximum enrichment, fractionation during hydrate formation has to be accompanied by fractionation during hydrate melting. It is necessary to carry out hydrate formation in the region of a P-T diagram most remote from a hydrate curve for normal water for producing drinking water not enriched with D_2O.

Crystallization in a column with a screw is suitable for fractionation of a HDO-D_2O mixture in H_2O which is a solid solution in a gas hydrate, when the raw material for a subsequent hydrate formation is a melt of a previous one. Transportation of deuterium in a column is done by diffusion in a liquid phase and by mass transfer from a solid phase into a liquid as a result of a sequence of hydrate formation and melting. Deuterium is the first to transform into a hydrate phase during hydrate formation, whereas protium is the first to go into liquid phase during hydrate melting. Having reviewed a physical model of a column crystallization of a solid solution of $H_2O + D_2O$ in a hydrate, we determined that the fractionation of D_2O resulting in a gradual enrichment of hydrate with deuterium is described by:

$$\frac{Y - Y_F}{Y_F - Y_W} = \exp\left(-\frac{z}{h}\right),$$

where

$$Y_W = \frac{L_e Y_e}{C(\alpha - 1) + L_e} \qquad (4.3)$$

$$h = \frac{1}{C(\alpha - 1) + L_e} \cdot \left[\pi D \rho S \varphi + \frac{\alpha(C^2 - L_e C}{kaS\rho}\right]$$

where

L, L_e, C are consumptions of washing water, productive concentrate of D_2O, and gas hydrate, accordingly (kg/s);

Y, X, Y_e, Y_W are current concentrations of deuterium in water and in gas hydrates along the column, and in concentrate and in washing water at level $z = 0$, accordingly (kg D_2O/kg of flow);

k is the mass transfer coefficient, m/s;

α is the surface area of mass transfer, m^2;

D is the diffusion coefficient, m^2/s;

S is the column cross-section, m^2;

ρ is the density, kg/m^3;

φ is the volume fraction of a liquid phase.

It is economically expedient to combine production of heavy water with desalinization of saline, especially sea water. Heavy water concentrator is a regular hydrate transformer (HT) with $z = 5$. Its operation is similar to the work of a desalinizing stage. The difference is that hydrate washed from brine does not go directly into melter after a separation-washing column (SWC), but initially into a rectification column where hydrate is enriched with deuterium. For example, energy consumption in a heat-pump HD (Figure 4-7) is 1500.5 MJ/kg of D_2O. Its exergy efficiency equals 0.03% which is several times higher than in some industrial technologies of D_2O production (electrolysis, rectification of liquid hydrogen, isotopic exchange with H_2S and their combinations).

Compressorless Increasing of Pressure

This section reviews the possibility of generating pressures up to several hundreds or even thousands of atmospheres by decomposition of a hydrate in a closed volume, and also by forming a hydrate from liquid hydrate formers in a closed volume.

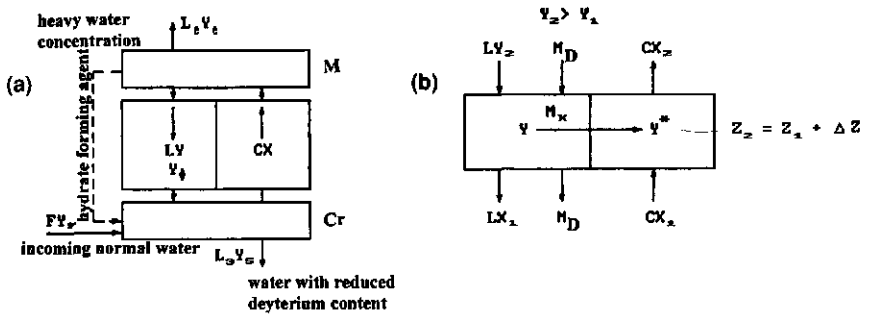

Figure 4-7 Physical model (a) and mass transfer (b) during contact crystallization of solid solution $H_2O + D_2O$ in gas hydrate.

Hydrates are compounds in which molecules of gas are in a compressed state inside a lattice of water molecules connected by hydrogen bonds. The smaller the size of a gas molecule located in a hydrate lattice formed by water molecules, i.e., the less loose is the water structure and less extended are hydrogen bonds, the smaller the number of water molecules required to fix a gas molecule and the higher is the pressure at which a gas molecule is in a hydrate. The larger the magnitude of decreasing a specific volume of gas during its transition into a hydrate state, the higher the increase of internal pressure of gas.

Loosening of water structure occurs during the transition into a hydrate state, and the specific volume of water increases by 26–32%. The voids formed in an open-work lattice of water molecules are filled with molecules of gas. Water molecules distributed in a volume of hydrate occupy a volume corresponding to their specific volume at specified temperature and pressure. Molecules of gas occupy the residual free volume.

A specific volume of hydrate forming gas molecules sharply decreases during the transition from a free state into a bound hydrate state. If the process of hydrate formation occurs at relatively low pressures, then the specific volume of a single gas molecule decreases by several orders of magnitude. There is a strict dependence between the magnitudes of an internal pressure of gas and the corresponding specific volume of gas.

The internal pressure of gas is released and can be used in various technological processes during decomposition of hydrates in a closed volume by increasing temperature. The magnitude of gas pressure during hydrate decomposition by increasing temperature depends on the density and composition of the hydrate, and on the characteristics of hydrate forming gas.

The density of hydrates can be determined by known methods (Chapter 2). The composition of a hydrate and a molar ratio of water and gas in it is determined by the laws of statistical mechanics (Chapter 1).

A mole of hydrate of any component contains about 22.4 liters of gas (at normal conditions) and n moles of water, i.e., for each mole of water there are 22.4/n liters of gas (at normal conditions). The ratio of the number of volumes of gas per one volume of water contained in a hydrate is determined based upon hydrate composition. The volume of gas contained in a unit volume of a hydrate and a mass ratio of water and gas also can be determined.

From Table 4-2 we see that a single volume of hydrate can contain from several tens to several hundreds of volumes of gas. A gas-water ratio on the order of 160–140 cm^3/cm^3 was obtained during an experimental study on conditions of hydrate formation from natural gases with

Table 4-2 Mass and volume of gas and water in the hydrates.

Component	CH_4	C_2H_6	C_3H_8	C_4H_{10}	CO_2	H_2S
Density of hydrate at $T = 0°C$ and hydrate formation pressure, g/cm³	0.91	0.959	0.866	0.901	1.117	1.04
Number of volumes of gas bounded in hydrate by one volume of water ($P = 0.1$ MPa, $T = 0°C$)	207.0	162.3	71.1	71.1	207.0	171.7
Number of volumes of gas in one volume of hydrate ($P = 0.1$ MPa, $T = 0°C$)	164.4	127.7	54.3	53.9	164.6	136.2
Mass of gas in a single volume of hydrate, kg/m³	117.0	171.2	110.0	142.0	323.3	220.0
Mass of water in a single volume of hydrate, kg/m³	793.0	786.6	770.0	748.0	793.7	820.0

a relative density of 0.6. The density of gas in a hydrate state is significantly higher than its density in a liquid or in a solid state, since the free volume per a single molecule of pure gas in a solid state is much higher than the volume per a single molecule of gas in a hydrate state—in a lattice formed by water molecules. For example, the volume per a single methane molecule in a solid state is 59×10^{-24} cm³, and 22.4×10^{-24} cm³ in a hydrate state.

Bounding of a significant volume of gas with one volume of water during transition into a hydrate yields high pressures of natural gas after hydrate decomposition in a closed volume. Knowing the quantitative content of water and gas in a unit volume of hydrate, and the dependence of their specific volume on pressure and temperature, one can determine the magnitude of internal pressure at which gas and water exist in a hydrate state, as well as the pressure of gas obtained after hydrate decomposition by increased temperature.

Let us consider an example of calculating decomposition pressures of ethane and of methane hydrates in a closed volume by increasing the temperature to 95°C:

a) 1. One mole of ethane hydrate: $C_2H_6 + n \times H_2O = 30 + 7.67 \times 18 = 168.1$ grams (Handa, 1986 b).

2. At the density of ethane hydrate of 0.95 g/cm³ at $T = 0°C$ one liter of hydrate contains $950/168.1 = 5.65$ moles of hydrate.

3. One cubic meter of ethane hydrate contains $30 \times 5.65 = 169.5$ kg of ethane and $7.67 \times 18 \times 5.95 = 821.5$ kg of water.

4. For a unit volume of hydrate the following condition must be satisfied:

$$\Sigma(V_G \gamma_G + V_W \gamma_W) = 1 \qquad \textbf{(4.4)}$$

where

V_G is the volume of gas in a unit volume of hydrate;

γ_G is the mass of gas in a unit volume of hydrate;

V_W is the volume of water in a unit volume of hydrate;

γ_W is the mass of water in a unit volume of hydrate.

Solving Equation 4.4 by a method of successive approximations for $T = 95°C$, we find that after decomposition of ethane hydrate and increasing the temperature to 95°C a pressure of 400 MPa corresponds to the specified correlation of components. Thus, a pressure of 400 MPa will be obtained after decomposition of ethane hydrate and raising the temperature to 95°C. [The following assumptions were made: (1) a change in the specific volume of water during dissolving of gas in it after hydrate decomposition was not considered; (2) a change of volume of free gas, because it dissolves in a bulk of water was not considered.] These assumptions have opposite signs and, probably, the resulting error is within the limits of acceptable accuracy. Note that the pressure of ethane hydrate formation at $T = 0°C$ equals 0.52 MPa. The internal pressure of ethane in a hydrate state increases by more than 500 times, and after ethane hydrate decomposition in a closed volume and raising the temperature to 95°C by 770 times.

b) For methane:

1. One mole of methane in the second quadruple point ($T = 0°C$) weighs:

$$16 + 6.0 \times 18 = 124 \text{ grams.}$$

2. Share of water in this weight is 108 grams.
3. At the density of methane hydrate in the conditions of the second quadruple point of 0.91 g/cm^3 the volume of hydrate is

$$124 / 0.91 = 134 \text{ cm}^3.$$

4. One liter of hydrate contains 7.33 moles of hydrate.
5. Share of water is 792 g, and 118 grams of methane.
6. 118 grams of methane occupy a volume of 208 cm^3 after hydrate decomposition. A pressure of 260 MPa corresponds to these parameters at 95°C, i.e., the pressure after methane hydrate decomposition in a closed volume and heating it to a temperature of 95°C exceeds the hydrate formation pressure at $T = 0°C$ by two orders of magnitude.

Figure 4-8 presents the curves of pressure that change during methane hydrate decomposition by heating. This method of a compressorless increase of gas pressure will receive wide implementation in a number of technological processes for transportation of liquid hydrocarbons (during stabilization of condensate using hydrates, for transportation of water and its solutions, etc.).

Thermal compression of gases is based on the fact that a hydrate former is packed in a hydrate state more compactly than in a gaseous state. The formation and subsequent melting of gas hydrates in a closed volume increases the pressure of gas (Makogon, 1970). A process of compression is machineless, single-stage at all degrees of compression, and close to isothermal. Thermal compression of gases having the first type of a phase diagram is accomplished until they liquefy.

The maximum pressure of thermal compression of gases (CH_4, natural gas, N_2, etc.) with the second type of a phase diagram is, according to an equation of state, at the temperature of hydrate melting by a minimum specific volume V_{min}

$$V_{min} = \frac{A}{\rho_H} - \frac{A-1}{\rho_W} \qquad (4.5)$$

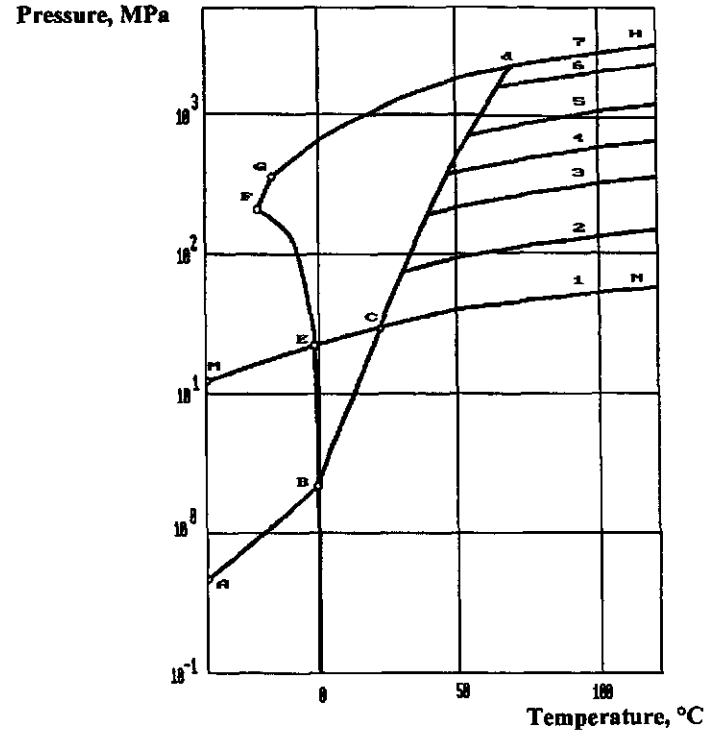

Figure 4-8 Pressure change with temperature during methane hydrate decomposition in fixed volume.

where

$A = nm_W/mA + 1$ - specific mass of hydrate, kg of hydrate/kg of agent; indices H, W, A represent gas hydrate, water, and agent, accordingly.

Thermal compressor (TC) generally consumes a low temperature heat (313–323 K) and is operable at a low difference in temperatures of a hot (T) and a cold (T_0) (ambient) heat source (20–35 K).

Constructively, TC is a regular GHT in which $z = 5$. Thermal compressors are classified in the order of increased efficiency as the following types (Figure 4-9):

- periodic—one apparatus periodically operates as a crystallizer and as a melter;
- continuous action with a pump—gas hydrate suspension is pumped from a crystallizer into a melter at a pressure of hydrate melting P_2;

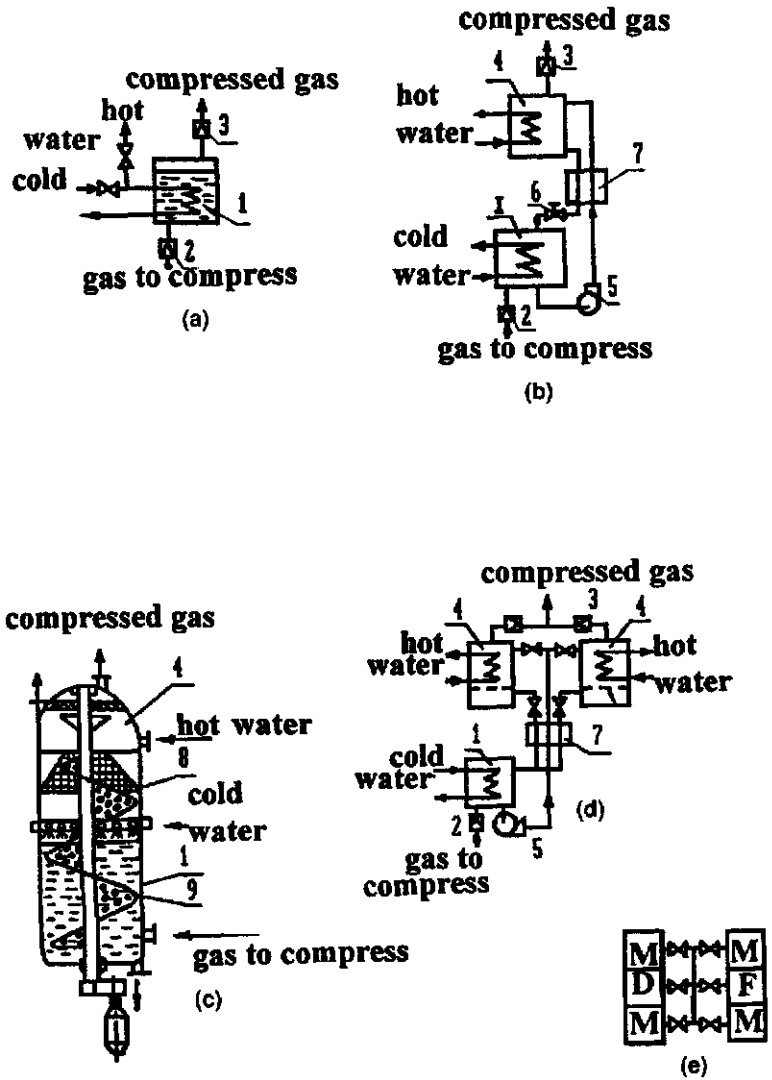

Figure 4-9 Schematics of thermal compressors (TC).

a: cyclic; b: continuous pumping; c: continuous with screw (TCS); d: continuous-cyclic (TCCC); e: continuous-cyclic with sectional melter (TCCCSM); M: melting; F: filling; D: drainage; 1: crystallizer; 2,3: back valve; 4: melter; 5: pump; 6: expansion valve; 7: heat exchanger; 8: filter; 9: screw.

- continuous action with a screw (TCS)—suspension is moved by a screw from a crystallizer into a melter at a variable pressure changing from a pressure of crystallization P_1 to a pressure melting P_2 (Smirnov, 1980);
- continuous-periodic action (TCCC)—suspension is moved under a pressure P_1 by a pump from a crystallizer which operates continuously into melters which operate by turns; and
- continuous-periodic action with a sectional melter (TCCCSM)—processes of filling melter sections with hydrate, melting of hydrate and draining water are done by turns in sections of melter.

The amount of gas left in melters in TCCC at pressure P_2 and specific volume V_2 after melting all hydrate is $x = V_{min}/V_2$ (kg of remaining agent/kg of agent which entered hydrate) where x cannot be used to release compressed gas at P_2, but has to be returned into a crystallizer. At pressure P_2, $1 - x$ of a comprised agent is obtained per 1 kg of agent. The difference $V_2 - V_{min}$ characterizes a dead space in TCCC. In order to decrease it in TCCCSM, pressure P_2 recovers at a sufficient number of sections in melter and $\times$ ® 0.

Energy consumption in TC is lower than in a regular compressor (C) of a volume gas compression The ratio of work done by a regular compressor l_C to that of a thermal compressor lTC continuously increases with the ratio P_2/P_1 (Figure 4-10). For example, for a TCCS:

$$\frac{l_C}{l_{TC}} = \frac{B_1}{(n\mu_B + \mu_A)(P_2 - P_1)B_2 + n\mu_B B_3} \qquad (4.6)$$

where

B_1, B_2, B_3 - constants.

Energy conservation lC / lTC is greater for those agents which have a more favorable aggregate of parameters:

- low initial pressure P_1 and small difference $(P_2 - P_1)$;
- low values of n and mA.

Although the degree of thermodynamic perfection of a TC is lower than in regular compressors (Figure 4-10), use of a cheap heat energy, often

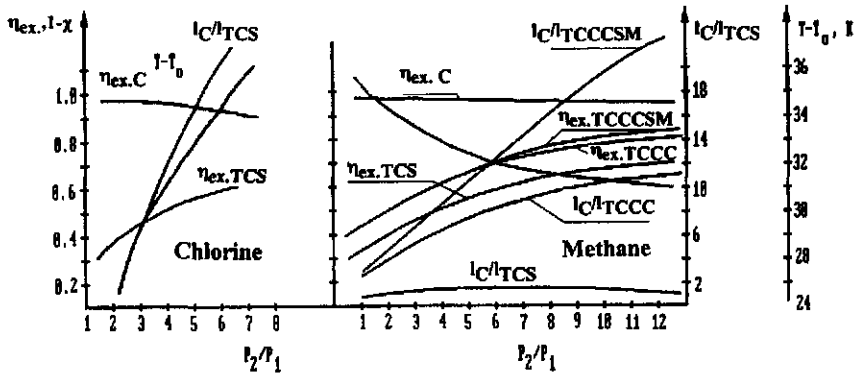

Figure 4-10 Energy characteristics of gas hydrate thermal compressors using chlorine and methane.

waste heat with a low potential, and a decrease in electric energy consumption by 2–20 times, improves the structure of energy consumption.

It is expedient to use TCCS for gases having the first type of a phase diagram according to thermodynamic and mass parameters and TCCC for gases with the second type.

Clathrate hydrate thermal compression complements industrial methods of volume compression, and in particular, allows us to generate with high productivity high pressures (50–1000 MPa) which are difficult to obtain using regular compressors with volume compression. Other advantages of TC also include a low final temperature of compression which does not exceed 313 K at all degrees of compression, single stage design, simplicity of construction, simple operation, smooth and economical control of productivity, absence of contamination of compressed gases with oil, possibility of compressing very moist gases, and an absence of noise.

Container Transportation of Gas

A proposal for a container transportation of natural gas in a hydrate state (Pat. No. 896854, 711758, 809783, 851877) is based on a property of compressibility of gas hydrate, closeness of their thermophysical properties to properties of ice, and on the fact that fusion of a surface of compressed hydrates slows hydrate decomposition under a fused surface during a decrease of pressure. It was proven experimentally that a piston made of a compressed hydrate retains its mechanical strength in a metastable state for several hours, and its fused surface has a low permeability for gas.

Gas is transformed into a hydrate in production and compressed into solid cylindrical blocks of hydrate (nonreturnable containers). These blocks are cooled to 271–281 K, transported through a pipeline on a gas cushion under pressure of a natural gas pressure differential, and melted in a place of gas consumption and release natural gas. The center of mass of a hydrate block is lowered with respect to its geometrical center axis by cutting out some hydrate on top and on the bottom of a block. Also, a Z-shaped hermetic cuff composed of a front lower, rear upper, and a longitudinal side locking belt is installed which decreases gas flow from a space behind a block with a higher pressure into a space in front of it with a lower pressure. A block can be complete or hollow to decrease hydraulic losses, and also for a simultaneous transportation of oil, gas condensate and massive dry loads like coal or ore. The outer surface of a block is hardened by cooling and has an ice or a hydrate crust. Blocks are transported separately, or in a joint form like a composition having a common Z-shaped cuff along the whole length, which is more energetically favorable.

A pressure drop is created at initial (A) and intermediate (B) stations by the thermal compression of gas existing between blocks. At station A, a hydrate is pressed into blocks, cut, shaped, and continuously cooled by hydrate converters (HC) connected directly to a transportation pipeline by a hydrate block distributor. Cooling is attained by an adiabatic pressure drop in HC. The pressure of gas is increased at station B and gas is cooled continuously. Station C melts hydrate blocks with water at 273–293 K producing compressed gas, fresh water, and cold.

Mass productivity of a pipeline by gas (kg/s) is

$$G = \frac{W_1 S \delta \beta}{\beta + 1}\left[\frac{1-\delta}{A \times V_G} + \frac{1+\delta\beta}{\beta V}\right] \qquad (4.7)$$

where

V_G, V are the specific volumes of hydrate and gas, accordingly (before transportation);

W_1 is the initial velocity of blocks after station B; $\beta = x/x_1'$;

x, x_1' are the lengths of blocks (or compositions) and intervals between blocks at the initial moment of motion, accordingly, m; $\delta = S'/S_\delta$;

S', S_δ are the cross sections of a hollow in a block, and of a block itself, accordingly, m^2.

The first square brackets in this formula represent the rate of gas flow in blocks and the second represent intervals between blocks.

A hydraulic resistance during transportation can be estimated by applying the first law of thermodynamics to a case of a steady discrete horizontal motion of blocks:

$$-VdP = (m + M)WdW + dL_{TR}^{Gas} + dL_{TR}^{Block} + dL_{TR}^{Bl.St}. \quad (4.8)$$

A work VdP of gas with mass, M, and volume, V, located in an interval between blocks is used to increase the kinetic energy of gas and a block with mass m moving at velocity, W, to friction of gas against a pipe wall dL_{TR}^{Gas}, to overcoming friction of a block against a viscous boundary layer near a pipe wall dL_{TR}^{Block}, and to immediate friction of a block against a pipe wall $dL_{TR}^{Bl.St}$. Integration of the written equation is done with simplifying assumptions: gas flow is close to isothermal, a multicomponent mixture obeys the ideal gas law, and the flow of gas through the clearance between a block and a pipe wall is negligibly small. Taking into account a flow continuity equation during discrete motion of a system $(m + M)$, isothermal expansion of gas, Darcy frictional pressure losses, resistance of a stationary gas boundary layer, friction of block against a pipe, and subtracting the hydrostatic compensating effect of a block weight we obtain:

$$-\int_{P_1}^{P_2} VdP = \frac{P_1 S_\delta \times (1 + \delta\beta)}{\beta} - In\left(\frac{P_1}{P_2}\right); \quad (4.9)$$

$$\int_{P_1}^{P_2} (m + M)WdW =$$

$$-\frac{S_\delta x\left[\varepsilon (1 - \delta)\rho_G + \frac{P_1(1 + \delta\beta)}{C\beta}\right] \times (1 + \delta\beta)W_1^2(P_2 - P_1)}{(\beta + 1)^2 P_2} \times$$

$$\left[\frac{(1 + \delta\beta)(P_1 + P_2)}{2P_2} + \beta\right] \quad (4.10)$$

$$\int_{P_1}^{P_2} dl^G = \frac{\lambda S_\delta x W_1^2 x_{ST} P_1}{2cd(\beta + 1)^2} \times$$

$$\left\{(1 + \delta\beta)\left[\frac{P_1(1 + \delta\beta)^2}{P_2\beta} + \frac{2P_1(1 + \delta\beta)}{P_2 - P_1}\ln\frac{P_2}{P_1} + \beta\right]\right\} -$$

$$\delta\left[\frac{3P_1(1 + \delta\beta)^2}{P_2 - P_1}\ln\frac{P_2}{P_1} + \frac{(P_2 + P_1)\beta^2}{P_1}\left(\frac{\delta^2}{2} - \delta + \frac{1}{2}\right) + \beta(1 + \delta\beta)(4 - 3\delta)\right] \quad (4.11)$$

$$\int_{P_1}^{P_2} dl^\delta = \frac{\xi\omega W_1^2 C_{ST}\beta}{C(\beta + 1)^2} \times \left[\frac{P_1^2(1 + \delta\beta)^2}{2(P_2 - P_1)\beta}\ln\frac{P_2}{P_1} + P_1(1 + \delta\beta)(1 - \delta) + \frac{\beta(P_2 + P_1)}{2}\left(\frac{\delta^2}{2} - \delta + \frac{1}{2}\right)\right] \quad (4.12)$$

$$\int_{P_1}^{P_2} dl^{\delta \times C} =$$

$$fx\left\{\varepsilon S_\delta (1 - \delta)\rho_H g x_{ST} + dx\left[(1 - \delta)(P_2 - P_1) + \frac{P_1(1 + \delta\beta)}{\beta}\ln\frac{P_2}{P_1}\right]\right\} \quad (4.13)$$

where

- d is the diameter of a block;
- w is the stream surface of a block;
- l, x, f are the coefficients of hydraulic friction, friction resistance, and motional friction of a block during its motion, accordingly; $C = PV$;
- X_{ST} is the distance between stations B;
- ε is the coefficient of a block mass decrease because of cut-outs;
- P_H is the density of hydrate;
- g is gravity;
- P_1, P_2 are the pressures of gas in front of and behind containers, accordingly.

At specified initial and final pressures of transportation, P_1 and P_2, characteristics of a pneumocontainer system, d, x, b, w, Sd, d, W_1, l, x, f, and properties of gas and hydrate the written equations define xST and input of each component of frictional losses and are usable for complete $(d = 0)$ and hollow blocks and compositons.

Results of computer calculations of transportation variants were analyzed according to a parameter of effectiveness of use of specific work of a flow

$$\Phi = \frac{-\int_{P_1}^{P_2} VdP}{MG^G L}, \quad (4.14)$$

which was compared to a particular parameter

$$\Phi' = \frac{\int_{P_1}^{P_2} dL^G}{MG^{Gas}_{\text{in intervals}} L} \tag{4.15}$$

where

G^G is the mass flow rate of gas contained in intervals between blocks.

Results of these calculations are presented in Figures 4-11 and 4-12.

The third and fourth members have the largest magnitude in the right part of Equation 4.9. Relative magnitude of the fifth member decreases with the increase of length of block x which is caused by the increase of a hydrostatic compensation of a block weight (DP increases), which increases its weight by 10–25% at short x (5–10 m) and by 80–100% during formation of compositions with a total length of 40–80 m (see Figure 4-12) and velocity which does not influence friction of a block against a pipe wall, and affects the third member as a quadratic function (see Figure 4-11).

Magnitudes of the third and the fourth members decrease with movement of hollow blocks open at the front end. In such cases, gas simulta-

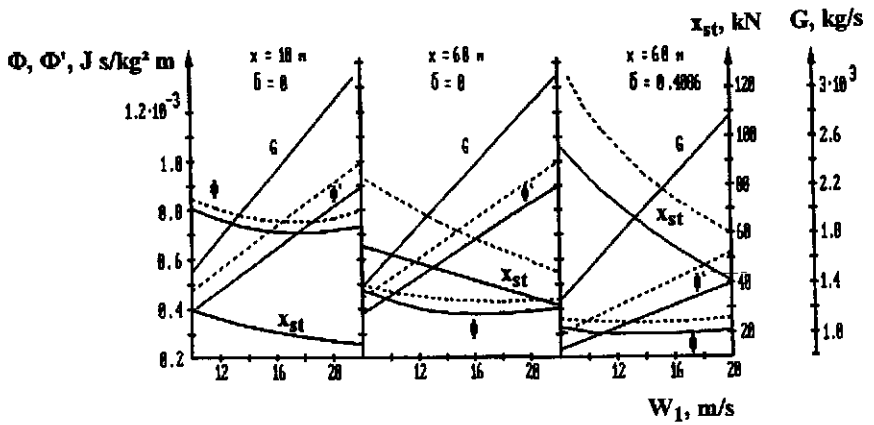

Figure 4-11 ϕ, ϕ', x_{st}, G as a function of W_1 at $P_1 = 7.5$ MPa and $\beta = 1$ for gas hydrate pipeline with $\alpha = 1.42$ m. (····· is $P_2 = 4$ MPa; —— is $P_2 = 5$ MPa).

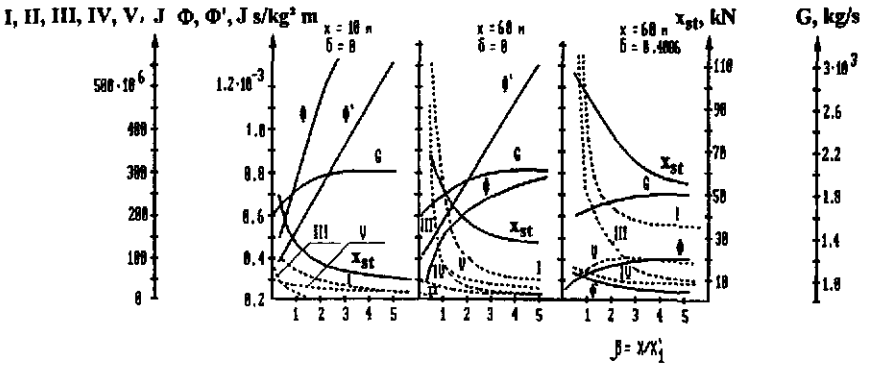

Figure 4-12 ϕ, ϕ', x_{st}, G and components I, II, III, IV, V of Equation 4.9 as a function of β at $P_1 = 7.5$ MPa, $P_2 = 5$ MPa and $W_1 = 12$ m/s for gas hydrate pipeline with $\alpha = 1.42$ m.

neously fills an interval between blocks and a hollow in a block of volume V_0 = const. Pushing is done by gas of volume V, and frictional losses is introduced only by a part of gas in an interval between blocks having a variable volume $V - V_0$. A decrease in G is small and as indicated by F, it is well compensated by a substantial decrease of the third member, and a noticeable decrease of the fifth member (because of a decrease in W).

Starting with W_1 = 12–15 m/s in a long, and the more so a hollow block, $F < F'$ which means a principally important fact of a decrease in hydraulic losses per unit of transportation work in a gas hydrate pipeline compared to a regular gas pipeline. $F = 0.25 - 0.5 \times 10^{-3}$ (J/kg)/(kg/s) × m at $W_1 = 12 - 15$ m/s, $x = 40 - 80$ m, $b = 1 - 4$, $x_{ST} = 60$–90 km, $P_1 = 7.5$–8 MPa, P_2 33 MPa, $d = 0.3 - 0.4$.

Table 4-3 presents the results of detailed energy, hydraulic, and economical calculations of a gas hydrate pipeline and its technical and economical comparison with other types of gas pipelines.

A gas hydrate pipeline has the following advantages compared to other industrial gas and high pressure cooled gas (203 K, 12 MPa) pipelines and liquefied natural gas pipelines (113 K).

- It has a significant increase (by 1.5–3 or more times) of capacity because of an increased density of methane packing in hydrate (compared to gas) to about 120 kg/m³ for a compressed hydrate block and an increase of the velocity of transportation to 12–25 m/s and higher. During an increase of hydrate blocks velocity to 18 m/s,

Table 4-3 Comparison of technical and economical parameters for various methods of natural gas transportation (d = 1.42 m = idem, $S \times ST$ = 3000 km = idem).

Parameters	*Methods*			
	Non-cooled Gas at Average Pressure	*Cooled Gas at High Pressure*	*Liquefied Gas*	*Gas in a Hydrate State**
Parameters of gas before transportation:				
temperature, K	283	203	113	279
pressure, MPa	7.6	12	4	7.5
Distance between intermediate stations, km	100	86	92.4	94.1
Gas pipeline capacity, billions m³/year	29.5	45.4	90	59.892†
Specific electric power, thou. kW/billns n.m³/yr.	60.1	49.4	43.9	30.1
Specific reduced expenses (1983 prices), million Rubles/billion normal cubic meters per year	16.5	13.65	10.4	10.26‡ / 7.5

*Gas composition (mass %): methane - 71.59, ethane - 10.05, propane - 8.13, isobutane - 2.97, n-butane - 3.42, pentane - 2.91, nitrogen - 0.93, W_1=12 m/s, δ=0.4086, composition length - 80 m, β=1, P_1=7.5 MPa, P_2=7.5 MPa, M=13611.4 kg, G=1655.3 kg/s, Φ=0.244 × 10^{-3} (J/kg)/(kg/s) × m, Φ'=0.296 × 10^{-3} (J/kg)/(kg/s) × m. Norms of construction and operation of pipelines accepted in gas industry were used during evaluation of capital expenses and economical indices. The following was assumed during calculation: northern variant of construction, construction of one gas pipeline, maximum coefficients of price increase for construction works, reservation of equipment, etc.

†At a rate of transportation W_1=12 m/s; at rates of 16-18 m/s productivity of a gas hydrate pipeline is greater than that of a liquefied natural gas pipeline.

‡numerator—without selling cold, denominator—with selling cold.

productivity of a gas pipeline also exceeds the capacity of a liquefied gas pipeline. Pipeline diameter can be decreased retaining the same capacity.

- It simplifies gas pumping installations by using a machineless thermal compression equipment of a high unit power and decreases the amount of compressed gas at intermediate stations by three to five times (only a part of liquid gas transported in intervals between blocks, whereas the gas in hydrate blocks is not treated at intermediate stations).
- It decreases requirements as to the quality of a pipeline steel due to non-extreme parameters of transportation (temperatures of 276–286 K and decreased pressures). During decrease of transportation pressure to 1–2 MPa (which is possible with transformation of a surface layer of hydrate blocks into ice) steel pipes can be substituted with glass-plastic-concrete pipes.
- The simultaneous transportation of fresh water from Northern regions of gas production (2.4–3.6 kg of water/kg of gas) and a concentrated isothermal cold (1.2–2 MJ of cold/kg of gas) generated during hydrate melting at a temperature of 273 K usable, for example, for air conditioning in centralized systems of cold supply is an advantage. Besides that, cold generation of a gas-cooled to about 200 K is 200–400 kJ/kg of gas. In principle, it is possible to transport oil, gas condensate, coal, and ore in hollow hermetically compressed blocks.

The transportation of liquid and dry materials (gas condensate, coal, etc.) in gas hydrate containers for relatively short distances (100–200 km) seems more realistic since it is difficult to assume the use of gas hydrate in the next 20 years for transporting natural gas.

Storage of Gas in a Hydrate State

Expediency of gas storage in a hydrate state comes from a gas-water molar ratio and an extremely high density of gas in a hydrate state. The specific density of methane in a hydrate lattice is higher than in a liquid state. The storage of gas in a hydrate state is most efficient at relatively low pressures when a lot more gas is contained in a unit volume at the same pressure in a hydrate state than in a free state.

The advantages of gas storage in a hydrate state result from a comparison of volumes of gas contained in a free state QF and in a hydrate state QH at various pressures. The volume of gas contained in a unit volume at different pressures is defined by the expression:

$$Q_F = \frac{VPT_0}{P_0TZ}, (m^3) \qquad \textbf{(4.16)}$$

The volume of gas contained in a similar volume of hydrate is defined by the expression:

$$Q_H = \frac{V_G \delta \times 10^3}{M_H}, (m^3) \qquad (4.17)$$

where

- V is the volume of a container;
- P is the pressure of gas storage;
- T_0, P_0 are the normal temperature and pressure;
- T is the temperature of gas storage;
- Z is the gas compressibility at normal temperature and pressure;
- V_G is the molar volume of gas;
- δ is the density of hydrate;
- M_H is the molar mass of hydrate.

Figure 4-13 presents the dependence of gas volumes contained in a unit volume in a free and in a hydrate state on temperature and pressure.

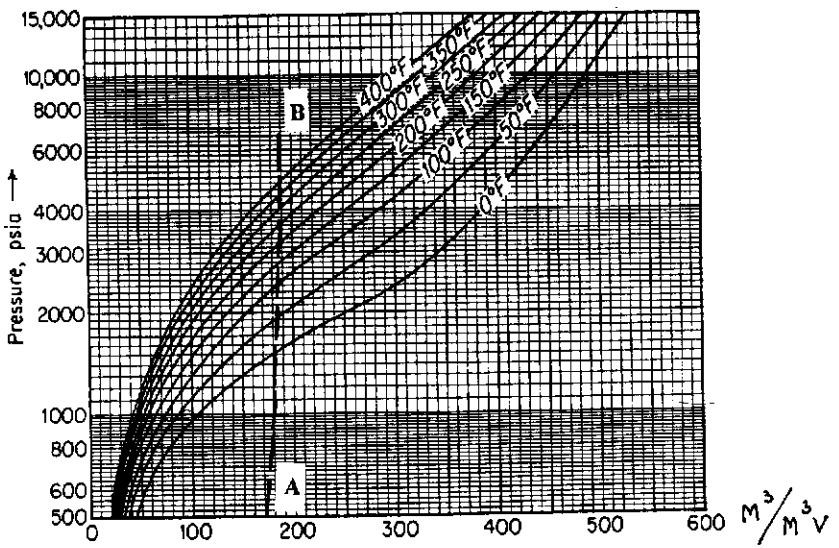

Figure 4-13 Amount of gas contained in the unit volume as a function of pressure and temperature. A-B: equilibrium hydrate formation P-T for natural gas 0.6 (Katz et al., 1959).

Creation of such gas storage facilities is the most efficient in permafrost regions where an insignificant deepening of containers provides a very economical creation of cooled gas hydrate storage to cover daily and seasonal variation in consumption in relatively small industrial centers.

Let us review an example of storage of gas having a relative density of 0.6 in a container of 100 m³ in a hydrate and in a free state at an ambient temperature of 0°C. It is necessary to determine the volume of gas stored in a hydrate state and the needed pressure of storing this gas in a free state. Using gas composition, the pressure of hydrate formation is found to be $P_0 = 1.0$ MPa and the molar mass of hydrate $M_H = 17.4 + 6 \times 18 = 125.4$. Density of a hydrate of this gas at the specified conditions is $\delta = 915$ kg/m³.

Therefore,

$$Q_H = \frac{100 \times 915 \times 22.4}{125.4} = 1.64 \times 10^3, \text{m}^3$$

and

$$\frac{P}{Z} = \frac{22.4 \times 915 \times 0.098}{125.4} \approx 16, \text{ Mpa} \qquad (4.18)$$

From here the advantages of storing gas in a hydrate state when there is no need for construction of containers and high pressure compressor stations are obvious.

The question about construction of underground gas storage facilities in regions with low ground temperatures appears to be interesting. It is known that layer isotherms follow the profile of layer deposition. Thus, an equilibrium isotherm of hydrate formation in layer condition also follows the profile of layer deposition. Starting from this, having determined the presence of a stratigraphic structure in a profile, it is easy to create a large underground storage of free gas in such a structure even without a lithological cover. A gas hydrate film formed at a lower boundary of hydrate formation then will serve as a cover. At that the danger of a cover breach with the increase of gas productivity floor and with the increase of pressure on the roof is excluded because thickness of the roof will increase, i.e., it will self-compact. Pressure will decrease at the roof and the lower part of the hydrate cover will decompose during a partial gas recovery from storage, i.e., gas transformed into a hydrate will not remain a dead weight.

Creation of gas storages with hydrate covers appears to be very possible in the eastern regions of Russia.

Killing a Blowout by Formation of Hydrate Plugs in a Well

Adhesive and strength properties of hydrates allow us to close strong uncontrollable gas and liquid flows during blowout of wells. It is most efficient to use hydrate blocking of a flow in wells with decreased flow temperatures, and also in conditions when other methods are extremely complicated or expensive. The method of a complete hydrate plug formation in a well in order to kill a blowout is very effective in wells with destroyed well-top equipment, destroyed upper part of a well bore, and useless well-top equipment for sealed access to a well, etc.

For example, in October 1981 technological testing of the Kumzha-9 well in the mouth of the Pechora River on a shore of the Arctic Ocean was initiated after its construction and mastering. Testing proceeded as a subsequent increase of production rate with intermediate stabilization of main parameters—pressure, temperature, and production rate. Testing was going well and enthusiasm was growing among the testing personnel. They were increasing the production rate each time. After the end of standard testing, a young geologist decided to find out what this well was capable of and removed the limiting washers. The well was set to a free rate: layer-atmosphere. Rate of production from the well had exceeded 1.5 million m^3/day. A strong vertical vibration started, and a column of fountain pipes tore off and fell into the well-bottom.

A breach of a production column occurred in the well bore and large cavities formed in a space outside the column during the removal of an emergency situation. The well-top equipment was destroyed and fountain tubes were thrown out of the well. The production column, technical column, and conductor were destroyed. A crater with a diameter of 120 m that formed to a depth of 157 m was filled with a mud-water pulp through which a powerful gas fountain was coming.

As a whole, the open blowout continued for 2,187 days. More than 4 billion cubic meters of gas and about 300,000 tons of condensate burned.

The traditional methods were used to kill the blowout:

- drilling of parallel wells in order to unload the well-top energy of the flow and to suppress the fountain by pumping water into the well and into the layer;
- drilling wells into the well bore of the emergency well; and
- a rock shift at a depth of 1470 m using a strong, including a nuclear, explosion. Overall, more than 20 additional wells were drilled. In one of these wells an electromagnetic self-guiding system for connection of the drilled and the emergency wells was used. Connection was established exactly in the calculated interval, at depth a of 1002 m. Water with temperatures of about 0°C was injected into the connection at a rate of 30 l/s. Two hydrate plugs formed in 40 minutes at depths of 500 m and 700 m from the well top after which the blowout well bore was cemented from well-bottom to the connection through the inclined connection well, and the well was saved.

Let us review briefly the technology of a hydrate plug formation in the well bore of the Kumzha-9 well. The directed inclined well No. 9 Kumzha was drilled to a depth 2893 m along well bore (2560 m vertically). The well bottom was located in a limestone of middle cretaceous period.

Well construction:

- conductor 324 mm–151.2 m; cement to well top;
- intermediate column 245 mm–1308 m; cement to well top;
- production column 146 mm–2866 m; cement to 300 m from well top.

Compressor pipes 73 x 60.3 mm were lowered to well bottom with a transition at depth of 1403 m. The following data in Table 4-4 were obtained during studies.

Layer pressure was 26.2 MPa; layer temperature 63°C; layer permeability (average) 77.2 millidarcy. Maximum production rate from the well was 1.5 × 106 m^3/day.

Composition and properties of gas:

- density 0.75 kg/m^3;
- relative density by air 0.622;
- composition (volume%): methane - 90.23, ethane - 1.56, propane - 0.54, isobutane - 0.08, n-butane - 0.25, isopentane - 0.1, pentane - 0.15, hexane and heavier - 0.1, hydrogen sulfide - 0.2;
- condensate factor 70 g/m^3.

Static pressure distribution with depth (vertically): 2835 m - 26.64 MPa, 2200 m - 26.38 MPa, 1600 m - 25.05 MPa, 800 m - 23.23 MPa, well top - 21.67 MPa. Temperature distribution in a closed well: 2350 m - 63.2°C, 2000 m - 52.6°C, 1500 m - 36.6°C, 1000 m - 21.3°C, 500 m - 14.5°C, 250 m - 9.0°C, 100 m - 8°C.

Table 4-4 Working parameters of Kumzha well.

Diaphragm Diameter, mm	*Pressure at Well Top, MPa*		*Well Bottom Pressure, MPa*	*Well Top Gas Temperature, °C*	*Gas Production Rate Thousand Normal Cubic Meter/Day*
	Outside Pipes	*Compressor Pipes*			
closed	21.4	21.4			0
4.0	21.3	21.3	26.0	+15	67.0
15.15	20.4	18.5	25.0	+23	595.2
22.2	18.9	14.5	23.1	+21	1060.0
29.75	14.8	12.1	18.1	+27	1287.5

As of November 5, 1981, the schematic state of well No. 9 was:

- well fountain was coming through a crater which formed around its top;
- heads of a 324 mm conductor and a 299 mm intermediate column were in the crater;
- head of production column is at depth of 157 m from well top;
- head of compressor pipes is at depth of 157 m;
- depth manometer and 1200 m of wire remained in the well since its testing.

The state of the Kumzha No. 9 well as of November 15, 1981 was: The well bore was in the same state as November 5 since none of the wells drilled previously for emergency removal approached the emergency well or its bottom. The No. 27-bis well was started especially to make connection with the well 9-Kumzha at a depth of about 1000 m in order to inject cooled drilling mud or water into the No. 9-K, which formed a hydrate plug in the interval of 800–400 m to suppress the blowout.

The use of a magnetic well guidance method allowed us to accurately approach the wellbore of No. 9-K, to cement the near-bore space and provide connection of bores of 27-bis and 9-K on May 15, 1987 by cutting through 245–146–73 mm columns (fragments of these columns were raised to the surface after cutting). Drilling mud at a temperature of about 0°C was injected at a pressure of about 12 MPa into the upgoing stream of gas and was cooling it during cutting into the space of production column and compressor column. A 40 m^3 volume of drilling mud at a temperature of about 0°C entered the well during cutting through columns using a milling cutter for three hours. This solution was thrown out by an upgoing gas flow into the crater and the blowout continued.

After cutting through all columns and a complete connection of bores water from a near-by lake with thawed water was injected with a temperature of about 0°C, water consumption was 30 l/s. Time of injection was 80 minutes; however, already after 45 minutes a gradual decrease in the intensity of the flare in the crater over the lake above well- top was noticed. Thirty-five minutes after the flare faded, the intensive blowout had stopped. An insignificant fountain continued after that for many days; however, this was a gas from a technogenic deposit which formed around the emergency well at the depth of well destruction. The degree of a gas and liquid flow subcooling was more than 10°C. A complete hydrate plug totally covered the well cross-section in 40 minutes.

After closing the well bore with a hydrate plug over 120 m^3 of loamy drilling mud with a density of 1.23 g/cm^3 at a rate of 30 l/s was injected into the well. An additional 500 m^3 of water with a temperature of 0°C was injected on May 16, 1987 at a specific rate of 20–50–100 l/s.

The level of pulp in the crater of well No. 9-K lowered by about 4.5 cm after closing the emergency gas fountain which was caused by a sharp decrease of an influx of gas into the liquid filling the crater (amount of gas bubbles in the pulp decreased). In order to control a complete closing of the open fountain in well No. 9-K with hydrates, 5200 m^3 of water was injected into the well. However, the level of liquid in the crater remained constant both during the injection of water into the well and after stopping the injection. This supports the fact of closing the bore of well No. 9-K between the point of connection to it and its top.

After fountain suppression the bore of emergency well was cemented from bottom to the place of connection of bores. Then the well was conserved.

It was shown by hydrodynamic calculations that in conditions of well No. 9-K drilling mud with a density of 1.23 g/cm^3 had to be injected into its bore at a rate of at least 75 l/s. Cutting and preparing of a connection hole was done at the well No. 9-K at a rate of 30 l/s of drilling mud. A hydrodynamic suppression with pure water would have required a rate of injection of over 90 l/s.

Technology of Removing a Blowout at the Well 9-Kumzha by Forming a Hydrate Plug in Well Bore

In a number of cases the control of gas well blowout is technologically difficult and expensive. It is especially difficult to remove strong blowouts on wells with a destroyed top when a mechanical closing of a well is impossible. The Kumzha-9 well is a classical example of the complexity of blowout control. The well with a depth of 2796 m, had its bottom displaced by 1286 m with respect to its top. The well top was destroyed, and a crater, over 120 m in diameter and 157 m in depth, formed. The crater is filled with a liquid pulp with a density of 1.4 g/cm^3. A seething flow of gas in the crater is constantly burning. Conductor, technological and production columns, and compressor tubes to a depth of 157 m were thrown out by the fountain. These factors significantly complicate the use of conventional methods of removing blowouts by supplying a suppression liquid into a near-well-bottom zone of a layer through an injection well or by a directed shift of rock with a special explosion.

The thermodynamic regime of the 9-K well blowout allowed us to use an effective method. An emergency blowout can be closed by forming a hydrate plug in the blowout well with a subsequent suppression and cementing of an emergency well bore. It is practically impossible to shift a hydrate plug formed in a well without its decomposition.

Composition of gas for the Kumzha-9 natural gas is presented in Table 4-5.

Equilibrium P-T conditions of hydrate formation from the gas of specified composition are given in Table 4-6.

Figure 4-14 presents a schematic of suppressing an emergency blowout by forming a hydrate plug in a bore, when cooled water or drilling mud is supplied into a blowout well through an injection well.

Figure 4-15 presents the main thermodynamic characteristics of the Kumzha-9 well operation at different regimes, including that with an open blowout. Dependencies of pressure and temperature at well-top, bottom, and along the well are shown in this figure. Also a dependence of an equilibrium temperature (TP) on pressure (P) is shown here.

Table 4-5 Gas composition for the Kumzha well.

	Gas						
	CH_4	C_2H_6	C_3H_8	C_4H_{10}	$C_5H_{12}+$	H_2S	*D*
Content, volume%	90.22	1.56	0.54	0.33	0.35	0.20	0.62

Table 4-6 Equilibrium P-T condition of hydrate formation from Kumzha gas well.

	Pressure, MPa					
	1.0	*1.8*	*3.4*	*6.3*	*13.5*	*33.0*
Temperature, °C	0	5	10	15	20	25

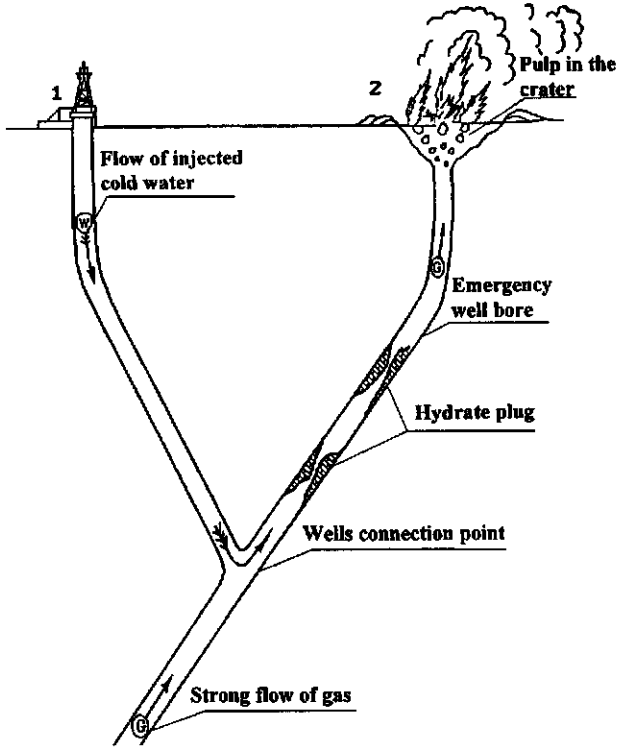

Figure 4-14 Schematic of emergency blowout extinguishing. 1: injection well; 2: blowout well.

Dependence of the well-top temperature of gas on the production rate was obtained from a hydrodynamic study of the well. As seen from the figure, conditions of hydrate formation in the Kumzha-9 well are present in the upper part of the bore at flow rates of up to 300–400 thousand m^3/day. At higher rates, including an open blowout regime, when the gas flow rate exceeds 1.5×10^6 m^3/day, hydrates do not form in the well bore because the temperature of the gas stream is higher by 2–7°C than hydrate equilibrium temperature, even at minimum temperatures.

It is possible to block the bore of a blowout well with a hydrate plug having created conditions for its formation and accumulation of hydrates in a well bore. This can be reached by an additional cooling of a gas stream by injecting cooled water into it. Cooled water is best injected directly into a well bore through an inclined injection well.

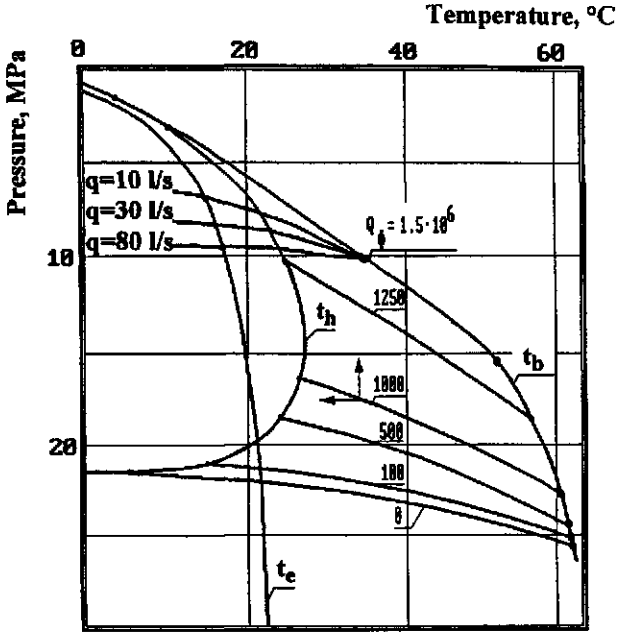

Figure 4-15 Dependence of temperature and pressure of gas flow at Kumzha-9 well on its flow rate and depth.

t: gas temperature; t_b: gas temperature at well bottom; t_h: gas temperature at well head; t_e: equilibrium hydrate formation temperature; Q_0: gas flow rate, thousands m^3/day.

Figure 4-16 shows the dependence of temperature of a fountain stream (T_F) with depth, and equilibrium temperature (T_{EQ}) on pressure in the 9-K well (P_F). The dependencies of a geothermal temperature and of an equilibrium temperature for a static (closed at well top) well (T_{EQ}^{ST}) are also presented here. The magnitude of temperature decrease needed for initiation of hydrate formation in a bore of a blowout well is shown in horizontal dashes. As seen from the curves, the minimum stream cooling is required at cool water injection depths of above 500 m. However, in real conditions, when the upper part of the column is thrown out, an extra length of column is required for cooling the stream and for adhesive formation of a strong hydrate plug in the production column and in the compressor tubing.

In this particular example it is most efficient to inject water cooled to a temperature of about 0°C into a bore of a blowout well at a depth of about 1000 m where the temperature of gas decreases significantly

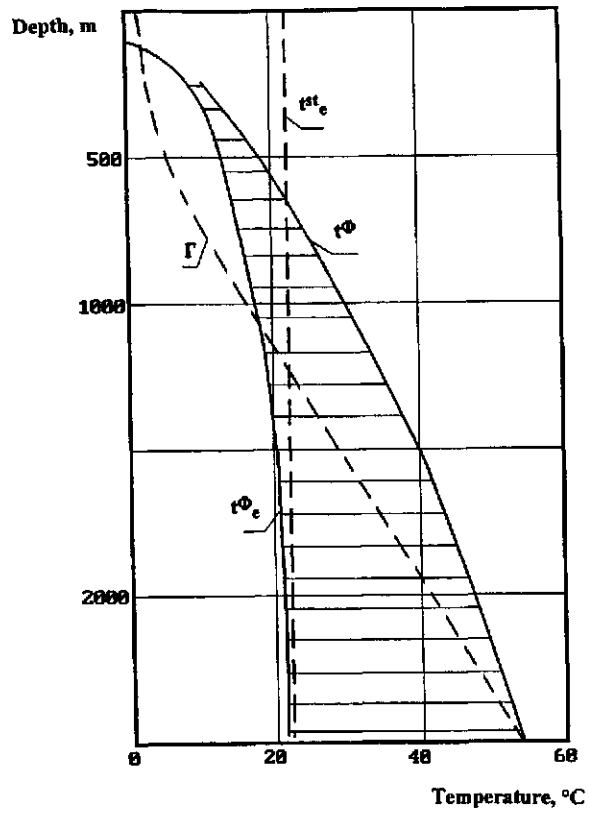

Figure 4-16 Kumzha-9 well operation.

because of a heat exchange with surrounding rock and because of throttling. The gas flow must be cooled by 14°C in order to ensure hydrate formation during injection of cooled water into the bore of a fountain well at a depth of 1000 m, by 25°C at 1860 m, and by 32°C at 2710 m. The depth of 1000 m is optimal for injection of cooled water, not only from the point of forming a hydrate plug in an emergency well, but also from the point of drilling an inclined injection well. As indicated by suppressing the fountain at the 9-K well, the interval of connection was the most optimal.

An estimate of the minimum amount of water (q_W) required to decrease the temperature of a gas stream in a blowout well to a temperature of an intensive hydrate formation can be done using the formula:

$$q_W = \frac{q_G C_P^0 (T_G - T_{EQ})}{\eta C_W (T_{EQ} - T_W^0)}, \text{ l/s} \qquad \textbf{(4.19)}$$

where

q_G is the gas flow rate, kg/s;

C_P^0 is the average heat capacity of gas, kJ/kg × °C;

C_W is the heat capacity of water, kJ/kg × °C;

T_G is the average temperature of gas in the point of injection of water into a gas stream, °C;

T_{EQ} is the equilibrium temperature of hydrate formation at a depth of injection, °C;

T_{W0} is the initial temperature of water at entrance into a fountain well, °C;

η is the heat exchange process efficiency for a gas-water system.

Notice that it is necessary to pump water with a minimum possible temperature 0–5°C into an injection well for effective cooling of a gas and water stream in the bore of a fountain well.

It is expedient to add 1–2 weight 5 of methyl or ethyl alcohol to water injected with a temperature of 0°C in order to prevent freezing of the water and to intensify the process of hydrate formation. The bore of an injection well has to be cooled before an injection of water into the stream of a fountain well. In drilling an injection well with a cooled mud there is no need for an additional cooling. The connection of wells has to be done in a cold regime.

Cooled drilling mud or water enter the stream already during the process of connection and the process of cooling the stream and hydrate formation in a fountain well proceeds. However, the well walls have to be cooled to a temperature below hydrate equilibrium in order to accumulate forming hydrate on well walls and to form a stable hydrate plug. An estimated volume of water (V_W) needed to cool bores of an injection well and fountain well to specified temperatures can be determined from the formula:

$$V_W = \frac{Q}{\eta C_W (T_F - T_H)/2}, \text{ m}^3 \qquad \textbf{(4.20)}$$

where

η is the efficiency of a heat exchange process between well walls and water, $\eta = 0.1$;

T_W is the temperature of injected water at injection well top, °C;

T_F is the average temperature of well walls in a blowout well bore in cooling interval, °C;

T_H is the average temperature in interval of hydrate formation, °C;

Q is the amount of heat which has to be removed from annular space adjacent to injection and fountain wells, kJ.

$$Q = V_R C_R \frac{T_I - T_H}{2} + V_F C_R \sum (T_{F_i} - T_{H_i}) \qquad (4.21)$$

where

V_R is the volume of cooled rock in annular space of injection well, m^3;

V_F is the volume of cooled rock in annular space of fountain well, m^3;

C_R is the heat capacity of rock, $kJ/m^3 \times °C$;

T_I is the average temperature of injection well walls, °C;

T_{Fi} is the average temperature of fountain well walls in i-th interval, °C;

T_{Hi} is the average equilibrium temperature of hydrate formation in i-th interval, °C.

Figure 4-17 shows the dependence of a hydrate plug formation starting time in a bore of the fountain well 9-K (at a production rate of $1.5 \times 10^6 m^3$/day) during an injection of cooled water as a function of connection depth, flow rate and temperature of injected liquid. From the picture, we see that at a flow rate of 30 l/s of injected solution at a depth of 1002 m with temperature of 0°C, the process of hydrate formation starts in 45 minutes. With a temperature of 5°C of injected liquid, a hydrate plug starts to form in a bore in 70 minutes and at 10°C in 200 minutes.

During injection at a depth of 2400 m, delay times change to 110, 160, and 430 minutes, accordingly. The minimum required volume of water (m^3) injected into a fountain well depends on the temperature and location of the injection and are presented in Table 4-7.

The time of a complete blockage of a well bore with internal diameter of 120 mm by a hydrate plug does not exceed 15–40 minutes after the start of hydrate formation during an intensive injection of cooled water into a gas stream. The time of a hydrate plug formation in a well depends on the intensity of water injection, degree of its subcooling, characteristics of the pipe's surface, and the presence of catalysts of a hydrate formation process in a gas and liquid flow.

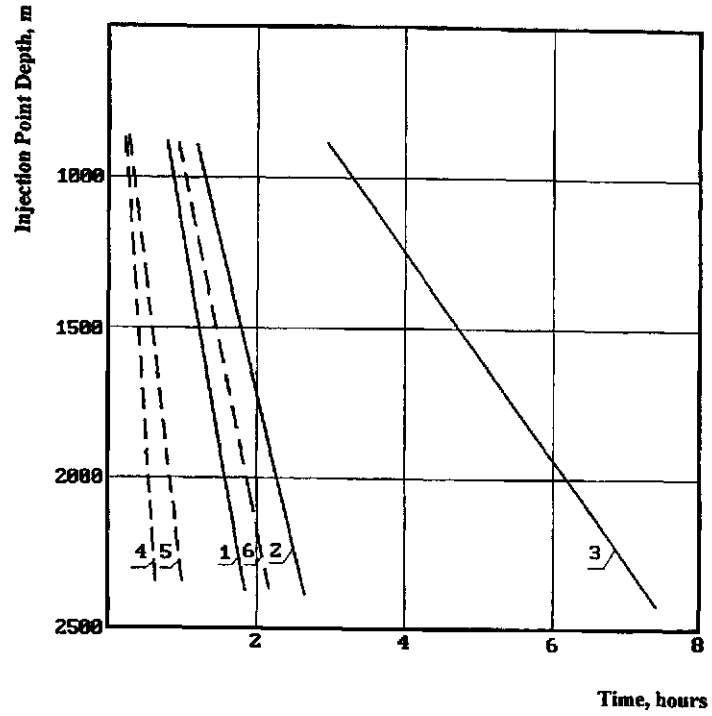

Figure 4-17 Dependence of hydrate formation start time on depth of water injection and its temperature at:
Flow rate 30 l/s: Line 1 is 0°C, Line 2 is 5°C, Line 3 is 10°C; Flow rate 100 l/s: Line 4 is 0°C, Line 5 is 5°C, Line 6 is 10°C.

Table 4-7 Volume of water (m^3) needed to form complete hydrate plugs in the well 9-K.

Depth of Cooled Water Injection (H), m	*Temperature of Injected Water, @C*		
	0	*5*	*10*
1000	81	126	360
2400	198	288	774

Formation of a hydrate plug in a well bore creates a local resistance. Pressure of gas before a plug gradually increases and, after a plug, it decreases. Velocity pressure of gas in a well decreases, and a possibility of an effective hydrodynamic suppression of a fountain well appears. During injection of a drilling mud with a density of 1.23 g/cm³ into the 9-K well at a rate of 30 l/s and a temperature of 1–2°C at a depth of 1002 m, the gas stream was closed by a forming hydrate plug during tens of minutes.

Figure 4-18 presents the dependencies of a minimum required flow rate of a liquid injected into a blowout for a hydrodynamic suppression of a gas well (a calculation was done for the conditions of the well 9-K). From the curves, we see that the flow rate of a drilling mud, having a density of 1.23 g/cm³ (actual), had to be 75 l/s in order to suppress the well 9-K, i.e., 2.5 times higher compared to an actual flow rate, and in case water was used as a liquid, its flow rate had to be increased to over 90 l/s.

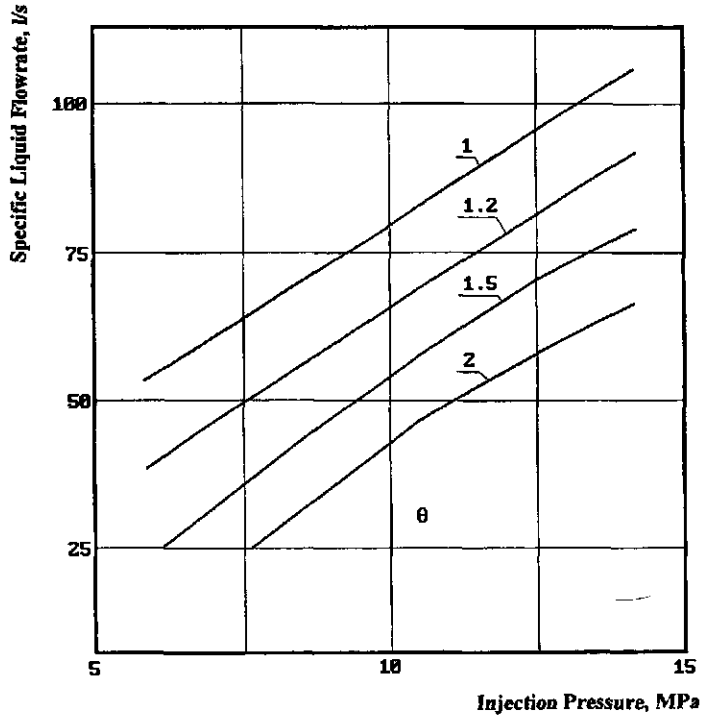

Figure 4-18 Dependence of liquid specific flow rate for hydraulic suppression of gas blowout on liquid density and pressure at injection point. θ is specific water flow rate at t = 0°C with blowout suppression with hydrate.

Even at the density of a drilling mud of 2 g/cm³, a specific liquid flow rate of 50 l/s would be required to suppress a fountain at the well 9-K in the specified regime.

In fact the specific flow rate of a drilling mud having a density of 1.23 g/cm³ was 30 l/s during suppression of the well 9-K, and its total consumption did not exceed 120 m³.

The Question of Using Gas Hydrates for Dissipation of Fogs

Methods of removing high-temperature fogs were developed as a result of studying the conditions of hydrate existence in a neutral medium, considering a large heat of vaporization of liquid hydrate formers and a relatively high temperature of hydrate formation at atmospheric pressure. The most investigated hydrate former for this application is propane (Krasnovskaya, 1976).

The development of high-speed aircraft required us to solve the problem of providing visibility for landing objects at all times of the year. Dense fog decreases the visibility of large objects at a distance of 50 m, moderate fog—to 500 m, and weak fog—to 1000 m. Fog is one of the reasons for air traffic delays.

Fog is a result of moisture condensation during the cooling of air. Most strong fogs form during mixing of warm moist air with cold air. Favorable conditions for fog formation are created by large industrial centers which are characterized by a high degree of heat dissipation and highly polluted atmospheres with microscopic dust—production waste. A noted distinction of these fogs is their high stability. They can form even in air not saturated with moisture.

A fog is an accumulation of droplets of water with a diameter of 0.1 to 100 microns. The amount of drops in a cubic centimeter of a weak fog ranges from 5 to 50, and 200–600 in a dense fog. The mass of water contained in a cubic meter of air reaches 0.05–1 g. Natural fogs are dissipated by the action of various agents providing a transition of small dispersed droplets of water into large aggregates with their subsequent precipitation from air.

Usually, a fog consists of drops of liquid water or ice crystals characterized by a certain water vapor pressure above them. Existing methods of fogs dissipation are based on the principle of decreasing water vapor pressure in a fog medium below the vapor pressure of water above the drops of water by creating microscopic zones of subcooling through an

instantaneous evaporation of dispersed substances. Chemicals such as solid carbon dioxide (dry ice), silver iodide, lead iodide, etc., are used for dispersion of which magnitudes of 10^{10}cm^3 provide an effective dissipation of fogs below –7°C. However, in practice, the so called high-temperature fogs whose temperature is close to ± 3°C are widespread.

In order to disperse such fogs it is expedient to use the property of gas hydrates to significantly decrease water vapor pressure. The essence of the influence of a hydrate or a volatile liquid on a fog consists of the following. A dispersed liquefied hydrate former whose high vapor pressure results in its quick evaporation is injected into a cloud of fog. Quick evaporation is accompanied by a significant temperature drop in a microscopic zone surrounding an evaporating droplet of a hydrate former. During this the supersaturation of the specified microscopic zone with moisture grows. Water vapor condenses and hydrate microcrystals form. Water vapor pressure decreases even more due to the formation of a solid hydrate phase. An intensive draining of moisture from liquid microdroplets to a surface of growing hydrate crystals, their coagulation and precipitation proceeds. The fog disappears.

One of the properties of hydrate crystals important for the purpose of artificial fog dissipation is the decreased water vapor pressure above the hydrate at the same temperatures. The volatility of water vapor above a hydrate can be determined from the equation:

$$\ln (f/r) = v(P - r)/RT \qquad \textbf{(4.22)}$$

where

P is the total pressure;

f is the volatility of water vapor above hydrate at specified P and T;

$\bar{v}$ is the molar volume of liquid water;

r is the saturated vapor pressure of water.

At specified temperatures the pressure of a water vapor above a hydrate is lower than the equilibrium pressure of a water vapor above ice (or liquid water). Equilibrium vapor pressure of water r_w above a hydrate is described by the expression:

$$\ln \rho_w = \ln \rho_w^0 + \frac{m}{(1+m)n} \ln(1 - Q_1) + \frac{1}{(1+m)n} \ln(1 - Q_2), \qquad \textbf{(4.23)}$$

where

n is the number of water molecules per one cavity (molar ratio of water and gas in a hydrate);

m is the ratio of the number of small cavities to the number of large cavities in a hydrate unit cell;

Q_1, Q_2 are the filling ratio of small and large cavities of a hydrate structure with hydrate former molecules, accordingly. The definition of values Q_1, Q_2 are given in Chapter 1.

It is necessary to introduce a certain number of active centers (hydrate crystals) into a fog zone in order to dissipate high-temperature fogs using the hydrate formation process. Effectiveness of fog removal changes with the number of active centers. The process will be slow and not effective at this small number, while at a large number many hydrate crystals will form which practically will not precipitate. In this case a fog will convert from a liquid-drop type into a crystal type and visibility will not improve. The optimum number of active centers of hydrate formation in a sphere of fogs at temperatures –3°C to +0.6°C equals $5 \times 10^6 - 5 \times 10^7$ per gram of propane. During introduction of a solid CO_2 the maximum effectiveness is noticed at its dispersion to $10^{10} - 10^{14}$ particles per gram.

The time of a nural fog dissipation using propane hydrate at temperatures –3°C to 0°C equals 12–14 minutes. The time of fog dissipation during freon action is about two times shorter than during propane action, which can be explained by the fact that water vapor pressure above a freon hydrate is lower in this temperature range than above a propane hydrate. Industrial testing of propane showed it to be effective for high-temperature fog dissipation.

5
CHAPTER

NATURAL GAS HYDRATES

Gas hydrates are molecular compounds of gas and water, solid crystals forming at certain pressures and temperatures. Hydrates can be divided into two clear groups according to their genesis: natural, which form and exist in nature without human intervention, and technogenic, which form in technological systems created and controlled by man. Although natural and technogenic gas hydrates are identical in their essence, problems generated by both groups, methods of solution, and research goals and consequences of the solutions are very different.

We will review only the conceptual problems of natural gas hydrates:

- conditions of formation, accumulation, stable existence and decomposition;
- spreading of hydrate formation zones on land and under sea;
- details of search and surveying gas hydrate deposits;
- resources of hydrocarbons accumulated in natural gas hydrates;
- methods of development of gas hydrate deposits and their influence on mastering oil and gas condensate fields in regions of gas hydrate deposits; and
- the influence of natural gas hydrates on regional ecology and global changes.

Natural gas hydrates, which are widespread on our planet, were discovered by Russian scientists. Natural gas hydrates are a powerful mineral energy resources and their use will significantly improve the energy balance of the world in future decades. According to the estimates of many experts the potential resources of natural gases accumulated on earth in a hydrate state are 15×10^{15} m^3, which is higher than the surveyed world

resources of hydrocarbon gases by two orders of magnitude. Natural gas hydrates, with a trained mastering, can provide humankind with cheap, ecological energy for many decades. At the same time their properties can, under certain conditions, be the cause of destruction and suffering.

Hydrates play a stabilizing role in climate changes by controlling heat flows on our planet, and a destabilizing role by releasing great volumes of methane into the atmosphere. We have to learn to control the state of natural gas hydrates. In-depth studies of the properties of natural gas hydrates, hydrate saturated rocks, conditions which affect the expression of these properties and controlling them is only beginning. Gas hydrate scientists have a responsibility and a concern that hydrates given to us by nature will be used effectively.

The first experiments studying gas hydrate formation conditions in synthetic and real core samples taken from productive layers indicate that natural gases form hydrates with rock water in porous media at appropriate P-T conditions (Makogon, 1965, 1966). Statements on determining the conditions of formation and decomposition of natural gas hydrates, on revealing the intervals of hydrate's location in rock profile, on calculating reserves of gas in gas hydrate deposits, and on mapping the zones of possible hydrate formation were formulated and the fundamentals of production of gas from gas hydrate deposits were laid in these works.

The first maps of spreading gas hydrate formation zones on the territory of the former USSR were presented in 1965–1968 (Makogon, 1965, Makogon and Medovskiy, 1968). The first world map of found gas hydrate deposit locations was reported in 1985 by the Department of Energy and Technology of West Virginia, USA in which 23 fields were shown. The map, published in 1988, already showed 39 fields and 57 fields in 1993 (Kvenvolden et al., 1988, 1993).

Gas hydrate accumulations were revealed in all regions where work aimed at finding hydrates was done. Unfortunately, more funds are spent in the modern world for prevention and removal of political conflicts than searching for new energy sources. This may result in a situation where no one will be able to use energy resources.

In December 1969 a scientific discovery, "A property of natural gases to exist in earth cover in a solid state at certain thermobaric (T-P) conditions and to form gas hydrate deposits" was registered in the USSR State Register (Sb. Otkrytiya, izobreteniya, tovarnye znaki, No. 10, 1970).

Lectures "On the Formation of Gas Pools of Solid Phase in Sedimentary Earth Cover" (Makogon, Trebin, Trofimuk, Cherskiy, 1970), and "Natural Gas Hydrates in Ocean" (Makogon, Bondarev, Tsarev, Cherskiy, 1970) were presented at the XI International Gas Congress

which took place in Moscow in 1970. After their presentations, the discovery of natural gas hydrates had received an international resonance and development. Since then, the problem of natural gas hydrates has been reviewed at many energy symposia. In July 1993 the first specialized international conference on natural gas hydrates took place in New Paltz, NY, USA, in July 1996 the second international conference on natural gas hydrates took place in Toulouse, France, and a detailed analysis of research was done, and perspectives were marked for the development of the natural gas hydrate problem.

Over the years of studying natural gas hydrates a majority of specialists have approached the problem from a position of putting hydrate resources into energy balance. However, reserves of natural gas practically fulfill modern energy needs. Aside from that, it should be recognized that despite numerous patented technologies there is almost no competitive method for effective production of gas from gas hydrate deposits located under sea, where about 99% of all gas hydrate resources are located. At the same time, lengthy experiences in the development of the Messoyakh gas hydrate deposit located in the sub-Arctic showed the possibility and economical expediency of gas production from such fields (Makogon et al., 1971, Krason and Finlay, 1992).

Mastering of traditional hydrocarbon fields on shelves and slopes offshore is complicated in a number of regions because of hydrate accumulations in bottom sediments where engineering installations such as platforms, oil and gas wells, pipelines, etc., are located. This is an aspect of the gas hydrate problem that results from capacitative and thermomechanical properties of gas hydrates and hydrate saturated rock. Absence of lithological covers over hydrate accumulations in sea and their metastable state require serious attention to solve environmental problems during gas hydrate and traditional oil and gas fields.

The importance of natural gas hydrates determines their active study in the world by laboratories having the latest equipment. The findings of research published in numerous works indicate that interesting results on the conditions of gas hydrates formation in earth, their spreading on land and under sea, and others were obtained. The study of natural gas hydrates is currently in a state where new problems and finding methods of their solution appear continuously.

The most acute problems in studying natural gas hydrates are:

- genesis of gas hydrate deposits (GHD), dynamics of their accumulation and destruction;
- search and surveying of GHD;

- determining regional resources of gas in GHD;
- properties of hydrate saturated rock;
- drilling wells through hydrate saturated layers;
- engineering mastering of GHD and of oil deposits under GHD;
- creation of effective ecological technologies for gas production from GHD;
- discovery of the effect of natural gas hydrates on geological processes and global changes;
- influence of the conditions of hydrate formation on processes in near and far space.

Composition of Gas and Conditions of Natural Gas Hydrates Formation

The first works devoted to natural gas hydrates described methane hydrates. Usually, calculations of potential energy resources accumulated in earth in a hydrate state are based on the content of methane in hydrates. However, numerous core samples extracted during drilling of wells in a hydrate formation zone indicated a large variation of gas composition in natural gas hydrates (Brooks et al., 1973–1994). Tables 5-1 and 5-2 present some characteristic data from analyses of composition of gas obtained from cores sampled in the Gulf of Mexico and in Kuparuk Bay Field at various depths in water and in sediments.

Compositional analysis of gas obtained from hydrate saturated cores can reveal a geological history of formation and long stable or metastable state of hydrates in a specified region. It also can determine a thermobaric history in rock profile.

In real conditions when generation of gas takes place in water-saturated sedimentary rock, an active redistribution and migration of gas and water occurs. At that volume and mass, ratios of water and gas are determined by a dynamics of thermobaric conditions in a profile, by phase states of components, etc.

Knowing the component and isotopic composition of gas in a hydrate, one can reveal the genesis of gas and stability of hydrate over the period of its existence. At a ratio $\frac{CH_4}{C_2H_6 + C_3H_8} \geq 100$, gas is, usually, of biogenic origin. At $\frac{CH_4}{C_2H_6 + C_3H_8} \leq 80$, gas has a thermogenic origin. A gas of a

Table 5-1 Gas composition and isotope distribution in the Gulf of Mexico hydrate samples.

Site	$\delta^{13}C$ CH_4	C_1	Composition of Gas, mole % C_2	C_3	$i\text{-}C_4$	$n\text{-}C_4$	CO_2	$\frac{C_1}{C_2+C_3}$
Biogenic Hydrate Samples								
Orca Basin	–71.3	99.1	0.34	0.28			0.24	159
Garden Banks-388	–70.4	99.5	0.12				0.26	829
Green Canyon-257	–69.2	99.7					0.26	>1000
Green Canyon-320	–66.5	99.7	0.08				0.12	1246
Thermogenic Hydrate Samples								
Green Canyon-184	–44.6	70.9	4.7	15.6	4.4	0.3	4.1	3.2
Green Canyon-204	–56.5	61.9	9.2	22.8	4.5	1.3	0.2	1.9
Green Canyon-234	–43.2	74.3	4.0	13.0	3.2	0.86	4.6	4.4
Mississippi Canyon	–48.2	93.4	1.2	1.3			4.0	37.4

(Brooks et al., 1986)

Table 5-2 Gas composition from hydrate containing cores, well No. 2, Kuparuk Field, volume % (Collett et al., 1988).

Depth, m	CH_4	C_2H_6	C_3H_8	CO_2	O_2	N_2
577–580	97.60	–	–	–	0.14	2.26
577–580	98.76	–	–	–	0.15	1.09
664–667	99.14	–	–	–	0.02	0.84
664–667	99.17	–	–	–	0.03	0.8
664–667	99.49	–	–	–	0.05	1.46

biogenic or a thermogenic origin can be determined by its isotopic composition from a correlation:

$$\delta_C^{13} \equiv \left[\frac{(^{13}C/^{12}C)_{sample}}{(^{13}C/^{12}C)_{PDB}} - 1\right] \times 10^3 \qquad (5.1)$$

where

PDB is the ratio in a standard sample of belemnite.

A value of $\delta_C^{13} > -55$ is characteristic for methane of a biogenic origin. A value of $\delta_C^{13} < -55$ is characteristic for methane of a thermogenic origin.

Figure 5-1 presents the schematic of distribution of gas in a hydrate, according to the origin of methane based on its isotopic characteristic. A complex study of gases in a zone of hydrate formation was reported in many works published by the group of Brooks (1973–1994).

It would be interesting to compare the results of measuring gas content in ocean water above a hydrate formation zone, in near-bottom pore water in a hydrate formation zone, and in pore water in rock underlying a hydrate formation zone with limiting the gas content in water in free and hydrate states. Unfortunately, it is impossible to make such a comparison today since all samples of pore water in a hydrate formation zone were taken in intervals of rock with nodular inclusions of hydrate. The size of hydrate nodules and distance between separate nodules are unknown. This prevents a conclusive interpretation of data on gas content in water.

Figure 5-2 shows the generalized diagram of a real change in ratio methane-water in ocean (curve a–b) (Sackett, Brooks, 1975) and in sedimentary rock—in pore water (curve c–d) (Brooks et al., 1979). The curve (efghi) represents the limiting solubility of methane in water in the considered ranges of temperature and hydrostatic pressure. The curves of dependence of gas content in a free (compressed state) in pore volume

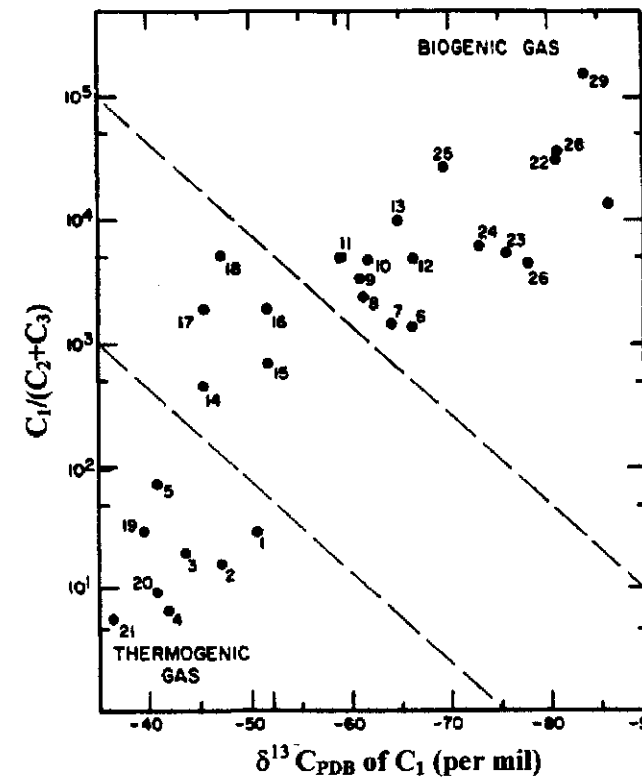

Figure 5-1 Cross plot of $C_1/(C_2 + C_3)$ against isotopic composition of C_1 to distinguish biogenic and thermogenic gas (reproduced with permission from Ann. Rev. Earth Planet. Sci., (Claypool and Kvenvolden, 1983)

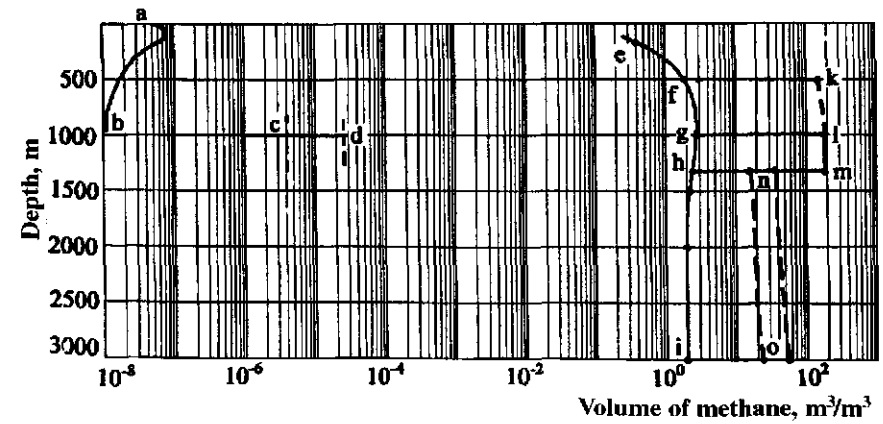

Figure 5-2 Methane concentrations in the: (a–b) sea water (Gulf of Mexico); (c–d) pore water; (e–f–g–h–i) solubility of CH_4 in free water; (k–l–m) methane in a hydrate state; (n–o) free gas in pore space.

(curve n-o) and the curve of a specific methane content in a hydrate state in a unit volume (curve k-l-m) are presented in the same figure.

As it is seen from the diagram, the volume ratio of methane and water in real conditions may vary by several orders of magnitude. For example, hydrate of methane discovered on the bottom surface of the Gulf of Mexico (Figure 5-3) at a temperature near 5°C and a pressure of 60 bars had the gas to water volume ratio of 182 m^3/m^3, and the carrying near-bottom water—1×10^{-8} m^3/m^3 (Brooks et al., 1993). Thus, one cubic meter of near-bottom water contains about 10 mm^3 of methane, which is over 10 orders of magnitude difference.

According to the known laws of physical chemistry, methane hydrate has to dissociate at such deficiency of gas content in carrying near-bottom water washing hydrate blocks on the ocean bottom. Nevertheless, hydrate does exist on the bottom of the ocean.

Usually, hydrate blocks lay on the ocean bottom in a zone of hydrate formation in regions characterized by a high influx of free methane from underlying sedimentary layers at insignificant subcooling when the process of hydrate formation is characterized by low rates.

The content of gas in the bound hydrate state in a profile of rock in a hydrate formation zone may exceed significantly the specific content of gas in free and dissolved states. The content of gas in a free state depends on pressure and temperature and is determined by the difference between the intensities of generation and of a diffusive influx and outflux through overlying rock and laterally migrating water. As a rule, the specific content of a free gas in a unit of the free volume of pores is determined by temperature and hydrostatic pressure. Gas content in a zone of hydrate formation is variable and depends not only on temperature and pressure, but also on the direction of phase transition processes. During hydrate formation a deficiency of dissolved gas occurs, while during hydrate decomposition, there is an excess up to the evolution of gas to a free state.

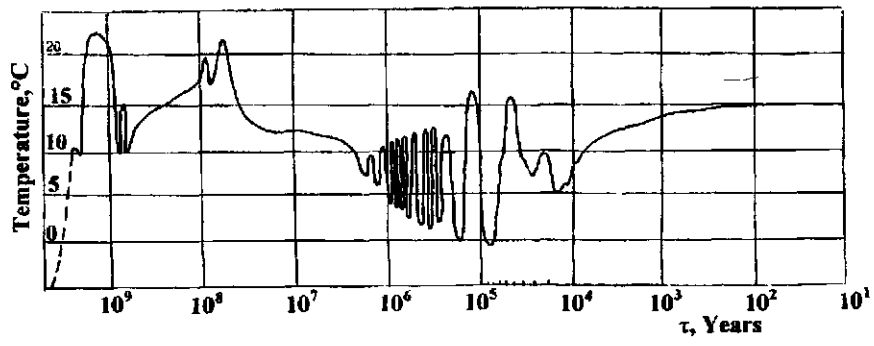

Figure 5-3 Average temperature change on the earth's surface.

A unit volume filled with hydrate contains from 70 to 220 volumes of gas at normal conditions, depending on hydrate composition. For example, a hydrate of methane has a density of 0.9 g/cm^3 in the region of low pressures and temperatures. Molecular ratio of water and gas is then near 5.9. One liter of hydrate contains 7.365 moles or 165 liters of methane. In similar P-T conditions one liter of a free (pore) volume may contain 30 to 50 liters of methane, i.e., several times less than in a hydrate state.

Composition of free and dissolved in water gas in a hydrate formation zone depends both on the type of crystallization and on the rate of hydrate formation and dissociation. Compositions of a free gas and a gas in a natural clathrate hydrate are different. Usually, a hydrate becomes enriched with heavy components contained in gas during hydrate formation.

Conditions of Natural Gas Hydrates Formation

In natural conditions hydrates form and stably exist in the presence of liquid water and gas at appropriate pressures and temperatures—in Earth, Mars, and other planets, on a solid surface (Mars, etc.), in atmosphere (Jupiter, Venus, etc.). In this section we consider only the specialties of hydrate formation in porous granular media, which is characteristic to the sedimentary cover of earth's crust in which the major resources of natural gas hydrate are accumulated.

The process of hydrate nucleation both in natural and in technogenic conditions has a common basis when hydrates form from free water and gas. However, additional conditions which are determined by capillary pressure, surface tension, salt content of the fluid, and capacitative properties of medium, etc., are applied during hydrate formation in a porous media.

In the simplest form, the formation of gas hydrate deposits has to be divided into two groups: 1) formation of hydrates from dissolved gas when the rate of hydrate accumulation is determined by the diffusive influx of gas from adjacent water and 2) from free gas contained in pores (gas or gas condensate deposit transforms into a gas hydrate one during a change in thermodynamic conditions. In the first case, the molecules of gas dissolved in water transform into a hydrate state encountering only a diffusive resistance of liquid water which is in contact with a surface of growing hydrates. In the second case the molecules of free gas contained in a pore bubble have to overcome the diffusive resistance of a hydrate growing on the boundary of a gas bubble in pore water in order to transform into a hydrate.

Primary gas hydrate deposits are formed in the first variant without the formation of a gas deposit. In the second variant—secondary gas hydrate

deposits are formed from gas or gas condensate deposits which formed earlier from supersaturated gas-water solutions under lithological covers. Primary gas hydrate deposits do not require an impermeable lithological cover. Hydrates which accumulate in porous sedimentary medium can be characterized by a very low permeability. In addition, at P-T conditions which correspond to hydrate formation, hydrates block a diffusive dissipation of vertically and laterally migrating gases.

In the very first experimental study of the conditions of natural gas hydrates (Makogon, 1966, 1974), a significant influence of the carrying porous rock on the process of hydrate formation was indicated—larger subcooling or overpressurization was required with the decreasing size of pores, compared to the process of hydrate formation at the free gas-water interface. Further investigation of the effect of porous medium on the process of hydrate formation (Handa, 1992, 1993; Sloan et al., 1991) have verified the hypothesis—the smaller the pore size, the higher the effect of porous medium on the process of hydrate formation.

The difference between the conditions of a pore water and a free water transformation into a hydrate is determined by the specificity of the properties and structure of a pore water. The physical state of water saturating rock varies. Free water migrates in rock at any, even the smallest gradients of pressure and can be moved by gravity. Capillary water is held in rock by physico-mechanical bonds in capillaries ($r > 10^{-8}$ m). It is capable of transmitting hydrodynamic pressure and does not release heat during wetting. Bounded water forms adsorbed water films which are attached directly to grains of rock. Heat is released during the formation of such films. Water is held by physico-chemical forces on the surface.

The effect of adsorption and surface tension forces results in the decrease of vapor pressure of bounded and capillary pore water. In their simplest statement, the conditions of hydrate formation in porous medium can be described by the expression (Makogon, 1985):

$$\ln\left(\frac{\rho_{SW}}{\rho_{0W}}\right) = \nu_1 \ln(1 - C_{A1}P) + \nu_2 \ln(1 - C_{A2}P) \qquad (5.2)$$

where

ρ_{SW} is the vapor pressure of saline water in pores of rock, MPa;
ρ_{0W} is the vapor pressure of water over empty hydrate lattice, MPa;
ν_1, ν_2 is the constants;
C_{A1}, C_{A2} is the Langmiur constants;
P is the equilibrium pressure of hydrate formation at conditions of a free gas-water contact.

Vapor pressure of pore water vapor ρ_m is determined from the expression:

$$\rho_m = \rho_W - \frac{2\sigma}{r}\frac{\delta_V}{\delta_W}, \qquad (5.3)$$

where

ρ_W is the vapor pressure of water above a free surface;
σ is the surface tension coefficient at a liquid-vapor interface, mN/m;
r is the radius of a capillary, cm;
δ_W is the density of water, g/cm^3;
δ_V is the density of vapor, g/cm^3, determined as :

$$\delta_V = P_C m_W / RT, \qquad (5.4)$$

where

P_C is the vapor pressure over the concave surface of water;
m_W is the molecular weight of water;
R is the gas constant.

Vapor pressure above the surface of water bounded in pores ρm can be determined from the formula (Skhaliaho, 1974):

$$\rho_m = \rho_W [\ 1 - \exp(WD/0.0126)2] \qquad (5.5)$$

where

ρ_W is the vapor pressure of water above a free gas-water interface;
W is the content of bounded water, millimoles/grams of porous medium (rock);
D is the mean particles diameter, mm.

The magnitude of decrease in vapor pressure above a solution of saline water in a porous sample of rock is determined by the expression:

$$\ln\frac{\rho_{W-} - \Delta\rho_m}{\rho_{0m}} = \frac{m}{(1+m)n}\ln\left(1 - \sum_{A,B,C,K}\Theta_1\right) + \frac{1}{(1+m)n}\ln\left(1 - \sum_{A,B,C,K}\Theta_1\right) \qquad (5.6)$$

where

$$\Delta\rho_m = \rho_W - \rho_m = \rho_W - \rho_W[1 - \exp(WD/0.0126)2] = \rho_W\{1 - [1 - \exp(WD/0.0126)2]\} \qquad (5.7)$$

Thus, the lower the diameter of particles which constitute porous medium and the lower the radius of capillaries of a medium, the higher the depression of water vapor pressure and the lower the temperature (or higher pressure) of the onset of hydrate formation in porous medium.

After the formation of crystal nuclei in porous medium its effect on the growth of hydrate crystals is not pronounced at conditions when $\rho_H \leq \rho_m$, i.e., when the vapor pressure of water above hydrate ρH is lower than above pore water. An experimental study of methane hydrate formation conditions in real core samples and in synthesized samples made of quartz sand indicated that starting with a capillary radius $r_m = 4$ μm the effect of porous medium on the process of hydrate formation is pronounced. A precise study done by Handa (1992) confirmed these results.

The effect of a porous medium increases with the accumulation of hydrates in pores. In real conditions up to 90% of pore water may be converted into a hydrate state. When a pore space is almost completely filled with hydrate, its permeability sharply decreases.

The start of a hydrate formation process is preferred, not in a deposit of gas where large bubbles of free gas are present in pores, but in a water deposit saturated with gas, and not during the period of increase of hydrostatic pressure, but during its decrease (even a short-term due to tectonic shifts or seismic vibration). It is important to notice that the lowering of temperature in a profile decelerates (and in some cases prevents) the process of hydrate formation which can be explained by the properties of water and gas in their solution. As seen in Figures 1.29 and 1.30, in real thermodynamic conditions, a decrease in temperature increases gas solubility, and oppositely, a decrease in pressure decreases solubility of gas. In a condition of complete saturation, a decrease in pressure results in the formation of microscopic bubbles of free gas in a bulk of water. Pressure in such microbubbles is significantly higher than the hydrostatic pressure (Chapter 1). Crystal nuclei form on the surface of these bubbles. Further growth or dissociation of these nuclei is determined by a thermodynamic or geochemical situation in a definite profile of rock. Thus, with temperature decrease above a saturated solution, the solution becomes undersaturated which prevents formation of hydrate nuclei. For example, the temperature decrease in a profile from 20°C to 10°C will result in an increase of solution capacity for gas from 3.0 m^3/m^3 to 4 m^3/m^3. The solution will be undersaturated and although the temperature is below hydrate equilibrium, hydrate will not be able to form. At the same time, a decrease in pressure, even by several atmospheres, will result in evolution of gas bubbles and hydrate formation.

Zone of Hydrate Formation

Generally a thickness of permeable, usually sedimentary rock whose P-T regime corresponds to the conditions of a stable existence of gas hydrates can be described as a hydrate formation zone (HFZ). For example, methane hydrates can exist in a broad range of temperatures—from 35 to 330 K in the conditions of high vacuum and at pressures above 17 kbar (Figure 1-14).

Due to the conditions of our planet, hydrates of hydrocarbon gases, mostly of methane at pressures ranging from 1 or 2 to 50 MPa and in temperature range from 264 to 300 K, are of interest. Beyond these temperatures hydrate accumulations are insignificant in resources and are hard to develop.

The size of an HFZ depends, in each case, on gas composition and salt content of formation water with all other thermodynamic conditions being equal. The most important property of gas hydrates is their ability to form from formation water undersaturated with gas; also a lithological screen is not necessary for a further storage of hydrates.

At certain pressures and temperatures the most thermodynamically favorable condition is not a free, but a hydrate state of gases. This property apparently played a large role during the initial formation of earth, its atmosphere and hydrosphere, and also during conservation and storage of hydrates in our planet. It has also significantly promoted the formation of modern industrial deposits of free natural gas, oil, and gas condensate.

Modern thermodynamic characteristics of the sedimentary cover of earth correspond to conditions of accumulation and the existence of natural gas in a solid hydrate state on 25% of land and nearly 70% of the sea. During the current billion years thermodynamic conditions have been changing on our planet rather sharply. As shown in Figure 5-3, the average temperature of earth's surface has changed from 23°C to 0°C (Makogon, 1980). The temperature gradient and temperature profile of rock has changed accordingly. During decreases of the average of earth's surface below 12°C, surface glaciers and permafrost have intensively developed, and hydrate accumulations formed when a generation of gas was present in rock. During the increase of the average temperature to 14–17°C, glaciers and permafrost degrade, hydrates decompose, the level of the ocean increases, and atmospheric pressure grows.

Figure 5-4 presents a curve of the ocean level change during the Phanerozoic Period (Sloan, 1990), and in Figure 5-5 a similar curve is shown for the Gulf of Mexico Basin during the past 60,000 years. A comparison of the curves in Figures 5-3 and 5-5 produces a correlation

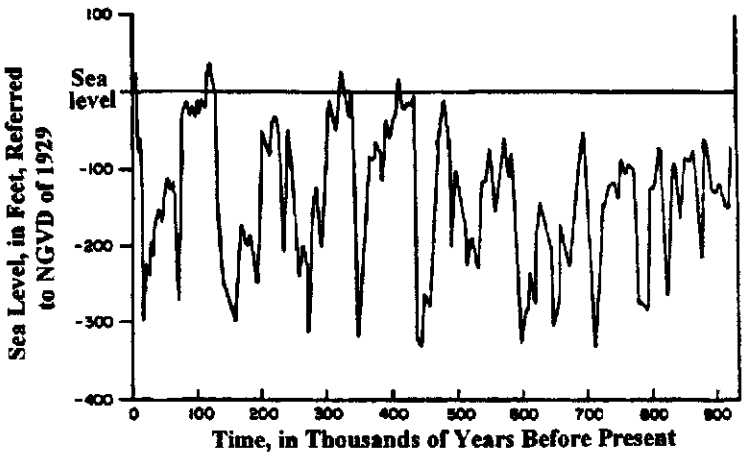

Figure 5-4 Changes in sea level during the last million years.

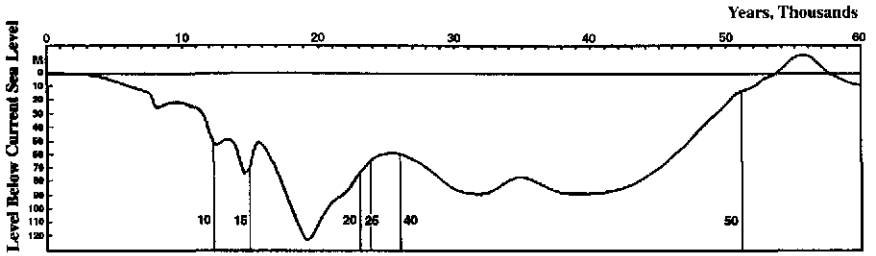

Figure 5-5 Sea level change in the Gulf of Mexico during the last 60,000 years.

between changes in the average of earth's surface temperature and the level of the ocean.

With changes in thermodynamic conditions, the zone of hydrate formation also changed its thickness and area on land and under oceans. The maximum thickness of HFZ on land is located near cooled profiles of earth's sedimentary cover. An analysis of modern thermobaric conditions in a profile of sedimentary cover on land indicates that on a significant part of land, an HFZ is located mainly in permafrost areas, although the contours of permafrost significantly come out of cryolithic zone boundaries on a regional scale.

Currently permafrost rock covers 34.5 million km^2 of earth which is near 23% of the total land on the planet. Permafrost in Alaska occupies

75%, and in Canada 63% of their territories. In Russia, permafrost is located on 10.6 million km^2, which is 62% of the country's territory.

The depth of frozen rock reaches 500–700 m, and in some areas it exceeds 1000 m. Thus, in the northwestern part of Yakutiya, zero-level temperatures were revealed during drilling of the Markhinskaya support well to a depth of 1450 m. In Canada and in Alaska permafrost rock reaches depths of 700 m, and under the Beaufort Sea relic permafrost was found at depths down to 925 m at temperatures as low as –6°C.

A large thick cryolithic zone and low temperatures in a profile in the presence of hydrocarbon gases create favorable conditions for the formation of natural gas accumulations in a solid hydrate state. On land the depth of an HFZ reaches 700–1500 m, and in a number of regions it reaches 2.5 kilometers. It is necessary to know the temperature of a neutral layer, temperature gradient in rock, salt content of formation water, and the characteristic of carrying rock in order to locate an HFZ in a certain region for a gas of known composition.

Figure 5-6 presents a schematic for locating an HFZ on land for methane and for natural gas with a relative density of 0.6. Points of intersection of equilibrium curves of hydrate formation with the rock thermal gradient curve determine thickness of HFZ. An HFZ for methane is at a depth of 250–1120 m for the specified conditions, and for a gas with Δ 0.6—at 100–350 m. The upper HFZ boundary is in a permafrost interval.

Regional geothermal profiles with equilibrium curves of hydrate formation are drawn in order to locate HFZ. During the construction of HFZ profiles it is necessary to consider the effect of size and structure of pores, salt content in water formation in a profile of rock, etc.

As indicated by an experimental study, the size of pores influences equilibrium conditions of a hydrate from a size of four microns. Salt content of formation water noticeably influences the size of HFZ. Figure 5-7 presents the actual profile of an HFZ in northwestern Yakutiya from which the effect of the salt content in pore water on the thickness of an HFZ can be seen. An HFZ can decrease in profile by a factor of two or more because of salt content in water.

Construction of geothermal profiles, accounting for the hydrostatic pressure and salt content, allows us to reveal the intervals of zone of a gas hydrate deposit's possible location and to determine natural gas resources for each particular area and for the whole region. Thermometric studies, reviewing archived geophysical data and taking core samples from supposed intervals of a HFZ made in Russia and in other countries, revealed a large number of potential regions and deposits of gas in a hydrate state.

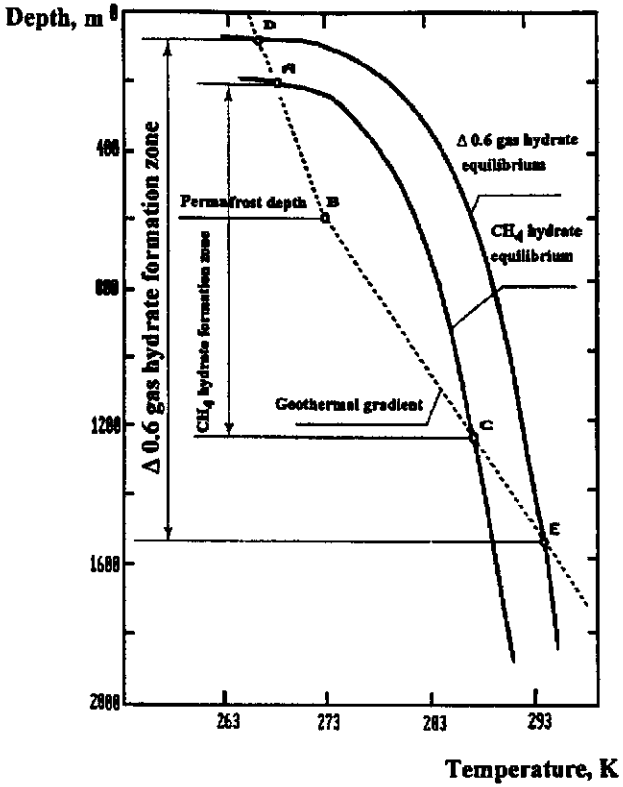

Figure 5-6 Schematic for determination of hydrate stability interval on continent with consideration of temperature gradient and gas composition.

In Russia, HFZs are more widespread in west and east Siberia and also in adjacent Arctic and far-east seas. Figure 5-8 presents a map of HFZs spreading in west Siberia (Cherskiy et al., 1982). Permafrost rock is characteristic in these regions. Permafrost depth in the sedimentary rock cover is the largest in Yakutiya. Thickness of the cryozone decreases from north to south in the northwest part of the mid-Siberian plateau. The geothermal gradient does not exceed 1.5°C per 100 m everywhere, except the northwest part where it reaches 2.5–3°C per 100 m, despite a thick cover of permafrost. Highly saline water which contains dissolved gases of methane-type composition is spread in the sedimentary cover all over the reviewed territory.

Lena-Tungusskian oil and gas bearing province embraces the largest structures (Tungusskian and Prisayano-Eniseyskian synclines, Anabarskian,

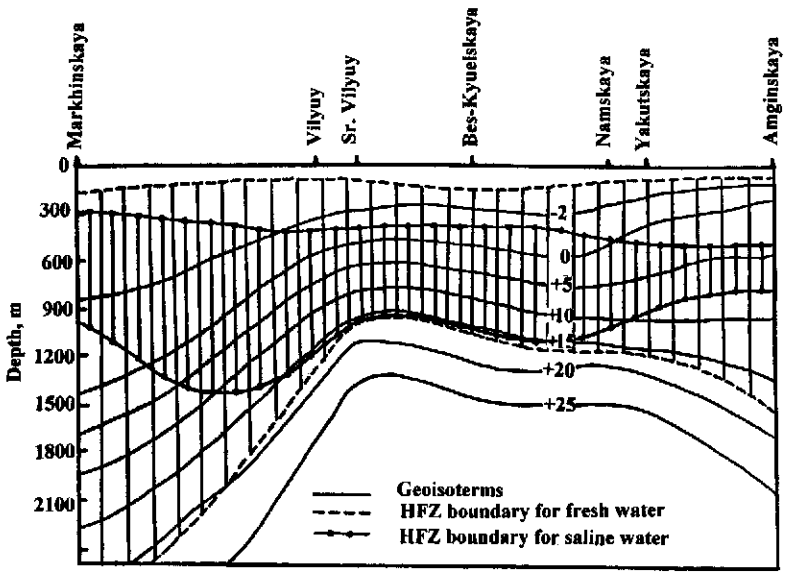

Figure 5-7 The profile of methane HFZ accounting for reservoir water salinity for the central part of the Yakutiya Autonomous Soviet Republic.

Aldanian and Nepsko-Botuobinskian anticlines, and Angaro-Lenan stage) and has the largest area of HFZs. In the central part of the platform an HFZ has maximum thickness and, apparently, includes the oil and gas bearing horizons of upper Paleozoic represented by alternating sandstone layers and packs of argyllyths, alevrolyths, and coal. As a whole, the zone of possible hydrate formation in the Lena-Tungusskian zone is over 2 million square kilometers.

The Khatagano-Viliuian oil and gas bearing province is also characterized by a significant spread of hydrate formation zones, and it includes the Yenisei-Khataganskian and Lena-Anabarskian mega-folds, Priverkhoyanskian edge fold, and the central part of the Viliuian syncline. The productive horizons are located in Permian, Triassic, and Jurassic layers. Thick and monotonous covers are absent in Predverkhoyanskian and Viliuian gas-bearing regions in a profile of the upper complex to a depth of 1 km. The thickness of the HFZ is 500–1200 m. Mostly terrigenic Mesozoic formations are present. A total area of the HFZ, whose development is possible everywhere, exceeds 600,000 km^2.

The Timano-Pechorian oil and gas bearing province is located at the Pechorian syncline and parts of Pre-Uralian edge fold adjacent from the east. The province is characterized by low values of geothermal gradient.

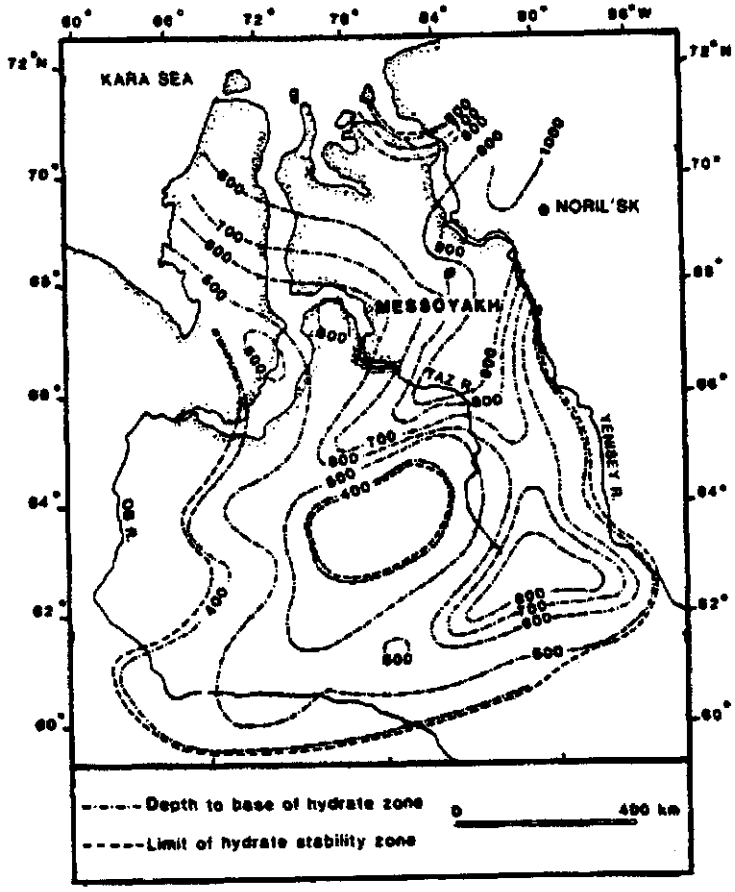

Figure 5-8 Distribution of the gas hydrate stability zone, West Siberian Basin, contour interval, 100 m (after Cherskiy et al., 1982).

Its upper water-bearing layers contain water with a low salt content. The thickness of the cryolythic zone increases from south to north. The area of HFZ spread is relatively small here (100 thousand km^2). Its exhibition is possible only in the northern parts of Izhma-Pechorian, Pechoro-Kolvinskian, Khoreiver-Morejusskian and north Pre-Uralian areas. The thickness of the HFZ is on average about 500 m. It includes the upper productive layers represented by Mesozoic deposits.

In northeast Russia, zones of potential hydrate formation are developed within the boundaries of Momo-Zyrianian and the Anadyrian oil and gas areas. The Anadyrian oil and gas area is located at the cavity bearing

the same name, whose sedimentary cover is represented by marine and continental deposit of the Cretaceous, Paleogenic, and Neogenic periods with a maximum thickness of up to 3–5 km. Only rock of Neogene complex with which the main perspectives for gas-bearing are related possess high collector properties. The area of the HFZ reaches 33,000 km^2, which include the productive horizons of Neogene.

North of west Siberia is one perspective region in which deposits of gas in a hydrate state can be discovered along with deposits of natural gas in a free state. This area is characterized by a high thick geocryolythical layer and relatively low geothermal gradients. During the cyclic cooling and glacier formation during Pleistocene deposits of gas at depths of 700–1200 m and more transformed into a hydrate state.

Cooling (mean annual temperatures during Pleistocene were 10–15°C lower than current temperatures), and consequently, the HFZ influenced already formed natural systems. As a result of that, oil and gas accumulation zones formed and disappeared here which resulted in a vertical and lateral migration of hydrocarbons. The maximum concentration of gas in an HFZ has to be in zones located near faults, salt and shale dyapirs. A stream of hydrocarbons was directed here from deeper horizons. Accumulations of free gas formed under the screening layer of sediments filled with hydrates. With favorable geological conditions, this gas could accumulate into deposits. At appropriate temperatures and excess pressures, gas dissolved in water can transform into a hydrate state avoiding a free state. Consequently, even formation water undersaturated with gas could be a source of hydrocarbons capable of forming large gas hydrate deposits.

It is necessary to know the vertical distribution of pressures and temperatures, chemical composition of hydrocarbons and salt content of water during the location of an HFZ. Within west Siberia the chemical composition of gas in oil and gas bearing complex is very homogeneous (up to 98–99% CH_4). Salt content of formation water does not exceed 15–19 grams/liter. Layer pressure is nearly equal to hydrostatic pressure.

Upper and lower boundaries of an HFZ are determined as points of intersection on the curve of equilibrium conditions of hydrate formation with the curve of temperature distribution in sedimentary layer, knowing the thickness of rock with sub-zero temperatures, geothermal gradients, composition of natural gas, and salt content of rock water. The geothermal gradient in a sedimentary cover changes from 1.0 to 2.5°C at the crossing of a zero-isotherm at 100 m. Studied periphery zones are distinguished by decreased geothermal gradients. This was reflected in a significant lowering of the lower HFZ boundary. Conditions for the transition of gas into a hydrate state were created during the formation of zones with decreased

temperatures. During the modern epoch a severe climate, hydrogeological and glaciological regimes promote the preservation of these conditions in the upper part of the sedimentary cover.

A geothermal study of the west-Siberian plateau allowed us to reveal a number of zones with temperature anomalies. So, the mean value of geothermal gradient varies between 2.7 and 5.2°C at 100 m, and the temperature at depths of 1000, 2000, and 2500 m is 19–59°C, 33–74°C, and 64–129°C. Distribution of the average geothermal gradient and temperature at various depths is related to a tectonic structure of a foundation, its material composition, age of consolidation, depth of its surface location, and with some tectonic faults.

For the west Siberian conditions for a gas with Δ0.6 the floor of an HFZ is at depths of 800–1000 m. Ob Bay and adjacent peninsulas, whose sedimentary cover is characterized by low permafrost thickness, by elevated heat flow in the central part of the Yavai peninsula, and by a low geothermal gradient in the periphery areas, can be considered as a perspective.

Thus, in the territory of Russia the hydrate formation zone is developed in four oil and gas bearing provinces and in four autonomous oil and gas bearing areas located in the northeast. Altogether it embraces 22 oil and gas bearing zones with a total area of over 3.5 million km^2, i.e., over 20% of Russian land has a developed zone of hydrate formation in which at least 50 trillion m^3 of natural gas are accumulated in a hydrate state.

On the North American Continent HFZs are developed in Alaska and in the sub-Arctic territories of Canada. According to the data from Judge (1994), Collett (1988), Kvenvolden (1991), at least 47 trillion m^3 of natural gas is accumulated in a hydrate state in North America. The total area of discovered gas hydrate deposits is over 300,000 km^2 (Malone, 1994).

Analysis of thermometric and logging data from 369 wells located on the Arctic islands of Canada and in Mackenzie Delta indicate that 1900–3900 Gt ($18 \times 10^{12} - 36 \times 10^{12}$ m^3) of methane is accumulated in a hydrate state in this sector alone (Judge et al., 1994). Among 369 wells in which surveying work to reveal hydrates was done, in 68% of the wells on Arctic islands and in 30% in the Mackenzie Eelta, hydrate-bearing layers were found. The thickness of the HFZ in these regions reaches 350–1300 m.

In Figure 5-9 a map of isopahites (lines of equal layer thickness) of hydrate-bearing rock in the central-northern slope of Alaska which was drawn according to the results of a geophysical logging in 124 wells (Collett, 1988). The Kuparuk Field (Figures 5-10, 5-11, 5-12) is the most surveyed and prepared for industrial development (Collett, 1994).

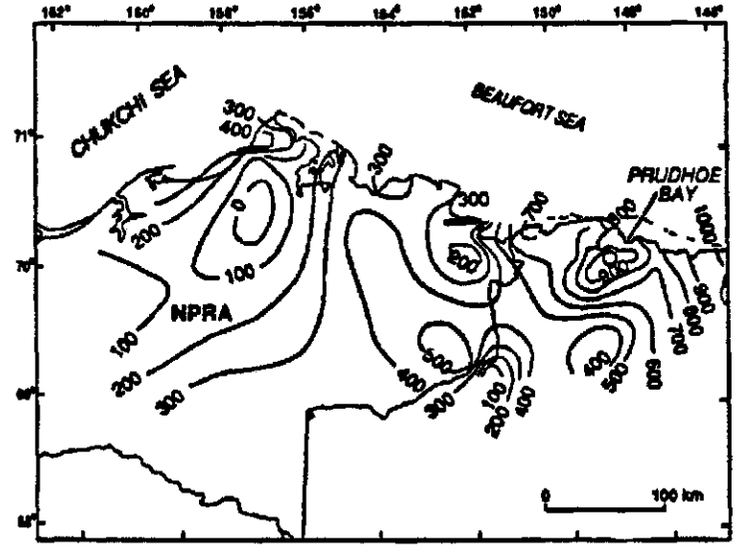

Figure 5-9 Isopach map of the Central North Slope showing calculated thickness (contour interval = 100 m) of the methane-hydrate stability field. Isopachs are based on gas hydrate stability calculations from 124 wells (Collett et al., 1988).

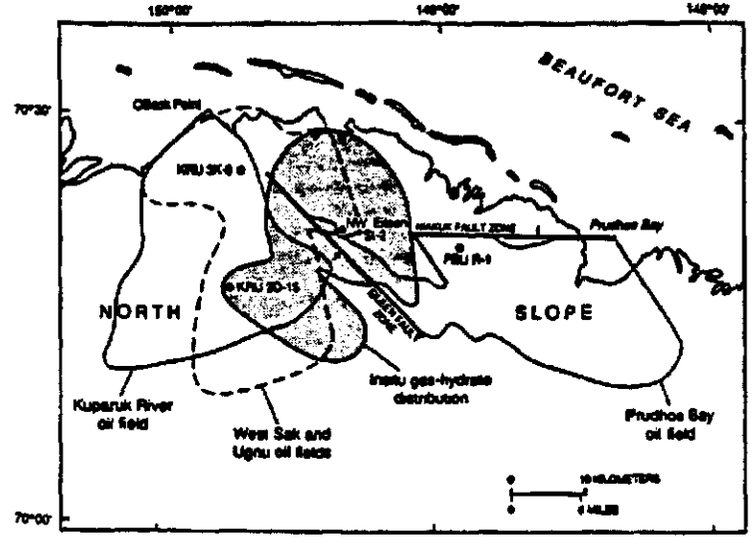

Figure 5-10 Distribution of in-siti gas hydrates and oil occurrences in Prudhoe Bay-Kuparuk River area. West Sak and Ugnu oil fields are shown as a single accumulation, enclosed by a dashed line. Major fault zones are indicated by bold lines; direction of dip shown by arrow. Oil well locations are shown by solid circles.

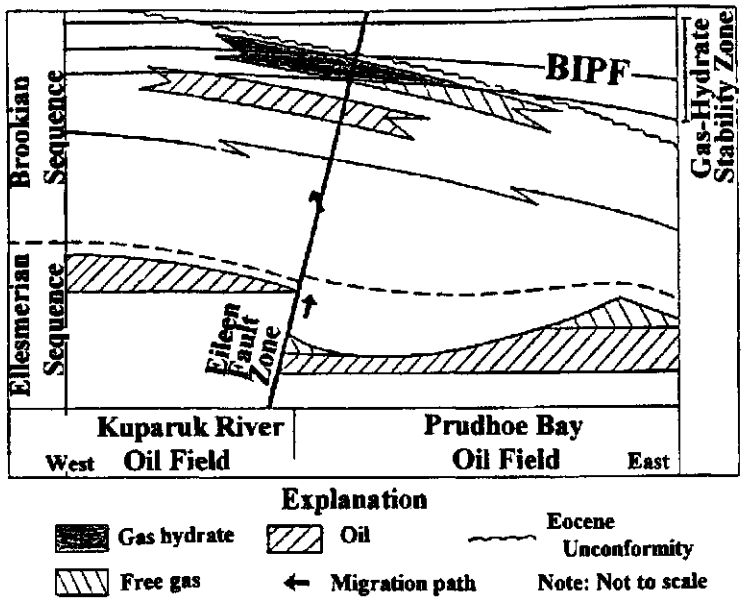

Figure 5-11 Schematic west to east cross section through Prudhoe Bay–Kuparuk River area illustrating possible gas migration paths and spatial relations between gas hydrates, free gas, oil, Eileen Fault Zone, base of ice-bearing permafrost, and gas-hydrate stability field (Carman and Hardwick, 1983).

Figure 5-13 presents a principal schematic for locating HFZs in sea, whose distinctive difference from that presented in Figure 5-6 is the presence of two temperature gradients—in water and in rock. A sharp change of slope can usually be noticed in the point of their intersection. In seas the upper boundary of an HFZ usually goes through a layer of water and the lower—through rock. The higher the temperature gradient, the thinner the HFZ. A real thickness of an HFZ in sea is located between the bottom of the sea and the lower point of intersection of a geothermal gradient and a curve of hydrate formation equilibrium. It should be noted that the thickness of an HFZ in sea is primarily determined by the temperature at the bottom, magnitude of geothermal gradient, hydrostatic pressure, gas composition, and capacity characteristics of rock in a profile. A change in a hydrostatic pressure plays a subordinate role compared to a change of bottom temperature and geothermal gradient (Figures 5-14, 5-15). During a decrease of bottom temperature at a depth of 600 m from 7°C to 3°C and a change of thermal gradient from 40°C/km to 20°C/km, the thickness of

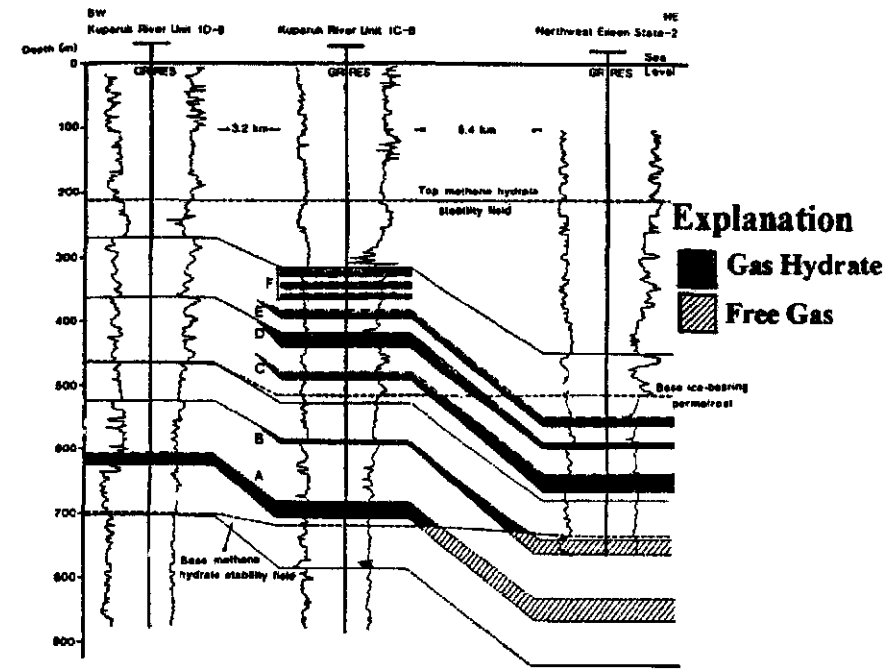

Figure 5-12 Three well cross-section showing lateral and vertical extent of gas hydrates and underlying free gas occurrences in the Prudhoe Bay–Kuparuk River area (Collett, 1994).

an HFZ for methane increases from 75 m to 500 m, and for a natural gas with Δ0.6—from 250 m to 900 m.

Figure 5-14 shows that during a decrease of the ocean level by 125 m an HFZ for methane at a thermal gradient of 30°C/km decreases from 360 m to 265 m. Similarly, during a temperature increase, by only 3°C at a constant geothermal gradient in a sedimentary cover and a constant level of ocean an HFZ decreases from 360 m to 175 m, and with a simultaneous decrease of ocean level—to 25 m.

The young Arctic Ocean is characterized by a broad spreading of relic permafrost whose thickness reaches 600 m or more in some regions, and the temperature of rock down to –6°C. Figure 5-16 presents a schematic for locating a P-T zone of hydrate formation in sea in the presence of a relic permafrost. The upper boundary for methane coincided with the surface of bottom (point A), the lower is point C. For a gas with Δ0.6 the upper boundary (point B) is in water, the lower is point E.

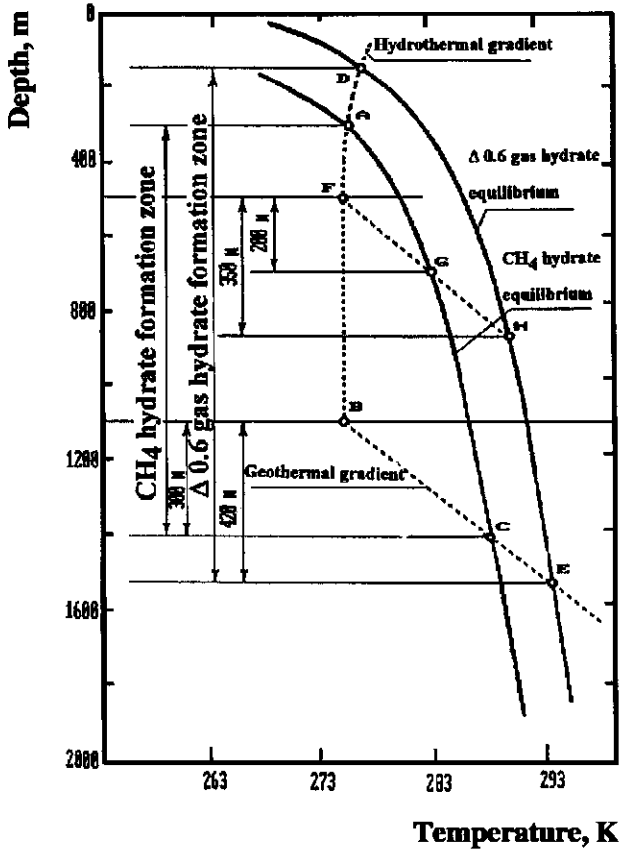

Figure 5-13 Schematic for determination of hydrate formation zone in the sea (Makogon, 1981).

Figure 5-17 presents a profile of rock in the Karski Sea with a highlighted P-T hydrate formation zone. A similar profile for the Barents Sea in the area of Shtockmanovskoe and Ledovoe gas condensate fields is shown in Figure 5-18. It is extremely important to know the change in a slope of a geothermal gradient at the lower boundary of an HFZ. If a thermal gradient in an HFZ interval is higher than in the underlying rock profile, then the processes of an intensive hydrate decomposition, formation of a metastable zone with decreased strength characteristics of carrying rock, high gas content in the profile, desalinization of pore water, etc. are characteristic to this HFZ interval.

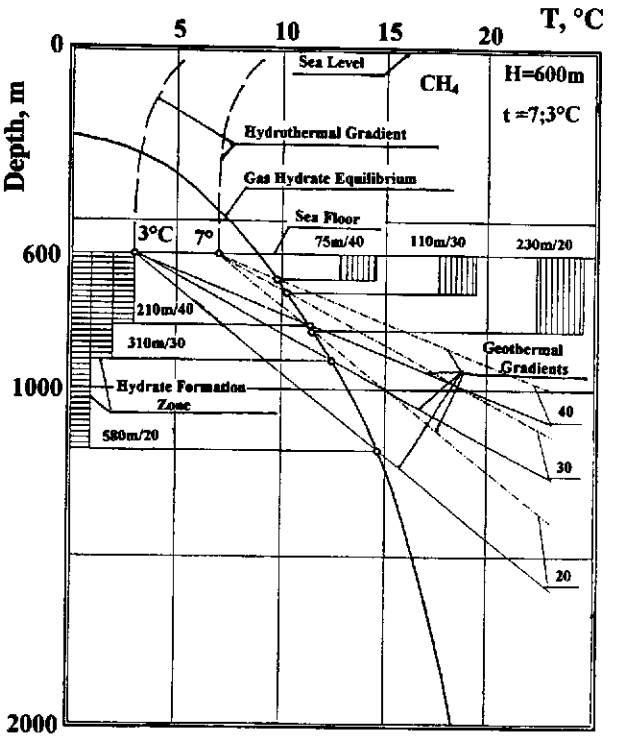

Figure 5-14 Schematic for determination of hydrate formation zone in sea, depending on the sea floor temperature, and geothermal gradient.

In case a geothermal gradient in an HFZ is lower than in the underlying rock, then the processes of hydrate accumulation for which a release of heat of crystallization is characteristic, a decreased gas content in pore water, increasing salt content of pore water, strengthening and increase of stress in carrying rock, etc. take place in this HFZ.

In the presence of a large, thick HFZ, several separate intervals with different thermal gradients can exist. These depend upon the direction of temperature fields at the upper and lower boundaries of an HFZ and on the change in salt content of laterally migrating rock water, composition of gas, heat conductivity of rock, etc. From the point of construction and operation of engineering objects those intervals of an HFZ are preferred in which the processes of hydrate accumulation and not hydrate decomposition take place. Such a rock has a large stability factor.

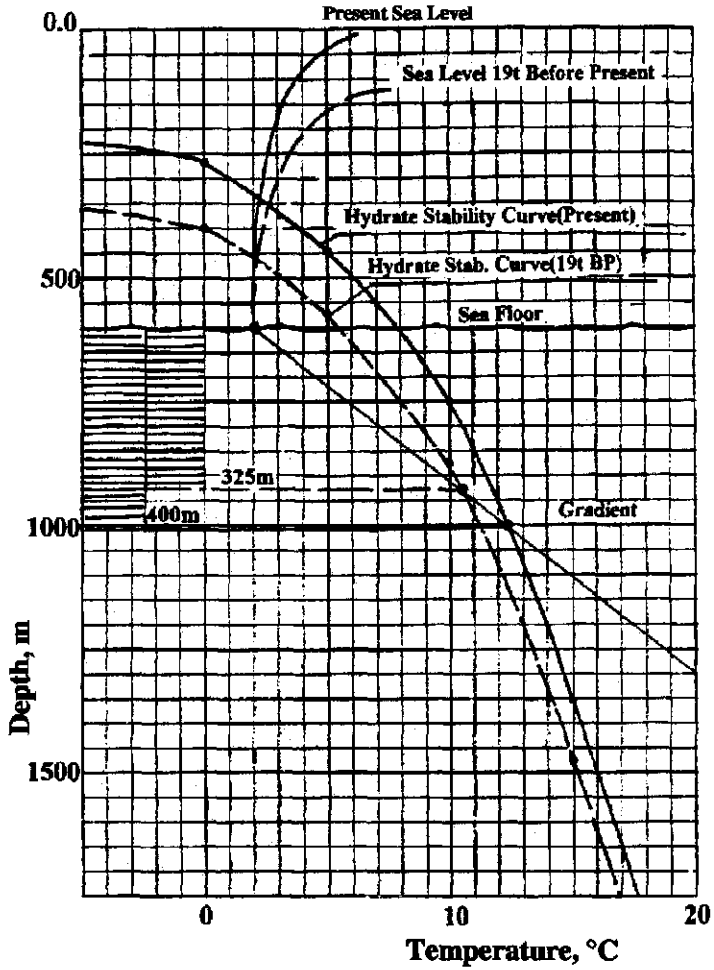

Figure 5-15 Dependence of hydrate formation zone on sea level in time.

Shtockmanovskoe Gas Field and Gas Hydrates

Several specialties of developing conventional hydrocarbon deposits in zones of hydrate formation in the Arctic sea can be shown from an example of the Shtockmanovskoe gas condensate field. The Shtockmanovskoe Field is located in the Barents Sea (Figure 5-18, Koulpin, 1994). The field is 650 km from shore. Water depth in the area of the field is 300–350 m. The depth of cover over the field deposits is 1800–2100 m. The temperature of sea water near bottom is about –1°C. Relic permafrost in the region

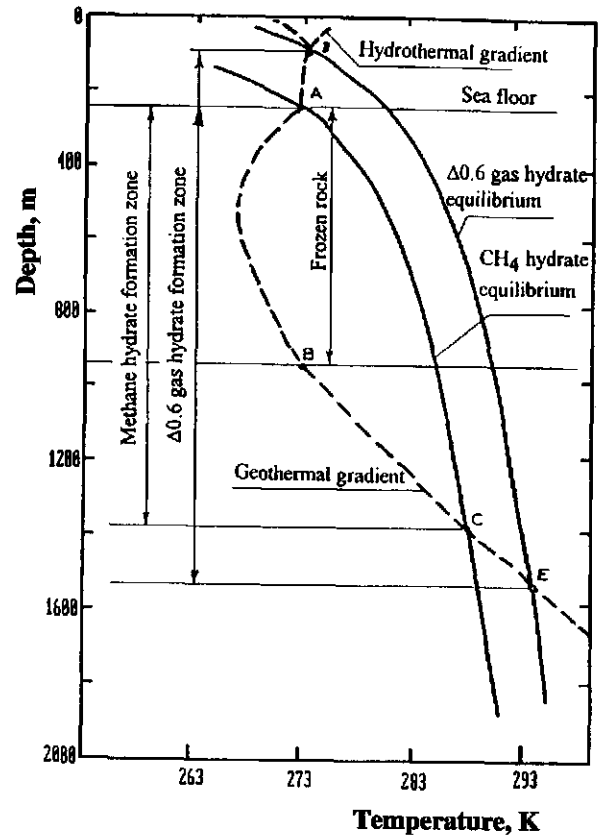

Figure 5-16 Schematic for calculation of interval of methane hydrate stability in Arctic Seas in presence of relic permafrost.

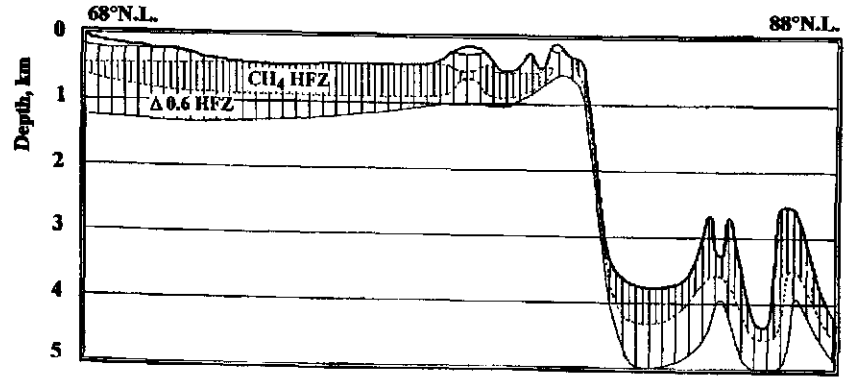

Figure 5-17 Qualitative schematic of hydrate formation zone (HFZ) depth variation.

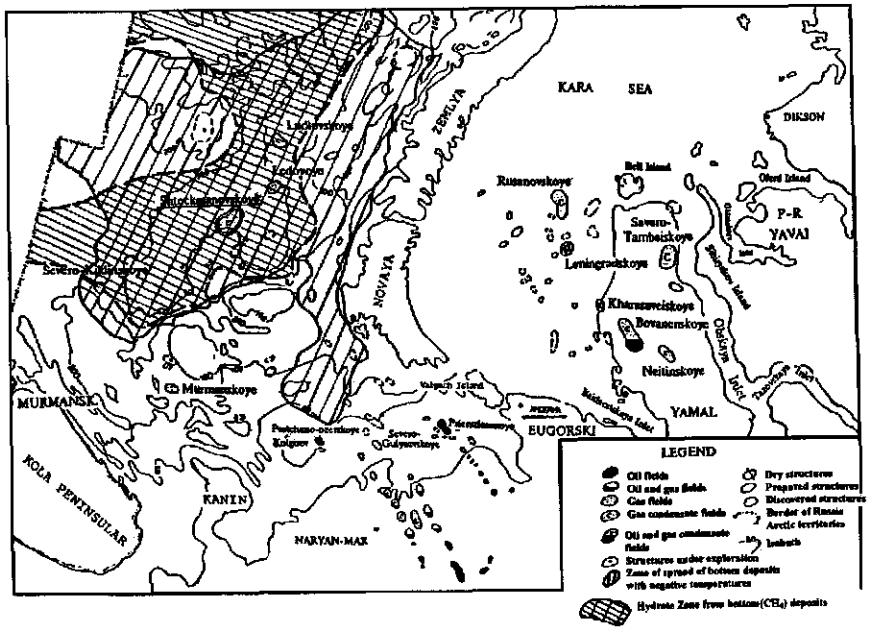

Figure 5-18 Location of Shtokmanskoye and Ledovoe gas fields on the Barents Sea.

of the field was not found. The geothermal characteristic of the rock is shown in Figure 5-19. Figure 5-19 shows the zone of hydrate formation in the area of the field is 180–330 m for methane hydrate and 550–640 m for a Δ0.6 gas. Notice that an HFZ for methane in this region is 240 km away from shore and 50 km away from shore for a Δ0.6 gas. Thus, all engineering objects, including product pipelines constructed in the region of the field have to be designed, constructed, and operated to account for the possible phase transitions in carrying rock and capacity and thermomechanical properties of hydrates.

A hydrate formation zone in bottom rock starts from the surface of a sea bottom. Special attention should be paid to the points of intersection between HFZ boundaries (points A and C, Figure 5-19) where excess strains may develop in pipelines. As seen from Figure 5-19, the lower boundary of an HFZ has a shape which depends on P-T conditions in a profile. Below the lower boundary of an HFZ (impermeable for gas) dome-like traps form under certain conditions in which free gas deposits may accumulate. In a number of cases, such deposits can have gas reserves of industrial significance.

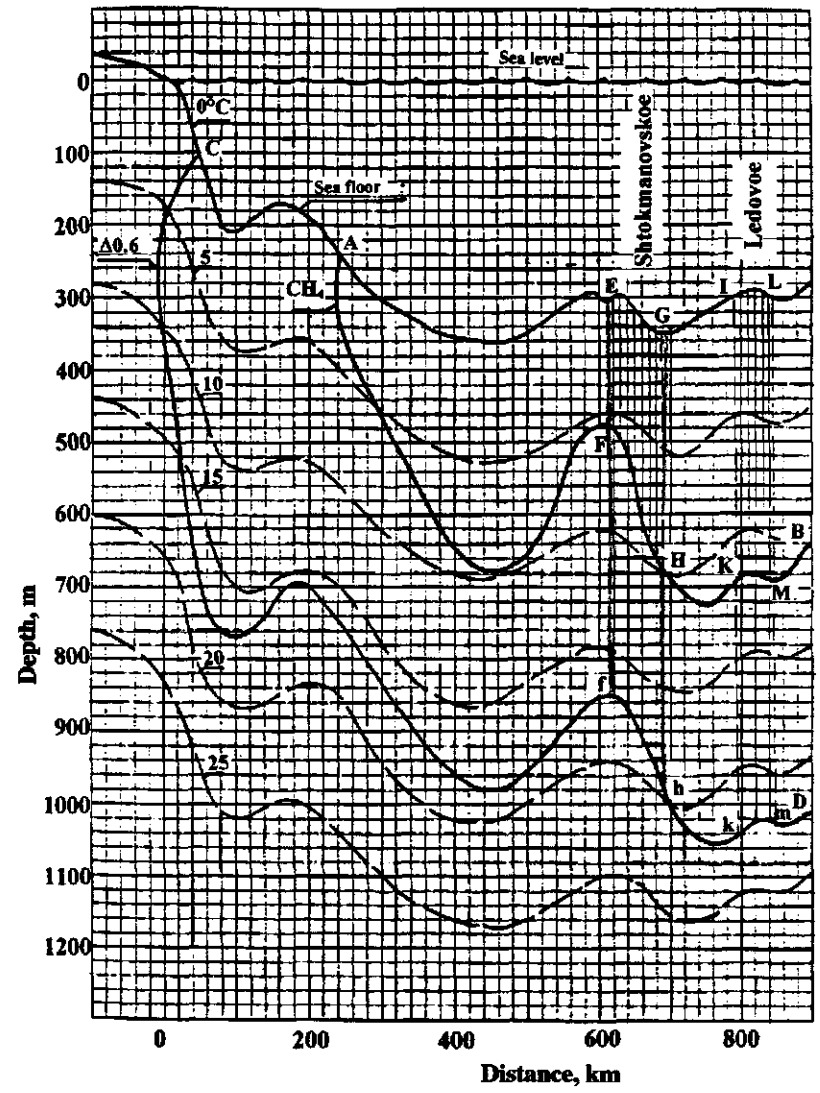

Figure 5-19 Cross-section through Shtokmanovskoe and Ledovoe fields in the Barents Sea.

Figure 5-20 shows the dependence of natural gas hydrate formation conditions (the CH_4 curve for methane and the Δ0.6 curve for a natural gas with relative density of 0.6). The conditions of hydrate formation in wells are also shown in this figure—the curve T_p. The curve of the geothermal gradient in the region of the field is labeled H. As seen from the curves, it

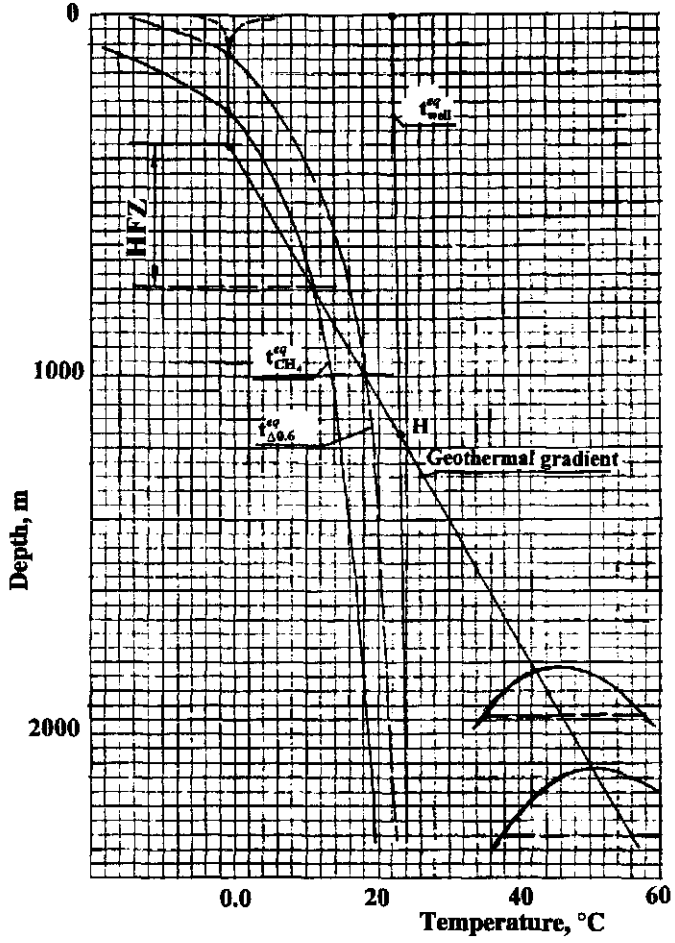

Figure 5-20 Hydrate formation condition in the Shtokmanovskoe field wells.

(HFZ) hydrate formation zone for a sea bottom deposit; ($t^{eq}_{CH_4}$) hydrate formation curve for CH_4; ($t^{eq}_{\Delta 0.6}$) hydrate formation curve for natural gas $\Delta 0.6$; (t^{eq}_{well}) hydrate formation temperature for shutdown well.

is necessary to take measures for the prevention of hydrate formation in well bores in all wells during the period of their mastering, testing, and conservation. Over the whole period of the field development, hydrates also may form in pipelines which connect the wells to a platform.

The dew point of water has to be lower than the minimum operating temperature in a product pipeline for a gas transported to shore terminals

after separation and drying on platforms. The operating temperature in a pipeline has to be below the temperature of hydrate decomposition in carrying (bottom) rock, especially in near-platform areas.

The majority of wells will operate in a hydrate regime but it is necessary to use means to prevent hydrate formation in well bores. During the period of well shutdowns hydrates may form in well bores at depths of up to 1000 m.

During the use of inhibitors the amount of inhibitor injection must be determined both by the conditions in a well and in pipelines which connect wells to a platform (Chapter 3).

Effect of Hydrate Formation Zone on Regional Tectonics

Although the major parameters which determine the change of an HFZ thickness in seas are changes in sea bottom temperature and in thermal gradient, a change of sea level in a number of regions can result in serious tectonic shifts, particularly underwater landslides, etc. Let us consider the conditions of formation of three landslides in the Sea of Norway which occurred approximately 30,000 and 7,000 years ago (Bugge et al., 1987).

Initial Information

A change in the temperature of the earth's surface in time is presented in Figure 5-4 (Makogon, 1980). As seen from the graph, in the last 100,000 years the average temperature on earth's surface has decreased several times below 12°C—below the limiting temperature of large glaciation accompanied by a change in the level of the ocean. Figure 5-3 (Gagliano et al., 1977) shows a graph of sea level change in the last 60,000 years, and Figure 5-5—during the Phanerozoic (Sloan, 1990). A good correlation between the temperature of the earth's surface and the sea level can be seen from comparing the curves in Figures 5-3, 5-4, and 5-5.

Amplitude of sea level variation in separate regions could differ by tens of meters because of regional tectonic shifts. Figures 5-3 and 5-5 show the sea level decreased to 125 m and the temperature of water near sea bottom remained practically constant at +1°C.

Figure 5-21 shows a profile of an active zone in the Sea of Norway (Bugge et al., 1987) where landslides developed. An analysis of the dynamics of hydrate accumulations and existing conditions in a rock profile in the specified region can help determine the cause of landslide development in this region.

The P-T situation in the Sea of Norway corresponds to the existence of methane hydrate in bottom sediments, starting with sea depths of 260–280 m. At sea depths of 1000 and 1500 m, a zone of hydrate formation for methane is 300 m and 350 m, accordingly. The sea bottom slope is 0.017 starting with a 260 m depth isocontour at a distance of 90–150 m. During the lowering of the sea level by 10–25 m, a zone of metastable hydrate state forms at the lower boundary of hydrate-saturated rock in an HFZ. A slow process of hydrate decomposition takes place. Free gas is released. The pressure of gas released from a hydrate is approximately 720 atm, which is much higher than hydrostatic and rock pressure. The intensity of hydrate decomposition and the release of a high pressure free gas in a metastable zone (ABDT, Figure 5-21) sharply increases during shaking of a rock profile. An effect of water boiling in a kettle occurs during shaking of a water ready to boil, evolution of vapor bubbles into water sharply increases.

Microbubbles of evolving high pressure gas rather freely enter near-bottom water in the interval AB, Figure 5-21 where an impermeable

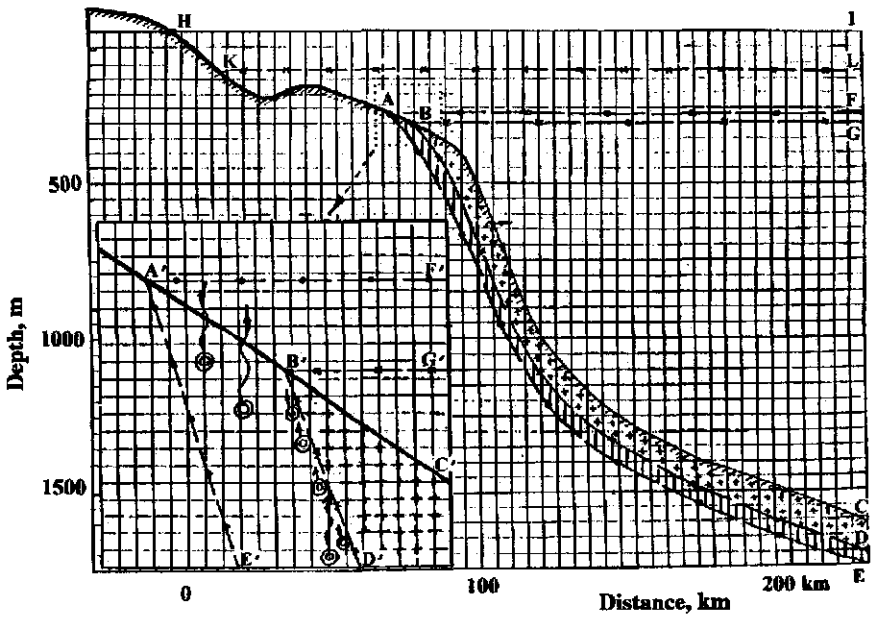

Figure 5-21 Cross-section of the Storegga Slide with metastable zone of hydrates.

(FAE) hydrate formation zone; (BDC) stable hydrate deposit; (A'B'–E'D' - metastable hydrate deposit; (ADE) metastable hydrate deposit; (HI–KL) difference in sea level (B'–C'–D') stable hydrate deposit.

hydrate cover is absent. However, at depth BC, Figure 5-21 there is an impermeable hydrate cover. The energy of gas bubbles released during decomposition of hydrates is consumed to expansion and moving of bubbles themselves, to moving (displacing) of pore water, to breaking of cementing bonds of carrying rock, to rising of overlying hydrate-saturated rock. In the presence of a slope, gravity may overcome friction in the overlying massive at a metastable boundary of a hydrate and the massive will start to slide down gaining speed and mass (Figure 5-22). An underwater landslide on a gas cushion of high pressure develops. In favorable conditions, the thickness of the metastable hydrate layer, which ensures the development of a large landslide, may be just a few centimeters.

Hydrate decomposition in a metastable layer at the lower boundary of an HFZ is especially active during geological vibrations (earthquakes, tectonic shifts). Technogenic vibrations–explosions, drilling, etc., also may initiate landslides on ocean slopes. The size of landslides may reach hundreds of kilometers in length and in width. The thickness of sliding rock may reach several hundred meters destroying every engineering object in the slide area. It is extremely important to know the geodynamic and thermodynamic situations in the regions of engineering development of slope regions in zones of hydrate formation.

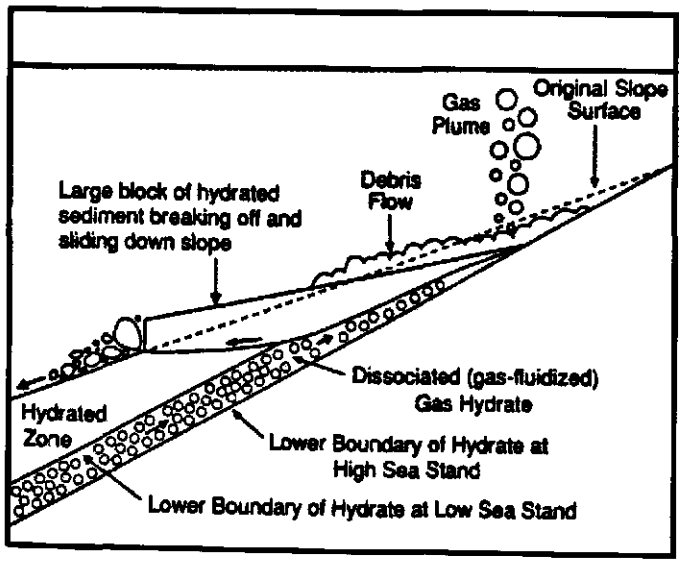

Figure 5-22 Diagram showing the effect of changes in pressure and temperature on submarine gas hydrate and the resulting sea floor failures and gas release (Kvenvolden, 1994).

In conclusion, favorable conditions for underwater landslides within shelf slopes exist in many regions. If we take a look at the profile presented in Figure 5-19 then it is obvious that barometric conditions for the development of landslides exist in the Barents Sea in the area of Shtokmanovskoe field at sea depths of 250 m for methane hydrate and 100 m for a Δ0.6 gas.

Locating Hydrate-Bearing Rock

Knowledge of the P-T zone of hydrate formation (HFZ) in a profile of rock does not mean that the whole interval of an HFZ is filled with gas hydrates. In porous sedimentary rock at P-T conditions of hydrate formation, the coefficient of hydrate saturation may vary between 0 and 1. The hydrate saturation coefficient and the properties of a pure hydrate determine many parameters of a rock profile in an HFZ-content of gas per unit volume, strength characteristics, acoustic permittivity, electrical resistivity, thermodynamic properties–heat capacity, thermal conductivity, permeability, density of hydrate-saturated rock, etc.

These specialties of hydrates and hydrate-saturated rock are laid in the basis during creation of instrumental search and surveying of gas hydrate accumulations by remote and direct contact methods. Gas hydrates are characterized by high electrical resistivity and acoustic permittivity (V_p, km/s). For water V_p = 1.478 km/s.

Natural hydrates whose massive samples were raised from near-bottom sediments had a sonic velocity of 3.1–4.4 km/s during testing, which is significantly higher that the sonic velocity in usual bottom sediments in which $V_p = 1.6^{-2}$ km/s. It was determined that V_p in porous rock filled with gas hydrates is 1.5^{-2} times higher than in a similar rock filled with gas and water (Max, 1990).

The density of natural hydrates is close to 0.9 g/cm^3, and the density of carrying sedimentary rock is 1.5–2 g/cm^3. Figure 5-23 shows the dependence on density of sonic velocity in a water-saturated rock (Dinakaran, 1994).

Hydrates in a rock mass have the maximum acoustic permittivity. In real conditions hydrate-saturated rock is often in direct contact with gas-saturated rock characterized by a minimum acoustic permittivity. In this case, if an HFZ is located under the sea and a hydrate-saturated rock is located in bottom sediments below which gas-bearing layers are located, then the diagram of acoustic permittivity looks like that presented in

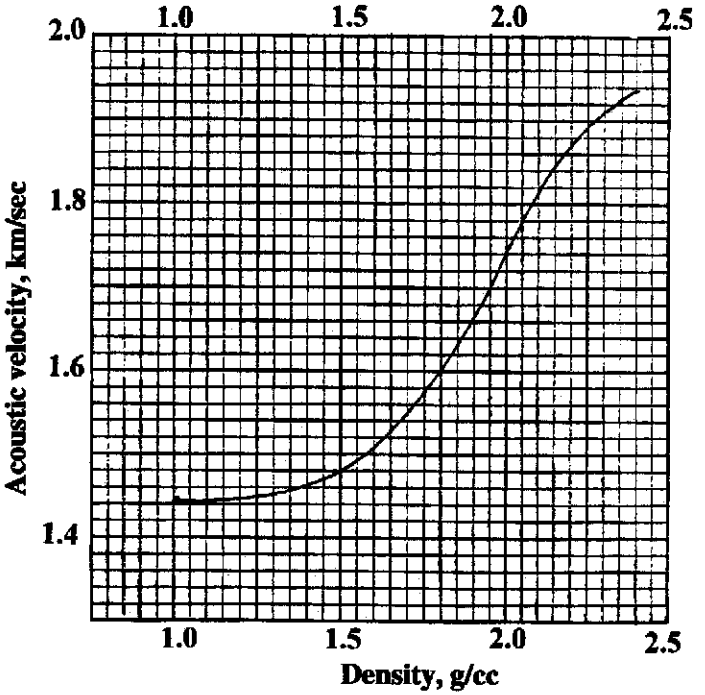

Figure 5-23 Plot of density and acoustic velocity, *v*.

Figure 5-24. Curve AB represents sonic velocity in water; BCKL—sonic velocity in sedimentary cover (BC—water-saturated layer of sediments above hydrates); DE—sonic velocity in a hydrate monolith; FG—sonic velocity in hydrate-saturated rock in which hydrate content is at least 30–40% which provide an impermeable cover for a free gas accumulating under a hydrate-saturated rock; HI—sonic velocity in a gas deposit below hydrate; KL—sonic velocity in a water-saturated profile of rock.

Having obtained such dependence in real conditions for a certain profile, the hydrate saturation coefficient of rock in an HFZ can be determined, and knowing the composition of a hydrate and a lateral spreading of gas hydrate accumulations, the reserves of gas in a gas hydrate deposit can be determined.

Figures 5-25, (a) and (b) present typical seismic logs on which the lower boundary of hydrate saturated layers—bottom simulating reflector (BSR) stands out. Also the gas-water boundary of an underlying gas deposit which formed under an impermeable hydrate cover stands out.

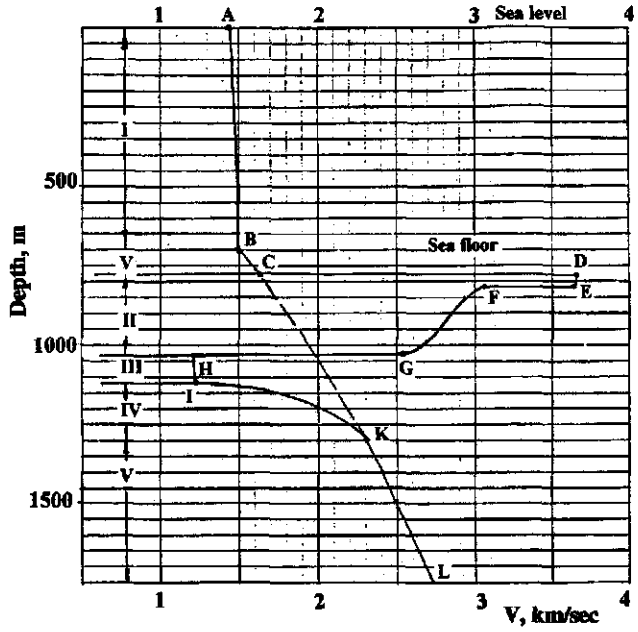

Figure 5-24 Geoacoustic (*Vp*) profile. (I) water; (II) gas hydrate layers; (III) free gas field; (IV) gas saturated sediments; (V) fluids in pore spaces.

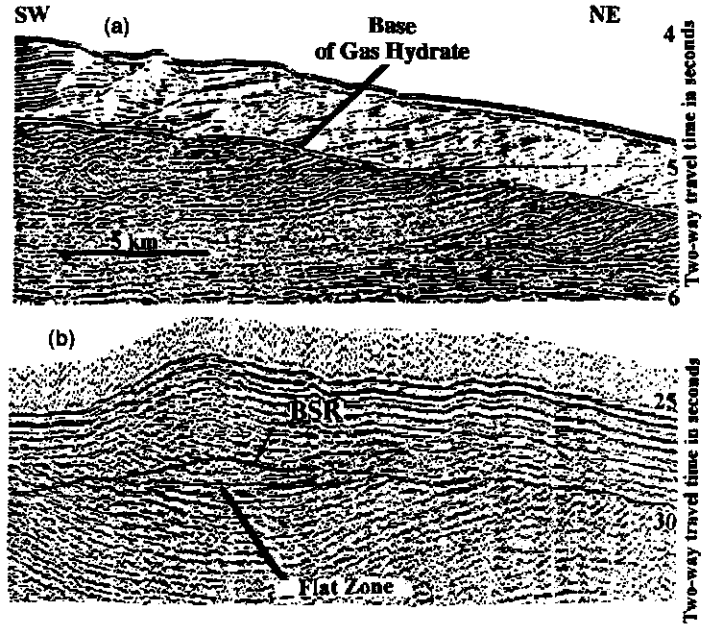

Figure 5-25 Bottom simulation reflector.

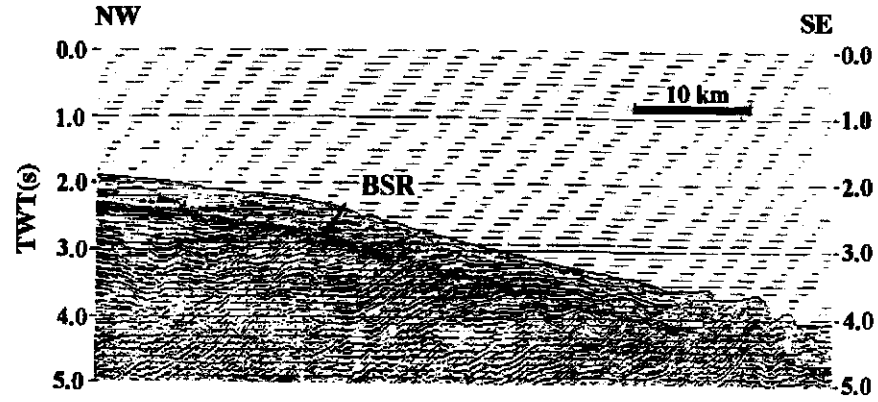

Figure 5-26 BSR on a Rio Grande slope near Brazil.

Figure 5-26 presents a similar seismic log taken in the Atlantic Ocean on a Rio Grande slope near Brazil. As seen from the seismic log, gas hydrate accumulations can be seen in this region for over 70 km (Fontana and Mussumeci, 1994).

Many natural gas hydrate accumulations were revealed in four oceans and on three continents based on the results of seismoacoustic probing, well drilling, core sampling and geophysical logging. Figure 5-27 presents regional schematic maps of gas hydrate deposits found in the Black Sea (Stupak, 1992). Figure 5-28 shows the map of gas hydrate deposits found around Japan (Okuda, 1996).

Electrical Conductivity of Hydrates

Hydrates are characterized by a high electrical resistivity. Figures 2-4 and 2-5 present some of the results of a study on electrical resistivity of hydrate-saturated rock. Figure 5-29 presents an actual curve of electrical resistivity in a profile of rock on which a hydrate-saturated interval is clearly indicated (Matthews et al., 1985).

There is a strong correlation between acoustic permittivity (V, km/s) and electrical resistivity of rock in a profile (λ, Ohm/m). A graph of electrical resistivity and seismic waves velocity in hydrate-saturated layer dependence is shown in Figure 5-30. If the product $V \times \lambda \geq 100$ then hydrate exists in a profile. The larger the product $V \times \lambda$, the larger the coefficient of hydrate saturation. An accurate interpretation of these two parameters allows us to determine one of the major parameters—coefficient of hydrate saturation of rock in a profile as a whole and in separate layers. If

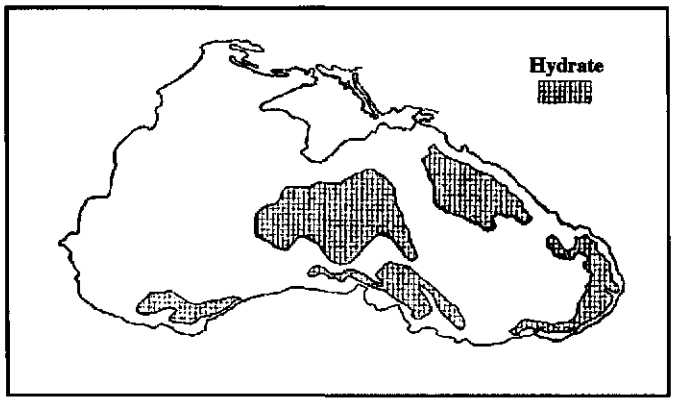

Figure 5-27 Location of gas hydrate fields in the Black Sea.

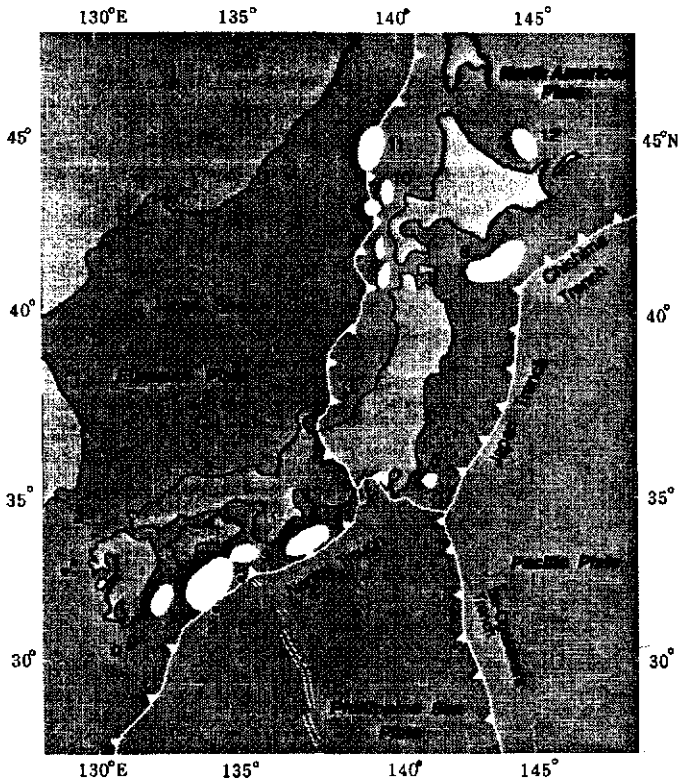

Figure 5-28 Location of gas hydrate fields in the Japan offshore.
1: Miyzaki; 2: Kochi; 3: Kii Strait; 4: Omaezaki-Kumano; 5: Boso; 6: Tokachi Hidaka; 7: Nishitugaru Basin; 8: Okushiri Basin; 9: Okushiri Ridge; 10: Shiribeshi Trough; 11: Tartary Trough; 12: Abasshin (Okuda, 1996).

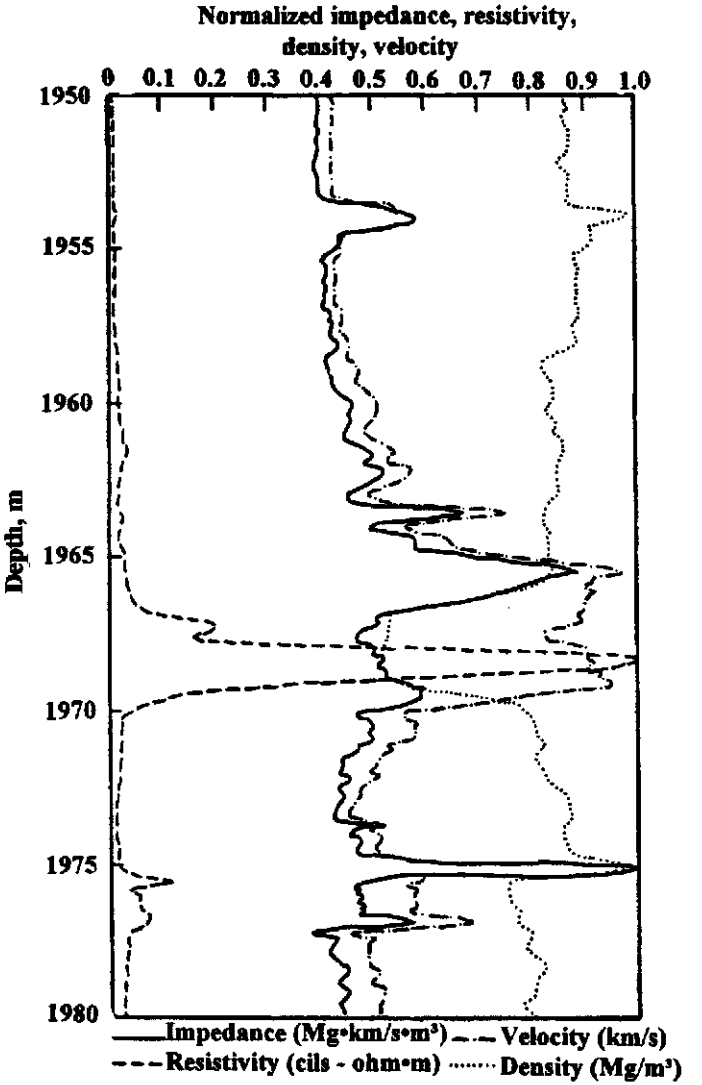

Figure 5-29 Some well logs at DSDP Site 570 (reproduced courtesy of U.S. Government, Mathews and von Huene, 1985).

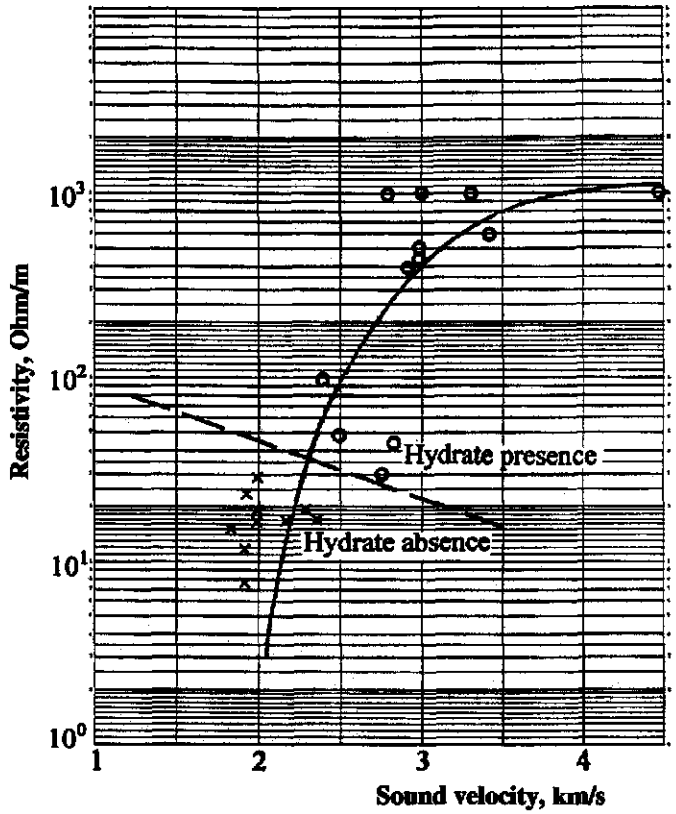

Figure 5-30 Resistivity and sound velocity in deposits depends on hydrate saturation.

$V \times \lambda \sim 400$, then the coefficient of hydrate saturation $H_S \sim 1$, i.e., there are layers of pure hydrate.

Permeability of Hydrate to Gas and Water

A monolith hydrate is practically impermeable to gas and water. Hydrate forming and accumulating in a pore space of granular rock blocks the channels of fluid migration (Bulavinov, 1964; Naden et al., 1988; Curtis et al., 1993).

Definition of a core permeability to gas K_G is described by the equation:

$$K_G = \frac{29.4 \times P \times Q \times \mu_G \times L}{F(P_1^2 - P_2^2)}, md \qquad (5.8)$$

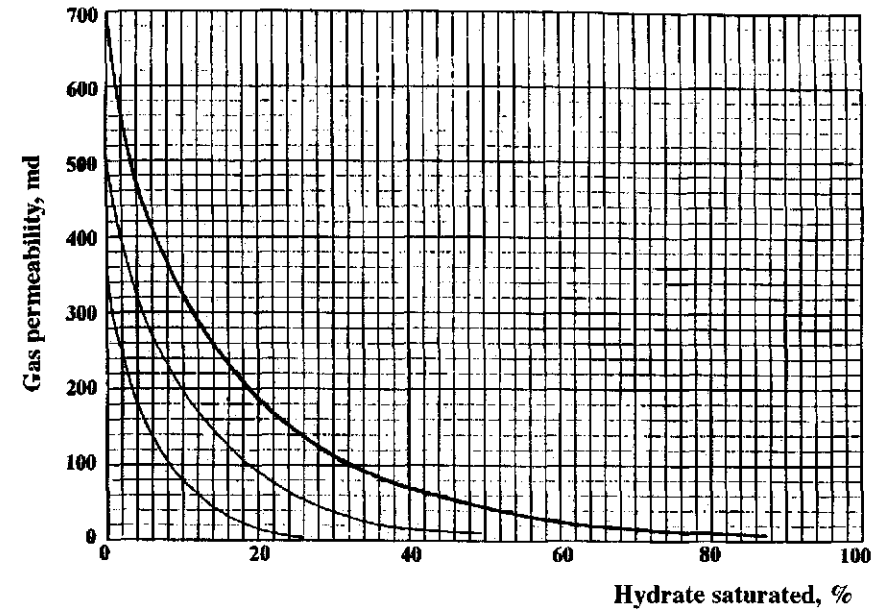

Figure 5-31 Gas permeability of hydrate saturated sample.

where

- P is the average pressure in a sample of length L and cross section F, cm^2; $P = (P_1 + P_2)/2$;
- P_1 is the sample inlet pressure;
- P_2 is the sample outlet pressure;
- Q is the average flowrate of gas through a sample at a pressure drop $P_1 - P_2$, cm^3/s;
- μ_G is the gas viscosity.

Figure 5-31 presents a number of curve decreases in core permeabilities depending on their saturation with gas (Naden, 1988). The slope of these curves depends on multiple factors: structure of porous matter, initial saturation with water and with gas, pore size, and time of hydrate accumulation, etc.

In real conditions at a coefficient of hydrate saturation of 25–35% of porosity, a rock is practically impermeable to free gas. Lateral migration of water is easily blocked. The process of migration of gas and water through a layer becomes a molecular diffusion process. Hydrate saturated

layers become lithological covers below which large deposits of oil and gas may form. This is a new statement in genesis of hydrocarbon deposits since it was traditionally thought that impermeable lithological covers were required for the formation of hydrocarbon deposits.

Low heat conductivity of hydrates also can be used effectively for well logging and for a remote contouring of gas hydrate accumulation in sedimentary cover of rock by logging the heat flow in a region. A decrease of a heat flow is characteristic above gas hydrate accumulations. The thicker a layer of gas hydrate saturated rock, the higher is a total heat flow in a region, and the higher the contrast at a gas hydrate deposit (GHD) boundary—a heat funnel is noticed above a GHD. Figure 5-32 presents a curve of rock thermal conductivity depending on density of rock, and Figure 2-8 shows the dependence of thermal conductivity of hydrates, hydrate

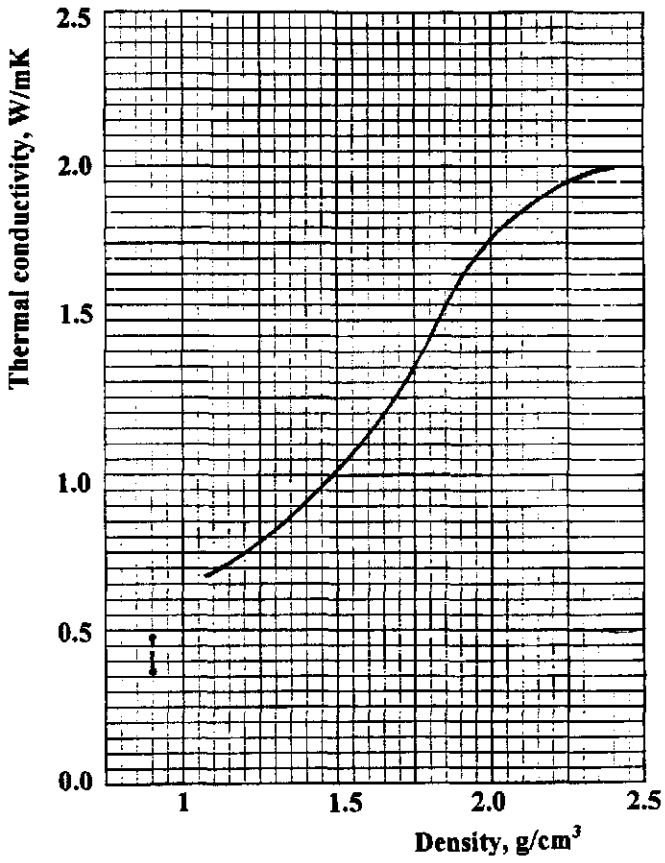

Figure 5-32 Plot of density and thermal conductivity.

saturated rock, ice and pure water. Layers of pure hydrate are clearly distinguished by logging in thermal conductivity, electrical resistivity, acoustic permittivity, and density, etc.

Well Logging

Locating remote gas hydrate deposits requires a detailed survey which is accomplished by a complex logging in wells which uncovered HFZs in the boundaries of located gas hydrate accumulations. A generalized characteristic of logging curves obtained using standard geophysical tools is shown in Figure 5-33. Anomalies of geophysical parameters caused by the presence of hydrates in layers and by hydrate properties are clearly indicated on the presented curves.

During interpretation of logging data it is necessary to consider that the electrical resistivity of gas bearing rock and of hydrates contained in a pore space goes to infinity because of the absence of any electronic ionic conductivity in them, while the electrical resistivity of pore water is determined only by its salt content.

Neutron properties of water and hydrates can be equated because methane hydrate and water contain practically the same number of protons which is close to 68×10^{21} per cm^3. The difference in their densities

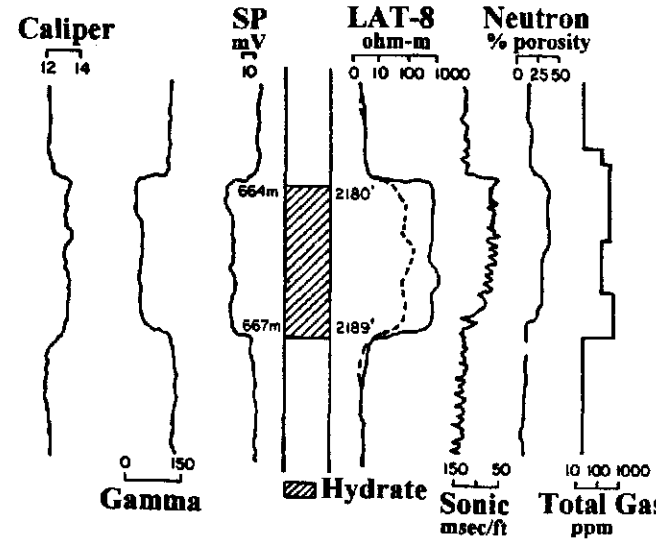

Figure 5-33 Typical well log responses to hydrates in permafrost (Collett, 1983).

does not exceed 10% which allows us to assume the total length of migration of neutrons and γ-quanta of radioactive capturing to be practically equal for hydrate and water.

Hydrate-bearing layers are characterized by insignificant anomalies of the natural electromagnetic field. A significant decrease in the amplitude of spontaneous polarization (PS) compared to gas saturated and water-saturated layers is related to the fact that, by plugging pores, hydrates decrease the intensity of diffusive and filtration processes. Besides cavities of increased size which form as a result of developing stresses during the formation and decomposition of hydrate in layers' pores and released during drilling, hydrate-bearing layers are marked on microprobe diagrams by very small increases in probe micropotential (PMP) over probe microgradient (PMG), i.e., these layers are noted as dense. This is related to a decrease in the permeability of layers which contain hydrate.

A specific electrical resistivity of a gas layer is significantly lower than that of a hydrate layer. The amplitude of PS for a gas layer is several times higher than for a hydrate layer. A presence of loamy crust is characteristic for a gas layer, while a presence of cavities is characteristic for a hydrate layer.

An increase in a probe micropotential over a probe microgradient is characteristic for a gas layer, whereas this increase is much smaller for a hydrate layer. Secondary gamma-activity is much higher for a free gas layer compared to a hydrate layer.

A detailed profile survey usually is performed to determine the thickness of interstitial layers and their saturation with gas and with hydrate during location of hydrate saturated layers in an HFZ. Core samples taken from an interval of hydrate-saturated layers are also closely studied. The rate of drilling and gas logging are analyzed. Usually, the rate of drilling during the uncovering of hydrate saturated layers decreases, and the gas content in a drilling mud significantly increases. Repeated timed logging usually provides a more certain confirmation which is related to decomposition of hydrate, relocation of a phase transition boundary from well walls into a layer.

A difference between the results of regular short-term logging and timed logging is explained by the consumption of a drilling mud by a zone saturated with hydrocarbons or by fresh water. Separation of a hydrate-saturated zone and a gas-saturated zone is made using the potential of a spontaneous polarization of a diagram of a two-probe induction logging.

A noticeable decrease in the peak of a spontaneous polarization potential can be seen on a diagram of a two-probe induction logging during comparison with the deviation of a specific resistivity inside a hydrate zone.

This is related to a decrease in filtration of drilling mud into a hydrate-saturated layer. Well logging also generates good information on acoustic permittivity and on electrical resistivity (Figures 5-24, 5-29, and 5-30).

Several surveys made by expeditions on land and in sea allowed us to locate over 60 large gas hydrate deposits with reserves of natural gas of over 700 trillion m^3 (Figure 1-4). Notice that only large accumulations of hydrate are shown on this map; no separate fields are shown. For example, in a sea near New Zealand nearly ten separate gas hydrate deposits were located which are shown on the map as a single point.

The data on gas hydrate deposits discovered in sea are shown in Table 5-3 (Kvenvolden et al., 1993). Of course, this is just the beginning of an era of revealing the development of gas hydrate resources, especially if compared to the history of mastering oil and gas resources. In 50–100 years our colleagues will remember with a smile and gratitude the pioneers of the gas hydrate epoch.

Estimation of Gas Reserves in a Gas Hydrate Deposit

It is necessary to know the volume of gas in a hydrate state in a profile of rock, not only for determining the energy resources in a specific region, but a detailed study of hydrate saturation of rock in a zone of hydrate formation is needed for forecasting the properties of a profile of rock in an HFZ, for choosing a proper technology during engineering of a region, construction of wells, construction of engineering objects built in an HFZ—basements of platforms, pipelines, etc., and below an HFZ. The higher the coefficient of hydrate saturation of rock, the larger the energy resources that are concentrated in this region.

Attention has to be given during engineering mastering of rock with a high hydrate saturation to the initial information about the properties of a profile, about their manifestation during changes in P-T conditions—during well drilling, operation of wells, pipelines, etc. An insufficient study of a profile may result in a serious emergency with severe consequences and tremendous economic loss. For example, a large accumulation of a free gas, which should not exist according to all geological signs, can reside below a hydrate layer. Uncovering such a deposit without the appropriate safety measures is related to an open fountain which is extremely difficult to remove using conventional methods. As a result, large sums of money can be lost and ecological harm can be done to a

Table 5-3 Summary of known and inferred gas-hydrate occurrences (Kvenvolden, 1994).

Designation	*Location*	*Evidence*
Onshore Deposits		
A	Messoyakhi (Siberia, Russia)	Samples
B	Ust'-Viliui (Siberia, Russia)	Samples
C	Pechori (Siberia, Russia)	BSR
D	Prudhoe Bay	Samples
E	Kuparuk	Samples
F	Resolute	Samples
G	Mastakh (Siberia, Russia)	Samples
Offshore Deposits		
Pacific Ocean		
P1	Panama	BSR
P2	Costa Rica (Middle America Trench)	BSR, Samples
P3	Nicaragua (Middle America Trench)	BSR
P4	Guatemala (Middle America Trench)	BSR, <Cl^-, Samples
P5	Mexico (Middle America Trench)	BSR, Samples
P6	Mexico (Gulf of California, Guaymas Basin)	BSR
P7	California, USA(Ed River Basin)	BSR, Samples
P8	Oregon, USA (Cascadia Basin)	BSR, Samples
P9	Vancouver Island, Canada (Cascadia Basin)	BSR
P10	Alaska, USA (Eastern Aleutian Trench)	BSR
P11	Alaska, USA (Middle Aleutian Trench)	BSR, <Cl^-
P12	Alaska, USA (Bering Sea)	VAMPs
P13	USA and Russia (Beringian Margin)	BSR
P14	Russia (Shirshov Ridge)	BSR
P15	Paramushir Island, UFRR (Okhotsk Sea)	Samples
P16	Japan (Japan Sea)	Sample
P17	Japan (Japan Trench)	<Cl^-
P18	Japan (Nankai Trough)	BSR, Sample
P19	New Zealand (Hikurangi Trough)	BSR
P20	Chile (Peru-Chile Trench)	BSR
P21	Peru (Peru-Chile Trench)	BSR, Samples
P22	Sahkalin Island, Russia (Okhotsk Sea)	Samples
Atlantic Ocean (including Black Sea)		
A1	Argentina (Central Argentine Basin)	BSR
A2	Brazil (Amazon Fan)	BSR
A3	Barbados(Barbados Ridge)	BSR
A4	Southern Caribbean Sea	BSR
A5	Panama and Colombia (Colombia Basin)	BSR
A6	Mexico (Western Gulf Of Mexico)	BSR
A7	Southern USA (Gulf of Mexico)	Samples

Table 5-3 continued

Designation	*Location*	*Evidence*
A8	Southeastern USA (Blake Outer Ridge)	BSR, Sample, <Cl^-
A9	Eastern USA (Carolina Trough)	BSR
A10	Eastern USA (Continental Rise)	BSR
A11	Newfoundland, Canada (Labrador Shelf)	BSR
A12	Norway (Continental Slope)	BSR, <Cl^-, Gas
A13	Crimea, Ukraine (Black Sea)	Samples
A14	Caucasus, Russia (Black Sea)	BSR
A15	Turkey (Black Sea)	BSR
Indian Ocean		
I1	Oman (Gulf of Oman, Makran Margin)	BSR
North (Arctic)		
N1	Alaska (Beaufort Sea)	BSR
N2	Canada(Beaufort Sea)	Logs
N3	Canada (Sverdrup Basin)	Logs
N4	Norway (Parents Sea)	BSR
N5	Svalbard (Fram Strait)	BSR
N6	Shtokmanskoe	BSR
South (Antarctic)		
S1	Antarctica (Wilkes Land Margin)	BSR
S2	Antarctica (Ross Sea)	Gas, <Cl^-
S3	Antarctica (Weddell Sea)	BSR
Other		
O1	Caspian Sea, Azerbaijan	Samples
O2	Lake Baikal, Russia	BSR

BSR, bottom-simulating reflection; < Cl^-, low chloride content of pore water; VAMPs, velocity amplitude pulldowns; Logs, well-log response.

region. Neither time nor materials to obtain reliable information about a profile of rock should be economized in an HFZ, since much larger sums will be spent to remedy the results of this lack of initial information.

Besides knowing a coefficient of hydrate saturation in a profile of rock, it is necessary to know the structure and type of hydrate inclusions. Hydrate inclusions in a profile of sedimentary rock can exist as fine-dispersed when the size of inclusions does not exceed the size of pores; dispersed—the size of inclusions exceeds the pore size, but there are no mechanical changes to a porous rock; nodular inclusions—the size of hydrate inclusions is larger than pore size and there are local structural

changes in carrying rock; lens-like inclusions between interstitial layers of rock with breaks in connections between layers; layer inclusions of large thickness and extent.

Nodular inclusions have a size from several millimeters to several tens of centimeters. Lens-like inclusions can have a thickness from several millimeters to tens of centimeters, and up to tens of meters in extent. Layer inclusions can reach a thickness from several centimeters to several meters and even tens of meters in favorable conditions of accumulation and storage, and from several hundreds of meters to several hundreds of kilometers in extent. Figure 5-26 presents a seismic profile of hydrate saturated rock in seas off Brazil with a length of about 700 km (Fontana and Mussumeci, 1994). Usually, hydrate lenses and layers exist between well permeable granular rock with a large thickness of generating layers.

A single volume of hydrate may contain different volumes of gas prorated for normal conditions, depending on hydrate composition and structure. The volume of gas in a volume of hydrate is determined by the expression:

$$Q_h = \frac{V_g \times \delta \times 10^3}{M_h}, m^3 \qquad \textbf{(5.9)}$$

where

V_g is the volume occupied by hydrate, m^3;

δ is the hydrate density (see Section 2);

M_h is the mass of hydrate.

A mass of hydrate $M_h = M_G \times n \times H_2O$ where M_G is a molecular weight of hydrate forming gas, n is the number of moles of water per a mole of gas in hydrate. In natural conditions, when hydrates form by a biogenic methane in bottom sediments, the value of n is 6.0–5.8; the magnitude of n may reach values of 7–12 or more during hydrate formation by depth catagenetic gases.

Let us consider an example of biogenic hydrate when n = 5.9 and hydrate former composition is close to methane (a volume of gas is equal to 22.4 m^3). At a density of hydrate δ = 900 kg/m^3, N moles of hydrate are contained in one cubic meter:

$$N = 900/M_h = 900/122 = 7.377,$$

and the volume of gas prorated for normal conditions contained in one m^3 of hydrate is:

$$Q = N \times 22.4 = 165.2 \text{ m}^3.$$

Knowing the volume of hydrate-saturated rock, structure of pores, content of free water and free gas and content of gas dissolved in water, the reserves of gas in a specified profile can be determined. Reserves of gas in a deposit which contains gas partially or completely in a hydrate state are determined by an equation:

$$Q = Q_G + Q_h + Q\lambda, \qquad \textbf{(5.10)}$$

where

Q is the total reserves of gas in a deposit, m^3;

Q_G is the reserves of gas in a free state, m^3;

Q_h is the reserves of gas in a hydrate state, m^3;

Q_λ is the reserves of a dissolved gas, m^3.

Reserves of free gas depend on a free volume of pore space, pressure and temperature. They are determined using an expression:

$$Q_G = V \times m \frac{PT_0}{P_1 T \times z}[1 - S_W(S_h V_h - S_h)] \qquad \textbf{(5.11)}$$

where

V is the volume of a deposit, m^3;

m is the total porosity of rock in a productive part, fraction of deposit volume;

P is the layer pressure, MPa;

T is the layer temperature, K;

z is the compressibility of free gas in a deposit;

S_W is the total content of pore water, fraction of m;

S_h is the part of pore water transformed into hydrate, fraction of S_W;

ϕ - coefficient of response, equals to the ratio of the number of volumes of gas at normal conditions per volume of water contained in one mole of hydrate;

λ is the solubility of gas in water being in contact with hydrate (see Chapter 1).

$$Q_h = V \times m \times S_W \times S_h \times \phi \qquad \textbf{(5.12)}$$

Reserves of gas dissolved in a free pore water:

$$Q_\lambda = V \times m \times S_W \times (1 - S_h) \times \lambda \qquad \textbf{(5.13)}$$

Figure 5-9 shows the comparison of volumes of gas contained in deposits of equal volume in a free and in a hydrate state (for methane hydrate). It can be seen from this figure we see that at depths up to 1.5–1.7 km in a gas hydrate deposit there are always larger reserves of methane than in a gas deposit of the same size. The amount of methane can be several times higher in a hydrate deposit.

The Role of Natural Gas Hydrates in Global Changes

Humans as a product and a part of nature remained in relative balance with the environment during the pre-industrial period. An intensive population growth and especially a growth of energy consumption promoted a disbalance of natural and antropogenic processes. Antropogenic activity exerts an ever increasing influence on the global processes taking place on our planet. Natural gas hydrates actively affect global changes both as a natural object and as a result of antropogenic activity.

Natural gas hydrates are one of the most widespread minerals present on our planet in a metastable state. The main components of natural gas hydrates are water and methane. The mass of methane in hydrates exceeds 10^4 Gt. However, 99% of hydrates are accumulated under sea, mostly in a transition zone shelf—oceanic slope. If the total volume of natural gas hydrates decomposed, the average radius of earth would have decreased by 8 cm. Local depressions of the level of sedimentary rock may reach 100–160 m. Wide spreading properties of hydrates exert a significant effect on many regional and global processes.

The main aspects of the influence of gas hydrates on global changes are:

- change in atmospheric composition;
- change in thermal regime of earth;
- activation of seismic processes;
- dynamics of geoelectric field;
- dynamics of hydrocarbon deposits;
- dynamics of Arctic shores and the level of the ocean bottom, etc.

The metastable state of methane hydrate ensures its active response to changes in a thermodynamic situation in the regions of hydrate accumulation which is accompanied by an influx of tremendous volumes of free methane into the atmosphere with all ecological consequences. On the other hand, gas hydrates possess a number of unique properties which ensure their influence on the temperature balance of earth, the dynamics of its surface, and the geography of its shore line in sub-Polar regions.

Gas hydrates have actively influenced the formation of earth as a planet, the formation of its atmosphere, hydrosphere, and continue to affect the formation and stability of hydrocarbon deposits (Trofimuk et al., 1983).

The sources of methane in the atmosphere are the least studied question in the problem methane-ecology. In this section only one of the most important sources is reviewed, gas hydrates, and a comparison is made for the effects of methane and other greenhouse gases. All components of the atmosphere make a certain contribution to its thermal regime by reflecting or by absorbing long-wave radiation and by increasing the temperature of earth's surface.

Methane affects the greenhouse effect of earth by several tens of times more aggressively than CO_2 (Rasmussen et al., 1989). The mass content of methane in the atmosphere is 140 times smaller than that of CO_2, but its contribution to the greenhouse effect is only 2.7 times smaller. Methane actively absorbs the heat radiation of earth at wave lengths of about 3 and 7 μm, ozone, at about 10 μm, and CO_2—at 2.7, 4.3, and 13-18 μm.

Isotopic analysis showed that over 20% of the methane contained in today's atmosphere was formed in a catagenetic zone in ancient times and comes from coal mines, gas and oil fields, permafrost rock, and depth breaches, etc.

Methane and CO_2 were always in earth's atmosphere. Today the source of methane entering the atmosphere are both natural and antropogenic sources. Table 5-4 presents average masses of methane entering the atmosphere from different sources.

Natural gas makes up about 25% of the total energy balance in the world, and in some countries 40% or more. Production, transportation, processing, and use of natural gas is related to the problem of prevention and removal of gas hydrates which form in the wells, gas and product pipelines, and in technological systems of gas treatment. Modern methods of preventing the processes of formation and removal of hydrates are ecologically negative. Alcohols and electrolytes are more widely used for these purposes in the world. For example, over 200 thousand tons of highly toxic methyl alcohol is used every year in Russia for fighting hydrates during production and transportation of natural gas. Methanol vapor escaping into the atmosphere of industrial buildings result in sharp breathing and sight disorders of service personnel. Methanol entering drinking water and human organisms through regenerative waste systems cause blood disorders in the organs of humans and animals.

Table 5-4 Sources of methane in atmosphere (Raynaud et al., 1988).

Source	*Mass, 10^9 tons/year*	*Fraction, %*
Forests and swamps	115	20
Animals	80	14
Termites	40	7
Oceans	10	2
Fresh water reservoirs	5	1
Soils	40	7
Rice fields	110	19
Drilling, production and Transport of oil and gas	45	7
Waste landfills	40	7
Coal mine gas	35	6
Burning biomass	55	9
Natural gas hydrates	50–500*	8–48

*During tectonic activity in hydrate formation zones.

Discharges of electrolytes from regeneration systems ($CaCl_2$, NaCl, BrCl, etc.) get into ground drinking water, and rivers, and lakes through drains, thus, disturbing the ecological balance in flora and fauna. In addition, practice indicates that the violation of technological regimes of operation of the systems of production, transportation, and processing of natural gas and light hydrocarbons is often accompanied by the formation of large hydrate plugs which results in shutdowns, and sometimes, explosions of technical equipment and pipelines. Removal of large hydrate plugs usually is related to the discharges of large volumes of methane and other components into the atmosphere with all of the accompanying ecological consequences.

A discharge of chemical agents, alcohols and electrolytes into the environment also significantly complicates the ecological situation of a region. For example, at least 2 m^3 of methanol or 4 m^3 of a 30% solution of CaC_2 is required for the removal of a hydrate plug whose volume is 1 m^3 at $T = 273$ K.

A faulty operation of a technological system results in a serious emergency due to hydrates. This can be crumpling or rupture of columns in gas or oil wells, gas or product pipelines, sudden thrust of a drilling mud during drilling of hydrate-saturated rock, or disturbance of well stability in an interval of hydrate saturated layers during their operation.

Table 5-5 Discharge of gases into the atmosphere, thousands of tons/year.

Department	*SO*	*CO*	*NO_2*	*Hydrocarbons*
Minenergo (energetics)	7549	175	2668	9.7
Minchermet (black metallurgy)	1081	6714	455	45.8
Mintsvetmet (color metallurgy)	4482	541	62	4
Minnefteprom (petroleum)	60	988	54	4140
Minneftehimprom (petroleum refining)	519	677	50	2241
Mingazprom (gas)	505	561	245	1358
Other	3456	5242	5451	681

Hydrates are a rock cementing component. During hydrate decomposition rock starts to flow. This is especially dangerous during the construction and operation of platforms and wells in seas where hydrate saturated layers are concentrated in near-bottom rock whose thickness may reach several hundreds of meters.

Significant amounts of methane enter the atmosphere during emergency discharges from wells and pipelines. For example, over 10^9 m^3 of gas went into the atmosphere during a blowout on the Kumzha-9 well which was drilled at the mouth of the Pechera River. Up to 10^7 m^3 of gas goes into the atmosphere during a venting of gas from just one section of a modern pipeline. Up to now in several countries the gas produced with oil is discharged into the atmosphere. Technogenic discharges of gas into the atmosphere have reached a tremendous magnitude. Table 5-5 presents the magnitude of discharges of several gases into the atmosphere by several industrial enterprises of the USSR in 1989.

Methane is the main component discharged. Figure 5-34 presents the dependence of a change in methane, NO_2 and CO_2 content over the period from 1700 until 1990. This information was obtained from an analysis of core samples of ice taken during drilling of wells in the Antarctica and in northern Greenland (Lorius, 1991). As seen from the curves, the rate of growth in CO_2 and NO_2 contents are practically the same, and the increase in methane content in the atmosphere during the industrial period sharply outruns the rates of increase of CO_2 and NO_2.

Technogenic sources of methane in the atmosphere provide an intensive accumulation and also increase the share of methane in the greenhouse effect on earth. Already in future decades the effect of methane in the greenhouse effect on earth may overcome the effect of CO_2, especially

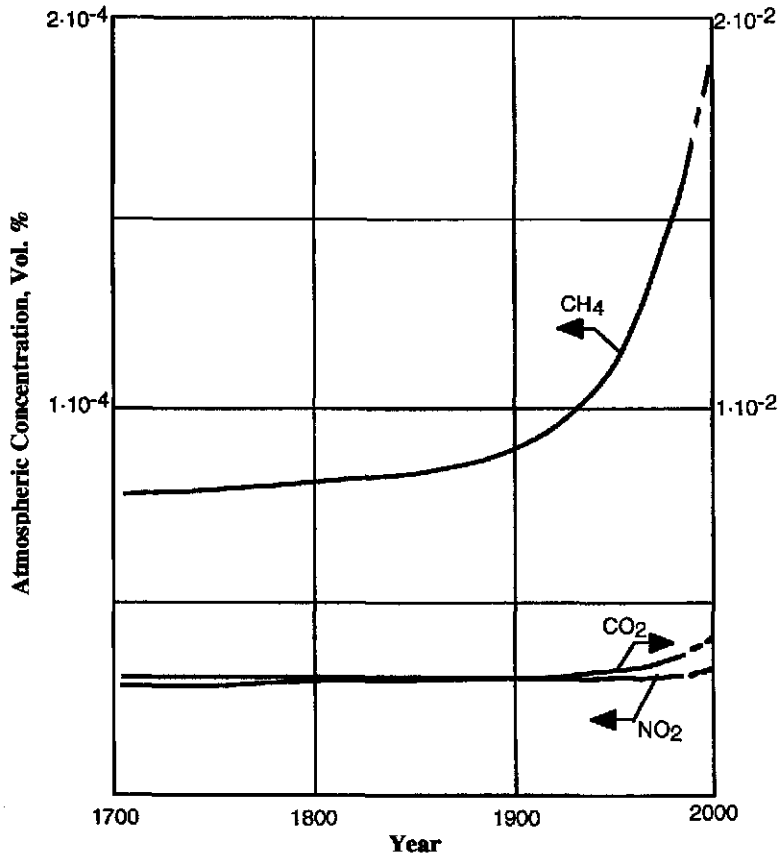

Figure 5-34 Change in atmospheric content of CH_4, NO_2, and CO_2 between 1700 and 1990 (Lorius, 1991).

if we take into consideration an impulse-like influx of methane from metastable zones of gas hydrate deposits in the ocean.

The sources of hydrate formation and of gas hydrate deposit formation are gaseous products of biochemical transformation of organic matter (CH_4, CO_2, H_2S, etc.), and also migration flows of catagenetic gases entering a zone of hydrate formation through tectonic breaches, gases of lateral migration of layer water, gases of upgoing diffusion, etc. Free gas and partially dissolved gases transform into a hydrate state after they enter a hydrate formation zone and form hydrate deposits. Deposits of free gas or oil may accumulate below an impermeable gas hydrate lithological cover.

Natural gas hydrates are a strong thermal screen on one hand, and an active source of methane into the earth's atmosphere on the other hand. Potential resources of methane in the earth are great:

- in a hydrate state—over 10^4 Gt;
- in a dissolved state in layer water—about 10^3 Gt;
- in collectors with low permeability—about 2×10^2 Gt;
- in gas, gas condensate and crude oil fields—about 4×10^2 Gt;
- in coal fields—on the order of 20 Gt;
- in the earth atmosphere—near 5 Gt;
- annually generated in a biosphere—about 0.5 Gt.

This mass of methane exists in a dynamic equilibrium. Intensity of methane influx into the atmosphere, rate of accumulation and oxidation depend on a number of interrelated factors—thermal regime of the system, seismic activity, dynamics of hydrostatic pressure, etc.

Depending on the conditions of deposition and variations in the P-T characteristic of a profile, gas hydrates accumulated in the earth exist in a stable solid or metastable state. At the present time, a P-T regime of a sedimentary cover of the earth's crust corresponds to the conditions of formation and stable existence of hydrates on land—on 25% of territory, and under nearly 90% of the sea. This does not mean that hydrate accumulations exist everywhere on these territories. Hydrates accumulate and stabily exist in those regions where sufficient sources of free hydrate forming gases at conditions of hydrate formation exist, and where was no cyclic temperatures increase above hydrate equilibrium in a profile of rock.

Thermophysical properties of water and hydrates provided more favorable conditions for the existence of hydrates in near-bottom sedimentary rock. Only secondary hydrate deposits formed from deposits of free natural gas during a change in a thermal regime of rock remained on land which is subjected to external heat action.

In seas, gas hydrate deposits are located near deep-water shelves and oceanic slopes. Large gas hydrate accumulations were not found on the sea floor due to an insignificant thickness of generating rock and a high temperature gradient.

Figure 5-35 presents a schematic of free methane migration in regions where a hydrate formation zone (HFZ) is present on land and under sea. On land gas hydrate deposits are accumulated in secondary deposits under lithological covers. Gases from these deposits do not significantly affect the gas balance in the earth's atmosphere. Two metastable zones of

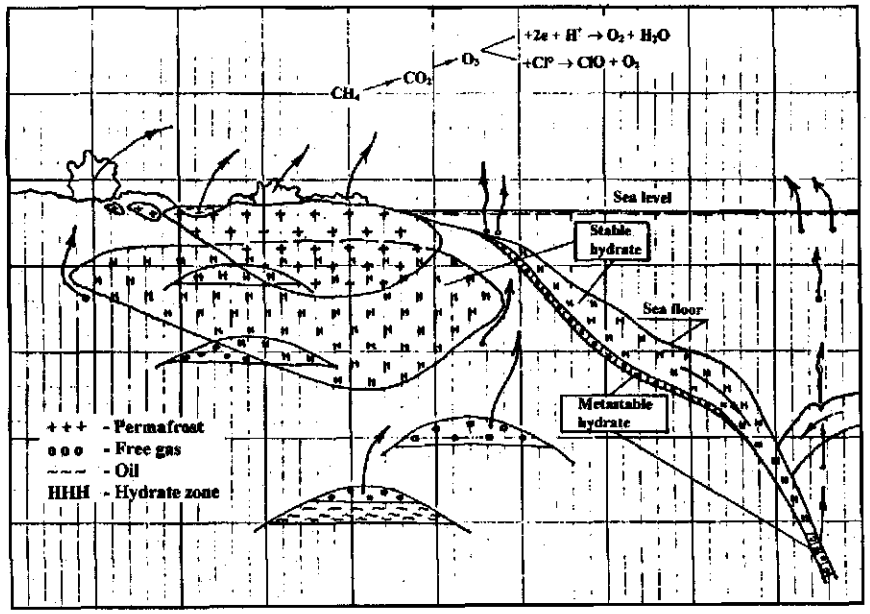

Figure 5-35 Schematic of methane release to the atmosphere.

hydrate which can supply large volumes of methane into the atmosphere exist under the sea where gas hydrate accumulations do not have lithological covers.

The first metastable zone underlies gas hydrate accumulations and exists near the lower boundary of an HFZ. The second one exists in a zone of immersion of hydrate saturated rock in a subduction region. The first metastable zone supplies a low pressure free methane; the second one in a zone of a dynamic immersion—high pressure methane. The first zone can supply methane both in a decay and in an impulse regime—during changes in hydrostatic pressure and in thermal gradient, and during seismic shakes of hydrate saturated profiles. Free methane accumulating under a layer of hydrate migrates to a shallow water boundary of hydrate accumulations and exits into the atmosphere through a layer of water. For example, up to 300 billion m^3 of CH_4 can evolve from a block the size of $1 \times 10^4 \times 10^6$ m at a hydrate saturation coefficient of 0.2, which is about 5% of the total amount of methane in the atmosphere. A metastable zone of hydrate under seas exists everywhere where a regression of water level or an increase of thermal gradient in a profile of hydrate saturated rock exist. A change of sea bottom temperatures by one degree may cause metastability of a hydrate in a layer of up to 75 m at a water depth of

600 m. Ocean levels vary many times with an amplitude of up to 25 m per 1000 years over the last 19 thousand years. At such rates of sea level change, up to 150 trillion m^3 of methane could enter the atmosphere from gas hydrate deposits.

Gas hydrates possess the unique property of concentrating gas in a unit volume. One volume of water in a hydrate state bounds 207 volumes of methane. A specific volume of water then increases by 26%. Figure 4-8 shows the dependence of pressure on gas temperature during decomposition of hydrates in a closed volume.

During hydrate decomposition in a closed volume, gas is released at a pressure which may be higher by several orders of magnitude than the initial equilibrium pressure of hydrate formation. This very property of hydrates provides the possibility of forming powerful impulse prolonged discharges of free methane in regions of active tectonic activity. The second depth metastable zone of gas hydrates appears in these regions (Figure 5-35).

In spite of a thick layer of rock covering hydrate saturated layers in regions of subduction, pressure of gas released during thermal decomposition of methane in a limited volume may overcome a hydrostatic and rock pressure and form a cold gas-water or gas-mud volcano. A single discharge of methane during this may reach several Gt. For example, during such a discharge in 1983 near Bennett Island of the Novo-Sibirski archipelago, a tail of methane had several tens of kilometers in a cross-section and up to 600 km in length. The volume of methane released into the atmosphere was then over one Gt. Since the lifetime of methane in the atmosphere is 8–12 years, such outbursts can make an impulse change of methane content in the atmosphere and change the thermal balance of earth's surface for many years.

With tectonic activity in subduction regions, impulse outbursts of gas released during decomposition of hydrates immersed into zones of elevated temperature may periodically repeat. Cycling of such outbursts is determined by the intensity of subduction, degree of hydrate saturation, permeability and plasticity of carrying rock, hydrate composition and a geothermal gradient in a region of consumption.

Methane and Ozone in the Earth Atmosphere

The atmosphere of the earth performs multiple functions. One of the most important ones is the function of thermal control. The most important components performing the thermal regulation function on our planet are CO_2, CH_4, and O_3. The effect of these gases on ecological parameters are not equivalent (Table 5-6), and their content in the atmosphere is different.

Table 5-6 Antropogenic gases and the greenhouse effect.

Component	Content in Atmosphere, Gt	Current Rate of Concentration Growth	Lifetime in Atmosphere Years	Effect of Doubling the Concentration on Temperature, °C	Current share in the Greenhouse effect	Increase of Thermal Influence as Compared to Pre-industrial Period, W/m²
CO_2	700	0.3–0.5	2	1.5–2.3	49	1.3
CH_4	5	1	8–12	0.3–1.4	18	0.6
O_3				0.9	6	0–0.2
Freon–11		5	75	0.1	14	0.06
Freon–12		5	110	0.02		0.12
NO_2		0.2	150	0.2	13	0.05
CO + other		1–2	3	0.3–1.1		0.05
Total						2.2

CO_2 is the fourth gas after N_2, O_2, and Ar by amount—0.046 wt. %. Ozone is on the tenth place by its content in the atmosphere—3.3×10^{-6} wt. %. Regarding methane, its position according to its content in the atmosphere, is not determined and its mass content is variable and, thus, not fixed. These three components share the same feature—all of them are strong absorbers of heat radiation. Their joint share in the greenhouse effect is 75% of all numerous components of the atmosphere.

A large number of studies have been devoted to these gases. In this section our positions regarding free methane and ozone in the atmosphere and their effect on the ecology of the earth are listed briefly. The thermal regime of earth's surface, climate, sea level, etc., depends, to a significant amount, on the content of free ozone and its even distribution in the atmosphere. However, direct studies of the atmosphere indicated that the content of ozone in the atmosphere is uneven. These so-called ozone holes, whose dimensions continuously vary, form in certain regions. A lot of attention has been paid during the last 20 years studying the factors which affect the stability and dynamics of ozone holes.

According to data from Arctic land-based stations and to measurements made from satellites, a constant (with small interruptions) decrease in ozone concentration which decreased more than twice during the periods of October was monitored during the 1980s (Farman, 1987). Losses of ozone are maximum in the interval of heights 10–25 km. The area of the ozone hole over the Antarctica is 10 million km². Destruction of the ozone layer also was noticed over the North Pole. Destruction of the ozone layer results in a significant warming of the climate and in an increased intensity of ultraviolet radiation in a short-wave region (< 290 nm) reaching the earth's surface. Starting with the 1970s, an idea of destruction of the ozone layer which absorbs hard solar radiation by technogenic freons has been popular. However, it is difficult to justify these statements if we take into account the fact that molecular density of freons is quite high and their diffusion in the atmosphere to the ozone layer is extremely complicated. Hydrogen and methane are 14 and 1.8 times lighter than air, accordingly, whereas the lightest among the used freons—freon-12 (CF_2Cl_2)–is four times heavier than air.

Free methane easily rises into the stratosphere where it aggregates with ozone. Destruction of the ozone layer then can follow two major paths: by forming hydrates of complex composition which enclathrate methane, ozone, and other gases, or by photochemical reactions.

The forecasting of scales to develop methods of preventing O_3 layer destruction harmful for the biosphere are possible only in the case of available and reliable information about the mechanics of this process. Hypotheses of this kind are divided into two main groups. The first group relates the dynamics of the O_3 content with the realization of the natural processes, and the second—with the action of antropogenic factors. Detection of products of human activity and their derivatives HF, HCl, freons (CF_2Cl_2, $CFCl_3$, etc.), ClO, $ClONO_2$, ClO_2, etc. in zones of ozone destruction points to a technogenic character of ozone destruction processes (Zurer, 1987). It is hypothesized that the products of photochemical transformations of freons—atomary chlorine (Cl^0), its oxygenated compounds—react with O_3 and convert it into oxygen.

The difficulty in using these hypotheses is that it is hard to explain how chemical reactions can proceed on a significant scale at very low temperatures of –70° to –90°C and low initial concentrations of reagents in air (with partial pressures on the order of nanobars). The hypothesis about concentration and reactions of ozone decomposition in clathrate hydrates formed by macrocomponents of air ($O_2 + N_2$, etc.) together with traces during reactions with water (water vapor) is more likely. During this process, molecular compounds of the type $M \times 5.75\ H_2O$ and more complex ones form, where M-molecules of O_2, N_2, CO_2, Ar, CO, CH_4, NO_2, O_3, CF_2Cl_2, $CFCl_3$, ClO, $ClONO_2$, ClO_2, Cl_2, etc. Vapor pressure of water above a hydrate is 2–3 times lower than above ice (Koshelev, 1971). Concentrations of ozone, freons, chlorine and its oxygenated compounds in a solid hydrate can be tens, thousands, or more times higher than in an equilibrium gas phase. One volume of hydrate contains 140–160 volumes of gas.

A very important property of clathrate hydrates is a significant decrease of the equilibrium pressure of a hydrate former (increase in stability of hydrates) during the increase of a partial pressure of water vapor in a system (Tsarev, 1976). An increase of water vapor pressure by 15–20% results in a decreased equilibrium pressure of hydrate-former gases by 4–6 or more times. Considering a significant subcooling of water vapor in clouds of stratosphere at temperatures as low as –90°C, the process of forming hydrates of air with traces of other gases, including O_3, becomes possible. Possibly, low temperature fogs in lower levels of atmosphere (at temperatures below –40° to –50°C) and traces of jet planes in the stratosphere have the same nature.

At moderately negative temperatures, artificial crystals of propane hydrate were obtained in zones of warm fog formation (Krasnovskaya, 1980). Also there were attempts to explain the nature of silver clouds in mesosphere at heights of 70–100 km (Tolkachev, 1988).

Activation of chemical reactions with the participation of small gas components of the atmosphere during formation of gas hydrates occurs not only as a result of concentrating of initial reactants, but also as a result of the cellular effect (Sergeev, 1978) when source reactant molecules appear to be close together in a lattice of clathrate hydrate lattice built with water molecules in conditions of limited mobility.

Molecules of hydrate forming gases and of water in a hydrate matrix (condensed phase) are subjected to a photolysis (*Science*, 1963, v. 142, No. 3590). Highly active products form during this process: `e - free electrons, Cl^0, H^0, O^0, and other free radicals, and different ion-radicals (H^+, Cl^-, F^-, etc.) which are stabilized at temperatures below –25°C by a hydrate lattice which significantly increases their lifetime. These very active oxidants and reducers react at high rates with O_3 present in the same matrix according to the following mechanism:

$$CH_4 \xrightarrow{h\nu} CH_3 + H$$

$$CH_4 \xrightarrow{h\nu} CH_2 + 2H$$

$$H + O_3 \rightarrow OH + O_2$$

$$O_3 + 2H \rightarrow H_2O + O_2$$

$$O_3 + Cl^0 \rightarrow ClO + O_2$$

$$ClO + O_3 \rightarrow ClO_2 + O_2$$

Besides that, H_2O_2, which can participate in forming a clathrate lattice (Tsarev, 1975), forms during a photolysis of H_2O and accelerates decomposition of O_3 in a weakly acidic medium according to the mechanism:

$$H_2O_2 + O_3 \rightarrow H_2O + 2O_2$$

Thus, methane in the upper layers of the atmosphere is subjected to a photolysis with evolution of hydrogen which enters into a reaction with ozone to form free water and oxygen.

Charge separation with a difference of potentials of up to 300 V occurs at phase boundaries during ice and clathrate hydrates formation-decomposition phase transitions of water. This difference of potentials is the driving force of electrochemical reactions in which free electrons

participate. In particular, a reaction of O_3 decomposition according to the mechanism proposed by Shamb et al. (1958):

$$O_3 + 2\grave{e} + H^+ \rightarrow O_2 + H_2O\,.$$

Thus, the formation of clathrate hydrates of air with the participation of trace gas components is a highly effective process which activates a chemical reaction of transformation of O_3 and other compounds. Considering the relatively high concentrations of O_3 in hydrates, this can be explained by their accumulation in hydrates and preservation of this unstable compound in a hydrate matrix which is used in technological processes (US Patent 1953. 2683651 KLNKI22-153).

A seasonal variation of ozone content during the use of a hydrate hypothesis can be explained by the fact that, at high latitudes during winter, hydrates accumulate and ozone concentrates during stabilization of minimum temperatures reaching –90°C (Chrigan, 1973). With the end of night and the beginning of an intensive photoradiation in spring, reactions of ozone decomposition activated by photoprocesses and by phase transitions of hydrate decomposition take place. Daily variations in free ozone and methane contents in the atmosphere can occur along with seasonal fluctuations—during the daytime their content increases, and during the night it decreases.

Encapsulation of trace gases (freons, ozone, chlorine compounds) takes place, especially in dynamic conditions of lowering temperatures, oversaturation of vapor and an abrupt process of hydrate formation. A kinetic effect of encapsulation of freons, chlorine oxides, ozone, etc. then works, which increases the effectiveness of their absorption by hydrates by several orders of magnitude.

Physical Principles and Models of Development of Gas Hydrate Deposits

It is necessary to solve problems of hydrate decomposition in layer conditions and to provide the prevention of their formation on the path of gas to a consumer during development of gas hydrate deposits. All known methods of decomposition of hydrates and prevention of their formation are based on shifting thermodynamic equilibrium in a three-phase system (water-hydrate-gas) which can be done by:

- injection of inhibitors of hydrate formation (alcohols, electrolytes) into a system;

- increasing the system temperature above the temperature of hydrate formation at a specified pressure; or
- decreasing the system pressure below the pressure of hydrate formation at a specified temperature.

In practice these methods may be combined. It is worth noting that the last two methods are tightly interrelated since a change in pressure (temperature) in the system generally results in a change of temperature (pressure).

Thermodynamic Model of Gas Hydrates Decomposition in Porous Medium during a Pressure Decrease

Production of gas from gas hydrate deposits and removal of hydrates from a well-bottom zone of wells presumes the creation of conditions required for a process of hydrate decomposition in a porous medium. Such conditions can be achieved by shifting the thermodynamic equilibrium by lowering pressure, increasing temperature, or affecting hydrate with inhibitors. Due to this the need arises to develop a thermohydrodynamic theory of gas hydrate decomposition in a porous medium.

Experimental studies indicate that decomposition of hydrates in a porous medium happens not in the whole volume, but in a certain narrow zone which can be treated as a surface. During this process the rate of hydrate decomposition is determined by the movement of a decomposition front, and not by the kinetics of this process. The movement of this front, in turn, depends on the magnitude of heat flow through it and on the specific heat of hydrate formation. Hydrate decomposition occurs during a temperature increase or because of the process of pressure redistribution in a layer during hydrate decomposition after a pressure decrease.

Thus, two zones, separated by a mobile boundary at which sources of heat and mass exist, are formed in a porous rock. A source of mass is caused by the release of water and gas during hydrate decomposition, and heat by the endothermic nature of the hydrate decomposition process.

The problem of hydrate decomposition by a pressure decrease was addressed in Makogon (1966, 1974) and Degtiarev and Bukhgalter (1976). Using an analog of the classical Stefan's problem for melting to describe the process of hydrate decomposition, a self-similar solution was obtained after linearization of Leibenzon's equations of the filtration of gas for the linear and radial flow of gas. Drawbacks of the model include no accounting for the release of water from a hydrate and an approximate mass balance at the surface of hydrate decomposition. These limitations were

removed in the work of Verigin et al. (1988). However, even this model does not account for a change of layer temperature during filtration.

Decomposition of hydrates during a temperature increase was first studied by Makogon and Khalikov (1981). In this work, a temperature field in a layer and the law of movement of the hydrate decomposition front were determined based on a mathematical model similar to Stefan's problem. However, the results obtained remain schematic since the filtration of gas and its influence on the temperature field was not considered in the statement of this problem.

Significant progress in this field was made by Bondarev and Cherskiy (1973). This study was conducted on the basis of a simultaneous solution of the equations of convective heat transfer and non-isothermal filtration of gas. As a result of this work, temperature and pressure fields in a layer were determined. Several specialties of a thermal method of development of gas hydrate fields were reviewed in Sheshukov (1984).

McGuirer (1981) should also be noticed. This study reviews a model for calculating the production of a gas from hydrate by flooding a gas hydrate layer with hot water, and a model for calculating the production of gas from hydrates from a system injection well—a production well connected by a fracture. Other interesting studies have been done by Kamath (1984), and by Kamath and Godbole (1987).

All of the studies mentioned contain mathematical models which do not account for the water released during hydrate decomposition. These works also assume that a porous medium is initially completely saturated with gas, although in real conditions, gas in a hydrate-saturated layer may be in a free state also.

Consideration of these factors was done in Makogon, Sayakhov, Khabibulin and Khalikov (1988). This work views hydrodynamic problems in a barotropic approximation, i.e., density of water and gas are assumed to be independent of temperature, which reflects the real picture rather well, since the majority of gas hydrate deposits are characterized by low layer pressures (up to 12 MPa) and temperatures (below 25°C). The second approximation is the condition of stationary water during hydrate decomposition. A mathematical model of a nonisothermal filtration of a two-phase system of water-gas was constructed which describes the process of hydrate decomposition during a pressure drop and accounts for a temperature change in a layer and for a filtration of water.

Linear One-Dimensional Problem of Hydrate Decomposition in a Porous Medium during a Pressure Drop

Let us assume that free gas, $m(1 - \beta,)$ and hydrate, $m\beta$, coexist in a pore space of a layer at some initial moment of time at pressure, P_e, and at temperature, T_e, where, m–porosity, and β–hydrate saturation of a layer. This situation corresponds to a lack of water in a layer for enclathrating free gas into a hydrate.

At some moment in time, the pressure in the gallery (at $x = 0$) sharply drops to a certain value $P_G < P_D < P_e$, where $P_D(T_D)$ is the decomposition pressure of a hydrate at the specified layer temperature. Then the pressure in a layer gradually decreases and two zones of gas filtration with different collector properties, separated by a moving boundary $l(t)$ appear.

During decomposition of a hydrate on the surface $l(t)$, water is released along with gas. However, in some cases the phase permeability of water can be assumed as zero, as shown below. Thus, let us consider the case when water does not move, and released at $l(t)$ it somewhat decreases the porosity and the phase permeability of gas in the first zone. Filtration of gas occurs in a direction towards a gallery, and the surface $l(t)$ moves in the opposite direction.

Distribution of pressure in the layer is described by the equations of gas filtration:

$$\frac{2m_n\mu_n}{k_n}\frac{\partial P_n}{\partial t} = \frac{\partial^2 P_n^2}{\partial x^2}, \qquad \textbf{(5.14)}$$

where

m is the viscosity;

k is the phase permeability of gas;

P is the pressure;

$m_1 = (1 - \sigma)$ m;

$m_2 = (1 - \beta)$ m;

σ is the water content of pores.

Hereinafter the index $n = 1$ is related to the region $0 < x < l(t)$, and the index $n = 2$ to the region $l(t) < x < \infty$.

The boundary conditions, $P_1(0, t) = P_G$, $P_2(x, 0) = P_2(\infty, t) = P_e$, are satisfied according to the statements above.

The surface of hydrate decomposition is a surface of discontinuity with sources of heat and mass. Then, according to the results obtained in the work of Verigin et al. (1984) it is possible to specify the following condition at this surface pressure is continuous and is related to temperature by the correlation of phase equilibrium between free gas and a hydrate:

$$P_1(l, t) = P_2(l, t) = P_D(T_D); \tag{5.15}$$

$$log\ P_D = a(T_D - T_0) + b(T_D - T_0)^2 + c$$

where

- $P_D(T_D)$ relates the pressure P_D and temperature of hydrate decomposition T_D, $T_0 = 273$ K;
- a, b, c are the empirical constants depending on hydrate composition and the interval of pressure and temperature variation.

At the surface $l(t)$ the conditions of gas and water mass balance are satisfied. Let us introduce the term *mass fraction of gas in a hydrate* (Bondarev et al., 1976).

$$\varepsilon = \frac{M}{18L + M} \tag{5.16}$$

where

- M is the molecular weight of a hydrate-former gas;
- L is the ratio of the number of water molecules per one molecule of gas in a hydrate;
- 18 is the molecular weight of water.

Thus, a unit mass of hydrate contains the mass of gas equal to ε and a mass of water $1 - \varepsilon$.

Mass balance for gas at the surface $l(t)$ is determined from the work of Verigin et al. (1980):

$$\rho_1 \upsilon_1 - \rho_2 \upsilon_2 = [\beta\varepsilon\rho_3 - (1 - \sigma)\rho_1 + (1 - \beta)\rho_2]m\frac{dl}{dt}$$

Since both on the right and on the left there is gas of the same composition, by using the continuity of pressure at l(t) and the equation of state for gas, we obtain

$$\rho_1(l, t) = \rho_2(l, t) = \rho_0 \frac{P_D T_0}{z P_0 T_D}$$

In this formula

- z is the compressibility of gas;
- ρ_0 is the density of gas at atmospheric pressure P_0 and temperature T_0.

With this expression the equation of gas balance at the decomposition front will be

$$\upsilon_1(l, t) - \upsilon_2(l, t) = -[\beta\varepsilon \frac{\rho_3 P_0 T_D}{\rho_0 P_D T_0} z - (\beta - \sigma)]m\frac{dl}{dt} \tag{5.17}$$

Thus, due to the presence of a source of mass and a step-like change in porosity and permeability, the rate of gas filtration at the front $l(t)$ undergoes a discontinuity.

In the case where a layer is initially completely saturated with hydrate ($\beta = 1$, $\upsilon_2 = 0$) and water released from a hydrate is not considered ($\sigma = 0$, $\varepsilon = 1$), the Equation 5.17 matches the condition obtained in the work of Bondarev et al. (1976).

The equation of balance for water released from a hydrate is:

$$\rho_w m\sigma = (1 - \varepsilon)\rho_3 m\beta,$$

$$\sigma = (1 - \varepsilon)\beta\rho_3/\rho_w.$$

Since water is stationary, and pressure and temperature are low in a gas hydrate layer, we can assume $\rho_w = \text{const}$, then also $\sigma_w = \text{const}$. Thus, the water saturation of a layer during decomposition of a gas hydrate is determined by its composition and saturation.

In general, the temperature field of a gas-saturated layer can be described by the equation which considers the convective and the conductive heat flows and a temperature change because of a throttling and adiabatic effects (Chekaliuk, 1964):

$$a_n \frac{\partial^2 T_n}{\partial x^2} = \frac{\partial T_n}{\partial t} - \frac{\rho_C k_n}{\alpha_n \mu}\frac{\partial P_n}{\partial x}\left(\frac{\partial T_n}{\partial x} - \delta\frac{\partial P_n}{\partial x}\right) - \eta\frac{m_n \rho_C}{\alpha_n}\frac{\partial P_n}{\partial t} \tag{5.18}$$

where

a_n, α_n is the thermal conductivity and heat capacity of zones, accordingly;

ρ_C is the volume heat capacity of gas;

δ, η is the throttling and adiabatic coefficients of gas, accordingly.

Let us review this equation in assumption $a_n = 0$, considering that the conductive heat flow in a porous medium is by several orders of magnitude less than the convective flow (Barenblatt et al., 1977). Then the following boundary conditions can be used for Equation 5.18:

$$T_2(\infty, t) = T_2(x, 0) = T_e, \qquad T_1(l(t), t) = T_2(l, t).$$

It is not difficult to demonstrate that this boundary-value problem allows a self-similar solution. Let us linearize Equation 5.14 by pressure squared in order to get a closed solution as proposed by Leibenzon. Such linearization does not result in a substantial error as shown by Charnyi (1963). The self-similar solution of linearized Equation 5.14 with the boundary conditions specified above is written as:

$$P_1^2 = P_\Gamma^2 - (P_\Gamma^2 - P_D^2)\frac{erf\ \lambda_1}{erf\ \alpha_1},$$

$$P_2^2 = P_e^2 - (P_D^2 - P_e^2)\frac{erfc\ \lambda_2}{erfc\ \alpha_2}, \qquad \textbf{(5.19)}$$

$$l(t) = \sqrt{\gamma t}$$

where

$$\lambda_n = \frac{x}{2\sqrt{\chi_n t}};\quad \alpha_n = \sqrt{\frac{\gamma}{4\chi_n}};\quad \chi_1 = \frac{k_1 P_G}{m(1-\sigma)\mu};\quad \chi_2 = \frac{k_2 P_e}{m(1-\beta)\mu};$$

$$erf\ \xi = \frac{2}{\sqrt{\pi}\int_0^\xi e^{-\eta^2} d\eta};\quad erfc\ \xi = 1 - erf\ \xi$$

Solution of Equation 5.18 is obtained as:

$$T_1 = T_D + A_1\delta\left[erf\ \lambda_1 - erf\ z_1 + \left(1 + \frac{\eta}{\delta}B_1\right)(\Phi_1(z_1) - \Phi_1(\alpha_1))\right] \qquad \textbf{(5.20)}$$

$$T_2 = T_e + A_2\delta\left[erfc\ z_2 - \left(1 + \frac{\eta}{\delta}B_2\right)\Phi_2(z_2)\right]$$

where

$$\Phi_1(\xi_1) = \frac{2}{\sqrt{\pi}}\int_0^{\xi_1}\frac{\eta e^{-\eta^2} d\eta}{\eta + C_1 e^{-\eta^2}};\qquad \Phi_2(\xi_2) = \frac{2}{\sqrt{\pi}}\int_{\xi_2}^{\infty}\frac{\eta e^{-\eta^2} d\eta}{\eta + C_2 e^{-\eta^2}};$$

$$A_1 = \frac{2}{erf\ \lambda_1}\frac{P_D^2 - P_G^2}{P_G};\qquad A_2 = \frac{2}{erfc\ \lambda_2}\frac{P_e^2 - P_D^2}{P_e};$$

$$B_1 = \frac{1}{4}\frac{P_G^2 m_1 \rho_{0C}}{P_0 \alpha_I};\qquad B_2 = \frac{1}{4}\frac{P_e^2 m_2 \rho_{0C}}{P_0 \alpha_{II}};$$

$$C_1 = \frac{P_D^2 - P_G^2}{P_G}\frac{\rho_{0C}}{\alpha_I}\frac{1}{2\sqrt{\pi} erf\ \lambda_1}\frac{k_1}{\mu\chi_1};\qquad C_2 = \frac{P_e^2 - P_D^2}{P_e}\frac{\rho_{0C}}{\alpha_{II}}\frac{1}{2\sqrt{\pi} erfc\ \lambda_2}\frac{k_2}{\mu\chi_2};$$

In the Equations 5.19 and 5.20, three values remain undefined: pressure and temperature at the front $l(t)$ and the parameter γ, which determines the motion of this surface. The temperature of hydrate decomposition, T_D, is determined at $z_2 = \alpha_2$ using Equation 5.20

$$T_D = T_e - A_2\delta \ln\left[erfc\ \alpha_2 - \left(1 + \frac{\eta}{\delta}B_2\right)\Phi_2(\alpha_2)\right] \qquad \textbf{(5.21)}$$

The magnitude of pressure is found according to Equation 5.15. Substituting Equation 5.19 into Equation 5.17, we obtain the equation to determine γ:

$$k_1\frac{P_D^2 - P_G^2}{\sqrt{\pi\chi_1}}\frac{e^{-\alpha_1^2}}{erf\ \alpha_1} - k_2\frac{P_e^2 - P_D^2}{\sqrt{\pi\chi_2}}\frac{e^{-\alpha_1^2}}{erf\ \alpha_2} = A\sqrt{\gamma} \equiv F(\gamma) \qquad \textbf{(5.22)}$$

$$A = \left[\beta\varepsilon\frac{\rho_3}{\rho_0}P_0\frac{T_D}{T_0}z - (\beta - \sigma)P_D\right]m\mu$$

Production rate of gas per unit length of a gallery is found from the expression:

$$Q = -\frac{k_1 h}{\mu}\frac{\partial P_1(0,t)}{\partial x} = \frac{k_1 h}{\mu}\frac{P_D^2 - P_G^2}{P_G}\frac{1}{erf\ \alpha_1}\frac{1}{2\sqrt{\pi\chi_1 t}} \qquad \textbf{(5.23)}$$

As expected, the production rate of gas decreases with time. The production rate depends on the thickness of a layer, h, and on its hydrodynamic and thermodynamic (via the quantity P_D) parameters of the first and the second regions.

Thus, Equation 5.20 allows us to determine all the major characteristics of the process of gas hydrates' decomposition during a pressure drop (distribution of pressure and temperature in a layer, temperature, pressure,

and rate of hydrate decomposition, production rate of gas, and water content of a layer during hydrate decomposition).

In conclusion, let us review the statements of general character.

a. The applicability of the model of a single-phase filtration is used above to describe decomposition of hydrates.

When the condition

$$\beta > \frac{\sigma_0}{1-\varepsilon}\frac{\rho_W}{\rho_3} = \beta_0$$

is satisfied, where σ_0 is the the value of water content at which the filtration of water starts, the hydrodynamic picture in the first region must be described by the equation of a two-phase filtration. It was determined experimentally that for the gas-water system $\sigma_0 \approx 0.2$. Then, at $\sigma_0 < 0.2$ the phase permeability of gas in the first region, in the presence of stationary water, can be determined from the correlation

$$k_1 = k\frac{(0.9-\sigma)^{3.5}}{0.9}(1+3\sigma),$$

where

k is the absolute permeability of the medium.

This applies to the region of above-zero °C temperatures. According to the existing notion, water released from a hydrate in gas hydrate layers with sub-zero temperatures transforms into ice and does not participate in filtration motion. Then σ should be considered as the ice content of a layer.

Thus, the model of a single-phase filtration described above adequately describes the decomposition of a hydrate for a whole range of values of hydrate content $0 < \beta < 1$ in the region of sub-zero temperatures and for a limited range of values of hydrate content $0 < \beta < \beta_0$ in the region of positive temperatures.

Particular cases of the problem. Assuming that $\beta = 1$ in the obtained expressions (in the case when $T_e < 273$ K) we obtain a solution of the problem about decomposition of a hydrate in a layer completely saturated with hydrate. During this $P_2 = P_e$ and filtration occurs only in the region $0 < x < l(t)$, and heat transfer occurs only by conduction in the region $l(t) < x < \infty$.

If we assume that $T_1(x, t) = T_2(x, t) = T_D = T_e$, then only the hydrodynamic part of the problem, which describes decomposition of hydrates during a pressure drop in isothermal approximation, makes sense. Such a problem was reviewed by Verigin, et al., (1980). Apparently, assumption of such an approximation is determined by the magnitude of a pressure drop in the first region.

b. The thermohydrodynamic problem with a free boundary reviewed above has a single solution.

Actually, when the conditions of the π-theorem and self-similarity of the problem are satisfied, the singularity of the initial boundary-value problem follows from the existence of the only solution of the system of transcendental Equations 5.15, 5.21, 5.22 which is not difficult to show.

Thus, in the case of an isothermal approximation, the singularity of the initial problem's solution follows from the existence of the only root of Equation 5.22. Analysis of this equation indicates that it has the only root since $F(0) = \infty$, $\lim_{\gamma\to\infty} F(\gamma) = -\infty$, $\frac{dF}{d\gamma} < 0$.

Axis-Symmetrical Problem on Decomposition of Gas Hydrates during a Pressure Drop

Let us consider the above problem in the case of planar-radial symmetry. Pressure and temperature change around a well with a radius r_0 during a production of gas with a constant flowrate Q and decomposition of hydrate initiates. The two regions of filtration of gas are formed in a layer. Pressure and temperature in these regions are described by the following equations:

$$\frac{k_n}{2m_n\mu_n}\left(\frac{\partial^2 P_n^2}{\partial r^2} + \frac{1}{r}\frac{\partial P_n^2}{\partial r}\right) = \frac{\partial P^2}{\partial t}, \quad (n = 1, 2) \tag{5.24}$$

$$\frac{a_n}{r}\frac{\partial}{\partial r}\left(r\frac{\partial T_n}{\partial r}\right) = \frac{\partial T_n}{\partial t} - \frac{\rho_n c_n k_n}{\mu_n}\frac{\partial P_n}{\partial r}\left(\frac{\partial T_n}{\partial r} + \delta\frac{\partial P_n}{\partial r}\right) - \frac{m_n\rho_n c_n\eta}{\alpha_n}\frac{\partial P_n}{\partial t}$$

At stationary boundaries the following conditions are satisfied:

$$\frac{\pi k_1 h}{\mu}\frac{\rho_0}{P_0}\left(r\frac{\partial P_1^2}{\partial r}\right)_{r=r_0} = Q$$

$$P_2(\infty, t) = P_2(x, 0) = P_e, \tag{5.25}$$

$$T_2(\infty, t) = T_2(x, 0) = T_e,$$

At the moving front of gas hydrate decomposition $R(t)$, the conditions of continuity of pressure and temperature, correlation of a gas-hydrate equilibrium and the mass balance of gas are satisfied:

$$P_1(R,t) = P_2(R,t) = P_D = f(T_D),$$

$$T_1(R,t) = T_2(R,t), \qquad \textbf{(5.26)}$$

$$k_1 \frac{\partial P_1(R,t)}{\partial r} - k_2 \frac{\partial P_2(R,t)}{\partial r} = \left[\varepsilon\beta \frac{\rho_3}{\rho_0} z \frac{P_0 T_D}{P_D T_0} - (\beta - \sigma)\right] m\mu \frac{dR}{dt}.$$

Assuming $a_n = 0$, we can write a self-similar solution of the problem (5.24, 5.25, 5.26):

$$P_1^2 = P_D^2 + \frac{Q\mu}{\pi k_1 h} \frac{P_0}{\rho_0}\left[E_i(-\lambda_1^2) - E_i(-\alpha_1^2)\right]_1$$

$$P_2^2 = P_e^2 + \left(P_D^2 - P_e^2\right)\frac{E_i(-\lambda_2^2)}{E_i(-\alpha_2^2)},$$

$$R(t) = \sqrt{\gamma t}, \quad E_i(-\xi) = -\int_\xi^\infty \frac{e^{-u}du}{u}, \qquad \textbf{(5.27)}$$

$$T_1 = T_D + A_1\left[\begin{array}{l} E_i(-\lambda_1^2) + (1+Q_1)E_i\left(-\lambda_1^2 - B_1 e^{-\lambda_1^2}\right) \\ -E_i(-\alpha_1^2) - (1+Q_1)E_i\left(-\alpha_1^2 - B_1 e^{-\alpha_1^2}\right)\end{array}\right]$$

$$T_2 = T_e + A_2\left[E_i(-\lambda_2^2) + (1+Q_2)E_i\left(-\lambda_2^2 - B_2 e^{-\lambda_2^2}\right)\right],$$

where

$$A_1 = \frac{Q\mu}{2\pi h k_1}\frac{\delta}{\rho_0}\frac{P_0}{P_D}, \quad A_2 = \frac{1}{2}\frac{\delta}{P_D}\frac{P_D^2 - P_e^2}{E_i(-\alpha_2^2)},$$

$$B_1 = \frac{Q}{\pi h \chi_1}\frac{c}{\alpha_I}, \quad B_2 = \frac{k_2}{\mu\chi_2}\frac{c_2\rho_0}{\alpha_{II}P_0}\frac{P_D^2 - P_e^2}{E_i(-\alpha_2^2)},$$

$$Q_1 = \frac{\eta}{\delta}\frac{mc\rho_0}{\alpha_I}\frac{P_D}{P_0}, \quad Q_2 = Q_1\frac{\alpha_I}{\alpha_{II}}, \quad \lambda_n = \frac{r}{2\sqrt{\chi_i t}}.$$

Notice that while solving Equation 5.26, a linearization by pressure squared was used, which does not result in a substantial error.

Thus, a good fit was shown for self-similar solutions of a non-linear axis-symmetrical problem and a linearized problem (Barenblatt et al., 1977), based on the study of the integral curves of a nonlinear equation.

A method described by Chekaliuk (1964) was used during the solution of Equation 5.24. The unknown temperature, T_D, is determined from Equation 5.27 at $\lambda_2 = \alpha_2$ and equals:

$$T_D = T_e + A_2\left[E_i(-\alpha_2^2) + (1+Q_2)Ei\left(-\alpha_2^2 - B_2 e^{-\alpha_2^2}\right)\right].$$

Then the quantity, P_D, is determined according to the correlation of phase equilibrium $P_D = f(T_D)$ whose explicit form can be taken according to the last expression of Equation 5.15. Substituting Equation 5.27 into Equation 5.26, we obtain a transcendental equation for determining the parameter γ:

$$\frac{Q\mu}{\pi h}\frac{P_0}{\rho_0}e^{-\alpha_1^2} + k_2\left(P_e^2 - P_D^2\right)\frac{e^{-\alpha_2^2}}{E_i(-\alpha_2^2)} = \alpha\chi_1\mu m\alpha_1 \equiv F(\gamma) \qquad \textbf{(5.28)}$$

where

$$\alpha = \beta\varepsilon\frac{\rho_3}{\rho_0}P_0 z - (\beta - \sigma)P_D, \quad \alpha_i = \sqrt{\frac{\gamma}{4\chi_i}}, \quad \alpha_2 = \alpha_1\sqrt{\frac{\chi_1}{\chi_2}}.$$

Thus, the Equations 5.27–5.28 and the correlation, $P_D = f(T_D)$, present the solution of the problem. Previous general comments also apply fully to this problem. For example, an analysis of Equation 5.28 indicates that

$$F(0) = \frac{Q\mu}{\pi h}\frac{P_0}{\rho_0} > 0, \quad \lim_{\gamma\to\infty} F(\gamma) = \infty, \quad \frac{dF}{d\gamma} < 0.$$

Then this equation and, consequently, the boundary-value problem in an isothermal approximation have a single solution.

However, notice that the following condition has to be satisfied in order to prevent the formation of a hydrate:

$$T(r,t) = T_D \qquad \textbf{(5.29)}$$

where T_D is determined according to the curve of gas-hydrate phase equilibrium $T_D = f(P_D)$ at pressure $P(r, t)$ in the specified point. Apparently, the maximum decrease in temperature will occur at a well wall, i.e., at $r = r_0$. It should be expected that if the condition (5.29) is satisfied at $r = r_0$, then hydrate formation in a layer is prevented.

It follows from Equation 5.27 that the temperature of gas in the first region depends on a mass flow rate of gas, Q, along with other parameters. Thus, the temperature and hydrodynamic fields in a layer can be

modified by varying the production rate of a well in order to prevent reuniting of gas and water into a hydrate.

Problem on Decomposition of Hydrates during a Pressure Drop with Account for Water Filtration

As presented earlier, at $\beta > \beta_0$ a simultaneous filtration of water and gas occurs in a zone of hydrate decomposition. The equations of heat transfer and filtration of gas reviewed above remain valid in region II. The filtration of a gas-water mixture in a region I (decomposition of hydrate) can be described by the following system of equations:

a) equations of motion

$$\vec{\upsilon}_B = -\frac{kk_B(\sigma)}{\mu_B}\nabla P_I, \quad \vec{\upsilon}_I = -\frac{kk_1(\sigma)}{\mu_1}\nabla P_I \tag{5.30}$$

b) continuity equations

$$m\frac{\partial\sigma}{\partial t} + div\,\vec{\upsilon}_B = 0, \quad m\frac{\partial\rho(1-\sigma)}{\partial t} + div\rho_1\vec{\upsilon}_1 = 0, \tag{5.31}$$

c) equations of state

$$\rho = \text{const}, \quad \rho_1 = \frac{P_I}{zRT_I} \tag{5.32}$$

Index *I* refers to gas. The system of Equations 5.30–5.32 is written without the consideration of an interphase capillary jump of pressure and neglecting the compressibility of water. These simplifications are quite acceptable for gas hydrate layers.

Phase permeabilities for the system gas-water can be taken as (Charnyi, 1963):

$$k_B(\sigma) = \left(\frac{\sigma - 0.2}{0.8}\right)^{3.5}, \quad 0.2 \le \sigma \le 1; \quad k_B(\sigma) = 0, \quad 0 < \sigma \le 0.2; \tag{5.33}$$

$$k_1(\sigma) = 0, \quad 0.9 \le \sigma \le 1; \quad k_1(\sigma) = \left(\frac{0.9 - \sigma}{0.9}\right)^{3.5}(1 + 3\sigma), \quad 0.2 \le \sigma \le 1;$$

According to Bondarev et al. (1976) the following equation can be used for calculating the temperature distribution in region I:

$$c_I\frac{\partial T_I}{\partial t} = div(\lambda_I\nabla T_I) - \vec{w}\,\nabla T_I + Q, \tag{5.34}$$

where

$$c_I = (1-m)c_0\rho_0 + m\sigma c_B\rho_B + m(1-\sigma)c_1\rho_1,$$

and

$$\lambda_I = (1-m)\lambda_0 + m\sigma\lambda_B + m(1-\sigma)\lambda_1$$

are the coefficients of heat capacity and thermal conductivity of a layer saturated with gas and water, averaged by volume,

$$\vec{w} = \rho_B c_B\,\vec{\upsilon}_B + \rho_1 c_1\,\vec{\upsilon}_1,$$

$$Q = c_1\delta_1\,\vec{\upsilon}_1\,\nabla P_I + m(1-\sigma)(c_1\delta_1\rho_1 + 1)\frac{\partial P_I}{\partial t} + \vec{\upsilon}_B\,\nabla P_1.$$

During the derivation of Equation 5.34, the effect of thermal expansion of water was not considered because of its insignificance in the range of temperatures studied.

Thus, a complete system of Equations 5.30–5.34 was constructed, which allows us to determine the saturation and velocity of the filtration of water and gas in a layer, and the distribution of pressure and temperature. The same boundary conditions are retained for pressure and temperature. The condition $\rho_B m\sigma = (1-\varepsilon)\rho_3 m\beta$ should be replaced with a more accurate correlation (accounting for the motion of water), i.e.:

$$\rho_B\left(\vec{\upsilon}_B - m\sigma\frac{d\vec{r}}{dt}\right) = m\beta(1-\varepsilon)\rho_3\frac{d\vec{r}}{dt}.$$

This condition represents a balance of water at the hydrate decomposition front. The value of water content at this surface $\sigma = \sigma\left(\vec{r}(t)\right)$ can be determined from this condition, if necessary. The initial condition for water content looks like $\sigma(t=0) = \sigma_e$, where σ_e is the residual water content of a gas hydrate layer.

Let us write the equations which describe thermohydrodynamic processes around a gas well in case of gas hydrate decomposition during a pressure drop accounting for a temperature change and water filtration using the equations obtained above. The Equations 5.30 and 5.31 are written as

$$\upsilon_B = -\frac{kk_B(\sigma)}{\mu_B}\frac{\partial P_I}{\partial r}, \quad \upsilon_I = -\frac{kk_1(\sigma)}{\mu_1}\frac{\partial P_I}{\partial r},$$

$$m\frac{\partial\sigma}{\partial t} + \frac{1}{r}\frac{\partial}{\partial r}(r\upsilon_B) = 0, \quad m\frac{\partial\rho_1\sigma}{\partial t} - \frac{\rho_1}{r}\frac{\partial}{\partial r}(r\upsilon_1) - \upsilon_1\frac{\partial P_I}{\partial r} = 0 \tag{5.35}$$

$$\rho_1 = \frac{P_l}{zRT_l}, \quad \rho_B = \text{const}$$

Here the phase permeabilities are determined according to Equation 5.33. Equation 5.34 for a case of planar-radial geometry is expressed by the formula:

$$c_l \frac{\partial T_l}{\partial t} = \frac{1}{r}\frac{\partial}{\partial r}\left(r\lambda_l \frac{\partial T_l}{\partial r}\right) - \vec{w}\frac{\partial T_l}{\partial r} + Q \qquad \textbf{(5.36)}$$

where

$$\vec{w} = -\rho_B c_B \frac{kk_B(\sigma)}{\mu_B}\frac{\partial P_l}{\partial r} - \rho_1 c_1 \frac{kk_1(\sigma)}{\mu_1}\frac{\partial P_l}{\partial r},$$

$$Q = c_1\delta_1\rho_1 \frac{kk_1(\sigma)}{\mu_1}\left(\frac{\partial P_l}{\partial r}\right)^2 + m(1-\sigma)(c_1\delta_1\rho_1 + 1)\frac{\partial P_l}{\partial t} - \frac{kk_B(\sigma)}{\mu_B}\left(\frac{\partial P_l}{\partial r}\right)^2.$$

Thus, the system of equations and boundary conditions together with Equation 5.24 at n = II and boundary conditions 5.25 and 5.26 represent a complete boundary-value problem about decomposition of gas hydrates in a layer during a pressure drop along with accounting for a change in temperature and filtration of the water.

A numerical solution of this system allows us to determine the temperature and pressure in a gas hydrate layer, the rate of gas hydrate decomposition, water, and gas contents of a layer, and with an appropriate reformulating of the first condition (5.25)—the flow rates of water and gas.

The problem appears sufficiently complicated. However, based on physical principles, it can be simplified. In particular, the transient processes of equilibration of temperature and pressure in a layer can be neglected and it can be assumed that only compositions explicitly depend on time (Bondarev, 1976).

Then, at $\frac{\partial P}{\partial t} = \frac{\partial T}{\partial t} = 0$ the pressure and temperature in Equations 5.35 and 5.36 have a stationary distribution and depend parametrically on compositions of phases which slowly change with time. The formulas 5.35 and 5.36 become the second order ordinary differential equations, and their analysis substantially simplified.

Another approximate approach can be used to estimate calculations. A self-similar variable $z = \frac{r}{\sqrt{t}}$ can be introduced and the order of equations

can be decreased. If we assume that the density of gas in gas layers is a weak function of temperature, i.e., if we assume that $\rho_l \approx \rho(P_l)$ and take into account the small value of the pressure gradient and assume that parts of the order $\left(\frac{\partial P}{\partial r}\right)^2$ are equal to zero, then the system of equations for P_l, T_l splits, and its study becomes significantly simpler.

The Principles of Development of Gas Hydrate Deposits by a High-Frequency Electromagnetic Field

One of the new methods of development of gas hydrate deposits is a high-frequency electromagnetic technology (Makogon et al., 1989). During this method, a strong high-frequency electromagnetic wave (HF EMW) is radiated from a well-bottom radiator (antenna) into a surrounding medium (productive gas hydrate layer). As the HF EMW propagates in a gas hydrate deposit, it interferes with the deposit. As a result, heat sources $q^{(e)}$, ponderomotive forces $\vec{F}^{(e)}$, and the momenta of forces of electromagnetic origin $\vec{K}^{(e)}$ appear distributed in the volume of a productive layer. Along with that, the presence of a high-frequency electromagnetic field (HF EMF) exerts a substantial influence on such physico-chemical phenomena as surface tension, electro-capillary and electro-kinetic processes, and also on the processes of diffusion, adsorption, and filtration in a porous medium.

As a result of an interaction between a hydrate-bearing porous rock and a strong HF EMF, its thermodynamic state changes. For example, the temperature increases because the internal heat sources appear. If the temperature reaches the value of a phase transition $T = T_p$, then a hydrate starts to decompose into gas and water. A high layer pressure is formed in this region, which promotes the filtration of water and gas to a well. Thus, gas can be produced from a hydrate deposit. This method has a number of principal differences from conventional methods. These specialties are the following: the energy is supplied into a layer as the energy of a HF EMW and not by means of hydrodynamic methods or by heat transfer. Therefore, the conditions of temperature distribution in a layer are mainly determined by its electrophysical properties.

A number of principally new problems need to be solved for scientific justification and development of a high-frequency electromagnetic technology for the production of gas from a gas hydrate deposit. These are: physico-mathematical problems of radiation and propagation of HF EMW in a porous medium saturated with a gas hydrate; filtration of liquid and gas in a porous medium in the presence of HF EMF; engineering-physical problems of supplying a high-frequency electromagnetic energy from a ground-based source to a well-bottom radiator; development of an effective underground radiator system; technological problems on the coupling of a technology for production of gas with channeling of a HF electromagnetic energy from a ground-based source to a well-bottom radiator and the radiation of HF EMW with the filtration of a gas and a liquid in a well.

Physical Bases of the Interaction of a High-Frequency Electromagnetic Field with a Hydrate-Bearing Porous Medium

Strong high-frequency sources usually generate electromagnetic fields at a fixed frequency. It is interesting to consider the interaction of a monochromatic HF EMF of the type:

$$\dot{\vec{E}} = \dot{\vec{E}}_0(r, \varphi, z)e^{j\omega t}; \quad \dot{\vec{H}} = \dot{\vec{H}}_0(r, \varphi, z)e^{j\omega t} \tag{5.37}$$

with a gas hydrate system. A hydrate-bearing rock from an electromagnetic point can be considered as a non-magnetic, weakly electrically conductive, polarizable medium which is characterized by the following electrophysical characteristics

$$\dot{\varepsilon}(\omega, T, P) = \varepsilon_0\left[\varepsilon'(\omega, T, P) - j\varepsilon''(\omega, T, P)\right] \tag{5.38}$$

$$\tan\delta(\omega, T, P) = \frac{\sigma + \omega\varepsilon_0\varepsilon''}{\omega\varepsilon_0\varepsilon'} \tag{5.39}$$

In the expressions 5.37–5.39

$\omega = 2\pi f$ - cyclic frequency

f is the frequency;

is the complex dielectric permittivity of a medium, which depends on the frequency ω, temperature T and pressure P;

$\varepsilon', \varepsilon''$ is the real (relative dielectric permittivity) and imaginary parts of the complex dielectric permittivity;

$\tan\delta$ is the tangent of the angle of dielectric losses;

ε_0, μ_0 is the dielectric and magnetic permittivities of vacuum, accordingly;

σ is the specific electrical conductivity;

$\dot{\vec{E}}(r, \varphi, z)$, $\dot{\vec{H}}(r, \varphi, z)$ are the complex amplitudes of the electric and magnetic components of a HF EMF, which depend on the space cylindrical coordinates r, φ, z.

As indicated by physical analyses and experimental studies, the electrical properties of a hydrate-bearing porous medium are determined by establishing the relations

$$\varepsilon' = \varepsilon'(\omega, T, P); \quad \tan\delta = \tan\delta(w, T, P); \quad \mu = \mu_0; \tag{5.40}$$

These relations are determined experimentally.

It is indicated by a physical analysis and by theoretical studies (Landau and Lifshits, 1959; Sayakhov and Fahretdinov, 1981; Sayakhov, 1986) that the energy and force interactions of an HF EMF of the type (5.37) with an operating medium characterized by the electrophysical properties of the type (5.38–5.40) are qualitatively and quantitatively characterized by the appearance of a ponderomotive force $\vec{F}^{(e)}$, momenta of forces $\vec{K}^{(e)}$, and heat sources $q^{(e)}$, whose densities are determined by the expressions:

$$\vec{F}^{(e)} = -\frac{\varepsilon_0(\dot{\vec{E}}_0\,\dot{\vec{E}}_0^*)}{\Delta}\nabla\varepsilon' + \nabla\left[\frac{\varepsilon_0(\dot{\vec{E}}_0\,\dot{\vec{E}}_0^*)}{\Delta}\rho\frac{\partial\varepsilon'}{\partial\rho}\right] \tag{5.41}$$

$$\vec{K}^{(e)} = -j\frac{\varepsilon_0\varepsilon''}{\Delta}\left[\dot{\vec{E}}_0\,\dot{\vec{E}}^*\right] \tag{5.42}$$

$$q^{(e)} = \frac{\omega\varepsilon_0\varepsilon'\tan\delta(\dot{\vec{E}}_0\,\dot{\vec{E}}_0^*)}{2} \tag{5.43}$$

Here a star * denotes a complex-conjugated value of the appropriate quantities; ρ - density of a medium. A complex amplitude of the strength of an

electric field $\vec{\dot{E}}(r,\varphi,z)$, depending on space coordinates, is determined from the solution of Maxwell's equations. Let us assume for a hydrate-saturated medium that the pore sizes, Δ, are significantly smaller than the wavelength of EMW λ, i.e. $\Delta \ll \lambda$. Then, from the linearity and isotropicity of electrophysical characteristics, and, assuming the absence of charges and currents, Maxwell's equations can be written as:

$$div\ \vec{\dot{D}}_0 = 0;\ div\ \vec{\dot{B}}_0 = 0;\ \vec{\dot{D}}_0 = \dot{\varepsilon}\vec{\dot{E}}_0;\ \vec{\dot{B}}_0 = \mu_0 \vec{\dot{H}}_0 \tag{5.44}$$

$$rot\ \vec{\dot{H}}_0 = j\omega\dot{\varepsilon}\left[1 - j\frac{\partial\varepsilon/\partial T}{\omega\dot{\varepsilon}}\frac{\partial T}{\partial t} - j\frac{\partial\varepsilon/\partial P}{\omega\dot{\varepsilon}}\frac{\partial P}{\partial t}\right]\vec{\dot{E}}_0 \tag{5.45}$$

$$rot\ \vec{\dot{E}}_0 = -j\omega\mu_0 \vec{\dot{H}}_0 \tag{5.46}$$

The function $\vec{\dot{E}}(r,\varphi,z)$ can be found from the solution of Equations 5.44–5.46. Indeed, Equations 5.44–5.46 can be brought to

$$\Delta\vec{\dot{E}}_0 + \Gamma^2\vec{\dot{E}}_0 = 0 \tag{5.47}$$

where the constant of propagation is determined by the expression

$$\Gamma^2 = \omega^2\mu_0\dot{\varepsilon}\left[1 - j\frac{\partial\varepsilon/\partial T\Sigma}{\omega\dot{\varepsilon}}\frac{\partial T}{\partial t} - j\frac{\partial\varepsilon/\partial P}{\omega\dot{\varepsilon}}\frac{\partial P}{\partial t}\right] \tag{5.48}$$

The following specialties of the obtained Helmholtz equation (Sayakhov, 1986) and of the expression for Γ should be noticed. The constant of propagation Γ is a complex quantity. Secondly, as seen from Expression 5.44, the constant of propagation Γ is determined by the equation of the electrodynamic state of an operating medium, i.e., by the dependence $\dot{\varepsilon} = \dot{\varepsilon}(\omega,T,P)$ or by dependencies $\varepsilon' = \varepsilon'(\omega,T,P)$; $\varepsilon'' = \varepsilon''(\omega,T,P)$; $\tan\delta = \tan\delta(\omega,T,P)$. This means that the character of distribution of an HF EMW is determined by the thermodynamic state of a medium.

The state of a medium changes with time because of the interference of an HF EMW with it, and the transformation of a part of EMW energy into heat. Qualitative changes in the character of an HF EMW propagation in a medium will be observed if phase transitions occur in a medium. Such a process is possible in the case of a hydrate-bearing porous medium. Indeed, the temperature of a medium will increase as a result of the appearance of internal heat sources during the propagation of an HF EMW, and with time, at appropriate conditions, it can reach the temperature of a phase transition, T_p, at which a hydrate starts to decompose into gas and water. A number of phase transitions are characterized by sharp changes in dielectric properties of a medium in a temperature range of a phase transition where large values of the quantity $\partial\dot{\varepsilon}/\partial T$ are possible. A sharp change of $\dot{\varepsilon}$ with temperature results in a step-like change of a wave resistance of a medium $z = \sqrt{\mu_0/\dot{\varepsilon}}$ on the surface of a phase transition. A change in wave resistance conditions the reflection of an HF EMW off the surface of a phase transition. Hence, a regime of a stationary HF EMW is established in the region of gas hydrate decomposition, and a regime of a running wave—behind the boundary of a phase transition. At that, the boundary of a phase transition will be moving with time. This circumstance points to the need to study a principally new class of problems related to solving Equation 5.47 and account for 5.48 and the thermohydrodynamic state of an operating medium. First, it is necessary to study the dielectric properties of gas hydrate systems as a function of frequency, temperature and pressure in order to obtain the solution to this equation. Initial results of such studies were presented in the works by Sayakhov, 1990.

Initial Equations of the Process-Mathematical Model of Gas Production from a Gas Hydrate Deposit

A schematic description of gas hydrate decomposition during its interaction with a strong HF EMW was presented above. The temperature in a productive layer increases near a well-bottom radiator during the operation of an HF EMW emitter, and after some time it reaches a value needed to start the process of decomposition of a gas hydrate which saturates a porous medium. If there exists a pressure gradient (it can be created in the process of interaction of HF EMF with a productive layer and as a result of physico-chemical processes occurring during this), then there can be a filtration of gas and liquid which form after a hydrate decomposition to a well. It is apparent that a moving boundary of gas hydrate decomposition in a layer $R(t)$ is formed.

It is interesting to determine the distributions of pressure and temperature, the law of a phase front $R(t)$ movement, and the rate of filtration of phases formed after hydrate decomposition, as well as other parameters which determine the technological indices of such a process.

Over time, as an HF EMW travels through an operating medium the thermodynamic state of the medium does not change significantly, and the character of the EMW can be considered unchanged. The processes of heat and mass transfer (changes of temperature and pressure, rate of diffusion, filtration, etc. in an operating medium) are inertial, and the following conditions are satisfied:

$$t_0 \gg 2\pi/\omega, \quad t_0 \gg l_0/\upsilon_\Phi, \quad \upsilon_\Phi = c\sqrt{\varepsilon'}$$

where

- υ_Φ is the phase velocity of a EMW in a medium;
- c is the speed of light in vacuum;
- t_0, l_0 are the characteristic time and length of a problem which determine the phenomena of heat and mass transfer.

The character and physico-chemical properties of a medium which saturate pores in a zone of gas hydrate location have a significance for further studies. Can we consider the saturating medium in a zone of hydrate decomposition as a gas and a liquid which flow independently? Or is some new elastic medium like a gassed liquid formed? Further, we will review a model of gas and liquid. First, we will specify the expressions for $\vec{F}^{(e)}$ and for $\vec{K}^{(e)}$ in order to write the equations of filtration of gas and liquid under the impact of an HF EMF. According to 5.42, $\vec{K}^{(e)}$ is not equal to zero only in the case of a rotating HF EMF for which $[\dot{\vec{E}}_0 \dot{\vec{E}}_0] \neq 0$. Such a field can be created in special UHF devices. This condition is not satisfied in a cylindrical HF EMW which is reviewed further, and therefore $\vec{K}^{(e)} = 0$.

A ponderomotive force $\vec{F}^{(e)}$ can also be neglected in a zone of filtration, since it is much smaller than the formed gradients of pressure ∇P. Therefore, taking into account the appearance of internal heat sources, the following equations of a non-stationary filtration can be written for the zone of gas hydrate decomposition $r \le R(t)$:

$$\frac{\partial(m\rho_i\sigma_i)}{\partial t} + \operatorname{div}(\rho_i\upsilon_i\tau_i) = \vartheta_i \tag{5.49}$$

$$\vec{W}_i = \frac{k(T,E)k_i}{\eta_i(T,E)} - \nabla P \tag{5.50}$$

$$C_{\Pi_1}\frac{\partial T_1}{\partial t} = \operatorname{div}(\chi_{\Pi_1}\nabla T_1) + \rho_i c_i \vec{W}_i \nabla T_1 + q_m + q_{\Pi_1}^{(e)} \tag{5.51}$$

$$\rho_i = \rho_i(P,T,E) \tag{5.52}$$

In these equations

- C_{π_1}, χ_{π_1} is the volume heat capacity and the coefficient of thermal conductivity of a productive rock in a zone of hydrate decomposition, accordingly;
- ρ_i, c_i are the density and specific heat capacity of gas and liquid;
- q_m is the density of heat sources formed during a hydrodynamic motion of gas and liquid;
- $q_{\pi_1}^{(e)}$ is the density of heat sources formed because of interference of a HF EMF with a productive layer in a hydrate decomposition zone;
- m is the porosity;
- k is the absolute permeability;
- k_i is the relative phase permeability;
- ϑ_i is the density of sources of phases;
- σ_i is the saturation of phases.

In a hydrate zone $R \ge R(t)$ it is clear that $\vec{W} = 0$, $q_m = 0$, and the equations take the form:

$$\frac{\partial(m\rho_2\sigma_2)}{\partial t} = 0 \tag{5.53}$$

$$C_{\Pi_2}\frac{\partial T_2}{\partial t} = \operatorname{div}(\chi_{\Pi_2}\nabla T_2) + q_{\Pi_2}^{(e)} \tag{5.54}$$

$$\rho_2 = \rho_2(P,T,E) = \text{const} \tag{5.55}$$

It is necessary to determine an analytical expression for the densities of heat sources in the first $q_{\pi_1}^{(e)}$ and in the second $q_{\pi_2}^{(e)}$ zones in order to theoretically study Equations 5.49–5.55 and to perform calculations on their basis. An electrodynamic problem, i.e., Equations 5.44–5.48 need to be solved for this.

We will limit ourselves to the solution of electrodynamic equations in the form of an axis-symmetrical cylindrical wave for the study of principal questions for the use of HF EMF energy during production of gas from a gas hydrate deposit. In order to do this, we will write the electrodynamic

equation in a cylindrical system of coordinates r, φ, z (z is located in the center of a productive layer, $r = 0$ on the axis of a well) assuming that

$$\partial / \partial\varphi = 0,\ \partial / \partial z = 0,\ \dot{E}_{0r} = \dot{E}_{0\varphi} = \dot{H}_{0r} = \dot{H}_{0\varphi} = 0$$

The non-zero components of a cylindrical HF EMW $\dot{E}_{0\varphi}$ and $\dot{H}_{0\varphi}$ are determined from the equations:

$$\frac{d^2 \dot{E}_{0z}}{dr^2} + \frac{1}{r}\frac{d \dot{E}_{0z}}{dr} + \Gamma^2 \dot{E}_{0z} = 0 \qquad \textbf{(5.56)}$$

$$\dot{H}_{0\varphi} = -\frac{j}{\omega\mu_0}\frac{d \dot{E}_{0z}}{dz}$$

These equations are obtained from 5.45 and 5.47 when they are written in a cylindrical set of coordinates taking into account the conditions listed above.

Here the expression for a constant electromagnetic wave Γ is used in the form:

$$\Gamma^2 = \omega^2 \dot{\varepsilon}_{\Pi} \mu_0 \left[1 - j\frac{\partial \dot{\varepsilon}_{\Pi} / \partial T}{\omega \dot{\varepsilon}_{\Pi}} \cdot \frac{\partial T}{\partial t} - j\frac{\partial \dot{\varepsilon}_{\Pi} / \partial P}{\omega \dot{\varepsilon}_{\Pi}} \cdot \frac{\partial P}{\partial t}\right] \qquad \textbf{(5.57)}$$

where

$\dot{\varepsilon}_{\Pi}, \tan\delta_{\Pi}$ are the dielectric characteristics of a layer, see the Equations 5.38, 5.39.

The constant of electromagnetic wave propagation changes with time, but slower than $\exp(j\omega t)$. Therefore, the wave character of an HF EMF propagation is retained in an operating medium. Hence, the solutions of a wave Equation 5.56 characterize the propagation of a UHF EMF in an operating medium.

Thus, the dependencies $\dot{\varepsilon}_{\Pi}(\omega, T, P)$ and $\tan\delta_{\Pi}(\omega, T, P)$ have a principal importance for the construction of the solutions of Equation 5.56 and for the process of interaction of an HF EMF with an operating medium. These dependencies can be determined only experimentally for such a complicated medium as a saturated porous medium to be used for calculations.

In the presence of phase transitions, sharp changes in the dielectric characteristics of a medium can occur in the process of interaction with an HF EMF. Such situations happen, for example, during the thawing of frozen ground and during formation and decomposition of gas hydrates (Makogon et al., 1988). Two zones at whose interface the dielectric properties undergo a step-change exist near the temperature of a phase transition during these processes. As a result, EMW reflects off a moving boundary of decomposition because of a sharp change in wave resistances of media $z = \sqrt{\mu_0 / \varepsilon_{\Pi_t}}$ at this boundary.

This can be seen from Figures 5-36 and 5-37 (Makogon et al., 1988) which present the dependencies of a relative static dielectric permittivity on temperature $\varepsilon'(T)$, and the dependencies of ε' and ε'' on the frequency for a gas hydrate. A phase transition occurs near $T = 160$ K—a jump of ε' is observed. The area of dispersion is located near the frequency of 10 MHz. According to the estimate made with these graphs, $\tan\delta_m = 0.35$. Such value of the tangent of the angle of dielectric losses is quite acceptable for performing a thermal influence on gas hydrates with HF EMF.

Separating an operating medium $r \geq r_0$ into two zones ($r_0 \geq r \geq R(t)$), and $r \geq R(t)$ and considering that an HF EMW reflected from a moving boundary can exist in the first region, the solutions of Equation 5.58 can be written as:

For the region $r_0 \leq r \leq R(t)$:

$$\dot{E}^{(1)}_{0z} = AH_0^{(1)}(\Gamma_1 r) + BH_0^{(2)}(\Gamma_1 r) \qquad \textbf{(5.58)}$$

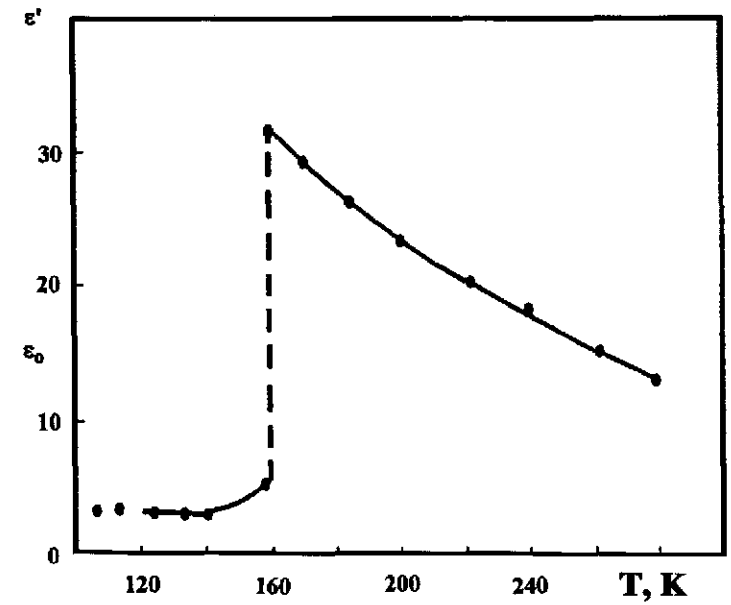

Figure 5-36 Dependence of the relative dielectric permeability of hydrate on temperature.

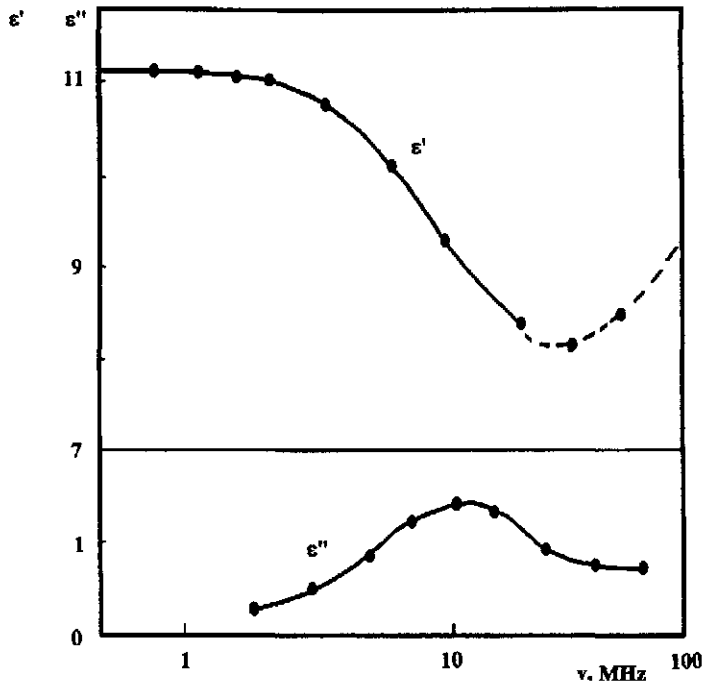

Figure 5-37 Dependence of ε' and ε" for hydrate on frequency.

$$\dot{H}_{0\varphi}^{(1)} = -\frac{\Gamma_1}{j\omega\mu}\left[AH_1^{(1)}(\Gamma_1 r) + BH_1^{(2)}(\Gamma_1 r)\right]$$

For the region $r \geq R(t)$:

$$\dot{E}_{0z}^{(2)} = CH_0^{(1)}(\Gamma_2 r) \qquad (5.59)$$

$$\dot{H}_{0\varphi}^{(2)} = -\frac{\Gamma_2}{j\omega\mu_0} CH_1^{(2)}(\Gamma_2 r)$$

In the expressions 5.58 and 5.59

A, B, C are arbitrary constants determined from the boundary conditions;

$\dot{H}_{0,1}^{(1)}(\Gamma_1 r)$, $\dot{H}_{0,1}^{(2)}(\Gamma_2 r)$ are Hankel functions of the first and second kind, of the zeroth and of the first order.

According to their asymptotic representations

$$H_0^{(1)}(x) = \sqrt{\frac{2}{\pi\chi}} e^{j\left(\chi - \frac{\pi}{2}\nu - \frac{\pi}{4}\right)}$$

$$H_0^{(2)}(x) = \sqrt{\frac{2}{\pi\chi}} e^{-j\left(\chi - \frac{\pi}{2}\nu - \frac{\pi}{4}\right)}$$

The functions $H_{0,1}^{(1)}\left(\dot{\Gamma} r\right)e^{j\omega t}$, $H_{0,1}^{(2)}\left(\dot{\Gamma} r\right)e^{j\omega t}$ are the solutions having the character of a cylindrical wave. The function $H_{0,1}^{(2)}\left(\dot{\Gamma} r\right)e^{j\omega t}$ corresponds to dispersing cylindrical waves (decreases at $r \to \infty$), and the function $H_{0,1}^{(1)}\left(\dot{\Gamma} r\right)e^{j\omega t}$—to converging cylindrical waves, Γ_j and Γ_2 - are related to the first and the second zones and are determined from Expression (5.59).

In order to determine the unknown constants A, B, and C, it is necessary to use the boundary conditions at $r = R(t)$, according to which the tangential components of the strengths of EMF are continuous during the transition through the boundary between two media. These conditions are mathematically written as:

$$\dot{E}_{0z}^{(1)} = \dot{E}_{0z}^{(2)} \text{ at } r = R(t)$$

$$\dot{H}_{0\varphi}^{(1)} = \dot{H}_{0\varphi}^{(2)} \text{ at } r = R(t)$$

$$AH_2^{(1)}(\Gamma_1 R) + BH_0^{(2)}(\Gamma_1 R) = CH_0^{(2)}(\Gamma_2 R)$$

$$\Gamma_1\left[AH_1^{(1)}(\Gamma_1 R) + BH_1^{(2)}(\Gamma_1 R)\right] = \Gamma_2 CH_1^{(2)}(\Gamma_2 R) \qquad (5.60)$$

One more condition is required in order to determine all three of the unknown constants. The expression can be used as this extra condition which indicates that the Umov-Poynting vector determines the power of a radiator at the surface of a radiator. The following can be written for complex values:

$$\frac{1}{2}\mathrm{Re}\left(\dot{H}_{0\varphi}\,\dot{E}_{0z}\right) = \frac{P_0}{2\pi r_0 h} \qquad (5.61)$$

where

P_0 is the power of a HF EMF emitted by a radiator (antenna);

r_0, h are the radius and length of a radiator, accordingly;

Re is the real component of a corresponding complex quantity.

From 5.60 we find:

$$A = C\frac{H_1^{(2)}(\Gamma_1 R)H_0^{(2)}(\Gamma_2 R) - (\Gamma_2/\Gamma_1)H_1^{(2)}(\Gamma_2 R)H_0^{(2)}(\Gamma_1 R)}{H_0^{(1)}(\Gamma_1 R)H_1^{(2)}(\Gamma_1 R) - H_0^{(2)}(\Gamma_1 R)H_1^{(1)}(\Gamma_1 R)}$$

$$B = C\frac{(\Gamma_2/\Gamma_1)H_0^{(1)}(\Gamma_1 R)H_1^{(2)}(\Gamma_2 R) - H_1^{(1)}(\Gamma_1 R)H_0^{(2)}(\Gamma_2 R)}{H_0^{(1)}(\Gamma_1 R)H_1^{(2)}(\Gamma_1 R) - H_0^{(2)}(\Gamma_1 R)H_1^{(1)}(\Gamma_1 R)}$$

Let us introduce the following notation in order to determine the constant C

$$A = \Phi_1(\Gamma_1,\Gamma_2,R)C; \qquad B = \Phi_2(\Gamma_1,\Gamma_2,R)C; \tag{5.62}$$

where

$$\Phi_1(\Gamma_1,\Gamma_2,R) = \frac{H_1^{(2)}(\Gamma_1 R)H_0^{(2)}(\Gamma_2 R) - (\Gamma_2/\Gamma_1)H_1^{(2)}(\Gamma_2 R)H_0^{(2)}(\Gamma_1 R)}{H_0^{(1)}(\Gamma_1 R)H_1^{(2)}(\Gamma_1 R) - H_0^{(2)}(\Gamma_1 R)H_1^{(1)}(\Gamma_1 R)} \tag{5.63}$$

$$\Phi_2(\Gamma_1,\Gamma_2,R) = \frac{(\Gamma_2/\Gamma_1)H_0^{(1)}(\Gamma_1 R)H_1^{(2)}(\Gamma_2 R) - H_1^{(1)}(\Gamma_1 R)H_0^{(2)}(\Gamma_2 R)}{H_0^{(1)}(\Gamma_1 R)H_1^{(2)}(\Gamma_1 R) - H_0^{(2)}(\Gamma_1 R)H_1^{(1)}(\Gamma_1 R)}$$

Now, assuming $\Gamma_i r_0 \ll 1$ and decomposing $H_{0,1}^{(1,2)}(\Gamma_2 r_0)$ from 5.58 and from 5.59 we find:

$$C^* = \frac{P_0}{h}\frac{\omega\mu_0}{2}\frac{1}{\mathrm{Im}[\Phi_1\Phi_2^*]} \tag{5.64}$$

From this we see that the constants A, B, and consequently, C, are determined through $R(t)$, Γ_1, Γ_2. Therefore, the densities of heat sources in zones 1 and 2 ($r \le R(t)$) and ($r \ge R(t)$) are determined by the same quantities. Hence a more complicated class of Stefan's problem emerges.

For a further study let us evaluate the dependence of a propagation constant Γ from 5.57 based on the following considerations

$$\frac{\partial\dot{\varepsilon}_\Pi/\partial T}{\omega\dot{\varepsilon}_\Pi}\frac{\partial T}{\partial t} \approx \frac{1}{\omega\dot{\varepsilon}_\Pi}\frac{\dot{\varepsilon}_\Pi}{T}\frac{T}{t_0} = \frac{1}{\omega t_0} \le 1$$

$$\frac{\partial\dot{\varepsilon}_\Pi/\partial P}{\omega\dot{\varepsilon}_\Pi}\frac{\partial P}{\partial t} \approx \frac{1}{\omega\dot{\varepsilon}_\Pi}\frac{\dot{\varepsilon}_\Pi}{P}\frac{P}{t_0} = \frac{1}{\omega t_0} \le 1$$

since the period of an HF EMF is much smaller than the characteristic time of this problem $2\pi/\omega \ll t_0$. Consequently, if temperature and pressure differ from the temperature and the pressure of a phase transition $T \neq T_\Phi$ and $P \neq P_\Phi$, then Γ in the zones ($r \le R(t)$) and ($r \ge R(t)$) is determined by the expression:

$$\Gamma^2 \approx \omega^2\dot{\varepsilon}_\Pi\mu_0$$

The effect of temperature and pressure changes of an operating medium on the value of Γ is determined by the dependence:

$$\varepsilon_\Pi = \varepsilon_0\varepsilon'_\Pi(\omega,T,P)\left[1 - j\tan\delta_m(\omega,T,P)\right].$$

The constant of propagation Γ is a complex quantity. Let us write it as $\Gamma = \beta - j\alpha$. After doing the appropriate transformations and assuming $\tan\delta \ll 1$, we obtain:

$$\beta = \omega\sqrt{\varepsilon_0\mu_0\varepsilon'_\Pi}, \quad \alpha = \frac{\omega}{2}\sqrt{\varepsilon_0\mu_0\varepsilon'_\Pi}\tan\delta$$

The above considerations allow us to solve electrodynamic and thermohydrodynamic problems independently. As stated above, the effect of a thermohydrodynamic state of a working medium on electromagnetic processes occurring in it is introduced through the dependencies of Γ_1 and Γ_2 on the temperature. At that, if we limit ourselves with the approximation $\tan\delta \ll 1$ used for estimate calculations, then $\dot{\varepsilon}_\Pi = \varepsilon_0\dot{\varepsilon}'_\Pi(\omega,T,P)$ hence

$$\Gamma^2 = \beta^2 = \omega^2\varepsilon_0\mu_0\varepsilon'_\Pi(\omega,T,P)$$

In this approximation we obtain the following expressions for heat sources in the zones 1 and 2 from 5.59 and 5.60. Then we express Hankel functions through Bessel's and Neumann's functions:

$$q_{\Pi_1}^{(e)} = \frac{\omega\varepsilon_0\varepsilon'_{\Pi_1}\tan\delta_{\Pi_1}}{2}\frac{|C|^2}{P^2}\left\{\begin{array}{l}\left[D_1J_0(\Gamma_1 r) + D_2N_0(\Gamma_1 r)\right]^2 + \\ \left[D_3N_0(\Gamma_1 r) + D_4J_0(\Gamma_1 r)\right]^2\end{array}\right\} \tag{5.65}$$

$$q_{\Pi_2}^{(e)} = \frac{\omega\varepsilon_0\varepsilon'_{\Pi_2}\tan\delta_{\Pi_2}}{2}|C|^2\left[J_0^2(\Gamma_2 r) + N_0^2(\Gamma_2 r)\right] \tag{5.66}$$

Here the following notation was used:

$$|C|^2 = \frac{\mu_0\omega P_0}{\pi r_0 h\Gamma_2}\frac{1}{J_0(\Gamma_2 R)N_1(\Gamma_2 R) - J_1(\Gamma_2 R)N_0(\Gamma_2 R)},$$

$$D = J_1(\Gamma_1 R)N_0(\Gamma_1 R) - J_0(\Gamma_1 R)N_1(\Gamma_1 R),$$

$$D_1 = J_1(\Gamma_1 R)N_0(\Gamma_2 R) - \sqrt{\varepsilon_{\Pi_1} / \varepsilon'_{\Pi_1}}\, J_0(\Gamma_1 R)N_1(\Gamma_2 R),$$

$$D_2 = J_1(\Gamma_1 R)J_0(\Gamma_2 R) - \sqrt{\varepsilon'_{\Pi_1} / \varepsilon'_{\Pi_2}}\, J_1(\Gamma_2 R)J_0(\Gamma_1 R),$$

$$D_3 = J_0(\Gamma_2 R)N_1(\Gamma_1 R) - \sqrt{\varepsilon'_{\Pi_1} / \varepsilon'_{\Pi_2}}\, J_1(\Gamma_2 R)N_1(\Gamma_1 R),$$

$$D_4 = N_1(\Gamma_1 R)N_0(\Gamma_2 R) - \sqrt{\varepsilon'_{\Pi_1} / \varepsilon'_{\Pi_2}}\, N_0(\Gamma_1 R)N_1(\Gamma_2 R),$$

J_0, J_1, N_0, N_1 are Bessel's and Neumann's functions of the zeroth and the first orders;

$$\Gamma_1 = \omega\sqrt{\varepsilon_0\mu_0}\sqrt{\varepsilon'_{\Pi_1}(\omega, T, P)},$$

$$\Gamma_2 = \omega\sqrt{\varepsilon_0\mu_0}\sqrt{\varepsilon'_{\Pi_2}(\omega, T, P)}.$$

A Model of Non-Isothermal Filtration during Gas Hydrate Decomposition in a Volume of Porous Medium under the Influence of a High-Frequency Electromagnetic Field

A question about decomposition of a hydrate located in a near-well zone arises during development of gas, gas-oil and gas condensate deposits. Decomposition of hydrates into gas and water with their subsequent production can be done in different ways—by lowering the pressure in a layer, by increasing the temperature, or by changing the chemical potentials of contacting phases.

In the present case, a possibility of decomposing gas hydrates in a near-well-bottom zone of a layer by heating it with a high-frequency electromagnetic field (HF EMF) is reviewed. In mathematical modeling of this process the two extreme mechanisms of decomposition of gas hydrates can be marked out. In-volume occurs when decomposition of hydrates takes place in a volume embraced by the effect of an EMF, and a contact one occurs when a separation boundary exists between hydrate-saturated and gas-saturated zones in a hydrate-saturated area. Different mathematical models of formation and decomposition of hydrates using both contact and in-volume mechanisms are reviewed in several works (Makogon et al., 1988; Makogon, 1985; Degtiarev and Bukhgalter, 1976; Bondarev and Babe, 1976). The results of Bondarev et al. (1989) are in favor of the existence of an extended zone of decomposition or formation of gas hydrates.

In the present work it is thought that decomposition of a hydrate takes place in a whole volume embraced by the effect of an HF EMF.

Let us consider a layer initially saturated with a hydrate and gas. Gas and hydrates exist in a state of thermodynamic equilibrium. During production of gas through a well, pressure decreases in a layer, and hydrate decomposes into gas and water which filtrate to a well. Simultaneously, we consider the electromagnetic influence on a layer through a well. At that, an irreversible transformation of the energy of an EMF into heat occurs in a layer around a well due to dielectric losses, which promotes an increase in the temperature. Thus, the method of production of gas from a gas-gas hydrate layer with combined pressure lowering and HF heating is reviewed.

Let

- m be the porosity of a layer;
- σ_1 be the gas content;
- σ_2 be the water content;
- β be the hydrate content of a layer;
- k be the absolute permeability of a layer.

Accounting for this we write Equations 5.49–5.51.

Continuity equation for the filtrating phases (gas and water) for a case of radial symmetry will look like:

$$m\frac{\partial(\rho_1\sigma_1)}{\partial t} + \frac{1}{r}\frac{\partial}{\partial r}\left(m\sigma_1\rho_1 \vec{\upsilon}_1 r\right) = -m\rho_3\varepsilon\frac{\partial\beta}{\partial t\Sigma} \qquad \textbf{(5.67)}$$

$$m\frac{\partial(\rho_2\sigma_2)}{\partial t} + \frac{1}{r}\frac{\partial}{\partial r}\left(m\sigma_2\rho_2 \vec{\upsilon}_2 r\right) = -m\rho_3(1-\varepsilon)\frac{\partial\beta}{\partial t\Sigma} \qquad \textbf{(5.68)}$$

$$\vec{\upsilon}_i = -\frac{kk_i(\sigma_i)}{\mu_i m_i}\,\mathrm{grad}P_i = -\frac{kk_i(\sigma_i)}{\mu_i m_i}\frac{\partial P_i}{\partial r}, (i = 1, 2) \qquad \textbf{(5.69)}$$

$$m_1 = m\sigma_1, \quad m_2 = m\sigma_2, \quad \sigma_1 + \sigma_2 + \beta = 1 \qquad \textbf{(5.70)}$$

Here index 1 relates to gas, 2—to water, 3 —to hydrate;

ρ_i, $\vec{\upsilon}_i$, k_i, μ_i, P_i - densities of phases, velocities of motion, relative phase permeabilities, viscosity coefficients, and pressures of phases, accordingly.

During derivation of the last equation from the equation of retention of impulses, inertial mass forces and inter-phase volume impulses are neglected. ε is determined from the equation:

$$\varepsilon = m_1/(m_1+nm_2),$$

where

m_1 is the molecular weight of a hydrate-forming gas;

m_2 is the molecular weight of water;

n is the number of water molecules associated with one gas molecule in a hydrate.

For methane hydrate $n = 6$, $m_2 = 18$, and $\varepsilon = 0.129$. Then the mass concentration of water

$$\varepsilon_2 = 1 - \varepsilon = 0.871.$$

Relative phase permeabilities, k_i, are determined experimentally. The following empirical dependencies of phase permeabilities, k, on saturations, σ_i, are suggested for a gas-water system:

$$k_1(\sigma_1) = \begin{cases} 0, & 1 \le \sigma_1 \le 0.1 \\ \left(\dfrac{\sigma_1 - 0.1}{0.9}\right)^{3.5}\left[1 + 3(1 - \sigma_1)\right], & 0.1 \le \sigma_1 \le 1 \end{cases} \quad (5.71)$$

$$k_1(\sigma_1) = \begin{cases} \left(\dfrac{0.8 - \sigma_1}{0.8}\right)^{3.5}, & 0 \le \sigma_2 \le 0.8 \\ 0, & 0.8 \le \sigma_2 \le 1 \end{cases}$$

This is a single-temperature model, hence we will write Equation 5.72 as:

$$C\frac{\partial T}{\partial t} = \operatorname{div}(\chi \operatorname{grad} T) - \vec{W}\operatorname{grad} T + q + q_\Phi + q_\Pi^{(e)} \quad (5.72)$$

Here

T is the temperature of medium;

C is the averaged heat capacity expressed through heat capacities of phases

$$C = (1 - m)\, C_0\rho_0 + m\sigma_1 C_1 P_1\rho_1 + m\sigma_2 C_2\rho_2 + m\beta C_3\rho_3 \quad (5.73)$$

where

C_i is the specific heat capacities of the according phases at a constant pressure; index "$_0$" relates to rock;

λ is the averaged coefficient of thermal conductivity:

$$\lambda = (1 - m)\chi_0 + m\sigma_1\chi_1 + m\sigma_2\chi_2 + m\beta\chi_3, \quad (5.74)$$

where

χ_i is the thermal conductivity coefficients of the according phases.

In Equation 5.72 $\vec{W}$ is the averaged vector of convective heat transfer:

$$\vec{W} = m\sigma_1 C_1\rho_1\,\vec{\upsilon}_1 + m\sigma_2 C_2\rho_2\,\vec{\upsilon}_2 \quad (5.75)$$

The term q represents the energy which is released per unit time in a unit volume of a medium as a result of work of forces of hydrodynamic pressure and the work of pseudo mass forces. The quantity q will be expressed in terms of components, each of which corresponds to a moving phase:

$$q = q_1 + q_2,$$

where

$$q_1 = P_1 m\frac{\partial\sigma_1}{\partial t} - h_1\rho_1 m\sigma_1\left(\frac{\partial P_1}{\partial t} + \vec{\upsilon}_1\operatorname{grad} P_1\right) + mP_1\,\vec{\upsilon}_1\operatorname{grad}\sigma_1 - m\sigma_1\rho_1 R_1\,\vec{\upsilon}_1,$$

$$q_2 = P_2 m\frac{\partial\sigma_2}{\partial t} - h_2\rho_2 m\sigma_2\left(\frac{\partial P_2}{\partial t} + \vec{\upsilon}_2\operatorname{grad} P_2\right) + mP_2\,\vec{\upsilon}_2\operatorname{grad}\sigma_2 - m\sigma_2\rho_2 R_2\,\vec{\upsilon}_2$$

Here, h_i, is the specific intrinsic heat of an isothermal change of pressure.

We assume that the work of forces of internal friction dissipates completely into heat during filtration. The expression for pseudo mass forces of resistance looks like (Bondarev and Babe, 1976):

$$\vec{R}_i = -\frac{\mu_i m_i\,\vec{\upsilon}_i}{kk_i(\sigma_i)\rho_i} + \frac{P_i}{m_i\rho_i}\operatorname{grad} m_i$$

Then the expressions for q_i will look like:

$$q_1 = P_i m\frac{\partial\sigma_i}{\partial t} - h_i\rho_i m\sigma_i\frac{\partial P_i}{\partial t} - m\vec{\upsilon}_i(h_i\rho_i\operatorname{grad} P_i + \operatorname{grad} P_i).$$

Let us introduce Joule-Thompson's coefficient δ and a coefficient of adiabatic expansion of gas η which are defined by the expressions:

$$\begin{cases} \delta = \dfrac{1}{C_P}\left(V - T\left(\dfrac{\partial V}{\partial T}\right)\right), \qquad V = \dfrac{1}{\rho} \\ \eta = \dfrac{T}{C_P}\dfrac{\partial V}{\partial T} \end{cases}$$

Then since $h = \left(\dfrac{\partial i}{\partial P}\right)_T - V$, where i - enthalpy, we can obtain a relation between h, δ, and η using the thermodynamic relations:

$$\left(\frac{\partial i}{\partial P}\right)_T = T\left(\frac{\partial S}{\partial P}\right)_T + V = -T\left(\frac{\partial V}{\partial T}\right)_P + V.$$

Then

$$h = T\left(\frac{\partial V}{\partial T}\right)_P.$$

Hence,

$$h\rho = -C_p\,\rho\,\delta - 1, \qquad h = C_p\eta\,.$$

Finally, the expression for q looks like:

$$q = m\left(P_1\frac{\partial \sigma_1}{\partial t} - P_2\frac{\partial \sigma_2}{\partial t}\right) + \rho_1 C_{P1}\eta_1 m\sigma_1\frac{\partial P_1}{\partial t} + \rho_2 C_{P2}\eta_2 m\sigma_2\frac{\partial P_{21}}{\partial t} +$$

$$\rho_1 m\sigma_1 CP_1\delta_1\vec{\upsilon}_1\,\mathrm{grad}P + \rho_2 m\sigma_2 CP_{21}\delta_2\vec{\upsilon}_2\,\mathrm{grad}P_2 \qquad \textbf{(5.76)}$$

In Equation 5.72 q_Φ is the energy released because of phase transitions and is determined by the expression:

$$q_\Phi = Lm\rho_3\frac{\partial \beta}{\partial t}, \qquad \textbf{(5.77)}$$

where

L is the specific heat of phase transitions.

$q_\pi^{(e)}$ is the energy released per unit time in a unit volume due to the interaction of an HF EMF. For zones 1 and 2, $q_m^{(e)}$ and $q_{\pi 2}^{(e)}$ are defined by Expressions 5.65 and 5.66.

In order to close the system 5.67–5.77, we will use the equation of a state of gas in a form:

$$P_l = z_l\frac{\rho_l RT}{\nu_l}, \qquad \textbf{(5.78)}$$

where

ν_l is the molecular weight of gas;

R is the universal gas constant;

z_l is the gas compressibility.

The condition of water incompressibility can be used as the equation of state for water:

$$\rho_j = \text{const.} \qquad \textbf{(5.79)}$$

A relation between the pressures of gas and liquid can be written in the most general form:

$$P_j - P_2 = P_K(\sigma_l, T), \qquad \textbf{(5.80)}$$

where

P_K is the capillary pressure at the gas-liquid interface, which is either defined by an empirical formula, or is neglected.

The system is completed by the equation which relates the temperature, T_D, and the pressure at the line of phase equilibrium

$$T_D = f(P_D) \qquad \textbf{(5.81)}$$

The boundary condition can be specified in the following way. Often the pressure at the well bottom, P_0, is specified, and the layer pressure, P_L, is known. Assuming that a well has a certain radius of influence, r_l, at which the pressure is equal to the layer pressure, then the boundary conditions for P can be written in the form:

$$P_j(r_0) = P_2(r_0) = P_0\,; \qquad P_j(r_l) = P_2(r_l) = P_L\,. \qquad \textbf{(5.82)}$$

Here r_l is the radius of well influence.

Boundary conditions for the temperature are also taken at the radius of influence and at well bottom:

$$T(r_1) = T_1; \quad \left.\frac{\partial T}{\partial r}\right|_{r=r_0} = 0 \tag{5.83}$$

Initial conditions will be written as

$$P_1(r, 0) = P_2(r, 0) = P_L, \qquad \sigma_1(r, 0) = \sigma_{10}, \tag{5.84}$$

$$T(r, 0) = T_L, \qquad \beta(r, 0) = \beta_0.$$

The system of Equations 5.67–5.83 is complete. Their solution can be obtained numerically using a computer. The solution of the problem will allow us to determine the main thermodynamic characteristics of the process: distributions of pressure and temperature in a layer, saturations of phases, rate of gas hydrates decomposition, amount of the produced gas, fraction of gas produced from hydrate, etc.

Let us consider the case when $\upsilon_2 = 0$, i.e., when there is no filtration of water since it remains in pores. Then the balance equations will look like:

$$m\frac{\partial(\rho_1\sigma_1)}{\partial t} + \frac{1}{r}\frac{\partial}{\partial r}(r\rho_1\upsilon_1) = m\rho_3\varepsilon\frac{\partial\beta}{\partial t}, \tag{5.85}$$

$$\rho_2\frac{\partial\sigma_2}{\partial t} = -\rho_3(1-\varepsilon)\frac{\partial\beta}{\partial t},$$

where $\upsilon_1 = -\dfrac{kk_1(\sigma_1)}{\mu m\sigma_1}\dfrac{\partial P_1}{\partial r}$ - rate of filtration of gas.

Using the correlation $\sigma_1 + \sigma_2 + \beta = 1$, we obtain

$$\frac{\partial\beta}{\partial t}\left[\frac{\rho_3}{\rho_2}(1-\varepsilon) - 1\right] = \frac{\partial\sigma_1}{\partial t}. \tag{5.86}$$

then from 5.85 we obtain

$$m\left[\rho_1 + \frac{\rho_2\rho_3\varepsilon}{\rho_3(1-\varepsilon)-\rho_2}\right]\frac{\partial\sigma_1}{\partial t} + m\sigma_1\frac{\partial P_1}{\partial t} - \frac{1}{r}\frac{\partial}{\partial r}\left(r\rho_1\frac{k}{\mu_1}k_1|\sigma_1|\frac{\partial P}{\partial r}\right) = 0 \tag{5.87}$$

In the equation of state 5.78 we assume that $z_1 = \text{const}$, or

$$\rho_1 = \frac{P_1}{\beta_1 T}, \text{ where } \beta_1 = \frac{z_1 R}{V_1} = \text{const}$$

Substituting the derivatives $\partial\rho_1/\partial t$ and $\partial\rho_1/\partial r$ in (5.87) and using the equation of phase equilibrium (5.81) we obtain:

$$m\left[\rho_1 + \frac{\rho_2\rho_3\varepsilon}{\rho_3(1-\varepsilon)-\rho_2}\right]\frac{\partial\sigma_1}{\partial t} + m\sigma_1\rho_1\left(\frac{1}{P_1} - \frac{f'_P}{T}\right)\frac{\partial P_1}{\partial t} -$$

$$\frac{kk_1}{\mu_1}\left[\frac{1}{r}\frac{\partial P_1}{\partial r} + \left(\frac{1}{P_1} - \frac{f'_P}{T}\right)\left(\frac{\partial P_1}{\partial r}\right)^2 + \frac{k\sigma_1}{k_1}\frac{\partial\sigma_1}{\partial r}\frac{\partial P_1}{\partial r} + \frac{\partial^2 P_1}{\partial r^2}\right] = 0 \tag{5.88}$$

In the equation of thermal conductivity which is written in this case as

$$C\frac{\partial T}{\partial t} = \frac{1}{r}\frac{\partial}{\partial r}\left(\lambda r\frac{\partial T}{\partial r}\right) - \rho_1\upsilon_1 C_1\frac{\partial T}{\partial r} + m\left(P_1\frac{\partial\sigma_1}{\partial t} + P_2\frac{\partial\sigma_2}{\partial t}\right) +$$

$$\rho_1 C_{P1}\eta_1 m\sigma_1\frac{\partial P_1}{\partial t} + \rho_2 C_2\eta_2 m\sigma_2\frac{\partial P_2}{\partial t} + \rho_1 C_{P1}\varepsilon_1\upsilon_1\frac{\partial P_1}{\partial t} + Lm\rho_3\frac{\partial\beta}{\partial t} + q^{(e)} \tag{5.89}$$

we neglect a capillary jump of pressure ($P_1 \approx P_2$), convective terms, and the terms related to adiabatic and throttling effects due to their small value. Then Equation 5.89 will simplify:

$$C\frac{\partial T}{\partial t} = m\frac{-P - LP_3}{1 - \dfrac{\rho_3}{\rho_2}(1-\varepsilon)}\frac{\partial\sigma_1}{\partial t} + q^{(e)} \tag{5.90}$$

from which the equation relative to P, σ can be obtained

$$Cf'_P\frac{\partial P_1}{\partial t} = m\frac{-P - LP_3}{1 - \dfrac{\rho_3}{\rho_2}(1-\varepsilon)}\frac{\partial\sigma_1}{\partial t} + q^{(e)} \tag{5.91}$$

Thus, we obtain two equations relative to P_1, σ_1 (5.88), (5.91) which can be used numerically. The boundary and the initial conditions which close this system look like:

$$P_1(r_0, t) = P_0 < P_L, \qquad P(r_1, t) = P_L,$$

$$P_1(r, 0) = P_L, \qquad \sigma_2(r, 0) = 0,$$

$$\beta(r, 0) = \beta_0 \tag{5.92}$$

From the second Equation 5.85 and from Equation 5.86 using the initial conditions (5.92), we can obtain a law of a change of water content in a layer:

$$\sigma_2(t) = \frac{\rho_3(1-\varepsilon)}{\rho_2}(\beta_0 - \beta(t)) \tag{5.93}$$

and a law of a change of gas content in a layer:

$$\sigma_1(t) = 1 - \beta(t) - \frac{\rho_3(1-\varepsilon)}{\rho_2}(\beta_0 - \beta(t)) \qquad (5.94)$$

A condition $\sigma_2(t) \le \sigma_2^*$ must be satisfied for $\sigma_2(t)$, where σ_2^* - value of water content at which filtration of water starts ($\sigma_2^* = 0.2 - 0.3$). If this condition is satisfied, then the initial assumption $k_2(\sigma_2) = 0$, $\upsilon_2 = 0$ is true. The moment in time t^* (from the moment of start of gas hydrate decomposition) when a single-phase filtration of gas will take place can be determined,

$$\beta(t^*) = \beta_0 - \frac{\sigma_2^*}{1-\varepsilon}\frac{\rho_2}{\rho_3} \qquad (5.95)$$

If a further decrease of β from a value $\beta_0 - \frac{\sigma_2^*}{1-\varepsilon}\frac{\rho_2}{\rho_3}$, the model of a single-phase filtration can not be valid.

The constructed mathematical model can be used for a numerical study of the processes of non-isothermal filtration during decomposition of a gas hydrate in a volume of a porous medium under the influence of a high-frequency electromagnetic field. This model can be used for making estimate calculations of the main technological indices of the process.

Considering the Wave-Conducting Effect during an HF Electromagnetic Influence on a Gas Hydrate Layer

If a productive layer has a limited thickness and its thickness is comparable to the electromagnetic wave (EMW) length, then the solutions of electrodynamic equations in a form of purely cylindrical waves are unacceptable. In real conditions productive layers are usually located between non-productive rock (roof and bottom), i.e., the zone of EMW propagation is a three-layer medium. At that, the electrical conductivity of a layer is usually small and the condition $(\sigma_L / \omega \varepsilon_0 \varepsilon'_П) \ll 1$ is satisfied, and for the roof and the bottom $(\sigma_R / \omega \varepsilon_0 \varepsilon'_R) \ge 1$, $(\sigma_{ВОТ} / \omega \varepsilon_0 \varepsilon'_{ВОТ}) > 1$. This means that we are dealing with a dielectric layer located between more conductive media.

If the thickness of such a dielectric layer, h, satisfies the condition, $\lambda \le 2h$, then the definition of a radio wave conductor can be applied to such a three-layer medium (Wait, 1963; Zverev et al., 1975). The so-called waves of types H and E can exist in a wave conductor roof-layer-bottom at certain conditions. In field conditions, we are interested in waves of

type E whose components, $\dot{E}_{0z}$, $\dot{H}_{0\varphi}$, $\dot{E}_{0r}$ are not equal to zero. It is necessary to study the conditions of excitation, propagation, and distribution of an electromagnetic field (EMF) for such waves at a finite thickness of a layer h.

For this type of wave the solutions of electrodynamic equations 5.45–5.46 look like:

In the region $r \le r < R(t)$

$$\dot{H}^{(1)}_{0\varphi П} = \left[AJ_1(\Gamma_1 r) + BN_1(\Gamma_1 r)\right] Sh\gamma_1 z \qquad (5.96)$$

$$\dot{E}^{(1)}_{0rП} = \gamma \frac{1}{j\omega \dot{\varepsilon}_{1П} F_1\left(\dot{\varepsilon}_{1П}, T, P\right)}\left[AJ_1(\Gamma_1 r) + BN_1(\Gamma_1 r)\right] Ch\gamma_1 z \qquad (5.97)$$

$$\dot{E}^{(1)}_{0zП} = \frac{\Gamma_1}{j\omega \dot{\varepsilon}_{1П} F_1\left(\dot{\varepsilon}_{1П}, T, P\right)}\left[AJ_0(\Gamma_1 r) + BN_0(\Gamma_1 r)\right] Sh\gamma_1 z \qquad (5.98)$$

$$\Gamma_1^2 = \gamma_1^2 + \omega^2 \mu_0 \dot{\varepsilon}_{1П}\left[1 - j\frac{\partial \dot{\varepsilon}_{1П}/\partial T}{\omega \dot{\varepsilon}_{1П}}\frac{\partial T}{\partial t} - j\frac{\partial \dot{\varepsilon}_{1П}/\partial P}{\omega \dot{\varepsilon}_{1П}}\frac{\partial P}{\partial t}\right] \qquad (5.99)$$

$$F_1\left(\dot{\varepsilon}_{1П}, T, P\right) = 1 - j\frac{\partial \varepsilon_{1П}/\partial T}{\omega \dot{\varepsilon}_{1П}}\frac{\partial T}{\partial t} - j\frac{\partial \varepsilon_{1П}/\partial P}{\omega \dot{\varepsilon}_{1П}}\frac{\partial P}{\partial t} \qquad (5.100)$$

In the region $r \ge R(t)$, $0 \le z \le h$

$$\dot{H}^{(2)}_{0\varphi П} = CH_1^{(2)}(\Gamma_2 r) Sh\gamma_2 z \qquad (5.101)$$

$$\dot{E}^{(2)}_{0rП} = \frac{\gamma_2}{j\omega \dot{\varepsilon}_{2П} F_2\left(\dot{\varepsilon}_{2П}, T, P\right)} CH_1^{(2)}(\Gamma_2 r) Ch\gamma_2 z \qquad (5.102)$$

$$\dot{E}^{(2)}_{0zП} = \frac{\Gamma_2}{j\omega \dot{\varepsilon}_{2П} F_2\left(\dot{\varepsilon}_{2П}, T, P\right)} CH_0^{(2)}(\Gamma_2 r) Sh\gamma \qquad (5.103)$$

$$\Gamma_2^2 = \gamma_2^2 + \omega^2 \mu_0 \dot{\varepsilon}_{2П}\left[1 - j\frac{\partial \dot{\varepsilon}_{2П}/\partial T}{\omega \dot{\varepsilon}_{2П}}\frac{\partial T}{\partial t} - j\frac{\partial \dot{\varepsilon}_{2П}/\partial P}{\omega \dot{\varepsilon}_{2П}}\frac{\partial P}{\partial t}\right] \qquad (5.104)$$

$$F_2\left(\dot{\varepsilon}_{2П}, T, P\right) = 1 - j\frac{\partial \varepsilon_{2П}/\partial T}{\omega \dot{\varepsilon}_{2П}}\frac{\partial T}{\partial t} - j\frac{\partial \varepsilon_{2П}/\partial P}{\omega \dot{\varepsilon}_{2П}}\frac{\partial P}{\partial t} \qquad (5.105)$$

In this case the densities of heat sources in the first and the second zones are determined by the expressions

$$q_{1\Pi}^{(e)} = \frac{\omega\varepsilon_0\varepsilon'_{1\Pi}\tan\delta_{2\Pi}}{2}\left(\left|\dot{E}_{0r\Pi}^{(1)}\right|^2 + \left|\dot{E}_{0z\Pi}^{(1)}\right|^2\right) \tag{5.106}$$

$$q_{2\Pi}^{(e)} = \frac{\omega\varepsilon_0\varepsilon'_{2\Pi}\tan\delta_{2\Pi}}{2}\left(\left|\dot{E}_{0r\Pi}^{(2)}\right|^2 + \left|\dot{E}_{0z\Pi}^{(2)}\right|^2\right) \tag{5.107}$$

The influence of surrounding medium ($|z| \geq h$) is, in essence, that transversal constants of propagation in a layer and outside of it are related by the expressions (Wait, 1972):

$$\gamma_C + \frac{\dot{\varepsilon}_C}{\dot{\varepsilon}_{1,2\Pi}}\gamma_{1,2\Pi}th\gamma_{1,2\Pi}h \tag{5.108}$$

$$\frac{\gamma_{2\Pi}}{\gamma_{1\Pi}} = \frac{\dot{\varepsilon}_{2\Pi}F_2}{\dot{\varepsilon}_{1\Pi}F_1} \tag{5.109}$$

Theoretical calculations of the distribution of EMF in a roof and a bottom were made. An appropriate function of distribution of the heat sources and other parameters of the system roof-layer-bottom represented it as a wave conductor with nonideally conducting walls, in accordance with the equations above.

The calculation indicates that for waves of type H_m and E_m their different components in such a wave conductor are described by the function of the form

$$E_m, N_m \sim \left\{\begin{matrix}\cos m\pi\dfrac{z}{h}\\ \cos m\pi\dfrac{z}{h}\end{matrix}\right\}\frac{e^{-\alpha r}}{\sqrt{\pi\beta r/2}}e^{-j\beta r}e^{j\omega t} \tag{5.110}$$

where m assumes only integer values $m = 0, 1, 2, \ldots$

$$\alpha = \frac{1}{2}\omega\sqrt{\varepsilon_\Pi\mu_0}(\tan\delta)_\Pi, \tag{5.111}$$

$$\beta = \sqrt{\left(\frac{m\pi}{h}\right)^2 - R^2}, \quad k = \omega\sqrt{\varepsilon_\Pi\mu_0} \tag{5.112}$$

Outside a layer (in roof and bottom) EMF quickly fades with growth of $|z|$ by exponential law, since for these $\alpha_R \gg \alpha_{BOT}$. On one hand, fading in a layer is determined by the quantity α_{BOT} with the formula 5.111. On the other hand, according to 5.112, if $(m\pi/h) < R$, then additional fading will be observed, and we have the distribution of a field without a consideration of wave-conducting effects. In the case $(m\pi/h) < R$ additional fading is not included, and the field will propagate along the wave conductor. Thus, a deep penetration of HF and UHF electromagnetic waves into a layer from a well radiator is realized for the main operating types of waves H_l, E_l ($m = 1$) because of wave conducting effects if the operating frequency of a generator is above some critical value determined by the expression

$$f_{CR} = \frac{m}{2h\sqrt{\varepsilon_\Pi\mu_0}} \tag{5.113}$$

Usually, the operating wavelength $\lambda_0 = c/f$ for a main wave $m = 1$ is chosen in the range

$$h\sqrt{\varepsilon'_\Pi} < 0 < 2h\sqrt{\varepsilon'_\Pi} \tag{5.114}$$

Thus, the expressions 5.113 and 5.114 are the conditions of choice of an operating frequency $f > f_{CR}$ or an operating wavelength of an HF generator in order to realize wave-conducting effects during an HF electromagnetic influence on a near-well-bottom zone of a layer.

Study of the dependence of the coefficient of general fading α_{GEN} and the constant of wave propagation β on the frequency obtained from a calculation of an exact electrodynamic problem for the case

$\varepsilon_{OTPP} = 2.2$, $\tan\delta\pi \approx 0.05$, $\varepsilon_{R.OTP} \approx \varepsilon_{BOT.OTP} = 4$,

$(\tan\delta)_R = (\tan\delta)_{BOT} = 0.15$, $h = 6$ cm

which corresponds to the parameters of the model used for an experimental study of wave-conducting effects indicated that if the condition $f = f_{CR} =$ 1670 MHz is satisfied, a wave-conducting effect is clearly displayed. This was confirmed by an industrial test. Notice that if the condition $f > f_{CR}$ (1900 MHz) is satisfied, the field is mainly concentrated in a layer, while outside of a layer it fades exponentially. If the condition $f > f_{CR}$ is not satisfied, then no selective concentration of HF energy in a layer is observed. It is quite evenly distributed across the model. With a further increase of frequency when the condition (5.113) is violated due to various electrodynamic effects, the concentration of the energy of an EMF in a layer weakens.

Principles and Experience of the Development of Gas Hydrate Deposits (GHD)

It is known that accumulations of hydrocarbons in the earth can exist in the three phase states: gaseous, liquid, and solid. In gas hydrate deposits, depending on the thermodynamic conditions, hydrocarbons exist in a solid hydrate, free, and dissolved pore-water states.

Gas hydrate deposits can be lithologically covered or open; equilibrated or supercooled; massive; one- or multi-layered with or without the lithological covers which separate the hydrate-saturated layers; and may contain hydrate in a dispersed, nodular, or monolith state.

Gas hydrate deposits can be at the stage of formation, stable, metastable, or dissociating. They can have anomalously high or low pressure, compared to the hydrostatic pressure. They can contact both on top and bottom with the deposits of a free gas. Gas hydrate deposits can be primary or secondary. One of the main parameters of GHDs is the hydrate saturation coefficient which varies between 0 and 1.

Selecting the drilling method and mastering and testing of wells in GHD depends on the geophysical characteristics of the field. The common principle of converting the gas from a hydrate into a free state and its consequent production using the regular methods underlies the modern methods of developing GHD. The methods of supplying energy to decompose a hydrate in GHD and methods of gas production are determined by the economic and the ecological requirements.

The unique experience of the development of the Messoyakh gas hydrate field has shown the technological possibility and economical suitability of developing GHD at the present time, especially in regions with low potential resources of traditional energy. The total production of natural gas from the gas hydrate deposit of the Messoyakh field was about 5 billion m^3. The cost of gas production from hydrate was 20% higher than traditional.

Development of GHD offshore has a number of special characteristics:

- small depths of the pay-zone location from the sea bottom;
- absence (often) of the impenetrable lithological covers above GHD;
- large area of GHD spreading;
- relatively low strength of the hydrate bearing and covering rock;
- presence of a large water cover over GHD;
- variable degree of GHD supercooling; and a number of other details.

Experiences in Hydrate Production (An Example of the Messoyakhi Field)

The Messoyakhi gas hydrate field was the catalyst in the problem of natural gas hydrates, similar to the hydrate plugs found by Hammerschmidt in pipelines.

It is known that the first publications about natural gas hydrates appeared in 1965–1966 (Makogon, 1965, 1966). However, the interest in the problem emerged after discovering the Messoyakhi gas hydrate deposit and developing it (Makogon et al., 1971).

In the early 1930s the Norilsk Metallurgical Plant was put into operation beyond the Arctic circle. This plant worked with expensive coal which had to be brought from afar. The geologists actively searched for a local source of oil or gas. As a result, in 1967 the Messoyakhi field was discovered 250 kilometers west of Norilsk on the left side of the Yenisei River (Figure 5-38).

This field was immediately put into industrial development. Gas was supplied to the plant through the 20-inch pipeline. About 70 wells were drilled on the field. It was found from the complex of geophysical, geochemical, and hydrodynamic testing that:

- the pay-zone area was 12.5 by 19 kilometers;
- the thickness of the pay-zone was 84 meters;
- layers of the pay-zone consist of shale and sandstone rock of the middle Jurassic, lower- and upper-Cretaceous and Pliocene ages, covered by the Quaternary sediments;
- open porosity coefficient varies between 16% and 38% with a 25% average;
- depth of the pay-zone cover was 730 meters;
- depth of the gas-water contact was 850 m;
- the residual water saturation was limited to 29–50%;
- permeability ranges within 10–1000 md (average is 125 mdarcy);
- rock water salt content was up to 1.5%;
- the natural gas composition at the initial temperature and pressure was CH_4 = 98.6%, C_2H_6 = 0.1%, C_3H_8+ = 0.1%, CO_2 = 0.5%, N_2 = 0.7%;
- the initial pressure was 7.8 MPa.

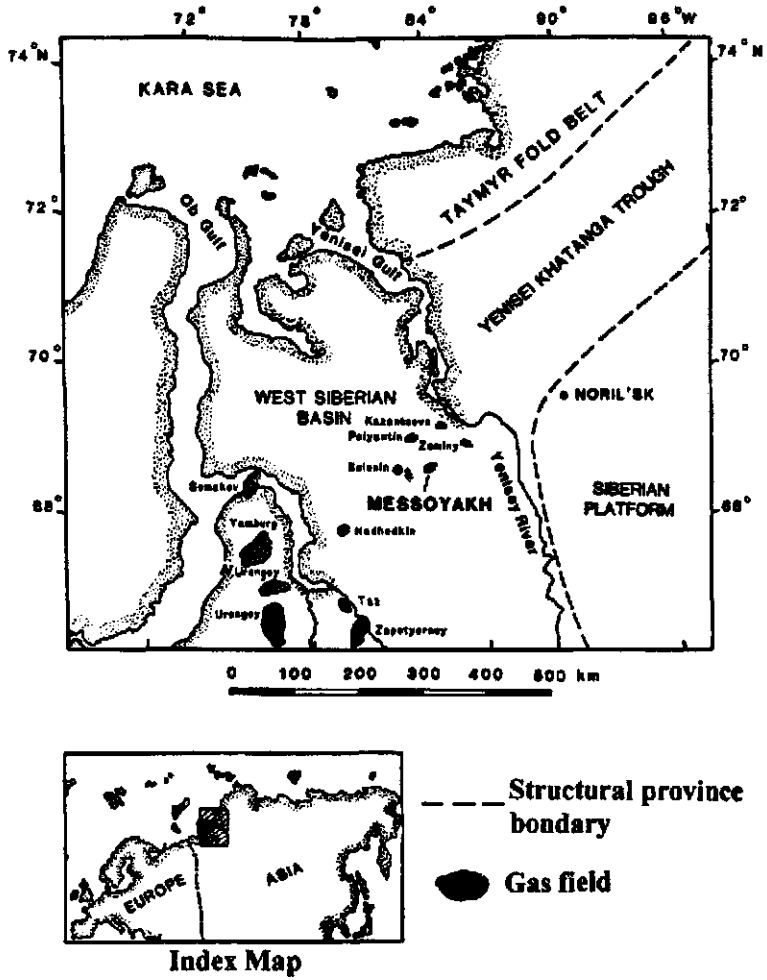

Figure 5-38 Map showing the Western Siberian Basin, the Messoyakhi field, other fields, and structural provinces.

The field is located in the permafrost region whose thickness over the field is 450 m. The field has a rigid thermodynamic characteristic. The roof of deposit temperature is 8°C, the bottom temperature is 12°C. The experimental equilibrium temperature of gas hydrate formation in the Messoyakhi field at P = 7.8 MPa equals 10°C, thus the +10°C geoisotherm is the lower boundary between the overlying gas hydrate deposit and the underlying gas deposit. The boundary is not flat but dome-like, following the geoisothermal surface which depends on the stratigra-

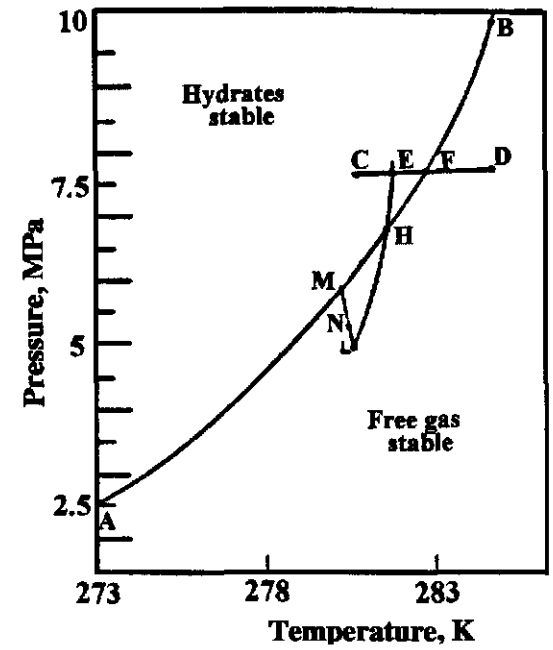

Figure 5-39 Pressure and temperature conditions of the Messoyakhi Reservoir.

phy of the deposit. The gas hydrate and the gas deposits have a common gas-water interface.

Other characteristics of the Messoyakhi field are:

- the hydrate saturation varies from 0.4 at the top of gas hydrate deposit to 0.2 at its bottom;
- effective thickness of the pay-zone is about 25 m;
- the total gas reserves are over 37×10^9 m^3 of which 15×10^9 m^3 are in a free state and the rest is in a hydrate state;
- the producing layers have non-producing lens-shaped inclusions and the open lithological windows at the gas-gas hydrate deposits interface.

Figure 5-38 shows a schematic map of the depths of a hydrate formation zone in the northwestern part of the West Siberia where the Messoyakhi field is located. In order to determine the hydrate formation conditions, the real core samples taken from the upper pay-zone intervals of the Messoyakhi field were studied. Figure 5-39 shows the curve of

equilibrium hydrate formation for gas and layer water of the Messoyakhi field. Figure 5-40 presents the stratigraphic column, and Figure 5-41, the thermal profile of the Messoyakhi field and the equilibrium curve of hydrate formation. Figure 5-41 shows that the hydrate deposit of the Messoyakhi field is metastable with an extremely low subcooling. The

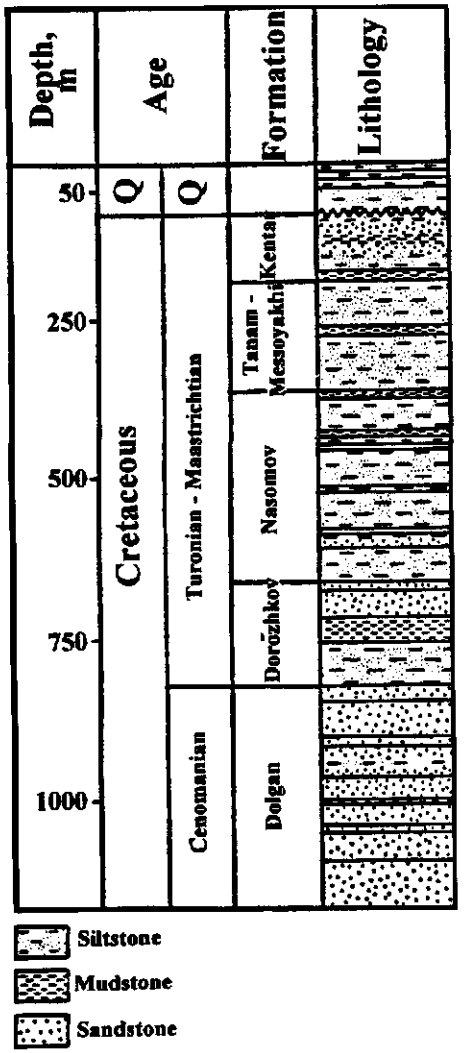

Figure 5-40 Schematic stratigraphic column, Messoyakhi gas field.

slightest decrease in the layer pressure or increase in temperature is accompanied by the decomposition of a hydrate in the layer. This statement is well supported by field development.

Figure 5-42 shows the fragment of the Messoyakhi field pay-zone profile. A large complex of geophysical, geochemical, and hydrodynamic tests on the Messoyakhi field were performed. Figure 5-43 shows the first results of a geophysical indication of gas hydrates obtained from one of the wells on the Messoyakhi field in 1968 (Sapir, 1973). Even the first geophysical logs of the pay-zone required additional tests for the dependence of various rock parameters on their hydrate content. The analysis of electric resistivity of rock compared to the other geophysical parameters (rate of drilling, cavity measurements, neutron and seismic logging, resistivity logging) produced good results and revealed hydrate saturated rock.

The effect of the layer temperature on the well production rate was found from the well testing. During the setting of perforation intervals

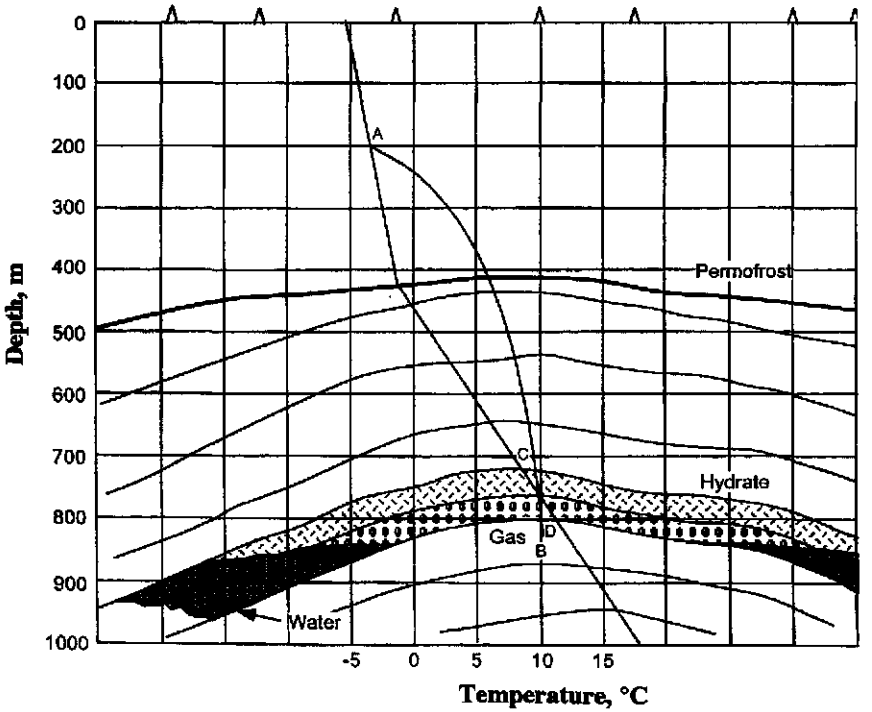

Figure 5-41 Thermal cross-section of Messoyakhi field.

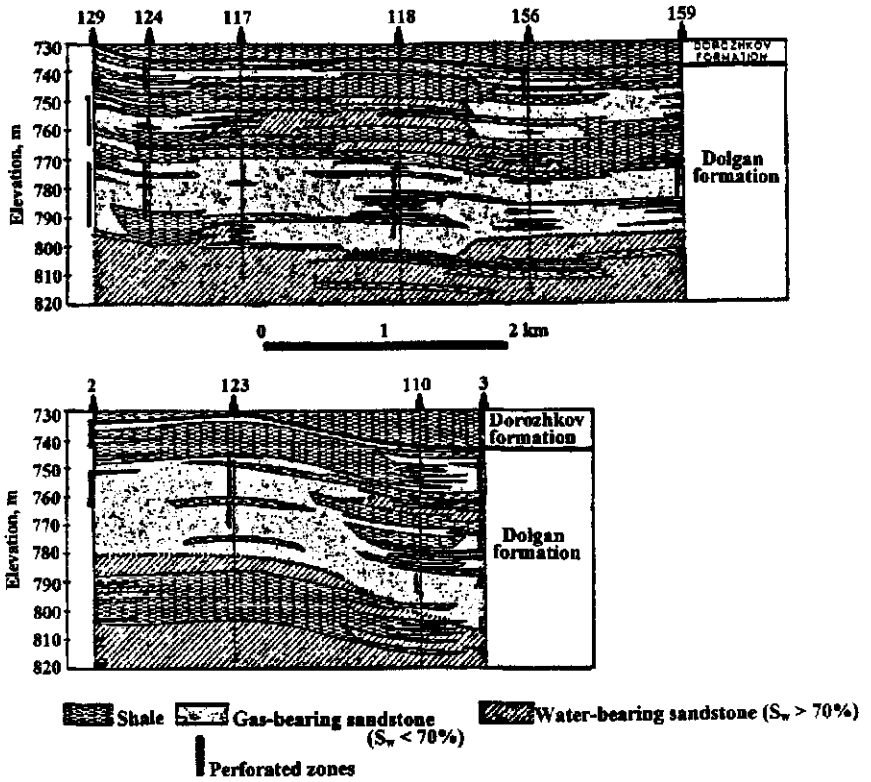

Figure 5-42 Cross-section of the Messoyakhi gas field, depths are subsea (adapted from Sapir et al., 1973).

upward from the lower boundary of the gas hydrate zone (10°C isotherm) a decrease of production rates was observed, and with the perforation intervals set below the hydrate boundary the production rates increased (Table 5-7).

The wells 109, 113, 120, and 121 drilled in the northwest part of the field gave no industrial gas production. The wells 109 and 113, which have opened the hydrate saturated and water-bearing layers, produced absolutely free rates of 133,000–137,000 m³/day during testing. After the methanol treatment of the hydrate saturated intervals, the industrial gas production rates were obtained (Table 5-8 and Figure 5-44).

There are mastered and operated wells on the field whose perforation opened simultaneously gas and hydrate saturated layers. According to the well-bottom production rate measurements, the magnitude of the gas

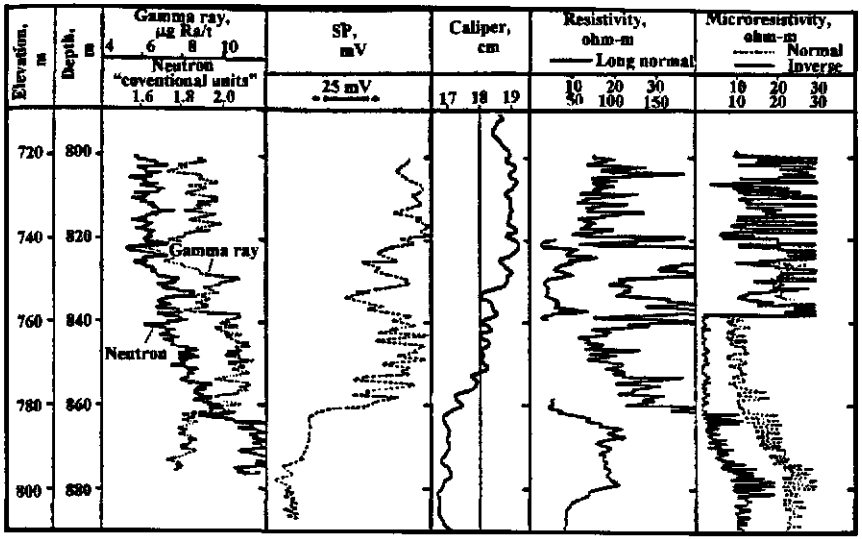

Figure 5-43 Logs of well 136, Messoyakhi gas field (adapted from Sapir et al., 1973).

Caliper and microresistivity log curves suggest the base of hydrate stability zone at –755 m, but SP, resistivity, and neutron curves indicate transition from hydrate to free-gas at –782 m.

Table 5-7 Dependence of free gas flow on depth of perforation.

Well Number	*Depth of Perforation Intervals, m*	*Depth of +10©C isotherm, m*	*Distance from Perforation Holes to +10©C isotherm, m*	*Absolutely Free Gas Flow, m³/day*
121	–716–727	–791	+64	26
109	–748–794	–800	+6	133
150	–741–793	–787	–6	413
195	–779–795	–766	–29	626
131	–771–793	–734	–59	1000

flow from the hydrate saturated layer varies between 0 and 36% of the total well production. Operation of the wells, which had opened simultaneously the gas and hydrate layers, is related to some complications caused by the influx of sand and water from the hydrate saturated intervals. During the initial period of exploitation of the field, the opinion of

Table 5-8 Results of methanol injection on gas flow.

Well Number	Before Treatment		After Treatment	
	Pressure Drop, kgf/cm²	Gas Flow, 1000 m³/day	Pressure Drop, kgf/cm²	Gas Flow, 1000 m³/day
133	3.5	25	0.4	50
	7.0	50	0.8	100
	14	100	1.1	150
	19	150	1.5	200
	22	200	2.0	250
142	8	5	0.4	50
	13	10	0.5	100
	19.5	25	0.7	150
	25	50	1.0	200
	30	100	1.4	
	33	150		

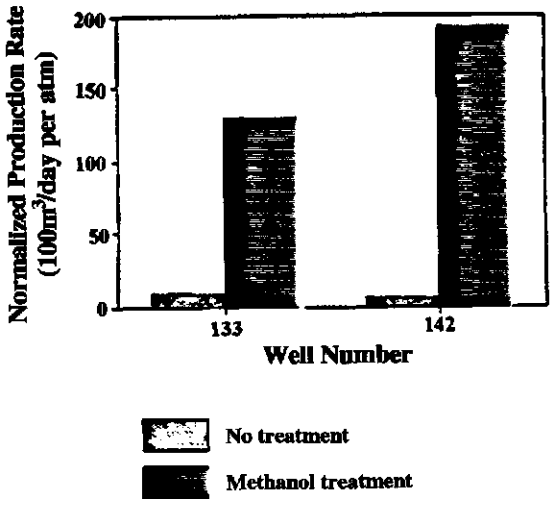

Figure 5-44 Effect of methanol injection on gas production rates (data from Makogon et al., 1971).

the management was that the hydrates formed in the well-bottom zone during the drilling process from the liquid filtered from the drilling mud. The field was already drilled and taking another core sample was impossible. That is why, in order to clear the incorrect opinion, thermochemical testing was performed. The hydrate saturated layers were revealed through controlling the temperature and composition of gas during the methanol injection. The measurements have shown the increase of well-bottom zone temperature during injection (due to methanol dissolving) and its consequent decreasing—during the decomposition of hydrate with methanol. This testing was performed in well No. 156 in which only two hydrate saturated intervals were opened at depths of 819–828 m and 830–836 m. From the materials of the field geophysical testing, the lower layer hydrate saturation coefficient was estimated at 0.2–0.3, and in the upper layer 0.3–0.4.

Prior to the methanol injection the well-head and the well-bottom static pressures were measured, and the temperature logging was done over the whole well interval. Four cubic meters of 96% concentration methanol were injected as follows—1 m^3 into the column, and 3 m^3 into the annular space. The temperature of the injected methanol was 4°C. The delay time after the injection was four days. Analysis of the obtained data and all consequent operation of the field indicated the presence of gas hydrate and gas deposits having a geothermal boundary. Thorough observations have shown the gradual increase in density of the produced gas, increase in volume, and decrease in salt content of the water produced with gas.

Mastering of wells on the Messoyakhi field at a temperature close to the equilibrium temperature of hydrate formation contains certain difficulties. Even an insignificant depression in the layer results in lowering the temperature of the gas due to throttling and to hydrate decomposition, which in turn, is accompanied by secondary hydrate formation in the well-bottom zone of the layer and in the wells.

Testing and operation of wells are performed with the continuous-cyclic injection of methanol in the layer. In order to decrease the amounts of sand coming into the wells, the operating depression is maintained at a fixed value of 0.2 MPa. The average production rate of the wells without the methanol treatment does not exceed 55,000 m^3/day, and with such treatment, 195 thousand m^3/day. Table 5-8 presents the data from some of the early comparisons of the gas production rates with and without the injection of methanol into the layer.

A Brief Analysis of the Field Development and Conservation

The Messoyakhi gas hydrate field was put into industrial operation in 1969. This is the first (and regrettably, the only) field which has industrially produced gas. Due to the discovery and operation of the larger, high-temperature Soleninsk gas field located closely, the Messoyakhi field was

operated intensively only during the first several years, after which it was conserved, and later reopened for experimental-industrial operation under special supervision. As indicated by the analysis of development, the most informative parameters are the layer pressure and composition of the produced gas and water. Water becomes less saline, gas becomes heavier, the layer pressure decreases significantly slower with gas production (at the constant level of the gas-water interface) than during the gas deposit production.

Figure 5-45 shows the values of the annual gas production (curve ABCDEFG), and the change in layer pressure over the period of the field exploitation (HIKLM—curve calculated from the gas field development conditions, and HINOPQ—actual curve reflecting the gas influx from the gas hydrate deposit). As seen from the curves in Figure 5-45, during the first three years the rate of gas production had been increasing sharply, and after putting the Soleninskoe field into exploitation, it decreased.

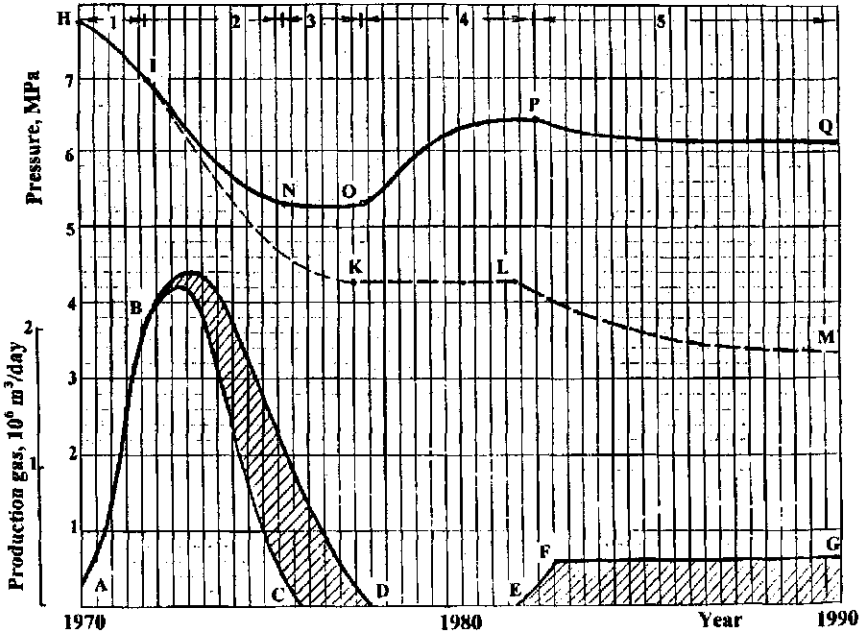

Figure 5-45 Pressure and produced gas as a function of time.

The long period of experimental-industrial operation of the Messoyakhi field can be divided into five characteristic stages:

1. The period of active production of the free gas from the gas deposit underlying the hydrate deposit (see the change of layer pressure curve H-I).
2. The period of production of gas coming from both the gas and the hydrate deposits. The layer pressure at this stage of development (curve I-N) is higher than the projected one (curve I-K), the magnitude of differential growing with the layer pressure decrease.
3. The period characterized by the gas produced only from the hydrate deposit due to the hydrate decomposition. The layer pressure stayed almost constant then (curve N-O). The period of the active field development lasted for eight years, after which the field was conserved.
4. The period of the field conservation lasted for almost four years. The hydrate decomposition has continued because at the time of conservation the layer pressure was below the hydrate equilibrium pressure. The layer pressure has increased to the equilibrium value, after which it stabilized (curve O-P). During the period of the active gas production (stages 1 and 2), the decrease in the layer temperature was observed which had reached 2 to 7°C below the initial temperature in the hydrate saturated layers. By the end of the conservation period, the temperature measurements in these wells have shown complete recovery of the temperature to its initial value.
5. The period of small gas production and practically constant layer pressure (curve P-Q). The produced gas was coming from the gas hydrate deposit due to the hydrate decomposition. It is worth emphasizing that during a gas hydrate field's development the layer pressure remains constant (taking into account the normal depression) until the total decomposition of hydrate in the deposit if the gas production rate does not exceed the volume of gas incoming from the decomposition of the hydrate in deposit at the current thermodynamic conditions of the layer.

The total amount of gas produced from the Messoyakhi field during its operation was over 16.4×10^9 m^3, 30% of which came from the hydrate

deposit. Analysis of the material on the development and conservation of the Messoyakhi gas hydrate field allowed us to reveal a number of special features of the operation of similar deposits. It allowed us to be absolutely sure about the presence of the gas hydrate deposit in the upper part of the field, has verified the character of the layer pressure change during the development process which was predicted by the laboratory research (Makogon, 1966), and has also indicated the real possibility of the development of similar fields by the available tools.

The Messoyakhi GHF development was analyzed by many researchers. The most complete out-of-Russia reviews of the conditions of development were made by E. D. Sloan (1990), and J. Krason and P. Finley (1992).

Gas Hydrates in Outer Space

Hydrates of gases in closed vessels have been known to exist since 1778 when J. Priestley obtained the first hydrate of SO_2. During the 1960s natural gas hydrates were discovered in a sedimentary cover of earth's crust.

Hydrates of gases can exist at appropriate thermodynamic conditions not only on our planet, but in space as well. If gas and water existed on some space body at appropriate thermodynamic conditions during its genesis, then hydrates accumulated and formed there. Hydrates continue to exist there if during the subsequent periods of existence of a planet or some other space body, the dispersion of matter into space did not result in a decrease of vapor pressure of a hydrate former below that above a hydrate.

Development of instrumental methods of research of planets allows us to determine the composition of planets' atmospheres, the magnitude of its pressure, and the temperature of a planet's surface. A determination of the presence of hydrates on a planet can be made by knowing the composition of gas, whether or not water is present, the value of pressure and temperature on a planet, and comparing them to the results of experimental investigations performed at appropriate conditions.

Experimental confirmation of the existence of hydrates in the conditions which are similar to planetary conditions has a large theoretical and practical significance for directing and developing the further study of planets.

Hydrates of gases can form and exist in a broad range of temperatures $2 \times 10^3 - 10^8$ MPa and temperatures 70–350 K. Hydrates of gases are characterized by a rather important property—water and gas in a hydrate state can exist at partial pressures significantly lower than is required for their existence in a pure (ideal) state. For example, at a temperature of –70°C, carbon dioxide can exist in a solid state at pressures above 0.2 MPa (see Figure 1-14), while in a solid hydrate state, the pressure of 2×10^{-2} MPa is sufficient.

Considering the property of hydrates to form hydrates which can exist at rather low pressures and the existence of thermodynamic conditions corresponding to the existence of hydrates, scientists can explain a number of contradictions which arise during interpretation of some investigations of space bodies. Let us review the possibility of interpreting some of the results of studies on Mars, considering the presence of hydrates on its surface.

From the results of studies of Mars by the Russian and American space stations, it was established that the atmosphere of Mars contains 90% CO_2. The remaining 10% are represented by water vapor, nitrogen, and other gases. Water content on Mars is insignificant, according to the data from automatic stations. Water vapor pressure is within the limits 3×10^{-7} -4×10^{-6} MPa which correspond to the vapor pressure of water over ice at –65°C to –53°C (i.e., at temperatures above –53°C, water exists only in a vapor state). It should be noticed that the moisture content on the surface of Mars at present time which is determined by measuring water vapor pressure is significantly underestimated (as well as CO_2 content) compared to their actual content.

With current thermodynamic characteristics, atmospheric pressure on Mars is determined by the volatilities of hydrate former vapors over their hydrates. Atmospheric pressure on Mars reaches 2×10^{-3} MPa, and the temperature on its surface varies within 150–290 K.

A low content of CO_2 and water do not yield a simple explanation for the size of polar caps on Mars whose sizes during summer significantly exceed the magnitude which corresponds to a solid state of CO_2 or water. So CO_2 can exist in a solid state at temperatures below –115°C ÷ –120°C, and ice—at temperatures below –60°C. However, if we consider the conditions of existence of CO_2 and water on Mars, considering the possibility of their existence in a hydrate state, we obtain that CO_2 and water can be in a solid state at significantly higher temperatures.

We have developed a method and experimentally investigated a section of a diagram in the temperature range 270–200 K in order to determine the conditions of the existence of a CO_2 hydrate at low temperatures. During this study, a hydrate was generated at $t > 0$°C from gaseous CO_2 and liquid water after which free water and vapor were displaced from a reactor cell by a low-boiling fraction of a neutral liquid and the pressure was decreased isothermally below the dissociation pressure of the

Table 5-9 Dissociation pressure for CO_2 hydrate.

	Temperature, °C								
	–5	*–10*	*–15*	*–20*	*–30*	*–40*	*–50*	*–60*	*–70*
Pressure, MPa	0.7	0.43	0.24	0.14	0.047	0.016	0.0058	0.0023	0.0017

hydrate. The pressure at which free CO_2 appeared in a vapor state determined the pressure of hydrate dissociation at a certain temperature.

The results of determining hydrate dissociation pressure are presented in Table 5-9.

In comparing the equilibrium parameters of CO_2 hydrate formation with the actual magnitude of pressure and temperature on the surface of Mars, hydrate of CO_2 exists at temperatures –127°C or to –40°C.

Since hydrates exist constantly on the surface of Mars and in the near-surface zone of granular rock, the magnitude of water vapor pressure in the atmosphere of Mars corresponds to the conditions of water existence in a hydrate state. The content of water vapor and the atmospheric pressure on Mars are not constant quantities, but are determined by a thermodynamic characteristic of the atmosphere on the planet. The total amount of hydrate on the planet decreases with temperature, and the atmospheric pressure increases.

As Mars travels away from the Sun, a part of the atmosphere transforms into a hydrate state with a temperature decrease, hydrates accumulate on its surface and the atmospheric pressure decreases. The atmospheric composition does not remain constant. With a pressure increase, the relative content of nitrogen and oxygen decreases, and with a pressure decrease it increases.

A hydrate of CO_2 can exist at temperatures up to –60°C or –40°C and at pressures from 2×10^{-3} to 2×10^{-2} MPa, considering decomposition in the conditions of Mars. In the regions on the surface of Mars where the temperature is below –60°C to –40°C, CO_2 and water are in a solid hydrate and a vapor state. In the regions with temperatures above –40°C, CO_2 and water are in a vapor state on the surface of Mars. Neither water, nor CO_2, can be in a liquid state at present thermodynamic conditions.

Based on the thermodynamic characteristic of Mars, we should notice that hydrates can exist not only on the planet's surface (in polar caps and in the atmosphere as clouds), but also in a profile of its rock. The thermal gradient of rock at $T < 273$ K is about 10 degrees per 1 km. Knowing the equilibrium curve of hydrate formation, the curves of the hydrostatic pressure, and the temperature gradient, it is easy to determine the depth of a hydrate formation zone in Mars, which generally is 6 km. In the polar regions, the depth of hydrate formation zone increases, and on the equator it decreases. A hydrate belt with a thickness of 6 km envelopes the whole planet.

It is noteworthy that the presence of hydrates should be accounted for during the calculation of CO_2 and water content on Mars based on their partial pressures in the atmosphere. Otherwise, the results of calculations will be underestimated. Based on the point that the hydrate belt is represented by granular rock and the hydrate saturation is 20%, we can calculate that 136 million km^3 of water exists on Mars in a bound hydrate state. For a comparison, we notice that 1460 million km^3 of water exist on Earth, i.e., if we consider the ratio of masses of Earth and Mars, we find that the content of water on these planets is practically proportional to their masses. This conclusion is of interest during a discussion of a hypothesis about origination of both these planets which existed in approximately similar thermodynamic conditions during their formation from the same initial materials.

Discovery of natural gas hydrates on earth poses a natural question about their presence and spreading on other objects of the Solar System and beyond—in interstellar medium, planetary systems of other stars in the Galaxy, and in general, in near and far space. A methodical foundation for a scientific statement of the problem is based on the following:

1. Establishing the conditions of existence and stability of a certain type of gas hydrate at specified P-T conditions;
2. Presence of the necessary P-T conditions and appropriate contents of hydrate forming chemical compounds and elements for these or other astrophysical objects;
3. Rather important are kinetic limitations and non-equilibrium of occurring processes;
4. Presence of many complicating astrophysical factors—hard UV, X-ray and other space radiations, a possibility of both catalytic and inhibiting reactions, etc.

Initially, the idea about the presence of gas hydrates on other objects of the Solar System was, probably, stated by G. Miller, who proposed a hypothesis in the 1950s about a possible gas hydrate content of comets'

nuclei. The difficulty of proving the existence of gas hydrates on remote astrophysical objects is witnessed by the fact that even after half a century of intensive spectral observations from earth and from space stations, there is no definite answer about a gas hydrate composition of comets. Nevertheless, astrophysical materials obtained in the last few years allows us to hope for a substantial advancement in this area already in the nearest decade.

Analysis of the actual materials obtained during the past visit of Halley's Comet indicated that the body of Halley's Comet is a block of gas hydrate (Makogon, 1987) and not of ice, as it was supposed earlier.

Conclusion

The presented upper estimate for the abundance of gas hydrates in interstellar medium is $\leq 10^{-5}$ of the total mass of the total matter in the galaxy is impressive, although, of course it needs further verification. It is necessary to continue the study of gas hydrate formation in nuclei of molecular clouds where ion-molecular reactions can play an important role. It is important to make more detailed calculations and laboratory experiments on destroying ice and gas hydrate mantles of dust specks and comet nuclei in the presence of a hard radiation at ranges of energies and flows of particles typical for interplanetary and interstellar medium.

CONCLUSION

Clathrate Hydrates of Hydrocarbons Are Our Dilemma and Hope

Nature has given a wonderful property to hydrate materials—the ability to exist in three phases depending on the pressure and temperature. This ability generates a great variety of states for different elements and their mixtures. Clathrate hydrates are an outstanding representative of natural minerals, whose properties greatly affect the processes taking place on earth and in the universe.

Although the history of hydrates extends back more than 200 years, we are still at the threshold of understanding hydrates, and have not yet started to use their capacity. Clathrate hydrates are a complex problem for science and industry.

Figure 1-1 presents the schematics of the hydrate problem which scientists have to work on in collaboration with industry. The modern study of hydrates has two major directions: natural and technogenic gas hydrates. The two directions have common goals in the study of formation conditions and properties of hydrates:

- to discover the genesis of natural hydrate formations;
- to create effective methods and means to control hydrate formation and decomposition in the pipelines;
- to design new technologies;
- to reveal the possibility of using the energy resources of natural gas hydrates; and
- to determine the effect of hydrates on the regional ecology, climate, and global changes.

Let us review briefly the sense of the main tasks. Formation, stable existence, and decomposition of both natural and technogenic gas hydrates are determined by composition and phase state of water and gas (or volatile liquids), pressure, and temperature. The processes of formation-decomposition have a strict kinetic, time-dependent characteristic.

Kinetics of the hydrate formation process is one of the most important and least studied characteristics of clathrate hydrates. Crystal nucleation occurs at the gas-water free interface, whereas the formation and accumulation of hydrates may occur both at the free interface and in bulk of water or gas. In addition, the process of hydrate formation may take place due to the surface adsorption (classic crystal growth) and the tunnel adsorption when the whiskery crystals grow. In order to properly model the kinetics of hydrate formation processes, one must know energetic and geometric characteristics of the hydrate formers at the molecular level. Their interrelation and interdependence—the surface tension and rate of free interface formation in the gas-oil-water flow, the structural state of water, viscosity, diffusive permeability, and gas content of water, moisture content of gas and oil, etc.—also should be understood.

Clathrate hydrate morphology—the function of the kinetic process—is studied very little. It has been found that formation of hydrate shape (and properties) is determined by the initial state of hydrate formers, the thermodynamic conditions of the process, and other factors. A large variety of hydrate crystal forms has been found; however, the factors that determine the shape of hydrate crystals have not been studied.

Almost no research has been done on the effect of external fields (electromagnetic, acoustic, etc.) on the process of hydrate formation and decomposition. The level of knowledge about the seismoacoustic properties of hydrates is at the initial stage. Without knowing the acoustic permeability and defining the pseudo boundary of hydrate accumulations in the sedimentary rock we cannot determine the hydrate saturation of the rock. This, in turn, prevents us from reliably estimating the hydrocarbon resources accumulated in the studied region. Dispersed accumulations of hydrates cannot be revealed using remote probing methods and expensive well drilling where complex geophysical logging is required.

Properties of hydrates and hydrate-saturated rock are the most important components in the problem of natural and technogenic gas hydrates. The current level of knowledge about hydrates gives a general picture of hydrate properties. This lack of information retards the creation of new methods for both preventing hydrate formation in wells and pipelines, and utilizing hydrate properties. Many characteristics must be investigated, including density of hydrates, heat of their formation, heat capacity, thermal conductivity, electrical resistivity, magnetic, diffusive, lateral, and acoustic permeability, thermodynamical and volumetric characteristics.

The crystallization pressure of hydrate formation has not yet been experimentally measured. The specific volume of water increases by 26–32% during its transition into a hydrate (compared to only 9% for water ice). The pressure of gas molecules in a hydrate cavity exceeds the equilibrium pressure of hydrate formation by two times. This property of hydrate is exhibited during the construction and operation of engineering projects, such as wells, pipelines, and platforms in the zone of hydrate formation, where hydrate is the cementing material for the rock. There have been cases when a well was destroyed by the gas hydrate formed in the well.

Resources of natural gas in a hydrate state are tremendous, exceeding surveyed global reserves of natural gas by two times. However, there is neither a reliable method of estimating their reserves, nor an effective and economical method of producing gas from hydrate deposits. Energy requirements during production from hydrate deposits (6.2%) are similar to energy consumption during oil production; however, it is difficult to ensure sealing and consequently ecological safety during the use of traditional methods of producing hydrocarbons. Methane, the main component of the natural hydrates, is a more active promoter of the greenhouse effect. The lower layers of hydrate in sedimentary rock are in a metastable state and are a powerful source of free methane for oceans and atmospheres on earth. This problem has yet to be resolved.

The presence of large areas of thick hydrate-saturated rock in Polar regions on land and under the sea, which have low thermal conductivity and high capacity (also considering phase transition heat), exerts a significant influence on the thermal balance of the earth's climate.

Hydrate-saturated rock is practically impenetrable for hydrocarbons and is the "lithological" roof for hydrocarbons generated below it, preventing their diffusion into the atmosphere. These problems are waiting to be solved.

The unique properties of hydrates allow creation of new technologies based on their utilization. These include:

- the storage and transportation of hydrocarbons;
- desalinization of water;
- compressorless increase of pressure;
- separation of gases and concentration of juices and wines;
- generation of electric power, etc.

Gas hydrates may be used as a fuel for marine, railroad, and automobile transportation vehicles. A number of these technologies are already created, but the perspectives are limited.

More than 1.2 million tons of methanol is currently used for prevention of hydrate formation in the world annually at a total cost of $400,000,000. Analysis of the world's experience indicates that removal of large hydrate plugs from wells and pipelines is 30 to 50 times more expensive than their prevention. It is significantly easier and cheaper to prevent hydrate formation (as in any disease) than to remove them.

Today the urgent gas hydrate problems are:

- creation of new methods of preventing the formation of large hydrate plugs in the gas-oil-water flows, in pipelines and wells, especially in conditions of deep-sea zones, including kinetic inhibitors;
- providing the stability of constructed and operated engineering objects in the hydrate formation zone;
- creation of new technologies based on hydrates;
- development of effective methods for discovery of gas hydrate deposits and for gas production from them;
- revealing the role of natural gas hydrates in global changes.

These tasks do not embrace all aspects of natural and technological hydrate problems, yet they are the most significant ones. Delay in their solution results in large material expenses or large losses from not using their resources. Those who solve these problems first will benefit, based on results of scientific and industrial research.

BIBLIOGRAPHY

Alexeyeff, V.A., et al. 1982. Details of hydrate layer formation around hydrophobic-hydrophilic nucleus in the crystalline structure of 34.5 water tri-N-butylphosphinoxide clathrate. *J. Struct. Chem.* 23:86–91.

Alexeyeff, W. 1876. *Ber.* 9:10–25.

Anderson, F.E., and J.M. Prausnitz. 1986. *AIChE J.* 32:13–21.

Andreassen, K., K. Hogstad, and K.A. Berteussen. 1990. Gas hydrates in the Barents Sea, indicated by a shallow seismic anomaly. 1(8):235–245.

Andryushchenko, F.K., and V.P. Vasilchenko. 1969. *Gasov. Prom.* 10:4. Moscow.

Aoki, Y., T. Tamano, and S. Kato. 1983. Studies in continental margin geology. J.S. Watkins and C.L. Drake, eds. *Amer. Assn. of Petrol. Geol. Mem No. 34*:309–322.

Aoyagi, K., et al. 1980. *Gas Processors Assn. Rsch. Rpt. No. 45.* Tulsa, OK.

Ariye, A.G. 1984. Physical gases of water fluid flow underground. Moscow. Nedra.

Ashworth, T., R.L. Johnson, and L.P. Lai. 1985. Thermal conductivity of pure ice and tetrahydrofuran clathrate hydrates. *High Temperature-High Pressures* 17:413–419.

Austvik, T. 1993. Modeling of hydrate formation and behavior in a pipeline. *International Conference on Natural Gas Hydrates,* p. 511. New York.

Avlonites, D. 1988. Multiphase equilibria in oil-water hydrate forming systems. *M.Sc. Thesis.* Heriot-Watt University, Edinburgh, Scotland.

Baker, P.E. 1974. In *Natural Gases in Marine Sediments,* ed. I.R. Kaplan, p. 227. Plenum, New York.

Barrer, R.M., and K.J. Ruzicka. 1962a. *Trans. Faraday Soc.* 58:22–53.

Barrer, R.M., and W.I. Stuart. 1957. *Proc. Roy Soc.* (London) A. No 1233. 243:172.

Berecz, E., and M. Balla-Achs. 1983. Gas hydrates. *Studies in Inorganic Chemistry* Vol 4. p. 343. Elsevier, New York.

Bermard, B.B., J.M. Brooks, and W.M. Sackett. 1977. A geochemical model for characterization of hydrocarbon gas sources in marine sediments. *Proceeding of the Ninth Annual Offshore Technology Conference,* OTC 2983, pp. 435–438. Houston, TX.

Bik, S.S., and V.I. Fomina. 1970. *Gas Hydrate*, M. VINITE 128.

Bik, S.S., Y.F. Makogon, and V.I. Fomina. 1980. *Gas Hydrates.* Khimiya, Moscow.

Bily, C., and J.W.L. Dick, 1974. *Bull. Can. Petr. Geol.* 22:340.

Bishnoi, P.R., and A. Vysniauskas. 1980. Kinetics of Gas Hydrate Formation, Pt. n, *Final Report to Gas Research Institute*. Chicago.

Bishnoi, P.R., V. Natarajan, and N. Kalogerakis. 1993. A unified description of the kinetics of hydrate nucleation, growth, and decomposition. *International Conference on Natural Gas Hydrates*, p. 311. New York.

Bondarev, E.A., G.D. Babe, A.G. Groysman, and M.A. Kanibolotsky. 1976. Mechanica of hydrate formation in the gas flows. *Novosibirsk*, p. 158. Nauka.

Booth, J.S., W.J. Winters, and W.P. Dillon. 1993. Circumstantial evidence of gas hydrate and slope failure associations on the United States Atlantic Continental Margin. *International Conference on Natural Gas Hydrates*, p. 487. New York.

Brockmann, A.R. 1992. Cloud-points of hydrocarbon systems-influence of pressure and methane addition. *Dr. Ing. (Ph.D.) Thesis*. The Norwegian Institute of Technology (NTH).

Brooks J.M., M.D. Field, and M.C. Kennicutt. 1990. Observations of gas hydrates in marine sediments, offshore northern California. *Marine Geology* 96:103–109.

Brooks, J.M., and W.R. Bryant. 1989. Geological and geochemical implications of gas hydrates in the Gulf of Mexico. U.S. Department of Energy, DOE, MC, 21088.

Brooks, J.M., et al. 1983. Molecular and isotopic compositions of hydrocarbons at site 533, Deep Sea Drilling Project Leg 76. In *Initial Reports of the Deep Sea Drilling Project* 76, ed. R.E. Sheridan et al., pp. 377–384. U.S. Government Printing Office, Washington, D.C.

Brooks, J.M., et al. 1986. Association of gas hydrates and oil seepage in the Gulf of Mexico. *Org. Geochem.* 10:221–234.

Brooks, J.M., et al. 1993. Hydrate occurrences in shallow subsurface cores by continental slope sediments. *International Conference on Natural Gas Hydrates*, p. 381. New York.

Bubnov, V.A., et al. 1969. *Trudy Vsesoyuznogo Soveshaniya po Ispolzovaniyu Energeticheskikh Resursov Yakutii*. Yakutsk.

Bugge, T., et al. 1987. A giant three-stage submarine slide off Norway. *Geo. Mar. Lett.* 7:191–198.

Buleyko, V.M., and Y.F. Makogon. 1989. *Dokl. Akad. Nauk SSSR*. 309, N3. Moscow.

Burruss, R.C. 1995. Crystallization of natural gas hydrate. *CSM*. Golden, Colorado.

Bylov, M., P. Rasmussen, and A. Calsep. 1996. A new technique for measuring gas hydrate kinetics. *2nd Intl. Conf. on Natural Gas Hydrates*. Toulouse, France.

Cameron, I., Y.P. Handa, and T.H.W. Baker. 1990. Compressive strength and creep behavior of hydrate-consolidated sand. *Can. Geotech. J.* 27:255.

Carpenter, G. 1981. Coincident sediment slump/clathrate complexes on the U.S. Atlantic continental slope. *Geo. Mar. Lett.* 1:29–32.

Carson, D.B., and D.L. Katz. 1942. *Trans. AIME* 146:150.

Chappellaz, J., et al. 1990. Ice core record of atmospheric methane over the past 160,000 years. *Nature* 345:127–131.

Cherskii, N.V., and Y.F. Makogon. 1970. Solid gas world reserves are enormous. *Oil and Gas, International* 10. 8:82–84.

Cherskii, N.V., V.P. Tsaarev, and S.P. Nikitin. 1982. Investigation and prediction of conditions of accumulaton of gas resources in gas-hydrate pools. *Petroleum Geology* 21:65–89.

Chrigan, A.H. 1973. Fizika atmosfernogo ozona (Physics of atmospheric ozone), Leningrad. Hydrometeoizdat.

Christiansen, R.L., and E.D. Sloan, Jr. 1993. Mechanisms and kinetics of hydrate formation. *International Conference on Natural Gas Hydrates*, p. 283. New York.

Cicerone, R.J., and R.S. Oremland. 1988. Biogeochemical aspects of atmospheric methane. *Global Biogeochem. Cycles* 2:299–327.

Ciesnik, M., and J. Krason. 1987. Geological evolution and analysis of confirmed or suspected gas hydrate localities: basin analysis, formation and stability of gas hydrates in the Black Sea. U.S. Department of Energy, DOE/MC/21181–1950, p. 11.

Claypool, G.E., and C.N. Threlkeld. 1983. Anoxic diagenesis and methane generation in sediments of the Blake Outer Ridge. Deep Sea Drilling Project Site 533, Leg 76. In *Initial Reports of the Deep Sea Drilling Project* 76, eds. R.E. Sheridan et al., pp. 391–402. Washington, D.C., U.S. Government Printing Office.

Claypool, G.W., and I.R. Kaplan. 1974. The origin and distribution of methane in marine sediments. In *Natural Gases in Marine Sediment,*. ed. I.R. Kaplan, pp. 99–139. Plenum Press, New York.

Claypool, G.E., and K.A. Kvenvolden. 1983. Methane and other hydrocarbon gasses in marine sediment. *Ann. Rev. Earth Planet. Sci.* 11:299–327.

Collett, T.S. 1983. Detection and evaluation of natural gas hydrates from well logs, Prudhoe Bay, Alaska, *M.S. Thesis*. U. Alaska. Fairbanks, AL.

Collett, T.S. 1992. Potential of gas hydrates outlined. *Oil & Gas J.* 90 25:84–87.

Collett, T.S. 1993. Permafrost-associated gas hydrate accumulations. *International Conference on Natural Gas Hydrates*, p. 247. New York.

Collett, T.S., S.P. Godbole, and C. Ehlig-Economomides. 1984. Quantification of gas hydrates on North Slope of Alaska. *Proceedings of the 35th Annual Meeting of Canadian Institute of Mining*. Calgary, Canada, June 10–12.

Collett, T.S., et al. 1988. Geologic interrelations relative to gas hydrates within the North Slope of Alaska. *U.S. Geol. Surv. Open File Rep.* 150:88–389.

Cox, J.L. 1983. *Natural Gas Hydrates: Properties, Occurrence and Recovery*. Butterworth Publishers, Woburn, MA.

Culberson, O.L., and J.J. McKetta. 1951. Phase equilibria in hydrocarbon-water systems. III - solubility of methane in water at pressures to 10,000 psia. *Petr. Trans. AIME* 192:223–226.

Davidson, D.W. 1973. Clathrate hydrates. In *Water: A Comprehensive Treatise*, 2d. ed. F. Franks. Chapter 3, p. 115.

———. August 1980. Gas hydrates as clathrate ices. *Amer. Soc. Simp.* Las Vegas, Nevada.

———. 1983a. Gas hydrates as clathrate ices. In *Natural Gas Hydrates: Properties, Occurrence and Recovery*, ed. J.L. Cox. Butterworths, Boston.

Davidson, D.W. 1987a. Natural gas hydrates in northern Canada. *National Research Council of Canada Proceedings 3rd International Conference on Permafrost* 1:938–943.

Davidson, D.W., and J.A. Ripmeester. 1978. *J. of Glaciology N* 85. 21:33–49.
———. 1974. *J. of Magn. Res.* 15:295–309.
Davidson, D.W., D.G. Leaist, and R. Hesse. 1983b. Oxygen-18 enrichment in the water of a hydrate. *Geochim. Cosmochim. Acta.* 47:2293–2295.
Davidson, D.W., et al. 1984. *Nature* 311, p. 142.
Davidson, D.W., et al. 1986. Laboratory analysis of a naturally occurring gas hydrate from sediment of the Gulf of Mexico. *Geochim. Cosmochim. Acta.* 50:619–623.
Davidson, D.W., Y.R. Handa, and J.A. Ripmeester. 1986. *J. of Phys. Chem.* 90:6549–6552.
Davidson, D.W., et al. 1987. Some physical and thermophysical properties of clathrate hydrates. *J. Incl. Phenom.* 5:219.
Davidson, D.W., J. El-Defrawy, and A.S. Judge. 1987b. Natural gas hydrates in northern Canada. *Proceedings of the Third International Permafrost Conference*1:938–943.
Davy, H. 1811. *Phil. Trans. Roy. Soc. London.* 101, p. 1.
de Forcrand, R. 1882. *Compt. Rend.* 95, p. 129.
———. 1897. *Compt. Rend.* 125, p. 109.
———. 1902. *Compt. Rend.* 135, p. 959.
———. 1923. *Compt. Rend.* 176, p. 355.
———. 1925. *Compt. Rend.* 181, p. 15.
de Forcrand, R., and P. Villard. 1888b. *Compt. Rend.* 106, p. 1357.
de la Rive, A. 1829. *Ann. Chem. Phys. Ser.* 2. 40, p. 405.
de Roo, J.L., et al. 1983. Occurrence of methane hydrate in saturated and unsaturated solutions of sodium chloride and water in dependence of temperature and pressure. *AIChE J.* 29:651–657.
Deaton, W.M., and E.M. Frost, Jr. 1946. Gas hydrates and their relation to the operation of natural gas pipelines. *U.S. Bureau of Mines Monograph* 8, p. 101.
———. 1937. *Oil & Gas J.* 36:*(1)*, p. 75.
Di Tolla, F.D., and M. Ronchetti. 1993. *Phys. Rev. E.* 48, p. 1726.
Dillon, W.P. 1991. Methane hydrate in sea floor sediments off of the southeastern U.S.; amounts and implication for climate change. *Geol. Soc. Am. Abstr. Progr.* 23, p. 23.
Dillon, W.P., J.A. Grow, and C.K. Paull. 1980. Unconventional gas hydrate seals may trap gas off southeast U.S. *Oil Gas J. (1)* 78:124–130.
Dillon, W.P., and C.K. Paull. 1983. Marine gas hydrates: II geophysical evidence. In *Natural Gas Hydrates: Properties, Occurrence and Recovery,* ed. J.L. Cox, pp. 73–90.
Dubinin, V.M., and G.G. Zhidenko. 1979. Transp. khranenie gaza *(Ref. Inf.)* 6, p. 20. Moscow.
Dufty, J.W., K.C. Mo, and K.E. Gubbins. 1991. *J. Chem.Phys.* 94:3132.
Dyadin, Y.A., and E.Y. Aladko. 1996. Decomposition of the methane hydrate up to 10kelar. NGHC. Toulousa.
Elperin, T., and A. Fominykh. 1996. Investigation of gas hydrates formation at the surface of rising bubbles and slugs of hydrate forming gas. *2nd Intl. Conf. on Natural Gas Hydrates.* Toulouse, France.

Emery, K.O. 1974. Pagoda structures in marine sediments. In *Natural Gases in Marine Sediments,* ed. I. R. Kaplan, pp. 309–317. Plenum, New York.
Englezos, P. 1986. A model for the formation kinetics of gas hydrates from methane, ethane and their mixtures. *M.S. Thesis,* U. Calgary.
Englezos, P. 1987b. *Chem. Eng. Sci.* 42, p. 2659.
Englezos, P., et al. 1987a. *Chem. Eng. Sci.* 42, p. 2467.
Englezos, P., and P.R. Bishnoi. 1988. *AIChE J.* 34, p. 1718.
Englezos, P., N. Kalogerakis, and P.R. Bishnoi. 1989. Formation and decomposition of gas hydrate of natural gas components. *J. Inclus. Phenom.* D.W. Davidson memorial volume.
Englezos, P., and S.G. Hatzikiriakos. 1993. Enviromental aspects of clathrate hydrates. *International Conference on Natural Gas Hydrates,* p. 270. New York.
English, C.A., and J.A. Venables. 1974. *Proc. R. Soc. Lond.* A340. 57.
Erickson, D., and T. Brown. 1993. Hydrate occurrence in multiphase flowlines. *International Conference on Natural Gas Hydrates,* p. 40. New York.
Falabella, B.J. 1975. A study of natural gas hydrates. *Ph.D. Dissertation,* U. Mass.
Faraday, M. 1823. *Phil. Trans. Royal Soc. London* 113:160.
Farman, L. 1987. *New Sci.* 116 n. 1586:50–54.
Finley, P., and J. Krason. 1986a. Geological evolution and analysis of confirmed or suspected gas hydrate localities: basin analysis, formation and stability of gas hydrates in the middle America trench. U.S. Department of Energy, DOE/MC/21181-1950, p. 9.
———. 1986b. Geological evolution and analysis of confirmed or suspected gas hydrate localities: basin analysis, formation and stability of gas hydrates of the Colombia Basin. U.S. Department of Energy, DOE/MC/21181-1950, p. 7.
Fontana, R.L., and A. Mussumeci. 1993. Hydrates offshore Brazil. *International Conference on Natural Gas Hydrate,* p. 106. New York.
Franks, F. ed. 1973. *Water: a Comprehensive Treatise* (7 volumes). Plenum, New York.
Frost, E.M. Jr., and W.M. Deaton. 1946. *Oil & Gas J.* 45(12):170.
Galimov, E.M., and K.A. Kvendvolden. 1983. Concentrations and carbon isotopic compositions of CH_4 and CO_2 in gas from sediments of the Blake Outer Ridge. Deep Sea Drilling Project Leg 76, In *Initial Reports of the Deep Sea Drilling Project,* 76. ed. R.E. Sheridan et al., pp. 403-407. U.S. Government Printing Office, Washington, D.C.
Galloway, T.J., et al. 1970. Experimental measurement of hydrate numbers for methane and ethane and comparison with theoretical values. *Ind. Eng. Chem. Fundam.* 9:237–243.
Ginsburg, G.D., et al. 1992. Gas hydrates of the Southern Caspian. *Int. Geol. Rev.* 34:765782.
Ginsburg, G.D., I.S. Gramberg, and V.A. Soloviev. 1994a. Gas hydrates of continental slopes. *Geologiya Nefti i Gaza* 11:43–45.
Ginsburg, G.D., and V.A. Soloviev. 1994. Submarine gas hydrates, p. 200. St. Petersburg.

Gmelins Handbuch der anorganischen Chemie. 1960. 8 auflage, Syst. No. 9, Schwefel. t.B, lfg. 2, S. 1100.
Godbole, S.P. 1981. Dissociation pressures of n-propane and i-butane hydrates below the ice point. *M.S. Thesis*, University of Pittsburgh.
Gorchilin, V.A., and L.I. Lebedev. 1991. On indications of gas hydrates in sedimentary cover of the Black Sea and possible type of hydrocarbon traps. *Geologicheskiy Zhurnal* 5:75–81.
Gray, G.R., and H.C.H. Darley. 1980. *Composition and Properties of Oil Well Drilling Fluids,* 4th ed. Gulf Publishing Co., Houston, TX.
Gregory, J.C. 1930. *The Scientific Achievements of Sir Humphrey Davy,* pp. 112–113. London, Milford.
Groysman, A.G. 1985. Thermophysical properties of gas hydrates. *Novosibirsk,* p. 95. Nauka.
Gryte, C.C. 1993. On the control of nucleation and growth by inhibition of gas hydrate formation. *International Conference on Natural Gas Hydrates,* p. 323. New York.
Halbouty, M.T., et al. 1970. World's giant oil and gas fields, geologic factors affecting their formation, and basin classification. *Geology of Giant Petroleum Fields.* AAPG Memoir 14:502555.
Hammerschmidt, E.G. 1934. Formation of gas hydrates in natural gas transmission lines. *Int. Eng. Chem.* 26:851–855.
———. 1934. *Ind. Eng. Chem.* 26:851.
———. 1939. *Gas* 15(5):30.
———. 1940. *Oil and Gas J.* 29(2):61. May 23.
Hand, J.H., D.L. Katz, and V.K. Verma. 1974. Review of gas hydrates with implication for oceanic sediments. In *Natural Gases in Marine Sediments,* ed. I.R. Kaplan, pp. 179–194. Plenum Press, New York.
Handa, Y.P. 1985. Heat capacities in the range 95 to 260 K and enthalpies of fusion for structure II clathrate hydrates of some cyclic ethers. *J. Chem. Thermodyn.* 17:201.
———. 1986. Composition dependence of thermodynamic properties of xenon hydrate. *J. Phys. Chem.* 90:5497.
———. 1986. Compositions, enthalpies of dissociation, and heat capacities in the range 85 to 270 K for clathrate hydrates of methane, ethane, and propane, and enthalpy of dissociation of isobutane hydrate, as determined by a heat-flow calorimeter. *J. Chem. Thermodyn.* 18:915.
———. 1988. A calorimetric study of naturally occurring gas hydrates. *Ind. Eng. Chem. Res.* 27:872.
———.1990. Effect of hydrostatic pressure and salinity on the stability of gas hydrates. *J. Phys. Chem.* 94:2652.
Handa, Y.P., R.E. Hawkins, and J.J. Murray. 1984. Calibration and testing of a Tian-Calvet heat-flow calorimeter. Enthalpies of fusion and heat capacities for ice and tetrahydrofuran hydrate in the range 85 to 270 K. *J. Chem. Thermodyn.* 16:623.
Handa, Y.P., and J.G. Cook. 1987. Thermal conductivity of xenon hydrate. *J. Phys. Chem.* 91:6327.
Handa, Y.P., and Stupin, D. 1992. Thermodynamic properties and dissociation characteristics of methane and propane hydrates in 70 Å radius silica gel pores. *J. Phys. Chem.* 96:8599.

Handa, Y.P., M. Zakrzewski, and C. Fairbridge. 1992. Effect of restricted geometries on the structure and thermodynamic properties of ice. *J. Phys. Chem.* 96:85–94.
Happell, J. 1993. New vistas for gas hydrate research and technology. In *International Conference on Natural Gas Hydrates,* p. 564. New York.
Harrison, W.E., and J.A. Curiale. 1982. Gas hydrates in sediments of holes 497 and 498A, Deep Sea Drilling Project Leg 67. eds. J. Aubouin et al. *Initial Reports Deep Sea Drilling Project,* U.S. Govemment Printing Office, Washington, D.C., 67:591–595.
Hesse, R., and W.E. Harrison. 1981. Gas hydrates (clathrates) causing pore-water freshening and oxygen isotope fractionation in deep-water sedimentary sections of terrigenous continental margins. *Earth Planet. Sci. Lett.* 55:453–462.
Hesse, R., J. Lebel, and J.M. Gieskes. 1985. Interstitial water chemistry of gas-hydrate bearing sections on the Middle America Trench slope, Deep-Sea Drilling Project Leg 84. In *Initial Reports of the Deep Sea Drilling Project,* 84, eds. R. von Huene et al., pp. 727–736. U.S. Government Printing Office, Washington, D.C.
Hidle, N., Dannelse og Opposning av Gasshydrtater. 1991. *Sivilingeniør Thesis,* Høgskolesenteret i Rogaland (in Norwegian).
Hitchon, B. 1974. Occurrence of natural gas hydrates in sedimentary basins. *Natural Gases in Marine Sediments,* ed. I.R. Kaplan, pp. 195–225. Plenum Press, New York.
Holder, G.D., and S.P. Godbole. 1982. *AIChE J.* 28:930.
Holder, G.D., and V.A. Kamath. 1982. The hydrates of propane/n-butane, propane/trans-2-butane, propane/isobutane, cis-2-butene and trans-2-butene below the ice point. Presented at *AIChE Meeting*, Los Angeles, November.
Holder, G.D., et al. 1982. *J. Petr. Tech.* 34:1127.
Holder, G.D., V.A. Kamath, and S.P. Godbole. 1984. The potential of natural gas hydrates as an energy resource. *Ann. Rev. Energy* 9:427–445.
———. 1976. *Am. Assoc. Petrol. Geol. Bull.* 60:981.
Holder, G.D., et al. 1993. Modeling thermodynamics and kinetics of hydrate formation. *International Conference on Natural Gas Hydrates,* p. 344. New York.
Hondoh, T. 1996. Clathrate hydrates in polar ice sheets. *2nd Intl. Conf. on Natural Gas Hydrates*. Toulouse, France.
Hooper, F.C., and F.R. Lepper. 1950. Transient heat flow apparatus for determination of thermal conductivity. *Heating, Piping and Air Conditioning* 56:129–134.
Hoover, W.G. 1985. *Phys. Rev. Letters* 31:1695.
Hwang, M.J., et al. 1989. An experimental study of crystallization and crystal growth of methane hydrates from melting ice. *J. Inclus. Phenom.* D.W. Davidson Memorial Volume.
Hyndman, R.D., and E.E. Davis. 1992. A mechanism for the formation of methane hydrate and seafloor bottom-simulating reflectors by vertical fluid expulsion. *J. Geophys. Res.* 97(B5):6683–6698, 7025–7041.
Istomin, V.A., and V.S. Yakushev. 1992. *Gas Hydrates in Natural Conditions.* Nedra, Moscow.

Jacoby, R.H. 1953. Vapor-liquid equilibrium data for use of methanol in preventing gas hydrates. *Proc. Gas. Hydr. Contr. Conf.* U. Oklahoma, Norman, OK.

Jansen, E. 1987. Large submarine slides on the Norwegian continental margin: sediments, transport and timing. *Mar. Geol.* 78:77–107.

Jeanjean, P. 1991. Hydrate detection by cone penetration testing. *M.S. Thesis*, Texas A&M University, College Station, TX.

Jeffrey, A.W.A. 1985. Isotopic analysis of core gases at sites. 565–570, Deep Sea Drilling Project Leg 84. In *Initial Reports of the Deep Sea Drilling Project* 84, ed. R. von Huene et al., pp. 719–726. U.S. Government Printing Office, Washington, D.C.

Jenden, P.D., and J.M. Gieskes. 1983. Chemical and isotopic compositions of interstitial water from Deep Sea Drilling Project sites 533 and 534. In *Initial Reports of the Deep Sea Drilling Project* 76, ed. R.E. Sheridan et al., pp. 453–461. U.S. Government Printing Office, Washington, D.C.

Jhaveri, J., and D.B. Robinson. 1965. Hydrates in methane-nitrogen system. *Canadian J. Chem. Eng.* 43:75-78.

Judge, A.S. 1981. Natural gas hydrates in Canada. In *Proceedings of the 4th Canadian Permafrost Conference,* ed. M.H. French. Ottawa: National Research Council of Canada, pp. 320–328.

Kamath, V.A. 1984. Study of heat transfer characteristics during dissociation of gas hydrates in porous media. *Ph.D. Dissertation.* U. Pittsburgh.

Kamath, V.A., and S.P. Godbole. 1987. *J. Petrol. Tech.* 39:1379.

Kamath, V.A., and G.D. Holder. 1987. *AIChE J.* 33:347.

Kamath, V.A., and S.L. Patil. 1993. Analogy between effect of inhibitors on hydrate equilibrium thermodynamics and hydrate decomposition kinetics. *International Conference on Natural Gas Hydrates,* p. 463. New York.

Katz, D.L. 1945. *Trans AIME* 160:140.

Katz, D.L. 1959. *Handbook of Natural Gas Engineering,* p. 802. McGraw-Hill, New York.

Katz, D.L., and R.L. Lee. 1990. *Natural Gas Engineering, Production and Storing*. McGraw Hill Publishing Co., New York.

Katz, H.R. 1981. Probable gas hydrate in continental slope east of the North Island, New Zealand. *J. Petrol. Geol.* 3:315–324.

Kayen, R.E. 1988. The mobilization of Arctic Ocean landslides by sea level fall induced gas hydrate decomposition. *M.Sc. Thesis*. Stanford University.

Kelland, M.A., T.M. Svartaas, and L.A. Dybvik. 1994. Control of hydrate formation by surfactants and polymers. *5th Intern. Oil Field Chemical Symposium.* Norway. March.

Kobayashi, R. 1951. Vapor-liquid equilibrium in binary hydrocarbon-water systems. *Ph.D. Dissertation*. University of Mich., Ann Arbor, MI.

Kobayashi, R., and D.L. Katz. 1949. Methane hydrate at high pressure. *Petrol. Trans. AIME* 186:66–70.

Kobayashi, R., and D.L. Katz. 1955. *Trans AIME* 204:262.

Kobayashi, R., K.Y. Song, and E.D. Sloan. 1987. In *Petrol. Eng. Hndbk.* Ch. 25, ed. H.B. Bradley. Society of Petrol Eng., Richardson, TX.

Koh, C.A., et al. 1993. Spectroscopic data on the kinetics of hydrate formation and decomposition. *International Conference on Natural Gas Hydrates,* p. 561. New York.

Koshelev, V.S., V.I. Fomina, and S.S. Bik. 1971. *J. Ph. Ch.* 45n. 11.

Kostic, S. 1991. Natural gas hydrates—only a nuiscance? Paper presented at the 1991 SPUNG Conference. Trondheim, September.

Kostic, S., and T.M. Svartaas. 1991. Naturgasshydrater-Fremtidens Drivstoff og Energikilde (Natural gas hydrates—A future fuel and energy source), *Kjemi*, N. 4, 4–5, (in Norwegian).

Krasnovskay, L.I. 1976. Mehanizm Vzaimodeistviya Gidratov s Vodnym Aerozolem (Mechanism of hydrate interaction with an aqueous fog), *Trudy TsAO*, N.104. Moscow.

Krason, J., and M. Ciesnik. 1985. Geological evolution and analysis of confirmed or suspected gas hydrate localities: gas hydrates in the Russian literature. U.S. Department of Energy, DOE/MC/21181-1950. 5:164.

———. 1986b. Geological evolution and analysis of confirmed or suspected gas hydrate localities: basin analysis, formation and stability of gas hydrates in the Panama Basin. U.S. Department of Energy, DOE/MC/21181-1950, p. 8.

———. 1987. Geological evolution and analysis of confirmed or suspected gas hydrate localites: basin analysis, formation and stability of gas hydrates of the Aleutian Trench and the Bering Sea. U.S. Department of Energy, DOE/MC/21181-1950, p. 10.

Krason, J., and W.I. Ridley. 1985a. Geological evolution and analysis of confirmed or suspected gas hydrate localities: Blake-Bahama Outer Ridge, U.S. East Coast. U.S. Department of Energy, DOE/MC/21181-1950, p. 1.

Krason, J., and W.I. Ridley. 1985b. Geological evolution and analysis of confirmed or suspected gas hydrate localities: Baltimore Canyon Trough and Environs-U.S. East Coast. U.S. Department of Energy, DOE/MC/21181-1950, p. 2.

Krason, J., and B. Rudloff. 1985. Geological evolution and analysis of confirmed or suspected gas hydrate localities: Offshore of Newfoundland and Labrador. U.S. Department of Energy, DOE/MC/21181-1950, p. 4.

Krason, J., P.D. Finley, and B. Rudloff. 1985. Geological evolution and analysis of confirmed or suspected gas hydrate localities: basin analysis, formation and stability of gas hydrates in the western Gulf of Mexico. U.S. Department of Energy, DOE/MC/21181-1950, p. 3.

Krason, J., and P. Finley. 1992. Messoyakh Gas Field—Russia West Siberian Basin. Structural Traps VII. *Treatise of Petroleum Geology Atlas of Oil and Gas Fields*. APGA, Tulsa, OK.

Kremlev, A.N., and G.D. Ginsburg. 1989. The first results of the search for submarine gas hydrates in the Black Sea (the 21st expedition of the *RV Yevpatoriya). Geologia i Geofizika* 4:110–111.

Kvamme, B. 1994. *Fluid Phase Equilibria* 101:157.

Kvamme, B. 1995. *International J. Thermophysics* 16:743.

Kvamme, B., and A. Lund. 1993. The influence of gas-gas interactions on the Langmuir Constants for some natural gas hydrates. *International Conference on Natural Gas Hydrates,* p. 545. New York.

Kvamme, B., and H. Tanaka. 1995. *J. Phys.Chem.* 99:7114.

Kvamme, B., G. Huseby, and O.K. Forrisdahl. 1996. Molecular dynamics simulations of PVP kinetic inhibitor in liquid water and hydrate/liquid water systems. *Molecular Physic.* 2. Porsgrunn, Norway.

Kvenvolden, K.A. 1982. Occurrence and origin of marine gas hydrates. In *Proceedings of the 4th Canadian Permafrost Conference*, ed. M.H. French. Roger, J.E., Brown Volume. Ottawa: National Research Council of Canada, pp. 305–311.

———. 1984. Geochemistry of a naturally occuring massive marine gas hydrate. *Org. Geochem.* 6:703–713.

———. 1988a. Methane hydrate—A major reservoir of carbon in the shallow geosphere? *Chem. Geol.* 71:41–51.

———. 1988b. Methane hydrates and global climate. *Global Biogeochem. Cycles* 2:221–229.

———. 1993. Natural Gas Hydrate Occurrence and Issues. *International Conference on Natural Gas Hydrates*, p. 232. New York.

Kvenvolden, K.A. 1983a. In *Natural Gas Hydrates*, p. 63, ed. J.L. Cox. Butterworths, Boston.

Kvenvolden, K.A., and G.E. Claypool. 1981. *Trans. Amer. Geophys. Union* 62(45):900.

Kvenvolden, K.A., and L.A. Barnard. 1983b. Hydrates of natural gas in continental margins, in studies in Continental Margin Geology, eds. J.S.Watkins and C.L. Drake. *Am. Assoc. Pet. Geol. Mern.* 34:631–640.

Kvenvolden, K.A., and L.A. Barnard. 1983c. Gas hydrates of the Blake Outer Ridge, Site 533, Deep Sea Drilling Project Leg 76. In *Initial Reports of the Deep Sea Drilling Project.* 76:353-365, ed. R.E. Sheridan et al. U.S. Government Printing Office, Washington, D.C.

Kvenvolden, K.A., and T.J. McDonald. 1985. Gas hydrates of the Middle America Trench, Deep Sea Drilling Project Leg 84. In *Initial Reports of the Deep Sea Drilling Project*, ed. R. von Huene et al. 84:667–682. U.S. Government Printing Office. Washington, D.C.

Kvenvolden, K.A., and A. Grantz. 1990a. Gas hydrates of the Arctic Ocean region. In *The Geology of North America, vol. L, The Arctic Ocean Region*, eds. A. Grantz, L. Johnson, and J.F. Sweeney, pp. 539–549. Geological Society of America, Boulder, CO.

Kvenvolden, K.A., and M. Kastner. 1990b. Gas hydrates of the Peruvian outer continental margin. In *Proceedings of the Ocean Drilling Program, Scientific Results* 112:517–526, ed. E. Suess et al. Ocean Drilling Program, College Station, TX.

Kvenvolden, K.A., G. D. Ginsburg, and V.A. Solovyev. 1993. Worldwide distribution of subaquatic gas hydrates. *Geo Mar. Lett.*

Laaksonen, A. P., and Stilbs. 1992. *Mol. Phys.* 74:747.

Larsen, R., et al. 1996. The influence of kinetic inhibitors in the morphology of sI and sII clathrate hydrates. *2nd Intl. Conf. on Natural Gas Hydrates.* Toulouse, France.

Leggett, J. 1990. The nature of the greenhouse threat. In *Global Warming, The Greenpeace Report*, ed. J. Leggett. 14–43. Oxford University Press, New York.

Lekvam, K. 1995. Kinetics of natural gas hydrates. *Ph.D. Dissertation.* University of Stavanger, Norway.

Lekvam, K., et al. 1992. Nonmonotonic reaction rates in the formation of methane hydrate from liquid water. Rogaland University Center (working paper). Norway.

Lekvam, K., and P. Ruoff. 1993. A reaction kinetic mechanism for methane hydrate formation in liquid water. *J. Am. Chem. Soc.* 115:8565–8569.

———. 1993. Reaction kinetic simulations of methane hydrate formation in liquid water. *International Conference on Natural Gas Hydrates*, p. 558. New York.

Levin and Associates. 1983. *Handbook of Gas Hydrate Properties and Occurrence.*

Lipkowski, J., et al. 1990. A novel clathrate hydrate structure of tetraisoamylammonium fluoride. *J. Inclusion Phenomena Mol. Recoan. Chem.* 9:275–276.

Lipkowski, J., et al. 1992. *J. Inclusion Phenomena* 13(3):295.

Lorius, C. 1991. Polar ice cores: climatic and environmental records. *Int. Conf. on the Role of the Polar Regions in Global Change.* University of Fairbanks, Fairbanks.

Lund, A. 1993. Comments to some preliminary results from the Exxon hydrate flow loop. *International Conference on Natural Gas Hydrates*, p. 447. New York.

Lysne, D. 1993. Hydrate plug dissociation by pressure reduction. *International Conference on Natural Gas Hydrates*, p. 514. New York.

MacDonald, G.T. 1990b. Role of methane clathrates in past and future climates. *Clim. Change* 16:247–281.

———. 1990a. The future of methane as an energy resource. *Ann. Rev. Energy* 15:53–83.

Makarenko, F.A., et al. 1972. *Geotermicheskaya Karta SSSR (Geothermal map of the USSR):* Scale 1:5,000,000. Geologicheskiy Institut Akademii Nauk SSSR, Moskva.

Makogon, T.Y., and E.D. Sloan. 1994. Phase equilibrium for methane hydrate from 190 to 262K. *J. Chem. Eng. Data* 39:351–353.

Makogon, Y. 1996. Formation of hydrates in shut-down pipelines in offshore conditions. *Offshore Technology Conference.* OTC-8235. Houston, TX.

———. 1996. Gas hydrate formation in porous medium. *2nd Intl. Conf. on Natural Gas Hydrates.* Toulouse, France.

Makogon, Y.F. 1960. Crystal hydrates of natural gases and their prevention. N.T.S. po gazovoy tekhnike, GOSINTI (Council on Gas Machinery GOSINTI), n. 3. Moscow.

———. 1965. Hydrate formation in gas-bearing layer in permafrost conditions. *Gazovaya Promyshelennost (Gas Industry)* 5:14–15. Moscow.

———. 1966b. Specialties of exploitation of the natural gas fields in permafrost conditions. *TsNTI Mingazprom.* Moscow.

———. 1970a. Effect of the state of water on gas hydrate formation conditions. *Ekspress informatsiya: VNIIEGazprom.* n. 20. Moscow.

———. 1970b. Method for gas storage. Pat. No. 270671.

———. 1970c. Method for increasing the pressure of natural gas. Pat. No. 23770.

———. 1972b. Natural gases of the ocean and the problem of hydrates. *Ekspressinformatsiya: VNIIEGazprom*, n. 11. Moscow.

———. 1978/1981. *Hydrates of Natural Gas*, Moscow, Nedra, Izadatelstro, p. 208, 1974. Translated from Russian by W.J. Cieslesicz, p. 237. PennWell Books, Tulsa, OK.

———. 1984a. Perspectives for the oil and gas industry in the world. *Gazovaya Promyshlennost (Gas Industry)*, n. 8. Moscow.
———. 1984b. Razrabotka gazogidratnoy zalezhi (Production from natural gas hydrate deposits). *Gazovaya Promishlennos.* 10:24–26. Moscow.
———. 1985. *Gas Hydrates: Prevention of Gas Hydrates Formation and Their Utilization.* Nedra, Moscow.
———. 1987. *La Recherche.* 18:1192.
———. 1988b. Natural gas hydrates: the state of study in the USSR and perspectives for its use. Paper presented at the Third Chemical Congress of North America, 5-10 June 1988, at Toronto, Canada, p. 20.
———. 1991. The role of natural gas hydrates in global changes. Geoph. Inst. Univ. Alaska, Fairbanks, II, XII.
———. 1993. Russia's contribution to the study of gas hydrates. *International Conference on Natural Gas Hydrates*, p. 119. New York.
Makogon, Y.F., and G.A. Sarkisyants. 1966a. *Prevention of Hydrate Formation during Production and Transportation of Gas.* Nedra, Moscow.
———. 1976. In *Prevention of Hydrate Formation in the Extraction and Transport of Gas,* ed. D.W. Davidson. National Research Council of Canada, Ottawa.
Makogon, Y.F., et al. 1970d. Natural gas hydrates—world energy resources. *XI International Gas Congress.*
———. 1973. Possible origin of natural gas hydrates at floors of seas and oceans. Akademiya Nauk, *Sibirskoye Otdeleniye Geologiya i Geofizika.* 4:3–6.
Makogon, Y.F., et al. 1971. Obnaruzheniye zalezhi prirodnogo gaza v tverdom (gazogidratnom) sostoyanii (Detection of a pool of natural gas in a solid [hydrate] state). *Doklady Akademii Nauk SSSR* 196, n.l, pp. 197–200, pp. 203–206.
Makogon, Y.F., V.I. Tsarev, and N.V. Cherskiy, 1972a. Formation of large natural gas fields in zones of permanently low temperatures. *Doklady Academii Nauk SSSR.* 205:700–703.
Makogon, Y.F., and F.L. Sayakhov. 1988. Physical principles and models of decomposition of the hydrates of natural gases. *VNIIEGazprom.* Moscow.
Maksimov, A.M. 1996. Coupled processes of gas hydrate dissociation in porous media. *Engineering Mechanics*, Vol. 1, ASCE. New York. pp. 220–223.
Malenko, E.V. 1974. *Respublikanskia Nauchno-Tekgnicheskaia Kenferentoria po Neftekhimii.* Zd. Guryev.
———. 1979. Study of the conditions of formation and decomposition of natural gas hydrate and of the inhibiting effect of nonelectrolytes. *Dissertation for Candidacy of Chemistry Science.* Gur'ev.
Maliniak A., A. Laaksonen, and J. Korppi-Tommola. 1990. *J. Am. Chem. Soc.* 112:89.
Malishev, A.G. 1979. Hydrates of havie hydrocarbons. *Ph.D Dis.*, p. 266 Tiymen Industrial Institute.
Malone, R. D. April 1985. Gas hydrates topical report. DOE/METC/SP-218, U.S. Department of Energy.
———. 1993. Overview: gas hydrate geology and geography. *International Conference on Natural Gas Hydrates,* p. 225. New York.

Manheim, F.T., and M.K. Horn. Composition of deeper subsurface waters along the Atlantic continental margin. *Southeastern Geology* 9:215–236.
Mann, S.L., et al. 1989. Vapor-solid equilibrium ratios for structure I and structure II natural gas hydrates. In *Proc. 68th Ann. Gas Proc. Assoc. Conv.* San Antonio, TX, 13–14 March.
Marcheti, M.C., and J.W. Dufty. 1981. *Phys. Rev.* A24:2116.
Marshall, D.R., S. Saito, and R. Kobayashi. 1964. *AIChE J.* 10:202, 723.
Mason, V., and M. Kurtz. 1952. Rapid measurement of the thermal resistivity of soils. *Transactions American Institute of Electrical Engineers* 71:570.
Mathews, M. 1986. Logging characteristics of methane hydrate. *Log Anal.* 27(3):26–63.
McCain, W.D. 1990. *The Properties of Petroleum Fluids.* PennWell Books. Tulsa, OK.
McGuire, P.L. 1982. In *Proc. Fourth Can. Permafrost Conf.,* ed. H.M. French, p. 356.
McIver, R.D. 1977. Hydrates of natural gas—Important agent in geological processes. *Geol. Soc. Am. Abstr. Programs* 9:1089–1090.
———. 1981. In *Long-Term Energy Resources,* eds. R.F. Meyer and H.C. Olson. Pitman Boston. 1:713.
McKee, R.L., and H. Neshan. 1993. Predicting and mitigating hydrates in deepwater production. *International Conference on Natural Gas Hydrates.* New York.
McKetta, J.J., and D.L. Katz. 1947. Phase relationships of hydrocarbons-water system. *Trans AIME.*
McKoy, V., and O. Sinanoglu. 1963. *J. Chem. Phys.* 38:2946.
McLeod, H.D., and J.M. Campbell. 1961. *J. Petrol Tech.* 13:590.
McMullan, R.K., and G.A. Jeffrey. 1965. *J. Chem. Phys.* 42:2725.
Melnikov, V., and A. Nesterov. 1996. Modeling of gas hydrates formation in porous medium. *2-NGHC.* Toulouse, France.
Miller, J.J., M.W. Lee, and R. von Huene. 1991. A quantitative analysis of a gas hydrate phase boundary reflection (BSR), offshore Peru. *AAPG Bull.* 7S:910–924.
Miller, S.L. 1969. Clathrate hydrates of air in Antarctic ice. *Scienc.* 165:489.
———. 1984. Natural gases in marine sediments, ed. I.R. Kaplan. *Marine Science* 3, p. 151. Plenum.
Mokshantcev, N.B., and N.V. Cherski. 1961. *General Features of Geological Composition in the Eastern Yakutia.* Yakutsk Academie.
Monfort, J.P., and A. Nzihou. 1993. Light scattering kinetics study of cyclopropane hydrate growth. *J. Crystal Growth* 128:1182–1186.
———. 1993. Crystallization of gas hydrates: experimental techniques for the kinetic measurement of cyclopropane hydrate crystal growth. *International Conference on Natural Gas Hydrates,* p. 555. New York.
Morgantown Energy Technology Center. 1984. METC Topical Report: Gas hydrates project. February 1984.
Mori, Y., and T. Mochizuki. 1996. Modeling of mass transfer across a hydrate layer intervening between liquid water. *2nd Intl. Conf. on Natural Gas Hydrates.* Toulouse, France.

Moshfeghian, M., and R.N. Maddox. 1993. HYDRATE+: simulation of high-pressure flowline hydrate formation conditions. *International Conference on Natural Gas Hydrates*, p. 508. New York.
Muller, H.R., and M. von Stackelberg. 1952. *Naturwis.* 39:20.
Nadem, S.L. 1988. Measurement of gas permeability in hydrate saturated unconsolidated cores. Paper presented at the *Third Chemical Congress of North America*, 5–10 June. Toronto.
Namiot, A.Y. 1991. *Solubility of Gas in the Water.* Nedra, Moscow.
Narita, H., and T. Uchida. 1996. Studies on formation/dissociation rates of methane hydrates. *2nd Intl. Conf. on Natural Gas Hydrates.* Toulouse, France.
Nerheim, A.R. 1993. Investigation of gas hydrate formation kinetics by laser light scattering. *Dr. Ing. (Ph.D). Thesis.* August. The Norwegian Institute of Technology (NTH).
Nerheim, A.R., T.M. Svartaas, and E.J. Samuelson. 1992. Investigation of hydrate kinetics in the nucleation and early growth stage by laser light scattering. In *Proceedings of the Second (1992) Interntional Offshore and Polar Engineering Conference* 1:620–627.
Nerheim, A.R., and T.M. Svartaas. April 1994. Laser light scattering studies of gas hydrate formation kinetics. *4th Intern. Offshore Confer.* Japan.
Ng, H.-J., and D.B. Robinson. 1976a. *I&EC Fundam.* 15:293.
———. 1976b. *AIChE Journal* 22:656.
———. 1977. *AIChE Journal* 23:477.
———. February 1980. Reprinted from *I&EC Fundamentals* 19:33.
———. April 1983. *Gas Proc. Assn. Rsch. Rpt. 66.* Tulsa, OK.
———. 1993. New developments in the measurement and prediction of hydrate formation for processing needs. *International Conference on Natural Gas Hydrates*, p. 450. New York.
Ng, H.-J., J.P. Petrunia, and D.B. Robinson. 1978. *Fluid Phase Equilibria* 1:283.
Ng, H.-J., C.J. Chen, and D.B. Robinson. September 1985. *Gas Proc. Assn. Rsch Rpt* 92. Tulsa, OK.
———. April 1987b. *Gas Proc. Assn. Rsch. Rpt.* 106. Tulsa, OK.
Ng, H.-J., C.J. Chen, and T. Saeterstad. 1987a. *Fluid Phase Equilibria* 36:99.
Nikitin, B.A. 1936. *Z. Anorg. Allg. Chem.* 227:81.
Nikitin, B.A. 1937. *Nature* 140:643.
Nikitin, B.A. 1939. *Zh. Obshch. Khim.* 9:1167–1176.
Nikitin, B.A. 1940. Izv. *Akad. Nauk SSSR, Otd. Khim.Nauk.* 1:39.
Nomokonov, V.P., and S.N. Stupak, 1988. Indications of gas hydrate deposits in the Black Sea. Izvestiya Vysshykh Utshebnykh Zavedeniy. *Geologia i Razvedka* 3:72–82.
Norvik, II, and K. Lekvam, 1994. Mass and heat transfer effects on gas hydrate growth. *International Offshore and Polar Engineering Conference.* Osaka, Japan.
Nose, S. 1984. *Mol. Phys.* 52:255.
Notz, P.K. 1993. Discussion of the paper "The study of separation of nitrogen from methane by hydrate formation using a novel apparatus." *International Conference on Natural Gas Hydrates*, p. 425. New York.

Pandit, B.I., and M.S. King. 1982. Elastic wave velocities of propane gas hydrates. In *Proceedings of the Canadian Permafrost Conference: the Roger J.E. Brown Memorial Volume*, ed. H.M. French, pp. 335–352. Ottawa, Canada (Canadian National Research Council).
Parameswaran, V.R., M. Paradis, and T.P. Handa. 1988. Strength of frozen sand containing tetrahydrofuran hydrate. *Proceedings of the Third Chemical Congress of North America.* Toronto, Canada.
———. 1989. Strength of frozen sand containing tetrahydrofuran hydrate. *Can. Geotech. J.* 26:479.
Paranjpe, S.G., et al. 1988. Hydrate formation in crude oils and phase behavior of hydrates in mixtures of methane, propane, isobutane, and n-butane. *Third Chemical Congress of North America*, 5–10 June. Toronto, Canada.
Parent, J.S., and P.R. Bishnoi. 1993. An apparatus for precise light scattering studies of the nucleation of natural gas hydrates. *International Conference on Natural Gas Hydrates*, p. 552. New York.
Parrish, W.R., and J.M. Prausnitz. 1972. *Ind. Eng. Chem. Proc. Des. & Dev.* 11:26.
Pauling, L. 1961. *Science* 134:15.
Paull, C.K., W. Ussler, and W.P. Dillon. 1991. Is the extent of glaciation limited by marine gas hydrates? *Geophysical Research Letters* 18:432–434.
Peng, D.Y., and D.B. Robinson. 1976a. *Ind. Eng. Chem. Fundam.* 15:59.
Perry, C.R. 1960. *Oil & Gas Journal* 58:71.
Pieroen, A.P. 1955. *Rec. Trav. Chim.* 74:995.
Pierre, J. 1848. *Ann. Chem. Phys. Ser. 3* 23:416.
Platteeuw, J.C., and J.H. van der Waals. 1959. *Rec. Trav. Chirn, Pays-Bas.* 78:126.
Poettmann, F.H. 1984. *Hydrocar. Proc.* 63(6):111.
Polderman, L.D. 1958. The glycols as hydrate point depressants in natural gas systems. *Proc. Gas Conditioning Conference.* Norman, OK.
Prausnitz, J.M. 1969. *Molecular Thermodynamics of Fluid-Phase Equilibria.* Prentice-Hall, Inc. Englewood Cliffs, NJ.
Priestley, J. 1790. Experiments and observations on different kinds of air, and other branches of natural philosophy, connected with the subject. Birmingham, Thomas Pearson. 2:359–362.
———. 1778–80. Versuche und Beobachtungen Über Vershiedene Gattungen der Luft, Th. 1-3, 3:359–362. Wien-Leipzig.
Reamer, H.H., F.T. Selleck, and B.H. Sage. 1952. *J. Petrol. Tech.* 4(8):197.
Reed, D.L., et al. 1990. Relations between mud volcanoes, thrust deformation, slope sedimentation, and gas hydrate, offshore north Panama. *Mar. Pet. Geol.* 7:44–54.
Reed, R.L., et al. 1993. Some preliminary results from a pilot-size hydrate flow loop. *International Conference on Natural Gas Hydrates*, p. 430. New York.
Ripmeester, J.A., and D.W. Davidson. 1981. *J. Mol. Struct.* 75:647.
———. 1977. *Mol. Cryst. Liq. Cryst.* 43:189.
Ripmeester, J.A., et al. 1987. *Nature* 325:135.
Ripmeester, J.A., et al. 1993. Molecular perspectives on structure and dynamics in clathrate hydrates. *International Conference on Natural Gas Hydrates*, p. 161. New York.

Robinson, D.B., and H.J. Ng. *Can. Petrol. Tech.*, 26, July–August.
———. December 1976. *Hydrocarbon Processing* 95.
Rodger, P.M. 1990. *J. Phys. Chem.* 94:6080.
———. 1994. *AIChE J.* 37:1511.
———. 1994. *Mol. Sim.* 5:315.
Roozeboom, H.W.B. 1884. *Rec. Trav. Chem. Pays-Bas.* 3:26.
———. 1885. *Rec. Trav. Chem. Pays-Bas.* 4:65.
Rouher, O.S., and A.J. Barduhn. 1969. *Desalination* 6:57.
Rozov, V.N., et al. 1986. *Gazov. Promst.* 10:11.
Rueff, R.M., E.D. Sloan, and V.F. Yesavage. 1988. *AIChE J.* 34:1468.
Saito, S., D.R. Marshall, and R. Kobayashi. 1964. *AIChE J.* 11:96.
Saltykova, N.A., V.A. Soloviev, and A.D. Pavlenkin. 1987. Seismic indications of submarine gas hydrates in the Bering Sea. *Geological-Geophysical Investigations of the World Oceans*, pp. 119–130. Sevmorgeologia, Lenigrad.
Sapir, M.H. 1973. *V.I., Geol. Nefti i Gaza.* 6:26.
Sarkisyants, G.A. 1958. Prevention of hydrate formation. *Gostoplekhizdat.* Moscow.
Sayakhov, F.L., M.A. Fathikhov, and N.M. Nasirov. 1990. Research of hydrate dissociation by high frequency electromagnetic field. *Int. Conf. Production of Gas.* Krasnodar.
Scauzillo, F.R. 1956. *Chem. Eng. Prog.* 52:324.
Schoenfeld, F.A. Ch. 1855. *Neue Reihe.* 19:19.
Schroeder, W. 1927. Die Geschichte der Gas Hydrate. Sammlung Chem. *Chem. Tech.* Vortrage 29, p. 98. F. Enke, Stuttgart.
Sego, D.C., and R.J. Wittebolle. 1984. Engineering behavior of sand containing hydrates. *Proceedings 3rd International Cold Regions Engineering Specialty Conference.* Edmonton, Canada. 2:589–602.
Selim, M.S., and E.D. Sloan. 1989. *AIChE J.* 35:1049.
Selleck, F.T., L.T. Carmichael, and B.H. Sage. 1952. *Ind. Eng. Chem.* 44:2219.
Sergeev, G.B. and V.A. Batiuk. 1978. *Kriokhimia. Moscow. Chem.*
Sharma, G.D. 1987. Development of Alaskan gas hydrate resources. Department of Energy. DOE/FE/61142608 (DE88010270). October.
Shepard, G.L. 1979. Shallow crustal structure and marine geology of a convergence zone, northwest Peru and southwest Ecuador. *Ph.D. Dissertation*, pp. 157–165, University of Hawaii.
Sheshukov, N.L. 1972. *Gazovoe Delo.* 6:8.
Sheshukov, N.L., et al. 1972. O zaleganii gaza v gidratnom sostoyanii na Mesoyakhskom mestorozhdenii (Occurrence of gas in the hydrate state in Messoyakh field.) *Gazovoe Delo.* 6:810.
Shipley, T.H., et al. 1979. Seismic reflection evidence for the widespread occurrence of possible gas-hydrate horizons on continental slopes and rises. *Amer. Assn. Petrl. Geol. Bull.* 63:2204–2213.
Shipley, T.H., and B.M. Didyk. 1982. Occurrence of methane hydrates offshore southern Mexico. In *Initial Reports, Deep Sea Drilling Project*, eds. J.S.Watkins et al. 76:353–365. U.S. Government Printing Office, Washington, D.C.
Shneidman, V.A., and M.C. Weinberg. 1992. *J. Chem. Phys.* 97:3621.

Sloan, E.D. 1984. *Proc. 63th Annual Convention, Gas Processors Association.* 63:163.
———. 1985a. *Proc. 64th Annual Convention, Gas Processors Association.* 64:125.
———. 1994. *Plenary Lecture, 12th Symposium on Thermophysical Properties.* 12–24 June. Boulder, CO.
Sloan, E.D. 1985b. In *Initial Reports of the Deep Sea DrillingProject*, eds. R. von Huene et al., 84:695. U.S. Government Printing Office Washington, D.C.
———. 1990. *Clathrate Hydrates of Natural Gas.* Marcel Dekker Inc., New York.
Sloan, E.D., F.M. Khoury, and R. Kobayashi. 1976. *Ind. Eng, Chem. Fundam.* 15:318.
Sloan, E.D., and W.R. Parrish. 1983. *Natural Gas Hydrates: Properties, Occurrence, and Recovery*, ed. J.L. Cox. Butterworths.
Sloan, E.D., et al. 1986. *Fluid Phase Equilibria.* 29:233.
———. 1987. *Ind. Eng. Che. Res.* 26:1173.
Smirnov, A.S. 1946. Hydrocarbon gases technology. *Gostoptekhizdat.* Moscow.
Smirnov, L.F. 1991. New techniques involving gas hydrates. *Teoreticheskie Osnovy Khimicheskoi Tekhnologii (Theoretical Bases of Chemical Engineering)*, n. 6.
———. 1993. *Thermodynamic Basis of Gas Hydrate Transformers.* Kiev.
Smirnov, L.F., and V.K. D'yaehenko. Method of production and storage of gas hydrates. Pat. No. 1723407.
Smith, S.L., and A. Judge. 1993. The distribution of natural gas hydrates in Canada. *International Conference on Natural Gas Hydrates*, p. 495. New York.
Solodovnikov, S.F. 1979. Crystallographic structure of the tetraisoamylphosphonium bromide clathrate hydrate (iso-$CSH_{11})_4PBr \cdot 32H_20$. *DAN SSSR* (USSR Academy of Sciences Reports) 247(2):357–360. Moscow.
Sparks, K.A. 1983. The water content of liquid ethane and propane in two phase equilibrium with hydrate. *M.Sc. Thesis T-2809.* Colorado School of Mines, Boulder, CO.
Stoll, R.D. 1974. Effects of gas hydrates in sediments. In *Natural Gases in Marine Sediments*, ed. I.R. Kaplan, pp. 235–348. Plenum Press, New York.
Stoll, R.D., J. Ewing, and G.M. Bryan. 1971. Anomalous wave velocities in sediments containing gas hydrates. *J. Geophys. Rsch.* 76:2090–2094.
Stoll, R.D., and G.M. Bryan. 1979. Physical properties of sediments containing gas hydrates. *J. Geophys. Rsch.* 84:1629–1634.
Strizhov, I.N., and I.E. Khodanovich. 1946. Gas production. *Gostoptekhizdat.* Moscow.
Sumets, V.I. 1974. Predotvrashchenie gidratobrazovaniya v prizaboynoy zone (Prevention of hydrate formation in well bottom zone). *Gazovaya Promyshlennost* 2:24–26.
Svartaas, T.M. November 1988. Overview of hydrate research at Rogalands-Forskning. Presented at BHRA Conference on Operational Consequences of Hydrate Formation and Inhibition Offshore, Cranfield, UK.

Svartaas, T.M. 1992. Formation and inhibition of hydrate crystals. *Report RF-249/92* (final report from NTNF-PROFF project).
Svartas, T.M. 1996. Kinetics of formation of natural gas hydrates. *2nd Intl. Conf. on Natural Gas Hydrates*. Toulouse, France.
Svartaas, T.M., and F.H. Fadnes. 1992. Methane hydrate equilibrium data for the methanewater-methanol system up to 500 bars. *Proceedings of the 2nd. International Offshore and Polar Engineering Conference* 1:614–619.
Svartaas, T.M., M. Kelland, and L. Dybvik. 1994. Control of hydrate formation by surfactants and polymers. *Proceedings of the 4th International Offshore and Polar Engineering Conference*. Japan.
Tanaka, H. 1992. *Chem. Phys. Lett.* 202:345.
Tanaka, H., and K. Kiyohara. 1993a. *J. Chem. Phys.* 98:4098.
———. 1993c. *Chem. Phys.* 98:8110.
Tanaka, H., and K. Nakanishi. 1994. *Mol. Sim.* 12:317.
Tolkachev, M.V. 1988. *Znaniya-Sila,* n. 1:12–13.
Torstein, Austvik 1992. Hydrate formation and behaviour in pipes. *Ph.D. Dissertation*. Trondheim, Norway.
Toxvaerd, S. 1990. *Mol. Phys.* 72:159.
Trofimuk, A.A. 1972. Mechanism of formation of natural gas hydrate accumulations. *Geologiya i Geofizika.* Novosibirsk N. 8.
Trofimuk, A.A., and N.V. Cherskii. 1974. Mekhanizm razdeleniya izotopov vody i gazov v zonakh gidratoobrazovaniya zemnoy kory (Mechanism of fractionation of isotopes of water and gas in crustal zones of hydrate formation). *Doklady Akademii Nauk SSSR* 215:210–212. Moscow.
Trofimuk, A.A., N.V. Cherskiy, and V.P. Tsarev. 1975. The biogenic methane resources in the oceans. *Doklady Academii Nauk SSSR* 225:936–943. Moscow.
———. 1973. Accumulation of natural gases in zones of hydrate formation in the hydrospere. *Doklady Akademii Nauk SSSR* 212:931–934. Moscow.
Trofimuk, A.A., N.V. Cherskiy, and V.P. Tsarev. 1979. Gas hydrates—new sources of hydrocarbons. *Priroda (Natura)* 1.18.27.
Trofimuk, A.A., et al. 1980. Possible gas reserves in the continental and marine deposits and the methods of their prospecting and development. Presented at the 11th ASA Conference on the Conventional and Unconventional World Natural Gas Resources, Laxenburg, Austria.
Trofimuk, A.A., Y.F. Makogon, and M.V. Tolkachev. 1981. *Geologiya Nefti i Gaza* 10:15.
Trofimuk, A.A., et al. 1982. *Geologiya i Geofizika* 23:3. Novosibirsk.
Tsarev, V.P. 1975. *J. Phys. Chem.* 49(1):2753–2755.
Tsarev, V.P. 1976. *Details of Gas Deposits Formation in Permafrost.* Yakutsk.
Tse, J.S. 1993. Dynamical properties and stability of clathrate hydrates. *International Conference on Natural Gas Hydrates,* p. 187. New York.
Tse, J.S., and D.W. Davidson. 1981. *Proc. Fourth Canadian Permafrost Conf.,* p. 329. Calgary, Alberta, 02–06 March. National Research Council of Canada, Ottawa.
Tse, J.S., et al. 1986. *J. Incl. Phenom.* 4:235.
Tse, J.S., W.R. McKinnon, and M. Marchi. 1987. *J. Phys. Chem.* 91:4188.

Tucholke, B.F., G.M. Bryan, and J.I. Ewing. 1977. Gas-hydrate horizons detected in seismic profiler data from the western North Atlantic. *Amer. Assn. of Petrol. Geo. Bull.* 61:698–707.
Tzirita, A. 1991. A study of electrical and thermal properties and their use to detect natural gas hydrates in ocean sediments. *Ph.D. Dissertation*. Texas A&M University, College Station, TX.
van Cleeff, A., and G.A.M. Diepen. 1960. *Rec. Trav. Chim.* 79:582.
van der Waals, J.H., and J.C. Platteeuw. 1959. Clathrate solutions. *Adv. Chem. Phys.* 2:1.
van der Waals, J.O. 1890. On the continuity of the gaseous and liquid state. *Dissertation*. Leiden.
Vasil'ev, V.G., Y.F. Makogon, F.A. Trebin, A.A. Trofimuk, and N.V. Chersky. 1970. The property of natural gases to occur in the Earth crust in a solid state and to form gas hydrate deposits. *Otkrytiya v SSSR* 1968–1969, pp. 15–17.
Verigin, N.N., I.L. Khabibullin, and G.A. Khalikov. 1980. Izv. *Akad. Nauk. SSSR, Mekhanika Zhidkosti Gaza* 1:174.
Verma, V.K. 1975. *J. Pet. Tech.* 27:223.
Villard, P. 1888. *Compt. Rend.* 106:1602.
———. 1890. *Compt. Rend.* 111:302.
———. 1896. *Compt. Rend.* 123:337.
von Stackelberg, M. 1949. *Naturwiss.* 36:327–359.
———. 1954. *Z. Electrochem.* 58:104.
———. 1956. *Rec. Trav. Chim. Pays-Bas.* 75:902.
von Stackelberg, M,. and H.R. Muller. 1951b. *J. Chem. Phys.* 19:1319.
———. 1951a. *Naturwiss.* 38:456.
von Stackelberg, M., and H. Frubuss. 1954. *Z. Electrochem.* 58:99.
von Stackelberg, M., and W. Jahns. 1954. *Z. Electrochem.* 58:162.
———. 1954. *Z. Electrochem.* 58:40.
von Stackelberg, M., and B. Meuthen. 1958. *Z. Electrochem.* 62:130.
Vysniauskas, A., and P.R. Bishnoi. 1983a. In *Natural Gas Hydrates: Properties, Occurrence and Recovery,* ed. J.L. Cox. Butterworths.
———. 1983. *Chem. Eng. Sci.* 38:1061.
———. 1985. *Chem Eng. Sci.* 40:299.
Waples, D.W. 1980. Time and temperature in petroleum formation: application of Lopatin's method. *AAPG Bulleti.* 64:916–926.
Watson, R.T., et al. 1990. Greenhouse gases and aerosols. In *Climate Change, The IPCC Scientific Assessment,* eds. J.T. Houghton, G.J. Jenkins, and J.J. Ephraums. 1–40, Cambridge University Press, New York.
Weast, R.C. 1977. *Handbook of Chemistry and Physics.* 58th ed., CRC, Florida.
Weaver, J.S., and J.M. Stewart. 1982. In situ hydrates under the Beaufort Sea Shelf. In *Proc. Fourth Canadian Permafrost Conf.*, ed. M.H. French, pp. 312–319. Calgary, Alberta, 02–06 March. National Research Council of Canada, Ottawa.
Whalley, E., et al. 1991. Some aspects of hydrogen bonding in the phases of water. *J. Mol. Struc.* 250:337.
Whalley, E., et al. 1986. Pressure melting below the glass transition: a new way of making amorphous solids. *Ann. New York Acad. Sci.* 484:81.

Wilcox, W.I., D.B. Carson, and D.L. Katz. 1941. *Ind. Eng. Chem.* 33:662.
Wroblewski, S.V. 1882. *Compt. Ren.* 94(212):1355.
Yamamoto, S., J.B. Alcauskas, and T.E. Crozier. 1976. Solubility of methane in distilled water and seawater. *J. Chem. Eng. Data* 21:78–80.
Yamano, M., et al. 1982. Estimates of heat flow derived from gas hydrates. *Geology* 10:339–343.
Yefremova, A.G., and B.P. Zhizhchenko. 1974. Occurrence of crystal hydrates of gas in sediments of modern marine basins. *Doklady Akademii Nauk SSSR* 214:1179–1181. Moscow.
Yefremova, A.G., and N.D. Gritchina. 1981. Gas hydrates in sediments beneath seas and the problem of their exploitation. *Geologiya Nefti i Gaza* 2:32–35. Moscow.
Zakerzewski, M., and Y.P. Handa. 1993. Thermodynamic properties of ice and of tetrahydrofuran hydrate in confined geometries. *J. Chem. Thermodyn.* 25:631.
Zeldovlch, Ya.B. 1943. *Acta Physicochim.* 11:1. USSR.
Zurer, P.S. 1987. *Chem. and Eng. News* 65(48):25–27.

INDEX